



**Université  
de Lille**



**UNIVERSITÀ  
DI TORINO** **DBios**

## **International co-tutorial Ph.D. thesis**

In agreement between

**Université de Lille**

**Faculté des Sciences et Technologies**

**Ecole Doctorale Biologie-Santé EDBSL**

**Laboratory of Cell Physiology INSERM U1003**

**France**

**Università degli Studi di Torino**

**Department of Life Sciences and Systems Biology**

**PhD School in Complex Systems for Life Sciences**

**Laboratory of Cellular and Molecular Angiogenesis**

**Italy**

Discipline: Physiologie 66  
Aspects moléculaires et cellulaires de la Biologie

Presented and publicly defended on 13/04/2023 by

**MADELAINE MAGALI AUDERO**

### **Acidic tumour microenvironment and Ca<sup>2+</sup> signalling interplay in Pancreatic Ductal Adenocarcinoma (PDAC) progression**

#### **Jury Members:**

Prof. Luis Pardo, Max Planck Institute, GE

Reviewer

Dr Sebastien Roger, University of Tours, FR

Reviewer

Prof. Ildiko Szabó, University of Padova, IT

Examiner

Prof. Dr. Albrecht Schwab, University of Münster, GE

Examiner

Prof. Natalia Prevarskaya, University of Lille, FR

Thesis supervisor

Prof. Alessandra Fiorio Pla, University of Turin, IT

Thesis Co-supervisor

# Abstract

Pancreatic ductal adenocarcinoma (PDAC) is the most common cancer affecting the pancreas, characterized by an unsatisfactory 5-year survival rate of around 10%. To date, there are no effective therapeutic options for PDAC. This is partly due to a highly desmoplastic and immunosuppressive microenvironment contributing to therapeutic failure. Moreover, the PDAC tumor microenvironment is featured by high acidosis ( $\text{pH}_e < 6.5$ ), a result of the metabolic reprogramming ("Warburg effect"), and hypoxic conditions, which offers important cues for its aggressiveness by selecting cancer cell phenotypes with competitive benefits for PDAC progression. On the other hand,  $\text{Ca}^{2+}$ -permeable ion channels are known to regulate several hallmarks of cancer; thus, they may play an important role in contributing to the PDAC malignancy by mediating tumor acidosis responses, as their  $\text{pH}_e$ -sensitivity allows them to transduce TME signals to activate intracellular downstream pathways linked to PDAC progression. Although the roles of tumor acidosis and  $\text{Ca}^{2+}$  signaling in cancer progression are well established, the hypothesis of acidic TME employing  $\text{Ca}^{2+}$  signaling as a preferential route for sustaining tumor progression has not yet been sufficiently explored.

My Ph.D. work aimed to study the phenotypic and genetic changes of PDAC cells upon acidic stress along the different stages of selection and to evaluate how tumor acidosis modulates  $\text{Ca}^{2+}$  signals and phenotypes in the PDAC cell lines, with a particular focus on  $\text{Ca}^{2+}$  oscillations and Store-Operated  $\text{Ca}^{2+}$  entry (SOCE). To this end, PANC-1 and Mia PaCa-2 cells were subjected to short- and long-term acidic pressure and recovery to  $\text{pH}_e 7.4$ . The latter treatment was to mimic PDAC edges and consequent cancer cell escape from the tumor. The impact of acidosis was assessed for cell morphology, proliferation, adhesion, migration, invasion, invadopodia activity, and epithelial-mesenchymal transition (EMT) via functional *in vitro* assays and RNA sequencing and for intracellular  $\text{Ca}^{2+}$  signals using Fura-2. Our results indicate that short acidic treatment limits the growth, adhesion, invasion, and viability of PDAC cells. As the acid treatment progresses, it selects cancer cells with enhanced migration and invasion abilities induced by EMT, further enhancing their metastatic potential when re-exposed to  $\text{pH}_e 7.4$ . RNA-seq analysis of PANC-1 cells exposed to short-term acidosis and  $\text{pH}_e$ -selected recovered to  $\text{pH}_e 7.4$  revealed distinct transcriptome

rewiring. We noted an enrichment of genes relevant to proliferation, migration, EMT, and invasion in acid-selected cells. Interestingly, PANC-1 cells are characterized by slower  $\text{Ca}^{2+}$  oscillations during short-term acid exposure compared to control cells and a tendency of ORAI1 downregulation at mRNA levels, while long-term acidosis and recovery to neutral  $\text{pH}_e$  determine the recovery of fast  $\text{Ca}^{2+}$  oscillations and upregulation of ORAI1. In all our cell models,  $\text{Ca}^{2+}$  oscillations are SOCE-dependent, as ORAI1 blockade with Synta66 and siORAI1 results in impaired  $\text{Ca}^{2+}$  oscillations' initiation and maintenance. These data correlate with SOCE in PANC-1 cells, which is decreased during the short-term acid treatment, and increased in acid-selected cells with and without recovery to  $\text{pH}_e$  7.4. Finally, ORAI1-mediated  $\text{Ca}^{2+}$  entry activates signaling cascades that increase migration and invasion of all the cell models exposed to acidic  $\text{pH}_e$ .

In conclusion, our findings show that acid-induced selection contributes to acquiring a more aggressive phenotype in PDAC cells, characterized by the upregulation of SOCE, required to generate fast  $\text{Ca}^{2+}$  oscillations, which may trigger  $\text{Ca}^{2+}$ -dependent signaling pathways involved in PDAC progression.

**Keywords:** Acidic tumor microenvironment; acid-selection; PDAC; EMT;  $\text{Ca}^{2+}$  signaling; Store-Operated  $\text{Ca}^{2+}$  Entry;  $\text{Ca}^{2+}$  oscillations.

# Résumé

L'adénocarcinome canalaire pancréatique (PDAC) est une maladie mortelle caractérisée par un micro-environnement tumoral (TME) extrêmement acide (<pHe 6,5) qui joue un rôle important dans son début et sa progression. Dans ce contexte, les canaux ioniques perméables au  $\text{Ca}^{2+}$  représentent de bons candidats cibles en raison de leur capacité à intégrer des signaux provenant de la TME. Les canaux  $\text{Ca}^{2+}$  sont en effet des capteurs de pH capables d'intégrer les signaux de la TME pour activer les voies intracellulaires en aval liées à la progression du PDAC. Bien que les rôles de l'acidose tumorale et de la signalisation du  $\text{Ca}^{2+}$  dans la progression du cancer soient bien établis, l'hypothèse d'une TME acide utilisant la signalisation du  $\text{Ca}^{2+}$  comme voie préférentielle pour soutenir la progression tumorale n'a pas encore été suffisamment explorée. Mon travail de doctorat visait à étudier les changements phénotypiques et génétiques des cellules PDAC lors d'un stress acide au cours des différentes étapes de sélection et à évaluer comment l'acidose tumorale module les signaux  $\text{Ca}^{2+}$  et les phénotypes dans les lignées cellulaires PDAC, avec un accent particulier sur les oscillations  $\text{Ca}^{2+}$  et Store-Operated  $\text{Ca}^{2+}$  entry (SOCE). À cette fin, les cellules PANC-1 et Mia PaCa-2 ont été soumises à une pression acide à court et à long terme et à une récupération à pHe 7,4. Ce dernier traitement visait à imiter les bords du PDAC et l'évasion consécutif des cellules cancéreuses de la tumeur. L'impact de l'acidose a été évalué sur la morphologie cellulaire, la prolifération, l'adhésion, la migration, l'invasion, l'activité des invadopodes et la transition épithélio-mésenchymateuse (TEM) par des tests fonctionnels in vitro et le séquençage de l'ARN, ainsi que sur les signaux  $\text{Ca}^{2+}$  intracellulaires avec Fura-2. Nos résultats indiquent qu'un court traitement acide limite la croissance, l'adhésion, l'invasion et la viabilité des cellules PDAC. Au fur et à mesure que le traitement acide progresse, il sélectionne les cellules cancéreuses ayant des capacités de migration et d'invasion accrues induites par l'EMT, ce qui augmente encore leur potentiel métastatique lorsqu'elles sont réexposées à un pHe 7,4. L'analyse RNA-seq des cellules PANC-1 exposées à une acidose de courte durée et récupérées à pHe 7,4 a révélé un recâblage transcriptomique distinct. Il est intéressant de noter que les cellules PANC-1 sont caractérisées par des oscillations  $\text{Ca}^{2+}$  plus lentes pendant une exposition à l'acide à court terme par rapport aux cellules de contrôle et par une tendance à la régulation négative d'ORAI1 au niveau de l'ARNm, tandis que l'acidose à long terme et le rétablissement à un pH neutre déterminent le rétablissement d'oscillations  $\text{Ca}^{2+}$  rapides et la



régulation positive d'ORAI1. Dans tous nos modèles cellulaires, les oscillations du  $\text{Ca}^{2+}$  sont dépendantes de SOCE, car le blocage d'ORAI1 par Synta66 et siORAI1 entraîne une altération de l'initiation et du maintien des oscillations du  $\text{Ca}^{2+}$ . Ces données sont en corrélation avec le SOCE dans les cellules PANC-1, qui est diminuée pendant le traitement acide à court terme, et augmentée dans les cellules sélectionnées pour l'acide avec et sans récupération à pHe 7,4. Enfin, l'entrée de  $\text{Ca}^{2+}$  médiée par ORAI1 pourrait être impliquée dans l'activation des cascades de signalisation qui conduisent à l'augmentation de la migration et de l'invasion de tous les modèles cellulaires exposés à un pHe acide, car le traitement par Synta66 et siORAI1 n'ont pas affecté l'invasion et la migration des cellules de contrôle.

En conclusion, nos résultats montrent que la sélection induite par l'acide contribue à l'acquisition d'un phénotype plus agressif dans les cellules de PDAC, caractérisé par une augmentation du SOCE, nécessaire à la génération d'oscillations rapides de  $\text{Ca}^{2+}$  qui peuvent activer des voies de signalisation  $\text{Ca}^{2+}$ -dépendantes impliquées dans la progression du PDAC

# Acknowledgments

During this journey, so many people have contributed in many different ways to this important achievement.

I want to express my sincere gratitude to my PhD defense jury members. First, **Prof. Luis Pardo** and **Dr. Sebastien Roger**, thank you for agreeing to review my thesis and for the dedicated time. You have assisted me in different places and roles these past 3 years, and your comments and suggestions have always s will be greatly appreciated. I would also like to thank **Prof. Ildiko Szabó** for accepting to be part of my jury, and I would like to renew my thanks for your valuable advice at our first meeting. **Prof. Dr. Albrecht Schwab**, *vielen Dank*, for accepting the role as President of my jury. In particular, thank you for the support, advice, suggestions, and many laughs you gave to other fellows and me during my journey within the pHioniC project.

A special “Thank you” to my thesis supervisor, **Prof. Natacha Prevarskaya**, first of all, thank you for accepting me in your Laboratory in 2018. You have provided fundamental insights and directed me in moments of indecision. Without your patience and reassuring guidance, it would certainly have been more difficult to extricate me from the pitfalls of the PhD. Not only, thank you for giving me a good example of leadership and female empowerment.

The second special “Thank you” to my co-supervisor, **Prof. Alessandra Fiorio Pla**. You have helped me on many occasions, from my Master’s studies to this last day, that I cannot count. You have opened for me the most important doors of my professional and scientific life, and your advice have been the sincerest. Besides your professional role, I will always cherish your funny and bright personality and your never-intrusive support that have, unknowingly, blown away many dark clouds during my journey and made me feel the burden of this experience less heavy. *Grazie davvero*.

I would also like to thank the past and present members of the Laboratory PhyCell for welcoming me at the beginning of my experience in France and for contributing in different manners. First, I would like to thank **Dr. Lina Mesilmany.**, my Habibi. I will always remember our first meet at my desk and the complete spontaneity and naturalness of the beginning of our friendship. We have shared innumerable experiences, hot chocolates and food, chats, travels, hugs and smiles and your friendship was a safe harbour during my Ph.D. *Shukran!* A big merci also to **Dr. Silviya**

**Radoslavova**, you have helped me a lot during these years, especially with the painful French bureaucracy, and only for this I am grateful for life! Thank you for the many chats and moments spent together in the lab and outside. Many thanks to **Dr Maya Yassine** for helping me with the hundreds of Western Blots for my first paper. Thank you to **Antoine Folcher, Dheeraj Kannancheri Puthooru, Dr Charlotte Dubois, Dr. Aurélien Haustrate, Dr Valerio Farfariello, Dr Loïc Lemonnier, Prof. Morad Roudbaraki, Dr Kateryna Kondratska, Prof. Dimitra Gkika, Dr. V'yacheslav Lehen'kyi, Emilie Desruelles, Nathalie Ziental-Gelus, and Sandy Despeghel** for your technical and scientific help and pieces of advice, for any antibody, solution, agonist or plasmid you shared with me, homemade sweets, for the random chats in any room of the Lab and the laughs. A special Merci to **Brigitte Macquart**, whose very efficient and fast administrative help with orders, missions, budgets, and much more made my Ph.D. easier.

I also deeply thank the members of the Laboratory of Cellular and Molecular Angiogenesis in Turin; **Dr. Giorgia Chinigò, Dr. Giorgia Scarpellino, Dr. Federico Ruffinatti, and Prof. Tullio Genova and Prof. Luca Munaron**, for your patience in helping me find the things every time I was coming back to the lab after some time, for your suggestions and bits of advice, for the collaborations and, especially, for the coffee breaks that I always missed once back to Lille.

My most sincere gratitude to all the Professors of the pHioniC consortium, who provided me with important suggestions and advice during each meeting. I am truly grateful for the opportunity of meeting so many passionate, kind, and humble scientists from different areas of research. It has been truly of inspiration. In particular, I thank **Prof. Stine Pedersen** for her generous support and kind words, **Prof. Stephan Reshkin** and **Dr Rosa Angela Cardone** for the amazing collaboration we established, and for all your valuable feedback. I also deeply thank my beloved pHioniC fellows; **Wiktoria Błaszczak, Ganga Deshar, Renata Ialchina, Jiayi Yao, Tiago Carvalho, Franco D'Alessandro, Julie Schnipper, Xiaoyi Shi, Sofie Hagelund, Roisin Mc Morrow** and, in particular, my beloved *Gipsy group*: **Elena Papacharisi, Marco Cozzolino, Micol Rugi e Jakub Mitreğa**. It was an honour to meet so many talented and amazing students and to learn from you, your works, and your cultural background. We have shared the European Marie Curie and the PhD experience, and we supported each other and enjoyed this journey like friends. I hope our friendship bond will be everlasting. *Cheers guys!*

My deepest thanks to **Mahdi Ghazal**. We are a very good team and we shared the lowest and highest moments of our Ph.Ds, together. Thank you for your company, endless laughs, patience, understanding and sincere love. You have taught me what determination and passion truly mean; you are an important reference point. Thanks to all the Ghazal family for accepting me and loving me like one of us.

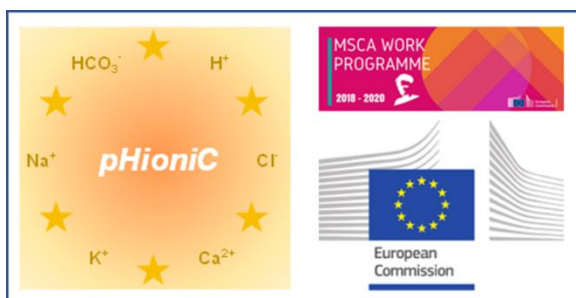
Thanks to all my friends scattered between Italy, France, Argentina, or any other European country for supporting me and cheering me during the PhD, particularly during Corona times, with your company, random and questionable videos, memes and silly songs.

Finally, I want to thank my family. **Meli** and **Barbi**, my big sisters, thank you for always being present and caring about me. I am almost 29 but you still consider me the little girl of the family. Thank you to my *babies*, **Ale**, **TinTin**, **Santi** and **Mimi**, whose innocence and joy have often redeemed me from dark moments. Thank you to **Anthoni** and **Salu** for being my “acquired” big brothers and being there for me when I need. **Mom**, I have no words to describe how much your presence, help and unconditional love have helped me during this PhD far away from home. Thank you because you have always respected my times and moods during the hardest times and you have always silently stood by my side, always. Your love and kindness are my strength. Thank you all for your pride in me and my work, with your support and love it all makes sense. *Los quiero de aquí hasta la luna ida y vuelta, a pasitos de tortuga ♥*.

Madelaine ☺

# Financial Support

This work was financially supported by the Marie Skłodowska Curie Innovative Training Network (#GA 813834 pHioniC-H2020-MSCA-ITN-2018) and PRIN-2017 “Lioness” project (#GA 754345) from the Italian Ministry for Education, University and Research (MIUR).



*Nothing in life is to be feared, it is only to be understood. Now is the time  
to understand more, so that we may fear less.*

*- Marie Curie*

***Para mi familia,***

# Table of content

Abstract.....	2
Résumé.....	4
Acknowledgments.....	6
Financial Support.....	9
List of Figures and Tables.....	15
Scientific Contributions .....	18
<i>First Author publications</i> .....	18
<i>Co-Author publications</i> .....	18
<i>Communications</i> .....	19
<i>Teaching and tutoring</i> .....	20
Chapter I.....	22
General context.....	22
1. <i>Physiology of the pancreas</i> .....	22
1.1 Endocrine component.....	23
1.2 Exocrine component.....	23
2. <i>Pancreatic Ductal Adenocarcinoma</i> .....	26
2.1 Risk factors.....	26
2.2 Pathogenesis .....	27
2.2.1 PDAC precursor lesions.....	27
2.2.2 PDAC gene mutations.....	29
2.3 Diagnosis .....	33
2.4 Prognosis and treatment.....	34
2.4.1 Surgical options .....	34
2.4.2 (Neo)Adjuvant Therapies: Chemotherapy and Radiotherapy.....	35
3. <i>Tumor microenvironment</i> .....	38
3.1 TME cellular component.....	39
3.2 TME molecular component.....	42
3.3 TME soluble component .....	43
3.4 PDAC desmoplastic microenvironment.....	45

3.5 Physico-chemical properties of the TME: hypoxia .....	46
3.5.1 Hypoxic tumor microenvironment.....	46
3.5.2 Contribute of hypoxia to PDAC progression and link with Warburg effect. ....	51
3.6 Physico-chemical properties of the TME: acidosis .....	54
3.6.1 pH-regulatory proteins in PDAC .....	57
Na <sup>+</sup> /H <sup>+</sup> exchangers (NHE): SLC9A-C .....	57
Monocarboxylate transporters (MCTs).....	58
Na <sup>+</sup> /HCO <sub>3</sub> <sup>-</sup> cotransporters (NBCs) .....	59
Carbonic Anhydrases (CAs).....	60
V-type H <sup>+</sup> ATPases .....	61
3.6.2 Acidic pHe as a driver of cancer .....	62
3.6.3 Acid-driven adaptation and differences with acid selection .....	66
3.6.4 Role of acidic pHe in PDAC progression: from physiology to pathology .....	68
4. Calcium signaling .....	71
4.1 Ca <sup>2+</sup> signaling toolkit .....	72
4.2 Ca <sup>2+</sup> -permeable channels in cancer: focus on PDAC .....	73
4.2.1 Ca <sup>2+</sup> -permeable channels: Focus on ORAI1 and STIM1 Ca <sup>2+</sup> sensor .....	75
4.2.2 Store-Operated Ca <sup>2+</sup> Entry mechanism .....	78
4.2.2.1 Store-Operated Ca <sup>2+</sup> Entry: ICRAC, ISOC, and homo- and heteromeric ORAI complexes .....	80
4.2.3 ORAI1/STIM1 role in the generation of Ca <sup>2+</sup> oscillations .....	82
4.2.4 Role of SOCE in cancer and its contradictions .....	86
4.2.4.1 Prostate cancer .....	86
4.2.4.2 Breast cancer .....	87
4.2.4.3 Ovarian Cancer .....	87
4.2.4.4 Leukaemia.....	88
4.2.4.5 Glioma.....	88
4.2.4.6 Melanoma .....	89
4.2.5 Role of STIM1 and ORAI1 in PDAC .....	91
4.4 Ca <sup>2+</sup> -permeable ion channels regulation by acidic pHe.....	93
5. Hypothesis and aim of the work .....	94
Chapter II .....	97
Materials and Methods.....	97



1.	<i>Cell culture</i> .....	97
2.	<i>Establishment of acid phenotypes in PDAC cells</i> .....	98
3.	<i>Reagents</i> .....	99
4.	<i>Immunofluorescence staining</i> .....	99
	4.1 Analysis of cell morphology: cell area and cell circularity .....	100
	4.2 Paxillin staining and confocal microscopy .....	100
5.	<i>Proliferation and viability</i> .....	101
	5.1 MTS .....	101
	5.2 EdU proliferation assay .....	102
	5.3 ATP quantification assay.....	102
	5.4 Trypan Blue exclusion assay .....	103
6.	<i>Cell-matrix adhesion assay</i> .....	103
7.	<i>Cell migration assays</i> .....	104
	7.1 Single-cell time lapse videomicroscopy .....	104
	7.2 Transwell migration assay with and without pH gradient.....	104
8.	<i>Cell invasion assays with and without pH gradient</i> .....	105
9.	<i>Invadopodia activity assay</i> .....	106
10.	<i>Cell transfection with siRNA</i> .....	107
11.	<i>Protein expression analysis</i> .....	108
	11.1 Protein extraction and quantification.....	108
	11.2 Western Blot .....	108
12.	<i>mRNA expression analysis</i> .....	109
	12.1 RNA extraction and Reverse Transcription.....	109
	12.2 qPCR.....	110
13.	<i>Intracellular pH measurements</i> .....	111
14.	<i>RNA-sequencing and analysis</i> .....	112
15.	<i>Calcium imaging</i> .....	113
	15.1 Ca <sup>2+</sup> oscillations induction protocol and analysis.....	114
	15.2 Store-Operated Ca <sup>2+</sup> entry (SOCE) protocol and analysis .....	114
16.	<i>Statistical analysis</i> .....	115
Chapter III.....		116
Results and discussion .....		116

<i>I. Acidic growth conditions promote epithelial-to-mesenchymal transition to select more aggressive PDAC cell phenotypes in vitro.</i> .....	116
Graphical Abstract.....	117
<i>II. pHe-sensitive Store-Operated Ca<sup>2+</sup> channels signals contribute to tumour acidic microenvironment-induced PDAC cells selection to more aggressive phenotypes.</i> .....	120
Abstract.....	120
Introduction .....	121
Materials and Methods .....	123
Results .....	128
I. Extracellular acidosis inhibits FBS-induced Ca <sup>2+</sup> -oscillations in PANC-1 cells. ....	128
II. FBS-induced Ca <sup>2+</sup> -oscillations are SOCE-dependent in all PANC-1 cell models.....	131
III. Intracellular Ca <sup>2+</sup> basal levels, Ca <sup>2+</sup> -release from ER and SOCE are affected by acidic pHe.....	133
IV. Acid selection promotes the upregulation of ORAI1 in PANC-1 cells.....	137
V. ORAI1 is involved in cell migration and invasion of acid-selected cells. ....	138
Discussion.....	140
Conclusions .....	143
References .....	144
Chapter IV.....	150
Conclusion and perspectives.....	150
<i>I. Acidic growth conditions promote epithelial-to-mesenchymal transition to select more aggressive PDAC cell phenotypes in vitro.</i> .....	150
<i>II. pHe-sensitive Store-Operated Ca<sup>2+</sup> channels signals contribute to tumor acidic microenvironment-induced PDAC cells' selection to more aggressive phenotypes.</i> .....	154
Annexe 1 .....	158
Bibliography .....	159

# List of Figures and Tables

## Introduction

Figure 1. Physiology of the pancreas.....	22
Figure 2. Organization of the exocrine pancreas and its cellular components. ....	24
Figure 3. Diagram depicting the channels and transporters localized in the basolateral membrane and apical membranes of pancreatic duct cells.....	25
Figure 4. H&E-stained histological images of normal pancreas, non-invasive precursor lesions (PanINs), intraductal papillary mucinous neoplasms (IPMNs), and mucinous cystic neoplasms (MCNs) and adenocarcinoma.. ....	28
Figure 5. Schematic with histological images from normal to PanIN lesions representing the PanIN progression model.....	29
Figure 6. Schematic showing the multi-step pathological and molecular PDAC carcinogenesis model.....	30
Figure 7. Schematic overview of all the current clinical treatment strategies for PDAC patients based on whether the patients have resectable, locally advanced, or metastatic PDAC.....	37
Figure 8. Schematic of the principal components of the tumor microenvironment, comprising cellular and non-cellular components.....	38
Figure 9. Schematic depicting the signaling interactions occurring in the tumor microenvironment during tumor progression.....	40
Figure 10. Schematic of the differences between the blood vasculature in healthy and tumor tissue .....	41
Figure 11. Schematic of the extracellular matrix of mammalian cells and its components. ....	42
Figure 12. Histological photographs showing the S&H staining for PDAC and normal pancreas...	45
Figure 13. Schematic of the contribution of MAPK cascades in the HIF-1 activation pathway.....	48
Figure 14. Schematic depicting the hypoxia-induced mechanism of NF- $\kappa$ B activation.. ....	50
Figure 15. Schematic showing the effects of ROS in cycling hypoxia on the activation of HIF-1 and NF- $\kappa$ B.. ....	51
Figure 16. Schematic showing the major molecules involved in pH regulation in cancer cells. ....	56

Figure 17. Schematic of main processes involved in tumor onset and progression, with indication (blue boxes) of those processes regulated by the acidic tumor microenvironment. ....	62
Figure 18. Schematic showing two examples of pH sensitivity curves for proliferation. ....	67
Figure 19. Schematic representing the hypothesis that acidic physiological microenvironment promotes PDAC onset and progression in concomitance of driving gene mutations and pre-neoplastic lesions. ....	70
Figure 20. Intracellular Ca <sup>2+</sup> signaling.....	72
Figure 21. Schematic of the structural differences among the ORAI protein family.....	77
Figure 22. Schematic depicting the structural differences among STIM proteins. ....	78
Figure 23. Molecular mechanism of store-operated Ca <sup>2+</sup> entry (SOCE) signaling.....	80
Figure 24. Illustration showing the frequencies and periods that modulate the different frequency-decoders.. ....	83
Figure 25. Schematic depicting the diversity in Ca <sup>2+</sup> signalling and its contribution to hallmarks of cancer.. ....	84

## Materials and Methods

Figure 26. Scheme of the different acidic pH <sub>e</sub> phenotypes established.....	99
---	----

## Results and discussion II

Figure 1. Effect of acidic pH <sub>e</sub> on intracellular FBS-induced Ca <sup>2+</sup> oscillations in PANC-1 cells.....	129
Figure 2. Effect of acute treatment with acidic pH <sub>e</sub> on PANC-1 Ca <sup>2+</sup> oscillations induced by 10% FBS.....	131
Figure 3. Ca <sup>2+</sup> oscillations are SOCE-dependent in PANC-1 cells.....	132
Figure 4. Effects of acidic pH <sub>e</sub> on cytosolic basal Ca <sup>2+</sup> levels, Ca <sup>2+</sup> -release from ER stores, and SOCE in PDAC cells. ....	134
Figure 5. Effects of acute exposition of acidic pH <sub>e</sub> SOCE in PDAC cells. ....	136
Figure 6. Effect of extracellular acidosis on ORAI1 channels and STIM1 expression in PANC-1 and Mia PaCa-2 cells. ....	138
Figure 7. Effect of ORAI1 silencing on cell migration and invasion in PANC-1 and Mia PaCa-2 cells and of Src kinase inhibition on cell adhesion and invasion in PANC-1 cells.....	139
Figure 8. Graphical abstract.....	143

## **Introduction**

Table 1. Ca <sup>2+</sup> -permeable ion channels profile expression and function in PDAC progression.....	74
--	----

## **Materials and Methods**

Table 1. Preparation of 500 ml of cell media with different pH.....	97
Table 2. Optimized siRNA transfection protocol for PDAC cells in 6-multiwell plate.....	107
Table 3. List of siRNA sequences.....	108
Table 4. List of primers sequences used for qPCR.....	110

## **Results and discussion II**

Table 1. List of siRNA sequences.....	125
Table 2. List of primer sequences used for qPCR.....	127

# Scientific Contributions

## First Author publications

1. **Audero, M.M.;** Ruffinatti, F.A.; Carvalho, T.; Kondratska, K.; Cardone, R.A.; Prevarskaya, N.; Fiorio Pla, A. pH<sub>e</sub>-sensitive Store-Operated Ca<sup>2+</sup> channels signals contribute to tumor acidic microenvironment-induced PDAC cells' selection to more aggressive phenotypes. *In preparation*.
2. **Audero, M.M.;** Carvalho, T.; Ruffinatti, F.A.; Loeck, T.; Yassine, M.; Chinigò, G.; Folcher, A.; Farfariello, V.; Schwab, A.; Reshkin, S.J.; Cardone, R.A.; Prevarskaya, N.; Fiorio Pla, A. Acidic growth conditions promote epithelial-to-mesenchymal transition to select more aggressive PDAC cell phenotypes *in vitro*. *Cancers* 2022. *Under revision*.
3. **Audero, M.M.;** Prevarskaya, N.; Fiorio Pla, A. Ca<sup>2+</sup> Signalling and Hypoxia/Acidic Tumour Microenvironment Interplay in Tumour Progression. *Int. J. Mol. Sci.* 2022, 23, 7377. <https://doi.org/10.3390/ijms23137377>

## Co-Author publications

1. Chinigò, G.; Grolez, G.P.; **Audero, M.M.;** Bokhobza, A.; Bernardini, M.; Cicero, J.; Toillon, R.-A.; Bailleul, Q.; Visentin, L.; Ruffinatti, F.A.; Brysbaert, G.; Lensink, M.F.; De Ruyck, J.; Cantelmo, A.R.; Fiorio Pla, A.; Gkika, D. TRPM8-Rap1A Interaction Sites as Critical Determinants for Adhesion and Migration of Prostate and Other Epithelial Cancer Cells. *Cancers* 2022, 14, 2261. <https://doi.org/10.3390/cancers14092261>
2. Carvalho, T.; Di Molfetta D.; **Audero M.M.;** Greco M.R.; Bincoletto V.; Arpicco S.; Fiorio Pla A.; Prevarskaya N.; Reshkin S.J.; Cardone R.A. Tumor microenvironment modulates invadopodia activity of pancreatic cancer cells and their sensitivity to gemcitabine and C-18 gemcitabine. *In preparation*.

# Communications

## Oral presentations

1. 14/10/2019. Oral presentation, pHioniC Summer School Workshop, Lille, France
2. 06/02/2020. Oral presentation, II pHioniC Progress meeting, Florence, Italy
3. 18/11/2020. Oral presentation, III pHioniC Progress meeting, Online
4. 17/03/2021. Oral presentation, IV pHioniC Progress meeting, Online
5. 17/09/2020. Oral presentation, PhD day organized by the Doctoral School in Complex Systems for Life Sciences, University of Turin, Italy
6. 03/11/2020. Oral presentation, PhD day organized by the Ecole Doctoral Biologie Santé, Lille, France
7. 24/08/2021. Oral presentation, V pHioniC Progress meeting, Gottingen, Germany, 24-27 August 2021
8. 25/08/2021. Oral presentation, 16th European Molecular Imaging Meeting –EMIM 2021, Gottingen, Germany, 24-27 August 2021
9. 30/09/2021. Oral presentation, PhD day organized by the Doctoral School in Complex Systems for Life Sciences, University of Turin, Italy
10. 08/11/2021. Oral presentation, PhD day organized by the Ecole Doctoral Biologie Santé, Lille, France
11. 28/01/2022. Oral presentation, VI pHioniC Progress meeting, Online
12. 17/03/2022. Oral presentation, ONCOLille PhD Students' Days, Lille, France
13. 15/05/2022. Oral presentation, VII pHioniC Progress meeting, Pistoia, Italy
14. 19/09/2022. Oral presentation, VIII pHioniC Progress meeting, Copenhagen, Denmark
15. 10/10/2022. Oral presentation, PhD day organized by the Doctoral School in Complex Systems for Life Sciences, University of Turin, Italy.

## Posters

1. 06/12/22. Poster presentation " pHe-sensitive Store-Operated Ca<sup>2+</sup> channels signals contribute to tumor acidic microenvironment-induced PDAC cells' selection to more aggressive phenotypes", Ion Channel & Cancer Meeting and Calcium Signaling in Cancer ECS session, 6-8 December 2022, Lille, France
2. 17/09/22. Poster presentation " pHe-sensitive Store-Operated Ca<sup>2+</sup> channels signals contribute to tumor acidic microenvironment-induced PDAC cells' selection to more aggressive phenotypes", Europhysiology Conference, 16-18 September 2022, Copenhagen, Denmark
3. 17/03/22. Oral presentation: "pHe-sensitive Store-Operated Ca<sup>2+</sup> signals contribute to acidic microenvironment-induced PDAC cells' selection", ONCOLille Ph.D. Days, 17-18 March 2022, Lille, France
4. 17/11/2021. Poster presentation: "Acidic microenvironment promotes PDAC cells selection inducing more aggressive cancer cells: role of Store Operated Ca<sup>2+</sup> signals", 17<sup>èmes</sup> Journées Annuelles du Cancéropôle GSO, Carcassonne, France.
5. 12/10/2021. Poster presentation and EYPS Best Poster Award: "Acidic microenvironment selects more aggressive cancer cell phenotypes in PDAC: role of Store Operated Ca<sup>2+</sup> signals", Young Physiologist's Symposium (EYPS) organized by the Federation of European Physiological Societies (FEPS), Online, 12 October 2021.
6. 08/09/2021. Poster presentation: "Acidic microenvironment selects more aggressive cancer cell phenotypes in PDAC: role of Store Operated Ca<sup>2+</sup> signals" in occasion of the 71st SIF National Congress, Online, 7-9 September 2021
7. 25/08/2021. Poster presentation: "pH and Ca<sup>2+</sup> signaling interplay in Pancreatic Ductal Adenocarcinoma progression", 16th European Molecular Imaging Meeting –EMIM 2021, Gottingen, Germany.

## Teaching and tutoring

1. 11/05/2021. Teaching lecture "pH homeostasis and regulation in cancer", Biophysics course, Master in Cellular and Molecular Biology, University of Turin, Italy: Teaching experience of 2h lecture about physiological and pathological pH regulation to Master students.



2. 17/05/2021. Teaching lecture "pH homeostasis and regulation in cancer", Régulation ionique de l'initiation et progression des cancers course, Master in Biologie Santé, University of Lille, France: Teaching experience of 2h lecture about physiological and pathological pH regulation to Master students.
3. 05/11/2021. Teaching lecture " pH-sensitive ion channels and role in tumor progression.", Cellular and Molecular Biophysics course, Master's Degree in Industrial Biotechnology, University of Turin, Italy: Teaching experience of 2h lecture about pathological pH regulation of ion channels to Master students.
4. 04/2021-07/2021. Student Supervision in the Laboratory of Cellular and Molecular Angiogenesis, University of Turin, Italy: Supervision of laboratory and thesis work of an undergraduate student from the University of Turin, Italy, for 3 months.
5. 01/09/2020-01/02/2021. Student Supervision in the Laboratory of Cell Physiology INSERM U1003, University of Lille, France: Supervision of an ERASMUS Master student from the University of Turin, Italy, for 6 months. I supervised his laboratory work (cell culture, cellular and molecular biology experiments). I helped in the redaction of his master thesis titled "Role of the microenvironment in pancreatic ductal adenocarcinoma (PDAC): Interplay between pH and Ca<sup>2+</sup> signals".

# Chapter I

## General context

### 1. Physiology of the pancreas

The human pancreas is a small organ that presents a 14-18 cm long extended form with a head, body, and tail<sup>1</sup>. It is located in the upper section of the abdominal cavity, behind the stomach and intestine. It serves the purpose of two organs in one since it has both an endocrine function, controlling the blood sugar levels, and an exocrine function related to digesting (Figure 1).

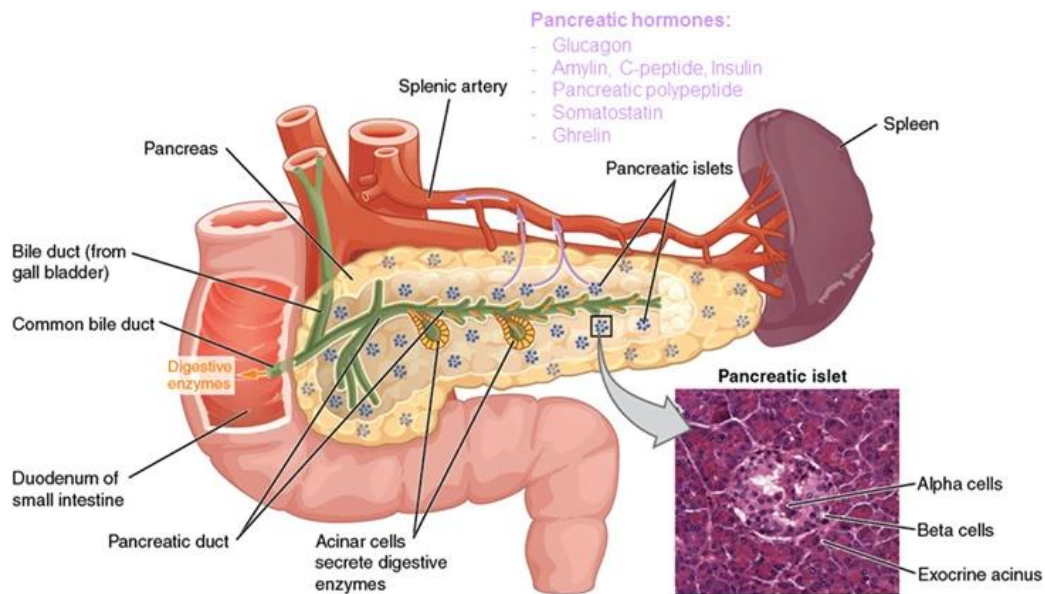


Figure 1. Physiology of the pancreas. Endocrine pancreas is involved in the production and secretion of insulin by beta cells and glucagon by alpha cells in the pancreatic islets (micrograph). The function of the exocrine pancreas is the production and secretion of enzymes by acinar and ductal cells which are involved in digestion. The image is adapted from [2].

## 1.1 Endocrine component

The endocrine component of the pancreas represents a small percentage of pancreatic tissue. It is often localized in the so-called Islets of Langerhans, more or less circular cellular formations spread throughout the pancreas and surrounded by a rich capillary network and in which highly specialized cell types are present, such as  $\alpha$ -,  $\beta$ -,  $\delta$ -,  $\gamma$ - and G cells, which produce and secrete into the bloodstream different hormones important for metabolism<sup>3</sup>. As mentioned before, the principal function of the endocrine pancreas is regulating glucose levels in the blood via two specific hormones, insulin, and glucagon. Insulin is secreted by  $\beta$ - cells after meals, and its primary function is to allow blood glucose to enter the cells to be used as an energy source. Therefore, it decreases blood sugar levels<sup>3</sup>. Its action is balanced by glucagon, secreted by  $\alpha$ -cells, and raises blood sugar concentrations when needed, for example, during fasting. This regulation is important for providing other organs (brain, liver, lungs, kidneys) with the adequate and constant glucose concentration necessary for their function<sup>3</sup>.

## 1.2 Exocrine component

The exocrine portion of the pancreas exerts a key role in the digestion process, containing glands for the production and secretion of enzymes needed for absorbing the various components of food. The exocrine pancreas consists of the acini and the ductal system<sup>4</sup>. Each basic functional unit consists of acinar secretory, centroacinar, and ductal cells arranged in rounded or tubular clusters (Figure 2). Pancreatic acinar cells cluster to form the acini and they are in charge of producing the pro-digestive enzymes, which are stored in zymogen granules and later secreted into the ductal system<sup>4</sup>. Centroacinar cells connect the acini and the ductal cells of the intercalated ducts, forming the initial part of the pancreatic duct system. They do not produce digestive enzymes as acinar cells but they secrete a bicarbonate-containing aqueous solution into the pancreatic duct which carries the inactive digestive enzymes to the duodenum lumen<sup>4</sup>. For the scope of the general work, particular attention will be addressed only to ductal cells.

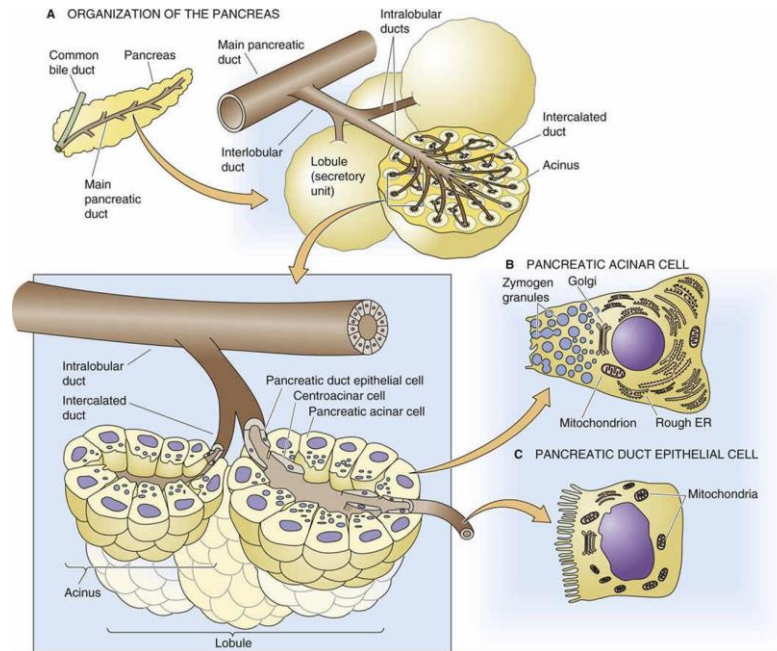


Figure 2. Organization of the exocrine pancreas and its cellular components. This image is adapted from [5]

As the centroacinar cells, the ductal cells form the intercalated ducts and participate in the secretion of pancreatic juice, which occurs during the digestive period, induced by hormonal and nervous stimuli<sup>4</sup>. The pancreatic juice is a colourless and alkaline liquid containing two secretion types: enzymatic and hydroelectrolytic. The enzymatic secretion is responsible for the hydrolysis of the nutritive substances in the food and is principally mediated by the acinar cells. In contrast, the hydroelectrolytic secretion acts as a vehicle for the enzymatic secretion and provides an alkaline medium required for the enzymes' function<sup>1</sup>. The chemical breakdown of the nutritive substances requires indeed the neutralization of the acid chyme in the duodenum, obtained by the high bicarbonate ( $\text{HCO}_3^-$ ) concentration in the pancreatic juice. The hydrolytic secretion consists mainly of water (98%) and in high  $\text{Na}^+$  and  $\text{HCO}_3^-$  concentrations, and it is stimulated by secretin hormone via the cAMP-induced activation of the Cystic fibrosis transmembrane conductance regulator (CFTR) chloride channel in the ductal cells' apical membrane, which allows  $\text{HCO}_3^-$  flux in the ductal lumen<sup>6</sup>. The activity of CFTR is coupled with  $\text{Cl}^-/\text{HCO}_3^-$  exchangers in the luminal membrane

and with  $\text{Na}^+\text{-HCO}_3^-$  cotransporters localized in the basolateral membrane<sup>7</sup>. The synergistic activity of these proteins promotes bicarbonate efflux into the ductal lumen (Figure 3).

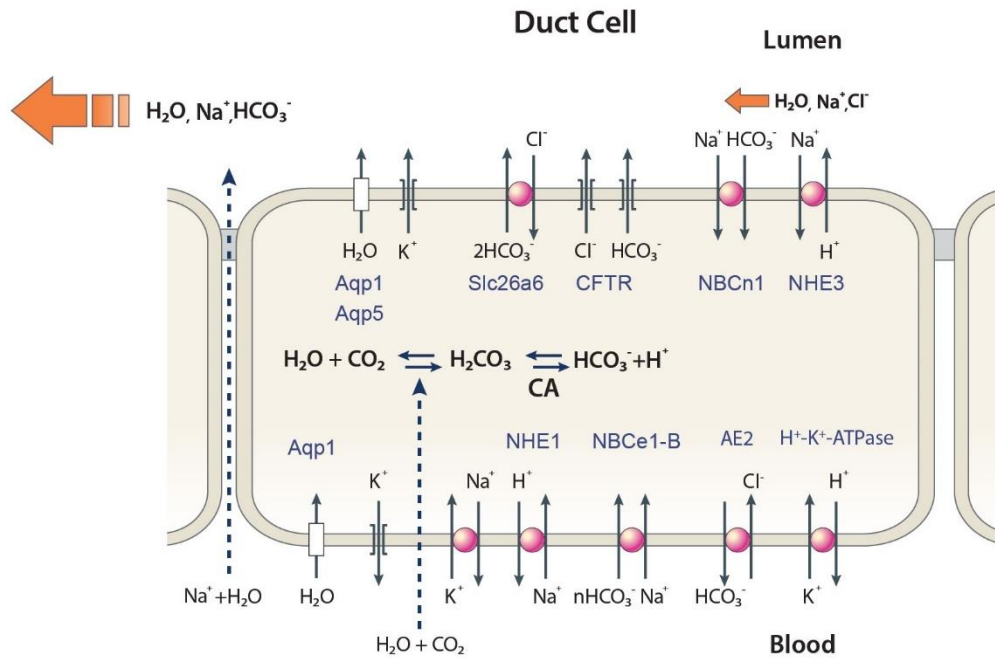


Figure 3. Diagram depicting the channels and transporters localized in the basolateral membrane and apical membranes of pancreatic duct cells. The image is adapted from [8].

This base secretion threatens ductal cells  $\text{pH}_i$  homeostasis; To prevent cytosolic acidification,  $\text{HCO}_3^-$  apical secretion is coupled to the extrusion of an equal amount of acid across the basolateral membrane by  $\text{H}^+\text{-K}^+\text{-ATPases}$  and  $\text{Na}^+\text{/H}^+$  exchanger (NHE1), releasing  $\text{H}^+$  in the pancreatic interstitium, therefore acidifying it<sup>9,10</sup> (Figure 3). This acid/base segmentation indicates that the pancreatic interstitial's  $\text{pH}_e$  will vary cyclically during the alternating phases of digestive stimulation of secretion, in which the extracellular  $\text{pH}$  reaches acidic values and resting phases<sup>11</sup>. Therefore, pancreatic ductal cells face dynamic temporal and spatial changes of  $\text{pH}_e$ , and they exist in a unique and dynamic  $\text{pH}_e$  environment in which their metabolism and proteins- as ion channels, transporters, and receptors- are tuned to this characteristic  $\text{pH}_e$  landscape. This notion assumes greater importance when collocated in the pathological context, as the dynamic situation of intermittent acidity in healthy pancreatic ductal cells trains them to cope with acidity. It represents a great advantage during pancreatic ductal adenocarcinoma (PDAC) onset.

## 2. Pancreatic Ductal Adenocarcinoma

Pancreatic ductal adenocarcinoma (PDAC) is the most common neoplasia of the exocrine pancreas, accounting for more than 90% of all pancreatic cancers<sup>12</sup>.

PDAC is a particularly aggressive neoplasm with little chance of response to medical treatment. It is the 12th most frequent type of cancer worldwide, with 495.773 new cases per year<sup>13</sup>, and the incidence is also high in Europe, where PDAC accounts for the 7<sup>th</sup> most common cancer in terms of new cases per year<sup>13</sup>.

With a 5-year survival of about 10%, one of the lowest among cancers, PDAC is among the few cancers with increasing mortality rates for both men and women, representing the seventh cancer for mortality rate in 2020, with 466.003 deaths per year<sup>13</sup> and prospective studies suggest that it will become the second leading cause of cancer-related deaths by 2030<sup>14</sup>. This trend is due to the increasing incidence and poor prognosis caused by the lack of striking symptoms, biomarkers for screening tests, and the limited efficacy of current chemotherapy treatments, which delay diagnosis<sup>15,16</sup>. Therefore, most patients are diagnosed at an advanced stage, where infiltration of lymph nodes and the vasculature are observed, as well as metastasis to the other organs, and less than 20% of cases are eligible for surgical resection<sup>17</sup>. The inefficacy of the therapeutic options is partly the result of the highly immunosuppressive, desmoplastic, hypoxic, and acidic PDAC microenvironment<sup>12</sup>.

### 2.1 Risk factors

The people most at risk of developing PDAC are those between 50-80 years. This type of cancer manifests at an average age of 55 and is very rare among people under 40. PDAC occurs in a slightly higher frequency (1.5-2 times) in men than women<sup>18</sup>. Moreover, black ethnicity represents another risk factor, as the incidence rate for Black people is 15.4 per 100.000 people, while for Asian, Hispanic and Non-Hispanic white people is 10.0, 11.6 and 13.2, respectively<sup>19</sup>.

Major risk factors for PDAC include smoking, which increases the probability of its insurgence by ~three times compared to non-smokers, and diet, considering the pancreas is a key digestive

organ. Moreover, obesity contributes to PDAC insurgence, particularly in concomitance with insulin resistance and type 2 diabetes<sup>18</sup>. Other risk factors are specific and rare genetic conditions such as von Hippel-Lindau syndrome<sup>20</sup>, and the presence of a family history of chronic pancreatitis, pancreatic, colon, or breast cancer might represent additional risk factors<sup>18,21,22</sup>, usually attributable to specific inherited genetic mutations, which play an important role in the onset of PDAC<sup>22,23</sup>.

## **2.2 Pathogenesis**

Considering that most PDAC patients are diagnosed at advanced stages, the identification and study of pre-invasive precursor lesions represent a major change for developing efficient screening and tailored therapies for earlier stages of pancreatic cancer, significantly improving patients' prognosis.

### **2.2.1 PDAC precursor lesions**

PDAC results from the accumulation of stepwise genetic alterations of the healthy mucosa to precursor and benign lesions of the exocrine pancreas that may eventually progress to an invasive malignancy. In this type of cancer, three distinct and non-invasive precursor lesions have been identified and characterized: pancreatic intraepithelial neoplasia (PanINs), intraductal papillary mucinous neoplasms (IPMNs), and mucinous cystic neoplasms (MCNs) (Figure 4)<sup>24</sup>. Each precursor lesion reflects a different route that pancreatic cancer might take, as they show specific clinicopathological manifestations and genetic features which define the genetic evolution of pancreatic cancer<sup>25</sup>. Unlike PanINs, IPMNs and MCNs are rare PDAC precursor lesions that imaging techniques can easily detect; therefore, they can be treated when detected in the pre-invasive stage<sup>26</sup>. For these reasons, a particular focus is given only to PanINs.

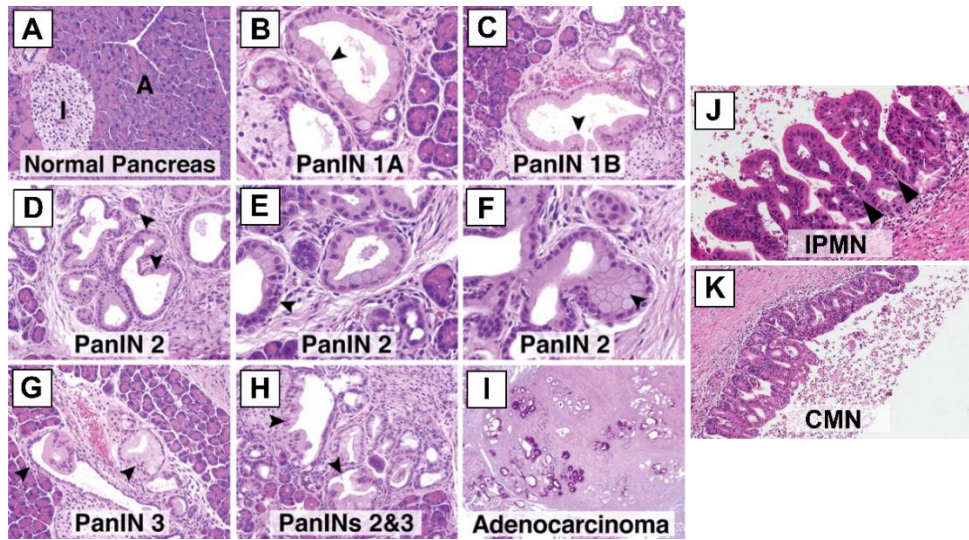


Figure 4. H&E-stained histological images of normal pancreas, non-invasive precursor lesions (PanINs), intraductal papillary mucinous neoplasms (IPMNs), and mucinous cystic neoplasms (MCNs) and adenocarcinoma. Modified from [27].

Pancreatic intraepithelial neoplasias (PanINs) represent the most common PDAC precursor lesions<sup>28</sup>. These are benign microscopic lesions with an indolent course that affect pancreatic ductal epithelial cells and are not easily detectable, partly due to the typical absence of symptoms. Depending on the extent of the lesions and DNA, RNA, and protein alterations, PanINs are classified into three distinct stages: PanIN-1A/B, PanIN-2, and PanIN-3 (Figure 5)<sup>28</sup>. Each stage coincides with a series of genetic alterations that become more prevalent and varied as PanIN advances and contribute to the progression from non-invasive lesions to invasive pancreatic cancer (See section 2.2.2)<sup>16,29</sup>.



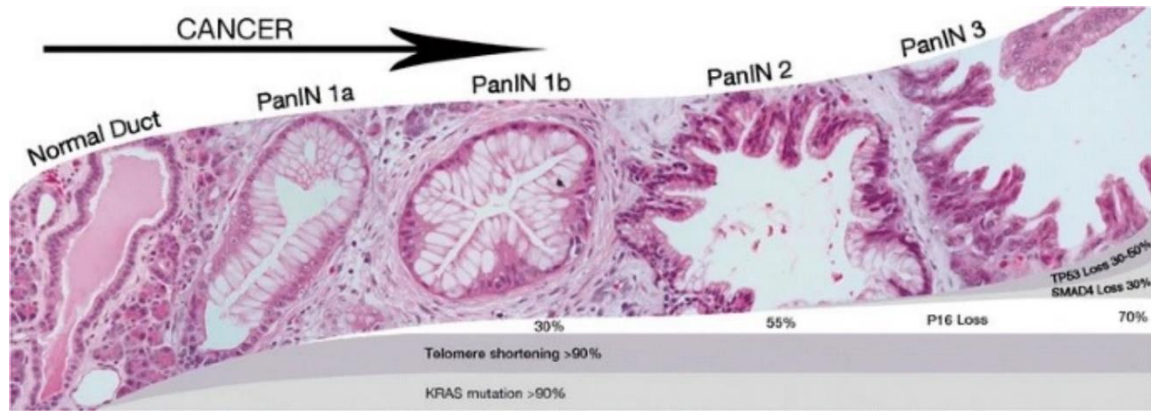


Figure 5. Schematic with histological images from normal to PanIN lesions representing the PanIN progression model. Image adapted from [30].

Low-grade dysplasia lesions with minimal cytologic and architectural involvement include PanIN-1A and PanIN-1B. PanINs-1A are described as flat duct lesions, PanINs-1B are papillary duct lesions, whereas PanINs-2 lesions display a slight increase in dysplasia, but they are still indicated as papillary duct lesions. PanINs-3 are also known as carcinoma *in situ* lesions, characterized by high-grade dysplasia that show significant morphological alterations and cancer features, yet not invasive ones (Figure 5)<sup>16,25</sup>. PanINs-3 are the only pancreatic lesions that may develop into a malignancy. This evidence is based on molecular analyses that demonstrated that PanINs harbour a similar number of gene mutations as invasive carcinoma, morphological associations between these pre-neoplastic lesions and invasive adenocarcinomas and reported cases of PanINs patients who have progressed to invasive pancreatic adenocarcinoma<sup>28,31</sup>.

The initiation of PanIN precursor lesions is related to a particular process of cell plasticity called acinar to ductal metaplasia (ADM), triggered by specific genetic mutations (see section 2.2.2), wherein pancreatic acinar cells lose their acinar traits and differentiate into ductal cells, favoring the development of high-grade PanINs which may progress to PDAC<sup>32</sup>.

## 2.2.2 PDAC gene mutations

As mentioned before, PDAC results from the progressive accumulation of genetic alterations from low-grade to high-grade pre-neoplastic lesions, which may progress to malignancy. For this

reason, the detection of these genetic mutations and their sequential occurrence represented the main effort of several studies, which uncovered several PDAC driver genes<sup>31,33,34</sup> (Figure 6).

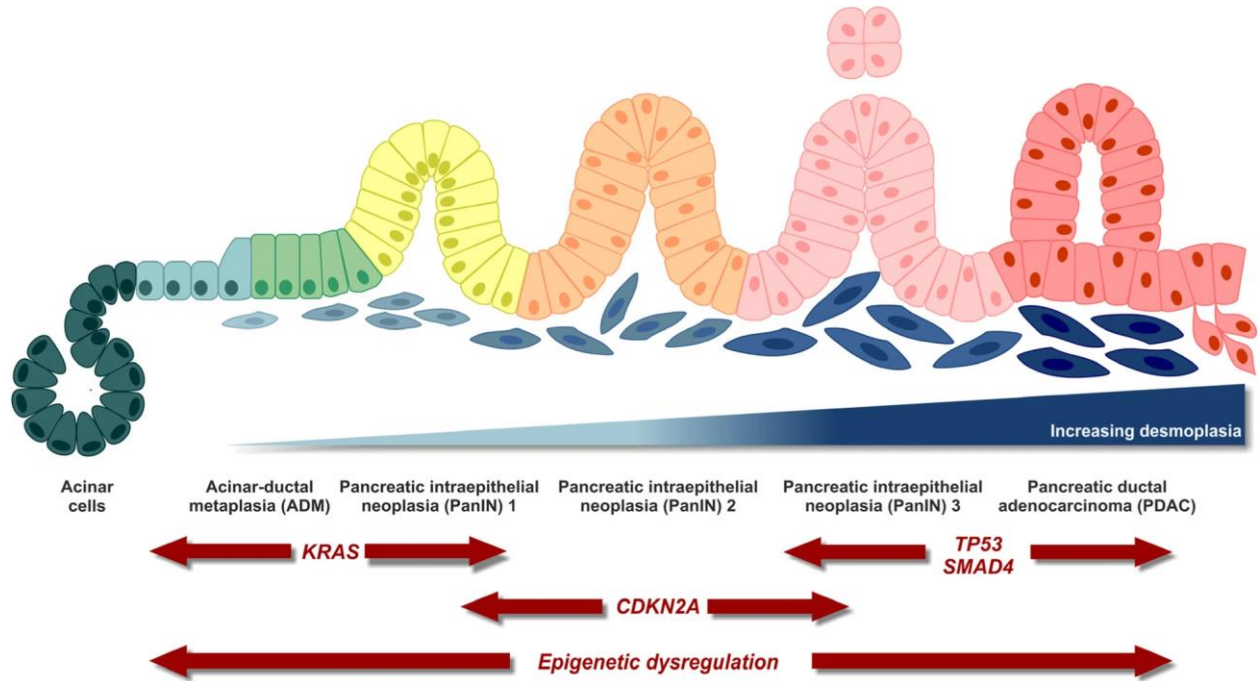


Figure 6. Schematic showing the multi-step pathological and molecular PDAC carcinogenesis model. Image adapted from [12].

*KRAS* belongs to the RAS family of small guanosine triphosphate (GTP)-binding proteins, which include *NRAS*, *HRAS*, and *KRAS*. It represents one of the major driver genes of pancreatic cancer, as activating mutations of this gene were reported in >95% of pancreatic cancer patients<sup>34</sup>. In 70-95% of cases, the *KRAS* gene harbours activating point mutations in correspondence with codon 12 (*KRAS*<sup>G12D</sup>), in which glycine residue is mutated in aspartic acid the majority of cases. Glycine replacements into valine or arginine residues in the same codon were also detected but in lower percentages<sup>35</sup>. Other codons, such as 11, 13, or 61, are among those that point mutations might impact, though less commonly than codon 12<sup>35</sup>. *KRAS* gene encodes for a cell membrane protein with intrinsic GTPase activity involved in the signaling transduction by growth factors and Ca<sup>2+</sup> ions<sup>36</sup>. These mutations result in a *KRAS* protein (p21-RAS) which is constitutively active, permanently promoting the activation of several downstream signaling pathways involved in PDAC cells' survival, proliferation, inflammation, migration, and invasion, such as MEK, PI3K, and RAF signaling<sup>36</sup>.

*KRAS* activating mutations represent an early event in PDAC, as they are detected in all three types of PDAC pre-neoplastic lesions (low-grade PanIN-1, IPMNs, MCNs)<sup>34</sup>, and they play an important role in PanINs initiation, as demonstrated in several genetically engineered mice models with endogenous mutated *KRAS* (*KRAS*<sup>G12D</sup>) expression in the pancreas, in which these mutations were sufficient to initiate pre-neoplastic lesions in all the mice models<sup>37,38</sup>. This process is further favoured by the induction of acute pancreatitis in inducible *KRAS*<sup>G12D</sup> mice, which promotes ADM and PanINs development<sup>39</sup>. However, *KRAS* mutation alone is necessary yet insufficient to induce the progression from pre-neoplastic lesions to invasive carcinoma, as only a small percentage of *Kras*<sup>G12D</sup> mice's PanINs evolve into pancreatic cancer<sup>37,39</sup>.

In dividing cells, chromosome ends have characteristic DNA-protein structures called telomeres that prevent DNA damage. Chromosome instability, typical of epithelial malignancies, can result from shortened telomeres. Telomere shortening is another early occurrence in PanIN-1 lesions, which may favour the insurgence of genetic abnormalities in PanINs<sup>40</sup>.

*KRAS* mutations are followed by other genetic alterations negatively affecting three major tumor suppressor genes: *CDKN2A*, *TP53*, and *SMAD4*. *CDKN2A* (Cyclin Dependent Kinase Inhibitor 2A, p16) is mutated in ~90% of PDAC cases<sup>41</sup>. The encoded protein p16 is involved in cell cycle arrest in correspondence with the G1-S phase transition by inhibiting cyclin-dependent kinase-4 and -6 (CDK-4/6); therefore, *CDKN2A* inactivation by transcriptional silencing results in uncontrolled proliferation of cancer cells<sup>42</sup>. Loss of p16 occurs later than *KRAS* mutations. It supports the concept that pre-neoplastic lesions are precursors to invasive pancreatic carcinoma, as *CDKN2A* mutations are present in the majority of intermediate PanIN-2 lesions<sup>34</sup> (Figure 6), and they promote the development of high-grade pre-neoplastic lesions, which rapidly progressed to invasive PDAC in inducible *KRAS*<sup>G12D</sup> mice<sup>43</sup>.

*TP53* is a tumor suppressor gene that regulates important cell functions, such as cell metabolism, cell cycle, apoptosis, and DNA repair<sup>36</sup>. This gene harbours heterogenic point mutations in 70% of PDAC patients, in particular missense point mutations<sup>44</sup>, leading to loss-of-function but also gaining new tumorigenic roles, determining cancer cell survival and uncontrolled proliferation, which further promotes genomic instability, contributing to cancer progression and the acquisition of aggressive behaviors<sup>45-47</sup>. *TP53* inactivating mutations are considered “late” ones, as they are detected in more advanced PanIN stages (PanIN-3)<sup>28,48</sup> (Figure 6), and important inducers of PDAC,

as inducible *KRAS*<sup>G12D</sup> mice with endogenous expression of mutant p53 developed metastatic PDAC faster than in the presence of null p53 allele<sup>38,49</sup>.

*SMAD4* is another common inactivated tumor suppressor gene in pancreatic cancer, in which mutations or homozygous deletions in one allele with loss of the second allele are detected in 55% of PDAC cases<sup>41</sup>. *SMAD4* mutations represent a “late” event in PDAC carcinogenesis, as low-grade PanIN-1 and -2 express wild-type *SMAD4*, but high-grade PanINs-3 lesions show a complete loss of *SMAD4* expression<sup>48,50</sup>. This gene encodes for the *SMAD4* protein, a transcription factor that mediates transforming growth factor  $\beta$  (TGF- $\beta$ ) signal transduction, which exerts anti-proliferative roles. Therefore, the loss of *SMAD4* protein in pancreatic cancer cells provides pancreatic cancer cells with a selective growth advantage<sup>51,52</sup> and was demonstrated *in vivo* using *Kras*<sup>G12D</sup> mice models with deletion of *SMAD4*, which developed greater fibrosis and faster high-grade PanIN lesions that progressed in some examples to invasive adenocarcinoma respect to *Kras*<sup>G12D</sup> mice alone<sup>53</sup>. This process was accelerated in the presence of *CDKN2A* mutation<sup>54</sup>.

TGF- $\beta$  signaling pathway exerts an anti-tumor role during the initial stages of carcinogenesis. At the same time, it switches to an oncogenic effect during more advanced stages, in particular in a *SMAD4*-independent manner, by activating alternative pathways, such as RhoA, MAPK, and PI3K<sup>55</sup>, but also via NFAT-mediated c-Myc expression, which enhances cancer cell growth<sup>56</sup>. Besides supporting cancer cell processes, the TGF- $\beta$  signaling pathway role is extended to the stromal components, such as pancreatic stellate cells (PSCs), which support PDAC progression. *In vivo* and *in vitro* studies have demonstrated that TGF- $\beta$ 's paracrine activity leads to PSCs activation and increased deposition of ECM proteins, particularly collagens, in pancreatic fibrosis<sup>57</sup>.

The genetic alterations of pre-neoplastic lesions described before are also present in PDAC, where these mutations occur more frequently. Besides the four major genes, other mutations can accompany the development and progression of pancreatic cancer. Gene-inactivating mutations, such as in *RNF43*, *ARID1A*, and *BRCA2*, are linked to PDAC initiation, although they are observed in a small percentage of PDAC cases<sup>58</sup>. *BRCA2* is involved in DNA repair. Its expression is also lost in high-degree PanINs, suggesting a late role in PDAC carcinogenesis<sup>59</sup>, and germline mutations significantly increase the risk of PDAC<sup>58</sup>. *GNAS* gene is commonly mutated in IPMN and PDAC and, to a minor extent, in MCN and PanINs<sup>58</sup>. Mutations in *PALB2*, *TGF $\beta$ R2*, and *ATM* have also been reported in PDAC<sup>58</sup>.

## 2.3 Diagnosis

As previously mentioned, early diagnosis represents one of the major clinical challenges of PDAC, contributing to its abysmal prognosis. The survival of patients correlates with the stage of the disease. Therefore, its early detection can significantly improve the probability of efficiently treating PDAC.

PDAC does not manifest itself with specific or visible symptoms during the early stages. Indeed, non-specific but frequent signs of pancreatic cancer are abdominal and back pain and weight loss, resulting from the impairment of the pancreatic synthesis of digestive enzymes and nutrient malabsorption<sup>18</sup>. These non-specific symptoms delay identification until the disease has already progressed. Almost all patients show locally or disseminated advanced PDAC at the diagnosis, with metastasis to the liver or lungs.

Besides unspecific symptoms, PDAC can cause diabetes in 20-50% of patients, leading to glucose intolerance<sup>60</sup>. In 80–90% of individuals, this cancer results in obstructive jaundice, gastrointestinal haemorrhage, and splenic vein blockage<sup>61</sup>.

In case of symptoms manifestation or PDAC suspect, the most common tests prescribed are abdominal computed tomography (CT) or magnetic resonance imaging (MRI). These techniques can assist in determining the presence of the tumor and whether cancer cells have metastasized to nearby organs, lymph nodes, and distant organs. A CT scan can be employed to evaluate if surgery would be an effective course of therapy<sup>16</sup>. Following these first-line imaging methods, the next step is endoscopic ultrasound for collecting biopsy samples for cytopathological studies, such as investigating mutations in the *KRAS* gene<sup>62</sup>, histologic diagnosis, and assessing surgical resectability<sup>16</sup>.

Besides the aforementioned imaging techniques, to date, there is no standardized PDAC screening technique available. Considering the high risk of misinterpreting benign lesions for PDAC or vice versa and the invasiveness of biopsy collection with these techniques, the need for less invasive diagnostic techniques, such as liquid biopsy or screening, to track patient response to therapy and direct therapeutic decisions, becomes urgent. For these reasons, the imaging techniques

are coupled with laboratory tests for potential biomarkers identification in patients' blood, pancreatic juice, and breath.

Serum carboxyhydrate Antigen 19-9 (CA 19-9) is secreted by a fraction of PDAC cells, and it can be used to screen individuals with high-risk factors, determine tumor resectability, and monitor patients' response to treatment after PDAC diagnosis<sup>16,63</sup>. Conventional protein biomarkers also consist of coagulation factors, such as Fibrinogen, D-dimer, haemostatic parameters, and inflammatory factors<sup>64</sup>. Moreover, increased alkaline phosphatase and bilirubin levels may indicate liver metastasization or bile duct obstruction<sup>65</sup>. Researchers have also focused on the detection of DNA mutations in pancreatic juice. Pancreatic intraepithelial neoplasia (PanIN) and invasive pancreatic cancer were associated with mutant P53 in the patients' pancreatic juice<sup>66</sup>. In addition, metabolomics can significantly help identify new PDAC plasma biomarkers for early diagnosing, where PDAC is still resectable, and for screening high-risk cohorts<sup>67</sup>. Other potential serum biomarkers are represented by circulating tumor cells (CTCs) and circulating tumor DNA (ctDNA), which can be more easily isolated from PDAC patients than biopsies or punctures, and understanding the molecular processes behind PDAC development and metastasis may be accomplished by performing different omics profiling on CTCs<sup>68</sup>. Several other biomarkers are currently under study for clinical validation, such as autotaxin, thrombospondin-2, lysophosphatidic acid, and insulin-linked binding protein 2<sup>64</sup>.

## **2.4 Prognosis and treatment**

Although the prognosis for pancreatic cancer varies depending on the stage and resectability, it is generally dismal (5-year survival: 10%), as many patients are diagnosed at a late stage, and the majority are declared surgically unresectable due to metastases. Only surgical resection and chemotherapy/radiation as adjuvant therapy have increased PDAC survival chances<sup>16</sup> (Figure 7).

### **2.4.1 Surgical options**

Once the medical team determines the diagnosis, treatment is evaluated to address the disease better. The main option remains surgery, immediate in the case of pancreatic tumors immediately classified as resectable (<20%)<sup>69</sup>. PDAC is then further classified as borderline resectable and unresectable (most locally advanced or metastatic)<sup>70</sup>. In the case of pancreatic cancer localized in the head of the organ, Whipple's procedure is considered the first choice for its resection. This procedure involves the removal of the head of the pancreas, the bile duct, the first portion of the intestine, and the gallbladder<sup>71</sup>. However, this technique is extremely difficult and linked to high post-operative morbidity due to incomplete excisions or development of metastasis, with 5-year survivals of ~20%.

For this reason, surgery is followed by adjuvant therapies<sup>69</sup>. In the case of borderline pancreatic tumors, which affect adjacent organs or vessels in a limited and localized way, neoadjuvant chemotherapy treatment aimed at reducing the extent of the tumor mass close to the blood vessels and organs concerned by the disease, may lead to subsequent surgery<sup>72</sup>. The same strategy is employed for locally advanced tumors. However, only a small percentage of cases (~30%) are considered for surgery following adjuvant therapy due to the important vascular involvement<sup>73</sup>, and the median survival equals resectable patients<sup>74</sup>. Metastatic pancreatic cancers (50-60% of PDAC cases) develop distant metastasis, and this determines the impossibility of their surgical excision; therefore, their treatment involves only a palliative chemotherapy regimen, yet survival of metastatic patients ranges around 5-9 months<sup>70,74</sup>.

#### **2.4.2 (Neo)Adjuvant Therapies: Chemotherapy and Radiotherapy**

Considering the high morbidity associated with PDAC excision surgery and the high percentage of patients with metastasis at the diagnosis, adjuvant therapies have emerged as important post-operative options to increase patients' survival rates<sup>69</sup>. Patients with resectable tumors can benefit from pre- and immediate post-operative adjuvant chemotherapeutic treatments for monitoring first and then limiting the chances of tumor relapse<sup>75</sup>. For these patients, adjuvant therapies consist of gemcitabine, alone or coupled with capecitabine<sup>76</sup>, or FOLFIRINOX, a combination of folic acid, 5-Fluorouracil (5-FU), oxaliplatin, and irinotecan. The choice of adjuvant therapy is guided by each patient's post-operative fitness<sup>75</sup>.

FOLFIRINOX and gemcitabine combined with paclitaxel can be administered as first-line neoadjuvant therapy for cases of resectable borderline and locally advanced pancreatic tumors to reduce their size and involvement of other organs and vessels and favour surgery resection<sup>77,78</sup>. For unresectable borderline, locally advanced, and metastatic pancreatic tumors, gemcitabine, alone or in combination with paclitaxel, and FOLFIRINOX represent the first-line standards of care, although other associations can be employed in case of bad patient fitness<sup>75</sup>.

Gemcitabine, in combination with capecitabine and 5-Fluorouracil, is often used in combination with radiotherapy. Although many in vitro studies and clinical trials have assessed the potential benefit of (chemo)radiotherapy in PDAC, there is an absence of consensus and conclusive evidence; therefore, the potential contribution of adjuvant radiation treatment to the improvement of patient outcomes in PDAC remains pending<sup>16,78</sup>.

The effectiveness of PDAC treatment remains poor despite the surgery and the variety of neo- and adjuvant therapies, representing a major challenge for basic and applied research, which needs to invest more of researchers' efforts in discovering new and alternative therapeutic options to replace or combine with current ones.



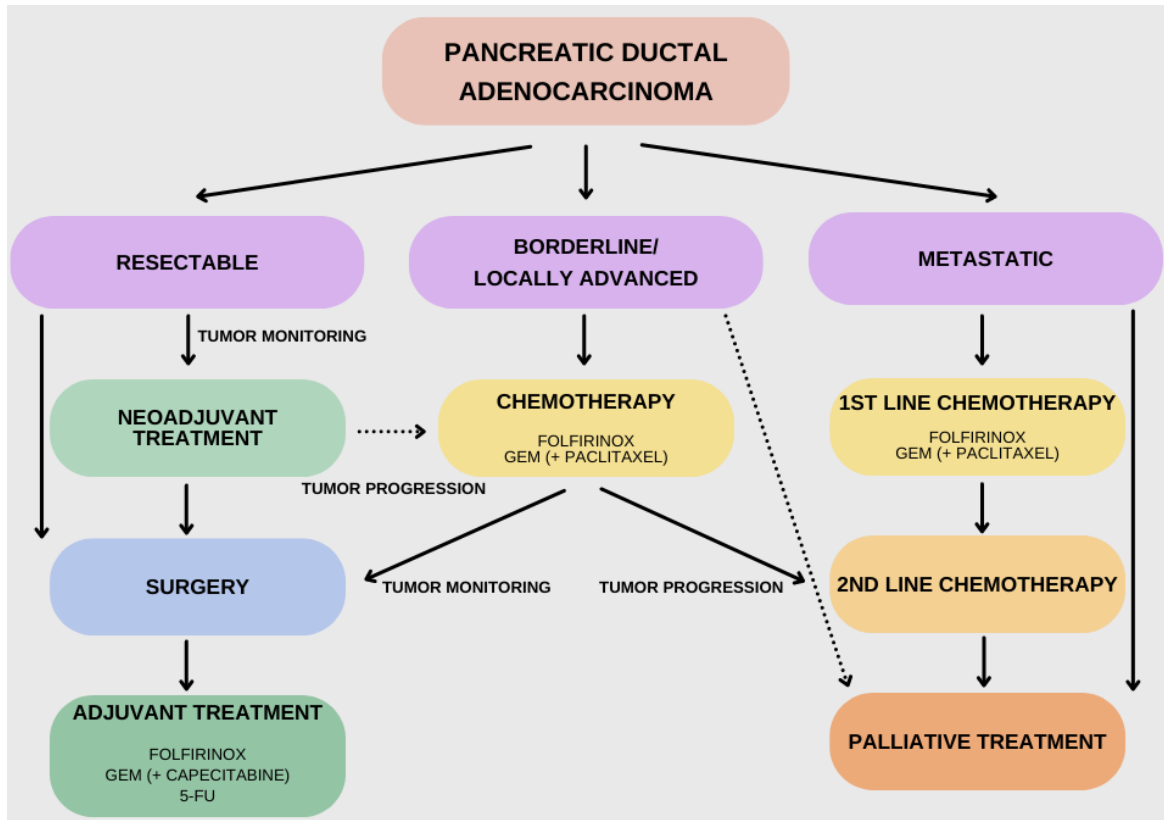


Figure 7. Schematic overview of all the current clinical treatment strategies for PDAC patients based on whether the patients have resectable, locally advanced, or metastatic PDAC. Image created with Biorender.

### 3. Tumor microenvironment

Tumors are caused by dysfunctions of certain cell types in the body, which then spread and proliferate uncontrollably outside the boundaries of the tissue in which they are located, leading to the development of tumor tissue whose properties differ from those of healthy tissue.

The concept of the tumor microenvironment (TME) was first introduced by the "seed-and-soil" theory developed by Stephen Paget in 1889 to explain the process of metastasis, in which cancer cells spread throughout the body<sup>79</sup>. According to this theory, metastatic cancer cells (the "seed") show preferences for specific organs when metastasizing, which are the result of the favourable interactions with the organ microenvironment (the "soil"). Therefore, this theory accords significant importance to the microenvironment in which cancer cells are placed. Since its elaboration, the notion of the tumor microenvironment has gained prominence in the cancer research field. Due to this interest in the tumor microenvironment, several features of tumor growth have been better understood, and novel medicines that target the tumor microenvironment have been developed.

The tumor microenvironment is the ensemble of cellular components, molecular components, and mechanical and chemical constraints that surround and interact with tumor cells, favoring tumor progression<sup>80</sup> (Figure 8).

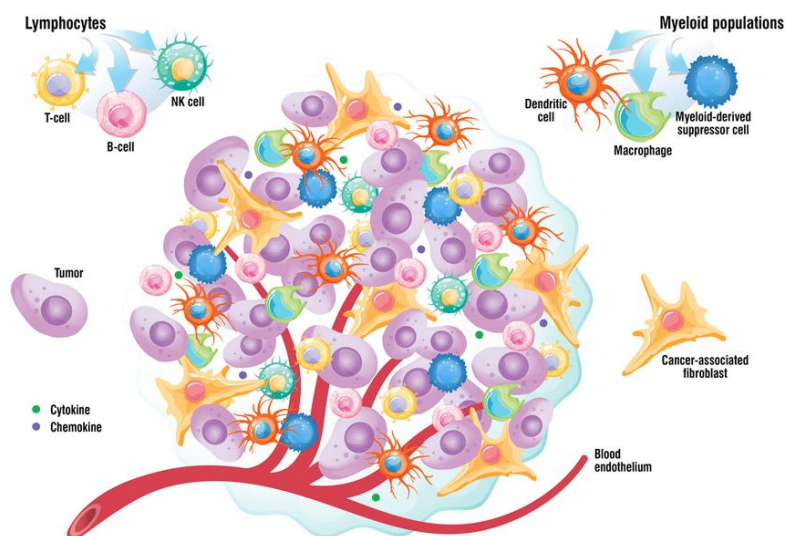


Figure 8. Schematic of the principal components of the tumor microenvironment, comprising cellular and non-cellular components. Image adapted from [81].

### 3.1 TME cellular component

The cellular component of the tumor microenvironment is constituted by stromal cells surrounding tumor cells. Stromal cells include infiltrating immune cells, mesenchymal cells of the connective such as fibroblasts, endothelial cells, which form blood and lymphatic vessels, nerve cells, and epithelial cells of the peri-tumoral healthy tissue. Cross-talks between these various cells cause cell activation, differentiation, and changes in the structural and biological characteristics of the ECM, resulting in the promotion of tumor growth, invasion, and metastatic spread. In addition to the abnormalities displayed by cancer cells in the tumor microenvironment, the surrounding stromal cells exhibit more different phenotypes than their healthy counterparts. Single-cell RNA seq analysis on mouse and human pancreatic tumors has recently revealed three different CAF subpopulations that exert different functions. Myofibroblastic CAFs (myCAFs) are the most abundant type in PDAC and derive from TGF- $\beta$ -activated pancreatic stellate cells, this phenotype is also characterized by high  $\alpha$ SMA expression, and is involved in the production of ECM components and in its remodelling, therefore playing a determinant role in PDAC desmoplasia and they are localized close to cancer cells<sup>82</sup>. Inflammatory CAFs (iCAFs) derived from IL1-activated pancreatic stellate cells but show low  $\alpha$ SMA expression, overexpressing instead different types of cytokines and chemokines, in particular IL6 and CXCL12, that promote PDAC progression and immune suppression<sup>82</sup>. myCAFs and iCAFs also share different localizations within the tumor; while myCAFs are localized close to cancer cells, iCAFs are found farther away from them in the stroma, suggesting a differential role related to their location. Moreover, these two types of CAFs are reversible states and can be converted into the other type based on their localization and the cues they are exposed to<sup>82</sup>. The third subpopulation expresses MHC class II genes similarly to antigen-presenting cells of the immune system; therefore, this CAF subpopulation was called antigen-presenting CAFs (apCAFs). These cells are thought to deactivate CD4<sup>+</sup> T cells and to contribute to suppress the immune system in PDAC<sup>82</sup>. Contrary to myCAFs and iCAFs, which originate from pancreatic stellate cells, studies suggest that apCAFs originate from mesothelial cells from normal pancreas<sup>83,84</sup>.

Mizutani et al. reported high Meflin/low  $\alpha$ SMA-expressing CAFs with an anti-tumor role in PDAC tissue samples. In fact, Meflin-positive CAFs correlated with better prognosis in PDAC patients and mouse model, suggesting that these stromal cells regulate differentiation in PDAC by

softening PDAC stroma and impairing its progression<sup>85</sup>. More recently, a new CAF subtype has been characterized. The metabolic CAFs (meCAFs) are characterized by elevated expression of marker genes related to glycolysis, suggesting a high glycolytic activity. The meCAFs are found in low desmoplasia PDAC patients and, despite they are associated to poor prognosis, patients with abundant meCAFs show a significant better response to immunotherapy, potentially due to the low desmoplastic reaction which promotes immune cells infiltration<sup>86</sup>.

Stromal cells interact dynamically with cancer cells to give them a more aggressive phenotype<sup>87</sup> (Figure 9). However, not all tumor-associated stromal cells will benefit the tumor, as for the case of recruited macrophages to the tumor site, where they can exert a pro- or anti-tumor role. Tumor-associated macrophages recruited by the tumor microenvironment can favour tumor progression via the synthesis of specific cytokines and chemokines, such as IL-6, growth factors, and hydrolytic enzymes for ECM remodeling, or by limiting the activity of other immune cells, leading to tumor immune escape<sup>88</sup>. Conversely, macrophages can act against the tumor by activating the macrophage-mediated programmed cell removal for tumor cell elimination or by secreting cytotoxic macromolecules<sup>88</sup>.

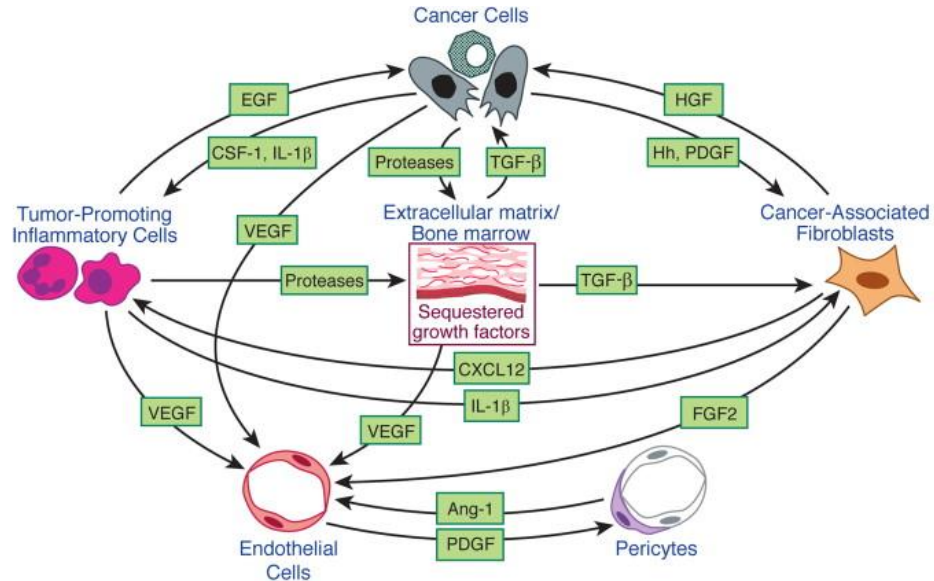


Figure 9. Schematic depicting the signaling interactions occurring in the tumor microenvironment during tumor progression. Image adapted from [89].

As for the vascular component of the TME, endothelial cells that form tumor capillaries display phenotypic and functional features which differ from healthy endothelial cells that results in a peculiar tumor microenvironment. In fact, normal tissues are characterized by well-organized and mature vasculatures and lymph vessels embedded in an ECM made up of a relaxed net of collagen and other fibers and a small number of fibroblasts and macrophages<sup>90</sup>. Conversely, TME is characterized by higher numbers of macrophages and fibroblasts and by a very intricate and dense network of collagen fibers that increases the interstitial tumor pressure<sup>91</sup>, further promoted by altered lymph vessels which are unable to drain the lymph fluid efficiently. In addition, tumor vasculature is aberrant, featured by frequently dilated and excessively branched vessels, with fenestrations, discontinuous basal membrane, and cancer cells embedded in the vessel's wall, causing the vessel to constrict. Due to these disordered and unpredictable abnormalities, blood flow is impaired in many tumors, further increasing interstitial pressure (Figure 10).

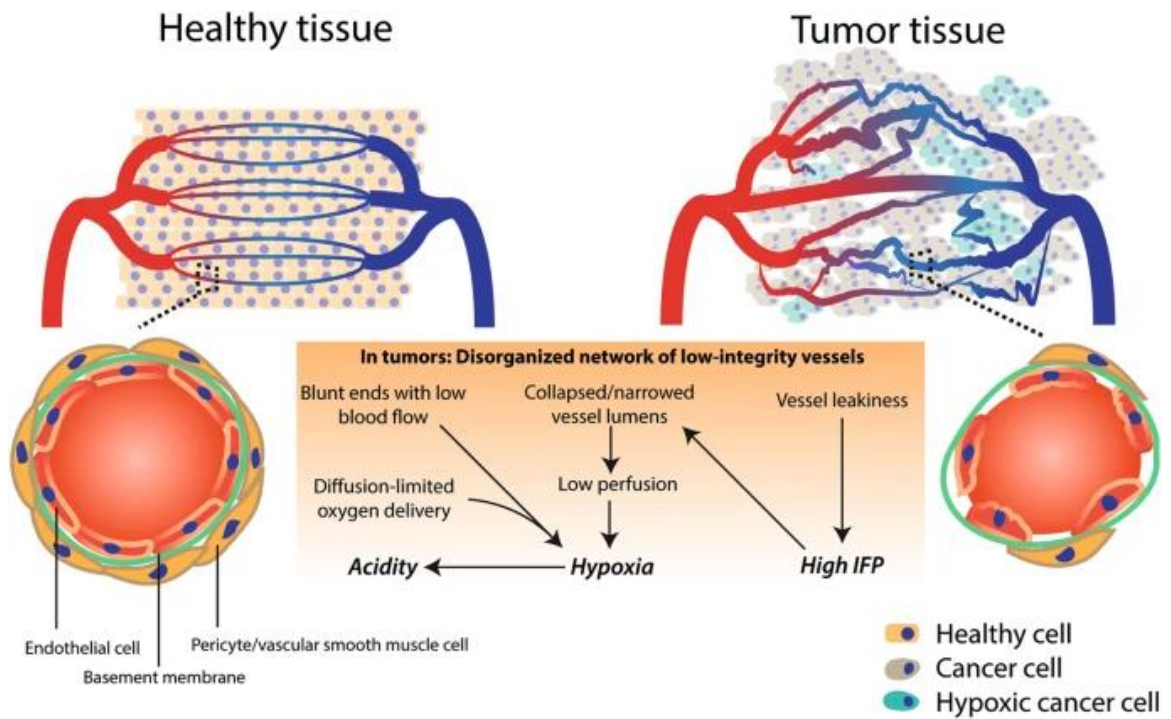


Figure 10. Schematic of the differences between the blood vasculature in healthy and tumor tissue. Image adapted from [92].

Tumor endothelial cells overexpress specific growth factors, such as Vascular Endothelial Growth Factor (VEGF) and its receptor (VEGF-R), promoting angiogenesis, and so their growth,

via autocrine signaling<sup>93</sup>. Tumor-associated endothelial cells also modify the interactions between cancer cells and ECM by increasing the expression of specific integrins involved in tumor cells' anchorage and growth, such as  $\alpha v \beta 3$  and  $\alpha v \beta 5$ <sup>94</sup> and potentiating tumor immune escape by cross-talking with tumor-associated macrophages<sup>88</sup>.

### 3.2 TME molecular component

Within the TME, the extracellular matrix (ECM) consists of a three-dimensional network of insoluble macromolecules. Within this mesh, cancer, and stromal cells, soluble molecules, such as enzymes, and soluble mediators of cell communication are embedded (Figure 11).

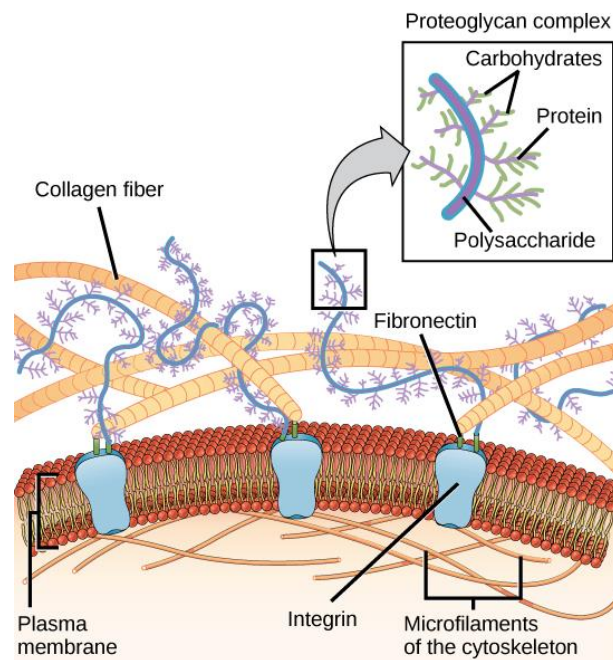


Figure 11. Schematic of the extracellular matrix of mammalian cells and its components. Image adapted from Wikimedia Commons<sup>95</sup>

The ECM comprises both polysaccharide and protein macromolecules. The extracellular matrix polysaccharides belong to the family of glycosaminoglycans; linear heteropolysaccharides are made up of repetitive disaccharide units. Polysaccharides include hyaluronic acid, chondroitin, dermatan, heparan, and keratan sulfates. The protein component of the extracellular matrix includes

glycoproteins such as collagen, laminin, fibronectin, and proteoglycans, and non-glycosylated proteins, such as elastin.

Fibroblasts synthesize collagens, a family of fibrous glycoproteins constituted by three  $\alpha$  polypeptide chains, each containing ~1000 amino acids with a particular peptide sequence (Gly-X-Y). Collagen largely contributes to ECM structure, and some types of collagens, such as type I and type IV, are overexpressed by tumor and stromal cells, promoting cancer progression, as demonstrated in pancreatic cancer<sup>96</sup> (See section 3.2.1).

Laminins are three-chain glycoproteins ( $\alpha$ ,  $\beta$ ,  $\gamma$ ) that constitute the basement membrane and type IV collagen. Laminins play an important role in many biological processes, including tumor migration, invasion, and dissemination, by promoting the synthesis of proteolytic enzymes that degrade the ECM<sup>97</sup>.

Fibronectins are glycoprotein dimers synthesized by fibroblasts and endothelial cells, which form fibrillar aggregates and participate in the organization and structuring of the ECM, playing a key role in cell adhesion, survival, growth, migration, and differentiation via integrin-mediated signaling<sup>98</sup>. They are frequently overexpressed in tumor tissue and involved in tumor progression and dissemination to other organs<sup>99</sup>.

Elastins are connective tissue proteins secreted by fibroblasts, smooth muscle cells, and endothelial cells in the form of tropoelastins, a precursor that is processed to elastin. These proteins exist as fibers and provide strength, toughness, and elasticity to the ECM of different tissues<sup>100</sup>. In the tumor context, elastin proteins are overexpressed by the modified ECM, having either favourable or unfavorable consequences on tumor progression. ECM elastin proteins cross-link with other extracellular matrix components and interact with tumor cells through specific receptors (EBP, Elastin-Binding Proteins), contributing to their metastatic phenotype and tumor-induced angiogenesis<sup>100</sup>.

### **3.3 TME soluble component**

Different soluble molecules are embedded within the ECM's insoluble protein and polysaccharide mesh. These include proteolytic enzymes involved in the ECM's remodeling,

playing a key role in processes such as cell differentiation, migration, proliferation, angiogenesis, and tissue repair<sup>101</sup>. Among the enzymes with proteolytic activity, we found the extracellular matrix proteases, which can belong to serine, cysteine, aspartate, and threonine proteases or the family of metalloproteases (MMPs), and glycosidases.

Glycosidases degrade the ECM polysaccharides, which are mainly glycosaminoglycans. Most of these hydrolases are localized intracellularly; therefore, glycosaminoglycans are first internalized in an endosome, where they undergo a first endolytic depolymerization to form oligosaccharides. The degradation continues after fusion with a lysosome, where oligosaccharides undergo enzymatic desulfation and exolytic depolymerization to form monosaccharides<sup>102</sup>. However, some glycosidases, such as those catalysing the degradation of hyaluronic acid, are secreted in the extracellular space (Jung H. et al., 2020).

Proteases can be integral membranes localized at the cell surface or secreted to the extracellular space. They are pleiotropic and pH-sensitive proteins that regulate the activity of several signaling molecules, the ECM turnover via the degradation of the ECM protein components, such as proteoglycans, fibronectin, and collagen, and the cleavage of precursor proteins to activate them<sup>101,103</sup>.

In addition to the physiological functions, proteolytic enzymes, in particular, all members of the metalloproteinase family, have been linked to tumor progression and metastasis, chronic inflammation, and subsequent tissue damage<sup>104</sup>. They have been recognized as biomarkers in various fields (diagnosis, monitoring, and treatment efficacy)<sup>105</sup>. Their role in cancer cells invasion and metastasis is closely linked to the acidic tumor microenvironment, as the acidic conditions promote the secretion and the activation of different proteases, leading to ECM degradation and cancer cells' enhanced migratory and invasive abilities<sup>106,107</sup>.



### 3.4 PDAC desmoplastic microenvironment

PDAC is a highly chemoresistant tumor, and this feature is the consequence of several factors; among them, we found the presence of a desmoplastic PDAC tumor microenvironment (Figure 12), which acts as a barrier that reduces the delivery of chemotherapy drugs.

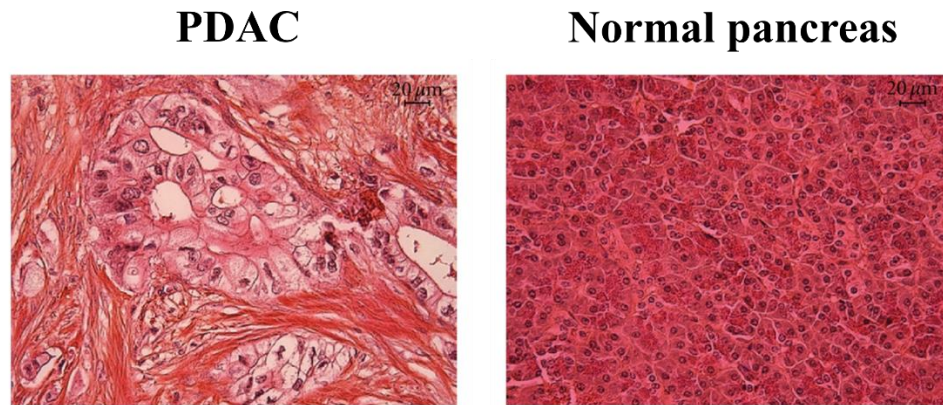


Figure 12. Histological photographs showing the S&H staining for PDAC and normal pancreas. Image adapted from [108].

PDAC is characterized by an extreme desmoplastic stroma surrounding the cancer cells, constituting 90% of the tumor volume<sup>109</sup>. This dense TME provides a scaffold for tumor growth, where stromal cells contribute to PDAC progression. Although cancer cells can produce ECM components, it is commonly assumed that the desmoplastic reaction results from cancer-associated fibroblasts (CAFs) activity, particularly pancreatic stellate cells (PSCs). During PDAC development, cancer cells secrete several factors, such as TGF- $\beta$ 1, platelet-derived growth factor (PDGF), sonic hedgehog (SHH), and fibroblast growth factor-2 (FGF2)<sup>110</sup>, for CAFs recruitment, activation, and proliferation<sup>110,111</sup>. When activated, PSCs start depositing high quantities of ECM, comprehending collagens I and V, fibronectins, hyaluronan, and laminins<sup>109</sup> to fuel the desmoplastic TME and promote a hypoxic microenvironment (see Section 3.6) and secreting different growth factors, immunosuppressive cytokines, and chemokines to promote mesenchymal and aggressive features of PDAC cells<sup>112–114</sup>. PDAC's dense ECM further promotes cancer progression by limiting immune cell accumulation via contact-mediated lymphocyte trapping<sup>115</sup> and activating the

integrin/FAK cascade in cancer cells<sup>116</sup>. Several works have demonstrated the pro-tumor role of PDAC desmoplasia and targeting both desmoplasias via pharmacologic inhibition and PDAC cells via chemotherapy has a greater effect than targeting cancer cells alone, highlighting its potential as a therapeutic target<sup>117,118</sup>.

### **3.5 Physico-chemical properties of the TME: hypoxia**

Tumor hypoxia is a chemical signature of the TME. Generally, this condition indicates low oxygen (O<sub>2</sub>) levels in the tissues (below 10 mmHg), which is caused by an unbalanced relationship between oxygen supply and demand. The role of hypoxia becomes more important in the tumor context, where the onset of this phenomenon brings several consequences closely associated with tumor progression and chemoresistance, thus contributing to a worse prognosis for the patient. The following sections provide an overview of the tumor hypoxic phenotype, the types of hypoxias, and the biological consequences.

#### **3.5.1 Hypoxic tumor microenvironment**

Cancer cells divide rapidly, resulting in tumor tissue growth. Angiogenesis fails to keep pace with this process, and it cannot supply the growing tumor with appropriate levels of oxygen, resulting in inner tumor regions with chronic low oxygen tension with respect to the surrounding healthy tissue due to the limited number of blood vessels. Therefore, tumor hypoxia results from an imbalance between O<sub>2</sub> demand and supply rate, and it can originate from different causes that depend on the time of exposure to low O<sub>2</sub> levels<sup>119</sup>. To mitigate this effect, cancer cells activate signaling pathways that promote angiogenesis in hypoxic conditions. However, as previously explained in paragraph 3.1, tumor angiogenesis is characterized by structural alterations in blood vessels with respect to healthy ones, displaying fenestrations that further impair blood circulation. This causes inefficient oxygen supply and reoxygenation in different tumor areas, leading to transient or cyclic hypoxia<sup>119</sup>.

Although transient and chronic hypoxia cannot always be distinguished completely in given tumor areas, chronic hypoxia typically occurs in cancer cells far from the blood supply and is brought on by restrictions in oxygen diffusion from tumor microvessels into the surrounding tissue.

On the other hand, acute or transient hypoxia arises closer to the blood vessels and is primarily caused by transient, local perturbations in blood perfusion<sup>119</sup>.

The effects of hypoxia on tumor cells are mediated by three proteins belonging to the hypoxia-inducible factor (HIF) family; HIF-1, HIF-2, and HIF-3. HIF-3 induces gene expression and inhibits the activity of HIF-1 and HIF-2 activity<sup>120</sup>. These last two proteins are closely related but target a different set of hypoxia-induced genes and have functions that only partially overlap. HIF-2 $\alpha$  subunits are expressed in conditions of intermediate hypoxia, whereas HIF-1 $\alpha$  is mostly expressed in severe and sustained hypoxic conditions<sup>121</sup>.

All three HIFs are heterodimers of two subunits,  $\alpha$ , and  $\beta$ . Most HIF transcriptional activity is mediated by HIF-1 $\alpha$  and HIF-2 $\alpha$  complexed with HIF-1 $\beta$ . Unlike  $\beta$  nuclear subunits, cytosolic  $\alpha$  subunits expression is regulated by alterations in oxygen levels via transcriptional regulation and proteolytic degradation<sup>122</sup>. In normoxic conditions, the HIF-1 $\alpha$  subunit is hydroxylated on different proline residues in the N-terminal oxygen-dependent degradation domain (NODD) and C-terminal oxygen-dependent degradation domain (CODD) by oxygen-dependent prolyl hydroxylase (PHD) enzymes<sup>123</sup>. This modification determines HIF-1 $\alpha$  ubiquitylation by 26S proteasome<sup>124</sup>. The active transcriptional  $\alpha/\beta$  complexes are not assembled without  $\alpha$  subunits. HIF- $\alpha$  activity is also negatively regulated by the factor inhibiting HIF (FIH), an oxygen-dependent enzyme that hydroxylates different asparagine residues in HIF-1 $\alpha$  and HIF-2 $\alpha$ <sup>125</sup>. This reaction prevents HIF- $\alpha$  subunit interaction with CBP/p300 co-activators, which is necessary for the transcriptional activity of HIF subunits<sup>126</sup>. Besides hydroxylation, HIF- $\alpha$  activity is also regulated by acetylation, which may lead to decreased or increased HIF- $\alpha$  stability and activity based on which residues are acetylated<sup>127</sup>.

Under hypoxia, the activity of PHD is decreased with consequent reduction of HIF- $\alpha$  hydroxylation and degradation. This results in an accumulation of HIF- $\alpha$  subunits in the cytosol and the increased dimerization of  $\alpha$  with  $\beta$  subunits in the nucleus to activate hypoxia-dependent gene expression by complexing of active HIF-1 with CBP/p300 at the level of the promoter of genes containing hypoxia response element (HRE) sequences. In chronic hypoxia, a high generation of reactive oxygen species (ROS) promotes HIF-1 stability by inhibiting PHD and FIH<sup>128</sup>.

Among the different signal transduction pathways induced by hypoxia, Mitogen-activated protein kinase (MAPK) signaling pathways are switched during chronic hypoxia and are crucial to the cancer cell response to low oxygen levels. Increased ROS levels are generated during hypoxia, and, together with the hypoxia-induced activation of L-type voltage-gated Ca<sup>2+</sup> channels and

consequent intracellular  $\text{Ca}^{2+}$  rise<sup>129</sup>, they activate c-Jun N-terminal kinase (JNK) MAPK, extracellular signal-regulated kinase (ERK) MAPK and p38 MAPK<sup>130</sup>. These kinases phosphorylate HIF-1 $\alpha$  subunits and enhance the stability, accumulation in the cell nucleus, and interaction with CBP/p300 co-activator, promoting the transcriptional activity of HIF-1<sup>131</sup>. Moreover, the activation of SIAH2 by p38 MAPK can also lead to the degradation of PHD3<sup>132</sup>, and chronic hypoxia inhibits the expression of dual specificity protein phosphatase (DUSP2). This enzyme dephosphorylates MAPK kinases, inactivating them<sup>133</sup> (Figure 13).

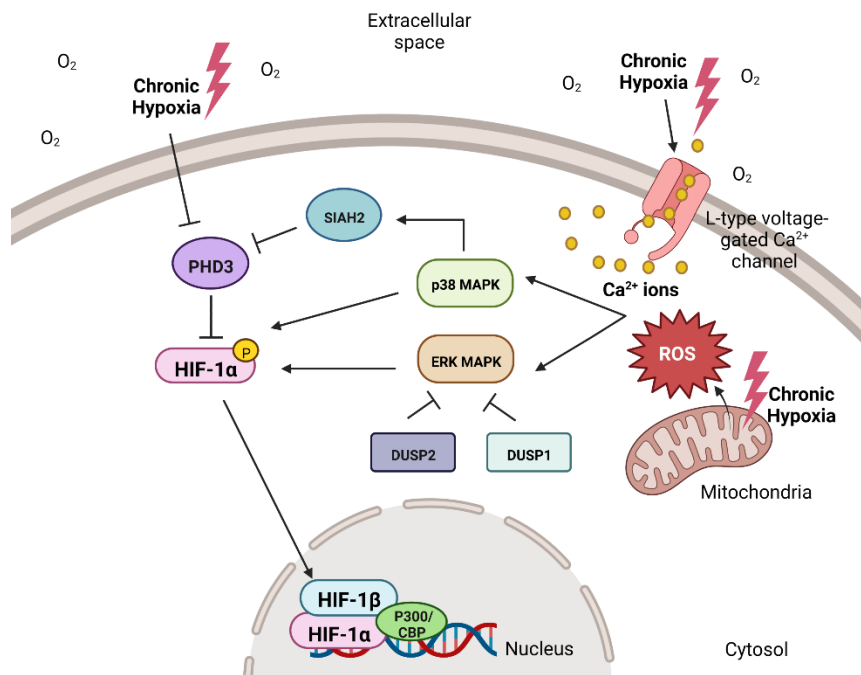


Figure 13. Schematic of the contribution of MAPK cascades in the HIF-1 activation pathway. Image adapted and modified from [134].

HIF-1 expression is also regulated by other pathways, including the NF- $\kappa$ B pathway. HIF1 $\alpha$  gene promoter contains NF- $\kappa$ B binding sequences, and in turn NF- $\kappa$ B induces the expression of HIF-1 $\alpha$ <sup>135</sup> as well as HIF-1 $\beta$ <sup>135</sup>. In particular, HIF-1 $\alpha$  activation is caused by p50 and p65/RelA NF- $\kappa$ B, but not c-Rel NF- $\kappa$ B. NF- $\kappa$ B expression is tightly linked to hypoxia, as it is upregulated at the beginning of chronic hypoxia, and this regulation occurs via several mechanisms.

In normal conditions, NF- $\kappa$ B is localized in the cytosol in an inactive form via interaction with I $\kappa$ B inhibitory proteins. In response to a stimulus triggered by inflammatory cytokines, viruses, bacteria, or different kinds of stress, IKK $\alpha/\beta$  kinases phosphorylate I $\kappa$ B inhibitory proteins, targeting them for proteasome-mediated degradation. As a result, NF- $\kappa$ B is free from the interaction

and can translocate to the cell nucleus, where it activates the expression of over 150 target genes involved in inflammation, immune response, and cancer progression<sup>136</sup>. IKK $\beta$  is a target of PHD1 for hydroxylation, and this modification leads to its degradation, reducing NF- $\kappa$ B activity<sup>137</sup>. In chronic hypoxia, decreased PHD1 activity results in reduced IKK $\beta$  degradation and, consequently, in an increase in NF- $\kappa$ B activity. As previously mentioned, intracellular Ca<sup>2+</sup> rises are observed during hypoxia, and this cytosolic increase activates Ca<sup>2+</sup>/calmodulin-dependent kinase 2 (CaMKII), which, in turn, triggers the activation of transforming growth factor- $\beta$  (TGF- $\beta$ )-activated kinase 1 (TAK1). Finally, this protein interacts with TAB, forming a complex that phosphorylates IKK $\beta$ , a modification necessary for activating NF- $\kappa$ B signaling<sup>137</sup>. These data indicate a positive feedback loop between hypoxia and NF- $\kappa$ B.

Alternatively, hypoxia promotes NF- $\kappa$ B activation via MAPK pathways. ERK MAPK catalyses the phosphorylation of p65/RelA NF- $\kappa$ B, activating it<sup>138</sup>. In addition, hypoxia-induced ROS production may lead to NF- $\kappa$ B activation through the PI3K/Akt/PKB pathway<sup>139</sup>, which shows different links to NF- $\kappa$ B activation. Akt serine/threonine kinase directly phosphorylates p65/RelA, activating it<sup>140</sup>, or acts upstream by catalysing IKK $\alpha$  and IKK $\beta$  phosphorylation via mTOR, therefore promoting I $\kappa$ B $\alpha$  degradation<sup>141</sup>. Finally, hypoxia upregulates alarmin receptors, playing an important role in mediated hypoxia responses in necrotic cells, which secrete damage-associated molecular patterns (DAMPs) when embedded in a hypoxic microenvironment. DAMPs bind to alarmin receptors and activate NF- $\kappa$ B indirectly<sup>142</sup> (Figure 14).

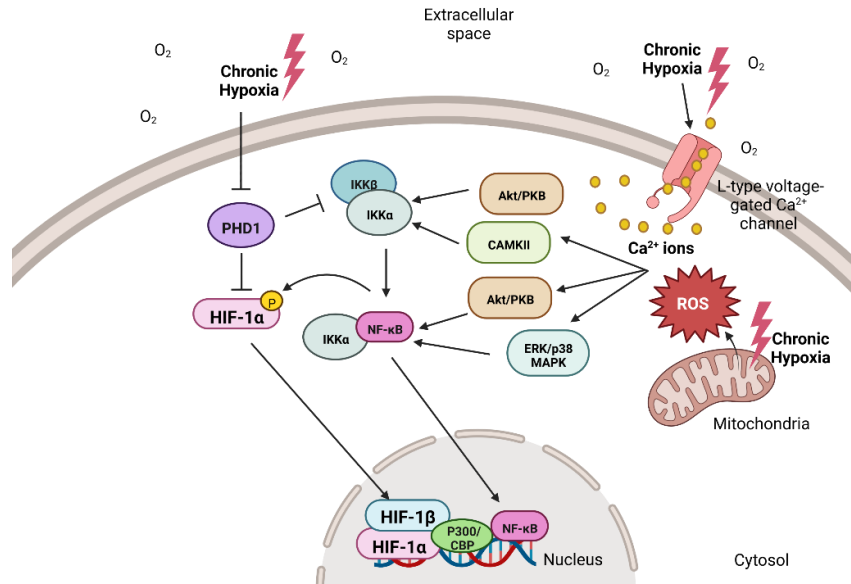


Figure 14. Schematic depicting the hypoxia-induced mechanism of NF- $\kappa$ B activation. Image adapted and modified from [134].

As described previously, transient hypoxia results from aberrant tumor vasculature; this translates to areas of the tumor that alternate between normoxic and hypoxic conditions, displaying fluctuations in oxygen tension that depend on the tumor type and size. The specificity of the pattern of these fluctuations is already observed at the level of the cell types from which the tumor originated *in vivo* studies<sup>143</sup>.

Compared to chronic hypoxia, transient hypoxia affects fewer genes, despite having a similar cellular response<sup>144</sup>. Similar to chronic hypoxia, transient hypoxia has a pro-inflammatory role, activating NF- $\kappa$ B via HIF-1 $\alpha$  and in a ROS-dependent way<sup>145,146</sup>. However, the two types of hypoxia show different NF- $\kappa$ B and HIF-1 $\alpha$  activation degrees and mechanisms. HIF-1 $\alpha$  is expressed at higher levels and for longer times in transient hypoxia compared to chronic hypoxia<sup>147,148</sup>. Moreover, as hypoxia cycles are repeated, the expression level of the protein HIF-1 increases; HIFs activation is greater when hypoxia cycles occur more frequently (high number of cycles/hour), translating into greater activation of NF- $\kappa$ B<sup>149</sup>. Transient hypoxia also has a much greater impact on specific genes expression than chronic hypoxia. Among these genes, we found epidermal growth factor (EGF) pathway-related genes, CXCL8, coding for IL-8, and PLAU, coding for Urokinase<sup>144</sup>.

Besides the pathways mentioned above, transient hypoxia generates ROS via the upregulation of NOX1, NOX2, and NOX4 and the mitochondrial electron transport chain<sup>150</sup>. ROS

promotes HIF-1 $\alpha$  expression and stability by reducing PHD activity and inactivating FIH<sup>125</sup>. Importantly, ROS is also a potent activator of the MAPK pathway, leading to the activation of activator protein-1 (AP-1) and of the mammalian target of rapamycin (mTOR) kinase via Ca<sup>2+</sup>-induced activation of protein kinase C (PKC) and protein kinase A (PKA), with final increased in HIF-1 $\alpha$  stability via phosphorylation<sup>150</sup> (Figure 15).

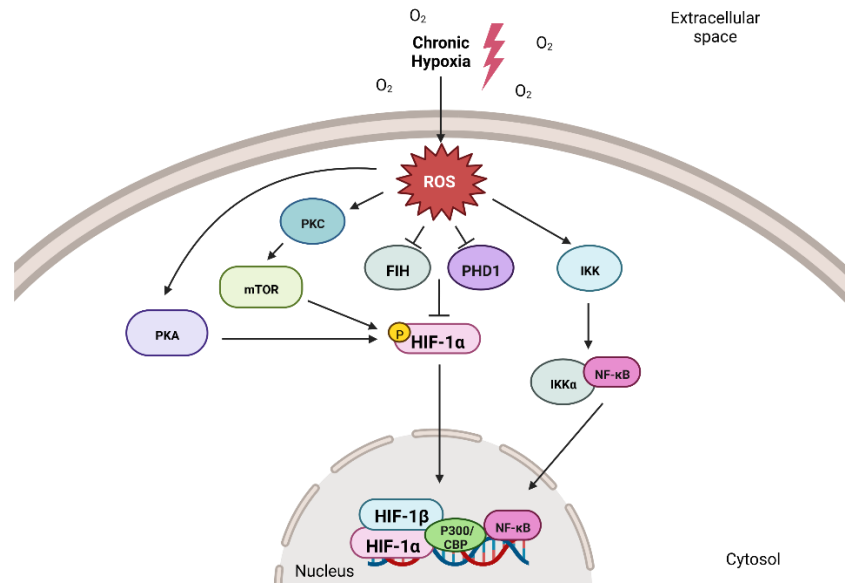


Figure 15. Schematic showing the effects of ROS in cycling hypoxia on the activation of HIF-1 and NF- $\kappa$ B. Image adapted and modified from [134].

### 3.5.2 Contribute of hypoxia to PDAC progression and link with Warburg effect.

PDAC is characterized by the rapid proliferation of cancer cells, hypovascularization, mitochondrial dysfunctions, and severe desmoplastic stromal response, which decreases the delivery of nutrients and oxygen and increases glycolysis and lactate accumulation. This translates into tumor areas that are highly hypoxic and not static. However, the tumor core is particularly hypoxic, with a median tissue partial oxygen pressure (pO<sub>2</sub>) of 0-5.3 mmHg compared to 24.3-92.7 mmHg in the adjacent healthy pancreas<sup>151</sup>. PDAC cells can rapidly adapt and grow in severe hypoxia, and this feature is linked to PDAC progression and aggressiveness, contributing to more aggressive PDAC cell phenotypes.

To meet their high demands for metabolites and energy in hypoxic conditions, pancreatic cancer cells evolve an effective adaptive metabolic response. Cancer cells show a metabolic shift compared to normal cells, and they are characterized by increased glucose uptake and a higher

reliance on glycolysis rather than mitochondrial oxidative phosphorylation for energy production, even under normoxic conditions<sup>152</sup>, such as close to blood vessels. The ATP pathway switch from OXPHOS to glycolysis was called Warburg effect. However, recent literature has demonstrated that several cancer types display an intact or upregulated OXPHOS. This indicates that although the Warburg effect is often present in cancer cells, oxidative phosphorylation still contributes to ATP synthesis, and the dependency of cancer cells on OXPHOS or glycolysis depends on the cell type, growth stage, and tumor microenvironment<sup>153</sup>. In recent years, many scientific works have demonstrated that Warburg supports PDAC aggressiveness by promoting EMT, distant dissemination, immunosuppression, stemness and angiogenesis<sup>154–161</sup>.

The Warburg effect represents one of the main intracellular responses to hypoxia. Indeed, it was reported that PDAC cells show a higher glycolytic and mesenchymal potential in a hypoxic environment compared to cells displaying only the Warburg effect, and the major lactate efflux from hypoxic PDAC cells fuels the growth of normoxic PDAC cells which surround the hypoxic core<sup>162</sup>. Indeed, the lactate secreted by hypoxic cancer cells is employed by surrounding stromal and normoxic cancer cells for immunosuppressive and growth purposes<sup>162</sup>. In this context, hypoxic tumor cells preferentially use glycolysis for ATP synthesis, and the lactate produced and extruded diffuses toward blood vessels, whereas normoxic tumor cells import it and oxidize it to produce energy. This means lactate efficiently replaces glucose to fuel cell respiration in normoxic cells. Hence, “unused” glucose diffuses in the extracellular space from the oxygenated tumor cell to support the glycolysis of distant, hypoxic tumor cells<sup>163</sup>. HIF-1 $\alpha$  role in promoting glycolytic phenotype in PDAC is further supported by the vascular epidermal growth factor (VEGF), which enables the transition from OXPHOS to glycolysis in PDAC cells by upregulating HIF-1 $\alpha$ <sup>164</sup>.

Hypoxia exerts its pro-tumor roles by generating ROS in both PDAC and stromal cells, and the function of ROS has two opposing edges, as ROS levels determine its pro- or anti-tumor effect. While excessive ROS induces oxidative stress and cell death in PDAC, a moderate production of ROS below a specific threshold level promotes glycolysis, tumor cell survival, and growth. Therefore, to avoid cell death by excessive ROS production by the hypoxic TME, PDAC and stromal cells exploit different strategies, such as hypoxia-induced upregulation of fibulin-5<sup>165</sup>, antioxidant enzymes such as heme oxygenase 1 (HO-1)<sup>166</sup>, and by tightly regulating ROS clearance<sup>167</sup>. ROS generation is independent of HIF-1 $\alpha$ , but it is required for its stabilization via the PI3K/Akt/p70S6 pathway, via MAPK pathway activation, or PHDs inactivation<sup>168</sup>.



Hypoxia results from the great desmoplastic reaction in PDAC, which is mainly due to the activation of pancreatic stellate cells (PSCs). Hypoxia-driven ROS production activates them and prompts them to secrete different soluble factors, such as hepatocyte growth factor (HGF), Osteopontin, VEGF, and inflammatory factors, which promote PDAC aggressive phenotypes<sup>169</sup>.

Cell responses to hypoxia also comprehend autophagy activation to promote PDAC stemness and progression<sup>170</sup>. Maintenance of stemness is further assured by autophagy-independent strategies, such as hypoxia-driven overexpression of Nestin via the TGF- $\beta$ 1/Smad4 pathway<sup>171</sup>, and via indirect ways, such as via upregulation of HO-1<sup>166</sup> and paracrine signaling of Osteopontin by pancreatic stellate cells<sup>172</sup>.

The hypoxia-mediated maintenance of stemness in pancreatic cancer cells is fundamental for acquiring migratory and invasive potential for tumor dissemination. However, hypoxia promotes metastatic phenotypes mostly in a HIF-1 $\alpha$  and NF- $\kappa$ B-dependent way, promoting the upregulation of several EMT markers<sup>173,174</sup>. However, HIF-2 $\alpha$  also contributes to EMT in PDAC, particularly by regulating Twist2 binding to the promoter of E-cadherin, leading to its downregulation<sup>175</sup>.

The acquisition of mesenchymal phenotypes favours the invasion and metastasis of PDAC cells. HIF-1 $\alpha$  is responsible for the transcriptional activation of genes involved in PDAC dissemination<sup>176</sup> and for the regulation of several ion channels, including Ca<sup>2+</sup>-permeable ion channels<sup>177</sup> and voltage-dependent K<sup>+</sup> channels<sup>178</sup>. PDAC stromal cells further foster PDAC cells' metastatic potential by secreting soluble factors that induce ECM digestion<sup>179</sup>.

The role of hypoxia covers almost all cellular processes determining the progression of PDAC. HIF-1 $\alpha$  also induces angiogenesis in pancreatic cancer by promoting the nuclear translocation of PKM2, which regulates HIF-1 $\alpha$ -induced VEGF transcription and secretion<sup>180</sup>. For the same purpose, hypoxia also promotes the cooperation between HIF-1 $\alpha$  and Stat3, which regulates VEGF expression in PDAC cells<sup>181</sup>, and enhances MUC1 activity, leading to the upregulation of several pro-angiogenic factors that are secreted by PDAC cells and promote endothelial cell tube formation<sup>182</sup>. However, targeting HIFs may not represent a successful strategy, as hypoxic PDAC cells can induce angiogenesis via HIF-1 $\alpha$ -independent ways<sup>183,184</sup>.

The enhancement of all these aggressive characteristics has inevitable consequences on the ability of pancreatic cancer cells to resist chemotherapeutic treatments, particularly gemcitabine treatment. The hypoxia niche activates Akt-related pathways that potentiates gemcitabine-induced stemness and resistance in PDAC cells<sup>185,186</sup>, and upregulates the ATP-binding cassette subfamily G member

2 (ABCG<sub>2</sub>), which decreases the gemcitabine sensitivity of PDAC cells<sup>187</sup>. In addition, some contribution of HIF-2 $\alpha$  in PDAC chemoresistance has also been reported, indicating HIF-2 $\alpha$ -induced SLC1A5 upregulation, which regulates glutamine-induced ATP synthesis and confers gemcitabine resistance to PDAC cells<sup>188</sup>.

### **3.6 Physico-chemical properties of the TME: acidosis**

All body tissues are net producers of acid due to mitochondrial respiration and CO<sub>2</sub> generation and fermentative metabolism that produces lactate. Protons concentration is commonly expressed on a pH scale and significantly affects the activity of all those proteins that undergo protonation. For example, the function of enzymes is closely linked to pH, and all can be ascribed to an optimal pH, and its changes deeply affect their activity. Furthermore, cytosolic enzymes, including glycolytic ones, are predicted to function optimally at a pH value of 7.3<sup>189</sup>; therefore, cells carefully regulate intracellular processes to maintain the cytoplasmic pH near that value. The acid-base status of normal tissues is generally stable, with extracellular pH (pH<sub>e</sub>) values ranging from 7.3 to 7.4. However specific epithelia, such as the pancreas, show fluctuations in their interstitial pH due to physiological acid and base secretions<sup>9</sup> (See Section 3.6.4).

In the context of tumorigenesis, it is well documented that the mean pH<sub>e</sub> value of TME is generally more acidic than the microenvironment of healthy tissues<sup>190</sup>. However, particular attention should be addressed to the heterogeneity and dynamism of TME, where pH<sub>e</sub> is variable within the tumor. This means that in the cancer, we can find highly acidic localized areas and other regions with a pH<sub>e</sub> close to physiological pH<sub>e</sub> (~ 7.4) and a pH<sub>e</sub> gradient from the tumor periphery to the core is associated with the development of a highly acidic necrotic tumor core. In general, most recorded pH<sub>e</sub> values in the tumor are in the range of 6.4-7<sup>191</sup>. The same heterogeneity is reflected for hypoxia and metabolic phenotypes, varying in time and space along tumor progression.

The acidic tumor microenvironment can be ascribed to different causes. Genetic and epigenetic alterations lead to oncogenic signaling, which may promote the activation of pH-regulatory members that mediate the extrusion of acid products to the TME<sup>152</sup>. Another cause is the cancer cells' metabolic reprogramming and hypoxic conditions described in the previous sections. The enhanced glycolysis produces a high output of lactate and protons, which are secreted into the extracellular space, acidifying it. Acidic areas correlate with areas of cells with an enhanced

glycolytic phenotype and invasive ability<sup>192</sup>. Cancer cells with OXPHOS phenotype and pentose phosphate pathway further contribute to producing acidic waste products in the form of CO<sub>2</sub>, which diffuses from cancer cells and accumulates in the TME, which is hydrated into protons and HCO<sub>3</sub><sup>-</sup> ions by CAs.

However, insufficient and inefficient tumor vascularization acts as a barrier that prevents the vascular dispersion of CO<sub>2</sub>-derived protons. In this case, diffusion distances can reach hundreds of μm and generate pH<sub>e</sub> gradients across the TME. Tumor acidosis can be potentiated mostly by the glycolytic metabolism, as lactate has a slower mobility than CO<sub>2</sub>, being also a stronger acid. Several studies have reported that hypoxic tumor regions overlap with acidic ones<sup>193</sup>. However, highly acidic areas can also be found in more oxygenated portions of the tumor, as at the interface with the stroma<sup>192</sup>. Moreover, although hypoxia and acidic pH<sub>e</sub> may induce similar programs in cancer cells, such as genomic alterations, EMT, and stemness properties, the cell metabolic responses to hypoxia differ from those caused by tumor acidosis. While hypoxic cancer cells enhance glycolytic phenotype and enhance glucose uptake, acidic ones promote the metabolic shift towards OXPHOS or Pentose Phosphate Pathway(PPP), limiting the use of glucose for lactate production also for protecting cancer cells from excessive ROS production<sup>194</sup>.

Acidic pH<sub>e</sub> is not only a consequence of a hypoxic microenvironment, but acidosis and hypoxia act synergically to induce HIFs. Filatova and colleagues have demonstrated that hypercapnic acidosis induces HIF1α and HIF2α expression already at normoxic conditions in glioblastoma cells. HIFs expression is further increased in presence of hypoxia within the pH<sub>e</sub> range 6.6-6.8. Therefore, acidosis and hypoxia cooperate in glioblastoma cells to activate the HIF signaling cascade that promote cancer stem cell maintenance<sup>195</sup>.

Moreover, the crosstalk between tumor acidosis and glycolysis is bidirectional, as a cytosolic acid pH (pH<sub>i</sub>) negatively regulates glycolytic enzymes<sup>196</sup>, potentially limiting cancer cell growth and survival.

Despite the significant production of acid products, cancer cells show a slightly more alkaline intracellular pH (7.1-7.7) than normal cells (around 7.2) under similar conditions<sup>191</sup>, a slight difference that is linked to tumor progression (see Section 3.6.2). However, the pH<sub>i</sub> of cancer cells is influenced by extracellular acidosis, as sudden and severe acidification of the extracellular space can negatively affect pH<sub>i</sub> steady-state, paving the way to cell death<sup>197</sup>. Therefore, considering Cancer cells increase their capacity for acid extrusion to maintain this alkaline pH<sub>i</sub> and avoid the

toxic effects of intracellular acidification. Still, this strategy also enhances their aggressiveness by promoting migration, invasion, immune escape, and chemoresistance. To maintain this alkaline  $pH_i$  value, transformed cells upregulate the expression and/or the activity of plasma membrane  $pH$  regulatory transporters and pumps, which extrude the excessive acid products from the cytosol. Bicarbonate transporters and exchangers (NBCs and AEs), the vacuolar-type  $H^+$ -ATPase (V-ATPase), the  $Na^+/H^+$  exchanger NHE-1 and its isoforms, the monocarboxylate transporters (MCTs) and carbonic anhydrases (CAs) CAIX and CAXII are constitutively expressed plasma membrane proteins that protect the intracellular space from acidification (Figure 16). In physiological conditions, these proteins collaborate to regulate  $pH$  homeostasis, which is required for correct cell signaling and metabolism. In cancer cells, these proteins are dysregulated, contributing to cancer cells' malignant and acid-resistant phenotype<sup>198</sup>. Additionally, the increased expression and/or activity of these proteins determines the  $pH$  gradient observed in transformed cells, characterized by a reversed  $pH$  gradient across the cell membrane, displaying an alkaline  $pH_i$  and an acidic  $pH_e$  compared to healthy cells<sup>191</sup>.

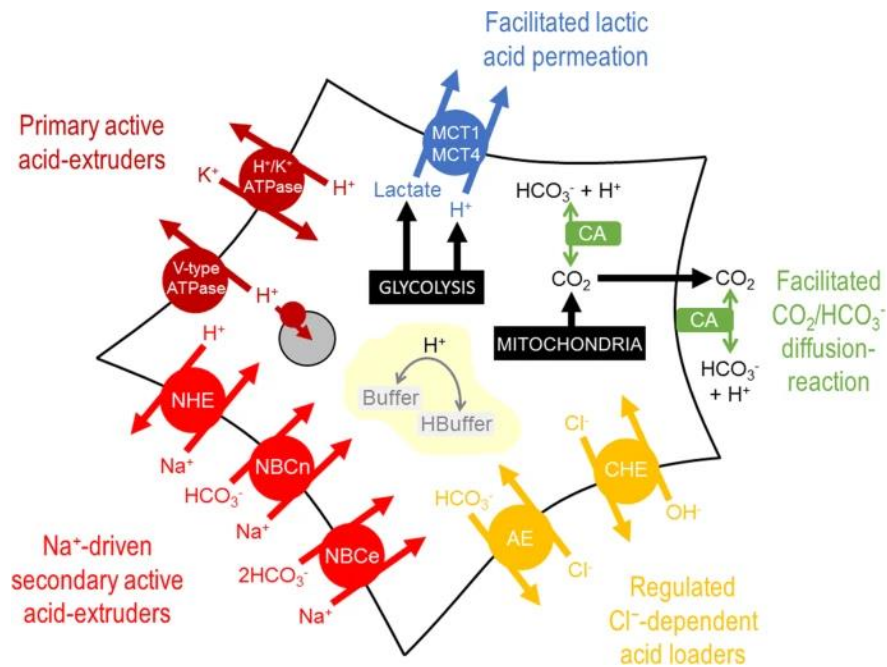


Figure 16. Schematic showing the major molecules involved in  $pH$  regulation in cancer cells. Image adapted from [197].

### 3.6.1 pH-regulatory proteins in PDAC

The main function of pancreatic ducts is the secretion of an alkaline fluid to neutralize the acidic chyme that comes from the stomach. This implies that pancreatic ductal cells secrete bicarbonate across their apical membrane while maintaining their  $\text{pH}_i$  stable, therefore representing a major challenge for their acid-base homeostasis. The pancreatic duct then exhibits a considerable capacity for acid-base transport, and studies have reported that several acid-base transport proteins are implicated in the aggressiveness of PDAC.

#### *Na<sup>+</sup>/H<sup>+</sup> exchangers (NHE): SLC9A-C*

The NHEs family comprehends 10 isoforms, and NHE1 is the most studied. NHE1 is a ubiquitously expressed plasma membrane protein and an important regulator of both  $\text{pH}_i$  and  $\text{pH}_e$ , and cell volume homeostasis via the electroneutral exchange of  $\text{Na}^+$  ions from the extracellular space with cytosolic protons. The NHE1-mediated changes in  $\text{pH}_i$  and the downstream signaling pathways are then required for the physiological regulation of cell differentiation, programmed cell death, migration, and proliferation<sup>199</sup>, and the integration of mechanical stimuli and hypoxia, and the NHE1 C-terminal tail is involved in the reorganization of the actin cytoskeleton through the binding with different actin-binding proteins<sup>200</sup>. Besides NHE1, NHE6 and NHE7 play an important role in  $\text{pH}_i$  regulation in the cancer context. In breast cancer cells and fibrosarcoma cells, hypoxia promotes the acidification of both TME and intracellular endosomes. The latter results from the translocation of NHE6, an endosomal exchanger, from the endosomal membranes to the plasma membrane of hypoxic cells. This relocation leads to hyper-acidification of endosomes, which drives intravesicular drug trapping and decreased sensitivity to Dox<sup>201</sup>. NHE9 also localizes in the endosomes in glioblastoma cells, where it alkalinizes endosomes' luminal pH to prevent EGFR turnover and to prolong its downstream signaling cascade involving MAPK and Akt to promote migration and tumor growth<sup>202</sup>.

The overexpression and/or activation of NHE1 have been reported to be an early event in tumorigenesis as it drives the intracellular alkalinization of cancer cells, and this acid extruder is

required for the acquisition of aggressive cancer cell phenotype by promoting cancer cells proliferation, migration, and invasion<sup>203–206</sup>.

In the pancreas, NHE1 has been demonstrated to play a major role in  $\text{pH}_i$  regulation in resting and muscarinic agonist-stimulated pancreatic acinar cells<sup>207</sup>. In PDAC, Neurotensin (NT) induces localized extracellular acidification via activation of NHE1, a requirement for cell aggressiveness<sup>208</sup>. Moreover, NHE1 expression, activity, and cell membrane accumulation are triggered by laminin subunit  $\gamma 2$  (LAMC2) via Akt-dependent signaling, modulating  $\text{pH}_e$  to induce EMT and the formation of actin-dependent pseudopodia for cell migration and invasion of PDAC cells<sup>209</sup>. Epidermal growth factors (EGF) and the EGF receptor (EGFR) play an essential role in PDAC, mediating the extensive desmoplastic stromal reaction, promoting PDAC cells aggressiveness<sup>210,211</sup>. Cardone et al. demonstrated that EGF promotes a pro-metastatic protein-protein complex composed of EGFR and NHE1 and mediated by  $\text{Na}^+/\text{H}^+$  exchanger regulatory factor 1 (NHEF1). This interaction stimulates NHE1 activity, leading to an increased 3D colony growth, invadopodial activity, and ECM digestion, then driving cell invasion<sup>212</sup>. NHE1 also promotes Merlin-induced invasiveness in PDAC cells<sup>213</sup>. These results suggest that NHE1 inhibition may potentially slow down PDAC progression.

Besides NHE1, other isoforms have been documented to be involved in the  $\text{pH}_i$  regulation of PDAC cells. In particular, NHE7 is upregulated in the most aggressive pancreatic cancer subtypes, regulating cell proliferation and cytosolic pH. This exchanger localizes in the trans-Golgi network for the latter purpose, regulating its luminal acidification to maintain an alkaline  $\text{pH}_i$  in PDAC cells. NHE7 abrogation leads to the alkalization of the trans-Golgi network and subsequent accumulation of protons in the cytosol that dysregulates actin fibers. Moreover, NHE7 KO inhibits tumor growth *in vivo*<sup>214</sup>.

### Monocarboxylate transporters (MCTs)

MTCs belong to the solute carrier 16 (SLC16) family of transmembrane proteins responsible for transferring monocarboxylated molecules, such as lactate and protons, across the plasma membrane. Among the 14 isoforms, MCT1 plays a pivotal role in PDAC under glucose restriction. It mediates lactate uptake that promotes colony formation and protects high MCT1 expressing-

PDAC cell lines from gemcitabine-induced cell death by promoting stemness properties<sup>215</sup>. MCT4 is also strongly involved in the  $\text{pH}_i$  regulation of PDAC cells. It is overexpressed in highly glycolytic PDAC cells, and its suppression compromises glycolysis but leads to the compensatory promotion of OXPHOS and autophagy. Its abrogation results in increased ROS production and subsequent cell death *in vitro*, significantly affecting tumor growth in xenograft models<sup>216</sup>. Next studies confirmed its localization to the plasma membrane with MCT1, where they mediate lactate influx. PDAC cell migration depends on MCT4 activity but not MCT1, while invasion and spheroid outgrowth are negatively affected by both MCT1 and MCT4 inhibition and knockdown<sup>217</sup>. Wu and colleagues confirmed these results by demonstrating that MCT1 is overexpressed in PDAC patients samples compared to healthy tissue and that the miR-124-mediated MCT1 inhibition leads to impaired glycolytic activity, lactate accumulation, and cytosolic acidification in PANC-1 cells, resulting in the inhibition of the cells' proliferation, viability, and migration *in vitro* and reduced tumor growth *in vivo*<sup>218</sup>. MCT1 and MCT4 are regulated by CD147 transmembrane glycoproteins. Silencing of CD147 results in decreased MCT1 and MCT4 expression in PDAC cells, leading to decreased lactate export and cytosolic acidification and weakening PDAC aggressiveness *in vitro* and *in vivo*<sup>219</sup>.

It is important to note that MCT outward activity is thermodynamically repressed by extracellular acidosis, impairing the lactate venting from the cytoplasm and affecting the metabolism and proliferation of cancer cells. For these reasons, cancer cells develop other venting strategies to operate in highly acidic microenvironments. Lactate can be exported via the connexin-assembled gap junctions<sup>220</sup>.

### *Na<sup>+</sup>/HCO<sub>3</sub><sup>-</sup> cotransporters (NBCs)*

NBCs play a key role in  $\text{pH}_i$  homeostasis through bicarbonate ( $\text{HCO}_3^-$ ) influx into cells and compensate for cytosolic protons. In the context of PDAC, more data is needed on the role of NBCs in its progression<sup>221</sup>. The electrogenic sodium bicarbonate cotransporter 1 isoform B (NBCe1-B) is the most abundant bicarbonate transporter in pancreatic ductal cells, where it mobilizes the bicarbonate inside the cells for later secretion in the duct lumen. Indeed, its silencing promotes cytosolic acidification and extracellular alkalinization both *in vitro* and *in vivo*<sup>222</sup>. In addition,

genetic and pharmacological targeting inhibits tumor growth and promotes mice survival by potentiating the immune response<sup>222</sup>. This protein is also the target of microRNA-223, which inhibits NBCe1 to promote the migration, invasion, angiogenesis, and tumorigenesis of PDAC cells<sup>223</sup>.

In addition, the electroneutral  $\text{Na}^+/\text{HCO}_3^-$  cotransporter 3 (NBC3) is overexpressed in PDAC tumors, and it is required for Ras-induced macropinocytosis in Ras mutant PDAC cells, a process that supports tumor growth, as silencing of NBC3 inhibits tumor growth *in vivo*<sup>224</sup>.

The sodium-bicarbonate cotransporter NBCn1 is overexpressed in PDAC cells compared to immortalized human pancreatic ductal epithelial (HPDE) cells and further increased by TGF- $\beta$ 1, and its knockdown inhibits Merlin-induced invasiveness in PDAC cells<sup>213</sup>.

### Carbonic Anhydrases (CAs)

$\text{CO}_2$  is a major acid source in cancer cells with enhanced OXPHOS phenotype or impaired glycolysis. The OXPHOS and the pentose phosphate pathway are the major producers of  $\text{CO}_2$ , which diffuses across cancer cell membranes, and blood perfusion drives  $\text{CO}_2$  out of cells. However, tumors are poorly perfused, and their distance from the closest capillary might increase significantly. This creates a barrier to  $\text{CO}_2$  diffusion, accumulating and acidifying the intracellular milieu. To improve  $\text{CO}_2$  clearance, cancer cells exploit specific enzymes that increase  $\text{CO}_2$  diffusivity by allowing a parallel transport of bicarbonate ions and protons. This reaction is catalyzed by the exofacial isoforms of carbonic anhydrases, such as CAIX and CAXII<sup>225</sup>. While bicarbonate ions are imported inside the cells by NBCs, protons are released in the TME. Then, this reaction reduces cytosolic acidification in cancer cells but leads to extracellular acidification<sup>226</sup>. CAIX activity is closely linked to the acquisition of more aggressive/invasive phenotypes in different types of tumors<sup>227</sup> and it is also upregulated by hypoxia<sup>228</sup>.

In PDAC, it was reported that CAIX is upregulated in PDAC tissues compared to normal tissues and also in PDAC cell lines. The abrogation of CAIX expression negatively affects the invasion and metastatic potential of PDAC cells, suggesting the important contribution of CAIX in PDAC progression<sup>229</sup>. Furthermore, hypoxia promotes the KRAS-dependent upregulation of CAIX and glycolytic phenotype, which correlates with PDAC cells' survival and poor patient prognosis.



CAIX abrogation results in intracellular acidification and increased sensitivity to gemcitabine in hypoxic conditions. CAIX's pro-tumor role was also confirmed *in vivo*, as CAIX knockout xenografts mice models show reduced tumor growth and decreased gemcitabine resistance, promoting mice survival<sup>230</sup>. These results support the notion that inhibiting CAIX might represent a successful strategy to alleviate PDAC patients from its progression.

### V-type H<sup>+</sup> ATPases

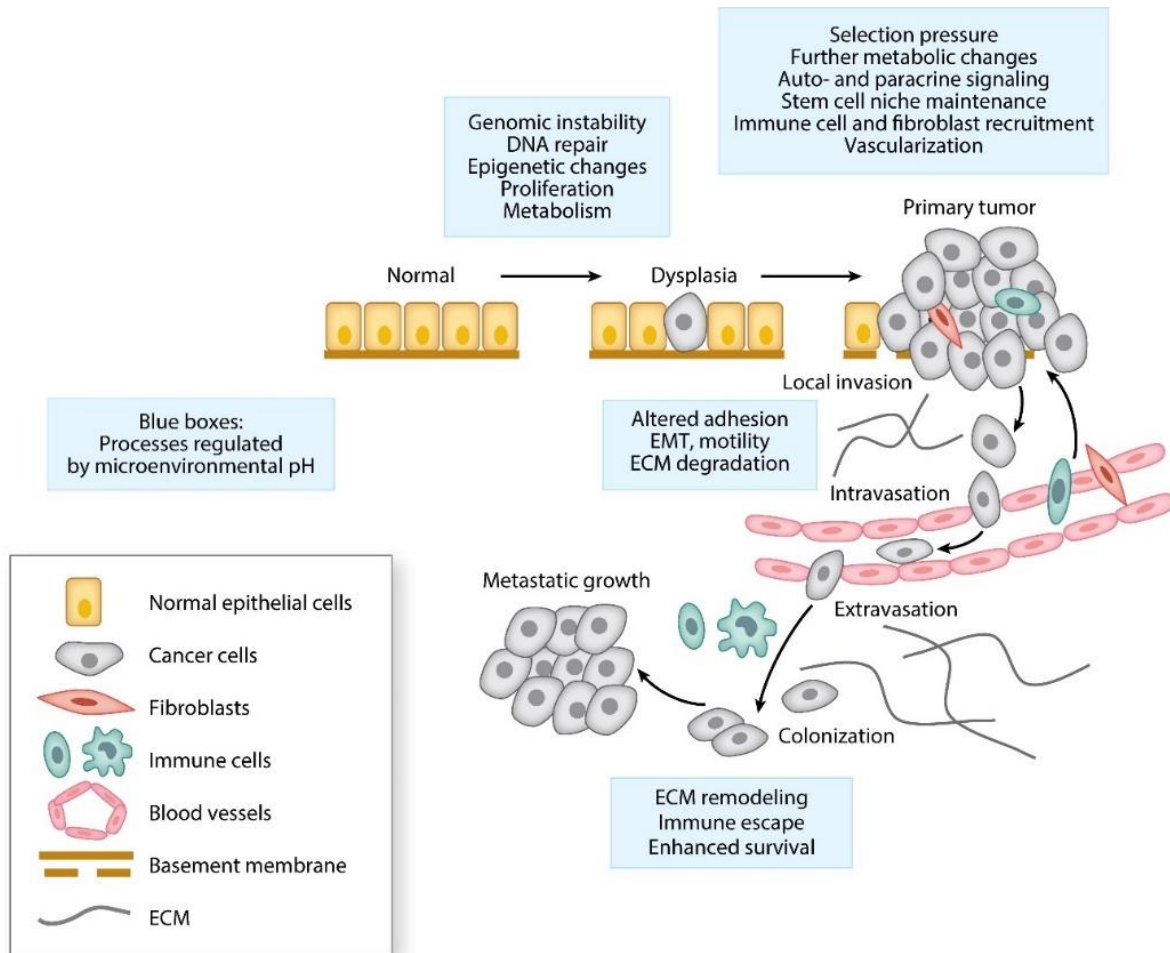
H<sup>+</sup> ATPases are electrogenic pumps that mediate the movement of protons against the electrochemical gradient by exploiting the energy of ATP hydrolysis. These transmembrane proteins are localized in different endomembrane organelles, such as lysosomes, endosomes, mitochondria, secretory granules, coated vesicles, and Golgi apparatus, but also at the cell plasma membrane level of specialized cell types and cancer cells, where they acidify the lumen of intracellular organelles and the extracellular space. Proton ATPases activity regulates different physiological processes, such as cell proliferation, cell fate and differentiation, lysosomal degradation, receptor endocytosis, insulin exocytosis, and vesicular trafficking via the activation of Notch, mTOR, and Wnt signaling cascades<sup>231–234</sup>. In tumorigenesis, H<sup>+</sup>-ATPases are required to maintain an alkaline cytosolic pH and for protons expulsion in the TME, features that promote cancer progression<sup>235</sup>.

H<sup>+</sup>-ATPases play an important role in PDAC, as they regulate lysosomal activity and nutrient scavenging, which PDAC relies heavily on for its aggressiveness<sup>236</sup>. Moreover, H<sup>+</sup>-ATPases tissue expression is correlated with the PDAC stage, being localized in the correspondence of invasive fronts of PDAC cell lines' plasma membrane with components of cell invasion apparatus, such as cortactin, where the pump's ability to extrude protons and acidify peri-cellular domains contributes to cell invasion by mediating MMP-9 release. The blockade of H<sup>+</sup>-ATPases negatively affects PANC-1 cells' MMP-9 activity and migratory and invasive abilities<sup>237</sup>. These results demonstrate that PDAC specimens overexpress H<sup>+</sup>-ATPases, which modulate specific MMPs release and cell invasion. In addition, Hayashi and colleagues previously demonstrated that bafilomycin A1 potently inhibits H<sup>+</sup>-ATPases in PDAC cells, inhibiting the transport of protons from the cytosol to the endosomes and secretory vesicles, thus impairing the protons transport across

the plasma membrane and leading to the acidification of the intracellular space, increasing the thermosensitivity of PDAC cells. These effects were potentiated with the combination of amiloride therapy, a known inhibitor of NHE1<sup>238</sup>.

### 3.6.2 Acidic pH<sub>e</sub> as a driver of cancer

Tumor acidosis plays an important role in each step of carcinogenesis, shaping its role based on the different stages (Figure 17).



Boedtker E, Pedersen SF. 2020. *Annu. Rev. Physiol.* 82:103–26

Figure 17. Schematic of main processes involved in tumor onset and progression, with indication (blue boxes) of those processes regulated by the acidic tumor microenvironment. Image adapted from [191].

Beside the role of genetic mutation in promoting acidic microenvironment, on the other way around, the insurgence and accumulation of random genetic alterations may depend on the

microenvironment pH, as it influences the stability of double-stranded oligonucleotides<sup>239</sup>. Normal cells may face acidosis following renal failure, diabetes, inflammation, metabolic changes, and ischemia. Acidic pH<sub>e</sub> promotes the transition from normal cells to cancer by directly causing DNA strand breakages and gaps, and its clastogenic role is cell-type-dependent<sup>240</sup>. The mechanisms by which acidosis induces genetic instability in normal cells may involve a decrease in the efficiency of DNA repair, leading to the stabilization of DNA double-stranded breaks and mutagenesis. The ability of acidosis to impair DNA repair mechanisms was shown almost 30 years ago in A459 cells subjected to lethal radiation damage (PLD). Acidic pH<sub>e</sub> inhibits PLD repair, blocking the re-joining of double-strand breaks, and the authors hypothesized that acidosis inhibited DNA repair by affecting pH-dependent DNA repair enzymes<sup>241</sup>. Massonneau and colleagues' work has further demonstrated that even slightly decreased optimal fibroblast pH<sub>e</sub> impairs the capacity of cells to repair the bleomycin-induced DNA double-strand breaks, promoting genome instability and potential carcinogenesis<sup>240</sup>. In addition, acidic pH<sub>e</sub> exerts a carcinogenic role in DMBA (a tumor initiator)-initiated papilloma skin mouse model, and it also upregulates p53 and other genes encoding DNA damage signaling proteins in breast cancer cells. Moreover, acidic pH<sub>e</sub>-induced mutagenesis involves Topoisomerase 2-mediated DNA single-strand breaks<sup>242</sup>. Reactive oxygen species (ROS) produced by acidosis are also considered potential carcinogens, as they cause double-strand DNA breaks and genomic instability. Zhang and colleagues demonstrated that acid exposure leads to double-strand breaks in Barrett's epithelial cells via ROS produced following acidosis-induced intracellular acidification<sup>243</sup>.

Besides inducing genomic instability, tumor low pH<sub>e</sub> also influences cell epigenetics, transcriptomic alterations, and changes in chromatin accessibility, for example, by inducing chromatin deacetylation in acidic conditions via upregulation of deacetylase 2 in the interface between acidic TME and stroma<sup>192</sup>. Histones deacetylation is required for the maintenance of pH<sub>i</sub>, in order to avoid intracellular acidification. Histones are also acetylated in presence of more alkaline pH<sub>i</sub> values, which are reached, for example, when cells are proliferating<sup>244</sup>. These results suggest that acidosis promotes genetic aberrations, transcriptomic changes, and potential cell transformation in preneoplastic stages. However, mutations will also be inhibited in their proliferation by acidic pH<sub>e</sub>, particularly those cells that did not yet acquire oncogenic mutations.

As noted previously, acidosis inhibits cell cycle progression and hence proliferation. Cells require an optimum mild alkaline pH<sub>i</sub> (7.0-7.2) for progress in the cell cycle through all the

checkpoints<sup>245</sup>. Transient increase in  $\text{pH}_i$  at the end of the S cell cycle phase promotes cancer cells' progress through the G2/M phases and suppresses mitotic arrest triggered by DNA damage checkpoint. Therefore, the alkaline  $\text{pH}_i$  of cancer cells allows them to bypass cycle checkpoints, promoting proliferation and genetic instability<sup>245</sup>. Acidification of the intracellular space is also a feature of mitochondria and death receptor-mediated apoptotic cells, which are required for caspase activation<sup>246</sup>. If acidic  $\text{pH}_e$  inhibits proliferation by lowering  $\text{pH}_i$ , it also promotes cell cycle progression by directly activating plasma membrane proteins, such as acid-sensing ion channels, which promotes proliferation in a  $\text{Ca}_{2+}$ -dependent way in pancreatic cancer (see also sub-chapter 4)<sup>177,247,248</sup>, or  $\text{pH}_e$ -sensitive receptors<sup>249</sup>.

To promote tumor growth, acidosis may also increase stemness properties in cancer cells, as reported in glioma cells. Hjelmeland and colleagues have demonstrated that 6 days-long exposure to  $\text{pH}_e$  6.5 maintains glioma stem cell-like phenotypes and prevents their differentiation by increasing the expression of several stem cell markers, including Olig2, Oct4, and Nanog, and angiogenic factors, including VEGF, probably via HIF2 $\alpha$ , leading to enhanced neurosphere formation capacity and promote tumor growth *in vivo*<sup>250</sup>. The group of Acker T. obtained similar results, showing that acidosis and hypoxia co-operate to induce HIF expression in a chaperone protein HSP90-dependent manner, resulting in enhanced stem cell properties of glioblastoma cells<sup>195</sup>. More recent work further elucidates the role of acidic  $\text{pH}_e$  in cell stemness, showing that acidosis promotes neurosphere formation and growth, mitochondrial respiration, and self-renewal in stem cell-like glioma cells via CYP24A1-mediated reduction of vitamin D, promoting and maintaining the stem properties of glioma cells<sup>251</sup>.

As described previously, during primary tumor growth, delivering oxygen and nutrients and removing waste products usually remain insufficient to match the increased metabolic demand of cancer cells. To counteract these limitations, cancer cells exploit tumor acidosis to promote angiogenesis. Lactate extruded by cancer cells is taken up by endothelial cells via MCT1, which use this acid product for triggering the NF- $\kappa$ B-dependent IL-8 production and subsequent activation of the IL-8 signaling pathway, that enhances endothelial cells migration and tube formation, promoting angiogenesis and tumor growth<sup>252</sup>. In the brain, lactate-induced acidosis can mediate the hypoxia-independent HIF-1 $\alpha$  activity, resulting in the increased expression and release of VEGF, VEGF receptor activation, and triggering of the angiogenic response<sup>253</sup>. However, other studies have reported that highly acidic  $\text{pH}_e$  promotes apoptosis and reduces proliferation, migration, cell-matrix

adhesion, and capillary tube formation of endothelial cells by inhibiting the secretion of VEGF and the activation of its downstream signaling cascade<sup>254</sup> or via downregulation of VEGFR-2 expression<sup>255</sup>.

Once the primary tumor is formed, cancer cells can disseminate to colonize distant organs and form metastasis. Tumor acidosis plays an important role acidosis in the different steps of the metastatic process. In particular, several studies have reported that tumor acidosis promotes EMT in different cancer cell types, enhancing the migratory and invasive potential in cancer cells, following both short- and long-acidic treatment and via different mechanisms. Extracellular acidosis can induce changes in EMT markers, as demonstrated in human melanoma cells subjected to 24h-long acidic treatment, showing increased expression levels of N-cadherin and Vimentin<sup>256</sup>, also confirmed by other works<sup>257,258</sup>, however, the EMT markers expression is cell-line specific. Acidosis can also promote EMT via the activation of HIF-2 $\alpha$ , promoting stem cells properties in glioma cells<sup>250</sup>. PDAC cancer cell line SUIT-2 activate EMT and autophagy under medium and prolonged acidic pressure (4-5 months to 10-12 months) as an early response to resist apoptosis<sup>259</sup>.

More specifically, acidosis may also promote EMT by driving the formation of lipid droplets for fuelling cancer cell invasiveness<sup>260</sup>. Other indirect mechanisms include pH<sub>e</sub>-induced TGF- $\beta$  secretion<sup>256</sup>, a known activator of EMT, or via factors in the glucose metabolic pathway, such as the downregulation of fumarate hydratase<sup>257</sup>. In addition, tumor acidosis may exploit pH<sub>e</sub>-sensitive ion channels for the activation of downstream signaling pathways involved in EMT, such as Ca<sup>2+</sup> signaling (as described in the sub-chapter 4).

Cell-cell adhesion and cell-matrix adhesion loss are required for tumor dissemination during the early stages of the metastatic cascade, and intercellular communication is significantly affected by low pH<sub>e</sub><sup>257,261,262</sup>. For example, acidosis regulates catenins, membrane-bound proteins required for cell-cell interaction at adherents junctions and which disruption is associated with EMT<sup>263</sup>. However, acid-adapted cells may show a different behaviour, increasing cell adherence in a cell-line-specific way<sup>257</sup>. The hypothesis is that tumor acidosis decreases the strength of cell-cell adherence by affecting the structure or the dynamics of the cytoskeleton<sup>264</sup>.

Other important steps in metastatic dissemination are cell migration and invasion. Several papers have shown that single-cell or population-directed or randomly oriented migration of tumor cells is modulated by acidosis, increasing it<sup>256,257,265,266</sup>, also in PDAC<sup>209,259</sup>. These effects are observed both following short acidic exposition or in acid-adapted cells and re-acclimated to pH<sub>e</sub>

7.4<sup>266</sup>, indicating the maintenance of the aggressive phenotype induced by acidosis. To invade the surrounding tissue and metastasize, cancer cells must digest the ECM. Several works have shown the  $\text{pH}_e$ -dependency of this process, as matrix metalloproteinases (MMPs) and cathepsins, are activated by acidic  $\text{pH}_e$  once secreted into the ECM, where they disrupt cell-substrate adhesions<sup>262</sup>. In particular, acid extruders play an important role in cell invasion, and a major one is played by NHE1 activity at invadopodia sites, where it is fundamental for generating the pericellular acidity that promotes the proteolytic activity of different proteinases<sup>206</sup>. Another key player is expected to be the CAIX, which acidifies the extracellular space to promote MMP14 activity<sup>267</sup> and metastasis *in vivo*<sup>268</sup> as previously mentioned in Section 3.6.1.

Finally, tumor acidosis promotes tumor progression by negatively affecting immune escape and chemoresistance<sup>269</sup>. The acidic tumor microenvironment inhibits T and NK cells' function and induces apoptosis<sup>270</sup>. At the same time, tumor acidosis activates immunosuppressive components such as regulatory T cells and myeloid cells<sup>156,271</sup>. Besides local immunosuppression, low  $\text{pH}_e$  can act systemically by impairing the distribution and bioactivity of antibodies, such as immune checkpoint inhibitors<sup>272</sup>. Acidic TME of solid tumors also represents a barrier (“ion trapping”) to drug delivery and efficacy for many chemotherapy drugs, inducing changes in drug structure and charge. An example is provided by doxorubicin, which is highly charged in acidic conditions, impairing its uptake by cancer cells<sup>273</sup>.

### **3.6.3 Acid-driven adaptation and differences with acid selection**

Considering the important impact of protonation on virtually all proteins and the influence of  $\text{pH}_e$  on  $\text{pH}_i$ , even a small change in  $\text{pH}_e$  is enough to significantly affect cell behaviour. The  $\text{pH}_e$  sensitivity of cancer cells and the range of their optimum  $\text{pH}_e$  can affect their survival in the hostile acidic microenvironment, for example in terms of proliferation (Figure 18A): indeed, cells with a broader pH sensitivity may be more adaptable to fluctuating pH as compared to cells presenting narrower pH sensitivity. Cancer cells are subjected to the selective pressure induced by the low  $\text{pH}_e$ , and in this situation, they may respond by developing strategies to gain competitive advantages over normal cells or other cancer subpopulations and survive<sup>274</sup>. For example, cancer cells may start an adaptation process by adjusting their optimum pH towards more acidic values and enhancing their metabolic rate, driving a further TME acidification that provides adapted cancer cells with a survival

advantage compared to normal cells or cancer cells with a more alkaline optimum pH, making the extracellular environment even more hostile for them (Figure 18B). Therefore, tumor acidosis selects the most aggressive cancer cell subtypes within the tumor.

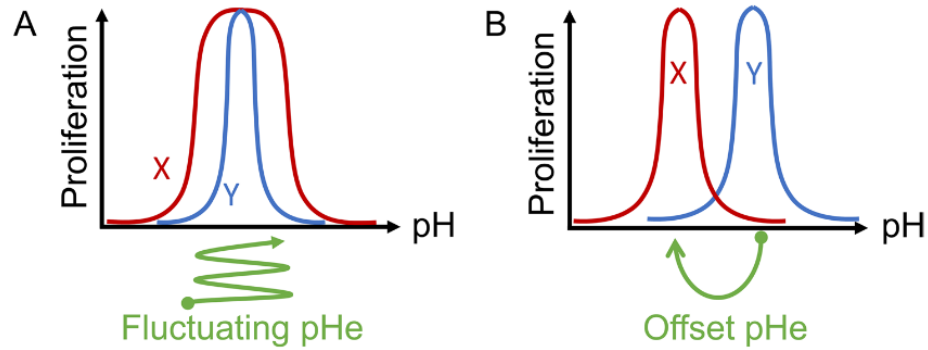


Figure 18. Schematic showing two examples of pH sensitivity curves for proliferation. A) Cell X has a larger pH optimum compared to cell Y; this indicates that its survival prospects are higher during fluctuations in pH. B) Cell X has an acid-shifted pH optimum compared to cell Y. If cell X also has a higher metabolic rate, it is likely to drive tissue pH to a lower level. This would provide the cell X with a survival advantage over cell Y. Image adapted from [274].

It is important to clarify that it is not acidosis *per se* that promotes tumor progression. Instead, it is the adaptation of cancer cells to acidic conditions, coupled or not with oncogenic mutations, to increase the capacity of cancer cells to survive in the hostile acidic microenvironment compared to non-adapted or normal cells. The adaptation will thus allow cancer cells to recover their proliferative potential via changes in gene and/or protein expression and to further increase it when  $pH_e$  conditions become less restrictive, as at the tumor boundaries<sup>192</sup>. Thus, only the “evolutionary fit” cancer cells will survive and be selected throughout the adaptation process, and their expansion will generate an acid-resistant population. The advantages acquired by tumor cells during acid adaptation were demonstrated by several works on different cancer cell types, with a particular focus on breast cancer and melanoma<sup>275–280</sup>, where they acquired new phenotypic characteristics that increased their survival and malignancy under acidic  $pH_e$  conditions. This aspect is more deeply discussed in our article “Acidic tumor microenvironment promotes epithelial-to-mesenchymal transition to select more aggressive PDAC cell phenotypes”, submitted to *cancers* journal (See Chapter 3).

For the purposes of the work in this Ph.D. thesis, it is important to note the differences between cancer cells acidic adaptation or selection. These responses depend substantially on the

experimental strategy chosen to achieve the target acidic  $\text{pH}_e$ <sup>274</sup>. Cancer cells will undergo an adaptation when they are exposed to graded changes in  $\text{pH}_e$  over an extended period, giving cancer cells time to respond and to adapt towards a more fitting phenotype. On the contrary, an abrupt decrease in  $\text{pH}_e$  maintained over time will promote a selection process where only a portion of the fitter cancer cell population survives. This last scenario is less experimentally characterized than adaptation processes, although theoretical models have described them<sup>281–283</sup>. Both acid-driven adaptation and selection lead to a similar output, although via different ways, providing cancer cells with survival benefits over host cells.

### **3.6.4 Role of acidic $\text{pH}_e$ in PDAC progression: from physiology to pathology**

As detailed in Section 1.2., exocrine pancreatic duct epithelium performs transepithelial acid-base transport; this suggests that apical and basal surfaces of ductal cells generate and are embedded in significantly different extracellular pH values, a characteristic further accentuated by the periodic nature of the apical alkaline secretion, leading to non-uniform temporal and spatial  $\text{pH}_e$  distributions.

More in detail, pancreatic ductal cells secrete an alkaline juice from the apical membrane to neutralize the acid chyme from the stomach. This base secretion is coupled to the extrusion of an equal amount of acid across the basolateral membrane, thereby acidifying the pancreatic interstitium, whose extracellular pH ( $\text{pH}_e$ ) will vary cyclically during the alternating phases of digestive stimulation of secretion, regulated by hormones and neurotransmitters and in which the extracellular pH reaches acidic values, and resting phases<sup>11</sup>. The pancreatic interstitium  $\text{pH}_e$  dynamics are further regulated by the blood flow and diffusional fluxes and by the acid buffering capacity of cells. Thus, pancreatic ductal cells face dynamic temporal and spatial changes of  $\text{pH}_e$ . Therefore, they exist in a unique and dynamic  $\text{pH}_e$  environment in which their metabolism and proteins- ion channels, transporters, and receptors- are tuned to this characteristic  $\text{pH}_e$  landscape. However, stromal cells and all the other types of cells residing in the interstitium will also be subjected to the changes in basolateral  $\text{pH}_e$ .

This dynamic situation of intermittent acidity in healthy pancreatic cells trains them to cope with acidity, representing a great advantage during PDAC onset. During chronic pancreatitis, considered as a risk factor of PDAC<sup>284</sup>, there is an increase in basal acidity, resulting in a decreased



interstitial pH, due to the inflammatory condition, and reduced blood perfusion until severe chronic pancreatitis is developed<sup>285</sup>. Chronic pancreatitis can result in intraepithelial neoplasias (PanIN-1, 2, 3), which represent the early stages of PDAC, in which pre-neoplastic lesions and inflammation may characterize pancreatic epithelium. During this phase, there is a further decrease in interstitium pH that becomes more independent from hormones-induced fluctuations. Once later stages of PDAC are reached, there is the development of a strongly desmoplastic, hypoxic, and acidic stroma<sup>286</sup>.

It is easy to hypothesize that the acidity intermittence of healthy pancreatic interstitium favours the dormancy of pre-malignant lesions due to the diverse and sometimes opposite and restrictive effects of acidosis on cancer cell functions, but, at the same time, it “preconditions” pancreatic ductal cells and stromal cells to increase their survival potential and aggressiveness when PDAC fully develops from early stages characterized by pre-neoplastic lesions and PDAC triggers mutations (Figure 19). This will provide cancer cells with a growth advantage and enhance their aggressiveness. This acid-preconditioning process results from the upregulation of many proteins and signaling cascades that enhance cell survival. Among these proteins, we can find pH<sub>e</sub>-sensitive ion channels, and in this thesis, particular attention was reserved for Ca<sup>2+</sup>-permeable ion channels.

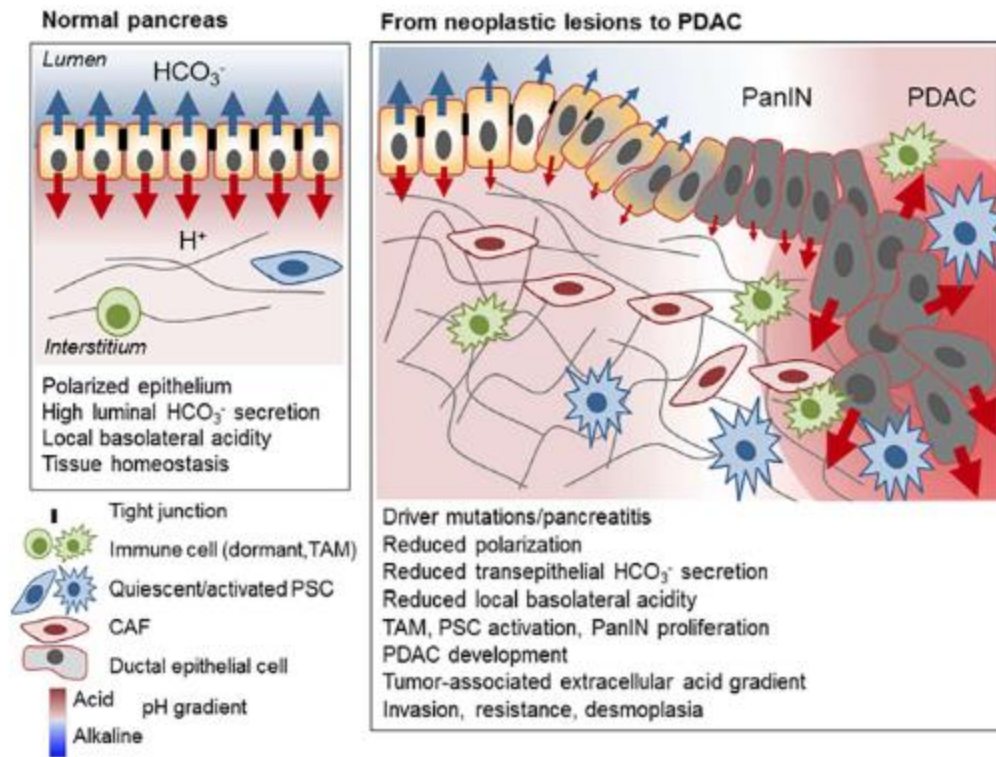


Figure 19. Schematic representing the hypothesis that acidic physiological microenvironment promote PDAC onset and progression in concomitance of driving gene mutations and pre-neoplastic lesions. Image adapted from [286].

## 4. Calcium signaling

$\text{Ca}^{2+}$  ions stand out among the other ions present in the intra- and extracellular environments for their crucial role as second messengers.  $\text{Ca}^{2+}$  ions interact with different signaling cascades via the activation and cooperation of the molecular components of the so-called “ $\text{Ca}^{2+}$  signaling toolkit” and by creating different spatio-temporal  $\text{Ca}^{2+}$  patterns to selectively regulate innumerable physiological cell processes, ranging from cell differentiation, proliferation, programmed cell death to gene transcription, among others<sup>287</sup>. Given the importance of  $\text{Ca}^{2+}$  ions in activating several signal transductions, cells require that intracellular  $\text{Ca}^{2+}$  homeostasis is highly regulated, keeping a low cytosolic free  $\text{Ca}^{2+}$  concentration (~100 nM) compared to the extracellular milieu (~1.2 mM) through the orchestrated work of several proteins that constitute the so-called  $\text{Ca}^{2+}$  signaling toolkit, including pumps ( $\text{Ca}^{2+}$  ATPases PMCA, SERCA) exchangers ( $\text{Na}^+/\text{Ca}^{2+}$  exchanger NCLX in mitochondria and NCX at the plasma membrane) or uniporters (MCU in mitochondria) and plasma membrane (PM) and endoplasmic reticulum (ER)  $\text{Ca}^{2+}$ -permeable channels.  $\text{Ca}^{2+}$  ions are also compartmented in different intracellular organelles, such as the nucleus, Golgi system, and mitochondria, where their concentration is comparable to the cytosolic one. At the same time, ER represents the major intracellular  $\text{Ca}^{2+}$  store, containing  $\text{Ca}^{2+}$  ions in a range of 100-800  $\mu\text{M}$ , followed by lysosomes having an internal  $\text{Ca}^{2+}$  concentration of ~500  $\mu\text{M}$  (Figure 20).

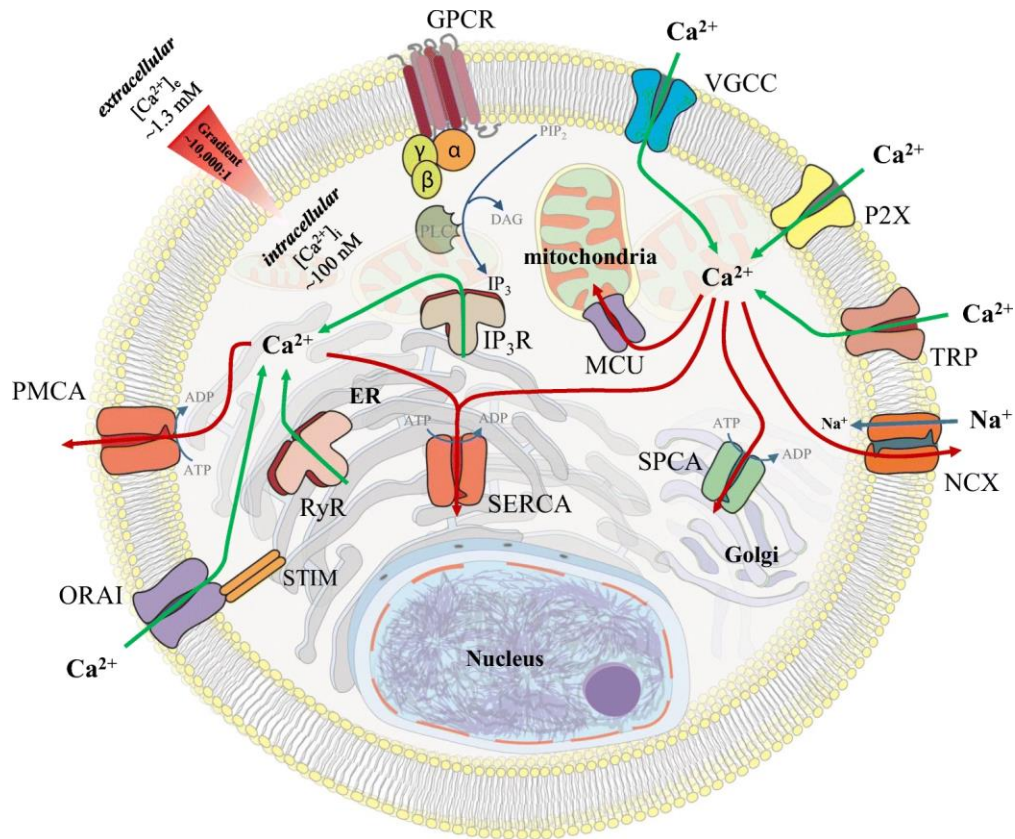


Figure 20. Intracellular  $\text{Ca}^{2+}$  signaling. Image adapted from [288].

To accomplish all the different cellular outcomes mediated by  $\text{Ca}^{2+}$  signals, they differ from each other in terms of amplitude, duration, location, and frequency<sup>289</sup>; high-amplitude calcium signals play a key role in cell death, transiently increased and highly localized intracellular  $\text{Ca}^{2+}$  levels are associated with processes as migration, while sustained high  $\text{Ca}^{2+}$  concentration in the ER and mitochondria are associated to apoptosis, the formation of  $\text{Ca}^{2+}$  microdomains in the proximity of plasma membrane calcium-permeable channels opening is linked to activation of gene transcription, as well as duration and frequency of  $\text{Ca}^{2+}$  oscillations, which regulate the activation of transcription factors.

#### 4.1 $\text{Ca}^{2+}$ signaling toolkit

The molecular components involved in  $\text{Ca}^{2+}$  homeostasis constitute the so-called “ $\text{Ca}^{2+}$  signaling toolkit”, composed of a great variety of proteins that act as  $\text{Ca}^{2+}$ -permeable channels, pumps, and exchangers and which, in an organized and coordinated way, regulate the  $\text{Ca}^{2+}$

concentrations in the compartments of the different cell and between the extra- and intracellular environment. Moreover, these  $\text{Ca}^{2+}$  sensors decipher the different  $\text{Ca}^{2+}$  patterns to activate the specific and downstream  $\text{Ca}^{2+}$ -dependent physiological activity.

Located at the endoplasmic reticulum's membrane, inositol trisphosphate receptors (IP3Rs) are large-conductance ion channels activated by IP3, inducing  $\text{Ca}^{2+}$  release from the ER store in the cytoplasm and involved in the so-called Store-Operated  $\text{Ca}^{2+}$  Entry (SOCE), a process of  $\text{Ca}^{2+}$  influx inside the cells that restore the homeostasis of intracellular  $\text{Ca}^{2+}$ <sup>290</sup> (See section 4.2.1). Therefore, SOCE is a  $\text{Ca}^{2+}$  influx process that is triggered internally. Refilling the ER  $\text{Ca}^{2+}$  store occurs through the action of SERCA channels in the ER membrane. SERCAs are  $\text{Ca}^{2+}$  ATPases that exploit ATP hydrolysis energy to transfer  $\text{Ca}^{2+}$  ions from the cytosol to the ER lumen, therefore, against their electrochemical gradient.

Others large intracellular  $\text{Ca}^{2+}$  reservoirs are the Golgi apparatus, nucleus, and mitochondria. Cytosolic  $\text{Ca}^{2+}$  levels are controlled by the activity of the  $\text{Ca}^{2+}$  ATPase Golgi-resident SPCA, sequestering  $\text{Ca}^{2+}$  free ions from the cytosol and inside the Golgi store<sup>291</sup> by the mitochondrial  $\text{Ca}^{2+}$  uniporter MCU, which mediates the  $\text{Ca}^{2+}$  uptake inside mitochondria, and  $\text{Na}^+/\text{Ca}^{2+}$  exchanger NCLX, which also regulates  $\text{Ca}^{2+}$ . ER and mitochondria further interact functionally and structurally to regulate  $\text{Ca}^{2+}$  exchange between the two organelles via the Mitochondrial Associated Membranes (MAMs).

At the plasma membrane level,  $\text{Ca}^{2+}$  ions extrusion is accomplished by the  $\text{Na}^+/\text{Ca}^{2+}$  antiporter NCX, which exploits the electrochemical gradient of  $\text{Na}^+$  ions to extrude  $\text{Ca}^{2+}$  ions from the cytosol to the extracellular space, and by the ATPase PMCA, which transport  $\text{Ca}^{2+}$  ions across the plasma membrane using the energy from ATP hydrolysis<sup>292</sup>. Instead,  $\text{Ca}^{2+}$  influx is resolved by the activity of transmembrane ion channels that are activated by external stimuli and allow the diffusional transport of  $\text{Ca}^{2+}$  ions inside the cell, according to their electrochemical gradient. Among all  $\text{Ca}^{2+}$ -permeable channels, examples are the family of Transient Receptor Potential channels (TRPs), Voltage-Gated  $\text{Ca}^{2+}$  Channels (VGCCs), and PIEZO channels.

#### **4.2 $\text{Ca}^{2+}$ -permeable channels in cancer: focus on PDAC**

$\text{Ca}^{2+}$ -permeable ions are located within the plasma membrane of all excitable cells and non-excitable, and in many intracellular organelles. They possess an aqueous pore through which  $\text{Ca}^{2+}$

ions are transported inside or outside the different compartments or across the plasma membrane. Considering the multifaced role of  $\text{Ca}^{2+}$  ions, several works have linked deregulations of  $\text{Ca}^{2+}$ -permeable ions with pathologies, including cancer<sup>293,294</sup>, making ion channels major players in cancer development (“Oncochannelopathies”)<sup>295</sup>. Loss of  $\text{Ca}^{2+}$  homeostasis contributes to its hallmarks: enhanced and uncontrolled proliferation, migration, invasion, immune and apoptosis escape, and neovascularization<sup>295</sup>. The remodeling of the  $\text{Ca}^{2+}$  network is a consequence of alterations at the genetic and/or protein levels, leading to dysregulations in the functionality and/or expression of the protein system in charge of regulating the flow of  $\text{Ca}^{2+}$  ions through the different compartments and cellular environments. In cancer, the aberrant  $\text{Ca}^{2+}$  signals-mediated events promote its progression.

Research indicates that PDAC growth and metastasis involve specific  $\text{Ca}^{2+}$ -permeable ion channels, whose alterations and functions in PDAC are listed in Table 1.

Table 1.  $\text{Ca}^{2+}$ -permeable ion channels profile expression and function in PDAC progression

<b>Channel</b>	<b>Profile expression</b>	<b>Function</b>	<b>Reference</b>
<i>Transient Receptor Potential channels (TRPs)</i>			
<b>TRPM2</b>	Upregulation	Proliferation, migration, invasion	296,297
<b>TRPM7</b>	Upregulation	Proliferation, migration, invasion, cell cycle progression, metastasis	298–301
<b>TRPM8</b>	Upregulation	Proliferation, migration, invasion, cell cycle progression, apoptosis	299,302–308
<b>TRPV1</b>	Upregulation	Apoptosis, proliferation	309,310
<b>TRPV4</b>	Upregulation	Fibrosis	311
<b>TRPV6</b>	Upregulation	Proliferation, migration, invasion, apoptosis, cell	307,312–314

		cycle regulation, metastasis	
<b>TRPC1</b>	Upregulation	Migration, invasion, Proliferation	308,315
<b>TRPC3</b>	Upregulation in PSCs	Migration and chemotaxis in PSCs	316
<b>TRPC6</b>	Upregulation in PSCs	Migration, cytokine secretion in PSCs	317
<b><i>Store-Operated Ca<sup>2+</sup> Entry channels (SOCs)</i></b>			
<b>ORA1/STIM1</b>	Upregulation	Cell survival, proliferation, invasion, EMT, chemoresistance Proliferation, cell cycle	312,318–321
<b>ORAI3</b>	Upregulation	progression, viability, mitotic catastrophe, apoptosis	322
<b><i>Other Channels</i></b>			
<b>PIEZO1</b>	Upregulation in PSCs	Cytoskeletal organization, invasion, pH-dependent mechanosensation	323,324
<b>CaCC (TMEM16A)</b>	Upregulation	Migration, the pathogenesis of acute pancreatitis	325–327
<b>ASIC1/ASIC3</b>	Upregulation	EMT, metastasis	328

#### 4.2.1 Ca<sup>2+</sup>-permeable channels: Focus on ORAI1 and STIM1 Ca<sup>2+</sup> sensor

ORAI proteins belong to the ORAI subfamily, which counts on three members; ORAI1, 2, and 3, which assemble to form homo- or heteromeric complexes. They were discovered quite recently, in 2006<sup>329–331</sup>, in an effort to identify the molecular components of the Store-Operated Ca<sup>2+</sup> entry (SOCE) (See Section 4.2.2). This relatively recent discovery is due to the absence of sequence

homology with any other known ion channel. In the same year, Yeromin et al. demonstrated that ORAI1 proteins form the so-called  $\text{Ca}^{2+}$  Release-Activated  $\text{Ca}^{2+}$  (CRAC) channel. They are the effector part of the SOCE<sup>332</sup>, while the group of Putney showed that the three ORAI proteins can generate different levels of SOCE, with ORAI1 inducing the larger SOCE, followed by ORAI2 and with ORAI3 providing the lowest SOCE<sup>333</sup>. The three homologs are expressed at mRNA and/or protein levels in all human tissues<sup>334</sup>.

From the structural point of view, the three ORAI homologs possess four transmembrane domains (TMs) with N- and C- termini facing the cytosol, resulting in two extracellular loops and one intracellular loop. In terms of sequence homology, the three ORAI proteins share about 60% of it, showing the largest differences in the topological domains in the N- and C-termini domains, which confer specific properties to each ORAI isoform. Among the conserved domains, the CaM binding domain in the N-terminus is responsible for the inactivation of the  $\text{Ca}^{2+}$ - channels formed by the ORAIs<sup>335</sup>, while the extended TM ORAI1 NH2-terminal (ETON) domain acts as a binding interface for the ORAI1 interaction with STIM1, further providing electrostatic gating elements to fine-tune the shape of the elongated pore<sup>336</sup>. The coil-coiled interaction domain also regulates the interaction between ORAI1-STIM1 and between ORAI proteins themselves in the C-termini of all three ORAI proteins<sup>337,338</sup>. All these domains were identified in ORAI1, the most studied ORAI protein, and are thought to be conserved in the other ORAIs due to the high level of sequence homology in these sites observed among the three homologs. The most conserved domains amongst the ORAIs are represented by the transmembrane domains, displaying 100% of sequence homology for TM1, while TM2 to TM4 show 81% sequence homology between ORAI1/ORAI2 and 87% for ORAI1/ORAI3<sup>339</sup> (Figure 21). Electrophysiological results have demonstrated that in the TM conserved domains, we found the two amino acid residues that are crucial for the high  $\text{Ca}^{2+}$ -selectivity of ORAI1; E106 in the TM1 and E190 in TM3<sup>340</sup>.



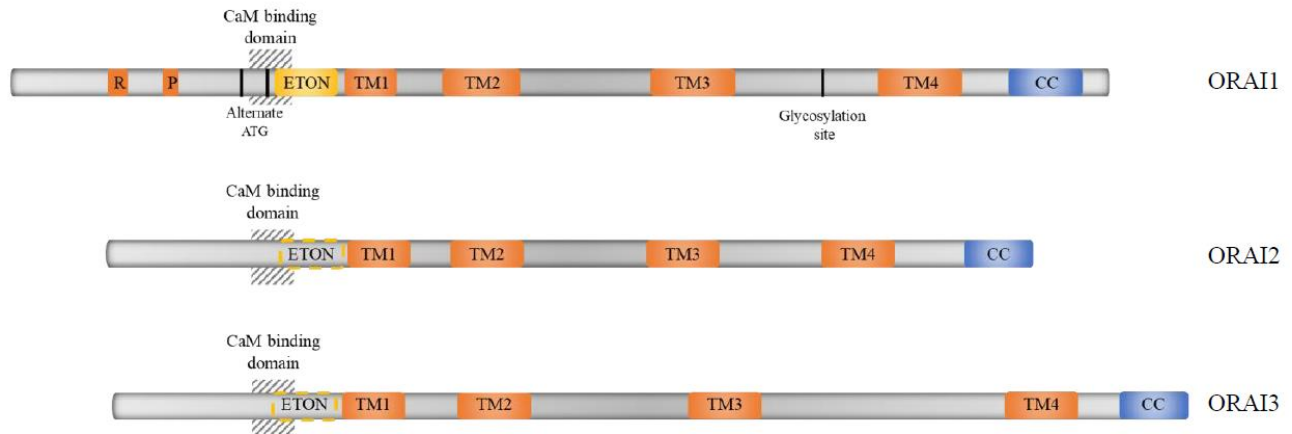


Figure 21. Schematic of the structural differences among the ORAI protein family. Image adapted from [341].

ORAI1 is the longest of the three ORAI isoforms, formed by 301 amino acids, while ORAI2 is 254 amino acids long and ORAI3 is 295 amino acids long. The increased length of ORAI1 is due to a proline/arginine-rich domain in its N-terminus that is absent from ORAI2/3, which is involved in the reactivation gating<sup>335</sup> and in STIM1-mediated SOCE<sup>342</sup>. The absence of this domain was also identified in one shorter isoform of ORAI1 named ORAI1  $\beta$ , the result of alternative translation initiation of the *ORAI1* gene. Despite the absence of the proline/arginine-rich domain, this isoform generates classic SOCE, although its current presents a stronger  $\text{Ca}^{2+}$ -dependent inhibition and a higher diffusion rate in the plasma membrane than ORAI1<sup>343,344</sup>. ORAI1 is also the only one among the ORAIs to present a site for N-glycosylation at the level of the second extracellular loop that may modulate the SOCE in a cell-type-specific manner<sup>345</sup>.

STIM proteins belong to the Stromal Interaction Molecule (STIM) family composed of two homologous proteins, STIM1 and STIM2, which are encoded by two different genes. The *STIM* gene was first cloned in 1996; however, no information about the role of STIM proteins was available until 2005, when two independent teams discovered the key role of STIMs in SOCE<sup>346,347</sup>. STIM1 and STIM2 proteins are ubiquitously expressed and mainly localized in the ER membrane. However, some evidence has indicated STIM1 at the plasma membrane level, regulating the CRAC-mediated  $\text{Ca}^{2+}$  entry<sup>348</sup> and in lysosome-related organelles and dense granules<sup>349</sup>.

At least three different isoforms were identified for STIM1 (STIM1, STIM1L and STIM1B) and STIM2 (STIM2.1, STIM2.2, the regular STIM2 isoform, and STIM 2.3). All the isoforms show

the same overall structure, displaying a short N-terminus facing the ER lumen, a single transmembrane domain, and a long C-terminus facing the cytosol (Figure 22).

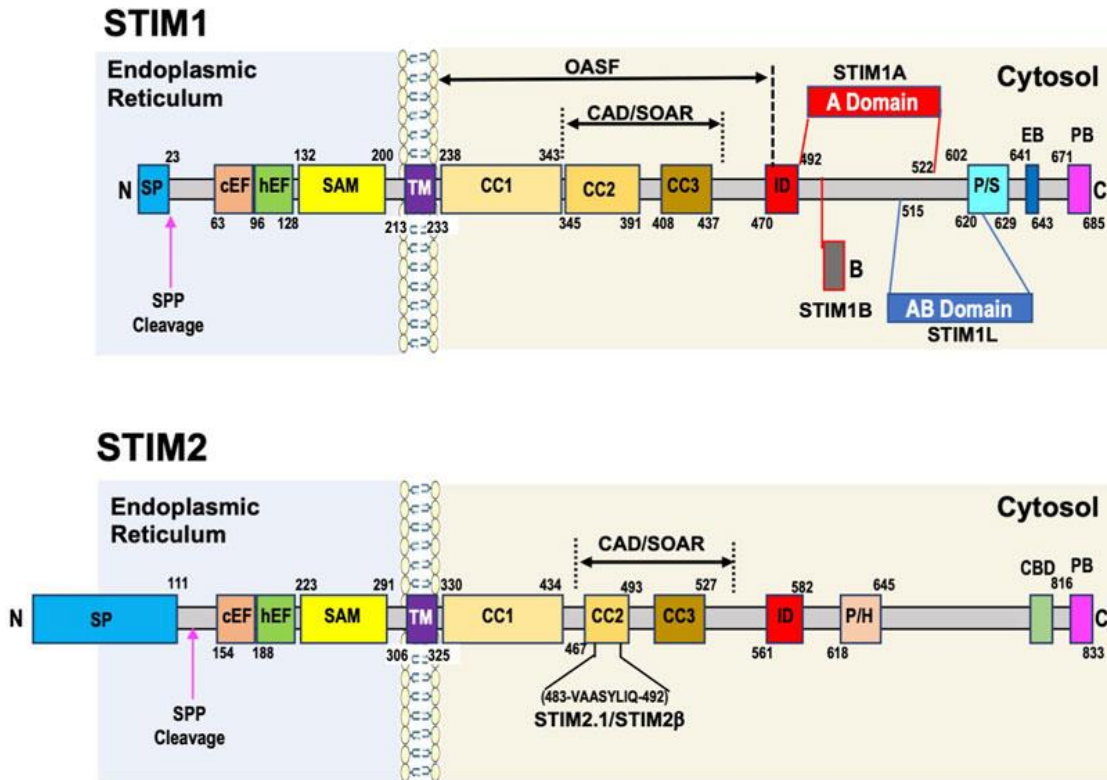


Figure 22. Schematic depicting the structural differences among STIM proteins. Image adapted from [350].

Moreover, both isoforms present an EF-hand motif associated with a sterile alpha motif (SAM) in the N-terminus region, which allows STIM proteins to detect changes in the  $\text{Ca}^{2+}$  concentration inside the ER. The EF-SAM domain is not identical in all the isoforms, providing them with different  $\text{Ca}^{2+}$ -sensitivities and selective activation depending on the extent of  $\text{Ca}^{2+}$  ER depletion. In the C-terminal region, we find three coil-coiled (CC) domains (CC1, CC2, CC3), where CC2 and CC3 form the CRAC-activating domain (CAD), also called STIM-ORAI-activating region (SOAR), which are involved in ORAI channel gating. Further domains include the STIM inactivation domain (ID), fundamental for the  $\text{Ca}^{2+}$  dependent inactivation (CDI) of the CRAC channel, microtubule end binding (EB) domain, required for STIM1 movements, and polybasic rich domain (PBD), which promotes STIMs localization to ER-plasma membrane junctions (Figure 22).

#### 4.2.2 Store-Operated $\text{Ca}^{2+}$ Entry mechanism

ORAI1s are  $\text{Ca}^{2+}$  release-activated  $\text{Ca}^{2+}$  channels (CRACs) that are major effectors, with STIM proteins, of the Store-Operated  $\text{Ca}^{2+}$  entry (SOCE) mechanism, first postulated in 1977 and formalized in 1986 by Putney<sup>351</sup>. ORAI1 channels constitute the pore-forming subunits of the store-operated CRACs, while STIM proteins are  $\text{Ca}^{2+}$ -sensors localized in the membrane of the endoplasmic reticulum. Concerning the molecular mechanism behind SOCE, it can be described in the following steps (Figure 23):

- 1) inositol triphosphate (IP3) is produced following the activation of a cell surface metabotropic receptor
- 2) IP3 binds to its receptor (IP3R), a  $\text{Ca}^{2+}$  channel situated in the ER membrane; this interaction leads to release of the ER-stored  $\text{Ca}^{2+}$  in the cytosol
- 3) The emptying of the ER  $\text{Ca}^{2+}$  content is sensed by the ER-resident protein STIM1, which undergoes a conformational change following  $\text{Ca}^{2+}$  decrease.
- 4) STIM1 protein translocate to ER-plasma membrane junctions where it interacts with the  $\text{Ca}^{2+}$  channel composed of ORAI proteins to form the  $\text{Ca}^{2+}$  release-activated  $\text{Ca}^{2+}$  channel (CRAC)
- 5) Binding of STIM1 to the CRAC channel determines a conformational change that opens the  $\text{Ca}^{2+}$  channel, allowing  $\text{Ca}^{2+}$  influx inside the cell.

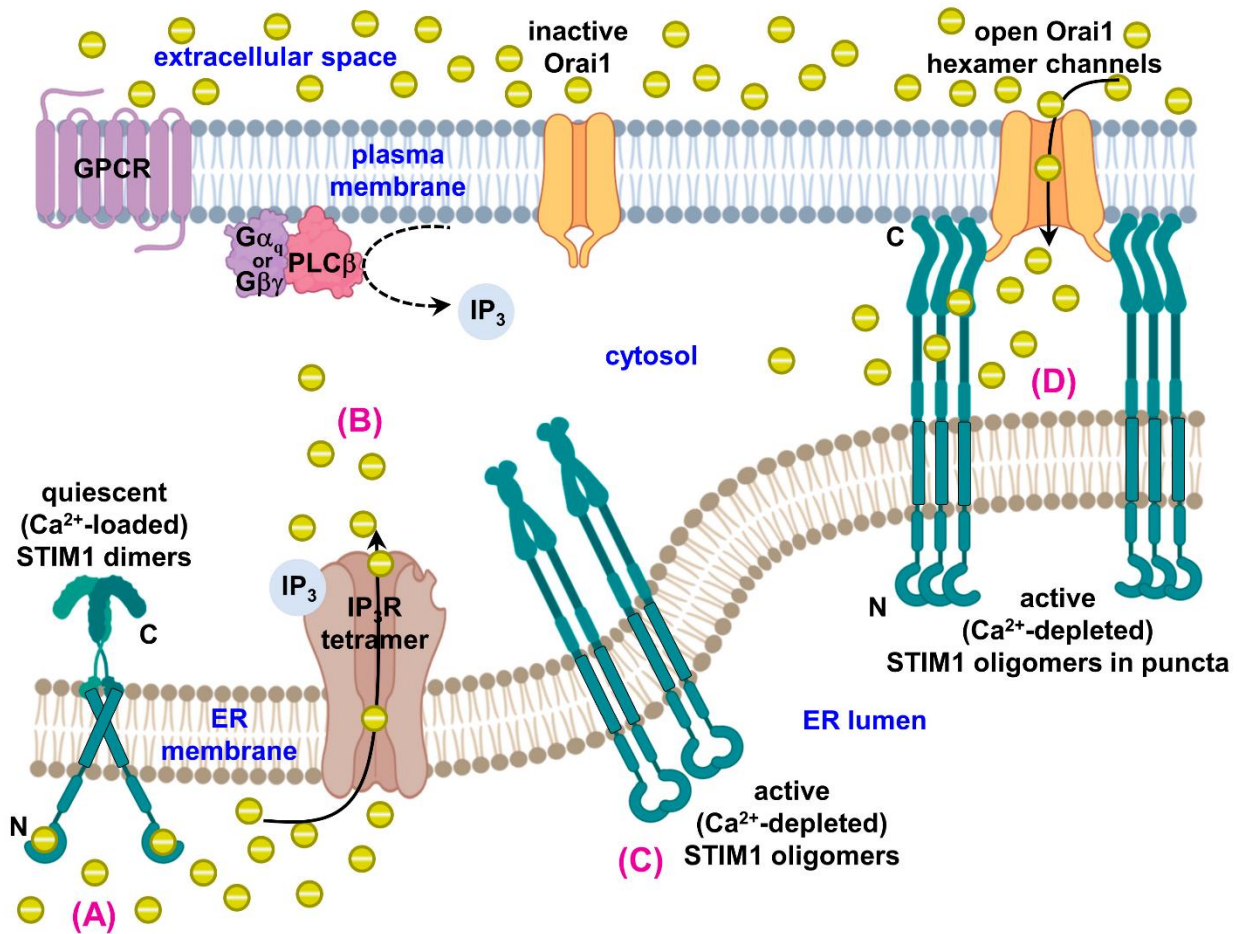


Figure 23. Molecular mechanism of store-operated Ca<sup>2+</sup> entry (SOCE) signaling. Image adapted from [352].

Early hypotheses saw SOCE solely as a mechanism to replenish intracellular ER calcium reserves<sup>353</sup>. However, several publications in the following years have demonstrated that the role of SOCE was wider than the sole refilling of ER Ca<sup>2+</sup> stores. Still, it is extremely important for signaling purposes, controlling physiological and pathological cellular processes such as secretion, differentiation, cell motility, cell proliferation, gene expression, apoptosis escape and cell invasion<sup>354</sup>.

#### 4.2.2.1 Store-Operated Ca<sup>2+</sup> Entry: IC<sub>RAC</sub>, ISOC, and homo- and heteromeric ORAI complexes

As mentioned previously, SOCE was studied before the identification of its molecular components, ORAIs and STIMs, and the current evoked by this mechanism was called IC<sub>RAC</sub> (Ca<sup>2+</sup>

release-activated  $\text{Ca}^{2+}$ )<sup>355</sup>, characterized by high  $\text{Ca}^{2+}$  selectivity, an inward rectification, a low single-channel conductance, and a  $\text{Ca}^{2+}$  dependent inactivation (CDI)<sup>356,357</sup>. This current was first characterized in T lymphocytes and mast cells; however, several studies have shown that SOCE current is cell-type specific and presents different ion selectivity among the different cell types. For this reason, these alternative currents from the classic  $I_{\text{CRAC}}$  evoked by SOCE were termed  $I_{\text{SOC}}$ . Other proteins were involved besides ORAI proteins, such as TRPs, identified ten years before ORAIs and were first considered the main players in  $I_{\text{CRAC}}$ . With the following characterization of ORAI and STIMs, it was possible to confirm that ORAI1 protein form homo-oligomers and mediate the Store-Operated  $\text{Ca}^{2+}$  Entry<sup>333</sup> because of the high levels of  $\text{Ca}^{2+}$  entry provided by ORAI1 compared to the other isoforms.

$I_{\text{SOC}}$  currents are characterized by different  $\text{Ca}^{2+}$  selectivity with respect to  $I_{\text{CRAC}}$  currents, suggesting that different proteins participate in SOCE. Among them, TRPC1 was indicated as a putative player involved in SOCE, as downregulation of TRPC1 resulted in the inhibition of SOCE in some cell types, such as endothelial cells, human platelets, and salivary gland cells<sup>358-360</sup>. Other studies demonstrated that ORAI and TRPC1 proteins could form heteromeric channels and interact with STIM1 for the  $\text{Ca}^{2+}$  entry<sup>361,362</sup>.

As explained before, ORAI1-only channels form the classic CRAC channels; however, some studies have shown that also ORAI2 and ORAI3 proteins can assemble in homomers to form functional channels that mediate the SOCE, in particular in HEK cells overexpressing ORAI2 and ORAI3 with STIM1<sup>363</sup>. Despite all ORAI channels being highly selective for  $\text{Ca}^{2+}$ , they also show different characteristics, with ORAI1 homomers displaying the greatest current amplitude and a  $\text{Ca}^{2+}$ -dependent inactivation (CDI). ORAI2-only channels display an intermediate current amplitude compared to ORAI1-only channels, the fastest activation, time, and the absence of a reactivation phase. ORAI3-only channels show the smallest current amplitude, the slowest activation time, and the absence of the reactivation phase, as for ORAI2. Moreover, all the ORAI channels show different sensitivities to 2-APB, which potentiates ORAI1-mediated SOCE at low concentrations and inhibits it at high concentrations while having no inhibitory effect on ORAI3-mediated SOCE, rather activating it<sup>363</sup>. Another difference regards the localization of ORAI proteins. The presence of ORAI2 was reported in the ER membrane, where it might represent a specific type of ER

channel<sup>364</sup>. Also, ORAI3 is located in the ER membrane in HeLa cells, where it plays a key role in avoiding ER Ca<sup>2+</sup> overload<sup>365</sup>.

ORAI proteins can also assemble into heteromeric channels<sup>363</sup>, forming ORAI1-ORAI2 and ORAI1-ORAI3 channels involved in SOCE. Inayama et al. demonstrated that ORAI2 and ORAI1 form a functional channel in the human chondrocyte cell line OUMS-27<sup>366</sup>. This result was later confirmed in mice T-cells, demonstrating that ORAI1-ORAI2 channels maintain the principal properties of the CRAC channel formed by ORAI1-only channels, showing only small differences in the I<sub>CRAC</sub> current generated by the heteromeric channel<sup>367</sup>. The same paper also demonstrated that the expression ratio between ORAI2 and ORAI1 modulates SOCE. Concerning ORAI1-ORAI3 channels, Yeast et al. recently reported that native CRAC channels are heteromers that display different sensitivities to Ca<sup>2+</sup> store depletion<sup>368</sup>. Moreover, ORAI1-ORAI3 channels are also involved in forming another type of channel which shows different properties and is not Store-Operated dependent, named arachidonate-regulated Ca<sup>2+</sup> (ARC) channel<sup>368</sup>. These results indicate that the stoichiometry of the ORAI1-ORAI2-ORAI3 channels are cell-type specific, resulting in different SOCE regulation and, therefore, in different physiological responses.

#### **4.2.3 ORAI1/STIM1 role in the generation of Ca<sup>2+</sup> oscillations**

Ca<sup>2+</sup> oscillations are ubiquitous signals in all cells that offer efficient ways to transfer biological information inside the cell, conferring signaling advantages over a sustained increase in Ca<sup>2+</sup> levels. High amplitude Ca<sup>2+</sup> signals are maintained only transiently during each oscillation. Therefore, the cytotoxic effect of a sustained rise in intracellular Ca<sup>2+</sup> levels is avoided. Moreover, Ca<sup>2+</sup> oscillations allow a prolonged stimulation of downstream responses, as they minimize the Ca<sup>2+</sup>-dependent inactivation of Ca<sup>2+</sup>-permeable channels and increase the signal-to-noise ratio by improving the capacity of low-intensity stimulation to elicit reactions. They can be generated spontaneously or upon receptor-ligand binding, leading the stable cytosolic Ca<sup>2+</sup> levels to oscillate respecting a specific oscillatory pattern, enabling the selective recruitment of downstream responses by imparting information in both amplitude and frequency and duration of the Ca<sup>2+</sup> transient. Besides these parameters, a major role is also played by the temporal and spatial profile of the Ca<sup>2+</sup> oscillation<sup>369</sup>. The oscillatory signals are then encoded by the downstream effectors present inside the cell, including phosphatases, kinases, and transcription factors, which are characterized by

multiple  $\text{Ca}^{2+}$ -binding residues that regulate the phosphorylation state of the protein, such as NF- $\kappa$ B, NFAT, calpain, PKC, mitochondrial dehydrogenases, MAPK and CAMKII, reported to exhibit decoding features which are dependent on frequency and duration (Figure 24). These proteins will decode the  $\text{Ca}^{2+}$  oscillatory pattern and activate specific cellular responses.

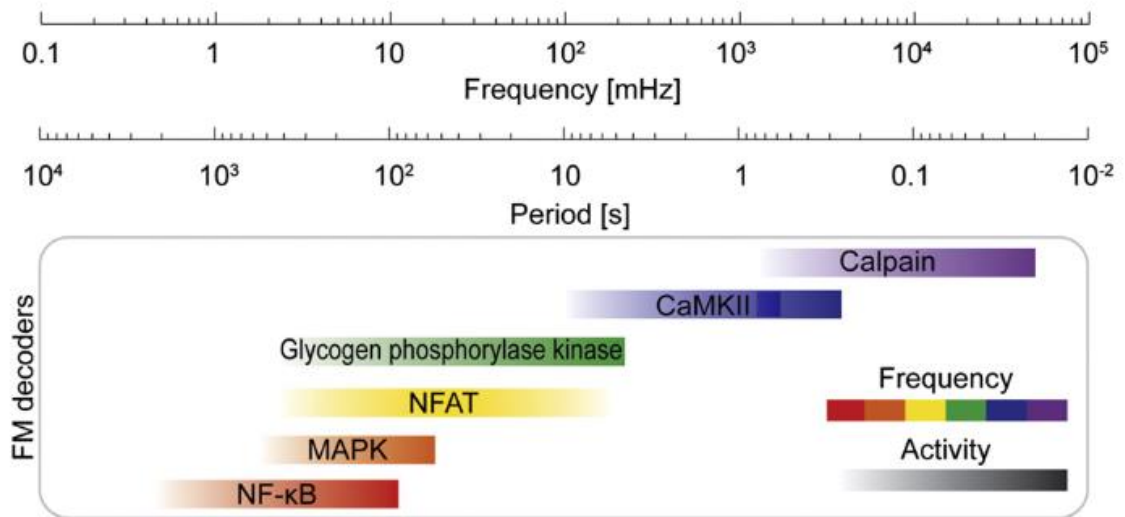


Figure 24. Illustration showing the frequencies and periods that modulate the different frequency-decoders. Image adapted from [369].

This signaling mechanism controls many cellular processes (Figure 25). In general, the degree of increase in cytosolic free  $\text{Ca}^{2+}$  concentration (amplitude modulation) is involved in cell fate decisions, including proliferation and cell death, and large and sustained increases in  $\text{Ca}^{2+}$  levels are linked to cell death. In many cases, the signal is carried by the oscillatory frequency, being involved in gene transcription, leading to different gene expression remodeling<sup>370</sup> in the contraction of pulmonary and arteriole smooth muscle<sup>371</sup>, and differentiation<sup>372</sup>. Moreover, highly localized transient alterations in cytosolic  $\text{Ca}^{2+}$  concentration called “ $\text{Ca}^{2+}$  flickers” may regulate directional migration at the edges of specific cell types<sup>289</sup>. Interestingly, it is important to specify that it appears that the signal might not be carried by the absolute frequency of the  $\text{Ca}^{2+}$  oscillations but rather by a change in their frequency, leading to high variability, even within the same cell type. Moreover, recent work has reported that fast  $\text{Ca}^{2+}$  oscillations play an important role in endothelial cells’ phenotype selection and vessel architecture<sup>373</sup>.



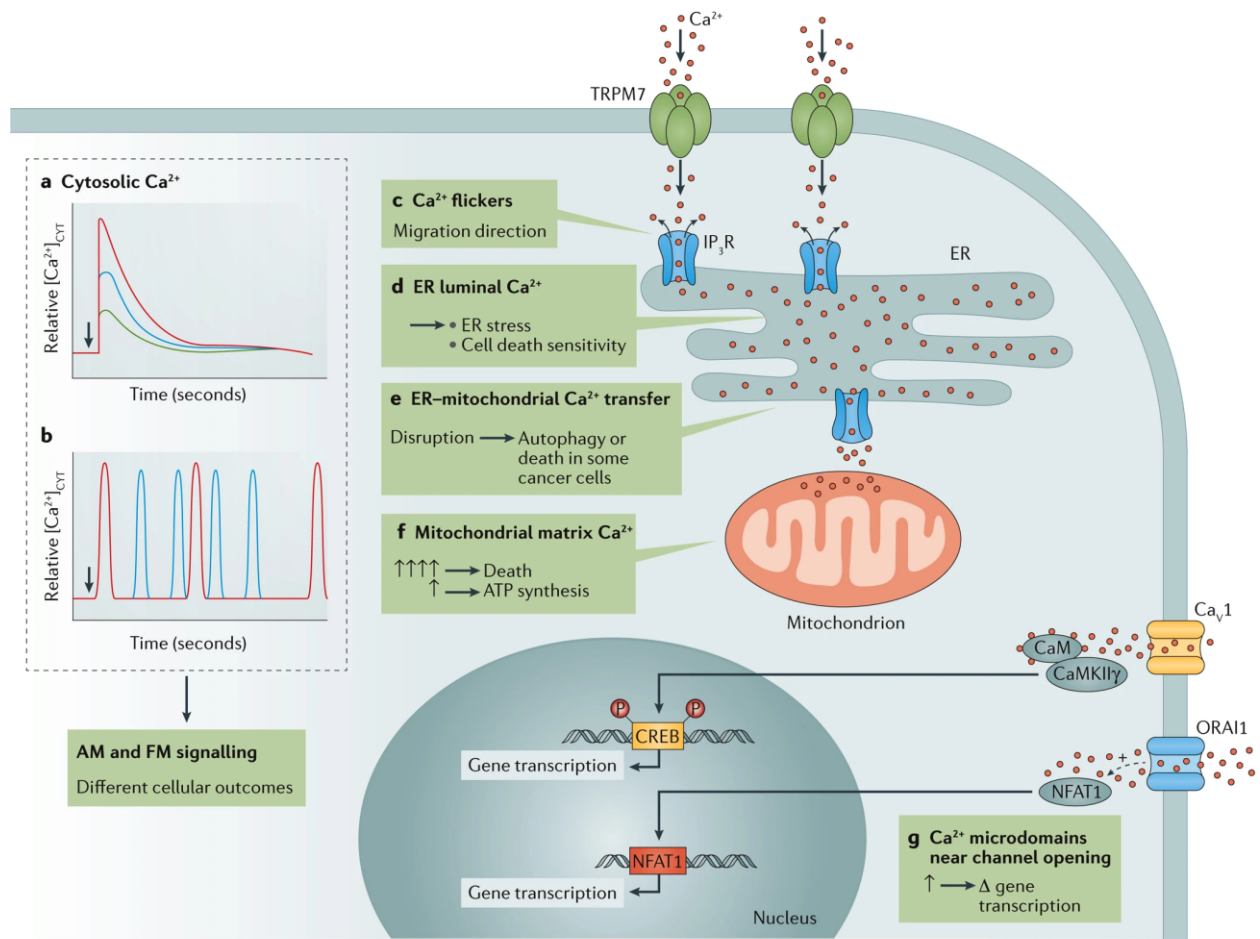


Figure 25. Schematic depicting the diversity in Ca<sup>2+</sup> signalling and its contribution to hallmarks of cancer. Image adapted from [289].

Upstream of the molecular decoders, cells exploit the components of the Ca<sup>2+</sup> toolkit, such as voltage-gated Ca<sup>2+</sup> channels, Ca<sup>2+</sup> ATPase pumps, or ER Ca<sup>2+</sup> channels, changing their spatial and temporal expression to control where and when the cytosolic Ca<sup>2+</sup> concentration is decreased or increased. To explain the generation of these oscillations, different experimental and mathematical models were developed, although a consensus regarding the mechanism still needs to be reached. Class I models assume that IP<sub>3</sub> receptors (IPRs) on ER membranes are rapidly activated by Ca<sup>2+</sup> and slowly inhibited by Ca<sup>2+</sup> ions. Step rises in cytosolic Ca<sup>2+</sup> concentration will result in a fast increase in the open probability of IPRs, followed by a slow decrease to a plateau. This results in the periodic opening and closing of IPRs, leading to cytosolic Ca<sup>2+</sup> oscillations at a constant IP<sub>3</sub> concentration<sup>374</sup>. Class II models consider both IP<sub>3</sub> and Ca<sup>2+</sup> concentrations as variables. These



types of  $\text{Ca}^{2+}$  oscillations are coupled to oscillations in the  $\text{IP}_3$  levels, as for the case of long-period  $\text{Ca}^{2+}$  oscillations in pancreatic acinar cells<sup>375</sup>. The last model describes those  $\text{Ca}^{2+}$  oscillations regulated by  $\text{Ca}^{2+}$  influx from the extracellular space, which will be described thereafter.

Several publications have demonstrated that  $\text{Ca}^{2+}$  entry via the SOCE is critical for agonist-induced calcium oscillations. These signals result from the coordinated release of  $\text{Ca}^{2+}$  ions from the ER and the enhanced  $\text{Ca}^{2+}$  influx across the plasma membrane following the activation of store-operated channels. The temporal pattern of  $\text{Ca}^{2+}$  oscillations then requires controlled on- and off-kinetics to return to basal  $\text{Ca}^{2+}$  concentrations after a  $\text{Ca}^{2+}$  rise. Before the identification of ORAI and STIMs, it was demonstrated that SOCE drives IPRs-independent  $\text{Ca}^{2+}$  oscillations in lymphocytes<sup>376</sup> and Liu X et al. later reported that intracellular  $\text{Ca}^{2+}$  oscillations directly depend on carbachol (CCh)-induced  $\text{Ca}^{2+}$  entry in HSG cells<sup>377</sup>.  $\text{Ca}^{2+}$  oscillations are mostly initiated by IPR-mediated  $\text{Ca}^{2+}$  release and maintained by SOCE in most cells<sup>378</sup>. Wedel et al. reported that  $\text{Ca}^{2+}$  oscillations in HEK293 cells are supported by  $\text{Ca}^{2+}$  entry, which depends upon STIM1 and ORAI1. The knockdown of STIM1 and ORAI1 determined a decrease in the frequency of  $\text{Ca}^{2+}$  oscillations following treatment with low concentrations of methacholine<sup>379</sup>. Other studies have recently confirmed this result by showing that ORAI1 is necessary to maintain  $\text{Ca}^{2+}$  oscillations in HEK293 cells<sup>368,380</sup>. SOCE is also important for sustaining the  $\text{Ca}^{2+}$  oscillations over a long period in airway smooth muscle cells<sup>381</sup>. Concerning other ORAI proteins, despite ORAI2 and ORAI3 do not contribute significantly to SOCE generation, they support  $\text{Ca}^{2+}$  oscillations, indicating that even minimal SOCE is enough to maintain  $\text{Ca}^{2+}$  oscillations<sup>368</sup>.

Concerning the other major component of SOCE, STIMs, early reports suggested that only STIM1 is required for  $\text{Ca}^{2+}$  oscillations<sup>379</sup>, however more recent studies demonstrated that both STIMs are involved in the regulation of  $\text{Ca}^{2+}$  oscillations, and this is dependent on the level of ER store depletion. STIM2 plays a key role in regulating  $\text{Ca}^{2+}$  oscillations by recruiting STIM1 to ER-plasma membrane junctions when ER stores are modestly depleted<sup>382-384</sup>. This indicates that with increasing agonist concentrations, SOCE is mediated first by STIM2 and incrementally by STIM1, allowing a fine modulation of  $\text{Ca}^{2+}$  entry dependent on the agonist concentration and the level of ER depletion.

In cancer, SOCE-mediated  $\text{Ca}^{2+}$  oscillation promotes cancer cell invasion by regulating the invadopodium formation and proteolytic activity by activating Src in melanoma cells and xenograft

mouse models. The inhibition of SOCE inhibited the recycling of MMP-containing vesicles to the plasma membrane, leading to decreased ECM degradation<sup>385</sup>. ORAI1-mediated Ca<sup>2+</sup> oscillations also promote the proliferation, migration, and invasion of esophageal squamous cells *in vitro* and attenuated tumor formation and growth *in vivo*<sup>386</sup>. SOCE is required to maintain Ca<sup>2+</sup> oscillations in liver cancer stem cells, where they play a key role in preserving the stemness properties of these cells. Indeed, the frequency of the Ca<sup>2+</sup> oscillation positively correlated with the self-renewal potential of the liver cancer stem cells<sup>387</sup>. In addition, it was reported that VEGF treatment induces cytosolic Ca<sup>2+</sup> oscillations via SOCE that promote the tubulogenesis and proliferation of endothelial progenitor cells (EPCs), which is important for the vascularization of solid tumors<sup>388</sup>. More recent work has further shown that transformed B-cells display SOCE-dependent Ca<sup>2+</sup>-oscillations that promote their proliferation and survival via NFAT signaling<sup>389</sup>.

#### **4.2.4 Role of SOCE in cancer and its contradictions**

Determining the contribution of Ca<sup>2+</sup>-dependent signalling in cancer represents a complicated task, because Ca<sup>2+</sup> ions play a key and dynamic role in activating different cell processes and because these activations are highly context-specific. This challenge extends to all types of Ca<sup>2+</sup> signals, in particular the Store-Operated Ca<sup>2+</sup> Entry. In the next section, the pro- or anti-tumor role of SOCE on different cancer types and cell processes will be examined, highlighting the contradictory effects when present.

##### **4.2.4.1 Prostate cancer**

Prostate cancer is the second most frequent diagnosed cancer among men worldwide<sup>390</sup>, strongly relying on the transcriptional activity of the androgen receptor (AR), which is regulated by Ca<sup>2+</sup><sup>391</sup>. STIM1 and Orai1 are differentially expressed depending on the stage of prostate cancer. *In vivo* overexpression of ORAI1 and STIM1 were detected in high-grade prostatic intraepithelial neoplasia and in clinically localized prostate cancer samples<sup>392</sup>. These results are supported by the consolidated role of SOCE in cell migration and invasion in prostate cancer cells<sup>393</sup>, in particular via the activation of the PI3K/AKT/mTOR pathway<sup>394</sup>. In addition, this signaling cascade interacts with AR signaling to promote treatment resistance<sup>395</sup>. Contrary, STIM1 and ORAI1 expression is downregulated in advanced castration-resistant prostate cancer stages<sup>392,396</sup>. ORAI1 downregulation

in later stages is consistent with the anti-apoptotic role of ORAI1 in prostate cancer revealed by our Laboratory<sup>397</sup>. Therefore, SOCE can be exploited as a marker of pancreatic cancer progression, as their expression levels are inversely correlated with Gleason Score<sup>396</sup> and directly correlated to AR status<sup>392</sup> and further regulated by AR<sup>398,399</sup>.

#### 4.2.4.2 Breast cancer

Breast cancer is the most common cancer detected in woman worldwide<sup>400</sup>. In this type of cancer, SOCE upregulation is crucial for its progression, in particular by enhancing its migration, invasion and ability to metastasise. Indeed, ORAI1-mediated SOCE regulates the phosphorylation status of ERK1/2 and the focal adhesion kinase (FAK), which is required for focal adhesion turnover, therefore migration and invasion<sup>401</sup>, and ORAI1 silencing was shown to inhibit lung metastasis *in vivo* due to impaired SOCE and focal adhesion turnover<sup>402</sup>. ORAI3 has also been reported to mediate to SOCE in estrogen receptor positive breast cancer cells to promote their aggressiveness<sup>403</sup>. In addition, SOCE pro-migratory and invasive role was further validated both *in vitro* and *in vivo* by several other studies<sup>404-406</sup>, and SOCE components were shown to be important initiators of hypoxia responses<sup>407</sup> and to be involved in acquired chemoresistance<sup>408,409</sup>.

#### 4.2.4.3 Ovarian Cancer

This cancer represents the 7<sup>th</sup> most common diagnosed cancer in women worldwide. Concerning the contribution of SOCE in its progression, it remains unclear at today and needs more study. SOCE components expression and Ca<sup>2+</sup> influx are increased in therapy resistant ovary carcinoma cells compared to therapy sensitive ones, promoting cell survival following cisplatin treatment in an Akt-dependent manner<sup>410</sup>. A more recent work have shown that placental growth factor (PIGF), a pro-tumor signaling protein produced by tumor cells, potentiates ORAI1 and STIM1 expression and SOCE, which promotes ovarian cancer progression by upregulating HIF-1 $\alpha$ <sup>411</sup>. The involvement of SOCE-mediated Ca<sup>2+</sup> influx in regulating focal adhesion assembly and disassembly was also reported in this type of cancer, where SOCE inhibition impaired focal adhesion turnover and the migratory and chemoresistance properties of chemoresistant IGROV1 ovarian cancer cells<sup>412</sup>.

#### 4.2.4.4 Leukaemia

Although most cancers exhibit an increase in SOCE to support their growth and progression, leukaemia is one of the few cancer types that decreases this  $\text{Ca}^{2+}$  entry mechanism for its progression. However, the mechanisms underlying this decrease and their link to leukaemia are still poorly understood. Soboloff J. and co-workers have measured the SOC-dependent  $\text{Ca}^{2+}$  influx in five different acute myeloid leukaemia (AML) cell lines, observing minimal SOCE in 3 out of 5 cell lines tested<sup>413</sup>. This output was later confirmed also in chronic myeloid leukaemia (CML) cells<sup>414</sup>, where decreased SOCE was linked to inhibition of apoptosis<sup>415</sup>.

One possible mechanism considers the activity of Wilms Tumor Suppressor 1 (WT1), known to negatively regulate STIM1 expression<sup>416</sup> and to be overexpressed in the majority of AML samples<sup>417</sup>. Indeed, murine 32D leukaemia cells, which do not express WT1, show high SOCE levels<sup>418</sup>. Given that leukocyte maturation shows loss of WT1 expression, and that AML is linked to lower SOCE, it is conceivable that the loss of SOCE might be exploited as a prognostic indicator for leukaemia. Another putative mechanism considers the dysregulations in the ORAI1/STIM1 stoichiometry. It has been shown that imbalances between ORAI and STIM ratios result in SOCE inhibition<sup>419</sup>. HL60 AML cells generally present low but functional SOCE, and mRNA overexpression of ORAI1 and ORAI2 and STIMs, but at disproportional levels. In these cells, SOCE is mediated by ORAI1 and ORAI2 and their knockdown negatively affects their migration via impairment of focal adhesion dynamics<sup>420</sup>.

#### 4.2.4.5 Glioma

This cancer represents the most common type of brain malignancy, which heavily relies on  $\text{Ca}^{2+}$  signaling, in particular SOCE. ORAI1 expression is high in both glioma cell lines and glioma samples compared with normal brain samples, where it plays a key role in tumor progression by promoting cell motility and invasion via of proline-rich tyrosine kinase 2 (Pyk2)-dependent regulation of EMT and focal adhesion turnover<sup>421</sup>. SOCE activity is also correlated to glioma stage, as it is higher in high grade gliomas than in low grade gliomas<sup>422</sup>. In addition, SOCE contributes to the maintenance of quiescence in glioma stem-like cells, a mechanism that protects them therapy-

induced cell death. In fact, SOCE regulates the switch from proliferative to quiescent states, as its inhibition suppresses the proliferative abilities of glioblastoma stem-like cells, which undergo quiescence. In this scenario, no changes in ORAI1 or STIM1 expression were detected between proliferating and quiescent glioma cells, but a major role seems to be played by ORAI3, which is upregulated in quiescent cells<sup>423</sup>. SOCE also contributes to the acquisition of stemness properties in glioblastoma cells, as its pharmacological inhibition reduces the proliferation, self-renewal, and the expression of the stem cell marker SOX2<sup>424</sup>. Previously, Motiani RK. and co-workers demonstrated that SOCE is increased in primary cell lines derived from brain tumor glioblastoma multiforme (GBM) patient explants compared to normal primary astrocytes and it also supports their aggressiveness of by promoting cell invasion<sup>425</sup>.

#### **4.2.4.6 Melanoma**

Among all the types of cancer mentioned above, melanoma probably represents the most interesting for portraying the contradictions of the role of SOCE in its progression. It is generally believed that SOCE promotes melanoma progression. In 2010, Feldman *et al.* first described the expression of ORAIs and STIMs and activity of SOCE in mouse melanoma cells. In these cells, SOCE is mediated by STIM1 and ORAI1 and no alterations between ORAI1 and STIM1 expression were detected when compared to non-malignant cells, although a higher SOCE was measured. By coupling with trans-mitochondrial Ca<sup>2+</sup> uptake, SOCE regulated proliferation and cell survival via activation of protein kinase B/AKT<sup>426</sup>. The same research group later demonstrated that lipid rafts are required for SOCE function and activation of protein kinase B/AKT<sup>427</sup>. Stanisz *et al.* later studied the role of SOCE in human melanoma cells, demonstrating that SOCE is mediated by ORAI1 and STIM2. Their silencing caused melanoma cells to proliferate more, although their invasive abilities decreased. Their role in promoting invasion was further supported by immunostaining on human melanoma patient samples, which revealed elevated ORAI1 and STIM2 expression in the invasive rims and lower expression in the central proliferative areas<sup>428</sup>. These results were partially confirmed the same year by another study, where SOCE inhibition suppressed the motility of melanoma cells *in vitro* and the metastasis *in vivo*. The authors also demonstrated that SOCE-downstream signalling pathway involves the CaMKII/Raf-1/ERK signaling cascade activation<sup>429</sup>. The pro-invasive role of SOCE in melanoma was supported by the work of Sun J. and co-workers in 2014, which showed that

ORAI1/STIM1-mediated  $\text{Ca}^{2+}$  oscillations facilitated invadopodium assembly via Src activation and promoted their proteolytic activity by recruiting the membrane type 1 matrix metalloproteinase for ECM degradation<sup>385</sup>. Despite the important role of STIM2 in mediating SOCE in melanoma cells elucidated by Stanisz *et al.*, its role was not explored in the study of Sun *et al.*

The studies mentioned above reported that invasive melanoma cells show a higher SOCE than melanocytes or primary melanoma cells. In opposition to these findings, the study published by Hooper *et al.* examined the role of SOCE in patients-derived invasive (characterized by high Wnt5a expression levels) and non-invasive melanoma cells (low Wnt5a expression levels) and showed that non-invasive melanoma cells displayed a higher SOCE than invasive ones. Interestingly, no alterations in gene and protein expression levels or localization were detected for STIMs and ORAIs, nor the transient overexpression of ORAI1 and STIM1 could restore the SOCE in the invasive melanoma cells. To explain the reduced SOCE, the authors were able to demonstrate that silencing of Wnt5a rescued SOCE in invasive cells, while overexpressing it in non-invasive led to reduced SOCE. Wnt5a regulates the activity of protein kinase C (PKC), which inhibits ORAI1. Indeed, PKC inhibition determines the recovery of SOCE in invasive melanoma cells<sup>430</sup>.

Additional contradictory results were later presented by a recent work of the same research group, which showed that SOCE can be suppressed to promote metastasis in melanoma<sup>431</sup>. The authors found that UV exposition inhibited SOCE in non-metastatic melanoma cells without affecting basal  $\text{Ca}^{2+}$  levels and ER  $\text{Ca}^{2+}$  release, promoting invasion and metastasis. Pharmacological SOCE targeting and reduction led to the same outcome, while its pharmacological activation decreased cell invasion but only in UV-exposed melanoma cells. This indicates SOCE inhibition as a mediator of UV-induced enhanced invasion. Interestingly, enhanced invasion was also obtained by ORAI1 overexpression, probably as a result of imbalanced ORAI1/STIM1 ratio. Surprisingly, complete SOCE abrogation with high concentrations of SOCE inhibitor reverted the pro-invasive effect, leading to diminished cell invasion. This indicates that minimum  $\text{Ca}^{2+}$  concentrations are required to promote melanoma cell invasion, as further confirmed by using an ORAI1 dominant negative mutant, which abrogated SOCE and reduced metastasis *in vivo*. Therefore, a modest decrease in SOCE is required for enhanced invasion, while SOCE ablation inhibits invasion. Since no differences in ORAIs and STIMs were detected between untreated and UV-treated melanoma cells, RNA-seq analysis revealed that cholesterol (CHL) biosynthesis pathway was upregulated in those melanoma

cells which showed reduced SOCE. Further results showed that UV treatment increased the CHL content and that inhibitors of CHL biosynthesis pathway restored SOCE in UV-treated melanoma cells and decreased cell invasion. In addition, high CHL levels were sufficient to mimic UV-induced metastasis *in vivo*. Finally, further RNA-seq analysis revealed that SOCE inhibition promoted the hexosamine biosynthetic pathway (HBP) activation. This pathway supports cancer progression by increasing N-acetyl-glucosamine (GlcNAc) formation, which O-GlcNAcylation mediated by the enzyme O-linked N-acetylglucosamine (GlcNAc) transferase results in enhanced EMT, cell survival and cell growth<sup>432</sup>. Indeed, melanoma cells showed enhanced O-linked N-acetylglucosamine (GlcNAc) transferase activity, which knockdown or pharmacological inhibition reduced melanoma cells invasion. The authors finally hypothesised that CHL-mediated SOCE inhibition results from CHL's known ability of interacting with ORAI1, inhibiting SOCE<sup>433</sup>.

These interesting results of the above-described papers reflect the non-linear relationship between SOCE and cancer metastasis, where its role is intricately and strongly context-specific, depending on the cancer type, Ca<sup>2+</sup> ions concentration and degree of change, and signalling environment.

#### **4.2.5 Role of STIM1 and ORAI1 in PDAC**

Despite ORAI1 and STIM1 roles' in carcinogenesis having been extensively studied in different types of cancer, relatively few studies have focused on their role in contributing to PDAC progression. One of these works belong to our Laboratory; Kondratska et al. have demonstrated that ORAI1 and STIM1 are expressed in different PDAC cell lines at both mRNA and protein levels, with PANC-1 displaying the highest levels of both proteins. Moreover, they mediate the SOCE in PANC-1, Capan-1, Mia PaCa-2, and AsPC-1 cells, as demonstrated by silencing experiments in Ca<sup>2+</sup> imaging. This study further elucidated the role of ORAI1 and STIM1 in cell survival following chemotherapeutic treatment. 5-FU chemotherapy drug induces cell survival in PDAC cells by upregulating the expression of ORAI1 and STIM1 and, therefore, increasing the SOCE, as demonstrated by the enhanced sensitivity to 5-FU and apoptosis in siSTIM1 and siORAI1 PANC-1 cells<sup>318</sup>. Unfortunately, the mechanisms behind this phenomenon are not yet clarified.

In 2015, Woods N. and co-workers reported that SOCE inhibition by SKF96365 treatment reduced the viability of PANC-1 and Mia PaCa-2 cells<sup>434</sup>. A more recent work by Khan et al.

reported a role for ORAI1 in the proliferation of PDAC cells by employing a recent CRAC channel inhibitor, RP4010. Cells treatment with this inhibitor negatively affected the proliferative and colony formation abilities of L3.6pl and MiaPaCa-2 cells. This effect was correlated with a decrease in Carbachol-induced SOCE upon RP4010 treatment. The authors further demonstrated that RP4010 decreased the gene and protein expression of pAKT and modulated the expression of proteins related to the AKT/mTOR signaling cascade. Therefore, they hypothesized that PDAC cells' proliferation is regulated via the AKT/mTOR pathway. More precisely, it was also demonstrated that both siORAI1 and RP4010-mediated CRAC inhibition inhibits NFAT1 translocation to the nucleus, suggesting that PDAC cells' proliferation is controlled by the AKT/mTOR/NFAT pathway<sup>319</sup>. In addition, RP4010 synergistically cooperates with gemcitabine and nab-paclitaxel to inhibit PDAC cells' proliferation, enhancing the anticancer activity of these chemotherapeutic drugs by downregulating NFAT, mTOR, and NF- $\kappa$ B signaling. This result was then validated *in vivo* using a patient-derived xenograft mouse model<sup>319</sup>. These results might explain the Ca<sup>2+</sup>-dependent pro-survival role of ORAI1 and STIM1 reported by Kondratska et al. Despite the ORAI1 upregulation reported in different PDAC cells compared to normal pancreatic ductal cells, an *in silico* analysis of 840 transportome genes in PDAC patients' tissues demonstrated a strong downregulation of ORAI1 (Fold Change = -13.31, *p*-value = 0.002)<sup>312</sup>, further supported by the microarray data set analysis of 36 PDAC patient tissues that indicated downregulation of ORAI1 in pancreatic cancer tissue compared to normal tissue (normal tissue Log<sub>2</sub> = 6.82 vs. Log<sub>2</sub> = 6.54 for tumor tissue *p*-value = 0.004)<sup>322</sup>.

Other works have focused on the contribution of STIM1 in PDAC progression. The work of Wang et al. showed that STIM1 is upregulated in PDAC tissues and involved in EMT in PDAC, as shRNA knockdown of STIM1 decreased the protein expression of Vimentin and upregulated E-cadherin levels, negatively affecting PDAC cells' proliferation and invasion<sup>321</sup>. The same work indicated that HIF-1 $\alpha$  is upregulated in PDAC tissues and promotes STIM1 expression at the transcriptional level in several PDAC cells, as demonstrated by the knockdown of HIF-1 $\alpha$ . This suggests that the highly hypoxic PDAC tumor microenvironment promotes PDAC aggressiveness by upregulating STIM1. STIM1 is upregulated following gemcitabine treatment, inducing a shift in Ca<sup>2+</sup> signaling and protecting pancreatic cancer cells from the pro-apoptotic ER stress response<sup>435</sup>.

Unfortunately, to date and my knowledge, data about the role of Ca<sup>2+</sup> oscillations in PDAC progression has yet to be available.



#### **4.4 Ca<sup>2+</sup>-permeable ion channels regulation by acidic pH<sub>e</sub>**

Ca<sup>2+</sup>-permeable channels are important mediators of two chemical signatures of the tumor microenvironment: acidic pH<sub>e</sub> and hypoxia. Our published review “Ca<sup>2+</sup> Signalling and Hypoxia/Acidic Tumour Microenvironment Interplay in Tumour Progression” aimed to overview the crosstalk between major chemical components of the tumor microenvironment, hypoxia, and acidic pH<sub>e</sub>, and Ca<sup>2+</sup>-permeable ion channels, with a major focus on TRPs, Store-Operated Ca<sup>2+</sup> channels, and PIEZO channels, summarizing the major Ca<sup>2+</sup>-mediated signaling pathways that are involved in hypoxia and acidic pH<sub>e</sub> responses in cancer cells (Annexe 1).

## 5. Hypothesis and aim of the work

PDAC is the 12th most frequent cancer disease worldwide, but despite being relatively infrequent, it is one of the deadliest and most aggressive human malignancies, showing an overall 5-years survival rate of less than 10%. This dismal prognosis is attributed to the lack of early detection and screening tests that lead to most of the patients with advanced, metastatic and unresectable PDAC, and which often show limited response to chemotherapy<sup>436</sup>. Moreover, pancreatic cancer cells are embedded in a highly desmoplastic, immunosuppressive, hypoxic, and acidic stroma, which creates a mechanical barrier to drugs and immune cell infiltration<sup>437</sup>. Current consensus states that PDAC develops in a stepwise manner with distinctive genetic alterations for each histologically distinct stage, starting from non-invasive preneoplastic lesions termed pancreatic intraepithelial neoplasia (PanIN), to more advanced lesions and to finally PDAC. This indicates that genomics provide us an important help for its understanding. However, beyond genomics, it is fundamental to also focus on the microenvironment, in particular on the microenvironment  $pH_e$  landscape in which pancreatic cancer cells, but also normal pancreatic ductal cells, are embedded. As explained in Section 3.7.5, pancreatic ductal cells face both spatial and temporal dynamic modifications in the interstitial  $pH_e$ , existing in a particular  $pH_e$  landscape where the intermittent acidity trains them to cope with acid stress, representing an important advantage during PDAC onset. In other words, when PDAC fully develops from PanIN lesions and driver mutations, it will be constituted by cancer and stromal cells that have been previously “preconditioned” by the acidity intermittence of the normal pancreatic interstitium to boost their survival capacity and aggressiveness. Therefore, PDAC will be an ensemble of cells that are adapted and preconditioned to an acidic microenvironment, which provided them with growth advantages.

This represents the notion at the basis of the pHioniC consortium which my PhD project belongs to, and the hypothesis of my work relies on this assumption, that is that the combination of the inherent ability of pancreatic ductal cells to withstand an heterogenous and intermittent acidic  $pH_e$  landscape and PDAC driver mutations, in the presence of early and pre-neoplastic lesions, results in the selection of a cancer cell population during the last phase which is acid-resistant and characterized by an aggressive phenotype, with enhanced invasive and metastatic potential.

The second important part of my project aims to provide an explanatory mechanism to the acid-driven selection in PDAC, by exploiting the expertise and knowledge of both the French (under Prof. Prevarskaya supervision) and Italian (under Prof. Fiorio Pla supervision) Laboratories I am affiliated to on  $\text{Ca}^{2+}$ -signaling in the context of cancer. As described in section 4,  $\text{Ca}^{2+}$  ions are a highly versatile intracellular signal capable of regulating different hallmarks of cancer via the generation of highly specific  $\text{Ca}^{2+}$  signals which are decoded by a plethora of proteins that constitute a unique set of  $\text{Ca}^{2+}$  signalling toolkit<sup>289</sup>. This complexity of  $\text{Ca}^{2+}$  signaling explains why its deregulation can be a feature of certain pathological states, including cancer, contributing to the acquisition of the malignant phenotypes.

Although the separate roles of tumor acidosis and  $\text{Ca}^{2+}$  signaling in cancer progression are well established, the hypothesis of acidic TME employing  $\text{Ca}^{2+}$  signaling as preferential route for sustaining tumor progression has not yet been sufficiently explored. Therefore, considering the major role that acidic tumor microenvironment plays in PDAC progression and also the major role of  $\text{Ca}^{2+}$  signaling in cancer-related processes and the pH-sensitivity of several  $\text{Ca}^{2+}$ -permeable ion channels, the main hypothesis of my PhD project is that the acidic tumor microenvironment and  $\text{Ca}^{2+}$  signalling could work in synergy to select the most aggressive PDAC cancer phenotypes.

Based on this idea, my work presents **two major aims**:

## **1. Evaluation of the impact of tumor acidosis-mediated selection on PDAC progression *in vitro*.**

The first part of my thesis was devoted to establishing and characterize the different genetic and phenotypic responses of PANC-1 and Mia PaCa-2 cells to acidosis along the different stages of acid selection. To this end, we subjected short-term exposition to acidic stress ( $\text{pH}_e$  6.6), in order to mimic the early stages of  $\text{pH}_e$  selection, and to long-term acidic pressure to obtain acid-selected cells, as it is established that the acidification of PDAC TME occurs over a sustained period. We also established a third acid model by assessing the impact of acid-mediated selection on reinforcing local invasion, establishing a model of acid-selected cells recovered in  $\text{pH}_e$  7.4. This last model aimed to mimic PDAC-stroma boundaries, areas in which  $\text{pH}_e$  is higher respect to the tumor core,

and therefore the cancer cell escape from the tumor. This aim is addressed in Chapter III with our article, currently under revision, titled: **“Acidic growth conditions promotes epithelial-to-mesenchymal transition to select more aggressive PDAC cell phenotypes *in vitro*”**.

## **2. Evaluation of the interplay between acidic $pH_e$ and $Ca^{2+}$ signaling in PDAC progression.**

The second part of my PhD project aimed at identifying acidic  $pH_e$ -inducible  $Ca^{2+}$  pathways that leads to one or more aggressive cell phenotypes in PDAC cancer cell lines. In particular, we focused on  $Ca^{2+}$  oscillations which are key players in sustaining cancer invasion. Our results clearly show that FBS-induced PANC-1  $Ca^{2+}$  oscillations are dependent on Store-Operated  $Ca^{2+}$  Entry (SOCE) mechanism and in particular on ORAI1 and STIM1. We further aimed to understand how the acidic PDAC microenvironment affects two important types of  $Ca^{2+}$  signals: Store-Operated  $Ca^{2+}$  Entry and  $Ca^{2+}$ -oscillations, and the impact of  $Ca^{2+}$ -permeable channels in the phenotypic characteristics of the different acidic models established in the point 1, with a focus on cell processes important for cancer, such as migration and invasion. The final aim is to target the selected ion channels and assess their potential clinical interest. This aim is addressed in Chapter III with our article in preparation titled **“ $pH_e$ -sensitive Store-Operated  $Ca^{2+}$  channels signals contribute to tumor acidic microenvironment-induced PDAC cells' selection to more aggressive phenotypes”**.

# Chapter II

## Materials and Methods

### 1. Cell culture

Human pancreatic ductal adenocarcinoma PANC-1 cells were obtained from the Institute for Experimental Cancer Research, Christian-Albrecht-University (CAU) of Kiel, Germany. Mia PaCa-2 cells were purchased from the American Type Culture Collection (ATCC). Control cells were cultured as monolayers in RPMI 1640 growth medium (Gibco, Cat# 31870-025) supplemented with 10% FBS (Biochrom, Cat# S0615), 2 mM L-Glutamine (Gibco, Cat# 25030-024), 1 mM sodium pyruvate (Gibco, Cat# 11360039) and antibiotics (penicillin/streptomycin 100 U ml<sup>-1</sup>, Life Technologies, Inc., Cat# 15070-063). For pH adjustments of the cell culture media to pH<sub>e</sub> 6.6, RPMI 1640 powder medium (Sigma, Cat# R6504) was complemented with NaHCO<sub>3</sub> according to the Henderson-Hasselbalch equation to derive the target pH<sub>e</sub> (Table 1). The osmolarity of the medium was balanced using NaCl. The different powders components were dissolved in UltraPure distilled water (Invitrogen, Cat# 10977-035), and the resulting medium was filtered in a sterile environment and supplemented with 10% FBS (Biochrom, Cat# S0615), 1 mM sodium pyruvate (Gibco, Cat# 11360039) and antibiotics (penicillin/streptomycin 100 U ml<sup>-1</sup>, Life Technologies, Inc., Cat# 15070-063). All cells were maintained at 37 °C in a humidified 5% CO<sub>2</sub> atmosphere.

Table 1. Preparation of 500 ml of cell media with different pH.

Component	Medium pH 7.4	Medium pH 6.6
	Quantity	Quantity
RPMI	4.2 grams	4.2 grams
NaCl	5 mM	25.2 mM
NaHCO <sub>3</sub>	24 mM	2 mM

FBS	10%	10%
Sodium pyruvate	1 mM	1 mM
L-Glu	2 mM	(already supplemented)
PenStrep	1%	1%
H <sub>2</sub> O	Up to 500 ml	Up to 500 ml

---

## 2. Establishment of acid phenotypes in PDAC cells

For the generation of the acidic phenotypes, PANC-1 and Mia PaCa-2 cells were exposed to pHe 6.6 for different time periods by changing the media pHe from 7.4 to 6.6. Control cells were cultured at pHe 7.4. For studying early stages of low pHe-selection («4 days pHe 6.6» cells) freshly split PANC-1 and Mia PaCa-2 cells were cultured in pHe 6.6 medium for 4 days. PDAC mimicking cells («pHe-selected» cells) were generated by a 1 month-long exposure to the acidic medium before performing the experiments. pHe-selected + 7.4 cells were maintained in pHe 6.6 for 1 month before they were put back to pHe 7.4 for 2 weeks (Figure 1). Experiments requiring pHe-selected + 7.4 cells were performed after a maximum of 2 weeks following recovery to pHe 7.4. Both pHe 7.4 and pHe 6.6 media were refreshed every other day, and acidic medium pH was monitored daily. For experiments requiring acute (1h) exposition to acidic pH, an aliquot of pHe 6.6 medium was maintained at 37 °C under a humidified 5% CO<sub>2</sub> atmosphere for at least 1h before the experiment to equilibrate the target pHe.

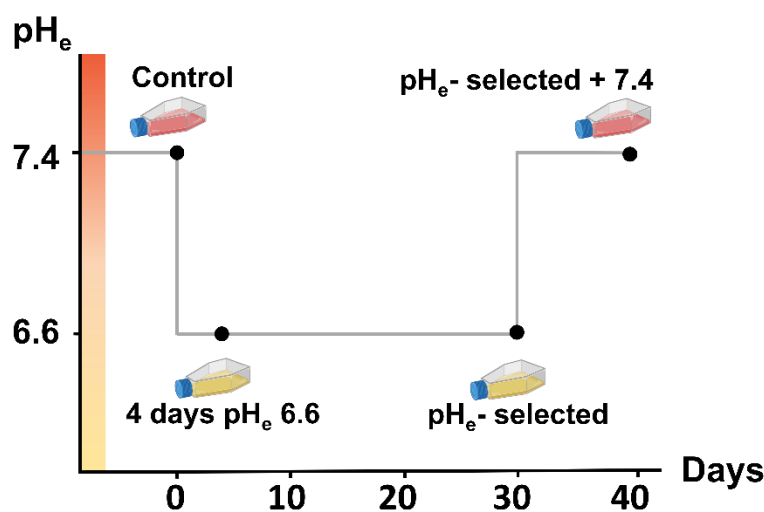


Figure 26. Scheme of the different acidic pHe phenotypes established. Control cells were kept in physiological pHe culture conditions (pHe= 7.4), while acidic phenotypes were constituted by PDAC cells exposed for different periods to acidic pHe: 4 days (cell model named “4 days pHe 6.6”), 1 month (pHe-selected) and 1-month long exposure followed by recover to physiological pHe for 2 weeks (pHe-selected + 7.4).

### 3. Reagents

Synta66 (TargetMol Chemicals Inc., Cat# T13047) was stored in DMSO stock solution at a concentration of 100 mM at -20°C. For experiments, a concentration of 10 μM was used. Src kinase inhibitor-1 was purchased from Sigma-Aldrich (Cat# S2075) and stored in 50 mM stock solution in DMSO at -20°C. It was diluted to 5 μM in cell culture medium for experiments. Fura-2 AM was purchased from Invitrogen (Cat# F1221), resuspended in DMSO stock solution, and kept at 4°C. It was used at a final concentration of 5 μM, while Thapsigargin (TG) was from Tocris (Cat# 1138) and used at a final concentration of 2 μM. The working concentration of Mitomycin C (MP Biomedicals™, Cat# 0219453202) was 10 μg/mL.

### 4. Immunofluorescence staining

PANC-1 and Mia PaCa-2 cells were stained with fluorescent phalloxin to label F-actin for cell morphology studies. Cells were plated in their corresponding pHe conditions in 1% gelatin-

coated coverslips inserted in 6-well plates at different densities to reach ~80% confluence on the day of the experiment. Cells were washed twice with PBS and fixed with 4% paraformaldehyde for 10 minutes at room temperature. After washing the samples twice with PBS, the fixed cells were incubated with a solution of 0.1% Triton X100 in PBS (PBST) for 5 minutes at room temperature for permeabilization. Solutions were decanted, and two washes with PBS followed. Fixed cells were incubated with PBS containing 1% BSA for 30 minutes and then stained with a staining solution containing 2 units/coverslip of fluorescent Alexa 488 phalloidin (2 U/200 ul per coverslip, Invitrogen™, Cat# A12379) in 1% BSA in PBS for 20 minutes at room temperature. Cells were washed two times with PBS, and cell nuclei were stained with a solution of 1:1000 DAPI in PBS for 15 minutes at room temperature. Cells were washed twice with PBS and air dried, and the coverslips were mounted on clean microscope glass slides using Glycergel mounting medium (Dako, Cat# C0563) and stored in the dark at 4°C. Glass slides were then examined using a confocal laser scanning microscope (LSM 700, Carl Zeiss MicroImaging GmbH) with a Plan Apochromat 40x/1.3 numerical aperture oil immersion objective. The images were analyzed in Zeiss LSM Image Browser software.

#### **4.1 Analysis of cell morphology: cell area and cell circularity**

Cells were plated in the appropriate pHe-target medium and grown to approximately 80% confluency. Four random fields of each cell condition were imaged using a brightfield microscope (Nikon Eclipse TS100). ImageJ software quantified cell area and circularity by manually segmenting the brightfield images. Over 500 cells for each condition were considered for cell area and circularity analysis.

#### **4.2 Paxillin staining and confocal microscopy**

PANC-1 cells seeded on 1% gelatin-coated coverslips were washed twice with cold phosphate-buffered saline (PBS) and fixed with 4% paraformaldehyde for 15 min at 4°C. After washing the samples twice with ice-cold PBS, the fixed cells were then incubated for 10 min at room temperature with PBS containing either 0.1% Triton X-100 (PBST) for permeabilization and blocking of unspecific binding of the antibody was obtained by incubating the cells with PBST containing 1% gelatin and 0.2 M glycine for 30 minutes. The solution was decanted, and a quick



wash with cold PBS followed. Cells were incubated in diluted Alexa Fluor® 647 Anti-Paxillin antibody (1:200, ab246719) in PBS containing 1% gelatin overnight at 4°C. The cells were then kept in the dark and washed three times in PBS for 5 minutes each, following DAPI staining for 10 minutes at room temperature. Cells were washed twice with PBS, and coverslips were mounted on glass slides with a drop of Glycergel. Coverslips were sealed with nail polish and stored in the dark at 4°C. Glass slides were then examined using a confocal laser scanning microscope (LSM 700, Carl Zeiss MicroImaging GmbH) with a Plan Apochromat 40x/1.3 numerical aperture oil immersion objective. Peripheral and cytosolic focal Adhesions (FAs) parameters were quantified with ImageJ (NIH, Bethesda, Maryland, USA) by manually selecting (ROI) at least 10 cells of 5 representative fields per biological replicate, and paxillin dots were distinguished from the background by applying a threshold and subsequently, FAs' area and density were automatically quantified by ImageJ software. FAs peripheral translocation was quantified by peripheral FAs to cytoplasmic FAs ratio. The mean numbers obtained from each biological replicate were used for statistical analysis. Three independent experiments were performed for each experimental condition.

## **5. Proliferation and viability**

Proliferation of PANC-1 and Mia PaCa-2 cells was studied using EdU staining assay, MTS assay, trypan blue exclusion assay, and ATP quantification assay.

### **5.1 MTS**

The MTS assay is a colorimetric method for indirectly determining the number of viable cells in proliferation which employs tetrazolium compound (MTS) and an electron coupling reagent (phenazine methosulfate, PMS). MTS is reduced into a formazan product by dehydrogenase enzymes found in metabolically active cells. The amount of formazan product is proportional to the number of viable cells. For MTS assays, cells were plated in 96-well plates at a density of 3000 cells/well for PANC-1 and 8000 cells/well for Mia PaCa-2 cells in 100 µl medium, letting them adhere overnight. Cell media of correspondent pH was refreshed the following day and cell

proliferation was assessed at 2h, 24h, 48h, 72h, and 96h using MTS CellTiter 96® Aqueous assay (Promega, Cat# G1111) following the manufacturer's instructions.

## 5.2 EdU proliferation assay

Cell proliferation was assessed via 5-ethynyl-2'-deoxyuridine (EdU) incorporation using Click-iT EdU Alexa Fluor 647 Imaging Kit (Invitrogen, Cat# C10340). Briefly, the different PANC-1 and Mia PaCa-2 cell models were plated in their corresponding pH<sub>e</sub> conditions in 1% gelatin-coated coverslips inserted in 6-well plates. Confluence was ~80 % on the day of the experiment. The culture medium was refreshed, and cells were incubated with 20 μM EdU for 2h at 37°C. Cells were then washed with phosphate buffered saline (PBS; pH 7.4; Gibco, Cat# 10010-015) and fixed with 4% paraformaldehyde (PFA) at room temperature for 15 minutes. Following two washes with 3% bovine serum albumin (BSA)-containing PBS, cells were permeabilized with 0.5% Triton X-100 in PBS at room temperature for 20 minutes and washed twice with 3% BSA-containing PBS. Cells were then stained with 100 μl Click-iT reaction cocktail per coverslip and incubated in the dark for 30 minutes. Following two washes with 3% BSA-containing PBS, cell nuclei were stained with Hoechst 33342 for 30 minutes and away from light. Coverslips were finally mounted on clean microscope glass slides using Glycergel mounting medium (Dako, Cat# C0563) and stored in the dark at 4°C. The EdU-positive cells were visualized using a confocal laser scanning microscope (LSM 700, Carl Zeiss MicroImaging GmbH) with a Plan Apochromat 40x/1.3 numerical aperture oil immersion objective. At least five photos per condition were taken, and analysis was performed by counting the cells using ImageJ software and calculating the percentage of EdU-positive cells over the total number of cells as follows:

$$\text{EdU-positive cell ratio (\%)} = (\text{Number of cells positive for EdU staining/number of total cells}) \times 100$$

## 5.3 ATP quantification assay

For ATP quantification assay, cells were plated in 96-well black-bottom polystyrene plates (Greiner Bio-One, Austria) at a density of 3000 cells/well for PANC-1 and 8000 cells/well for Mia PaCa-2 cells in 100 ul medium volume and let adhere overnight in physiological pH<sub>e</sub> conditions for

control, 4 days pHe 6.6 and pHe- selected + 7.4 cell models, while pHe-selected cells were plated in acidic conditions. Acidic cell models were treated with fresh acidic pHe (pHe 6.6) medium the following day, and ATP quantification was assessed at 1h, 48h, and 96h. The number of metabolically active cells was quantified based on the ATP amount using CellTiter-Glo® 2.0 Luminescent Cell Viability Assay (Promega, Cat# G9241) following the manufacturer's indications. Luminescence was recorded using a microplate reader (FilterMax F5, Multi-Mode Microplate Reader, Molecular Devices). Each condition was tested in eight technical replicates, and three independent experiments were performed for each experimental condition.

#### **5.4 Trypan Blue exclusion assay**

Trypan blue exclusion assays were used to determine the viability of PANC-1 and Mia PaCa-2 cell models after exposition to pHe 6.6 for different time points (2h, 24h, 48h, 72h, and 96h, 15 days, and 30 days). PANC-1 and Mia PaCa-2 cells were seeded in 6-well plates at a density of  $2 \times 10^5$  cells/well and let adhere overnight. Cells were then treated with the acidic medium for the different time points. Cells were trypsinized at specific time points and stained with trypan blue to assess the live/dead cell counts following counting on a haemocytometer. Data from treated cells with acidic pHe was compared to those from PANC-1 and Mia PaCa-2 cells kept in pHe 7.4. Three independent experiments were performed for each experimental condition.

### **6. Cell-matrix adhesion assay**

Adhesion assays quantified the ability of PDAC cells to remain adhered to 1% gelatin-coated wells when exposed to a detachment force. PANC-1 and Mia PaCa-2 cells were plated in 96-well plates at a density of 3000 cells/well, and 6000 cells/well, respectively, in 100  $\mu$ l of the appropriate growth medium containing 10% FBS. PANC-1 and Mia PaCa-2 were incubated at 37°C and 5% CO<sub>2</sub> for 1 and 2 hours, respectively, to let the cells adhere to the well surface. Each condition of each independent experiment was performed in eight technical replicates. Media was discarded, and non-adherent cells were further removed with two washes with cold PBS containing Ca<sup>2+</sup> and Mg<sup>2+</sup>. Adherent cells were fixed with cold methanol for 15 minutes at 4°C, followed by two washes with

cold PBS containing  $\text{Ca}^{2+}$  and  $\text{Mg}^{2+}$ . Nuclei were stained with DAPI in PBS for 15 minutes at room temperature, and cells were then washed and kept in PBS. Image acquisition was performed using a Nikon Eclipse Ti fluorescence microscope (Nikon Corporation, Tokyo, Japan) with a 4× objective. Cell nuclei of adherent cells of 4 different fields per well were counted in ImageJ for a total of 32 images per condition/ biological replicate. The mean numbers of adherent cells obtained from the 32 images of each biological replicate were used for statistical analysis. Three independent experiments were performed for each condition tested.

## **7. Cell migration assays**

### **7.1 Single-cell time lapse videomicroscopy**

PANC-1 cells were plated in technical duplicate in 1% gelatin-coated wells at a density of 5000 cells/well in 500 ul volume in 24-well plates and incubated at 37°C overnight. Before time-lapse imaging, media was changed to remove detached cells. For time-lapse image acquisition, cells were kept at 37°C and under 5%  $\text{CO}_2$  in an incubator chamber (Okolab). Cells' random migration was followed in phase contrast illumination at 20X magnification using Eclipse Ti-E Nikon inverted microscope, selecting five representative fields per well, resulting in a total of ten fields per condition and each image stack containing 60 frames. Images were acquired every 10 minutes for 10 hours with a CCD video camera using NIS-Element software (Nikon). Image stacks were analysed with ImageJ software, and cells were manually tracked using the MtrackJ plugin. Dividing cells and cells exiting the recorded field were excluded from data analysis, and cells' migratory velocity was used as the parameter. Three independent experiments were performed for each experimental condition.

### **7.2 Transwell migration assay with and without pH gradient**

Transwell migration assays were performed using 6.4 mm cell culture inserts with 8  $\mu\text{m}$  pore-size polyethylene terephthalate (PET) membrane (Corning, Cat# 353097) placed into Falcon® 24-well Permeable Support Companion Plate (Corning, Cat# 353504). Cells were pretreated with 10  $\mu\text{g}/\text{mL}$  of cell cycle inhibitor mitomycin C for 2 hours before seeding. The lower chamber was

filled with 500  $\mu$ l of growth medium pH 7.4 or 6.6 containing 10% FBS.  $75 \times 10^3$  PANC-1 and  $10 \times 10^4$  Mia PaCa-2 cells/insert were seeded in 300  $\mu$ l of the corresponding pH target growth medium supplemented with 10% FBS. Thereby, we avoided a FBS gradient between the two compartments. The cells were allowed to migrate through the pores of the insert membrane overnight at 37°C and 5% CO<sub>2</sub>.

Regarding pH gradient experiments, one major limitation of the Transwell system is the inability to maintain a stable pH gradient throughout the experiment (18 hours). The pH gradient established by this system is transient due to the diffusion of the acidic medium to the lower compartment with pH 7.4, which dissipates the pH gradient. Measurements of the medium pH present in the upper chamber revealed that the pH gradient along the Transwell system starts to decrease within ~5 hours of the experiment in the absence of the matrigel coating. For these reasons, experiments with pH gradient were performed in a 5-hour time window, allowing the pH gradient to remain present (Supplementary Figure 3a). After incubation, cells were washed with PBS, and non-migrating cells were removed from the upper side of the membrane using a cotton swab; cell fixation with cold methanol for 15 minutes at 20°C was then performed. Cells were stained with 0.4% crystal violet solution at room temperature in the dark for 30 minutes and imaged under a light microscope (10 $\times$  magnification). Migrated cells were counted in five representative fields of view per condition. The mean numbers of cells obtained from the five images of each biological replicate were used for statistical analysis. Three independent experiments were performed for each experimental condition.

## **8. Cell invasion assays with and without pH gradient**

Transwell invasion assays were performed using 6.4 mm cell culture inserts with 8  $\mu$ m pore-size polyethylene terephthalate (PET) membrane (Corning, Cat# 353097) placed into Falcon® 24-well Permeable Support Companion Plate (Corning, Cat# 353504). Cells were pretreated with 10  $\mu$ g/mL of cell cycle inhibitor mitomycin C for 2 hours before seeding. The lower chamber was filled with 500  $\mu$ l of growth medium pH 7.4 or 6.6 containing 10% FBS.  $75 \times 10^3$  PANC-1 and  $10 \times 10^4$  Mia PaCa-2 cells/insert were seeded with matrigel coating (diluted in growth medium in ratio 1:5, Corning, Cat# 354230) in 300  $\mu$ l of the corresponding pH target growth medium supplemented

with 10% FBS. Thereby, we avoided a FBS gradient between the two compartments. The cells were allowed to invade through the pores of the insert membrane overnight at 37°C and 5% CO<sub>2</sub>.

Regarding pH gradient experiments, one major limitation of the Transwell system is the inability to maintain a stable pH gradient throughout the experiment (18 hours). The pH gradient established by this system is transient due to the diffusion of the acidic medium to the lower compartment with pHe 7.4, which dissipates the pH gradient. Measurements of the medium pH present in the upper chamber revealed that a substantial dissipation of the pH gradient occurred after ~7 hours in the presence of the matrigel coating. For these reasons, experiments with pH gradient were performed in a 5-hour time window, allowing the pH gradient to remain present (Supplementary Figure 3a). After incubation, cells were washed with PBS, and non-invasive cells were removed from the upper side of the membrane using a cotton swab; cell fixation with cold methanol for 15 minutes at 20°C was then performed. Cells were stained with 0.4% crystal violet solution at room temperature in the dark for 30 minutes and imaged under a light microscope (10× magnification). Invasive cells were counted in five representative fields of view per condition. The mean numbers of cells obtained from the five images of each biological replicate were used for statistical analysis. Three independent experiments were performed for each experimental condition.

## **9. Invadopodia activity assay**

Invadopodia focal ECM digestion experiments were conducted as previously described[43]. Cells were seeded onto a layer of 90% matrigel:10% collagen I (3.6 mg/ml matrigel and 0.4 mg/ml collagen I) in which quenched BODIPY linked to BSA (DQ-Green-BSA) was mixed at a final concentration of 30 µg/ml. The matrix mix was used to cover 12-mm round glass coverslips at the bottom of a 24-well plate. Matrigel containing the fluorescent dye was allowed to polymerize for 30 minutes in a humidified incubator at 37°C. Then, 30×10<sup>3</sup> cells/coverslip were seeded on the top of polymerized ECM at both pHe 7.4 and pHe 6.6 and incubated overnight. Cells were fixed with paraformaldehyde 3.7% in PBS, stained for F-actin with Phalloidin–Tetramethylrhodamine B isothiocyanate (1:5000 in 0.1% gelatin in PBS, Sigma-Aldrich Cat# p1951), and processed for immunofluorescence. Invadopodia-dependent ECM digestion was evaluated microscopically.

Invadopodia-ECM digestion emits green fluorescence on a black background, which quantitatively reflects their ECM proteolytic activity. The quantity of invadopodia ECM proteolysis for 100 cells was then calculated as follows:

$$\text{Digestion Index} = \% \text{ of cells positive for invadopodial ECM digestion} \times \text{mean pixel density of focal ECM digestion/cell.}$$

## 10. Cell transfection with siRNA

A double-pulse approach with Lipofectamine™ 3000 Reagent (Invitrogen) was used to transfect PDAC cells with siRNAs. Cells were plated the day prior the transfection in 6-well plates in order to reach 80% of confluency the day of transfection. The optimized cell density, siRNA concentration and lipofectamine are listed in Table 2, while the siRNA sequences are listed in Table 2.

Table 2. Optimized siRNA transfection protocol for PDAC cells in 6-multiwell plate

PDAC cell line	Cell density	Mix A	Mix B	siRNA final concentration (nM)	Final Volume (ml)
<b>PANC-1</b>	150×10 <sup>3</sup> /2 ml	125 µl SFM + 5 ul Lipofectamine™ 3000 Reagent	125 µl SFM + siRNA	50	2,5
<b>Mia PaCa-2</b>	200×10 <sup>3</sup> /2 ml	125 µl SFM + 5 ul Lipofectamine™ 3000 Reagent	125 µl SFM + siRNA	50	2,5

The day of the transfection, mix A was prepared in RPMI without FBS (SFM) and antibiotics. Mix B then was prepared without the P3000™ Reagent when diluting the siRNA. Mix A was mixed with Mix B, gently vortexed and kept for 12 minutes at room temperature. During the incubation time, cell culture medium was replaced in each well and 2,250 ml of fresh RPMI

containing 10% FBS was added in each well. After the incubation time, 250  $\mu$ l of the Mix A+B was added as drop in each well. The entire process was repeated for the double pulse the following day and the experiments were performed 48h following the second pulse.

Table 3. List of siRNA sequences.

siRNA	Sequence Forward (5' to 3')	Sequence Reverse (5' to 3')
Control siRNA duplex negative control	Cat. Number: SR-CL000-005 (Eurogentec)	/
siORAI1	UGAGCAACGUGCACAUCU	AGAUUGUGCACGUUGCUCU

## 11. Protein expression analysis

### 11.1 Protein extraction and quantification

PANC-1 and Mia PaCa-2 cells were washed with ice-cold PBS and lysed in RIPA buffer (1% Triton X-100, 0.1% sodium deoxycholate, 150 mM NaCl, 20 mM PO<sub>4</sub>Na<sub>2</sub>/K, pH 7.2, 5 mM EDTA) containing protease (10  $\mu$ l/ml) and phosphatase inhibitor (1:10 from stock 10X) cocktails (Sigma-Aldrich and Thermo Scientific™, respectively). Cells were kept in ice and scraped, and the protein lysates were collected in a cold Eppendorf, vortexed and left on ice for 30 minutes. Protein lysates were then sonicated (3 cycles of 10 seconds), centrifuged for 10 minutes at 12000 rpm at 4°C for pelleting cell debris, and the supernatant was collected in a new Eppendorf. All protein lysates were conserved at -20°C. Protein concentrations were determined with the Bicinchoninic Acid protein assay (Thermo Fisher Scientific), and 30  $\mu$ g of denatured protein lysate for each condition was used.

### 11.2 Western Blot

Samples were loaded in sodium dodecyl sulfate-polyacrylamide gels (7 or 12%) of 1.5-mm thickness and electrophoresed in tris-glycine migration buffer (25 mM tris base, 192 mM glycine,



and 0.1% SDS, pH 8.3-8.5) at 80 V in stacking gel and 120 V in resolving gel. Protein samples were transferred from the polyacrylamide gel onto a nitrocellulose membrane using a Pierce G2 Fast Blotter System (Thermo Scientific) at 2.5 V and 3 A constant for 15 minutes. Nitrocellulose membranes were blocked with 3% BSA in 1X TNT buffer (15 mM Tris-HCl, 140 mM NaCl, 0.05% Tween 20, pH 7.5) for 1 hour at room temperature followed by an overnight incubation at 4°C with the following specific primary antibodies preparing in 3% BSA in 1X TNT supplemented with 0.02% sodium azide: anti-E-cadherin (1:1000, Cat# MAB3199), anti-N-cadherin (1:200, Cat# SC59987), anti-Vimentin (1:1000, Cat# SC5565), anti-Actin (1:1000, Cat# A5441), anti-Calnexin (1:1000, Cat# MAB3126). Following overnight incubation, three washes of 5 minutes each and one wash of 10 minutes in 1X TNT were performed before membranes were incubated with 3% BSA in TNT solution containing goat anti-rabbit IgG (Jackson ImmunoResearch, Cat# 211-032-171, 1:50,000) or goat anti-mouse IgG (Jackson ImmunoResearch, Cat# 115-035-174, 1:25,000) horseradish peroxidase-conjugated secondary antibodies for 1 hour at room temperature. Membranes were then washed for 3×5 minutes and 1×10 minutes in 1X TNT. Peroxidase activity was revealed using SuperSignal West Dura or SuperSignal West Femto chemiluminescent substrate (Thermo Fisher Scientific), according to the manufacturer's instructions. Chemiluminescent signals were captured on Amersham Imager 600 (GE Healthcare Life Sciences) and quantified using the densitometric analysis option in ImageJ/Fiji version 1.53 software. All band density values were normalized to  $\beta$ -actin or Calnexin, used as loading controls, and then compared to the control condition.

## **12. mRNA expression analysis**

### **12.1 RNA extraction and Reverse Transcription**

Total RNA was isolated from cultured PANC-1 and Mia PaCa-2 cell models using the NucleoSpin RNA Plus kit (Macherey Nagel Bioanalysis™) according to the manufacturer's instructions. RNA concentration was determined by absorbance at 260 nm, and quality control was performed by evaluating the absorbance at 260/280 nm ratio (for protein contamination) and at 260/230 nm (for solvent contamination). Reverse Transcription synthesized cDNA in a final 20- $\mu$ l

reaction mixture containing 2 µg total RNA, 1 µl dNTPs (10 mM) and 1 µl Random Hexamers (50 µM/100 µl) and water up to 12 µl. This hybridization mix was heated for 5 minutes at 65°C, then put in ice and centrifuged at 10000g for 30 seconds. The 7 µl-RT mix containing 4 µl 1x First strand buffer, 1 µl RNase inhibitor (20 U/µl) and 2 µl DTT (0.1 M) was added to the hybridization mix and incubation at 37°C for 2 minutes and finally 1 µl M-MLV reverse transcriptase (200 U) were added. After 10 minutes incubation at room temperature for hybridization, an elongation step followed by incubating the reaction mixture at 37°C for 50 min, which activates the M-MLV reverse transcriptase for cDNA synthesis start. This step was followed by a 15-minutes long incubation at 70°C for inactivating the enzyme. Reaction mixture was then put in ice, centrifuged at 10000g for 30 seconds and stored in -80°C.

## 12.2 qPCR

Real-time qPCR was performed in a 20 µl-reaction mixture containing 5 µl cDNA (10ng/µl), 10 µl SYBR™ Green PCR Master Mix (ThermoFisher Scientific), and 0.6 µl forward and reverse primers for each gene of interest (400 nM) and water. qPCR reactions were performed in technical triplicates. The primers used are listed in Table 4. The analysis was performed in a real-time thermal cycler Cfx C1000 (Bio-Rad). Hypoxanthine Phosphoribosyltransferase-1 (HPRT-1) was used for normalization. Relative mRNA levels were quantified using the  $2^{-\Delta\Delta CT}$  method.

Table 4. List of primers sequences used for qPCR.

Gene name	Primer probe	Sequence (5' to 3')
hORAI1	Forward	ATGGTGGCAATGGTGGAG
	Reverse	CTGATCATGAGCGCAAACAG
hORAI2	Forward	GCAGCTACCTGGAAGTGGTC
	Reverse	CGGGTACTGGTACTGCGTCT
hORAI3	Forward	AAGTCAAAGCTTCCAGCCGC

	Reverse	GGTGGGTACTCGTGGTCACTCT
hSTIM1	Forward	TGTGGAGCTGCCTCAGTAT
	Reverse	CTTCAGCACAGTCCCTGTCA
hE-cadherin	Forward	GAACGCATTGCCACATACAC
	Reverse	GAATTCGGGCTTGTTGTCAT
hN-cadherin	Forward	CCTGAGGGATCAAAGCCTGGAAC
	Reverse	TTGGAGCCTGAGACACGATTCTG
hVimentin	Forward	TCTACGAGGAGGAGATGCGC
	Reverse	GGTCAAGACGTGCCAGAGAC
hSnai1	Forward	CTTCCAGCAGCCCTACGAC
	Reverse	CGGTGGGGTTGAGGATCT
hTwist	Forward	AGCAAGATTCAGACCCTCAAGCT
	Reverse	CCTGGTAGAGGAAGTCGATGTACCT
hSlug	Forward	TGTTTGCAAGATCTGCGGC
	Reverse	TGCAGTCAGGGCAAGAAAA
hKi67	Forward	TGACCCTGATGAGAAAGCTCAA
	Reverse	CCCTGAGCAACACTGTCTTTT
hG0S2	Forward	AAGGGGAAGATGGTGAAGCTG
	Reverse	CTGCACACAGTCTCCATCAGG
hHPRT1	Forward	AGTTCTGTGGCCATCTGCTT
	Reverse	CAATCCGCCCAAAGGGA ACT

### 13. Intracellular pH measurements

The intracellular pH of PANC-1 cells was measured using fluorescent live-cell imaging (Axiovert TV100, Zeiss, Oberkochen, Germany) as described previously[42]. Cells were loaded with the fluorescent pH indicator 2',7'-bis(carboxyethyl)-5-carboxyfluorescein (BCECF-AM) (3  $\mu$ M) for up to 2 min. The excitation wavelength alternated between 490 nm and 440 nm. The emitted fluorescence was detected at 510 nm. The mean fluorescence of each cell was measured in 10

seconds intervals. Data acquisition and the polychromator (Visitron Systems, Puchheim, Germany) were controlled by the program VisiView (Visitron Systems). The cells were superfused with prewarmed (37°C) CO<sub>2</sub>/HCO<sub>3</sub><sup>-</sup>-buffered Ringer's solution (116 mM NaCl; 24 mM NaHCO<sub>3</sub>; 5,4 mM KCl; 0.8 mM MgCl<sub>2</sub>; 1,2 mM CaCl<sub>2</sub>; 5,5 mM Glucose) at pH 7.4. NaHCO<sub>3</sub> was lowered to 4.7 mM for pH 6.6. pH measurements were calibrated with a two-point calibration (130 mM KCl; 1.2 mM CaCl<sub>2</sub>; 0.8 mM MgCl<sub>2</sub>; 10 mM Hepes; 5.5 mM Glucose; pH 7.5 and pH 6.5; supplemented with 10 μM Nigericin) (Sigma-Aldrich, Merck KGaA, Darmstadt, Germany). For data analysis, the mean fluorescence intensity of the cell area was measured and corrected for background fluorescence. Afterward, the 490 nm/440 nm ratio was determined, and the pHi was calculated with a linear regression of pH 6.5 and 7.5.

## 14. RNA-sequencing and analysis

Total RNA was isolated from cultured PANC-1 cells using the NucleoSpin RNA Plus kit (Macherey Nagel Bioanalysis™) according to the manufacturer's instructions. Libraries for the RNA-Seq analysis were prepared with 200 ng of RNA using the Illumina Stranded mRNA Prep Kit according to the manufacturer's protocol. All the libraries were sequenced on an Illumina NovaSeq 6000 system using paired-end NovaSeq 6000 S2 Reagent Kit (200 cycles). Raw sequencing reads were first trimmed using BBDuk (from BBTools suite v35.85) to remove possible adapter contamination and then aligned to the reference genome (Ensembl Release 106) using STAR aligner v2.5. RSEM v1.3.0 was used to quantify transcript abundances, while differential expression analysis was carried out using the package DESeq2 v1.14.1 (in R/Bioconductor environment). False discovery rate (FDR) was controlled at level  $\alpha = 0.05$  through the Benjamini-Hochberg procedure. Genes with an adjusted p-value smaller than 0.05 and featuring a  $|\log_2FC| > 1$  were considered significantly deregulated. ToppFun web tool (from Topmen Suite, <https://toppgene.cchmc.org/>, accessed on 04 August 2022) was used to identify significantly overrepresented GO terms and pathways. Finally, log<sub>2</sub> fold changes determined with DESeq2 were used to rank genes for Gene Set Enrichment Analysis (GSEA v4.2.2) with the MSigDB database v2022.1.Hs (updated August 2022). Probes were collapsed into unique gene symbols before the analysis, and a standard

(weighted) enrichment statistic was chosen for the computation of the Normalized Enriched Score (NES). Within the context of the GSEA, the q-values cut-off was set to 0.25.

## 15. Calcium imaging

Ca<sup>2+</sup> imaging is a microscopy technique that allows to measure in real time the variations in intracellular Ca<sup>2+</sup> levels by using Ca<sup>2+</sup> indicators, fluorescent molecules that are able to chelate Ca<sup>2+</sup> ions and whose fluorescence properties are altered upon binding with the Ca<sup>2+</sup> ions. For assessing cytosolic Ca<sup>2+</sup> levels, we took advantage of a membrane-permeant derivative of Fura-2 called Fura-2 AM. This is a ratiometric fluorescent dye that it is able to cross the cell plasma membranes and, once in the cytosol, cellular esterases remove the acetoxymethyl groups to generate Fura-2, which is now retained in the intracellular space. This Ca<sup>2+</sup> indicator possesses an excitation spectrum at 380 nm when it is not binding Ca<sup>2+</sup> ions. When it is in the Ca<sup>2+</sup>-bound form, the excitation spectrum is shift to 340 nm. Independently of the absence or presence of Ca<sup>2+</sup> ions, Fura-2 shows a single emission wavelength at 510 nm. This indicates that rises in intracellular Ca<sup>2+</sup> levels excites the fluorescent probe in the 340 nm, along with a reduction in the fluorescence intensity at 380 nm from the Ca<sup>2+</sup>-free form. The ratio of the emissions at 340 and 380 is therefore a direct indicator of the intracellular Ca<sup>2+</sup> concentration. The double emission spectra indicates that Fura-2 is a ratiometric probe, and the use of the 340/380 ratio allows to cancel variables such as local differences in Fura-2 concentration and cell thickness.

Cells were plated in glass coverslips to reach an 80% confluency the day of the experiment. The cells were then loaded with 5 uM Fura-2 AM (Interchim, Cat# FP-42776C) diluted in cell culture medium and incubated for 45 minutes at 37 °C and 5% CO<sub>2</sub>. The cells were then gently washed three times with standard Hank's Balanced Salt solution (HBSS) (composition: 140 mM NaCl, 5 mM KCl, 2 mM CaCl<sub>2</sub>, 1 mM MgCl<sub>2</sub>, 0.3 mM NaH<sub>2</sub>PO<sub>3</sub>, 0.4 mM KH<sub>2</sub>PO<sub>4</sub>, 10 mM N-(2-hydroxyethyl)-piperazine-N'-ethanesulfonic acid (HEPES), 5 mM glucose, pH adjusted to 7.35 with NaOH) before fluorescence acquisition. Coverslips were then transferred to POCmini-2 Cell chambers on the stage of an Eclipse Ti-inverted series microscope (Nikon) and measurements were performed using an S Fluor 20×/0.75 NA objective lens (Nikon), by exciting Fura-2 fluorescence alternatively at 340 and 380 nm with a monochromator (Polychrome IV, TILL Photonics GmbH)

and collected at 510 nm through a CCD camera (QImaging) controlled with Metafluor software (Molecular Devices). Calcium imaging traces were analysed with Clampfit 10.7 software (Molecular Devices) and GraphPad Prism 7 software (GraphPad Corporation).

### **15.1 Ca<sup>2+</sup> oscillations induction protocol and analysis**

For Ca<sup>2+</sup> oscillations protocol, cells were starved overnight in serum-free RPMI 1640 (pH<sub>e</sub> 7.4 or pH<sub>e</sub> 6.6) the day prior the experiment. Following loading with Fura-2 and incubation, cells were washed three times in HBSS containing 2 mM Ca<sup>2+</sup> and the coverslips mounted in the POCmini-2 Cell chamber and observed at the microscope. Cells were maintained in 2 mM Ca<sup>2+</sup> solution for 100 seconds, in order to measure basal Ca<sup>2+</sup> concentrations. At 100 seconds, a HBSS solution containing 10% FBS was administered, and the Fura-2 emission signals were recorded for at least 500 seconds. For assessing the effect of acute treatment with acidic pH<sub>e</sub>, cells were bathed in HBSS solution pH 6.6 + 10% FBS at 600 seconds and the Ca<sup>2+</sup> signals were recorded for at least 200 seconds. The effect of Synta66 on Ca<sup>2+</sup> oscillations initiation was assessed by bathing the cells with HBSS + 10% FBS + 10 μM Synta66 at 100 seconds, while its effect on the maintenance of Ca<sup>2+</sup> oscillations was assessed by treating the cells with HBSS containing 10% FBS and 10 μM Synta66 at least 500 seconds following the Ca<sup>2+</sup> oscillations initiation. For the quantification of basal Ca<sup>2+</sup> levels and the mean Ca<sup>2+</sup> peak amplitude, we considered the same time frame for all the conditions tested, assuming a Δt of 50 seconds for the basal Ca<sup>2+</sup> levels and a Δt of 500 seconds for the peak amplitudes.

### **15.2 Store-Operated Ca<sup>2+</sup> entry (SOCE) protocol and analysis**

For SOCE protocol, we employed the irreversible SERCA pump inhibitor thapsigargin (TG) in Ca<sup>2+</sup>-free HBSS solution to induce Ca<sup>2+</sup> release and emptying of the ER stores. Following addition of HBSS solution containing 2 mM Ca<sup>2+</sup> maximally activates SOCE. Following loading with Fura-2 and incubation, cells were washed three times in HBSS containing 2 mM Ca<sup>2+</sup> and the coverslips mounted in the POCmini-2 Cell chamber and observed at the microscope. Cells were maintained in 2 mM Ca<sup>2+</sup> solution for 100 seconds, in order to measure basal Ca<sup>2+</sup> concentrations. At 100 seconds, a Ca<sup>2+</sup>-free HBSS solution was administered, while at 200 seconds cells were

bathed with Ca<sup>2+</sup>-free HBSS solution containing 2 μM TG. The 2 mM Ca<sup>2+</sup> solution was re-introduced following the complete emptying of the ER Ca<sup>2+</sup> stores and the stabilization of the Ca<sup>2+</sup> signals, around 500-600 seconds. SOCE signals were recorded for 300 seconds. To evaluate the effects of acute exposition to pH 6.6 solution, HBSS acid solution was administered following SOCE and recorded for 200 seconds.

For the quantification of basal Ca<sup>2+</sup> levels, a Δt of 50 seconds was considered for all the conditions, while for the mean peak amplitude and area of Ca<sup>2+</sup> release from ER was considered a Δt of 200 seconds. For the quantification of the mean peak amplitude and area of SOCE, Δt of 300 seconds was taken into consideration. Finally, the quantification of the SOCE signals in presence of acidic pH acute treatment was assessed by measuring the Ca<sup>2+</sup> signals in a time frame of 200 seconds, and these signals were compared to the 200 seconds immediately preceding the introduction of the acidic solution.

## 16. Statistical analysis

The data were analysed using GraphPad Prism 7 software (GraphPad Corporation). The Shapiro-Wilk normality test was used to assess the normality of distribution of the continuous variables, which were reported as mean and standard deviation (SD) or standard error of the mean (SEM). In contrast, non-normally distributed variables were reported as a median and 95% Confidence Interval. The Student's *t*-test was used to compare the means of two continuous variables with normal distribution. In contrast, the Mann-Whitney *U* test was used for non-normal distributed variables. Means of more than two groups of variables were compared using One-way ANOVA or Kruskal-Wallis *H*-test. A *p*-value < 0.05 was considered significant.

# Chapter III

## Results and discussion

### *I. Acidic growth conditions promotes epithelial-to-mesenchymal transition to select more aggressive PDAC cell phenotypes in vitro.*

Madelaine Magali Audero<sup>1,2</sup>, Tiago Carvalho<sup>3</sup>, Federico Ruffinatti<sup>2</sup>, Thorsten Loeck<sup>4</sup>, Maya Yassine<sup>1</sup>, Giorgia Chinigò<sup>2</sup>, Antoine Folcher<sup>1</sup>, Valerio Farfariello<sup>1</sup>, Albrecht Schwab<sup>4</sup>, Stephan J. Reshkin<sup>3</sup>, Rosa Angela Cardone<sup>3</sup>, Natalia Prevarskaya<sup>1†\*</sup> and Alessandra Fiorio Pla<sup>1,2†\*</sup>

<sup>1</sup> U1003—PHYCEL—Laboratoire de Physiologie Cellulaire, Inserm, University of Lille, Villeneuve d'Ascq, 59000 Lille, France; madelaine.audero@univ-lille.fr (M.M.A.); mhy06@mail.aub.edu (M.Y.); valerio.farfariello@inserm.fr (V.F.); antoine.folcher@inserm.fr (A.F.); alessandra.fiorio@unito.it (A.F.P.); natacha.prevarskaya@univ-lille.fr (N.P.)

<sup>2</sup> Laboratory of Cellular and Molecular Angiogenesis, Department of Life Sciences and Systems Biology, University of Turin, 10123 Turin, Italy; federicoalessandro.ruffinatti@unito.it (F.A.R.)

<sup>3</sup> Department of Biosciences, Biotechnologies and Environment, University of Bari, 70126 Bari, Italy; tiagomac94@gmail.com (T.C.); stephanjoel.reshkin@uniba.it (S.J.R.); rosaangela.cardone@uniba.it (R.A.C.)

<sup>4</sup> Institute of Physiology II, University of Münster, 48149 Münster, Germany; loeck@uni-muenster.de (T.L.); aschwab@uni-muenster.de (A.S.)

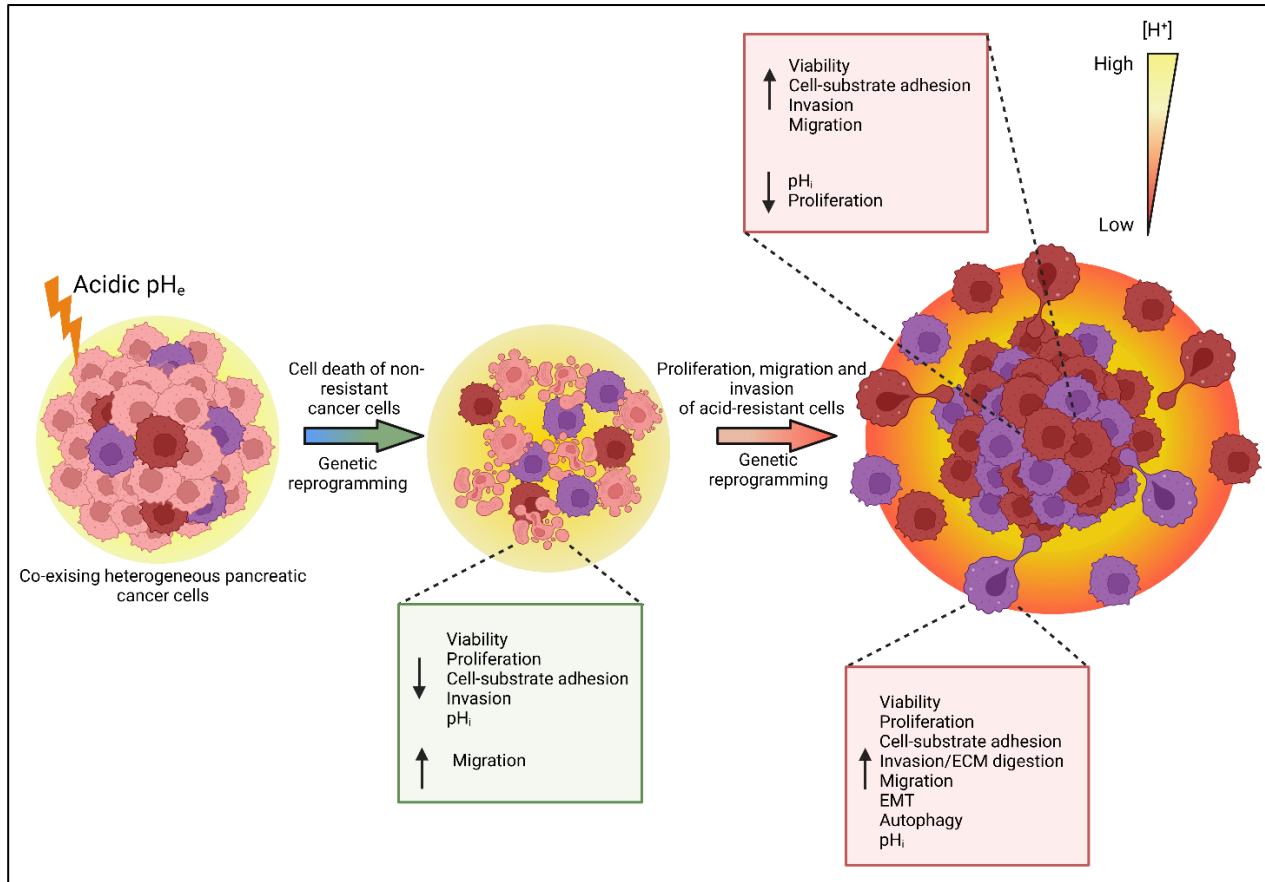
\* Correspondence: alessandra.fiorio@unito.it; Tel.: +39-0116704660, natacha.prevarskaya@univ-lille.fr; Tel.: +33-320336423

† These authors contributed equally to this work.

**Submitted to Cancers journal and currently under positive revisions.**



## Graphical Abstract



Extracellular acidosis is a feature of most solid tumors, including Pancreatic Ductal Adenocarcinoma (PDAC), result of a metabolic reprogramming that starts early in carcinogenesis and that results in the so-called “Warburg effect”, i.e., the selection for a highly glycolytic phenotype in cancer cells that finally leads to production and extrusion of lactate, which acidifies the tumor microenvironment. In addition, the aberrant vascularization that results in hypoxic areas and the  $CO_2$  hydration in better perfused tumor areas further contribute to the generation of a highly acidic tumor microenvironment (TME). Together with the overexpression of several  $pH$ -regulatory proteins, all the processes mentioned above determine a “reversed  $pH$  gradient” in cancer cells, considered a hallmark of cancer and promoter of several cancer-associated processes<sup>438</sup>. In the

context of PDAC, it is hypothesized that, in combination with PDAC driver mutations, the dynamic and physiological  $\text{pH}_e$  landscape in the pancreas provides pancreatic epithelial cells with the ability to survive to different  $\text{pH}_e$  conditions, favoring the adaptation and selection of acid-resistant and aggressive cancer cell phenotype, which may promote PDAC onset and/or progression<sup>286</sup>.

Due to the lack of a comprehensive evaluation of the effects of tumor acidosis-induced selection of PDAC cell lines, the aim of this work was to characterize the phenotypic changes occurring in PANC-1 and Mia PaCa-2 cells along the low  $\text{pH}_e$ -induced selection. To accomplish this, we established different cell models that were compared to control cells ( $\text{pH}_e$  7.4):

- 1) Cells exposed to short-term acidic treatment (4 days in  $\text{pH}_e$  6.6) to mimic the early stages of acidic selection.
- 2) Cell exposed to long-term acidic treatment (30 days in  $\text{pH}_e$  6.6).
- 3) Cell exposed to long-term acidic treatment (30 days in  $\text{pH}_e$  6.6) + recovery to  $\text{pH}_e$  7.4 for 2 weeks. This “metastatic” model was established to assess the impact of acid selection on local invasion.

We first demonstrated that acidic treatment affects PDAC cells’ morphology, and our *in vitro* results indicated that low  $\text{pH}_e$  is a stressor factor during the early stages of acid selection, increasing the percentage of cell death and impairing the proliferative and cell-matrix adhesive capacities of PDAC cells, leading to decreased cell invasion but, interestingly, enhanced single-cell and population cell motility. PANC-1 cells RNA-seq, which allowed us to identify the different genetic signatures of the short-term and long-term (and recovery to  $\text{pH}_e$  7.4) acid models, allowed us to confirm these results, as we observed the acid-induced increase of cell death-related genes expression and the decrease of cell proliferation, adhesion and invasion-related genes expression during the early stages of acid selection.







Along the acid selection period, the most acid-resistant and aggressive cancer subpopulation is selected via EMT, as demonstrated by an increase in the mRNA and protein levels of EMT markers and confirmed by dbEMT2 database. The acquisition of mesenchymal properties resulted in increased migration and cell invasion. Importantly, this aggressive phenotype is further accentuated when PDAC cells are re-exposed to physiological  $\text{pH}_e$ , that is when cells find themselves at the interface between tumor acidic regions and stroma, characterized by better blood perfusion and, therefore, less acidic. In this scenario, acid-selected and recovered to  $\text{pH}_e$  7.4 cells

showed enhanced proteolytic activity in correspondence of focal adhesion, indicative of ECM degradation. We further validated that different gene sets of cell proliferation, EMT, migration, invasion and ECM remodelling are linked to the acid-selected phenotypes recovered to physiological pH<sub>e</sub>.

Our work emphasizes the important of tumor acidosis in the selection of cancer cells' phenotypes that show enhanced survival and aggressiveness in a hostile microenvironment. This tumor acidosis-mediated selection occurs via a genetic reprogramming that results in the acquisition of increased proliferative, mesenchymal, migratory and invasive properties, fundamental for PDAC progression.

## Article

# Acidic Growth Conditions Promote Epithelial-to-Mesenchymal Transition to Select More Aggressive PDAC Cell Phenotypes In Vitro

Madelaine Magali Audero <sup>1,2</sup>, Tiago Miguel Amaral Carvalho <sup>3</sup>, Federico Alessandro Ruffinatti <sup>2</sup>, Thorsten Loeck <sup>4</sup>, Maya Yassine <sup>1</sup>, Giorgia Chinigò <sup>2</sup>, Antoine Folcher <sup>1</sup>, Valerio Farfariello <sup>1</sup>, Samuele Amadori <sup>2</sup>, Chiara Vaghi <sup>2</sup>, Albrecht Schwab <sup>4</sup>, Stephan J. Reshkin <sup>3</sup>, Rosa Angela Cardone <sup>3</sup>, Natalia Prevarskaya <sup>1,\*,†</sup> and Alessandra Fiorio Pla <sup>1,2,\*,†</sup>

- <sup>1</sup> U1003—PHYCELL—Laboratoire de Physiologie Cellulaire, Inserm, University of Lille, Villeneuve d'Ascq, 59000 Lille, France
- <sup>2</sup> Laboratory of Cellular and Molecular Angiogenesis, Department of Life Sciences and Systems Biology, University of Turin, 10123 Turin, Italy
- <sup>3</sup> Department of Biosciences, Biotechnologies and Environment, University of Bari, 70126 Bari, Italy
- <sup>4</sup> Institute of Physiology II, University of Münster, 48149 Münster, Germany
- \* Correspondence: [natacha.prevarskaya@univ-lille.fr](mailto:natacha.prevarskaya@univ-lille.fr) (N.P.); [alessandra.fiorio@unito.it](mailto:alessandra.fiorio@unito.it) (A.F.P.); Tel.: +33-320336423 (N.P.); +39-0116704660 (A.F.P.)
- † These authors contributed equally to this work.

**Simple Summary:** Acidosis represents a key chemical marker of the Pancreatic Ductal Adenocarcinoma (PDAC) microenvironment (TME). It induces the selection of aggressive cancer cell phenotypes and promotes its progression. Here, we describe the impact of an acidic TME on different PDAC hallmarks such as proliferation, migration, extracellular matrix digestion, invasion, and epithelial–mesenchymal transition. This was executed after establishing a model of pH<sub>e</sub>-selected cells that were cultured for different time periods in an acidic environment and then re-acclimated back to pH<sub>e</sub> 7.4. Our findings show that the acid selection contributes to PDAC cells' response and adaptation to the hostile acidic microenvironment, which is a requirement for the acquisition of an aggressive phenotype of PDAC cells.



**Citation:** Audero, M.M.; Carvalho, T.M.A.; Ruffinatti, F.A.; Loeck, T.; Yassine, M.; Chinigò, G.; Folcher, A.; Farfariello, V.; Amadori, S.; Vaghi, C.; et al. Acidic Growth Conditions Promote Epithelial-to-Mesenchymal Transition to Select More Aggressive PDAC Cell Phenotypes In Vitro. *Cancers* **2023**, *15*, 2572. <https://doi.org/10.3390/cancers15092572>

Academic Editor: Jurgen Dittmer

Received: 16 November 2022

Revised: 28 March 2023

Accepted: 26 April 2023

Published: 30 April 2023



**Copyright:** © 2023 by the authors. Licensee MDPI, Basel, Switzerland. This article is an open access article distributed under the terms and conditions of the Creative Commons Attribution (CC BY) license (<https://creativecommons.org/licenses/by/4.0/>).

**Abstract:** Pancreatic Ductal Adenocarcinoma (PDAC) is characterized by an acidic microenvironment, which contributes to therapeutic failure. So far there is a lack of knowledge with respect to the role of the acidic microenvironment in the invasive process. This work aimed to study the phenotypic and genetic response of PDAC cells to acidic stress along the different stages of selection. To this end, we subjected the cells to short- and long-term acidic pressure and recovery to pH<sub>e</sub> 7.4. This treatment aimed at mimicking PDAC edges and consequent cancer cell escape from the tumor. The impact of acidosis was assessed for cell morphology, proliferation, adhesion, migration, invasion, and epithelial–mesenchymal transition (EMT) via functional in vitro assays and RNA sequencing. Our results indicate that short acidic treatment limits growth, adhesion, invasion, and viability of PDAC cells. As the acid treatment progresses, it selects cancer cells with enhanced migration and invasion abilities induced by EMT, potentiating their metastatic potential when re-exposed to pH<sub>e</sub> 7.4. The RNA-seq analysis of PANC-1 cells exposed to short-term acidosis and pH<sub>e</sub>-selected recovered to pH<sub>e</sub> 7.4 revealed distinct transcriptome rewiring. We describe an enrichment of genes relevant to proliferation, migration, EMT, and invasion in acid-selected cells. Our work clearly demonstrates that upon acidosis stress, PDAC cells acquire more invasive cell phenotypes by promoting EMT and thus paving the way for more aggressive cell phenotypes.

**Keywords:** acidic tumor microenvironment; acid-selection; PDAC; cell proliferation; cell adhesion; cell migration; cell invasion; EMT

## 1. Introduction

Pancreatic ductal adenocarcinoma (PDAC) is the most common neoplastic condition affecting the pancreas. It is characterized by an unsatisfactory 5-year survival rate of around 10%, far below that for other forms of solid cancer [1]. In the early stages, PDAC does not manifest itself with striking symptoms and lacks useful screening tests for evaluating asymptomatic patients. This condition often delays diagnosis, when metastases have usually/already spread throughout the body [2]. To date, there are no effective therapeutic options for PDAC. This is in part due to an immunosuppressive microenvironment and a strong desmoplastic reaction that occurs during tumor development [3]. Moreover, this type of cancer is distinguished by a characteristic chemical signature, an acidic extracellular microenvironment ( $\text{pH}_e < 6.5$ ), common to many other malignancies, which offers important cues for its progression and aggressiveness [4,5].

The PDAC acidic microenvironment is the result of a shift to glycolytic metabolism (the “Warburg effect”) that leads to the production and excretion of lactate and  $\text{H}^+$ , even in the presence of oxygen [4]. The excretion of these acidic products, together with the hydration of  $\text{CO}_2$ , the aberrant vascularization which causes a continuous hypoxic state, and the overexpression and activity of acid transporters, determine a “re-versed pH gradient” with cancer cells, in contrast to normal cells, showing an alkaline  $\text{pH}_i$  and acidic  $\text{pH}_e$ . This pH gradient reversal is now considered to be an emerging “hallmark of cancers” [6]. Additionally, the acidic PDAC microenvironment also finds its roots in the physiology of the exocrine pancreas, where the intermittent exposition of pancreatic ductal cells to stroma acidification results from their bicarbonate secretion across their apical membranes into pancreatic ducts. This has been considered to promote the adaptation of acid-resistant phenotypes aiding in PDAC initiation and progression in concomitance with driving mutations [4].

While the reversed pH gradient represents a driving force for cancer progression, tumor acidosis may disrupt this pH balance, fostering genomic instability and imposing considerable selective pressure on cells [7–10]. The acidic microenvironment of the tumor may negatively affect cancer cell survival [11,12] and promote the selection of acid-resistant cancer subclones characterized by defense mechanisms against acidotic stress, such as autophagy [13].

Moreover, an acidic  $\text{pH}_e$  in the tumor microenvironment represents an escape strategy for tumor cells to promote EMT, cell migration, and local invasion [5,13–22], posing a threat to the efficacy of PDAC therapy. The role of the acidic  $\text{pH}_e$  at the peritumoral regions has been previously described by the Gillies group [17,21]. It plays a role in the degradation of the extracellular matrix at the periphery of the tumor and subsequent local invasion in melanoma and breast cancers [21]. In this complex tumor microenvironment, cells adapted to acidic  $\text{pH}_e$  survive due to adaptive mechanisms.

While several teams have focused on the effects of short-term extracellular acidification on different cancer cell types [9,14,23–38], these have provided a limited understanding of how tumor cells respond to this acute acidic exposure. Moreover, as regarding the effects of long-term adaptation and selection to extracellular acidosis [13,15–17,39–42], few data are available on PDAC [43,44] and a clear role of acid selection in cell invasion still needs to be elucidated.

Due to the lack of a comprehensive characterization of the different cell phenotypes induced by acid selection in PDAC and, in particular, re-acclimation in physiological pH in pancreatic cancer, we aimed to describe the impact of the tumor acidic microenvironment on PDAC progression. We therefore established and characterized the different phenotypic alterations occurring in two PDAC cell lines (PANC-1 and Mia PaCa-2). Cells were subjected to a short-term (4 days) exposition to acidic  $\text{pH}_e$  ( $\text{pH}_e 6.6$ ), in order to mimic the early stages of  $\text{pH}_e$  selection and also a long-term (1 month) exposition, as the acidification of PDAC tumor microenvironment occurs over a sustained period. To evaluate the impact of acid selection on promoting local invasion, we also established a model of  $\text{pH}_e$ -selected cells recovered in  $\text{pH}_e 7.4$ . Our *in vitro* results, confirmed by RNA-seq, indicate that low  $\text{pH}_e$

acts as a stressor factor during the acute exposition, limiting PDAC cell growth and viability and impairing cell adhesion and invasion. This paves the way for a more aggressive cancer cell subpopulation, induced by the epithelial–mesenchymal transition. Migratory and invasive activity rise as the acid treatment progresses. Importantly, this process further enhances metastatic potential when cells are re-exposed to  $\text{pH}_e$  7.4 as can occur during local cyclic waves of acidification and alkalization. These data emphasize the importance of an extracellular acidification in cancer cell selection and adaptation to hostile environments that promotes the development of more aggressive PDAC cell phenotypes.

## 2. Materials and Methods

### 2.1. Cell Culture and Generation of PANC-1 and Mia PaCa-2 Acidic Phenotypes

Human pancreatic ductal adenocarcinoma PANC-1 cells were obtained from the Institute for Experimental Cancer Research, Christian-Albrecht-University (CAU) of Kiel, Germany. Mia PaCa-2 cells were purchased from the American Type Culture Collection (ATCC). Control cells were cultured as monolayers in RPMI 1640 growth medium (Gibco, Cat# 31870-025) supplemented with 10% FBS (Biochrom (Cambridge, UK); Cat# S0615), 2 mM L-Glutamine (Gibco (Carlsbad, CA, USA); Cat# 25030-024), 1 mM sodium pyruvate (Gibco; Cat# 11360039), and antibiotics (penicillin/streptomycin 100 U mL<sup>-1</sup>; Life Technologies, Inc. (Carlsbad, CA, USA); Cat# 15070-063). For pH adjustments of the cell culture media to  $\text{pH}_e$  6.6, RPMI 1640 powder medium (Sigma (Macquarie Park, NSW, Australia); Cat# R6504) was complemented with NaHCO<sub>3</sub>, according to the Henderson–Hasselbalch equation to derive the target  $\text{pH}_e$ . The osmolarity of the medium was balanced using NaCl. The different powder components were dissolved in UltraPure distilled water (Invitrogen (Waltham, MA, USA); Cat# 10977-035), and the resulting medium was filtered in a sterile environment and supplemented with 10% FBS (Biochrom; Cat# S0615), 1 mM sodium pyruvate (Gibco; Cat# 11360039), and antibiotics (penicillin/streptomycin 100 U mL<sup>-1</sup>; Life Technologies, Inc.; Cat# 15070-063). All cells were maintained at 37 °C in a humidified 5% CO<sub>2</sub> atmosphere.

For the generation of the acidic phenotypes, PANC-1 and Mia PaCa-2 cells were exposed to  $\text{pH}_e$  6.6 for different time periods by changing the media  $\text{pH}_e$  from 7.4 to 6.6. Control cells were cultured at  $\text{pH}_e$  7.4. For studying early stages of low  $\text{pH}_e$ - selection («4 days  $\text{pH}_e$  6.6» cells), freshly split PANC-1 and Mia PaCa-2 cells were cultured in  $\text{pH}_e$  6.6 medium for 4 days. PDAC mimicking cells (« $\text{pH}_e$ -selected» cells) were generated by a 1 month-long exposure to the acidic medium before performing the experiments.  $\text{pH}_e$ -selected + 7.4 cells were maintained in  $\text{pH}_e$  6.6 for 1 month before they were put back to  $\text{pH}_e$  7.4 for 2 weeks. Experiments requiring  $\text{pH}_e$ -selected + 7.4 cells were performed after a maximum of 2 weeks following recovery to  $\text{pH}_e$  7.4. Both  $\text{pH}_e$  7.4 and  $\text{pH}_e$  6.6 media were refreshed every other day, and acidic medium pH was monitored daily. For experiments requiring acute (1 h) exposition to acidic pH, an aliquot of  $\text{pH}_e$  6.6 medium was maintained at 37 °C under a humidified 5% CO<sub>2</sub> atmosphere for at least 1 h before the experiment to equilibrate the target  $\text{pH}_e$ .

### 2.2. Cell Proliferation and Viability

Proliferation of PANC-1 and Mia PaCa-2 cells was studied using EdU staining assay, MTS assay, trypan blue exclusion assay, and ATP quantification assay. For MTS assays, cells were plated in 96-well plates at a density of 3000 cells/well for PANC-1 and 8000 cells/well for Mia PaCa-2 cells in 100 µL medium, letting them adhere overnight. Cell media of correspondent pH was refreshed the following day and cell proliferation was assessed at 2 h, 24 h, 48 h, 72 h, and 96 h using MTS CellTiter 96<sup>®</sup> AQueous assay (Promega (Madison, WI, USA); Cat# G1111) following the manufacturer's instructions.

Cell proliferation was assessed via 5-ethynyl-2'-deoxyuridine (EdU) incorporation using Click-iT EdU Alexa Fluor 647 Imaging Kit (Invitrogen; Cat# C10340). Briefly, the different PANC-1 and Mia PaCa-2 cell models were plated for 4 days in their corresponding  $\text{pH}_e$  conditions in 1% gelatin-coated coverslips inserted in 6-well plates. The culture

medium was refreshed every two days, and cells were incubated with 20  $\mu$ M EdU for 2 h at 37 °C. Cells were then washed with phosphate-buffered saline (PBS; pH 7.4; Gibco; Cat# 10010-015) and fixed with 4% paraformaldehyde (PFA) at room temperature for 15 min. Following two washes with 3% bovine serum albumin (BSA)-containing PBS, cells were permeabilized with 0.5% Triton X-100 in PBS at room temperature for 20 min and washed twice with 3% BSA-containing PBS. Cells were then stained with 100  $\mu$ L Click-iT reaction cocktail per coverslip and incubated in the dark for 30 min. Following two washes with 3% BSA-containing PBS, cell nuclei were stained with Hoechst 33342 for 30 min and away from light. Coverslips were finally mounted on clean, microscope glass slides using Glycergel mounting medium (Dako (Santa Clara, CA, USA); Cat# C0563) and stored in the dark at 4 °C. The EdU-positive cells were visualized using a confocal laser scanning microscope (LSM 700; Carl Zeiss MicroImaging GmbH, Oberkochen, Germany) with a Plan Aplanachromat 40 $\times$ /1.3 numerical aperture oil-immersion objective. At least five photos per condition were taken, and positive cells were counted using ImageJ software (v1.54d).

Trypan blue exclusion assays were used to determine the viability of PANC-1 and Mia PaCa-2 cell models after exposition to pH<sub>e</sub> 6.6 for different time points (2 h, 24 h, 48 h, 72 h, and 96 h, 15 days, and 30 days). PANC-1 and Mia PaCa-2 cells were seeded in 6-well plates at a density of  $2 \times 10^5$  cells/well and allowed to adhere overnight. Cells were then treated with the acidic medium for the different time points. Cells were trypsinized at specific time points and stained with trypan blue to assess the live/dead cell counts following counting on a hemocytometer. Data from treated cells with acidic pH<sub>e</sub> were compared to those from PANC-1 and Mia PaCa cells kept in pH<sub>e</sub> 7.4. Three independent experiments were performed for each experimental condition.

### 2.3. Cell Adhesion

Adhesion assays quantified the ability of PDAC cells to remain adhered to 1% gelatin-coated wells when exposed to a detachment force. PANC-1 and Mia PaCa-2 cells were plated in 96-well plates at a density of 3000 cells/well, and 6000 cells/well, respectively, in 100  $\mu$ L of the appropriate growth medium containing 10% FBS. PANC-1 and Mia PaCa-2 were incubated at 37 °C and 5% CO<sub>2</sub> for 1 and 2 h, respectively, to allow the cells to adhere to the well surface. Each condition of each independent experiment was performed in eight technical replicates. Media was discarded, and non-adherent cells were further removed with two washes with cold PBS containing Ca<sup>2+</sup> and Mg<sup>2+</sup>. Adherent cells were fixed with cold methanol for 15 min at 4 °C, followed by two washes with cold PBS containing Ca<sup>2+</sup> and Mg<sup>2+</sup>. Nuclei were stained with DAPI in PBS for 15 min at room temperature, and cells were then washed and kept in PBS. Image acquisition was performed using a Nikon Eclipse Ti fluorescence microscope (Nikon Corporation, Tokyo, Japan) with a 4 $\times$  objective. Cell nuclei of adherent cells of 4 different fields per well were counted in ImageJ for a total of 32 images per condition/biological replicate. The mean numbers of adherent cells obtained from the 32 images of each biological replicate were used for statistical analysis. Three independent experiments were performed for each condition tested.

### 2.4. Cell Migration and Cell Invasion

Transwell migration and invasion assays were performed using 6.4 mm cell culture inserts with 8  $\mu$ m pore-size polyethylene terephthalate (PET) membrane (Corning (New York, NY, USA), Cat# 353097) placed into Falcon® 24-well Permeable Support Companion Plate (Corning, Cat# 353504). Cells were pretreated with 10  $\mu$ g/mL of cell cycle inhibitor mitomycin C for 2 h before seeding. The lower chamber was filled with 500  $\mu$ L of growth medium pH<sub>e</sub> 7.4 or 6.6 containing 10% FBS. The  $75 \times 10^3$  PANC-1 and  $10 \times 10^4$  Mia PaCa-2 cells/insert were seeded without Matrigel coating (migration assay) or with Matrigel (diluted in growth medium in ratio 1:5; Corning; Cat# 354230) coating in 300  $\mu$ L of the corresponding pH<sub>e</sub>-target growth medium supplemented with 10% FBS. Thereby, we avoided a FBS gradient between the two compartments. The cells were allowed to migrate

or invade through the pores of the insert membrane overnight (around 18 h) at 37 °C and 5% CO<sub>2</sub>.

Regarding pH gradient experiments, one major limitation of the Transwell system is the inability to maintain a stable pH gradient throughout the experiment (18 h). The pH gradient established by this system is transient due to the diffusion of the acidic medium to the lower compartment with pHe 7.4, which dissipates the pH gradient. Measurements of the medium pH present in the upper chamber revealed that the pH gradient along the Transwell system starts to decrease within ~5 h of the experiment in the absence of the Matrigel coating, while a substantial dissipation of the pH gradient occurred after ~7 h in the presence of the Matrigel coating. For these reasons, experiments with a pH gradient were performed in a 5-h time window, allowing the pH gradient to remain present (Figure S3a (Supplementary Materials)). After incubation, cells were washed with PBS, and non-migrating/invading cells were removed from the upper side of the membrane using a cotton swab; cell fixation with cold methanol for 15 min at –20 °C was then performed. Cells were stained with 0.4% crystal violet solution at room temperature in the dark for 30 min and imaged under a light microscope (10× magnification). Invasive cells were counted in five representative fields of view per condition. The mean numbers of cells obtained from the five images of each biological replicate were used for statistical analysis. Three independent experiments were performed for each experimental condition.

### 2.5. Immunofluorescence Staining

PANC-1 and Mia PaCa-2 cells were stained with fluorescent phalloxin to label F-actin for cell morphology studies. Cells were plated in their corresponding pHe conditions in 1% gelatin-coated coverslips inserted in 6-well plates at different densities to reach ~80% confluence on the day of the experiment. Cells were washed twice with PBS and fixed with 4% paraformaldehyde for 10 min at room temperature. After washing the samples twice with PBS, the fixed cells were incubated with a solution of 0.1% Triton X-100 in PBS (PBST) for 5 min at room temperature for permeabilization. Solutions were decanted, and two washes with PBS followed. Fixed cells were incubated with PBS containing 1% BSA for 30 min and then stained with a staining solution containing 2 units/coverslip of fluorescent Alexa 488 phalloidin (2 U/200 µL per coverslip; Invitrogen™; Cat# A12379) in 1% BSA in PBS for 20 min at room temperature. Cells were washed two times with PBS, and cell nuclei were stained with a solution of 1:1000 DAPI in PBS for 15 min at room temperature. Cells were washed twice with PBS and air dried, and the coverslips were mounted on clean microscope glass slides using Glycergel mounting medium (Dako; Cat# C0563) and stored in the dark at 4 °C. Glass slides were then examined using a confocal laser scanning microscope (LSM 700; Carl Zeiss MicroImaging GmbH) with a Plan Aplanachromat 40×/1.3 numerical aperture oil-immersion objective. The images were analyzed in Zeiss LSM Image Browser software.

### 2.6. Analysis of Cell Morphology: Cell Area and Cell Circularity

Cells were plated in the appropriate pHe-target medium and grown to approximately 80% confluency. Four random fields of each cell condition were imaged using a brightfield microscope (Nikon Eclipse TS100). ImageJ software quantified the cell area and circularity by manually segmenting the brightfield images. Over 500 cells for each condition were considered for the cell area and circularity analysis.

### 2.7. RNA Extraction and qPCR

Total RNA was isolated from cultured PANC-1 and Mia PaCa-2 cell models using the NucleoSpin RNA Plus kit (Macherey Nagel Bioanalysis™, Bethlehem, PA, USA), according to the manufacturer's instructions. RNA concentration and quality were determined by absorbance at 260 nm. Reverse Transcription synthesized cDNA in a 20-µL reaction mixture containing 2 µg total RNA, 10 mM dNTPs, 50 µM/100 µL Random Hexamers, 1× First strand buffer, 20U RNase inhibitor, 0.1 M DTT, and 200 U M-MLV reverse transcriptase.



Real-time qPCR was performed in a 20  $\mu$ L-reaction mixture containing 10 ng/ $\mu$ L cDNA, SYBR<sup>TM</sup> Green PCR Master Mix (ThermoFisher Scientific), and 400 nM forward and reverse primers for each gene of interest. qPCR reactions were performed in technical triplicates. The primers used are listed in Table 1. The analysis was performed in a real-time thermal cycler Cfx C1000 (Bio-Rad, Hercules, CA, USA). Hypoxanthine Phosphoribosyltransferase-1 (HPRT-1) was used for normalization. Relative mRNA levels were quantified using the  $2(-\Delta\Delta CT)$  method.

**Table 1.** List of primers for qPCR.

Gene Name	Primer Probe	Sequence (5' to 3')
hE-cadherin	Forward	GAACGCATTGCCACATACAC
	Reverse	GAATTCGGGCTTGTGTGCAT
hN-cadherin	Forward	CCTGAGGGATCAAAGCCTGGAAC
	Reverse	TTGGAGCCTGAGACACGATTCTG
hVimentin	Forward	TCTACGAGGAGGAGATGCCG
	Reverse	GGTCAAGACGTGCCAGAGAC
hSnail	Forward	CTTCCAGCAGCCCTACGAC
	Reverse	CGGTGGGGTTGAGGATCT
hTwist	Forward	AGCAAGATTCAGACCCTCAAGCT
	Reverse	CCTGGTAGAGGAAGTCGATGTACCT
hSlug	Forward	TGTTTGCAAGATCTGCCGG
	Reverse	TGCAGTCAGGGCAAGAAAAA
hKi67	Forward	TGACCCTGATGAGAAAGCTCAA
	Reverse	CCCTGAGCAACACTGTCTTTT
hG0S2	Forward	AAGGGGAAGATGGTGAAGCTG
	Reverse	CTGCACACAGTCTCCATCAGG
hHPRT1	Forward	AGTTCTGTGGCCATCTGCTT
	Reverse	CAATCCGCCCAAAGGGAAC

## 2.8. Protein Extraction and Western Blot

PANC-1 and Mia PaCa-2 cells were washed with ice-cold PBS and lysed in RIPA buffer (1% Triton X-100, 0.1% sodium deoxycholate, 150 mM NaCl, 10 mM  $\text{PO}_4\text{Na}_2/\text{K}$ , pH 7.4) containing protease and phosphatase inhibitor cocktails (Sigma-Aldrich and Thermo Scientific<sup>TM</sup>, respectively). Protein concentrations were determined with the Bicinchoninic Acid protein assay (Thermo Fisher Scientific, Waltham, MA, USA), and 30  $\mu$ g of denatured protein lysate was used for each condition. Samples were loaded in sodium dodecyl sulfate-polyacrylamide gels (7 or 12%) of 1.5-mm thickness and electrophoresed in tris-glycine migration buffer (25 mM tris base, 192 mM glycine, 0.1% SDS, pH 8.3–8.5) at 80 V in stacking gel and 120 V in resolving gel. Protein samples were transferred from the polyacrylamide gel onto a nitrocellulose membrane using a Pierce G2 Fast Blotter System (Thermo Scientific) at 2.5 V and a 3 A constant for 15 min. Nitrocellulose membranes were blocked with 3% BSA in 1X TNT buffer (15 mM Tris-HCl, 140 mM NaCl, 0.05% Tween 20, pH 7.5) for 1 h at room temperature followed by an overnight incubation at 4 °C with the following specific primary antibodies preparing in 3% BSA in 1X TNT supplemented with 0.02% sodium azide: anti-E-cadherin (1:1000, Cat# MAB3199), anti-N-cadherin (1:200, Cat# SC59987), anti-Vimentin (1:1000, Cat# SC5565), anti-Actin (1:1000, Cat# A5441), anti-Calnexin (1:1000, Cat# MAB3126). Following overnight incubation, three washes of 5 min each and one wash of 10 min in 1X TNT were performed before membranes were incubated with 3% BSA in TNT solution containing goat anti-rabbit IgG (Jackson ImmunoResearch (West Grove, PA, USA); Cat# 211-032-171, 1:50,000) or goat anti-mouse IgG (Jackson ImmunoResearch; Cat# 115-035-174, 1:25,000) horseradish peroxidase-conjugated secondary antibodies for 1 h at room temperature. Membranes were then washed for 3  $\times$  5 min and 1  $\times$  10 min in 1X TNT. Peroxidase activity was revealed using SuperSignal West Dura or SuperSignal West Femto chemiluminescent substrate (Thermo Fisher Scientific, Waltham, MA, USA), according to the manufacturer's instructions. Chemiluminescent signals were captured

on Amersham Imager 600 (GE Healthcare Life Sciences, Chicago, IL, USA) and quantified using the densitometric analysis option in ImageJ/Fiji version 1.53 software. All band density values were normalized to  $\beta$ -actin or Calnexin, used as loading controls, and then compared to the control condition.

### 2.9. Intracellular pH Measurements

The intracellular pH of PANC-1 cells was measured using fluorescent live-cell imaging (Axiovert TV100, Zeiss, Oberkochen, Germany) as described previously [45]. Cells were loaded with the fluorescent pH indicator 2'7'-bis(carboxyethyl)-5-carboxyfluorescein (BCECF-AM) (3  $\mu$ M) for up to 2 min. The excitation wavelength alternated between 490 nm and 440 nm. The emitted fluorescence was detected at 510 nm. The mean fluorescence of each cell was measured in 10 s intervals. Data acquisition and the polychromator (Visitron Systems, Puchheim, Germany) were controlled by the program VisiView (Visitron Systems). The cells were superfused with prewarmed (37 °C) CO<sub>2</sub>/HCO<sub>3</sub><sup>-</sup>-buffered Ringer's solution (116 mM NaCl; 24 mM NaHCO<sub>3</sub>; 5.4 mM KCl; 0.8 mM MgCl<sub>2</sub>; 1.2 mM CaCl<sub>2</sub>; 5.5 mM Glucose) at pH 7.4. NaHCO<sub>3</sub> was lowered to 4.7 mM for pH 6.6. pH measurements were calibrated with a two-point calibration (130 mM KCl; 1.2 mM CaCl<sub>2</sub>; 0.8 mM MgCl<sub>2</sub>; 10 mM HEPES; 5.5 mM Glucose; pH 7.5 and pH 6.5; supplemented with 10  $\mu$ M Nigericin) (Sigma-Aldrich, Merck KGaA, Darmstadt, Germany). For data analysis, the mean fluorescence intensity of the cell area was measured and corrected for background fluorescence. Afterward, the 490 nm/440 nm ratio was determined, and the pH<sub>i</sub> was calculated with a linear regression of pH 6.5 and 7.5.

### 2.10. Invadopodia Activity Assay: Fluorescent-Matrigel Layer Preparation and ECM Digestion Index Assay

Invadopodia focal ECM digestion experiments were conducted as previously described [46]. Cells were seeded onto a layer of 90% matrigel:10% collagen I (3.6 mg/mL Matrigel and 0.4 mg/mL collagen I) in which quenched BODIPY linked to BSA (DQ-Green-BSA) was mixed at a final concentration of 30  $\mu$ g/mL. The matrix mix was used to cover 12-mm round glass coverslips at the bottom of a 24-well plate. Matrigel containing the fluorescent dye was allowed to polymerize for 30 min in a humidified incubator at 37 °C. Then, 30  $\times$  10<sup>3</sup> cells/coverslip were seeded on the top of polymerized ECM at both pH<sub>e</sub> 7.4 and pH<sub>e</sub> 6.6 and incubated overnight. Cells were fixed with paraformaldehyde 3.7% in PBS, stained for F-actin with Phalloidin-Tetramethylrhodamine B isothiocyanate (1:5000 in 0.1% gelatin in PBS, Sigma-Aldrich Cat# p1951), and processed for immunofluorescence. Invadopodia-dependent ECM digestion was evaluated microscopically. Invadopodia-ECM digestion emits green fluorescence on a black background, which quantitatively reflects their ECM proteolytic activity. The quantity of invadopodia ECM proteolysis for 100 cells was then calculated as follows:

Digestion Index = % of cells positive for invadopodial ECM digestion  $\times$  mean pixel density of focal ECM digestion/cell.

### 2.11. RNA-Sequencing and Analysis

Total RNA was isolated from cultured PANC-1 cells using the NucleoSpin RNA Plus kit (Macherey Nagel Bioanalysis™), according to the manufacturer's instructions. Libraries for the RNA-Seq analysis were prepared with 200 ng of RNA using the Illumina Stranded mRNA Prep Kit (Illumina, Inc., San Diego, CA, USA), according to the manufacturer's protocol. All the libraries were sequenced on an Illumina NovaSeq 6000 system using paired-end NovaSeq 6000 S2 Reagent Kit (200 cycles). Raw sequencing reads were first trimmed using BBDuk (from BBTools suite v35.85) to remove possible adapter contamination and then aligned to the reference genome (Ensembl Release 106) using STAR aligner v2.5 [47]. RSEM v1.3.0 [48] was used to quantify transcript abundances, while differential expression analysis was carried out using the package DESeq2 v1.14.1 [49] in R/Bioconductor environment. False discovery rate (FDR) [50] was controlled at level

$\alpha = 0.05$  through the Benjamini–Hochberg procedure. Genes with an adjusted  $p$ -value smaller than 0.05 and featuring a  $|\log_2\text{FC}| > 1$  were considered significantly deregulated. The ToppFun web tool (from Topmen Suite, <https://toppgene.cchmc.org/>, accessed on 4 August 2022) was used to identify significantly overrepresented GO terms and pathways [51]. Finally,  $\log_2$  fold changes determined with DESeq2 were used to rank genes for Gene Set Enrichment Analysis (GSEA v4.2.2) with the MSigDB database v2022.1.Hs (updated August 2022) [52]. Probes were collapsed into unique gene symbols before the analysis, and a standard (weighted) enrichment statistic was chosen for the computation of the Normalized Enriched Score (NES). Within the context of the GSEA, the  $q$ -values cutoff was set to 0.25.

### 2.12. Statistical Analyses

The data were analyzed using GraphPad Prism 7 software (GraphPad Corporation, San Diego, CA, USA). The Shapiro–Wilk normality test was used to assess the normality of distribution of the continuous variables, which were reported as mean and standard deviation (SD) or standard error of the mean (SEM). In contrast, non-normally distributed variables were reported as a median and 95% Confidence Interval. The Student's  $t$ -test was used to compare the means of two continuous variables with normal distribution. In contrast, the Mann–Whitney  $U$  test was used for non-normal distributed variables. Means of more than two groups of variables were compared using One-way ANOVA or the Kruskal–Wallis  $H$ -test. A  $p$ -value  $< 0.05$  was considered significant.

## 3. Results

### 3.1. Extracellular Acidification Selection Affects PANC-1 Intracellular pH and PDAC Cell Line Morphology

The role of an acidic  $\text{pH}_e$  in determining phenotypic changes was assessed in PANC-1 and Mia PaCa-2 pancreatic cancer cell lines. They are characterized by a mesenchymal phenotype and are poorly differentiated [53]. We chose  $\text{pH}_e$  6.6 which is in the typical  $\text{pH}_e$  range of solid tumor areas ( $\text{pH}_e$  6.4 to 7.2), including pancreatic cancer [54]. The cells were subjected to  $\text{pH}_e$  6.6 for a short-term period («4 days  $\text{pH}_e$  6.6» cells) or long-term period (« $\text{pH}_e$ -selected» cells) to simulate and study the early and late stages of low  $\text{pH}_e$  selection (see also the Materials and Methods section for details) (Figure 1a). Moreover, to mimic the heterogeneity of the tumor pH landscape and, in particular, the tumor edges at the interface with peritumoral tissue, PDAC cell lines were recovered at  $\text{pH}_e$  7.4 after pH selection (« $\text{pH}_e$ -selected + 7.4» cells) (Figure 1a).

The first step in evaluating the role of the extracellular acidic tumor microenvironment was to monitor its effect on intracellular pH ( $\text{pH}_i$ ). It is a key parameter for all types of cells, profoundly affecting several cell processes, including those promoting cancer progression [7]. This value does not always correspond to the extracellular  $\text{pH}_e$  value in cancer cells but is influenced by it. Figure 1b shows the mean traces of PANC-1 cells' resting intracellular pH measurements, obtained by superfusing each cell model with  $\text{CO}_2/\text{HCO}_3^-$ -buffered Ringer's solution at the appropriate  $\text{pH}_e$  for 3 min. Extracellular acidification at  $\text{pH}_e$  6.6 treatment slightly influences the intracellular pH that became more acid compared to the control condition, although the difference is not statistically significant ( $\text{pH}_i$   $6.99 \pm 0.12$  control conditions;  $\text{pH}_i$   $6.72 \pm 0.10$  4 days  $\text{pH}_e$  6.6;  $\text{pH}_i$   $6.57 \pm 0.21$   $\text{pH}_e$ -selected cells). In contrast, recovery to  $\text{pH}_e$  7.4 following the 1-month-long  $\text{pH}_e$  6.6 treatment determines a significant cytosolic alkalinization compared to  $\text{pH}_e$ -selected cells, although not statistically significant compared to control cells ( $p$ -value = 0.50) ( $\text{pH}_i$   $7.31 \pm 0.17$ ) (Figure 1b,c). These results indicate that extracellular acidosis leads to a mild intracellular acidification, affecting PANC-1 cells exposed to acidic  $\text{pH}_e$  for extended periods. As opposed to this phenomenon, 1-month acidic treatment followed by a  $\text{pH}_e$  7.4 exposition recovers and alkalinizes the  $\text{pH}_i$ .

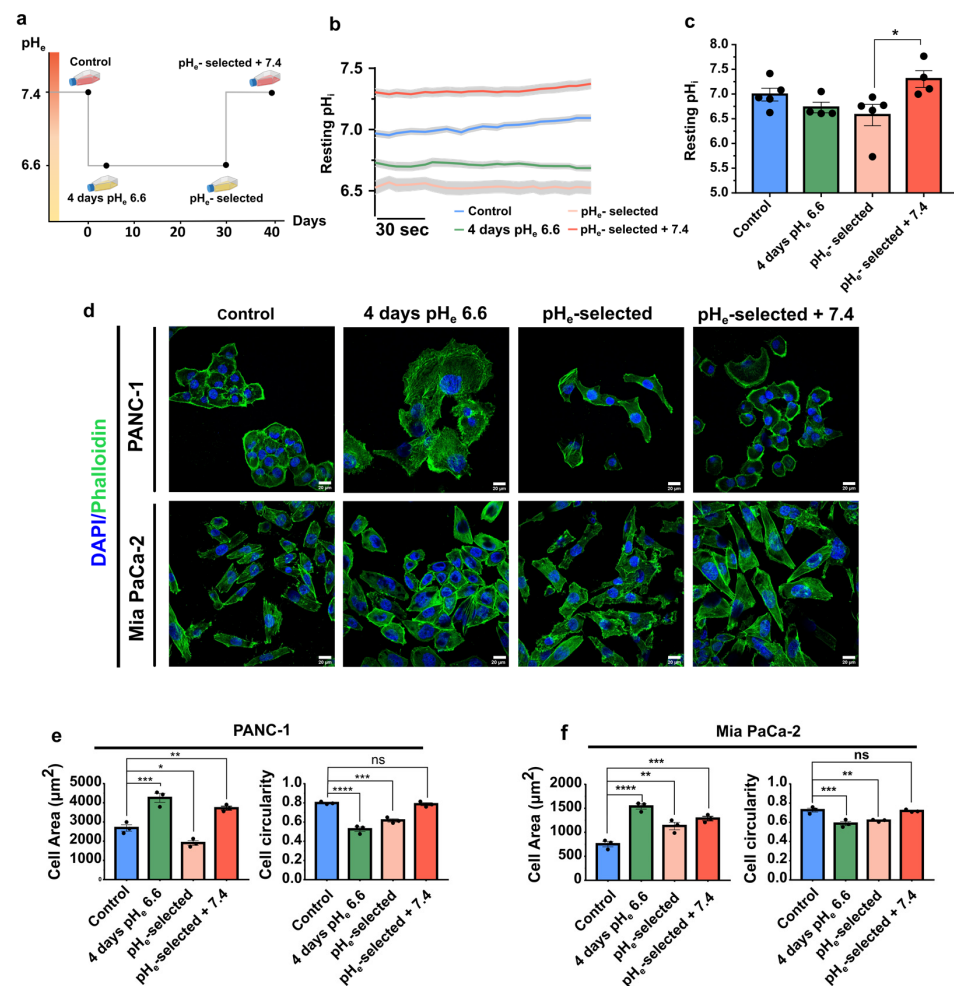


**Figure 1.** Effects of acidic  $pH_e$  on PANC-1 cells' intracellular pH and PDAC cells' morphology. (a) Scheme of the different acidic  $pH_e$  phenotypes established. Control cells were kept in physiological  $pH_e$  culture conditions ( $pH_e = 7.4$ ), while acidic phenotypes were constituted by PDAC cells exposed for different periods to acidic  $pH_e$ : 4 days (cell model named "4 days  $pH_e$  6.6"), 1 month ( $pH_e$ -selected), and 1-month long exposure followed by recovery to physiological  $pH_e$  for 2 weeks ( $pH_e$ -selected + 7.4). (b) Mean traces ( $\pm$  SEM) of at least 4 independent experiments illustrating the resting  $pH_i$  values in PANC-1 control cells (blue) and the different acidic phenotypes. Cells were loaded with 3  $\mu M$  BCECF, and  $pH_i$  values were recorded for 3 min as a fluorescent ratio (490/440 nm) changes following exposition to  $pH_e$  6.6 for 4 days (green), 1 month (light orange), and 1-month prior recovery to  $pH_e$  7.4 for 2 weeks (red). (c) Quantification of  $pH_i$  values in PANC-1 control and acidic phenotypes from 3 min recording. Each dot indicates the mean value of one independent experiment ( $n \geq 108$  cells for each condition). Data were analyzed using the Kruskal–Wallis  $H$ -test and Dunn's multiple comparison test, \*  $p < 0.05$ , ns = not significant. (d) Alexa Fluor 488-phalloidin (F-actin, green) and DAPI (nucleus, blue) staining of the different PANC-1 (top) and Mia PaCa-2 (bottom) cell models on a 1% gelatin-coated surface. Scale bar 20  $\mu m$ . (e) Quantification of cell area in  $\mu m^2$  (left) and cell circularity index (right) of the different PANC-1 and (f) Mia PaCa-2 cell models. Data were reported as mean ( $\pm$  SEM) of 5 representative regions per condition; 3 independent experiments were performed for each condition. Data were analyzed using One-way ANOVA with Dunnett's multiple comparisons test. \*  $p < 0.05$ , \*\*  $p < 0.01$ , \*\*\*  $p < 0.001$ , \*\*\*\*  $p < 0.0001$ , ns = not significant.

To examine the role of short- or long-term acidification on PDAC cell lines, we evaluated the morphology of PANC-1 and Mia PaCa-2 cells after labeling the cells with Alexa 488 phalloidin and DAPI (Figure 1d–f). Both cell lines display a more spread-out morphology in the initial days of the acidic  $pH_e$  exposure (4 days  $pH_e$  6.6), compared to control

cells (Figure 1d). This is accompanied by an increase in cell area and a decrease in cell circularity (Figure 1e,f, green bars). This spread-out and elongated shape is still maintained in PANC-1 and Mia PaCa-2 selected cells + 7.4 (Figure 1d–f, red bars). Interestingly, Mia PaCa-2 cells show similar behavior after 1-month of acid selection (Figure 1d,f, pink bars). This treatment induces a significant decrease in the cell area of PANC-1 cells (Figure 1d,e, pink bar).

### 3.2. Extracellular Acidification Decreases Cell Proliferation in PANC-1 and Mia PaCa-2 Cells

Cell proliferation is strictly regulated by the  $\text{pH}_e/\text{pH}_i$  ratio. We quantified DNA-synthesizing cells by using EdU incorporation, and the metabolic activity as an indication of the proliferative state of cells was quantified by MTS assay. The data showed a significant inhibition of both PANC-1 and Mia PaCa-2 cell proliferation by extracellular acidification independently of the time of acidic  $\text{pH}_e$  exposure. Indeed, the ratio of Edu positive/Hoechst cells is reduced and the absorbance of the MTS reagent is reduced in 4 days  $\text{pH}_e$  6.6 and  $\text{pH}_e$ -selected cells when compared to the control groups (Figure 2a–f, Figure S1a,b). Data were also confirmed by quantifying the ATP production (Figure S1c,d). Interestingly, a significant increase in the fraction of EdU-positive cells or increase in MTS absorbance is detected in  $\text{pH}_e$ -selected + 7.4 cells, demonstrating that  $\text{pH}_e$  7.4 treatment following long-term acid exposure enhances cell proliferation in both PDAC cell lines as compared to control conditions (Figure 2c–f).

The enhancement in cell viability in  $\text{pH}_e$ -selected cells after recovery at  $\text{pH}_e$  7.4 is further confirmed in PANC-1 by quantification of the ATP production by metabolically active cells. However, no significant differences are detected between Mia PaCa-2 control and  $\text{pH}_e$ -selected + 7.4 (Supplementary Figure S1a). The reduced proliferation observed in PANC-1 and Mia PaCa-2 cells following a 4 days-long treatment with acidic  $\text{pH}_e$  is the consequence of an increase in cell death, as detected by the trypan blue exclusion assay. The latter shows that the percentage of dead cells reaches almost 50% after 4 days in acidic  $\text{pH}_e$  media for PANC-1 cells and nearly 30% in Mia PaCa-2 cells (Figure 2g). However, this phenomenon appears to be overcome as the acidic treatment continued. After 15 days-long acidic treatment, the percentage of live cells recovers, reaching almost 90% after 1 month in low  $\text{pH}_e$  conditions (Figure 2h). These results indicate that acute acidification promotes significant cell death in both PDAC cell lines (Figure 2h) within the first 96 h after seeding, selecting a subpopulation of cells that outgrows and is viable under acidic conditions, with a higher proliferation rate as compared to non-selected PANC-1 cells (Figure 2e,\* and \$ symbol), which is consistent with more aggressive phenotype. To better clarify the acquired proliferative and more acid-resistant behavior of PDAC  $\text{pH}_e$ -selected + 7.4 cells, they were subjected to a 4-days long treatment with  $\text{pH}_e$  6.6. Cell viability was assessed at the end of the treatment, obtaining no significant differences in the percentage of live cells when compared with the same cells kept in  $\text{pH}_e$  7.4 and control cells (Figure 2i). These results indicate that PDAC control and  $\text{pH}_e$ -selected + 7.4 cells respond differently to low  $\text{pH}_e$ , thus suggesting a selection of acid-resistant cells whose phenotype is also maintained after recovering in  $\text{pH}_e$  7.4.



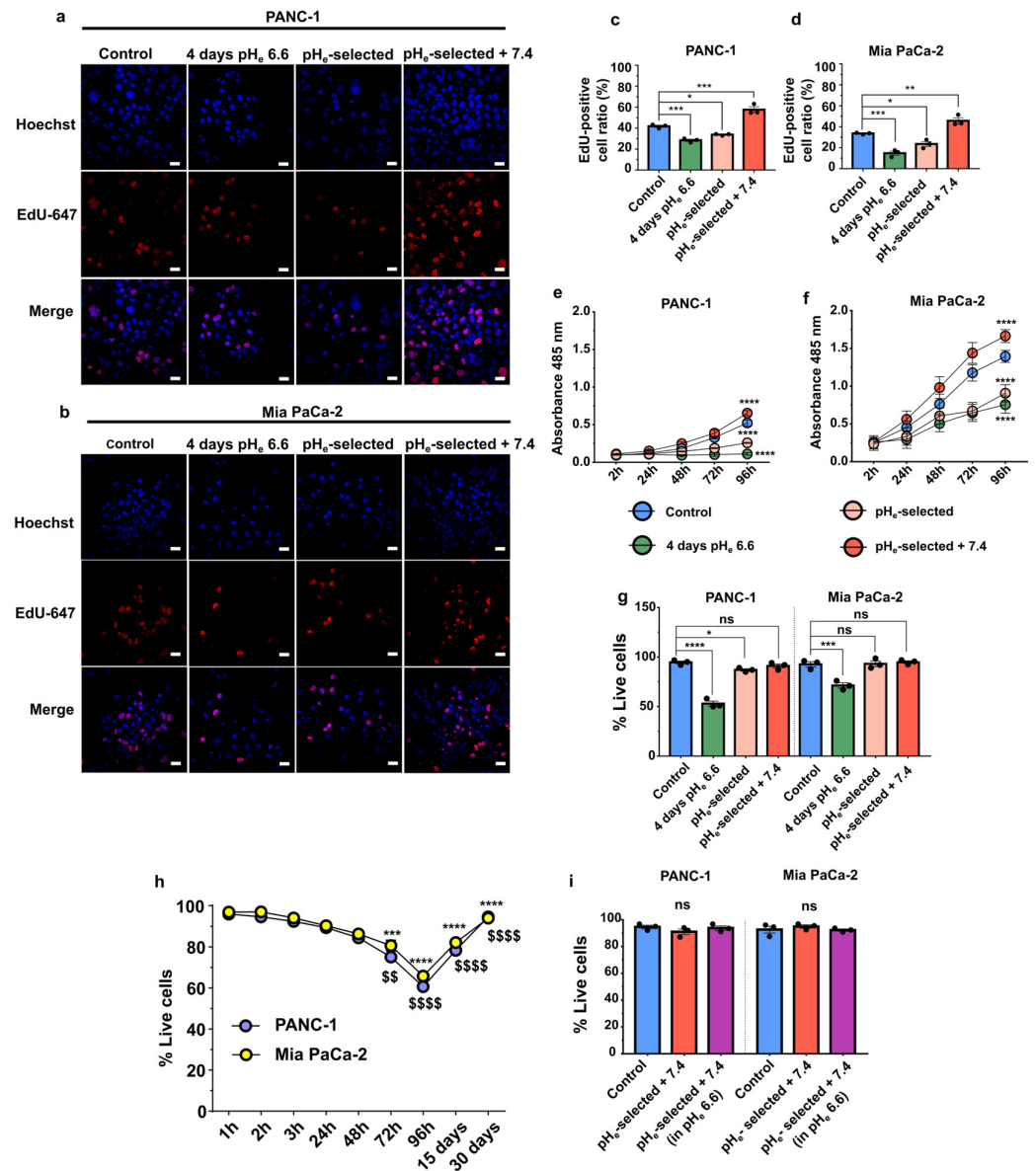


**Figure 2.** Effects of acidic pH<sub>e</sub> on PDAC cells' viability and proliferation. (a) Representative fluorescence images of PANC-1 and (b) Mia PaCa-2 cell proliferation obtained by EdU staining assay (red, Alexa Fluor 647) and Hoechst (blue) nuclear staining. Scale bar = 20 μm. (c) Quantification of the percentage of PANC-1 and (d) Mia PaCa-2 EdU-positive cells upon treatment with acidic pH<sub>e</sub>. Data were reported as the percentage of EdU/Hoechst-positive cell mean ± SEM from 4 representative regions for each condition. Time course of proliferation of the different models of (e) PANC-1 and (f) Mia PaCa-2 cells assessed by an MTS assay. Significant differences between control cells vs. all other conditions at 96 h. (g) Determination of PANC-1 (left) and Mia PaCa-2 (right) cell viability by trypan blue exclusion assay in control cells (pH<sub>e</sub> 7.4), 4 days pH<sub>e</sub> 6.6, pH<sub>e</sub>-selected (1 month in pH<sub>e</sub> 6.6) and pH<sub>e</sub> selected + 7.4 (1 month in pH<sub>e</sub> 6.6 followed by 2 weeks in pH<sub>e</sub> 7.4). (h) Time course of PANC-1 (blue) and Mia PaCa-2 (yellow) cell viability by trypan blue exclusion assay in control cells exposed to acidic pH<sub>e</sub> for different times. Significant differences in PANC-1 (\*) or Mia PaCa-2 cells (\$) at each time point of acidic treatment vs. 1 h. (i) Determination of PANC-1 (left) and Mia PaCa-2 (right) cell viability as assessed by trypan blue exclusion assay in control cells (pH<sub>e</sub> 7.4) and pH<sub>e</sub> selected + 7.4 (1 month in pH<sub>e</sub> 6.6 followed by 2 weeks in pH<sub>e</sub> 7.4) cells in pH<sub>e</sub> 7.4 and following 96 h treatment in pH<sub>e</sub> 6.6. Data were presented as mean ± SEM using One-way ANOVA with Dunnett's multiple comparisons test. All data shown were obtained from three independent experiments, \* *p* < 0.05, \*\* *p* < 0.01, \*\*\* *p* < 0.001, \*\*\*\* *p* < 0.0001, \$\$, *p* < 0.01, \$\$\$\$ *p* < 0.0001, ns = not significant.

### 3.3. Acid Selection at $pH_e$ 6.6 Promotes Adhesion, Migration, and Invasion of PANC-1 and Mia PaCa-2 Cells

The role of acidic  $pH_e$  on cell migration and invasion was initially investigated by studying their ability to adhere to gelatin. A period of 4 days of extracellular acidification significantly inhibits both PANC-1 and Mia PaCa-2 cell adhesion compared to the control condition (~50 % reduction; Figure 3a,b). The inhibitory effect of acidic  $pH_e$  is already present after 1 h of acidic exposure of PANC-1 cells growing at  $pH_e$  7.4 (control cells) (Figure S1e). On the contrary, one-month extracellular acidification ( $pH_e$ -selected cells) promotes an increase in PANC-1 and Mia PaCa-2 adhesion compared to their respective control groups. A similar positive effect on cell adhesion is observed on adhesion of PANC-1  $pH_e$ -selected + 7.4 cells (Figure 3a). However, surprisingly Mia PaCa-2  $pH_e$ -selected + 7.4 cells decrease their adhesion ability as compared to control (Figure 3b). Mia PaCa-2 cells are less sensitive to a 1 h acid treatment, which does not affect the adhesive properties of  $pH_e$ -selected cells (Figure S1f).

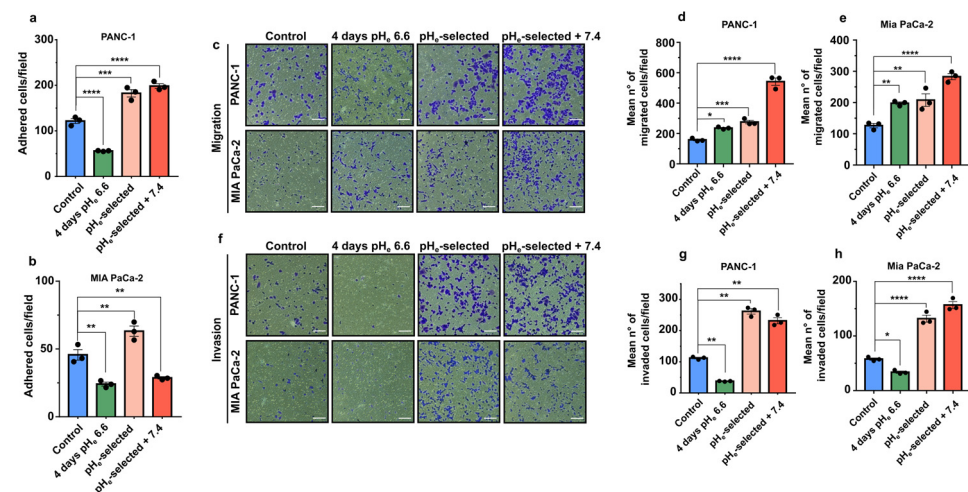


**Figure 3.** Effects of acidic  $pH_e$  on PDAC cell adhesion, migration, and invasion. (a) Quantification of PANC-1 and (b) Mia PaCa-2 cell adhesion assays. Cells were exposed to acidic conditions for different periods. Data were reported as mean  $\pm$  SEM from at least 4 representative regions for each condition. (c) Representative brightfield microscopic images of crystal violet-stained PDAC cell (in blue) that migrated through the transwell membrane in the migration assay. Scale bar = 100  $\mu$ m. Quantification of the mean number of migrated (d) PANC-1 and (e) Mia PaCa-2 cells determined in a transwell 18-h long migration assay. Data were reported as mean  $\pm$  SEM. (f) Representative images of PDAC cell models that invaded through the Matrigel-coated transwell membrane in the invasion assay. Scale bar = 100  $\mu$ m. Quantification of the mean number of invaded cells of the 18-h long transwell invasion assay in (g) PANC-1 and (h) Mia PaCa-2 cells. Data were reported as mean  $\pm$  SEM of three independent experiments and analyzed using One-way ANOVA with Dunnett's multiple comparisons test. All data shown were obtained from three independent experiments, \*  $p < 0.05$ , \*\*  $p < 0.01$ , \*\*\*  $p < 0.001$ , \*\*\*\*  $p < 0.0001$ .

In the second set of experiments, the migratory ability of PDAC cells was evaluated using Transwell migration assays. The data presented in Figure 3c–e show that cell migration is significantly enhanced during the early stages of  $pH_e$  treatment (4 days  $pH_e$  6.6) and in  $pH_e$ -selected cells, with a maximal effect in  $pH_e$ -selected + 7.4 (Figure 3c–e). Time-lapse video-microscopy assays were also performed to confirm the enhanced migratory activity at the single-cell level after 4 days of acidic  $pH_e$  treatment in PANC-1 cells (Figure S2a,b). This increase in PANC-1 cell migration nicely correlates with the higher recruitment of paxillin, a central Focal Adhesion (FA)-adaptor protein and a marker for nascent focal adhesion [55] toward the cell periphery and by larger FAs compared to control (Figure S2c–f).

The correlation between migratory cell properties and cell invasion was studied by using Matrigel-coated Transwell filters. Interestingly, early stages of acidic selection (4 days  $\text{pH}_e$  6.6) significantly inhibit the invasive abilities of both PANC-1 and Mia PaCa-2 cells (Figure 3f–h). The effect is reversed with a prolonged exposition to acidic  $\text{pH}_e$  conditions ( $\text{pH}_e$ -selected cells) at a similar rate as  $\text{pH}_e$ -selected + 7.4 cells (Figure 3f–h).

The role of  $\text{pH}_e$  selection on both migration and invasion in the context of a microenvironmental  $\text{pH}_e$  gradient was evaluated by experimentally establishing a  $\text{pH}_e$  gradient in the Transwell system. This experimental condition would mimic the interface between acidic cancer edges and neighboring healthy tissues and blood vessels. To simulate this situation, PDAC cells were plated in  $\text{pH}_e$  6.6 media and allowed to migrate or to invade (through the Matrigel coating) toward  $\text{pH}_e$  7.4 media overnight. Migration assay clearly demonstrates that all three acid-treated PDAC cell models (4 days  $\text{pH}_e$  6.6;  $\text{pH}_e$ -selected and  $\text{pH}_e$ -selected + 7.4) respond to the  $\text{pH}_e$  gradient more avidly than the control cells (Figure 4a–c). In contrast, invasion of PANC-1 and Mia PaCa-2 cells exposed to  $\text{pH}_e$  6.6 for a short term (4 days  $\text{pH}_e$  6.6 cells) along the alkalizing  $\text{pH}_e$  gradient is significantly inhibited compared to control cells (Figure 4d–f). On the contrary, prolonged treatment with acidic media enhances the invasion of both PDAC  $\text{pH}_e$ -selected cells towards the compartment filled with  $\text{pH}_e$  7.4 as compared to control. This invasive behavior is maintained in PANC-1 and Mia PaCa-2  $\text{pH}_e$ -selected + 7.4 cells (Figure 4d–f).

Cancer cells digest extracellular matrix (ECM) on their way to local or distant metastases. To accomplish this task, cells employ specialized structures called invadopodia, F-actin-rich membrane protrusions that mediate protease-dependent proteolysis of ECM components. Previous works have elucidated the critical role of extracellular acidosis in invadopodial function and invasion [46,56–60]. Therefore, we next assessed whether the extracellular acidosis could promote the invadopodia-mediated proteolytic degradation of the ECM by performing an in situ zymography in both PANC-1 and Mia PaCa-2 cells. To this purpose, cells were plated on quenched DQ-Green-BSA-containing Matrigel-coated slides the invadopodia-mediated focal ECM digestion was quantified via the measurement of the ECM Digestion Index (Figure 4g,h), which derives from the combination of % of cells positive for invadopodial ECM digestion  $\times$  mean pixel density of focal ECM digestion/cell (see Section 2.10) that are presented as single parameters in Figure S3b–e. The invadopodia-mediated ECM digestion assay was performed in both PDAC control and  $\text{pH}_e$ -selected + 7.4 cells subjected to an overnight exposition to acidic  $\text{pH}_e$  ( $\text{pH}_e$  6.6) or physiological  $\text{pH}_e$  ( $\text{pH}_e$  7.4) (same protocol as in Figure 4a–f). Acidic overnight treatment ( $\text{pH}_e$  6.6) of both PANC-1 and Mia PaCa-2 control cells reduces the invadopodial Digestion Index compared to control cells exposed to  $\text{pH}_e$  7.4 (Figure 4g,h). On the contrary, the Digestion Index is very much higher in both PANC-1 and Mia PaCa-2  $\text{pH}_e$ -selected + 7.4 cells compared to the control cells at  $\text{pH}_e$  7.4 and  $\text{pH}_e$  6.6. Moreover, extracellular acidosis further increases the Digestion Index of  $\text{pH}_e$ -selected + 7.4 cells compared to the same cells at physiological  $\text{pH}_e$ . Thus, prolonged exposure of PDAC cells to acidic conditions selects cells with higher proteolytic invadopodial activity, conferring a more aggressive and invasive phenotype to these cells.



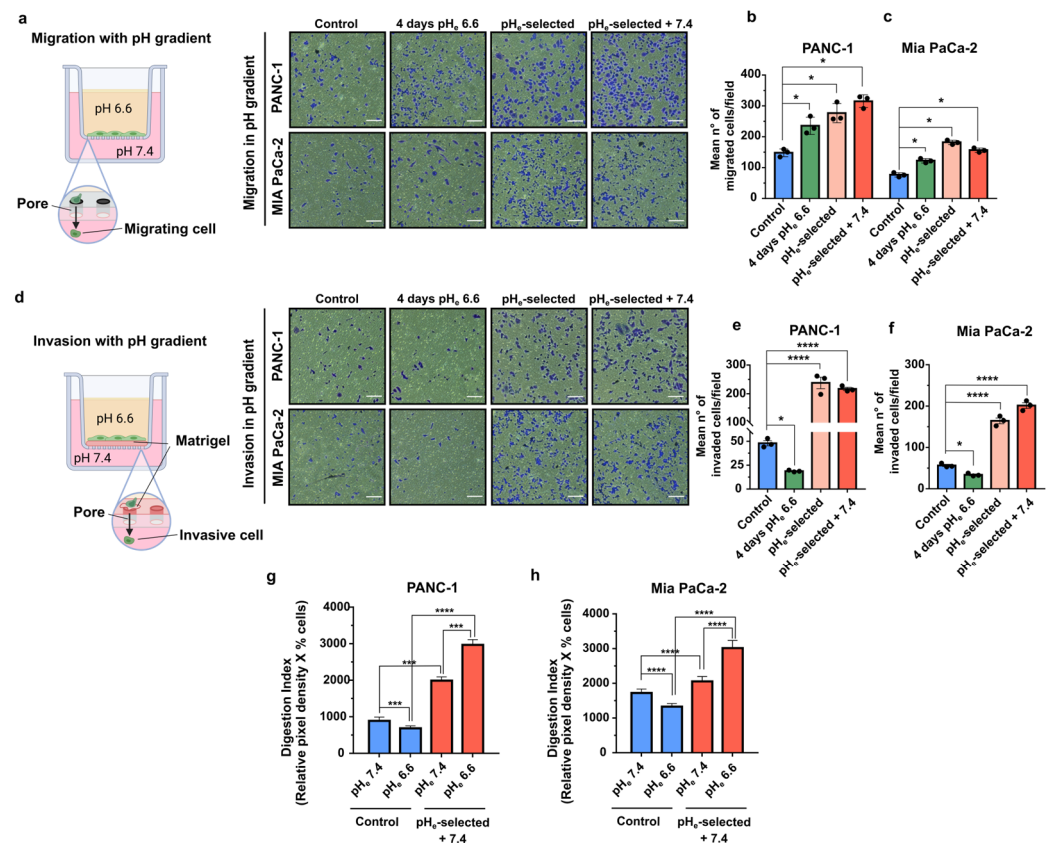


**Figure 4.** Effects of a pH<sub>e</sub> gradient on PDAC cells migration, invasion, and invadopodia activity. (a) Representative microscopic images of PDAC cells' migration assay, showing cells that migrated through the transwell membrane in a pH gradient, allowing cells to move from an acidic compartment to the pH 7.4 bottom part of the transwell. Scale bar = 100  $\mu$ m. (b) Quantification of the mean number of migrated cells of the transwell migration assay in PANC-1 and (c) Mia PaCa-2 cells in the presence of a pH gradient. (d) Representative microscopic images of PDAC cell invasion assay, showing cells that invaded through the Matrigel-coated transwell membrane in a pH gradient. Scale bar = 100  $\mu$ m. (e) Quantification of the mean number of invaded cells of the transwell invasion assay in PANC-1 and (f) Mia PaCa-2 cells in the presence of a pH gradient. (g) Effect of acidic pH<sub>e</sub> on the Digestion Index of both PANC-1 and (h) Mia PaCa-2 control and pH<sub>e</sub>-selected + 7.4 cells. The percentage of cells that produced invadopodia and their ECM degradation was determined by in situ zymography. The mean total invadopodia proteolytic activity was calculated as follows: Digestion Index = % of cells positive for invadopodia ECM digestion  $\times$  mean pixel density of focal ECM digestion/cell. Data were reported as mean and  $\pm$  SEM and analyzed using One-way ANOVA with Dunnett's multiple comparisons test with Tukey's multiple comparisons test for (g,h). All data shown were obtained from three independent experiments, \*  $p < 0.05$ , \*\*\*  $p < 0.001$ , \*\*\*\*  $p < 0.0001$ .

### 3.4. Effects of pH<sub>e</sub> 6.6 on Epithelial-Mesenchymal Transition and Proliferation Markers of PANC-1 and Mia PaCa-2 Cells

Considering the previous results and the more aggressive behavior showed by acid-selected cells, we assessed whether acidic pH<sub>e</sub>-induced selection determines the acquisition of mesenchymal properties in PDAC cell lines. Therefore, different EMT markers were evaluated at mRNA levels by qPCR. As previously demonstrated [53], PANC-1 and Mia PaCa-2 cell lines are characterized by low E-cadherin mRNA expression levels, which are not affected by the different acidic pH<sub>e</sub> exposures (Figure 5a,b and Figure S3f).

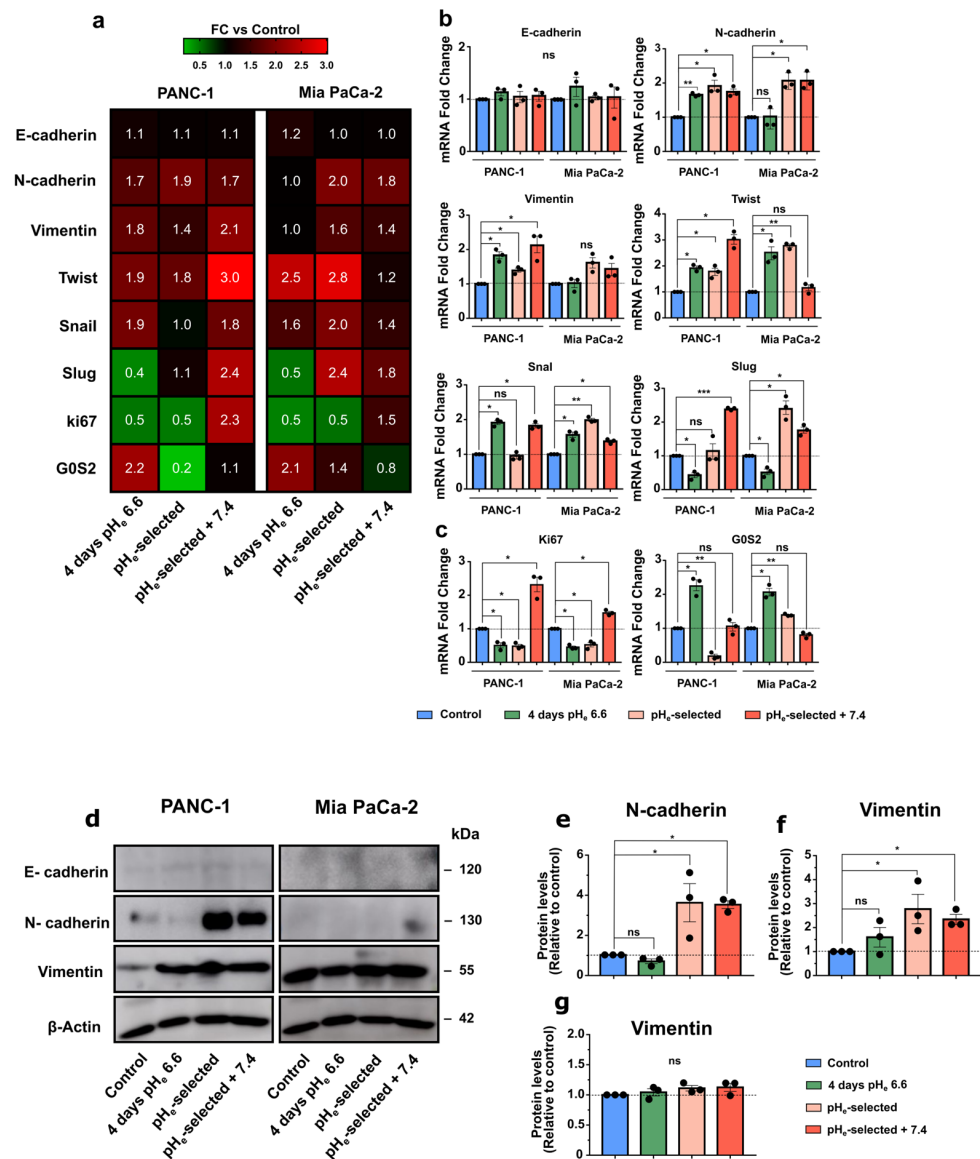


**Figure 5.** Effects of acidic pH<sub>e</sub> on epithelial–mesenchymal transition and proliferation markers of PDAC cell. (a) Heatmap of mRNA levels for epithelial–mesenchymal transition (EMT) markers in PANC-1 and Mia PaCa-2 cells. Columns represent each condition of the different PDAC cell lines, while rows indicate each differentially expressed gene. The value indicated is the mean value of the fold change of triplicate samples relative to control. Fold changes relative to control are visualized using a green-to-red gradient color scale. (b) mRNA expression levels of the different EMT markers and (c) proliferation (Ki67) and cell-cycle arrest (G0S2) markers in PANC-1 and Mia PaCa-2 cells subjected to acidic treatment for different periods and presented as fold change values, obtained by RT-qPCR. The effects of pH<sub>e</sub> 6.6 treatment on EMT and proliferation marker expression were compared with control samples (dotted lines). Fold changes were quantified using the 2<sup>-ΔΔCq</sup> method and normalized to HPRT reference gene. (d) Representative Western blot results that illustrate the effect of different times of exposure to acidic pH<sub>e</sub> on EMT proteins in PANC-1 and Mia PaCa-2 cells. (e) Relative densitometric quantification of Western blot results, showing the abundances of N-cadherin and (f) Vimentin proteins in PANC-1 cells and (g) Vimentin protein levels in Mia PaCa-2 cells compared to control conditions after normalization with β-actin. Data were presented as mean and ± SEM and analyzed using one-way ANOVA with Dunnett’s multiple comparisons test. All data reported were obtained from three independent experiments, \* p < 0.05, \*\* p < 0.01, \*\*\* p < 0.001, ns not significant. The uncropped blots are shown in Supplementary File S11—Uncropped Western Blots Membranes.

E-cadherin and N-cadherin mRNA expression levels were then validated at the protein level in both cell lines (Figure 5d,e). Although the PANC-1 cell line shows increased N-cadherin expression during the different exposures to acidic pH<sub>e</sub> at mRNA level (Figure 5a,b), it reaches significant protein upregulation only in pH<sub>e</sub>-selected + 7.4 cells (Figure 5d,e). Mia PaCa-2 cells follow a similar mRNA expression pattern in the different acidic conditions (Figure 5b). The acidic treatment-induced shift towards the acquisition of a more mesenchymal phenotype in PANC-1 and Mia PaCa-2 cells is confirmed by the increased mRNA expression of additional mesenchymal markers, Twist1 and Snail. (Figure 5a,b), while Vimentin mRNA levels are significantly increased in PANC-1 cells (Figure 5a,b) but not in Mia PaCa-2 cells, as confirmed by protein quantification (Figure 5d,g). Vimentin overexpression is confirmed by Western blot, showing a significant increase in PANC-1 cells exposed to 1 month to pH<sub>e</sub> 6.6 and those subsequently recovered to pH<sub>e</sub> 7.4 (Figure 5d,f). Both PDAC cell lines express Slug at low mRNA levels (Figure S3f). However, its gene downregulation is detected following 4 days-long acidic treatment (Figure 5a,b), while a clear upregulation emerges in pH<sub>e</sub>-selected cells recovered to pH<sub>e</sub> 7.4. These results reinforce the idea that the acidic tumor microenvironment promotes the acquisition of more aggressive cellular phenotypes via the epithelial–mesenchymal transition, especially in PANC-1 cells.

To further support the previous proliferation results (Figure 2 and Figure S1), PANC-1 and Mia PaCa-2 cells were tested for the mRNA expression of Ki67, an important proliferation marker, and G0S2, a protein involved in the maintenance of hematopoietic stem cells in a quiescent state [61] (Figure 5c). Ki67 upregulation is confirmed in PANC-1 and Mia PaCa-2 pH<sub>e</sub>-selected + 7.4 cells, indicating their enhanced proliferative potential compared to control cells, while its expression is decreased in 4 days- and 1-month-long acidic treatment (Figure 5c). Both PDAC cell lines exposed for 4 days to pH<sub>e</sub> 6.6 then display a proliferation arrest in the G0 phase, as demonstrated by the enhanced mRNA expression of the G0S2 marker. The reversibility of this cell-cycle arrest is shown by the progressive decrease in the G0S2 marker expression in cells following 1-month-long pH<sub>e</sub> 6.6 treatment and further recovered to physiological pH<sub>e</sub>, particularly in PANC-1 cells (Figure 5c).

### 3.5. Differential Transcriptomic Profiles in PANC-1 Cells in Response to Acidosis

To study the effects of the acidic pH<sub>e</sub> on gene expression profile in PANC-1 cells, RNA samples from control, 4 days pH<sub>e</sub> 6.6, and pH<sub>e</sub>-selected + 7.4 cell models were subjected to RNA-sequencing.

Raw paired-end reads were first trimmed to remove adapter contamination; then, STAR aligner was used with RSEM to obtain the count table at gene level as detailed in the Materials and Methods section. Principal component analysis (PCA) was conducted to check the consistency of the three experimental groups (Figure S4a,b); then, the DESeq2 Bioconductor package was used to assess differential gene expression. Our results lead to the identification of 772 differentially expressed genes (DEGs) in PANC-1 cells exposed for 4 days to pH<sub>e</sub> 6.6 compared to control samples (398 genes downregulated and 374 genes upregulated), while 989 DEGs are identified between control and pH<sub>e</sub>-selected + 7.4 samples (530 genes downregulated and 459 genes upregulated) (Figure 6a–d and Files S1 and S2 for the full DEG lists and the related statistics). Notably, just 134 genes (8.2% of the total DEGs) are in common between the two experimental conditions of pH<sub>e</sub> manipulation (see Venn diagram in Figure 6e), representing the transcriptional correlate of that specificity already observed through functional assays.

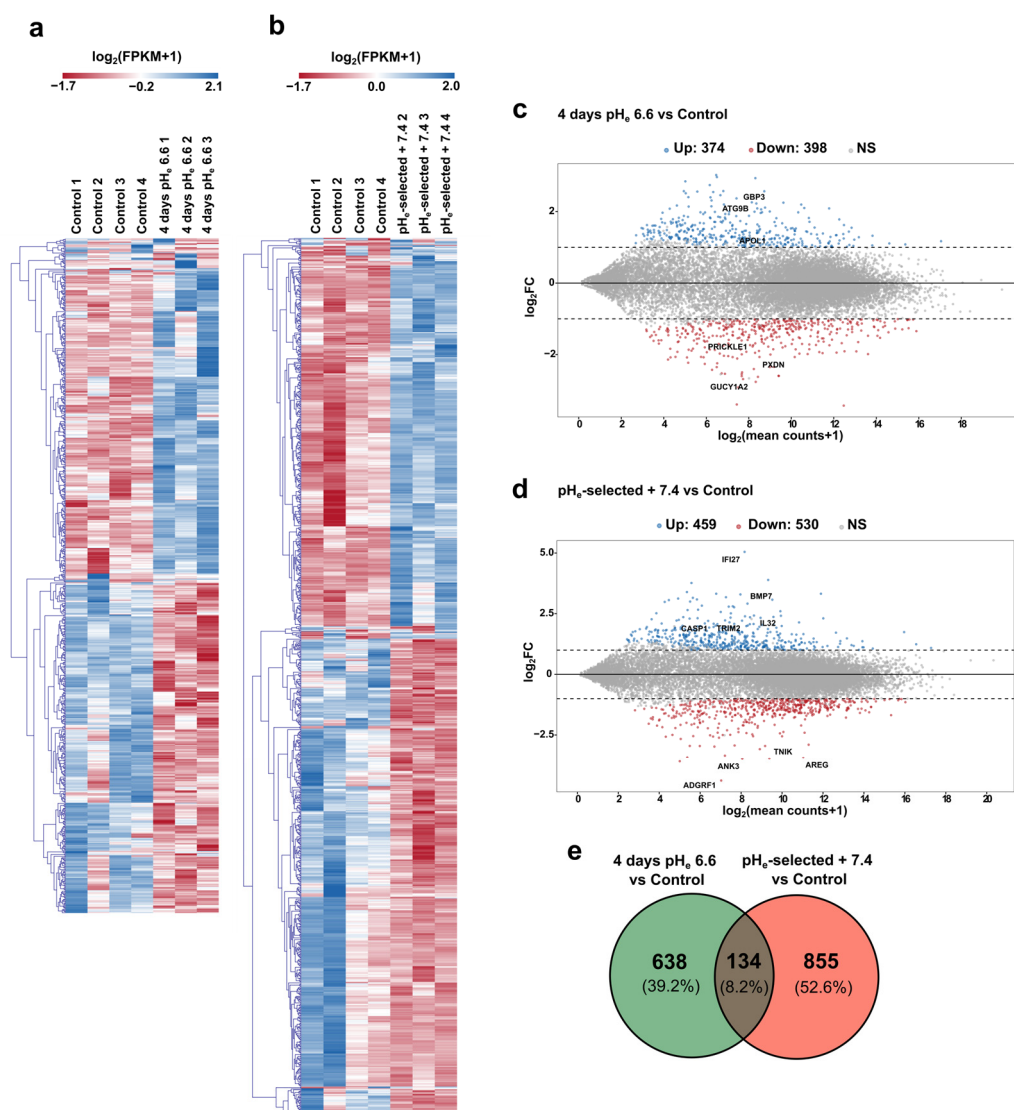


**Figure 6.** Differential transcriptomic profiles in PANC-1 cells in response to acidosis. (a) Heatmaps of RNA-Seq transcriptomic data relative to the differentially expressed genes (DEGs) detected comparing PANC-1 control condition against 4 days pH<sub>e</sub> 6.6 cells and (b) PANC-1 pH<sub>e</sub>-selected + 7.4 cells, respectively. Rows of the heatmaps represent the DEGs detected in the two comparisons, while columns are the individual biological replicates. Gene expression values are shown as gene-wise median-centered “ $\log_2(\text{FPKM}+1)$ ” (FPKM = Fragments Per Kilobase of sequence per Million mapped reads) according to a red-to-blue color gradient. (c) MA-plots showing gene differential expression observed in PANC-1 after 4 days at pH<sub>e</sub> 6.6 and (d) in PANC-1 pH<sub>e</sub>-selected + 7.4 cells compared to Control. “ $M = \log_2(\text{FC})$ ” vs. “ $A = \log_2(\text{mean counts}+1)$ ”. Downregulated genes are in red, while upregulated DEGs are in blue. Grey dots indicate non-significant gene expression changes. (e) Venn diagram summarizing the number of differentially expressed genes in PANC-1 4 days pH<sub>e</sub> 6.6 cells vs. Control and pH<sub>e</sub>-selected + 7.4 cells vs. Control; the number of genes deregulated in both acidic conditions is represented by the overlap between the two circles.

Highly upregulated genes in 4 days pH<sub>e</sub> 6.6 cells includes GBP3, a member of the guanylate-binding protein family, which induces caspase-dependent apoptosis in leukemia cells [62] and exerts an anti-tumor role in colorectal cancer [63]. However, its pro-tumor role has also been previously reported [64]. Among the top five downregulated genes in 4 days pH<sub>e</sub> 6.6 cells, we find PXDN, coding for Peroxidase, a heme peroxidase which has been associated with proliferation in endothelial cells [65] and with cancer cells in-

vative phenotype [66,67], Guanylate Cyclase 1 Soluble Subunit Alpha 2 coding gene (GUCY1A2), which mediates cell growth and survival in different cancer cell types [68–72], and PRICKLE1, prickle planar cell polarity protein 1, a member of the planar cell polarity (PCP) pathway which is involved in cancer cell metastasis [73,74]. Stronger gene deregulations are observed for pH<sub>e</sub>-selected + 7.4 cells, where the top 10 upregulated genes include Interferon Alpha Inducible Protein 27 (IFI27), a prognostic marker for pancreatic cancer [75] that promotes PDAC cell proliferation, migration, and invasion [76]; bone morphogenetic protein 7 (BMP7), a member of the transforming growth factor- $\beta$  (TGF- $\beta$ ) family reported to be involved in tumor metastasis, including pancreatic cancer where it promotes EMT and invasiveness in PANC-1 cells via matrix metalloproteinase (MMP)-2 upregulation [77]; Interleukin-32 (IL32), involved in PDAC cells invasiveness [78]; tripartite motif-containing 2 (TRIM2), which increases PDAC tumorigenesis both in vitro and in vivo [79]. Among top downregulated genes, amphiregulin (AREG) is involved in EMT and growth in different types of cancer, including PDAC [80], while Adhesion G Protein-Coupled Receptor F1 (ADGRF1) has an important role in inducing quiescence and chemoresistance in breast cancer [81]. Other downregulated genes include Traf2- and Nck-interacting kinase (TNIK), involved in colorectal carcinogenesis via modulation of Wnt signaling pathway [82], and Ankyrin-3 (ANK3), whose knock-down was reported to decrease the growth of prostate cancer cells while promoting their invasion both in vitro and in vivo [83], and to inhibit invasive abilities of thyroid cancer cells and their tumorigenesis when ectopically expressed [84].

To deepen the role of pH<sub>e</sub> selection and recovery in EMT process, we performed a hypergeometric test to measure the significance of the overlap between our DEG list and the set of genes involved in EMT as provided by dbEMT 2.0 (<http://dbemt.bioinforminzhao.org>) [85]. Interestingly, the data clearly show a 1.7-fold enrichment of the EMT gene set in our DEG list ( $p$ -value =  $7.27 \times 10^{-7}$ ) in pH<sub>e</sub>-selected + 7.4 cells as well as in 4 days pH<sub>e</sub> 6.6 cells ( $p$ -value =  $9.91 \times 10^{-6}$ , fold enrichment = 1.7) (Figure 7a,b; see Files S3 and S4 for a complete list of EMT DEGs). These data agree with the significant increase in EMT markers expression in both early and late stages of acidosis adaptation (Figure 5), thus supporting the hypothesis that acidosis selects more invasive cell phenotypes by promoting EMT and thus paving the way for more aggressive cell phenotypes.

To corroborate the functional assays and results obtained in vitro, up- and downregulated DEG lists were separately tested for over-representation through hypergeometric distribution by ToppFun web tool (see Materials and Methods section). The analysis of 4 days pH<sub>e</sub> 6.6 downregulated genes returned many enriched GO terms (biological processes) related to cell adhesion, cell growth, proliferation, and (negative regulation of) migration (Figure 7c), whereas very few terms resulted in upregulated PANC-1 cells exposed to short-term acidosis (Figure 7e). Pathway analysis further confirmed the involvement of 4 days pH<sub>e</sub> 6.6 downregulated genes in cell adhesion-related processes (such as  $\beta$ 1 integrin cell surface interactions and focal adhesions) as well as a significant contribution to cholesterol biosynthesis and NOD-like receptor signaling pathway coming from the upregulated genes (Figure S4c–d, respectively). As for the pH<sub>e</sub>-selected + 7.4 condition, GO terms (biological processes) linked to the negative regulation of cell cycle and cell growth are significantly over-represented within the set of the downregulated genes (Figure 7d), while biological processes associated with cell adhesion, cell migration, and EMT are significantly enriched in the upregulated gene list (Figure 7f). Accordingly, pathway analysis points at a significant alteration in cell cycle-associated processes due to the genes downregulated in pH<sub>e</sub>-selected + 7.4 condition, while the upregulated ones are mostly involved in the cadherin signaling pathway, interferon signaling, and cell invasion-associated processes, including degradation of the extracellular matrix and DUB metalloproteases (Figure S4e,f). The complete lists of all the enriched terms returned by such an over-representation analysis are provided in the Supplementary Materials (see Files S5–S8).



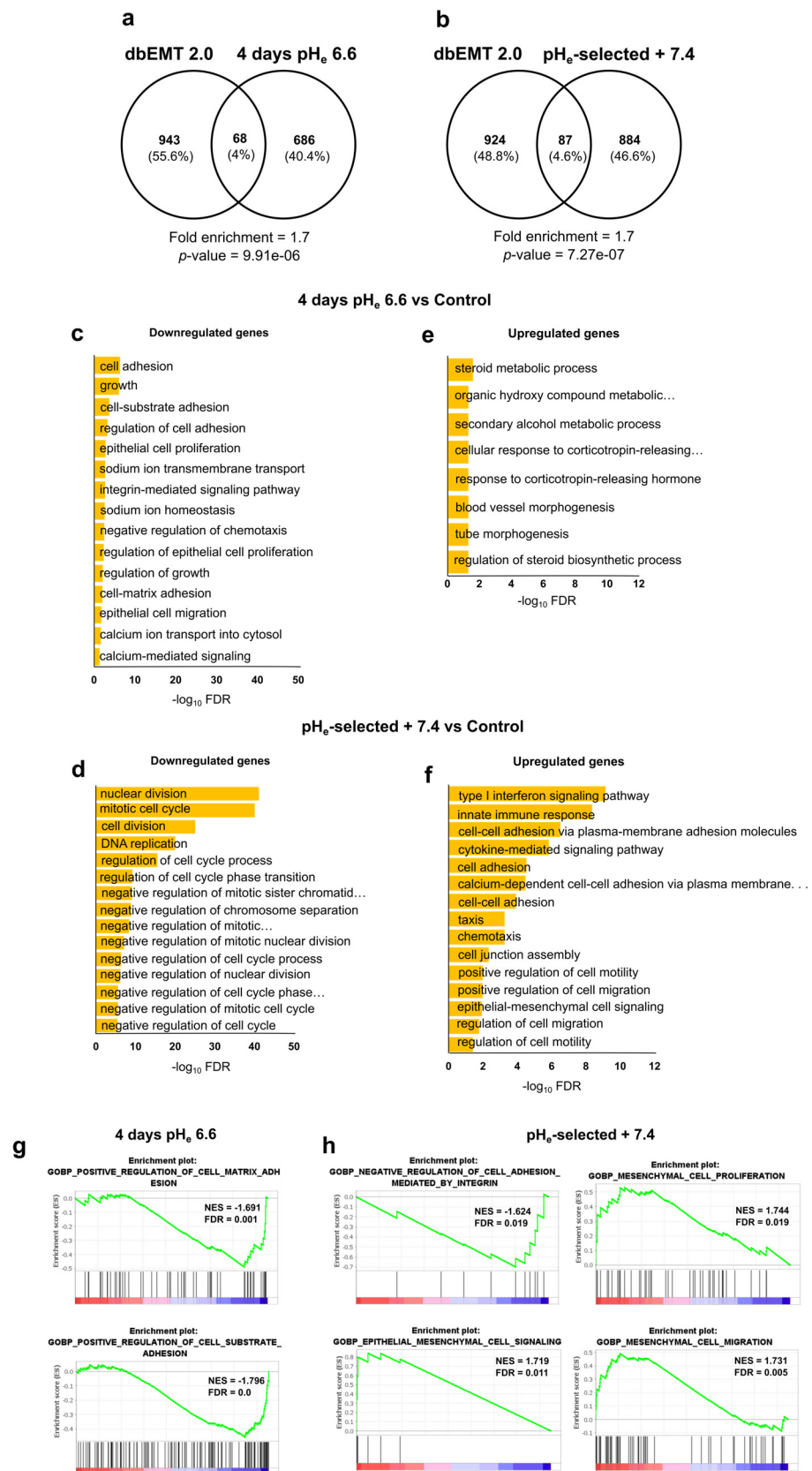


**Figure 7.** Gene ontology (GO) and gene set enrichment analysis (GSEA) of differentially expressed genes in PANC-1 cells in response to acidosis. (a) Venn plots showing overlapped dbEMT2.0 curated genes and differentially expressed genes (DEGs) in PANC-1 4 days pH<sub>e</sub> 6.6 and (b) PANC-1 pH<sub>e</sub>-selected cells + 7.4. (c) Bar chart of the most relevant enriched biological processes as defined in

GO database and resulting from the analysis of genes downregulated in PANC-1 4 days pHe 6.6 cells vs. Control, and (d) in PANC-1 pHe-selected + 7.4 cells vs. Control, and of genes upregulated in (e) PANC-1 4 days pHe 6.6 cells vs. Control, and (f) in PANC-1 pHe-selected + 7.4 cells vs. Control. (g) RNA-Seq data of PANC-1 4 days pHe 6.6 and (h) pHe-selected + 7.4 cells analyzed using gene set enrichment analysis (GSEA) and presented as enrichment score (ES) plots. GSEA showed significant enrichment of cell-substrate adhesion, and migration-related gene sets in the two acidic conditions, and of proliferation-related gene set for pHe-selected + 7.4. *y*-axes in GSEA plots represent the ES function, while *x*-axes display a red-blue color scale corresponding to the ranked list of DEGs (from the most up- to the most downregulated one, respectively) following one of the two acidic treatments. Vertical black lines above the red-blue scale in each plot refer to the position of each gene of the selected gene set along the ranked gene list as returned by the differential expression analysis of experimental data.

Finally, to validate and deepen these results, the GO database was also interrogated using GSEA software (see Section 2.11 for more details on parameter settings). GSEA results are in good agreement with the previous ones, showing that 4 days exposure of PANC-1 cells to pHe 6.6 decreases cell adhesion properties (Figure 7g). The long-lasting selection protocol induces a general enhancement of cell adhesion, proliferation, and migration in relation to the mesenchymal-like phenotype of PANC-1 cells kept under acidic conditions (Figure 7h). The full tables of significant terms resulting from GSEA can be found in Files S9 and S10.

#### 4. Discussion

In the same way as most other cancers, Pancreatic Ductal Adenocarcinoma is characterized by a highly acidic microenvironment resulting from the aberrant blood perfusion and the metabolic rearrangement that cancer cells put in place to meet the increased demand for energy and nutrients needed for their growth. In this study, we characterized the response of PDAC cell lines, PANC-1 and Mia PaCa-2, to short term (4 days) or long-lasting (1 month) acidosis (pHe 6.6) exposure on PDAC cellular hallmarks. Although previous research already showed that prolonged treatment induce a phenomenon of acid adaptation in pancreatic cells [41,43,86,87] little is known about the metastatic potential of the acid-selected cancer cells. To this purpose we established a model by re-exposing acidic selected cells to pHe 7.4 for two weeks. This treatment mimics the interface between acidic microenvironment of the tumor and the physiological pHe of the adjacent non-tumorous tissue. Indeed, tumor acidosis is not restricted to its hypoxic core, but it extends toward the interface between the tumor and normal tissue which delineates the margin of a malignant tumor when cells invade neighboring healthy tissues and blood vessels [21,88].

Our data indicate that acidic pHe selects for more aggressive pancreatic cancer cells via the increase in cell death during the short-term exposition (4 days). This leads to the survival of acid-resistant cells to low pHe stress that further outgrew and underwent EMT to acquire a more aggressive and invasive phenotype when exposed to pHe 7.4.

One feature of cancer cells is the pH gradient reversal compared to their healthy counterparts, leading to extracellular acidification coupled with the relative alkalinization of the intracellular space [7,89]. pHi homeostasis is important for the correct functioning of various physiological and pathological cellular processes. Despite the interest of the cancer cell to maintain a stable pHi, it is subjected to variations in external pH; therefore, sudden acidification of the extracellular space can result in the disruption of the pHi steady-state, which may pave the way toward selective pressures as a survival mechanism [6,90]. Our results indicated that short and long acidic exposure induces a slight decrease, although not significant, in the PANC-1 basal pHi (Figure 1b,c), in accordance with previous reports [43,91,92]. Our data demonstrated that the basal pHi value is not only recovered but further increased when PANC-1 pHe-selected cells face back pHe 7.4 (Figure 1b,c),

supporting recent evidences in same cell type [43], a feature that may represent a driving force for cancer progression, as suggested for other cancer types [7,93–95].

The results on  $\text{pH}_i$  levels correlated well with functional assays, as those PANC-1 cells exposed to acidic  $\text{pH}_e$  for 4 days had both a decrease in the proliferation rate and lower  $\text{pH}_i$  values than control cells. After 1 month of acidic  $\text{pH}_e$  exposure, the growth rate of PDAC cells was comparable to that of cells exposed for 4 days to  $\text{pH}_e$  6.6. We confirmed this output in Mia PaCa-2 cells, although the inhibition of proliferation was less evident in these cells. Validation of the Ki67 proliferation marker and G0S2 quiescence marker mRNA levels confirmed our proliferation results (Figure 5c). These results agree with the well-established notion that internal acidification, probably due to external acidic  $\text{pH}_e$ , inhibits cell proliferation in pancreatic cancer [43,86]. Finally, PDAC cell proliferation was restored and further boosted by recovery in  $\text{pH}_e$  7.4. These results clearly demonstrate that the acidic tumor microenvironment selects for cells with reduced growth capacities in acidic conditions but which display greater proliferative abilities when they come into contact with areas of physiological  $\text{pH}_e$  [10].

We showed that cell growth inhibition results from an increase in cell death, which gradually increased until it reached the maximum percentage of cell death at 4 days (Figure 2g,h). The reduced cell viability is the result of energy deprivation caused by glycolysis inhibition [96], as demonstrated by ATP shortage (Figure S1a,b) and by intracellular acidification (Figure 1b,c). We observed a subsequent, progressive, and almost complete recovery of cell viability (Figure 2g,h). This is likely due to the selection of a subset of cells resistant to the tumor acidosis-induced toxicity around the middle of the 1-month treatment. Consequently, almost all cells were alive at the end of the 1-month acidic exposure. Such a behavior was also observed in other cancer cell types [24,30,39,43,97].

Potential in cell migration and invasion represents a key feature of aggressive cancer progression. Quantification of the adhesive abilities of PANC-1 and Mia PaCa-2 cells to gelatin-coated wells under different acidic conditions (Figure 3) confirmed that cell-matrix interactions are inhibited under acidic conditions during the early phase of acidotic stress (4 days  $\text{pH}_e$  6.6), as previously demonstrated in other works [19,29,31]. On the contrary, acid selection enhanced the ability of PDAC cells to adhere, maintaining this feature once PANC-1 cells face back physiological  $\text{pH}_e$  7.4 (Figure 3a,b). The acidic treatment led to PDAC cells with an increased migratory potential at population (Figure 3c–e) and single-cell level (Figure S2a,b), with further accentuation in cells re-acclimated to  $\text{pH}_e$  7.4 (Figure 3c–e). Of particular interest are the results obtained from  $\text{pH}_e$ -taxis experiments, which confirmed that the same behavior was observed in the presence of a  $\text{pH}_e$  gradient, allowing the cells to migrate from an acidic compartment to a  $\text{pH}_e$  7.4 one (Figure 4a–c). These data support the hypothesis of acidic selection of a more invasive phenotype as observed on the edges of the tumor. Interestingly, this behavior is not common to immune cells which instead tends to move toward a more acidic  $\text{pH}_e$  [98].

Despite the inhibition of cell attachment of PANC-1 and Mia PaCa-2 cells exposed for 4 days to low  $\text{pH}_e$ , those cells migrated faster in acidic conditions.

The apparent contradictory behavior induced at early stages of acidic  $\text{pH}_e$  selection (4 days), i.e., lower cell-matrix adhesion properties and increased migration velocity, could be explained by an early acidic  $\text{pH}_e$  selection. In line with this hypothesis, the few PANC-1 cells that survived and remained attached to the gelatin-coated surfaces at the early stages of  $\text{pH}_e$  6.6 exposure might have already evolved sufficiently into a more aggressive phenotype characterized by faster cells, as suggested by the greater percentage of PANC-1 cells characterized by high-velocity respect to control cells (Figure S2d). The acquisition of this migratory phenotype might not require longer acidic treatment or acclimation to  $\text{pH}_e$  7.4. In this context, focal adhesions (FAs) might be involved. They play a key role in cell migration, as these multi-protein assemblies represent the main linkage between the intracellular cytoskeleton and extracellular matrix, promoting membrane protrusion at the leading edge of migrating cells [99]. Our immunostaining results on PANC-1 cells might confirm this, as cells exposed for 4 days to  $\text{pH}_e$  6.6 were faster than control cells



and showed increased paxillin recruitment to the cell periphery, with larger FAs compared to control (Figure S2c–f). On the contrary, the acute acidic treatment did not affect the size of FAs, their number, nor their plasma membrane recruitment in Mia PaCa-2 cells (Figure S2g–i).

One major step in tumor metastasis is local tumor cell invasion, a process promoted by acidic TME [10,21]. Our results indicated that, although PDAC invasive capacities are impaired during the early stages of low  $\text{pH}_e$  selection, they were indeed potentiated during long-term acidic treatment (1 month). More interestingly this pro-metastatic phenotype is conserved following cell re-acclimation to physiological  $\text{pH}_e$  (Figure 3f–h). Transwell invasion experiments performed with  $\text{pH}_e$  gradient (Figure 4d) demonstrated that the increased invasive properties acquired by acid-selected cells were further potentiated when cells found themselves at the interface with less acidic areas mimicking tumor-stroma boundaries, where cells are in contact with better perfused, and therefore less acidic, regions. Indeed, invadopodial activity was increased in PDAC  $\text{pH}_e$ -selected + 7.4 cells, leading to a more pronounced digestion of the ECM. Although we did not provide the molecular mechanisms involved, a major role in low  $\text{pH}_e$ -induced matrix degradation is expected for  $\text{Na}^+$ - $\text{H}^+$  exchanger (NHE1), localized in the invadopodia [100–102] and which promotes the proteolytic activity of different proteinases [46,58,59], and by Carbonic Anhydrase IX (CAIX), which acidifies the extracellular space to promote MMP14 activity [60,103] and metastasis in vivo [104].

These results highlight the metastatic potential of  $\text{pH}_e$ -selected cells in vitro and indicate that the increased invasiveness results from a gradual selection of aggressive cell phenotypes induced by the acidic  $\text{pH}_e$ . However, our results following a short-term acid exposure contrast with previous reports with PDAC cells [20], which may explain the different strategies employed for creating the acidic conditions, and other cancer types [14,25,40,59]. In fact, particular attention should be addressed to the different responses that a specific maneuver of  $\text{pH}_e$  may induce in cancer cells [8]. Our results suggest that the impact of acidic  $\text{pH}_e$  on cell invasion depends on the strategy used for manipulating the pH, which can produce distinct responses based on the deregulation of specific proteins involved in  $\text{pH}_e$ / $\text{pH}_i$  sensing and transduction. Moreover, the adaptation/selection process might produce different outcomes and take different times to activate/inhibit specific cell processes based on the cell type. We found that some extent of selection is observable after 15 days of acid treatment, concurrently with the progressive recovery of cell viability.

A section of the paper was devoted to underlining the role of acidic pH selection toward a mesenchymal phenotype. Indeed, EMT is another crucial step in disseminating tumor cells from the primary sites to other organs, providing cancer cells with invasive properties [105]. Our work showed that  $\text{pH}_e$  selection induced a mesenchymal phenotype in both PDAC cells, as demonstrated by an increase in the mRNA levels of several EMT markers. Moreover, PANC-1 exposed to  $\text{pH}_e$  6.6 for 4 days and  $\text{pH}_e$ -selected + 7.4 cells showed a significant enrichment of the EMT gene set (as provided by dbEMT 2.0) in our DEG list (Figure 7a,b), including several metalloproteases and integrins genes. Interestingly, among the EMT genes enriched in the  $\text{pH}_e$ -selected + 7.4 cells DEG list, we also observed a significant increase in the FGFR2 expression, confirming the role of this receptor in PDAC cell EMT as recently suggested [106]. The EMT phenotype was confirmed by qPCR data, showing a significant decrease in Slug gene expression in the 4 days  $\text{pH}_e$  6.6 models, which might correlate with the decrease in proliferative and invasive abilities in the early stages of  $\text{pH}_e$  selection, as suggested in colorectal cancer [107]. Several publications support the notion that extracellular acidosis promotes EMT [15,19,26,86]. In our work, RNA sequencing on PANC-1 cells allowed us to identify the different genetic signatures of the short-term and long-term (and recovery to  $\text{pH}_e$  7.4) acid models, observing the acid-mediated downregulation of genes involved in cell growth, invasion, and adhesion or the upregulation of cell death-related genes during the early stages of  $\text{pH}_e$  selection (Figures 6c and 7c,e,g). We also validated that different gene sets of cell proliferation, ECM remodeling, migration, and invasion were associated with the acid-selected phenotypes

recovered to  $pH_e$  7.4, whose migratory and invasive phenotypes were related to epithelial–mesenchymal transition induction (Figures 6d and 7d,f,h). These results are in accordance with previous RNA-seq data on 1-month acid-adapted PANC-1 cells [41] and microarray data on other pancreatic cancer cells adapted to low  $pH_e$  [86].

## 5. Conclusions

This work reports that the acidic tumor microenvironment provides certain PDAC cell subpopulations with selective survival benefits that allow them to survive under acidic stress conditions. They do so via genetic reprogramming toward the expression of proliferation, migration, invasion, autophagy, and EMT-related markers, leading to PDAC cells with enhanced metastatic potential which promote cancer progression (Figure 8).

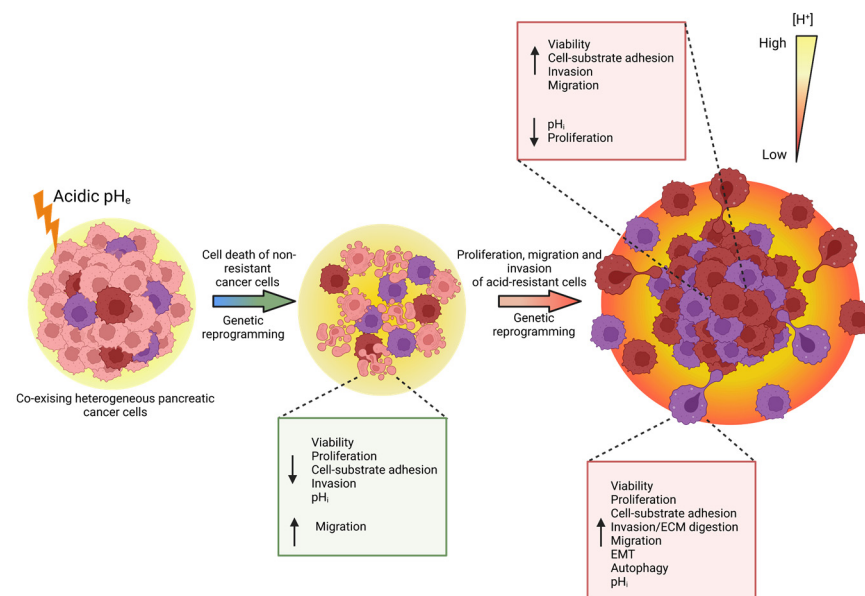


**Figure 8.** PDAC cells exposed to acidic extracellular conditions undergo a process of selection, characterized by acid-induced genetic and phenotypic alterations. This results in increased cell death due to the cytotoxic effect of low  $pH_e$  and decrease in cell-substrate adhesion, proliferation, and cell invasion. Along with the acid exposition, further genetic rewiring provides surviving cancer cells with more aggressive properties in terms of adhesion, migration, and invasion. Limited proliferative capacities are overcome when cells are acclimated to  $pH_e$  7.4 following 1 month-long  $pH_e$  6.6 treatment. ↓ arrow indicates downregulation, ↑ arrow indicates upregulation. The figure was created with [www.Biorender.com](http://www.Biorender.com).

**Supplementary Materials:** The following supporting information can be downloaded at: <https://www.mdpi.com/article/10.3390/cancers15092572/s1>, Figure S1: Effect of acidic  $pH_e$  on ATP production and of acidic  $pH_e$  acute treatment of cell-substrate adhesion in PANC-1 and Mia PaCa-2; Figure S2: Effect of acidic  $pH_e$  on single cell migration in PANC-1 cells and on Focal Adhesions (FAs) membrane recruitment on PANC-1 and Mia PaCa-2 cells; Figure S3: Establishment of a pH gradient in the Transwell system and effect of acute exposition to acidic  $pH_e$  on PANC-1 and Mia PaCa-2 cells' invadopodia activity and epithelial–mesenchymal transition; Figure S4: Principal component analysis (PCA) of RNA-seq-based expression data and gene ontology (GO) pathway enrichment analysis of PANC-1 differentially expressed genes (DEGs) in response to acidosis. Supplementary File S1: DEGs PANC-1–4 days  $pH_e$  6.6 vs. Ctrl; Supplementary File S2: DEGs PANC-1– $pH_e$ -selected + 7.4 vs. Ctrl; Supplementary File S3: EMT DEGs—4 days  $pH_e$  6.6 vs. Ctrl; Supplementary File S4: EMT DEGs— $pH_e$ -selected + 7.4 vs. Ctrl; Supplementary File S5: GO analysis PANC-1—4 days  $pH_e$  6.6 vs. Ctrl—Downregulated; Supplementary File S6: GO analysis PANC-1—4 days  $pH_e$  6.6 vs. Ctrl—Upregulated; Supplementary File S7: GO analysis PANC-1— $pH_e$ -selected + 7.4 vs. Ctrl—Downregulated; Supplementary File S8: GO analysis PANC-1— $pH_e$ -selected + 7.4 vs. Ctrl—

Upregulated; Supplementary File S9: GSEA PANC-1—4 days pH<sub>e</sub> 6.6 vs. Ctrl; Supplementary File S10: GSEA PANC-1—pH<sub>e</sub>-selected + 7.4 vs. Ctrl; Supplementary File S11—Uncropped Western Blots Membranes.

**Author Contributions:** Conceptualization, M.M.A., A.F.P. and N.P.; methodology, M.M.A., T.M.A.C., T.L., F.A.R., M.Y., G.C., A.F., S.A., C.V. and V.F.; software, F.A.R.; validation, M.M.A., T.M.A.C., F.A.R., T.L., M.Y., G.C., S.A., C.V., A.S., S.J.R., R.A.C., A.F.P. and N.P.; formal analysis, M.M.A., T.M.A.C., F.A.R., T.L., M.Y. and G.C.; investigation, M.M.A., T.M.A.C., F.A.R., T.L. and M.Y.; resources, A.S., S.J.R., R.A.C., A.F.P. and N.P.; data curation, M.M.A.; T.M.A.C., F.A.R., T.L., M.Y., G.C., S.A., C.V., A.S., S.J.R., R.A.C., A.F.P. and N.P.; writing—original draft preparation, M.M.A., T.M.A.C., F.A.R., T.L. and A.F.P.; writing—review and editing, M.M.A., T.M.A.C., F.A.R., T.L., M.Y., G.C., A.S., S.J.R., R.A.C., A.F.P. and N.P.; visualization, M.M.A., A.F.P. and N.P.; supervision, A.S., S.J.R., R.A.C., A.F.P. and N.P.; project administration, M.M.A., A.F.P. and N.P.; funding acquisition, A.S., S.J.R., R.A.C., A.F.P. and N.P. All authors have read and agreed to the published version of the manuscript.

**Funding:** This research was funded by Marie Skłodowska Curie Innovative Training Network (#GA 813834 pHioniC-H2020-MSCA-ITN-2018); ANR-AAPG219 Mécanismes calcium-dépendants d’activation des cellules pancréatiques stellaires—Calstell Project; PRIN-2017 “Lioness” project (#GA 754345) from Italian Ministry for Education, University and Research (MIUR), by the Programma Operativo Complementare Ricerca e Innovazione, Asse I “Investimenti in Capitale Umano”—Azione I.1 “Dottorati innovativi con caratterizzazione industriale” del PON R&I 2014–2020, Deutsche Forschungsgemeinschaft (GRK 2515/1, Chembion and SCHW407/22-1); C.V. is funded by PhD scholarship D.M. 351/2022 (M4C1 – Inv. 4.1)/PNRR Research.

**Institutional Review Board Statement:** Not applicable.

**Informed Consent Statement:** Not applicable.

**Data Availability Statement:** The data presented in this study are available in this article and supplementary material.

**Acknowledgments:** We are grateful to Ania Trauzold, University of Kiel, Germany for kindly providing us with PANC-1 cells and we thank the Plateforme de Genotypage/Séquençage, Institut du Cerveau/Paris Brain Institute, ICM, Hôpital de la Pitié-Salpêtrière CNRS UMR 7225—Inserm U 1127—Sorbonne Université UM75, for performing the RNA-seq.

**Conflicts of Interest:** The authors declare no conflict of interest.

## References

1. Khalaf, N.; El-Serag, H.B.; Abrams, H.R.; Thrift, A.P. Burden of Pancreatic Cancer: From Epidemiology to Practice. *Clin. Gastroenterol. Hepatol.* **2021**, *19*, 876–884. [[CrossRef](#)] [[PubMed](#)]
2. McGuigan, A.; Kelly, P.; Turkington, R.C.; Jones, C.; Coleman, H.G.; McCain, R.S. Pancreatic Cancer: A Review of Clinical Diagnosis, Epidemiology, Treatment and Outcomes. *WJG* **2018**, *24*, 4846–4861. [[CrossRef](#)] [[PubMed](#)]
3. Orth, M.; Metzger, P.; Gerum, S.; Mayerle, J.; Schneider, G.; Belka, C.; Schnurr, M.; Lauber, K. Pancreatic Ductal Adenocarcinoma: Biological Hallmarks, Current Status, and Future Perspectives of Combined Modality Treatment Approaches. *Radiat. Oncol.* **2019**, *14*, 141. [[CrossRef](#)] [[PubMed](#)]
4. Pedersen, S.F.; Novak, I.; Alves, F.; Schwab, A.; Pardo, L.A. Alternating PH Landscapes Shape Epithelial Cancer Initiation and Progression: Focus on Pancreatic Cancer. *BioEssays* **2017**, *39*, 1600253. [[CrossRef](#)] [[PubMed](#)]
5. Carvalho, T.M.A.; Di Molfetta, D.; Greco, M.R.; Koltai, T.; Alfouk, K.O.; Reshkin, S.J.; Cardone, R.A. Tumor Microenvironment Features and Chemoresistance in Pancreatic Ductal Adenocarcinoma: Insights into Targeting Physicochemical Barriers and Metabolism as Therapeutic Approaches. *Cancers* **2021**, *13*, 6135. [[CrossRef](#)]
6. Zheng, T.; Jäättelä, M.; Liu, B. PH Gradient Reversal Fuels Cancer Progression. *Int. J. Biochem. Cell Biol.* **2020**, *125*, 105796. [[CrossRef](#)]
7. Webb, B.A.; Chimenti, M.; Jacobson, M.P.; Barber, D.L. Dysregulated PH: A Perfect Storm for Cancer Progression. *Nat. Rev. Cancer* **2011**, *11*, 671–677. [[CrossRef](#)]
8. Blaszczyk, W.; Swietach, P. What Do Cellular Responses to Acidity Tell Us about Cancer? *Cancer Metastasis Rev.* **2021**, *40*, 1159–1176. [[CrossRef](#)]
9. Stock, C.; Gassner, B.; Hauck, C.R.; Arnold, H.; Mally, S.; Eble, J.A.; Dieterich, P.; Schwab, A. Migration of Human Melanoma Cells Depends on Extracellular PH and Na<sup>+</sup>/H<sup>+</sup> Exchange: Extracellular Protons Modulate Cell Migration. *J. Physiol.* **2005**, *567*, 225–238. [[CrossRef](#)]
10. Boedtker, E.; Pedersen, S.F. The Acidic Tumor Microenvironment as a Driver of Cancer. *Annu. Rev. Physiol.* **2020**, *82*, 103–126. [[CrossRef](#)]

11. Lagadic-Gossmann, D.; Huc, L.; Lecureur, V. Alterations of Intracellular PH Homeostasis in Apoptosis: Origins and Roles. *Cell Death Differ.* **2004**, *11*, 953–961. [[CrossRef](#)] [[PubMed](#)]
12. Matsuyama, S.; Llopis, J.; Deveraux, Q.L.; Tsien, R.Y.; Reed, J.C. Changes in Intramitochondrial and Cytosolic PH: Early Events That Modulate Caspase Activation during Apoptosis. *Nat. Cell Biol.* **2000**, *2*, 318–325. [[CrossRef](#)] [[PubMed](#)]
13. Wojtkowiak, J.W.; Rothberg, J.M.; Kumar, V.; Schramm, K.J.; Haller, E.; Proemsey, J.B.; Lloyd, M.C.; Sloane, B.F.; Gillies, R.J. Chronic Autophagy Is a Cellular Adaptation to Tumor Acidic PH Microenvironments. *Cancer Res.* **2012**, *72*, 3938–3947. [[CrossRef](#)] [[PubMed](#)]
14. Suzuki, A.; Maeda, T.; Baba, Y.; Shimamura, K.; Kato, Y. Acidic Extracellular PH Promotes Epithelial Mesenchymal Transition in Lewis Lung Carcinoma Model. *Cancer Cell Int.* **2014**, *14*, 129. [[CrossRef](#)]
15. Andreucci, E.; Peppicelli, S.; Ruzzolini, J.; Bianchini, F.; Biagioni, A.; Papucci, L.; Magnelli, L.; Mazzanti, B.; Stecca, B.; Calorini, L. The Acidic Tumor Microenvironment Drives a Stem-like Phenotype in Melanoma Cells. *J. Mol. Med.* **2020**, *98*, 1431–1446. [[CrossRef](#)]
16. Sutoo, S.; Maeda, T.; Suzuki, A.; Kato, Y. Adaptation to Chronic Acidic Extracellular PH Elicits a Sustained Increase in Lung Cancer Cell Invasion and Metastasis. *Clin. Exp. Metastasis* **2020**, *37*, 133–144. [[CrossRef](#)]
17. Damaghi, M.; Gillies, R. Phenotypic Changes of Acid-Adapted Cancer Cells Push Them toward Aggressiveness in Their Evolution in the Tumor Microenvironment. *Cell Cycle* **2017**, *16*, 1739–1743. [[CrossRef](#)]
18. Wang, H.; Cai, J.; Du, S.; Wei, W.; Shen, X. LAMC2 Modulates the Acidity of Microenvironments to Promote Invasion and Migration of Pancreatic Cancer Cells via Regulating AKT-Dependent NHE1 Activity. *Exp. Cell Res.* **2020**, *391*, 111984. [[CrossRef](#)]
19. Li, S.; Xiong, N.; Peng, Y.; Tang, K.; Bai, H.; Lv, X.; Jiang, Y.; Qin, X.; Yang, H.; Wu, C.; et al. Acidic PH Regulates Cytoskeletal Dynamics through Conformational Integrin B1 Activation and Promotes Membrane Protrusion. *Biochim. Biophys. Acta (BBA) Mol. Basis Dis.* **2018**, *1864*, 2395–2408. [[CrossRef](#)]
20. Shin, S.C.; Thomas, D.; Radhakrishnan, P.; Hollingsworth, M.A. Invasive Phenotype Induced by Low Extracellular PH Requires Mitochondria Dependent Metabolic Flexibility. *Biochem. Biophys. Res. Commun.* **2020**, *525*, 162–168. [[CrossRef](#)]
21. Estrella, V.; Chen, T.; Lloyd, M.; Wojtkowiak, J.; Cornnell, H.H.; Ibrahim-Hashim, A.; Bailey, K.; Balagurunathan, Y.; Rothberg, J.M.; Sloane, B.F.; et al. Acidity Generated by the Tumor Microenvironment Drives Local Invasion. *Cancer Res.* **2013**, *73*, 1524–1535. [[CrossRef](#)]
22. Corbet, C.; Bastien, E.; Santiago de Jesus, J.P.; Dierge, E.; Martherus, R.; Vander Linden, C.; Doix, B.; Degavre, C.; Guilbaud, C.; Petit, L.; et al. TGF $\beta$ 2-Induced Formation of Lipid Droplets Supports Acidosis-Driven EMT and the Metastatic Spreading of Cancer Cells. *Nat. Commun.* **2020**, *11*, 454. [[CrossRef](#)] [[PubMed](#)]
23. Rabiee Motmaen, S.; Tavakol, S.; Joghataei, M.T.; Barati, M. Acidic PH Derived from Cancer Cells as a Double-edged Knife Modulates Wound Healing through DNA Repair Genes and Autophagy. *Int. Wound J.* **2020**, *17*, 137–148. [[CrossRef](#)] [[PubMed](#)]
24. Yang, O.C.Y.; Loh, S.-H. Acidic Stress Triggers Sodium-Coupled Bicarbonate Transport and Promotes Survival in A375 Human Melanoma Cells. *Sci. Rep.* **2019**, *9*, 6858. [[CrossRef](#)] [[PubMed](#)]
25. Rofstad, E.K.; Mathiesen, B.; Kindem, K.; Galappathi, K. Acidic Extracellular PH Promotes Experimental Metastasis of Human Melanoma Cells in Athymic Nude Mice. *Cancer Res.* **2006**, *66*, 6699–6707. [[CrossRef](#)] [[PubMed](#)]
26. Riemann, A.; Rauschner, M.; Gießelmann, M.; Reime, S.; Haupt, V.; Thews, O. Extracellular Acidosis Modulates the Expression of Epithelial-Mesenchymal Transition (EMT) Markers and Adhesion of Epithelial and Tumor Cells. *Neoplasia* **2019**, *21*, 450–458. [[CrossRef](#)]
27. Bohloli, M.; Atashi, A.; Soleimani, M.; Kaviani, S.; Anbarlou, A. Investigating Effects of Acidic PH on Proliferation, Invasion and Drug-Induced Apoptosis in Lymphoblastic Leukemia. *Cancer Microenviron.* **2016**, *9*, 119–126. [[CrossRef](#)]
28. Marino, M.L.; Pellegrini, P.; Di Lernia, G.; Djavaheri-Mergny, M.; Brnjic, S.; Zhang, X.; Hägg, M.; Linder, S.; Fais, S.; Codogno, P.; et al. Autophagy Is a Protective Mechanism for Human Melanoma Cells under Acidic Stress. *J. Biol. Chem.* **2012**, *287*, 30664–30676. [[CrossRef](#)]
29. Chen, Y.; Chen, C.-H.; Tung, P.-Y.; Huang, S.-H.; Wang, S.-M. An Acidic Extracellular PH Disrupts Adherens Junctions in HepG2 Cells by Src Kinases-Dependent Modification of E-Cadherin. *J. Cell. Biochem.* **2009**, *108*, 851–859. [[CrossRef](#)]
30. Gilbert, H.T.J.; Hodson, N.; Baird, P.; Richardson, S.M.; Hoyland, J.A. Acidic PH Promotes Intervertebral Disc Degeneration: Acid-Sensing Ion Channel -3 as a Potential Therapeutic Target. *Sci. Rep.* **2016**, *6*, 37360. [[CrossRef](#)]
31. Kondo, A.; Yamamoto, S.; Nakaki, R.; Shimamura, T.; Hamakubo, T.; Sakai, J.; Kodama, T.; Yoshida, T.; Aburatani, H.; Osawa, T. Extracellular Acidic PH Activates the Sterol Regulatory Element-Binding Protein 2 to Promote Tumor Progression. *Cell Rep.* **2017**, *18*, 2228–2242. [[CrossRef](#)] [[PubMed](#)]
32. Lee, S.; Shanti, A. Effect of Exogenous PH on Cell Growth of Breast Cancer Cells. *Int. J. Mol. Sci.* **2021**, *22*, 9910. [[CrossRef](#)] [[PubMed](#)]
33. Zhou, Z.; Song, J.; Li, W.; Liu, X.; Cao, L.; Wan, L.; Tan, Y.; Ji, S.; Liang, Y.; Gong, F. The Acid-Sensing Ion Channel, ASIC2, Promotes Invasion and Metastasis of Colorectal Cancer under Acidosis by Activating the Calcineurin/NFAT1 Axis. *J. Exp. Clin. Cancer Res.* **2017**, *36*, 130. [[CrossRef](#)] [[PubMed](#)]
34. Hu, P.; Li, S.; Tian, N.; Wu, F.; Hu, Y.; Li, D.; Qi, Y.; Wei, Z.; Wei, Q.; Li, Y.; et al. Acidosis Enhances the Self-Renewal and Mitochondrial Respiration of Stem Cell-like Glioma Cells through CYP24A1-Mediated Reduction of Vitamin D. *Cell Death Dis.* **2019**, *10*, 25. [[CrossRef](#)] [[PubMed](#)]



35. LaMonte, G.; Tang, X.; Chen, J.L.-Y.; Wu, J.; Ding, C.-K.C.; Keenan, M.M.; Sangokoya, C.; Kung, H.-N.; Ilkayeva, O.; Boros, L.G.; et al. Acidosis Induces Reprogramming of Cellular Metabolism to Mitigate Oxidative Stress. *Cancer Metab.* **2013**, *1*, 23. [[CrossRef](#)]
36. Peppicelli, S.; Bianchini, F.; Toti, A.; Laurenzana, A.; Fibbi, G.; Calorini, L. Extracellular Acidity Strengthens Mesenchymal Stem Cells to Promote Melanoma Progression. *Cell Cycle* **2015**, *14*, 3088–3100. [[CrossRef](#)]
37. Hofschroer, V.; Koch, K.A.; Ludwig, F.T.; Friedl, P.; Oberleithner, H.; Stock, C.; Schwab, A. Extracellular Protonation Modulates Cell-Cell Interaction Mechanics and Tissue Invasion in Human Melanoma Cells. *Sci. Rep.* **2017**, *7*, 42369. [[CrossRef](#)]
38. Tang, X.; Lucas, J.E.; Chen, J.L.-Y.; LaMonte, G.; Wu, J.; Wang, M.C.; Koumenis, C.; Chi, J.-T. Functional Interaction between Responses to Lactic Acidosis and Hypoxia Regulates Genomic Transcriptional Outputs. *Cancer Res.* **2012**, *72*, 491–502. [[CrossRef](#)]
39. Moellering, R.E.; Black, K.C.; Krishnamurty, C.; Baggett, B.K.; Stafford, P.; Rain, M.; Gatenby, R.A.; Gillies, R.J. Acid Treatment of Melanoma Cells Selects for Invasive Phenotypes. *Clin. Exp. Metastasis* **2008**, *25*, 411–425. [[CrossRef](#)]
40. Anemone, A.; Consolino, L.; Conti, L.; Irrera, P.; Hsu, M.Y.; Villano, D.; Dastrù, W.; Porporato, P.E.; Cavallo, F.; Longo, D.L. Tumour Acidosis Evaluated in Vivo by MRI-CEST PH Imaging Reveals Breast Cancer Metastatic Potential. *Br. J. Cancer* **2021**, *124*, 207–216. [[CrossRef](#)]
41. Yao, J.; Czaplinska, D.; Ialchina, R.; Schnipper, J.; Liu, B.; Sandelin, A.; Pedersen, S.F. Cancer Cell Acid Adaptation Gene Expression Response Is Correlated to Tumor-Specific Tissue Expression Profiles and Patient Survival. *Cancers* **2020**, *12*, 2183. [[CrossRef](#)] [[PubMed](#)]
42. Zhou, Z.-H.; Wang, Q.-L.; Mao, L.-H.; Li, X.-Q.; Liu, P.; Song, J.-W.; Liu, X.; Xu, F.; Lei, J.; He, S. Chromatin Accessibility Changes Are Associated with Enhanced Growth and Liver Metastasis Capacity of Acid-Adapted Colorectal Cancer Cells. *Cell Cycle* **2019**, *18*, 511–522. [[CrossRef](#)] [[PubMed](#)]
43. Schnipper, J.; Kouba, S.; Hague, F.; Girault, A.; Telliez, M.-S.; Guénin, S.; Ahidouch, A.; Pedersen, S.F.; Ouadid-Ahidouch, H. Acid Adaptation Promotes TRPC1 Plasma Membrane Localization Leading to Pancreatic Ductal Adenocarcinoma Cell Proliferation and Migration through Ca<sup>2+</sup> Entry and Interaction with PI3K/CaM. *Cancers* **2022**, *14*, 4946. [[CrossRef](#)] [[PubMed](#)]
44. Czaplinska, D.; Ialchina, R.; Andersen, H.B.; Yao, J.; Stigliani, A.; Dannesboe, J.; Flinck, M.; Chen, X.; Mitrega, J.; Gnosa, S.P.; et al. Crosstalk between Tumor Acidosis, P53 and Extracellular Matrix Regulates Pancreatic Cancer Aggressiveness. *Int. J. Cancer* **2023**, *152*, 1210–1225. [[CrossRef](#)] [[PubMed](#)]
45. Schwab, A.; Rossmann, H.; Klein, M.; Dieterich, P.; Gassner, B.; Neff, C.; Stock, C.; Seidler, U. Functional Role of Na<sup>+</sup>–HCO<sub>3</sub><sup>−</sup> Cotransport in Migration of Transformed Renal Epithelial Cells: Na<sup>+</sup>–HCO<sub>3</sub><sup>−</sup> Cotransport and Cell Migration. *J. Physiol.* **2005**, *568*, 445–458. [[CrossRef](#)] [[PubMed](#)]
46. Busco, G.; Cardone, R.A.; Greco, M.R.; Bellizzi, A.; Colella, M.; Antelmi, E.; Mancini, M.T.; Dell’Aquila, M.E.; Casavola, V.; Paradiso, A.; et al. NHE1 Promotes Invadopodial ECM Proteolysis through Acidification of the Peri-invadopodial Space. *FASEB J.* **2010**, *24*, 3903–3915. [[CrossRef](#)]
47. Dobin, A.; Davis, C.A.; Schlesinger, F.; Drenkow, J.; Zaleski, C.; Jha, S.; Batut, P.; Chaisson, M.; Gingeras, T.R. STAR: Ultrafast Universal RNA-Seq Aligner. *Bioinformatics* **2013**, *29*, 15–21. [[CrossRef](#)]
48. Li, B.; Dewey, C.N. RSEM: Accurate Transcript Quantification from RNA-Seq Data with or without a Reference Genome. *BMC Bioinform.* **2011**, *12*, 323. [[CrossRef](#)]
49. Love, M.I.; Huber, W.; Anders, S. Moderated Estimation of Fold Change and Dispersion for RNA-Seq Data with DESeq2. *Genome Biol.* **2014**, *15*, 550. [[CrossRef](#)]
50. Benjamini, Y.; Drai, D.; Elmer, G.; Kafkafi, N.; Golani, I. Controlling the False Discovery Rate in Behavior Genetics Research. *Behav. Brain Res.* **2001**, *125*, 279–284. [[CrossRef](#)]
51. Chen, J.; Bardes, E.E.; Aronow, B.J.; Jegga, A.G. ToppGene Suite for Gene List Enrichment Analysis and Candidate Gene Prioritization. *Nucleic Acids Res.* **2009**, *37*, W305–W311. [[CrossRef](#)]
52. Subramanian, A.; Tamayo, P.; Mootha, V.K.; Mukherjee, S.; Ebert, B.L.; Gillette, M.A.; Paulovich, A.; Pomeroy, S.L.; Golub, T.R.; Lander, E.S.; et al. Gene Set Enrichment Analysis: A Knowledge-Based Approach for Interpreting Genome-Wide Expression Profiles. *Proc. Natl. Acad. Sci. USA* **2005**, *102*, 15545–15550. [[CrossRef](#)] [[PubMed](#)]
53. Deer, E.L.; González-Hernández, J.; Coursen, J.D.; Shea, J.E.; Ngatia, J.; Scaife, C.L.; Firpo, M.A.; Mulvihill, S.J. Phenotype and Genotype of Pancreatic Cancer Cell Lines. *Pancreas* **2010**, *39*, 425–435. [[CrossRef](#)] [[PubMed](#)]
54. Hao, G.; Xu, Z.P.; Li, L. Manipulating Extracellular Tumour PH: An Effective Target for Cancer Therapy. *RSC Adv.* **2018**, *8*, 22182–22192. [[CrossRef](#)]
55. Deakin, N.O.; Turner, C.E. Paxillin Comes of Age. *J. Cell Sci.* **2008**, *121*, 2435–2444. [[CrossRef](#)]
56. Kato, Y.; Lambert, C.A.; Colige, A.C.; Mineur, P.; Noël, A.; Frankenne, F.; Foidart, J.-M.; Baba, M.; Hata, R.-I.; Miyazaki, K.; et al. Acidic Extracellular PH Induces Matrix Metalloproteinase-9 Expression in Mouse Metastatic Melanoma Cells through the Phospholipase D-Mitogen-Activated Protein Kinase Signaling. *J. Biol. Chem.* **2005**, *280*, 10938–10944. [[CrossRef](#)] [[PubMed](#)]
57. Magalhaes, M.A.O.; Larson, D.R.; Mader, C.C.; Bravo-Cordero, J.J.; Gil-Henn, H.; Oser, M.; Chen, X.; Koleske, A.J.; Condeelis, J. Cortactin Phosphorylation Regulates Cell Invasion through a PH-Dependent Pathway. *J. Cell Biol.* **2011**, *195*, 903–920. [[CrossRef](#)]
58. Lucien, F.; Brochu-Gaudreau, K.; Arsenaault, D.; Harper, K.; Dubois, C.M. Hypoxia-Induced Invadopodia Formation Involves Activation of NHE-1 by the P90 Ribosomal S6 Kinase (P90RSK). *PLoS ONE* **2011**, *6*, 11. [[CrossRef](#)]
59. Greco, M.R.; Antelmi, E.; Busco, G.; Guerra, L.; Rubino, R.; Casavola, V.; Reshkin, S.J.; Cardone, R.A. Protease Activity at Invadopodial Focal Digestive Areas Is Dependent on NHE1-Driven Acidic PHe. *Oncol. Rep.* **2014**, *31*, 940–946. [[CrossRef](#)]

60. Debreova, M.; Csaderova, L.; Burikova, M.; Lukacikova, L.; Kajanova, I.; Sedlakova, O.; Kery, M.; Kopacek, J.; Zatovicova, M.; Bizik, J.; et al. CAIX Regulates Invadopodia Formation through Both a PH-Dependent Mechanism and Interplay with Actin Regulatory Proteins. *Int. J. Mol. Sci.* **2019**, *20*, 2745. [[CrossRef](#)]
61. Yamada, T.; Park, C.S.; Burns, A.; Nakada, D.; Lacorazza, H.D. The Cytosolic Protein G0S2 Maintains Quiescence in Hematopoietic Stem Cells. *PLoS ONE* **2012**, *7*, e38280. [[CrossRef](#)] [[PubMed](#)]
62. Luo, Y.; Jin, H.; Kim, J.H.; Bae, J. Guanylate-Binding Proteins Induce Apoptosis of Leukemia Cells by Regulating MCL-1 and BAK. *Oncogenesis* **2021**, *10*, 54. [[CrossRef](#)]
63. Britzen-Laurent, N.; Lipnik, K.; Ocker, M.; Naschberger, E.; Schellerer, V.S.; Croner, R.S.; Vieth, M.; Waldner, M.; Steinberg, P.; Hohenadl, C.; et al. GBP-1 Acts as a Tumor Suppressor in Colorectal Cancer Cells. *Carcinogenesis* **2013**, *34*, 153–162. [[CrossRef](#)] [[PubMed](#)]
64. Xu, H.; Sun, L.; Zheng, Y.; Yu, S.; Ou-yang, J.; Han, H.; Dai, X.; Yu, X.; Li, M.; Lan, Q. GBP3 Promotes Glioma Cell Proliferation via SQSTM1/P62-ERK1/2 Axis. *Biochem. Biophys. Res. Commun.* **2018**, *495*, 446–453. [[CrossRef](#)] [[PubMed](#)]
65. Lee, S.; Kim, H.; Naidansuren, P.; Ham, K.A.; Choi, H.S.; Ahn, H.; Kim, M.; Kang, D.H.; Kang, S.W.; Joe, Y.A. Peroxidase Is Essential for Endothelial Cell Survival and Growth Signaling by Sulfilimine Crosslink-dependent Matrix Assembly. *FASEB J.* **2020**, *34*, 10228–10241. [[CrossRef](#)] [[PubMed](#)]
66. Kurihara-Shimomura, M.; Sasahira, T.; Shimomura, H.; Kirita, T. Peroxidase Plays a Tumor-Promoting Role in Oral Squamous Cell Carcinoma. *Int. J. Mol. Sci.* **2020**, *21*, 5416. [[CrossRef](#)]
67. Paumann-Page, M.; Kienzl, N.F.; Motwani, J.; Bathish, B.; Paton, L.N.; Magon, N.J.; Sevcnikar, B.; Furtmüller, P.G.; Traxlmayr, M.W.; Obinger, C.; et al. Peroxidase Protein Expression and Enzymatic Activity in Metastatic Melanoma Cell Lines Are Associated with Invasive Potential. *Redox Biol.* **2021**, *46*, 102090. [[CrossRef](#)]
68. Cai, C.; Chen, S.-Y.; Zheng, Z.; Omwancha, J.; Lin, M.-F.; Balk, S.; Shemshedini, L. Androgen Regulation of Soluble Guanylyl Cyclase1 Mediates Prostate Cancer Cell Proliferation. *Oncogene* **2007**, *26*, 1606–1615. [[CrossRef](#)]
69. Babykutty, S.; Suboj, P.; Srinivas, P.; Nair, A.S.; Chandramohan, K.; Gopala, S. Insidious Role of Nitric Oxide in Migration/Invasion of Colon Cancer Cells by Upregulating MMP-2/9 via Activation of CGMP-PKG-ERK Signaling Pathways. *Clin. Exp. Metastasis* **2012**, *29*, 471–492. [[CrossRef](#)]
70. Schwappacher, R.; Rangaswami, H.; Su-Yuo, J.; Hassad, A.; Spittler, R.; Casteel, D.E. CGMP-Dependent Protein Kinase  $\beta$  Regulates Breast Cancer Cell Migration and Invasion via a Novel Interaction with the Actin/Myosin-Associated Protein Caldesmon. *J. Cell Sci.* **2013**, *126*, 1626–1636. [[CrossRef](#)]
71. Ronchetti, S.A.; Pino, M.T.L.; Cordeiro, G.; Bollani, S.N.; Ricci, A.G.; Duvilanski, B.H.; Cabilla, J.P. Soluble Guanylyl Cyclase A1 Subunit Is a Key Mediator of Proliferation, Survival, and Migration in ECC-1 and HeLa Cell Lines. *Sci. Rep.* **2019**, *9*, 14797. [[CrossRef](#)] [[PubMed](#)]
72. Zhou, J.; Gao, S.; Hsieh, C.-L.; Malla, M.; Shemshedini, L. Peptide B Targets Soluble Guanylyl Cyclase A1 and Kills Prostate Cancer Cells. *PLoS ONE* **2017**, *12*, e0184088. [[CrossRef](#)]
73. Daulat, A.M.; Bertucci, F.; Audebert, S.; Sergé, A.; Finetti, P.; Josselin, E.; Castellano, R.; Birnbaum, D.; Angers, S.; Borg, J.-P. PRICKLE1 Contributes to Cancer Cell Dissemination through Its Interaction with MTORC2. *Dev. Cell* **2016**, *37*, 311–325. [[CrossRef](#)] [[PubMed](#)]
74. Jiang, D.; He, Y.; Mo, Q.; Liu, E.; Li, X.; Huang, L.; Zhang, Q.; Chen, F.; Li, Y.; Shao, H. PRICKLE1, a Wnt/PCP Signaling Component, Is Overexpressed and Associated with Inferior Prognosis in Acute Myeloid Leukemia. *J. Transl. Med.* **2021**, *19*, 211. [[CrossRef](#)]
75. Huang, S.; Zhao, J.; Song, J.; Li, Y.; Zuo, R.; Sa, Y.; Ma, Z.; OuYang, H. Interferon Alpha-Inducible Protein 27 (IFI27) Is a Prognostic Marker for Pancreatic Cancer Based on Comprehensive Bioinformatics Analysis. *Bioengineered* **2021**, *12*, 8515–8528. [[CrossRef](#)]
76. Lao, M.; Zhang, X.; Ma, T.; Xu, J.; Yang, H.; Duan, Y.; Ying, H.; Zhang, X.; Guo, C.; Qiu, J.; et al. Regulator of Calcineurin 1 Gene Isoform 4 in Pancreatic Ductal Adenocarcinoma Regulates the Progression of Tumor Cells. *Oncogene* **2021**, *40*, 3136–3151. [[CrossRef](#)] [[PubMed](#)]
77. Gordon, K.J.; Kirkbride, K.C.; How, T.; Blobe, G.C. Bone Morphogenetic Proteins Induce Pancreatic Cancer Cell Invasiveness through a Smad1-Dependent Mechanism That Involves Matrix Metalloproteinase-2. *Carcinogenesis* **2009**, *30*, 238–248. [[CrossRef](#)]
78. Takagi, K.; Shimomura, A.; Imura, J.; Mori, H.; Noguchi, A.; Tanaka, S.; Minamisaka, T.; Nishida, T.; Hatta, H.; Nakajima, T. Interleukin-32 Regulates Downstream Molecules and Promotes the Invasion of Pancreatic Cancer Cells. *Oncol. Lett.* **2021**, *23*, 14. [[CrossRef](#)]
79. Sun, Q.; Ye, Z.; Qin, Y.; Fan, G.; Ji, S.; Zhuo, Q.; Xu, W.; Liu, W.; Hu, Q.; Liu, M.; et al. Oncogenic Function of TRIM2 in Pancreatic Cancer by Activating ROS-Related NRF2/ITGB7/FAK Axis. *Oncogene* **2020**, *39*, 6572–6588. [[CrossRef](#)]
80. Wang, L.; Wang, L.; Zhang, H.; Lu, J.; Zhang, Z.; Wu, H.; Liang, Z. AREG Mediates the Epithelial-mesenchymal Transition in Pancreatic Cancer Cells via the EGFR/ERK/NF- $\kappa$ B Signaling Pathway. *Oncol. Rep.* **2020**, *43*, 1558–1568. [[CrossRef](#)]
81. Abdulkareem, N.M.; Bhat, R.; Qin, L.; Vasaikar, S.; Gopinathan, A.; Mitchell, T.; Shea, M.J.; Nanda, S.; Thangavel, H.; Zhang, B.; et al. A Novel Role of ADGRF1 (GPR110) in Promoting Cellular Quiescence and Chemoresistance in Human Epidermal Growth Factor Receptor 2-positive Breast Cancer. *FASEB J.* **2021**, *35*, e21719. [[CrossRef](#)]
82. Masuda, M.; Uno, Y.; Ohbayashi, N.; Ohata, H.; Mimata, A.; Kukimoto-Niino, M.; Moriyama, H.; Kashimoto, S.; Inoue, T.; Goto, N.; et al. TNIK Inhibition Abrogates Colorectal Cancer Stemness. *Nat. Commun.* **2016**, *7*, 12586. [[CrossRef](#)] [[PubMed](#)]

83. Wang, T.; Abou-Ouf, H.; Hegazy, S.A.; Alshalalfa, M.; Stoletov, K.; Lewis, J.; Donnelly, B.; Bismar, T.A. Ankyrin G Expression Is Associated with Androgen Receptor Stability, Invasiveness, and Lethal Outcome in Prostate Cancer Patients. *J. Mol. Med.* **2016**, *94*, 1411–1422. [[CrossRef](#)] [[PubMed](#)]
84. Zeng, C.; Long, J.; Deng, C.; Xie, L.; Ma, H.; Guo, Y.; Liu, S.; Deng, M. Genetic Alterations in Papillary Thyroid Carcinoma with Hashimoto's Thyroiditis: ANK3, an Indolent Maintainer of Papillary Thyroid Carcinoma. *Front. Oncol.* **2022**, *12*, 894786. [[CrossRef](#)] [[PubMed](#)]
85. Zhao, M.; Liu, Y.; Zheng, C.; Qu, H. DbEMT 2.0: An Updated Database for Epithelial-Mesenchymal Transition Genes with Experimentally Verified Information and Precalculated Regulation Information for Cancer Metastasis. *J. Genet. Genom.* **2019**, *46*, 595–597. [[CrossRef](#)] [[PubMed](#)]
86. Wu, T.-C.; Liao, C.-Y.; Lu, W.-C.; Chang, C.-R.; Tsai, F.-Y.; Jiang, S.-S.; Chen, T.-H.; Lin, K.M.-C.; Chen, L.-T.; Chang, W.-S.W. Identification of Distinct Slow Mode of Reversible Adaptation of Pancreatic Ductal Adenocarcinoma to the Prolonged Acidic PH Microenvironment. *J. Exp. Clin. Cancer Res.* **2022**, *41*, 137. [[CrossRef](#)]
87. Hagelund, S.; Trauzold, A. Impact of Extracellular PH on Apoptotic and Non-Apoptotic TRAIL-Induced Signaling in Pancreatic Ductal Adenocarcinoma Cells. *Front. Cell Dev. Biol.* **2022**, *10*, 768579. [[CrossRef](#)]
88. Rohani, N.; Hao, L.; Alexis, M.S.; Joughin, B.A.; Krismer, K.; Moufarrej, M.N.; Soltis, A.R.; Lauffenburger, D.A.; Yaffe, M.B.; Burge, C.B.; et al. Acidification of Tumor at Stromal Boundaries Drives Transcriptome Alterations Associated with Aggressive Phenotypes. *Cancer Res.* **2019**, *79*, 1952–1966. [[CrossRef](#)]
89. Corbet, C.; Feron, O. Tumour Acidosis: From the Passenger to the Driver's Seat. *Nat. Rev. Cancer* **2017**, *17*, 577–593. [[CrossRef](#)]
90. Swietach, P. What Is PH Regulation, and Why Do Cancer Cells Need It? *Cancer Metastasis Rev.* **2019**, *38*, 5–15. [[CrossRef](#)]
91. Riemann, A.; Schneider, B.; Ihling, A.; Nowak, M.; Sauvant, C.; Thews, O.; Gekle, M. Acidic Environment Leads to ROS-Induced MAPK Signaling in Cancer Cells. *PLoS ONE* **2011**, *6*, e22445. [[CrossRef](#)] [[PubMed](#)]
92. Pedersen, S.F.; Jørgensen, N.K.; Damgaard, I.; Schousboe, A.; Hoffmann, E.K. Mechanisms of PHi Regulation Studied in Individual Neurons Cultured from Mouse Cerebral Cortex. *J. Neurosci. Res.* **1998**, *51*, 431–441. [[CrossRef](#)]
93. White, K.A.; Grillo-Hill, B.K.; Barber, D.L. Cancer Cell Behaviors Mediated by Dysregulated PH Dynamics at a Glance. *J. Cell Sci.* **2017**, *130*, 663–669. [[CrossRef](#)] [[PubMed](#)]
94. Persi, E.; Duran-Frigola, M.; Damaghi, M.; Roush, W.R.; Aloy, P.; Cleveland, J.L.; Gillies, R.J.; Ruppin, E. Systems Analysis of Intracellular PH Vulnerabilities for Cancer Therapy. *Nat. Commun.* **2018**, *9*, 2997. [[CrossRef](#)] [[PubMed](#)]
95. Russell, S.; Xu, L.; Kam, Y.; Abrahams, D.; Ordway, B.; Lopez, A.S.; Bui, M.M.; Johnson, J.; Epstein, T.; Ruiz, E.; et al. Proton Export Upregulates Aerobic Glycolysis. *BMC Biol.* **2022**, *20*, 163. [[CrossRef](#)]
96. Bevington, A.; Walls, J. Protein Catabolism in Metabolic Acidosis: Inhibition of Glycolysis by Low PH Suggests a Role for Glucose. *Biochem. Soc. Trans.* **1995**, *23*, 464S. [[CrossRef](#)]
97. de Bem Prunes, B.; Nunes, J.S.; da Silva, V.P.; Laureano, N.K.; Gonçalves, D.R.; Machado, I.S.; Barbosa, S.; Lamers, M.L.; Rados, P.V.; Kurth, I.; et al. The Role of Tumor Acidification in Aggressiveness, Cell Dissemination and Treatment Resistance of Oral Squamous Cell Carcinoma. *Life Sci.* **2022**, *288*, 120163. [[CrossRef](#)]
98. Oster, L.; Schröder, J.; Rugi, M.; Schimmelpennig, S.; Sargin, S.; Schwab, A.; Najder, K. Extracellular PH Controls Chemotaxis of Neutrophil Granulocytes by Regulating Leukotriene B<sub>4</sub> Production and Cdc42 Signaling. *J. Immunol.* **2022**, *209*, 136–144. [[CrossRef](#)]
99. Nagano, M.; Hoshino, D.; Koshikawa, N.; Akizawa, T.; Seiki, M. Turnover of Focal Adhesions and Cancer Cell Migration. *Int. J. Cell Biol.* **2012**, *2012*, 310616. [[CrossRef](#)]
100. Cardone, R.A.; Casvola, V.; Reshkin, S.J. The Role of Disturbed PH Dynamics and the Na<sup>+</sup>/H<sup>+</sup> exchanger in metastasis. *Nat. Rev. Cancer* **2005**, *5*, 786–795. [[CrossRef](#)]
101. Brisson, L.; Reshkin, S.J.; Goré, J.; Roger, S. PH Regulators in Invasosomal Functioning: Proton Delivery for Matrix Tasting. *Eur. J. Cell Biol.* **2012**, *91*, 847–860. [[CrossRef](#)] [[PubMed](#)]
102. Reshkin, S.J.; Cardone, R.A.; Harguindey, S. Na<sup>+</sup>/H<sup>+</sup> Exchanger, PH Regulation and Cancer. *Recent Pat. Anti-Cancer Drug Discov.* **2012**, *8*, 85–99. [[CrossRef](#)]
103. Swayampakula, M.; McDonald, P.C.; Vallejo, M.; Coyaudo, E.; Chafe, S.C.; Westerback, A.; Venkateswaran, G.; Shankar, J.; Gao, G.; Laurent, E.M.N.; et al. The Interactome of Metabolic Enzyme Carbonic Anhydrase IX Reveals Novel Roles in Tumor Cell Migration and Invadopodia/MMP14-Mediated Invasion. *Oncogene* **2017**, *36*, 6244–6261. [[CrossRef](#)] [[PubMed](#)]
104. Lee, S.-H.; McIntyre, D.; Honess, D.; Hulikova, A.; Pacheco-Torres, J.; Cerdán, S.; Swietach, P.; Harris, A.L.; Griffiths, J.R. Carbonic Anhydrase IX Is a PH-Stat That Sets an Acidic Tumour Extracellular PH in Vivo. *Br. J. Cancer* **2018**, *119*, 622–630. [[CrossRef](#)] [[PubMed](#)]
105. Yilmaz, M.; Christofori, G. EMT, the Cytoskeleton, and Cancer Cell Invasion. *Cancer Metastasis Rev.* **2009**, *28*, 15–33. [[CrossRef](#)]
106. Ranieri, D.; Guttieri, L.; Raffa, S.; Torrisi, M.R.; Belleudi, F. Role of FGFR2c and Its PKCε Downstream Signaling in the Control of EMT and Autophagy in Pancreatic Ductal Adenocarcinoma Cells. *Cancers* **2021**, *13*, 4993. [[CrossRef](#)]
107. Qian, J.; Liu, H.; Chen, W.; Wen, K.; Lu, W.; Huang, C.; Fu, Z. Knockdown of Slug by RNAi Inhibits the Proliferation and Invasion of HCT116 Colorectal Cancer Cells. *Mol. Med. Rep.* **2013**, *8*, 1055–1059. [[CrossRef](#)]

**Disclaimer/Publisher's Note:** The statements, opinions and data contained in all publications are solely those of the individual author(s) and contributor(s) and not of MDPI and/or the editor(s). MDPI and/or the editor(s) disclaim responsibility for any injury to people or property resulting from any ideas, methods, instructions or products referred to in the content.

*Supplementary*

# **Acidic Growth Conditions Promote Epithelial-to-Mesenchymal Transition to Select More Aggressive PDAC Cell Phenotypes In Vitro**

**Madelaine Magali Audero, Tiago Miguel Amaral Carvalho, Federico Alessandro Ruffinatti, Thorsten Loeck, Maya Yassine, Giorgia Chinigò, Antoine Folcher, Valerio Farfariello, Samuele Amadori, Chiara Vaghi, Albrecht Schwab, Stephan J. Reshkin, Rosa Angela Cardone, Natalia Prevarskaya and Alessandra Fiorio Pla**

## **Materials and Methods**

### *ATP quantification assay*

For ATP quantification assay, cells were plated in 96-well black-bottom polystyrene plates (Greiner Bio-One, Austria) at a density of 3000 cells/well for PANC-1 and 8000 cells/well for Mia PaCa-2 cells in 100 ul medium volume and let adhere overnight in physiological pHe conditions for control, 4 days pHe 6.6 and pHe- selected + 7.4 cell models, while pHe-selected cells were plated in acidic conditions. Acidic cell models were treated with fresh acidic pHe (pHe 6.6) medium the following day, and ATP quantification was assessed at 1h, 48h, and 96h. The number of metabolically active cells was quantified based on the ATP amount using CellTiter-Glo® 2.0 Luminescent Cell Viability Assay (Promega, Cat# G9241) following the manufacturer's indications. Luminescence was recorded using a microplate reader (FilterMax F5, Multi-Mode Microplate Reader, Molecular Devices). Each condition was tested in eight technical replicates, and three independent experiments were performed for each experimental condition.

### *Single-cell time-lapse cell random migration*

PANC-1 cells were plated in technical duplicate in 1% gelatin-coated wells at a density of 5000 cells/well in 500 ul volume in 24-well plates and incubated at 37°C overnight. Before time-lapse imaging, media was changed to remove detached cells. For time-lapse image acquisition, cells were kept at 37°C and under 5% CO<sub>2</sub> in an incubator chamber (Okolab). Cells' random migration was followed in phase contrast illumination at 20X magnification using Eclipse Ti-E Nikon inverted microscope, selecting five representative fields per well, resulting in a total of ten fields per condition and each image stack containing 60 frames. Images were acquired every 10 minutes for 10 hours with a CCD video camera using NIS-Element software (Nikon). Image stacks were analyzed with ImageJ software, and cells were manually tracked using the MtrackJ plugin. Dividing cells and

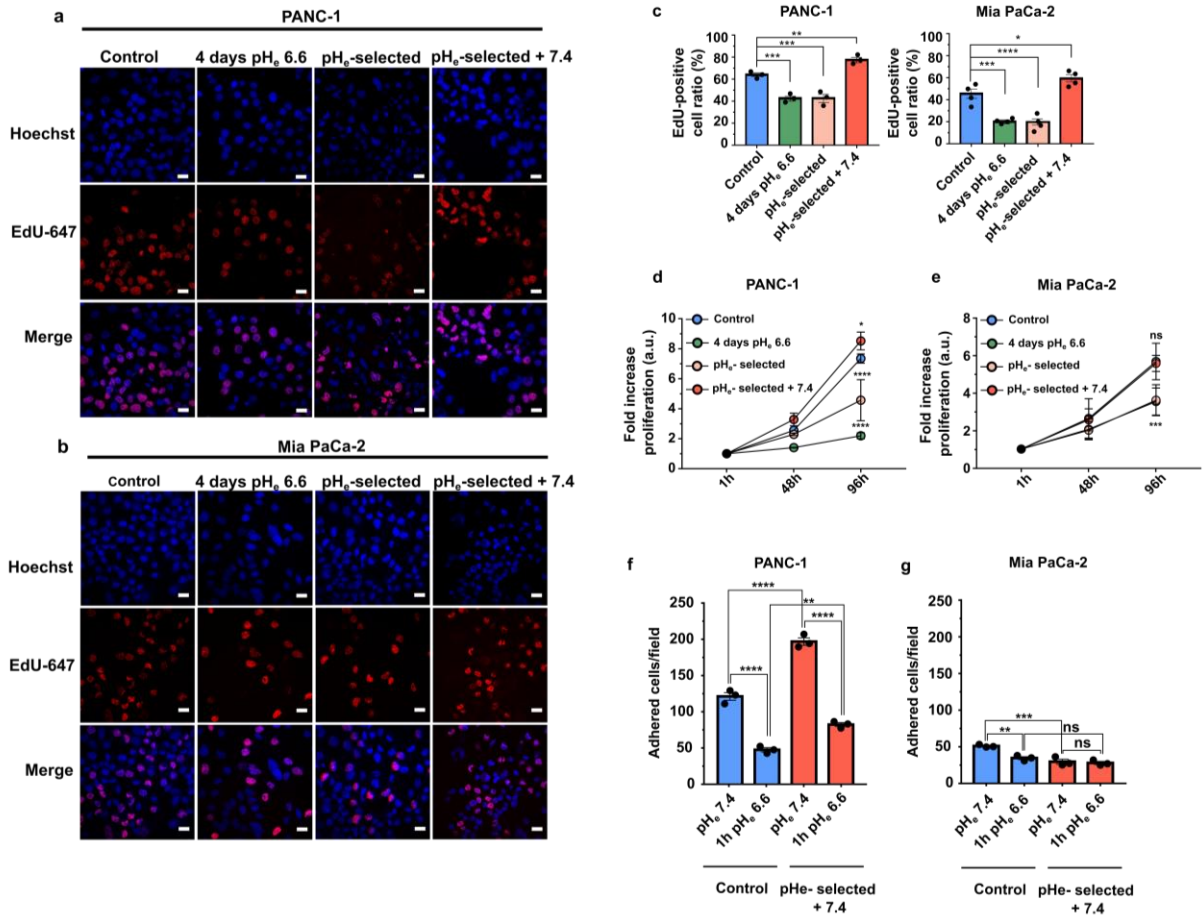


cells exiting the recorded field were excluded from data analysis, and cells' migratory velocity was used as the parameter. Three independent experiments were performed for each experimental condition.

#### *Immunofluorescence paxillin staining and confocal microscopy*

PANC-1 cells seeded on 1% gelatin-coated coverslips were washed twice with cold phosphate-buffered saline (PBS) and fixed with 4% paraformaldehyde for 15 min at 4°C. After washing the samples twice with ice-cold PBS, the fixed cells were then incubated for 10 min at room temperature with PBS containing either 0.1% Triton X-100 (PBST) for permeabilization and blocking of unspecific binding of the antibody was obtained by incubating the cells with PBST containing 1% gelatin and 0.2 M glycine for 30 minutes. The solution was decanted, and a quick wash with cold PBS followed. Cells were incubated in diluted Alexa Fluor® 647 Anti-Paxillin antibody (1:200, ab246719) in PBS containing 1% gelatin overnight at 4°C. The cells were then kept in the dark and washed three times in PBS for 5 minutes each, following DAPI staining for 10 minutes at room temperature. Cells were washed twice with PBS, and coverslips were mounted on glass slides with a drop of Glycergel. Coverslips were sealed with nail polish and stored in the dark at 4°C. Glass slides were then examined using a confocal laser scanning microscope (LSM 700, Carl Zeiss MicroImaging GmbH) with a Plan Aplanachromat 40x/1.3 numerical aperture oil immersion objective. Peripheral and cytosolic focal Adhesions (FAs) parameters were quantified with ImageJ (NIH, Bethesda, Maryland, USA) by manually selecting at least 10 cells as region of interest (ROI) of 5 representative fields per biological replicate, and paxillin dots were distinguished from the background by applying a threshold, and subsequently, FAs' area and density were automatically quantified by ImageJ software. FAs peripheral translocation was quantified by peripheral FAs to cytoplasmic FAs ratio. The mean numbers obtained from each biological replicate were used for statistical analysis. Three independent experiments were performed for each experimental condition.

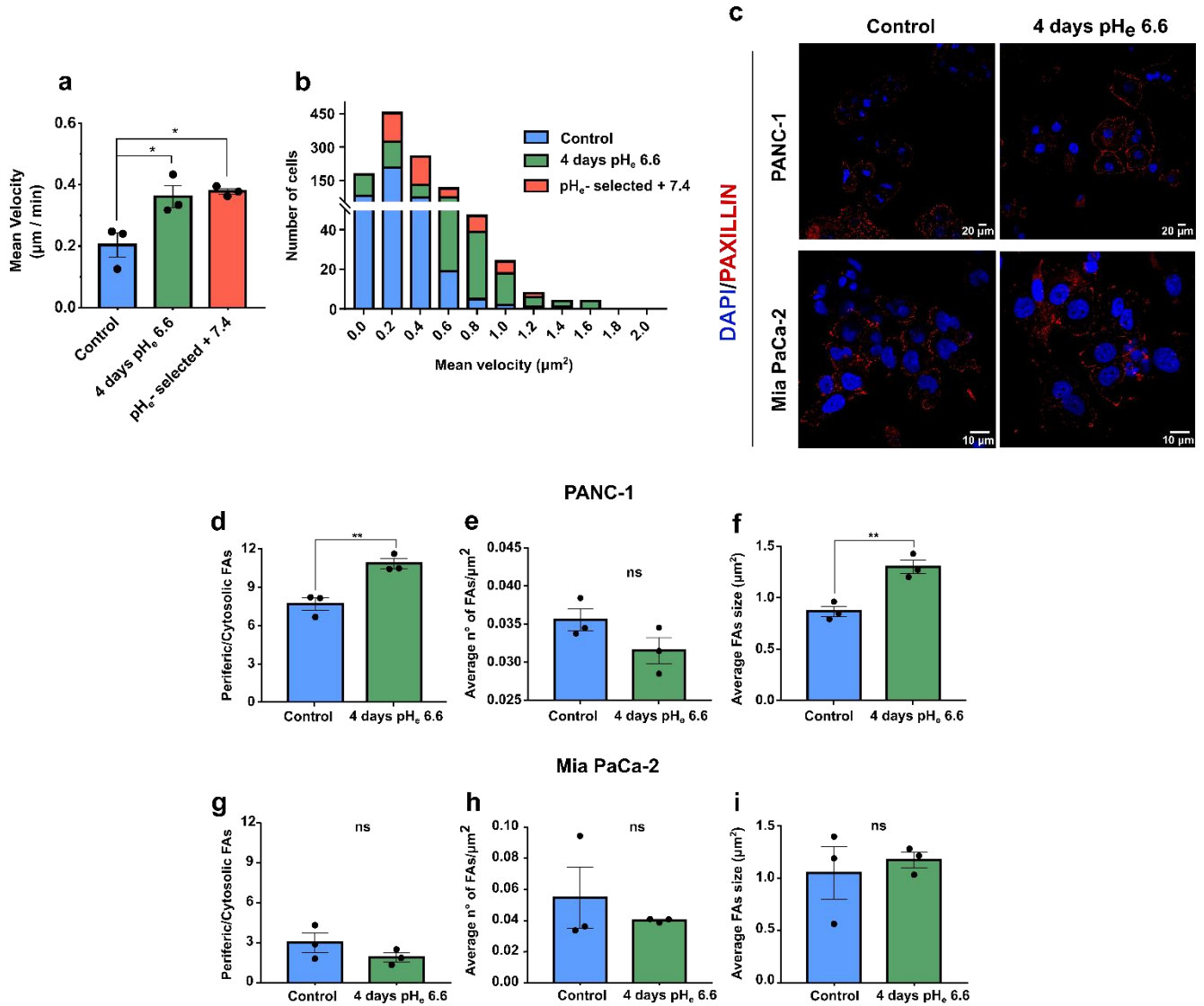
Supplementary Figure S1:



Effect of acidic pH<sub>e</sub> on cell proliferation, ATP production and of acidic pH<sub>e</sub> acute treatment of cell-substrate adhesion in PANC-1 and Mia PaCa-2. **a)** Representative fluorescence images of PANC-1 and **b)** Mia PaCa-2 cell proliferation obtained by EdU staining assay (red, Alexa Fluor 647) and Hoechst (blue) nuclear staining. Scale bar = 20 μm. **c)** Quantification of the percentage of PANC-1 (left) and Mia PaCa-2 EdU-positive cells (right) upon treatment with acidic pH<sub>e</sub>. Data were reported as the percentage of EdU/Hoechst-positive cell mean ± SEM from 4 representative regions for each condition. **d)** Fold increase in proliferation rate in PANC-1 and **e)** Mia PaCa-2 cells' models assessed by ATP quantification at 1h, 48h, and 96h. Significant differences between PANC-1 or Mia PaCa-2 control vs. all at 96h. **f)** Cell adhesion assay performed on PANC-1 and **g)** Mia PaCa-2 control and pH<sub>e</sub>-selected cells + 7.4 exposed for 1 hour to pH<sub>e</sub> 6.6 (acute treatment) before fixation and counting of cells. Data were collected from 4 representative regions for each condition. Each condition was repeated in 8 technical replicates. All data were presented as mean ± SEM from three independent experiments and analyzed using Two-way

ANOVA with Dunnett's multiple comparisons test and One-way ANOVA with Tukey's multiple comparisons test for e) and f), \*  $p < 0.05$ , \*\*  $p < 0.01$ , \*\*\*  $p < 0.001$ , \*\*\*\*  $p < 0.0001$ .

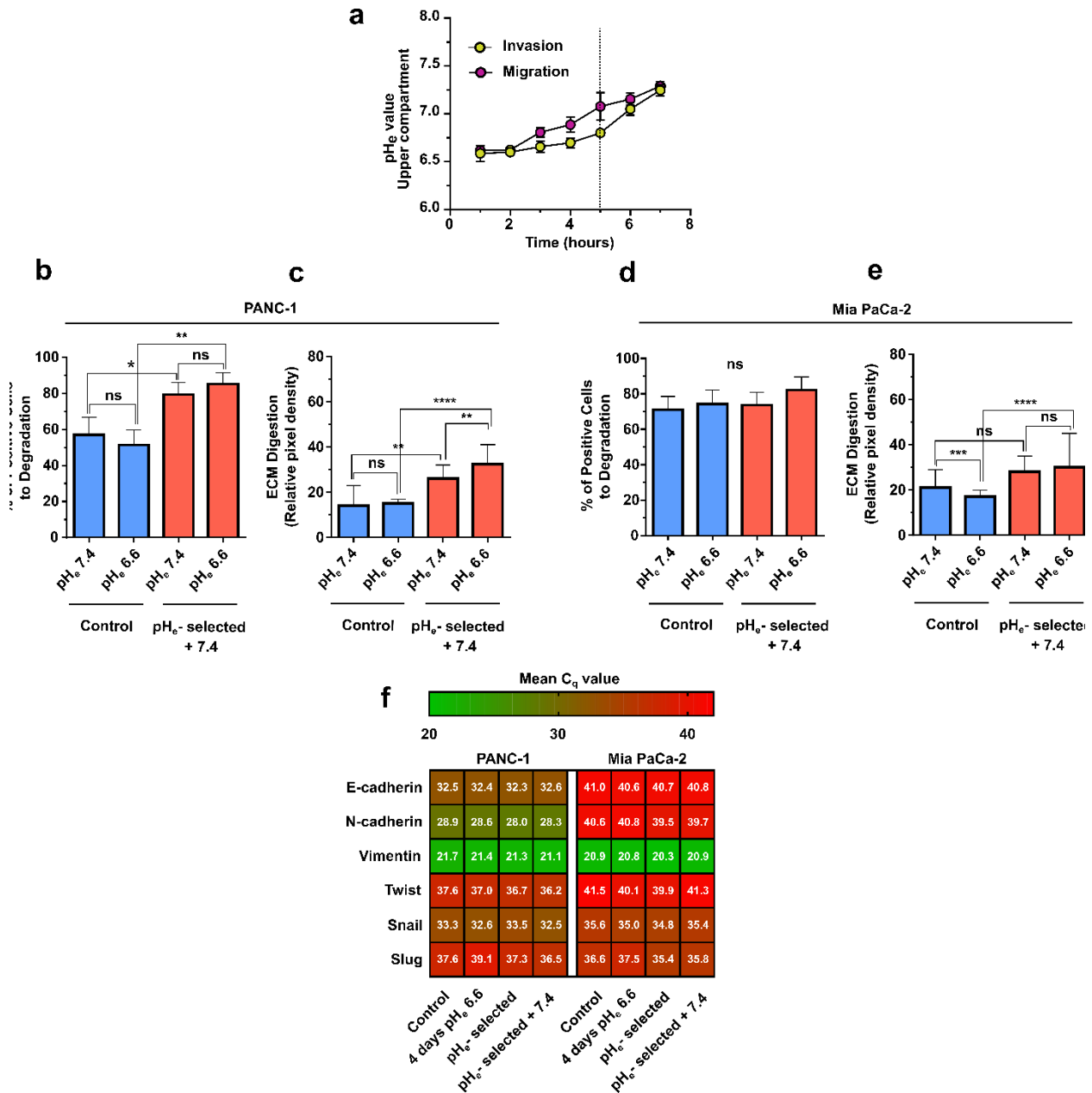
**Supplementary Figure S2:**



**Effect of acidic pH<sub>e</sub> on single cell migration in PANC-1 cells and on Focal Adhesions (FAs) membrane recruitment on PANC-1 and Mia PaCa-2 cells.** **a)** Quantification of PANC-1 control, 4 days pH<sub>e</sub> 6.6 and pH<sub>e</sub>-selected + 7.4 cells' mean velocity (µm/min) obtained by single-cell time-lapse videomicroscopy. Data were collected from five representative regions for each condition (n= 390 cells for control, n= 387 cells for 4 days pH<sub>e</sub> 6.6, n= 311 cells for pH<sub>e</sub>- selected + 7.4). **b)** Histogram showing the frequency distribution of PANC-1 migration velocities in control cells and in response to 4 days- and 1 month-long (followed by acclimation in 7.4) treatments

in pH<sub>e</sub> 6.6 (n= 390 cells for control, n= 387 cells for 4 days pH<sub>e</sub> 6.6, n= 311 cells for pH<sub>e</sub>- selected + 7.4). **c)** DAPI (blue) nuclei staining and Paxillin (Alexa Fluor 647, red) immunofluorescence staining of PDAC control and 4 days pH<sub>e</sub> 6.6 cells on gelatin-coated coverslips, obtained by confocal microscopy (Scale bar= 20 μm for PANC-1 cells and 10 μm for Mia PaCa-2 cells). Focal adhesions were observed by staining for paxillin (red). The photos are representative of one field of one experiment. **d and g)** Quantification of the peripheric/cytosolic focal adhesions (FA) ratio, indicative of paxillin recruitment to the focal adhesion, of **e and h)** the average number of focal adhesions (FAs) per μm<sup>2</sup> and of **f and i)** average size (μm<sup>2</sup>) of FAs in PANC-1 and Mia PaCa-2 control cells and 4 days pH<sub>e</sub> 6.6 cells following paxillin staining (n= 162 cells for control, n= 160 cells for 4 days pH<sub>e</sub> 6.6 for PANC-1 cells, n= 88 cells for control, n= 45 cells for 4 days pH<sub>e</sub> 6.6 for Mia PaCa-2 cells). All data were reported as mean ± SEM from three independent experiments. Data were analyzed using One-way ANOVA with Dunnett's multiple comparisons test and using an unpaired t-test for d), e), f), g), h), and i), \* p < 0.05, \*\* p < 0.01, ns not significant.

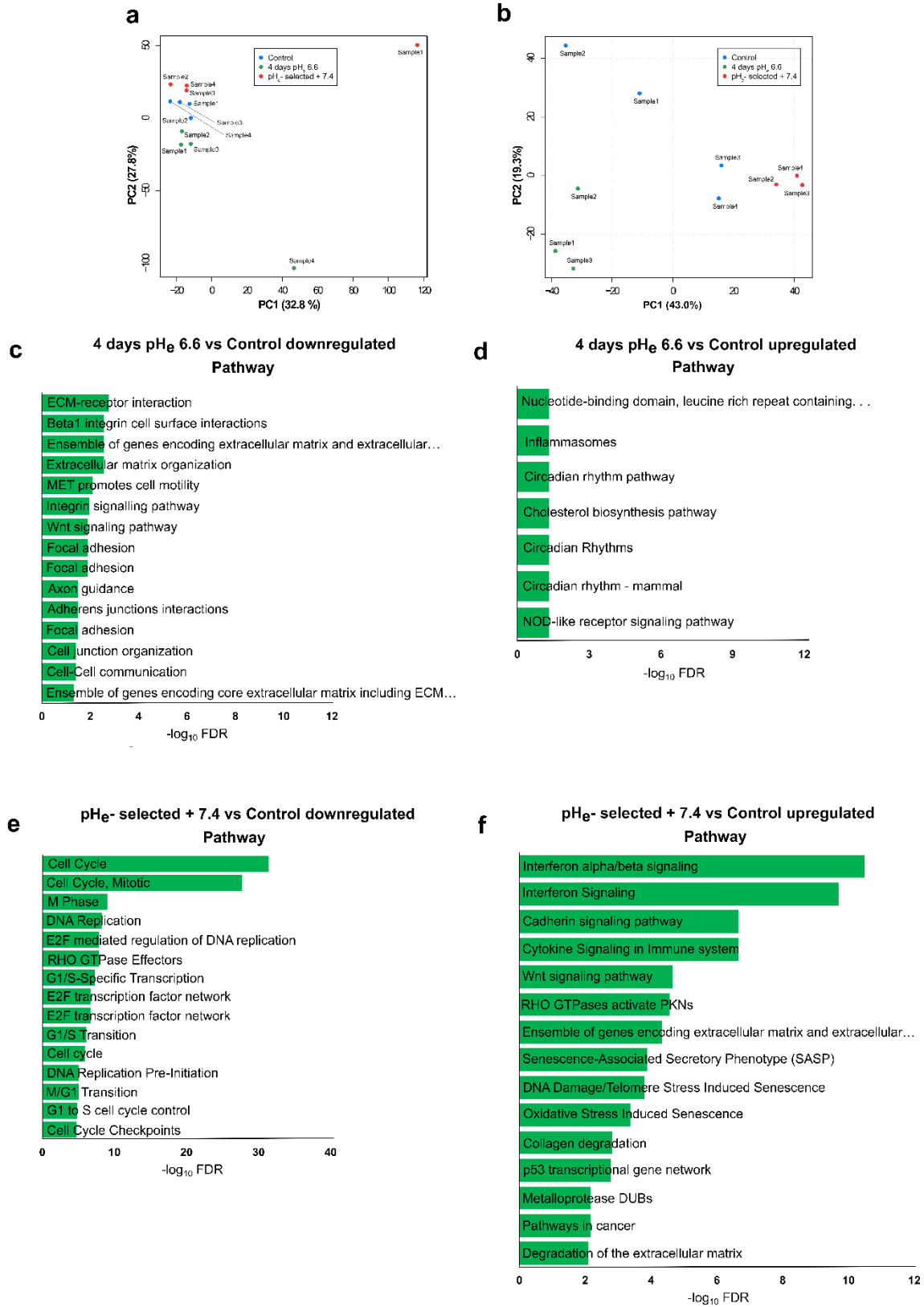
Supplementary Figure S3:



Establishment of a pH gradient in the Transwell system and effect of acute exposition to acidic  $pH_e$  on PANC-1 and Mia PaCa-2 cells' invadopodia activity and epithelial-mesenchymal transition. **a)** Time course indicates the maintenance of pH values of the acidic medium ( $pH_e$  6.6) in the upper compartment of the Transwell system in the presence of  $pH_e$  7.4 in the lower chamber, the presence or absence of a matrigel coating. Cell plates containing the Transwell systems were maintained in the incubator at 37°C and 5%  $CO_2$  to allow pH to equilibrate. Measurements were recorded every hour for 8 hours immediately after removing the plate from the incubator by using pH strips to minimize the time outside the incubator and the alkalization of the acidic

medium in the upper compartment. **b)** Quantification of the percentage of positive cells to ECM digestion and of **c)** the mean number of invadopodia per cell in PANC-1 control cells and pH<sub>e</sub><sup>-</sup> selected + 7.4 exposed or not to an overnight exposure to pH<sub>e</sub> 6.6. **d)** Quantification of the percentage of positive cells to ECM digestion and of **e)** the mean number of invadopodia per cell in Mia PaCa-2 control cells and pH<sub>e</sub><sup>-</sup> selected + 7.4 exposed or not to an overnight exposure to pH<sub>e</sub> 6.6. **f)** Heatmap showing the RT-PCR mean cycle thresholds (C<sub>q</sub>) of PANC-1 and Mia PaCa-2 control, 4 days pH<sub>e</sub> 6.6, pH<sub>e</sub><sup>-</sup> selected, and pH<sub>e</sub><sup>-</sup> selected + 7.4 cells. Columns represent each condition of the different PDAC cell lines, while rows indicate the mean C<sub>q</sub> value of triplicate biological samples, and they are visualized in green and red color scales. All data were reported as mean (± SEM) from three independent experiments, and they were analyzed using Kruskal-Wallis H-test and Dunn's multiple comparison test, \* p < 0.05, \*\* p < 0.01, ns not significant, \*\*\* p < 0.001, \*\*\*\* p < 0.0001, ns not significant.

Supplementary Figure S4:



**Principal component analysis (PCA) of RNA-seq-based expression data and gene ontology (GO) pathway enrichment analysis of PANC-1 differentially expressed genes (DEGs) in response to acidosis.** **a)** Three-dimensional PCA scatter plots of the first two principal components (PC1, x-axis, PC2, y-axis). PCA was conducted to infer the quality of the RNA-seq data. Each point indicates an RNA-seq sample, and biological replicates are represented with the same colors (red= control, green= 4 days pHe 6.6, blue= pHe- selected + 7.4). The processed RNA data formed spatially distinct clusters within the same sample group in the first (PC1) and second (PC2) principal components, indicating similar gene expression profiles. The PCA analysis also revealed differences among RNA-seq data of corresponding conditions (4 days pHe 6.6 replicate 2 and pHe- selected + 7.4 replicate 1), mostly due to biological variability of cell populations, therefore the replicates aforementioned were excluded from the samples cohort and **b)** PC analysis was re-performed, showing the segregation of control samples from both acidic conditions. **c)** Bar chart of the most relevant enriched pathway as defined in GO database and resulting from the analysis of genes downregulated in PANC-1 4 days pHe 6.6 cells vs. Control, and **e)** in PANC-1 pHe- selected + 7.4 cells vs. Control, and of genes upregulated in **d)** PANC-1 4 days pHe 6.6 cells vs. Control, and **f)** in PANC-1 pHe- selected + 7.4 cells vs. Control.



## ***II. $pH_e$ -sensitive Store-Operated $Ca^{2+}$ channels signals contribute to tumour acidic microenvironment-induced PDAC cells selection to more aggressive phenotypes.***

Madelaine Magali Audero<sup>1,2</sup>, Federico Ruffinatti<sup>2</sup>, Kateryna Kondratska<sup>1</sup>, Luca Munaron<sup>2</sup>, Natalia Prevarskaya<sup>1</sup>†\* and Alessandra Fiorio Pla<sup>1,2</sup>† \*

<sup>1</sup> U1003—PHYCEL—Laboratoire de Physiologie Cellulaire, Inserm, University of Lille, Villeneuve d'Ascq, 59000 Lille, France; madelaine.audero@univ-lille.fr (M.M.A.); mhy06@mail.aub.edu (M.Y.); valerio.farfariello@inserm.fr (V.F.); antoine.folcher@inserm.fr (A.F.); alessandra.fiorio@unito.it (A.F.P.); natacha.prevarskaya@univ-lille.fr (N.P.)

<sup>2</sup> Laboratory of Cellular and Molecular Angiogenesis, Department of Life Sciences and Systems Biology, University of Turin, 10123 Turin, Italy; federicoalessandro.ruffinatti@unito.it (F.A.R.)

\* Correspondence: alessandra.fiorio@unito.it; Tel.: +39-0116704660, natacha.prevarskaya@univ-lille.fr; Tel.: +33-320336423

† These authors contributed equally to this work.

### **Paper in preparation**

### **Abstract**

Pancreatic ductal adenocarcinoma (PDAC) represents one of the deadliest cancers, whose aggressiveness is partly due to a highly acidic tumour microenvironment (TME), a key player in PDAC onset and progression. Indeed, cancer cells are subjected to the selective pressure induced by the low  $pH_e$ . In this situation, they respond by developing strategies to gain competitive advantages over normal cells or other cancer subpopulations and survive. In this context, ion channels, particularly  $Ca^{2+}$ -permeable channels, are key proteins in the interaction between the TME and cancer cells, acting as  $pH$  sensors and transducing signals to activate intracellular downstream pathways linked to PDAC progression. Their deregulation also contributes to several

cancer hallmarks. Despite their importance, the interplay between the  $\text{Ca}^{2+}$  signals and acidic TME in PDAC still needs to be sufficiently addressed. Here, we aimed to investigate  $\text{Ca}^{2+}$  signal responses to acidic stress along different stages of acid selection in PDAC cells. We showed that PANC-1 cells generate different patterns of SOCE-dependent  $\text{Ca}^{2+}$  oscillations under acidic selection, characterised by low frequencies and downregulation of SOCE and ORAI1 during early stages of  $\text{pH}_e$ -selection and recovery of faster  $\text{Ca}^{2+}$  waves, increased SOCE and upregulation of ORAI1 with long-term acidic treatment and recovery to  $\text{pH}_e$  7.4. ORAI1-mediated  $\text{Ca}^{2+}$  entry might be involved in the increased migration and invasion of all the cell models exposed to acidic  $\text{pH}_e$ , as Synta66 treatment and siORAI1 didn't affect control cells' invasion and migration. Our work demonstrates that acid selection and recovery to physiological  $\text{pH}_e$  may employ ORAI1-mediated  $\text{Ca}^{2+}$  signals to promote increased aggressiveness, cell migration, and invasion in PDAC cells.

## Introduction

Pancreatic ductal adenocarcinoma (PDAC) is the most common type of pancreatic cancer, representing the 7th leading cause of cancer death worldwide<sup>1</sup> and characterised by a dismal prognosis (5-year survival rate of ~10%), a result of the lack of screening tests, late diagnosis, and ineffective therapeutic options<sup>2</sup>. To develop improved therapy options, there is an urgent need to deeply investigate the mechanisms that lead to PDAC onset and progression. One major player in PDAC development is the dysregulation of its physiological dynamic pH microenvironment. Pancreatic ductal epithelial cells secrete an alkaline juice from their apical membrane into the pancreatic ducts to neutralise the acidic chyme. To maintain intracellular pH ( $\text{pHi}$ ) homeostasis, the apical secretion is coupled to the extrusion of protons from the basolateral membrane, acidifying the stroma. The pancreatic interstitium extracellular pH ( $\text{pH}_e$ ) will then vary cyclically during digestion and resting phases, leading to a dynamic and unique  $\text{pH}_e$  landscape<sup>3,4</sup>. It was suggested that this intermittent acidification preconditions normal ductal cells to acidity, selecting for acid-resistant cancer subpopulations with acquired survival advantages during PDAC onset<sup>4</sup>. Once PDAC develops, its microenvironment further acidifies due to the Warburg effect and hypoxia<sup>5</sup>, potentiating different cancer-related processes that sustain its advance<sup>6</sup>. In our previous work (submitted), we demonstrated that the genetic and phenotypic responses of PDAC cells change according to the different stages of selection induced by the acidic TME, which selects via epithelial-

to-mesenchymal transition more aggressive PDAC cells in terms of migration and invasion, and the malignant phenotypes are further accentuated when acid-selected cells encounter a more neutral  $\text{pH}_e$  microenvironment, as during local invasion.

To exert its pro-tumour function, the acidic TME relies on several pH-sensitive transmembrane proteins, which intercept its signals and respond accordingly<sup>7,8</sup>. Ion channels are transmembrane proteins whose alterations in gene expression and/or activity have been extensively documented<sup>9</sup>. Ion channels can act as extracellular pH sensors by integrating signals from the TME as changes in  $\text{pH}_e$ , leading to the activation of intracellular signalling pathways involved in cancer development<sup>9</sup> and progression<sup>7,10</sup>. Among ion channels,  $\text{Ca}^{2+}$ -permeable ion channels exert a multifaced role by cross-talking with different cell signalling cascades to selectively regulate innumerable cancer-related processes, such as proliferation, migration, invasion, EMT, chemoresistance, angiogenesis, and cell survival<sup>9</sup>. Oscillatory variations in the cytosolic  $\text{Ca}^{2+}$  levels represent a common cell signalling mechanism that encodes different biological outcomes.  $\text{Ca}^{2+}$  oscillations seem to be a feature of highly metastatic cancer cells<sup>11</sup>, where they contribute to cancer progression by promoting invasion<sup>12</sup>, proliferation and migration<sup>13</sup>, stemness<sup>14</sup> and tumour angiogenesis<sup>15</sup>.  $\text{Ca}^{2+}$  oscillations are documented in pancreatic acinar cells, where elevations in  $[\text{Ca}^{2+}]_i$  and faster  $\text{Ca}^{2+}$  oscillations have been linked to pancreatitis<sup>16</sup>.  $\text{Ca}^{2+}$  oscillations have also been reported in PANC-1 cells following treatment with different agonists, such as ATP, UTP<sup>17</sup> and insulin<sup>18</sup>. However, to our knowledge, the role of  $\text{Ca}^{2+}$  oscillations in PDAC onset or development has yet to be explored. Among the mechanism sustaining  $\text{Ca}^{2+}$  oscillations, the so-called Store-Operated  $\text{Ca}^{2+}$  Entry (SOCE) and its major molecular components ORAI1 and the  $\text{Ca}^{2+}$  sensor STIM play an essential role in the generation of  $\text{Ca}^{2+}$ -oscillations<sup>19,20</sup>. Several pieces of evidence have indeed demonstrated that SOCE signals are often remodelled in cancer due to alterations at the gene or protein level or in the activity of its components. This remodelling affects  $\text{Ca}^{2+}$  homeostasis to promote cell transformation and cancer progression<sup>21</sup>. SOCE signals are also modulated by tumour acidosis<sup>10</sup>, although the consequences of low  $\text{pH}_e$ -mediated SOCE alterations in cancer, particularly PDAC, have not yet been sufficiently explored. Moreover, the hypothesis that acidic TME exploits  $\text{Ca}^{2+}$  signalling as the main route for selecting aggressive cell phenotypes and sustaining PDAC progression needs further attention. Therefore, in this study, we exploited different acidic PDAC cell models previously characterized (see Results I section of the manuscript) to assess the impact of tumour acidosis on  $\text{Ca}^{2+}$  oscillations and Store-Operated  $\text{Ca}^{2+}$  entry (SOCE) in PDAC. Our results

show that short-term acidosis (4 days in  $\text{pH}_e$  6.6) inhibits SOCE in PDAC cells, probably due to the downregulation of ORAI1. This translates into a reduced  $\text{Ca}^{2+}$  entry for fuelling  $\text{Ca}^{2+}$  oscillations, which display minor frequencies compared to control cells. As the acid exposure increases to 1 month, acid-selected cells recover control-like fast  $\text{Ca}^{2+}$  oscillations, with upregulation of SOCE. This output is stronger in  $\text{pH}_e$ -selected cells recovered to  $\text{pH}_e$  7.4. Our results also show that acidic  $\text{pH}_e$  may require ORAI1-mediated  $\text{Ca}^{2+}$  influx to regulate the migratory and invasive capacities of all the acidic models, as both silencing and chemical inhibition of this channel did not affect these abilities in control cells. This highlights the key role of ORAI1 channels as mediators of acidic TME signals in PDAC progression.

## Materials and Methods

### Cell culture

Human pancreatic ductal adenocarcinoma PANC-1 cells were obtained from the Institute for Experimental Cancer Research, Christian-Albrecht-University (CAU) of Kiel, Germany. Mia PaCa-2 cells were purchased from the American Type Culture Collection (ATCC). Control cells were cultured as monolayers in RPMI 1640 growth medium (Gibco, Cat# 31870-025) supplemented with 10% FBS (Biochrom, Cat# S0615), 2 mM L-Glutamine (Gibco, Cat# 25030-024), 1 mM sodium pyruvate (Gibco, Cat# 11360039) and antibiotics (penicillin/streptomycin 100 U ml<sup>-1</sup>, Life Technologies, Inc., Cat# 15070-063). For pH adjustments of the cell culture media to  $\text{pH}_e$  6.6, RPMI 1640 powder medium (Sigma, Cat# R6504) was complemented with  $\text{NaHCO}_3$  according to the Henderson-Hasselbalch equation to derive the target  $\text{pH}_e$  (Table 2). The osmolarity of the medium was balanced using NaCl. The different powders components were dissolved in UltraPure distilled water (Invitrogen, Cat# 10977-035), and the resulting medium was filtered in a sterile environment and supplemented with 10% FBS (Biochrom, Cat# S0615), 1 mM sodium pyruvate (Gibco, Cat# 11360039) and antibiotics (penicillin/streptomycin 100 U ml<sup>-1</sup>, Life Technologies, Inc., Cat# 15070-063). All cells were maintained at 37 °C in a humidified 5%  $\text{CO}_2$  atmosphere. For the generation of the acidic phenotypes, refer to Audero M.M. et al., 2022 (see Results I section of the manuscript).

## **Reagents**

Synta66 (TargetMol Chemicals Inc., Cat# T13047) was stored in DMSO stock solution at a concentration of 100 mM at -20°C. For experiments, a concentration of 10 µM was used. Src kinase inhibitor-1 was purchased from Sigma-Aldrich (Cat# S2075) and stored in 50 mM stock solution in DMSO at -20°C. It was diluted to 5 µM in cell culture medium for experiments. Fura-2 AM was purchased from Invitrogen (Cat# F1221), resuspended in DMSO stock solution, and kept at 4°C. It was used at a final concentration of 5 µM, while Thapsigargin (TG) was from Tocris (Cat# 1138) and used at a final concentration of 2 µM. The working concentration of Mitomycin C (MP Biomedicals™, Cat# 0219453202) was 10 µg/mL.

## **Cell migration and invasion assays**

Transwell migration and invasion assays were performed using 6.4 mm cell culture inserts with 8 µm pore-size polyethylene terephthalate (PET) membrane (Corning, Cat# 353097) placed into Falcon® 24-well Permeable Support Companion Plate (Corning, Cat# 353504). Cells were pretreated with 10 µg/mL of cell cycle inhibitor mitomycin C for 2 hours before seeding. The lower chamber was filled with 500 µl of growth medium pH<sub>e</sub> 7.4 or 6.6 containing 10% FBS. 75×10<sup>3</sup> PANC-1 and 10×10<sup>4</sup> Mia PaCa-2 cells/insert were seeded without matrigel coating (migration assay) or with matrigel coating (diluted in growth medium in ratio 1:5, Corning, Cat# 354230) in 300 µl of the corresponding pH<sub>e</sub> target growth medium supplemented with 10% FBS. Thereby, we avoided an FBS gradient between the two compartments. The cells were allowed to migrate or invade through the pores of the insert membrane overnight at 37°C and 5% CO<sub>2</sub>.

## **Cell transfection with siRNA**

A double-pulse approach with Lipofectamine™ 3000 Reagent (Invitrogen) was used to transfect PDAC cells with siRNAs. Cells were plated the day before the transfection in 6-well plates to reach 80% of confluency on the day of transfection.

On the day of the transfection, mix A was prepared in RPMI without FBS (SFM) and antibiotics. Mix B was prepared without the P3000™ Reagent when diluting the siRNA (50 nM final concentration). The siRNA sequences are listed in Table 1. Mix A was then mixed with Mix B, gently vortexed and kept for 12 minutes at room temperature. During the incubation time, the cell culture medium was replaced in each well, and 2,250 ml of fresh RPMI containing 10% FBS was added to each well. After the incubation, 250 µl of Mix A+B was added as a drop in each well. The entire process was repeated for the double pulse the following day, and the experiments were performed 48h following the second pulse.

*Table 1. List of siRNA sequences.*

<b>siRNA</b>	<b>Sequence Forward (5' to 3')</b>	<b>Sequence Reverse (5' to 3')</b>
Control siRNA		
duplex	Cat. Number: SR-CL000-005	/
negative	(Eurogentec)	
control		
siORAI1	UGAGCAACGUGCACAAUCU	AGAUUGUGCACGUUGCUCU

### **Calcium Imaging**

Cells were plated in glass coverslips to reach an 80% confluency on the day of the experiment. The cells were then loaded with 5 µM Fura-2 AM (Interchim, Cat# FP-42776C) diluted in cell culture medium and incubated for 45 minutes at 37 °C and 5% CO<sub>2</sub>. The cells were then gently washed three times with standard Hank's Balanced Salt solution (HBSS) (composition: 140 mM NaCl, 5 mM KCl, 2 mM CaCl<sub>2</sub>, 1 mM MgCl<sub>2</sub>, 0.3 mM NaH<sub>2</sub>PO<sub>3</sub>, 0.4 mM KH<sub>2</sub>PO<sub>4</sub>, 10 mM N-(2-hydroxyethyl)-piperazine-N'-ethanesulfonic acid (HEPES), 5 mM glucose, pH adjusted to 7.35 with NaOH) before fluorescence acquisition. Coverslips were then transferred to POCmini-2 Cell chambers on the stage of an Eclipse Ti-inverted series microscope (Nikon), and measurements were performed using an S Fluor 20×/0.75 NA objective lens (Nikon) by exciting Fura-2 fluorescence alternatively at 340 and 380 nm with a monochromator (Polychrome IV, TILL Photonics GmbH) and collected at 510 nm through a CCD camera (QImaging) controlled with Metafluor software

(Molecular Devices). Calcium imaging traces were analysed with Clampfit 10.7 software (Molecular Devices) and GraphPad Prism 7 software (GraphPad Corporation).

### **Ca<sup>2+</sup> oscillations induction protocol and analysis**

PANC-1 cells were starved overnight in serum-free RPMI 1640 (pH<sub>e</sub> 7.4 or pH<sub>e</sub> 6.6) the day before the experiment. Following loading with Fura-2 and incubation, cells were washed three times in HBSS containing 2 mM Ca<sup>2+</sup>, and the coverslips were mounted in the POCmini-2 Cell chamber and observed at the microscope. Cells were maintained in a 2 mM Ca<sup>2+</sup> solution for 100 seconds to measure basal Ca<sup>2+</sup> concentrations. At 100 seconds, an HBSS solution containing 10% FBS was administered, and the Fura-2 emission signals were recorded for at least 500 seconds. For assessing the effect of acute treatment with acidic pH<sub>e</sub>, cells were bathed in HBSS solution pH 6.6 + 10% FBS at 600 seconds, and the Ca<sup>2+</sup> signals were recorded for at least 200 seconds. The effect of Synta66 on Ca<sup>2+</sup> oscillations initiation was assessed by bathing the cells with HBSS + 10% FBS + 10 μM Synta66 at 100 seconds, while its effect on the maintenance of Ca<sup>2+</sup> oscillations was assessed by treating the cells with HBSS containing 10% FBS and 10 μM Synta66 at least 500 seconds following the Ca<sup>2+</sup> oscillations initiation. For the quantification of basal Ca<sup>2+</sup> levels and the mean Ca<sup>2+</sup> peak amplitude and area, the same time frame for all the conditions tested was considered, assuming a Δt of 50 seconds for the basal Ca<sup>2+</sup> levels and a Δt of 500 seconds for the peak amplitudes and area.

### **Store-Operated Ca<sup>2+</sup> entry (SOCE) protocol and analysis**

For SOCE protocol, we employed the irreversible SERCA pump inhibitor thapsigargin (TG) in Ca<sup>2+</sup>-free HBSS solution to induce Ca<sup>2+</sup> release and emptying of the ER stores. Following the addition of HBSS solution containing 2 mM Ca<sup>2+</sup> maximally activates SOCE. Following loading with Fura-2 and incubation, cells were washed three times in HBSS containing 2 mM Ca<sup>2+</sup>, and the coverslips were mounted in the POCmini-2 Cell chamber and observed at the microscope. Cells were maintained in a 2 mM Ca<sup>2+</sup> solution for 100 seconds to measure basal Ca<sup>2+</sup> concentrations. At 100 seconds, a Ca<sup>2+</sup>-free HBSS solution containing 2.5 mM EGTA was administered, while at 200 seconds, cells were bathed with Ca<sup>2+</sup>-free HBSS solution containing 2.5 mM EGTA + 2 μM TG. The 2 mM Ca<sup>2+</sup> solution was re-introduced following the complete emptying of the ER Ca<sup>2+</sup> stores and the stabilisation of the Ca<sup>2+</sup> signals, around 500-600 seconds. SOCE signals were recorded for 300 seconds. To evaluate the effects of acute exposition to pH 6.6 solution, HBSS acid solution was administered following SOCE and recorded for 200 seconds. For the quantification of basal Ca<sup>2+</sup>

levels, a  $\Delta t$  of 50 seconds was considered for all the conditions, while the mean peak amplitude and area of  $\text{Ca}^{2+}$  release from ER was considered a  $\Delta t$  of 200 seconds. For quantifying the mean peak amplitude and area of SOCE,  $\Delta t$  of 300 seconds was considered. Finally, the quantification of the SOCE signals in the presence of acidic pH acute treatment was assessed by measuring the  $\text{Ca}^{2+}$  signals in a time frame of 200 seconds. These signals were compared to the 200 seconds immediately preceding the introduction of the acidic solution.

### RNA extraction and qPCR

RNA extraction and qPCR Total RNA was isolated from cultured PANC-1 and Mia PaCa-2 cell models using the NucleoSpin RNA Plus kit (Macherey Nagel Bioanalysis™) according to the manufacturer's instructions. RNA concentration and quality were determined by absorbance at 260 nm. Reverse Transcription synthesised cDNA in a 20- $\mu\text{l}$  reaction mixture containing 2  $\mu\text{g}$  total RNA, 10 mM dNTPs, 50  $\mu\text{M}$ /100  $\mu\text{l}$  Random Hexamers, 1x First strand buffer, 20U RNase inhibitor, 0.1 M DTT, and 200 U M-MLV reverse transcriptase. Real-time qPCR was performed in a 20  $\mu\text{l}$ -reaction mixture containing 10ng/ $\mu\text{l}$  cDNA, SYBR™ Green PCR Master Mix (ThermoFisher Scientific), and 400 nM forward and reverse primers for each gene of interest. qPCR reactions were performed in technical triplicates. The primers used are listed in Table 2. The analysis was performed in a real-time thermal cycler Cfx C1000 (Bio-Rad). Hypoxanthine Phosphoribosyltransferase-1 (HPRT-1) was used for normalisation. Relative mRNA levels were quantified using the  $2^{(-\Delta\Delta\text{CT})}$  method.

*Table 2. List of primer sequences used for qPCR*

Gene name	Primer probe	Sequence (5' to 3')
hORAI1	Forward	ATGGTGGCAATGGTGGAG
	Reverse	CTGATCATGAGCGCAAACAG
hORAI2	Forward	GCAGCTACCTGGAAGTGGTC
	Reverse	CGGGTACTGGTACTGCGTCT
hORAI3	Forward	AAGTCAAAGCTTCCAGCCGC
	Reverse	GGTGGTACTCGTGGTCACTCT



hSTIM1	Forward	TGTGGAGCTGCCTCAGTAT
	Reverse	CTTCAGCACAGTCCCTGTCA
hHPRT1	Forward	AGTTCTGTGGCCATCTGCTT
	Reverse	CAATCCGCCCAAAGGGA ACT

## Statistical analyses

The data were analysed using GraphPad Prism 7 software (GraphPad Corporation). The Shapiro-Wilk normality test was used to assess the normality of distribution of the continuous variables, which were reported as mean and standard error of the mean (SEM). The Student's t-test was used to compare the means of two continuous variables with normal distribution. Means of more than two groups of variables were compared using One-way ANOVA. A  $p$ -value  $< 0.05$  was considered significant.

## Results

### I. Extracellular acidosis inhibits FBS-induced $\text{Ca}^{2+}$ -oscillations in PANC-1 cells.

Intracellular  $\text{Ca}^{2+}$  oscillations are peculiar, transducing and sustaining cancer hallmarks. We, therefore, investigated whether early or long-lasting acidic exposure affected PDAC cells oscillatory behaviour. For this purpose, experiments were performed on PANC-1, which spontaneously generated cytosolic  $\text{Ca}^{2+}$  oscillations when bathed in standard HBSS solution pH 7.4 containing 2 mM  $\text{Ca}^{2+}$  and challenged with FBS (Figure 1a-c), while this phenomenon was not observed for Mia PaCa-2 cells (Supplementary figure 1a). All PANC-1 cell models showed a similar percentage of FBS response (Figure 1d) and of FBS-induced oscillating cells (around 70% of cells oscillating in the dish) (Figure 3e). The quantification of the mean  $\text{Ca}^{2+}$  peak amplitude demonstrated that both short- and long-term acidosis and the recovery to  $\text{pH}_e$  7.4 increased the mean peak amplitude of the  $\text{Ca}^{2+}$  oscillations compared to control cells (Figure 1f). This result was supported by the increased  $\text{Ca}^{2+}$  oscillations area in all acidic models (Figure 1g). We further confirmed the enhanced basal  $\text{Ca}^{2+}$  levels in PANC-1 cells exposed for 4 days to  $\text{pH}_e$  6.6 compared to the other conditions (Supplementary Figure 1b).

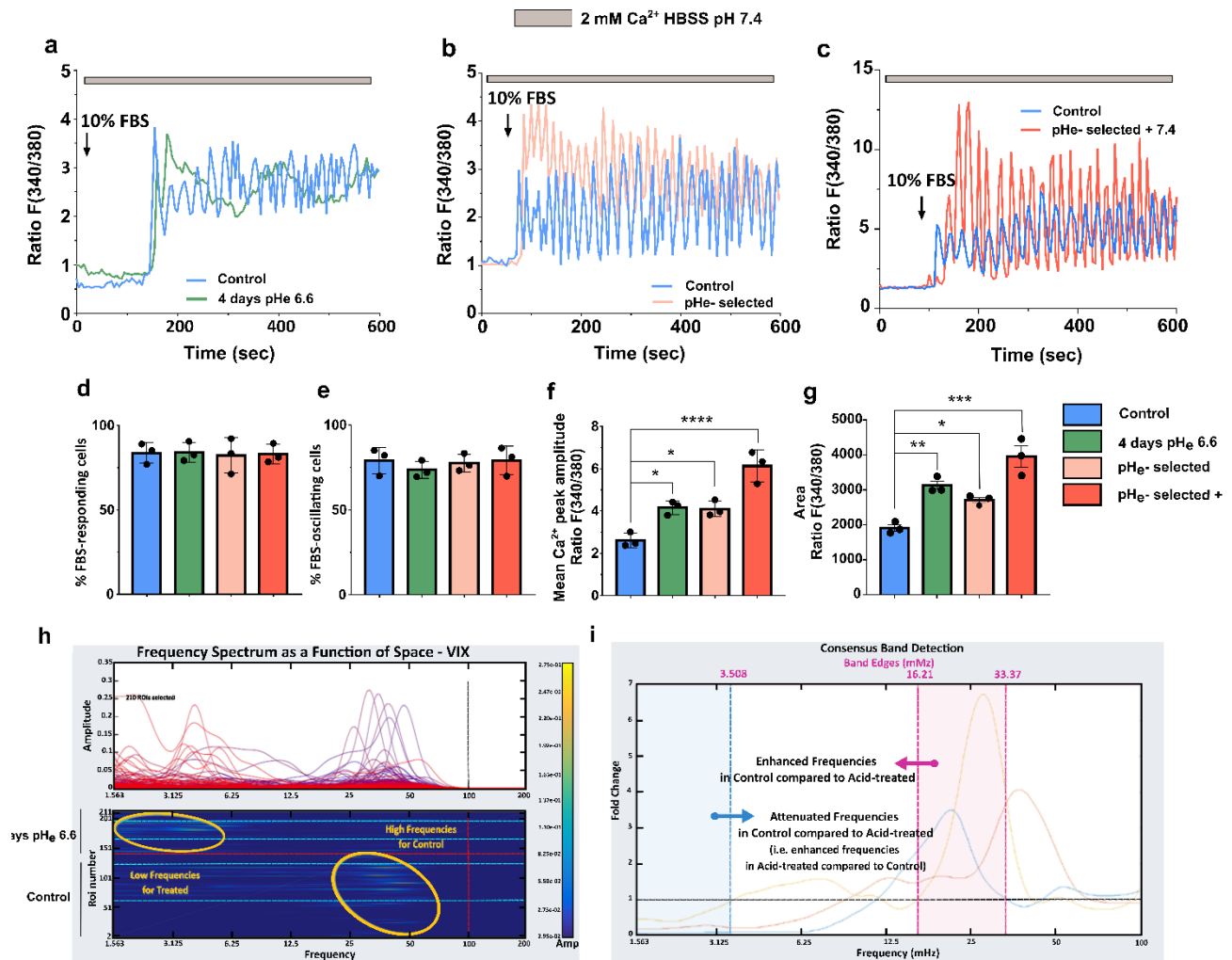


**Figure 1. Effect of acidic pH<sub>e</sub> on intracellular FBS-induced Ca<sup>2+</sup> oscillations in PANC-1 cells.** **a)** Representative traces of FBS-induced Ca<sup>2+</sup> oscillations in PANC-1 control cells (blue) and PANC-1 4 days pH<sub>e</sub> 6.6 (green), **b)** in PANC-1 control cells (blue) and PANC-1 pH<sub>e</sub>-selected cells (light orange) and **c)** in PANC-1 control cells (blue) and PANC-1 pH<sub>e</sub>-selected + 7.4 (red). **d)** Quantification of the percentage of PANC-1 FBS-responding cells and **e)** of the percentage of oscillating cells in PANC-1 cells. **f)** Quantification of the mean Ca<sup>2+</sup> peak amplitude and **g)** mean area of Ca<sup>2+</sup> oscillations in PANC-1 control, 4 days pH<sub>e</sub> 6.6, pH<sub>e</sub>-selected and pH<sub>e</sub>-selected + 7.4. cells. **h)** Wavelet-based analysis of FBS-induced calcium oscillations in PANC-1 control and 4 days pH<sub>e</sub> 6.6 cells. Frequency spectra of each oscillating cell from the three biological replicates (superimposed and heat mapped in the upper and lower panel, respectively). **i)** Control-to-acid treated ratios of the mean spectra from the three experimental replicates. The frequency enhanced in control cells is within the red band, while those enhanced in 4 days pH<sub>e</sub> 6.6 are within the blue one. Data were reported as mean ± SEM and are from 3 independent experiments. Data were analysed using One-way ANOVA with Dunnett's multiple comparison test, \* p < 0.05, \*\* p < 0.01, \*\*\* p < 0.001, \*\*\*\* p < 0.0001.

A more quantitative analysis of the Ca<sup>2+</sup> oscillations led us to assess the impact of pH<sub>e</sub> in terms of another important parameter: the frequency of the Ca<sup>2+</sup> oscillations. PANC-1 cells exposed

for 4 days to  $\text{pH}_e$  6.6 showed the slowest  $\text{Ca}^{2+}$  oscillations among all cell models (Figure 1a). For this reason, to uncover the effect of acidosis on the  $\text{Ca}^{2+}$  oscillatory behaviour, we quantitatively analysed the frequency of the  $\text{Ca}^{2+}$  oscillations of control and 4 days  $\text{pH}_e$  6.6 cells using a wavelet-based algorithm<sup>22,23</sup>. From the summary of the frequency spectra (Figure 1h), we observed that high frequencies (representing the most rapid events, i.e., the sharpest peaks) were confined in the control samples, while the 4 days  $\text{pH}_e$  6.6 cells (here also called “acid-treated”) were dominated by low-frequency  $\text{Ca}^{2+}$  oscillations. To better quantify the range of frequencies affected by the treatment, the paired control-to-4 days  $\text{pH}_e$  6.6 cells ratio of the mean spectra for each of the three experiments was computed (Figure 1i). The analyses described the difference between control and 4 days  $\text{pH}_e$  6.6 conditions in terms of enhanced and attenuated frequencies induced by the acidic  $\text{pH}_e$ . High frequencies were enhanced (ratio > 1), while low frequencies resulted in depressed (ratio < 1) in control cells compared to 4 days  $\text{pH}_e$  6.6 samples. The frequency bands affected by the treatment were finally measured by a consensus approach, defining the range of frequencies enhanced by the acidic treatment. PANC-1 cells exposed to short-term acidosis displayed  $\text{Ca}^{2+}$  oscillations characterised by a frequency range below 3.5 mHz (Figure 1i, blue band), slower than the  $\text{Ca}^{2+}$  oscillations exhibited by control cells, which frequency falls in the range from 16 to 33 mHz (Figure 1i, red band).

We next questioned whether acute acidosis might affect the oscillatory behaviour by allowing the cells to oscillate first and then bathing them in HBSS pH 6.6 containing 10% FBS (Figure 2a-d). We observed that this strategy resulted in the damping of  $\text{Ca}^{2+}$  oscillations in 71.89% of control cells, while 4 days long acidic pre-incubation of cells reduced the impact of the inhibitory effect of the acute acidic treatment, observing damping in  $\text{Ca}^{2+}$ -oscillations in 52.05% of cases and 56.19% in  $\text{pH}_e$ -selected cells. Interestingly,  $\text{pH}_e$ -selected cells recovered to  $\text{pH}_e$  7.4 were the most affected by acidic  $\text{pH}_e$ , showing damped  $\text{Ca}^{2+}$ -oscillations in 83.71% of the cells (Figure 2e).

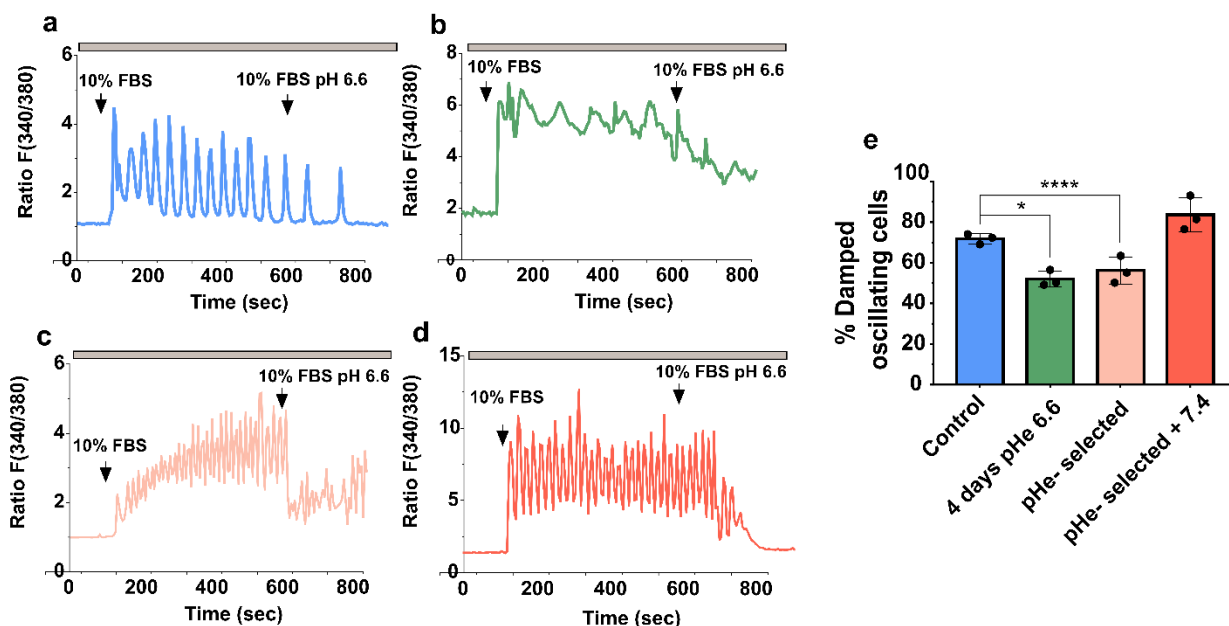


**Figure 2. Effect of acidic pH<sub>e</sub> on the amplitude and effect on the frequency of PANC-1 Ca<sup>2+</sup> oscillations induced by 10% FBS by Wavelet analysis.** a) Representative traces of FBS-induced Ca<sup>2+</sup> oscillations with acute acidic treatment in PANC-1 control, b) 4 days pH<sub>e</sub> 6.6, c) pH<sub>e</sub>-selected and d) pH<sub>e</sub>-selected + 7.4. e) Quantification of the percentage of damped oscillating cells following acidic treatment in PANC-1 cells. Data were reported as mean ± SEM and are from 3 independent experiments. Data were analysed using One-way ANOVA with Dunnett's multiple comparison test, \* p < 0.05, \*\*\*\* p < 0.0001.

## II. FBS-induced Ca<sup>2+</sup>-oscillations are SOCE-dependent in all PANC-1 cell models.

Different evidence throughout the years has demonstrated that Ca<sup>2+</sup> oscillations are mediated and sustained by SOCE<sup>19</sup>, which major molecular components are STIM1 and ORAI1 proteins. For this reason, the putative role of these channels, in particular the Ca<sup>2+</sup>-permeable channels ORAI1, as initiators or contributors of the Ca<sup>2+</sup> oscillations observed, was investigated using siRNA technology and tested by means of Ca<sup>2+</sup> imaging (Figure 3, Supplementary Figure 1c).

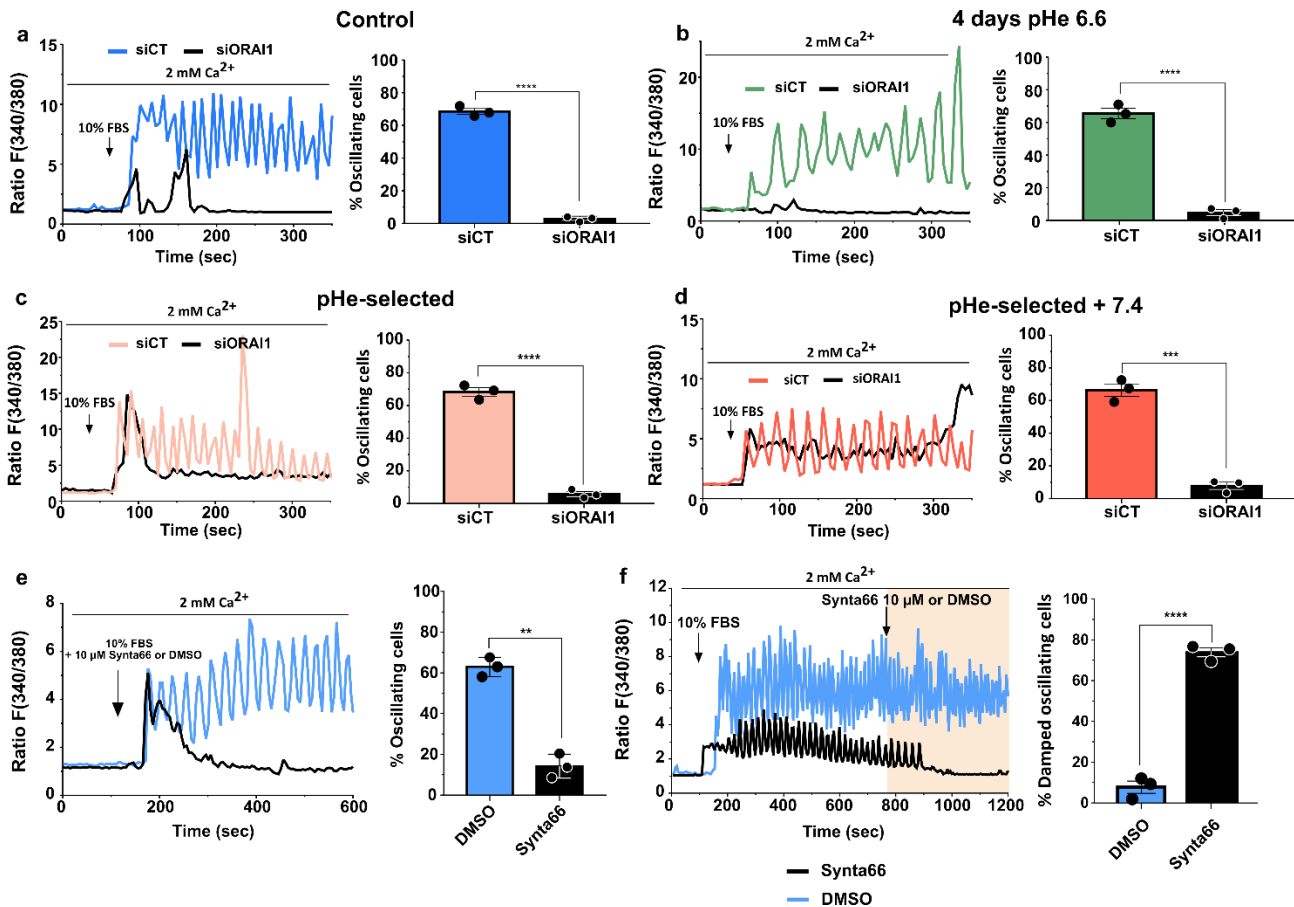


**Figure 3.**  $\text{Ca}^{2+}$  oscillations are SOCE-dependent in PANC-1 cells. **a)** Representative traces of FBS-induced  $\text{Ca}^{2+}$  oscillations in PANC-1 cells treated with siCT and siORAI1 (left) with quantification of the percentage of oscillating cells in both conditions in PANC-1 control, **b)** PANC-1 4 days  $\text{pH}_e$  6.6, **c)** in PANC-1  $\text{pH}_e$ -selected cells and **d)** in PANC-1  $\text{pH}_e$ -selected + 7.4. **e)** Representative traces of FBS-induced  $\text{Ca}^{2+}$  oscillations in PANC-1 control cells treated with DMSO or Synta66 in concomitance with FBS stimulation (left) with quantification of the percentage of oscillating cells in both conditions. **f)** Representative traces of FBS-induced  $\text{Ca}^{2+}$  oscillations in PANC-1 control cells treated with DMSO or Synta66 500 seconds after the FBS stimulation (left) with quantification of the percentage of oscillating cells in both conditions. Data were reported as mean  $\pm$  SEM and are from 3 independent experiments. Data were analysed using Student *t*-test, \*\*  $p < 0.01$ , \*\*\*  $p < 0.001$ , \*\*\*\*  $p < 0.0001$ .

Silencing of ORAI1 expression resulted in the abolishment of cytosolic  $\text{Ca}^{2+}$  oscillations compared to control PANC-1 cells (siCT) in both control and acidic conditions (Figure 5a-d). Interestingly silencing of ORAI1 did not affect the basal  $[\text{Ca}^{2+}]_i$  of both control of PANC-1 grown in acidic conditions (Supplementary Figure 1d). The data suggest that ORAI1 is not responsible for the higher basal  $[\text{Ca}^{2+}]_i$  observed in PANC-1 after 4 days at  $\text{pH}_e$  6.6. As an additional strategy, we tested the pharmacological inhibition of ORAI1 using Synta66, a selective CRAC ( $\text{Ca}^{2+}$  release-activated  $\text{Ca}^{2+}$ ) channel inhibitor (Supplementary Figure 1e, f), in concomitance or not with FBS

treatment. Simultaneous treatment of PANC-1 control cells with 10% FBS and 10  $\mu$ M Synta66 resulted in the abolishment of  $\text{Ca}^{2+}$  oscillations compared to untreated cells (Figure 3e), while 73.4% of PANC-1 cells showed damped  $\text{Ca}^{2+}$  oscillations after Synta66 treatment (Figure 3f). These results indicate that ORAI1 plays an important role in initiating and sustaining  $\text{Ca}^{2+}$  oscillations induced by FBS treatment in PANC-1 cells.

### **III. Intracellular $\text{Ca}^{2+}$ basal levels, $\text{Ca}^{2+}$ -release from ER and SOCE are affected by acidic $\text{pH}_e$ .**

To further decipher the intracellular  $\text{Ca}^{2+}$  signals of PDAC acidic models, we imaged the cytosolic basal  $\text{Ca}^{2+}$  levels ( $[\text{Ca}^{2+}]_i$ ) in PANC-1 and Mia PaCa-2 cell models. In PANC-1 cells, short-term acidic exposure (4 days  $\text{pH}_e$  6.6) strongly increased basal  $[\text{Ca}^{2+}]_i$  compared to control cells (Figure 4a). In contrast, long-term acidic treatment ( $\text{pH}_e$ -selected cells) and recovery to  $\text{pH}_e$  7.4 ( $\text{pH}_e$ -selected + 7.4) led to the restoration of the basal  $[\text{Ca}^{2+}]_i$  observed in control cells (Figure 4a). No differences in basal  $[\text{Ca}^{2+}]_i$  were observed in Mia PaCa-2 cells following the different acidic treatments (Figure 4b). To characterise the role of acidic exposure on intracellular  $\text{Ca}^{2+}$  homeostasis, we focused on intracellular  $\text{Ca}^{2+}$  store content and SOCE, applying the  $\text{Ca}^{2+}$  add-back protocol. This strategy stimulates the  $\text{Ca}^{2+}$  release from Endoplasmic Reticulum (ER) stores in Fura-2-loaded cells bathed with  $\text{Ca}^{2+}$ -free standard Hank's Balanced Salt Solution (HBSS,  $\text{pH}$  7.4) containing the SERCA-inhibitor thapsigargin (TG; 2  $\mu$ M). The ER  $\text{Ca}^{2+}$  stores emptying is followed by the switch to  $\text{Ca}^{2+}$ -containing HBSS (2 mM  $\text{Ca}^{2+}$ ) to measure the SOCE (Figure 4c-n). Switching from  $\text{Ca}^{2+}$ -containing medium to a  $\text{Ca}^{2+}$ -free HBSS significantly affected basal  $[\text{Ca}^{2+}]_i$  of short-term acidic exposure (4 days  $\text{pH}_e$  6.6) in PANC-1 (Figure 4d) but not Mia PaCa-2 cells (Figure 1h), suggesting that the increased basal  $[\text{Ca}^{2+}]_i$  previously observed is due to an increased  $\text{Ca}^{2+}$  entry (Supplementary Figure 1g). TG treatment in  $\text{Ca}^{2+}$ -free conditions showed that  $\text{Ca}^{2+}$  release from ER is significantly decreased in both PANC-1 and Mia PaCa-2 cells exposed to short-term acidosis (Figure 4k and m). For PANC-1 cells, this result was associated with a decrease in the SOCE (Figure 4l). Unexpectedly, we observed an opposite effect in Mia PaCa-2 cells, which showed an increase in SOCE compared to control cells (Figure 1n). In contrast,  $\text{Ca}^{2+}$  release from ER was strongly increased in PANC-1  $\text{pH}_e$ -selected cells and those recovered to  $\text{pH}_e$  7.4 (Figure 4k), and this was associated with an increase in the SOCE component (Figure 4l). Despite no changes in  $\text{Ca}^{2+}$  release from ER were

detected in Mia PaCa-2 pH<sub>e</sub>-selected and recovered to pH<sub>e</sub> 7.4 (Figure 4m), they showed enhanced SOCE compared to control cells (Figure 4n).

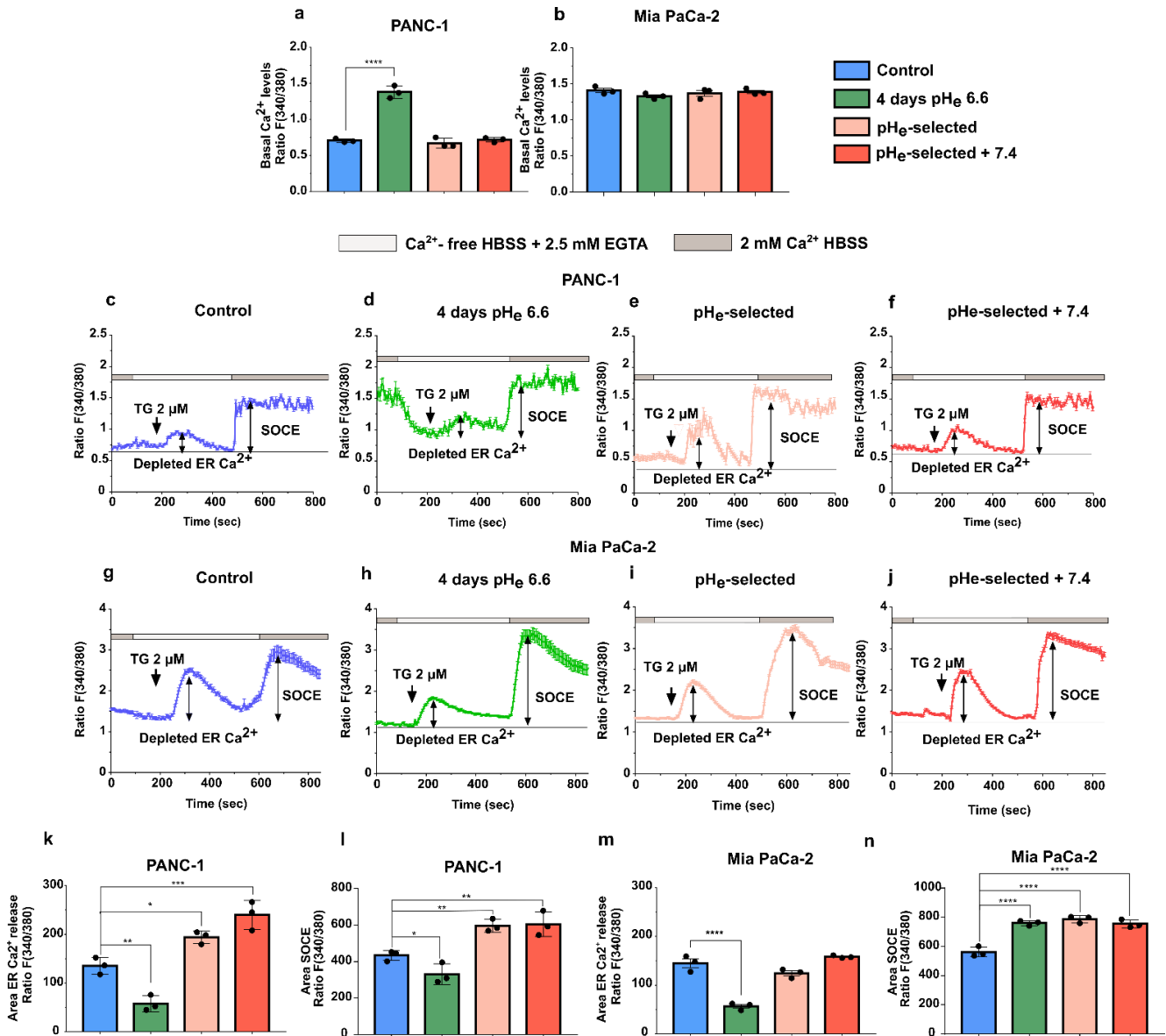


**Figure 4. Effects of acidic pH<sub>e</sub> on cytosolic basal Ca<sup>2+</sup> levels, Ca<sup>2+</sup>-release from ER stores and SOCE in PDAC cells.** a) Basal Ca<sup>2+</sup> levels in PANC-1 and b) Mia PaCa-2 cells. c) Mean trace of TG-induced SOCE in PANC-1 control cells, d) PANC-1 4 days pH<sub>e</sub> 6.6, e) PANC-1 pH<sub>e</sub>-selected cells and f) PANC-1 pH<sub>e</sub>-selected cells + 7.4. g) Mean trace of TG-induced SOCE in Mia PaCa-2 control cells, h) Mia PaCa-2 4 days pH<sub>e</sub> 6.6, i) Mia PaCa-2 pH<sub>e</sub>-selected cells and j) Mia PaCa-2 pH<sub>e</sub>-selected cells + 7.4. Cells were initially treated with 2 μM thapsigargin (TG) in absence of extracellular calcium ions to induce the depletion of intracellular calcium stores. Administration of 2 mM Ca<sup>2+</sup> solution with physiological pH-induced calcium entry (SOCE). D) Quantification of resting Ca<sup>2+</sup> levels in the 3 PANC-1 models.

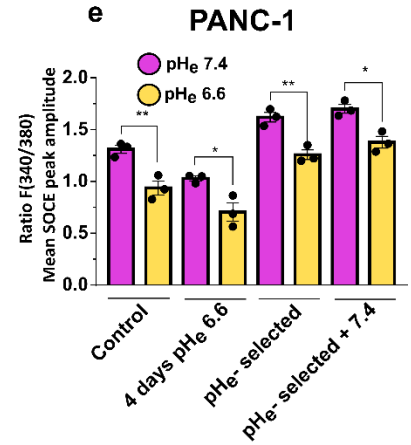
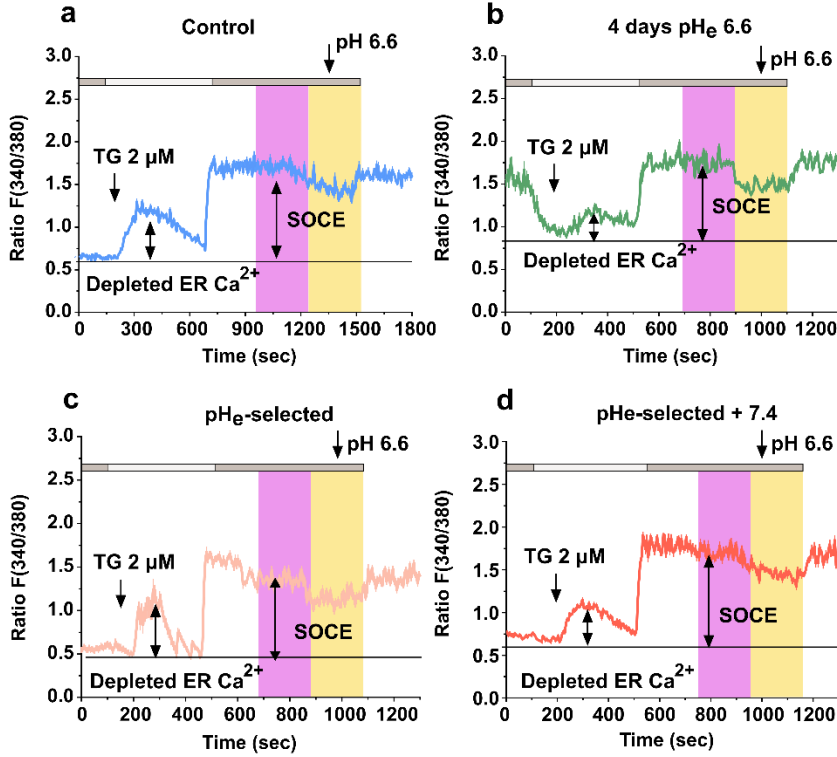
**k)** Quantification of the area of the  $\text{Ca}^{2+}$  release after depletion of ER store with thapsigargin in PANC-1 cells and **l)** of SOCE area in PANC-1 cells. **m)** Quantification of the area of the  $\text{Ca}^{2+}$  release after depletion of ER store with thapsigargin in Mia PaCa-2 cells and **l)** of SOCE area in Mia PaCa-2 cells. Data were reported as mean  $\pm$  SEM and are from 3 independent experiments. Data were analysed using One-way ANOVA with Dunnett's multiple comparison test, \*  $p < 0.05$ , \*\*  $p < 0.01$ , \*\*\*  $p < 0.001$ , \*\*\*\*  $p < 0.0001$ .

We next investigated the effects of acute exposition to acidic  $\text{pH}_e$  on intracellular  $\text{Ca}^{2+}$  homeostasis. Both PANC-1, as well as MiaPaCa-2 cells, showed a strong SOCE inhibition when challenged with standard HBSS solution at pH 6.6 and for 200 seconds following  $\text{Ca}^{2+}$  entry (Figure 5a-j), observing a decrease in the mean peak amplitude of the SOCE signal in all the cell models (Figure 5e and j). The data are in agreement with previous results<sup>24,25</sup>. Taken together, these results indicate that extracellular acidosis differentially affects the cytosolic basal  $\text{Ca}^{2+}$  levels, the extent of  $\text{Ca}^{2+}$  release from ER and the  $\text{Ca}^{2+}$  entry in PDAC cells before and after the acid selection and recovery.



Ca<sup>2+</sup>- free HBSS + 2.5 mM EGTA    2 mM Ca<sup>2+</sup> HBSS

### PANC-1



### Mia PaCa-2

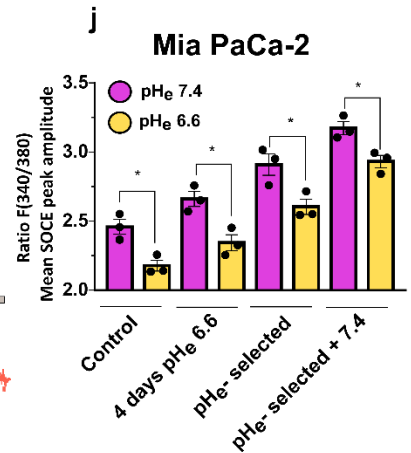
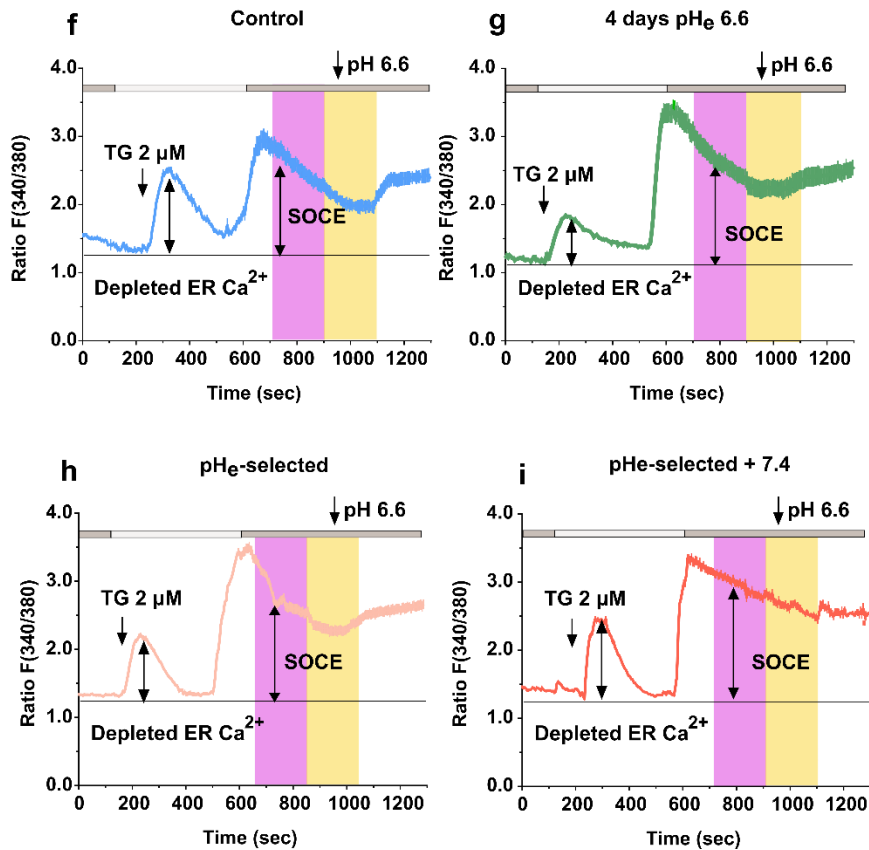


**Figure 5. Effects of acute exposition of acidic pHe SOCE in PDAC cells.** **a)** Mean SOCE trace with acute low pHe solution treatment in PANC-1 control cells, **b)** PANC-1 4 days pHe 6.6, **c)** PANC-1 pHe-selected cells and **d)** PANC-1 pHe-selected cells + 7.4. **e)** Quantification of mean SOCE peak amplitude before (pHe 7.4) and during (pHe 6.6) treatment with acidic solution in PANC-1 cells. **f)** Mia PaCa-2 pHe-selected cells + 7.4 in Mia PaCa-2 control cells, **g)** Mia PaCa-2 4 days pHe 6.6, **h)** Mia PaCa-2 pHe-selected cells and **i)** Mia PaCa-2 pHe-selected cells + 7.4. **j)** Quantification of mean SOCE peak amplitude before (pHe 7.4) and during (pHe 6.6) treatment with acidic solution in Mia PaCa-2 cells. Data were reported as mean  $\pm$  SEM and are from 3 independent experiments. Data were analysed using Students *t*-test, \*  $p < 0.05$ , \*\*  $p < 0.01$ .

#### **IV. Acid selection promotes the upregulation of ORAI1 in PANC-1 cells.**

To evaluate the expression of the two major SOC components in PDAC cell lines, qPCR analysis was performed for ORAI1 and STIM1. As shown in Figure 6, ORAI1 was downregulated in PANC-1 cells following a short-term acidosis. Acid-selected cells showed a tendency of upregulation of ORAI1, which becomes significant after the recovery to pHe 7.4 (Figure 6a). On the contrary, no differences in ORAI1 channel expression were revealed in Mia PaCa-2 cells (Figure 6b). The accessory protein STIM1 showed no mRNA changes in all conditions and cell lines tested (Figures 6c and d). We further investigated the mRNA expression of other SOC channels implicated at the different extents in SOCE, identifying ORAI2 overexpression in pHe-selected + 7.4 cells (Figure 6a) and ORAI3 downregulation in all Mia PaCa-2 acidic conditions (Figure 6b).

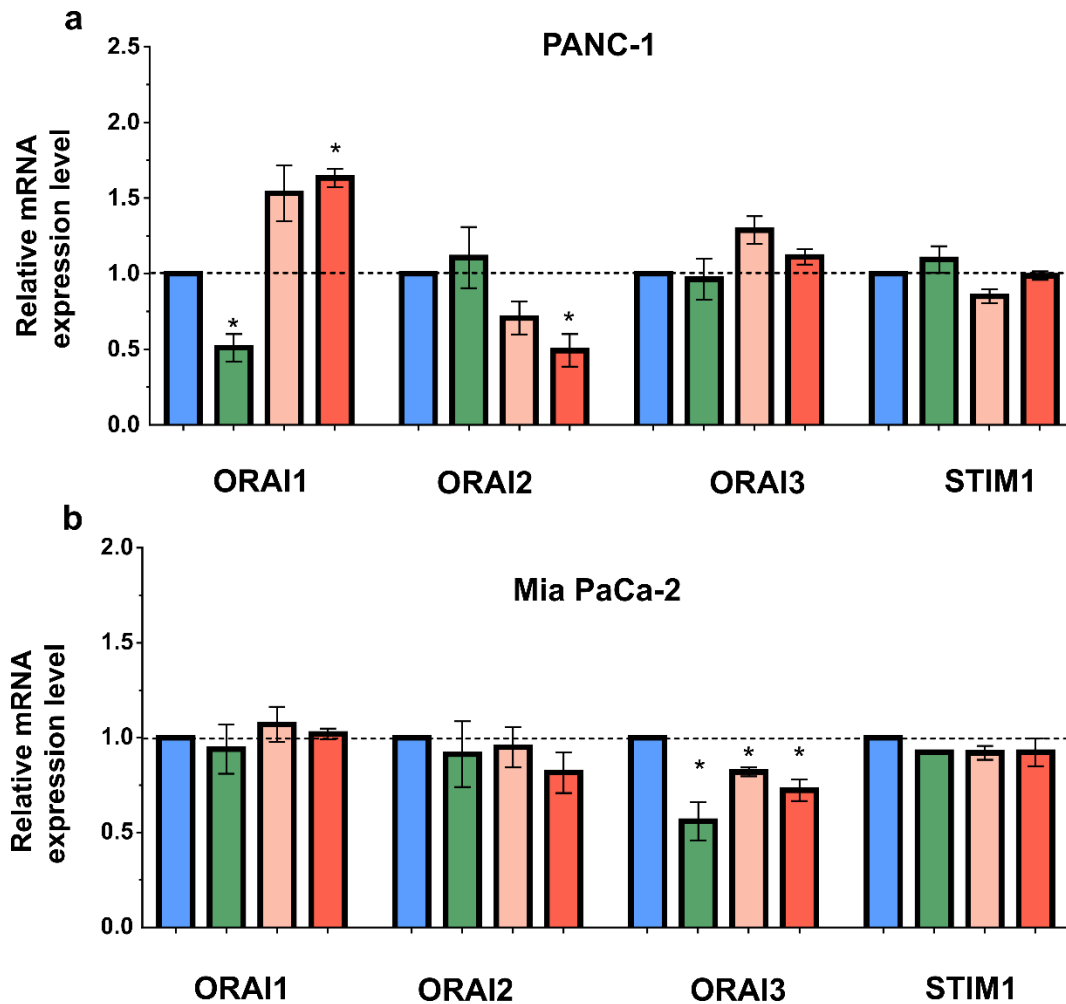


**Figure 6. Effect of extracellular acidosis on ORAI1 channels and STIM1 expression in PANC-1 and Mia PaCa-2 cells. a)** mRNA expression levels of ORAI1, ORAI2, ORAI3 channels and STIM1 in PANC-1 and **b)** Mia PaCa-2 cells subjected to acidic treatment for different periods and presented as fold change values, obtained by RT-qPCR. The effects of pHe 6.6 treatment on SOCs and STIMs expression were compared with control samples (dotted lines). Fold changes were quantified using the  $2^{-\Delta\Delta Cq}$  method and normalised to HPRT reference gene. Data were presented as mean and  $\pm$  SEM and analysed using One sample *t* test. All data reported were obtained from three independent experiments, \*  $p < 0.05$ .

## V. ORAI1 is involved in cell migration and invasion of acid-selected cells.

To address the putative contribution of ORAI1 in PDAC aggressiveness, the functional significance of ORAI1 silencing was investigated using Transwell migration and matrigel invasion assays (Figure 7). While the migratory abilities of PANC-1 control cells were not affected by siRNA treatment compared to siCT, they were strongly inhibited in all the acidic models, with a major effect on pHe-selected + 7.4 cells (Figure 7a). Interestingly, we observed the same pattern of results

for Mia PaCa-2 cells, although the extent of the siORAI1-mediated inhibition was milder than in PANC-1 cells (Figure 7b). Cell invasion almost followed the same trend, being negatively affected in pH<sub>e</sub>-selected cells, with greater effects in pH<sub>e</sub>-selected cells recovered to pH<sub>e</sub> 7.4. Contrary to migration, short-term acidosis did not affect the invasive abilities of PANC-1 cells (Figure 7c). As previously, PANC-1 cell invasion results were replicated in Mia PaCa-2 cells, where siORAI1-treated pH<sub>e</sub>-selected cells and recovered to pH<sub>e</sub> 7.4 displayed a less dramatic decrease in their cell invasion compared to PANC-1 cells (Figure 7d). Given the accentuated inhibitory effects of siORAI1 on pH<sub>e</sub>-selected + 7.4 cells, we confirmed cell invasion results using Synta66 in both PDAC cell lines (Supplementary Figure 2a-d).

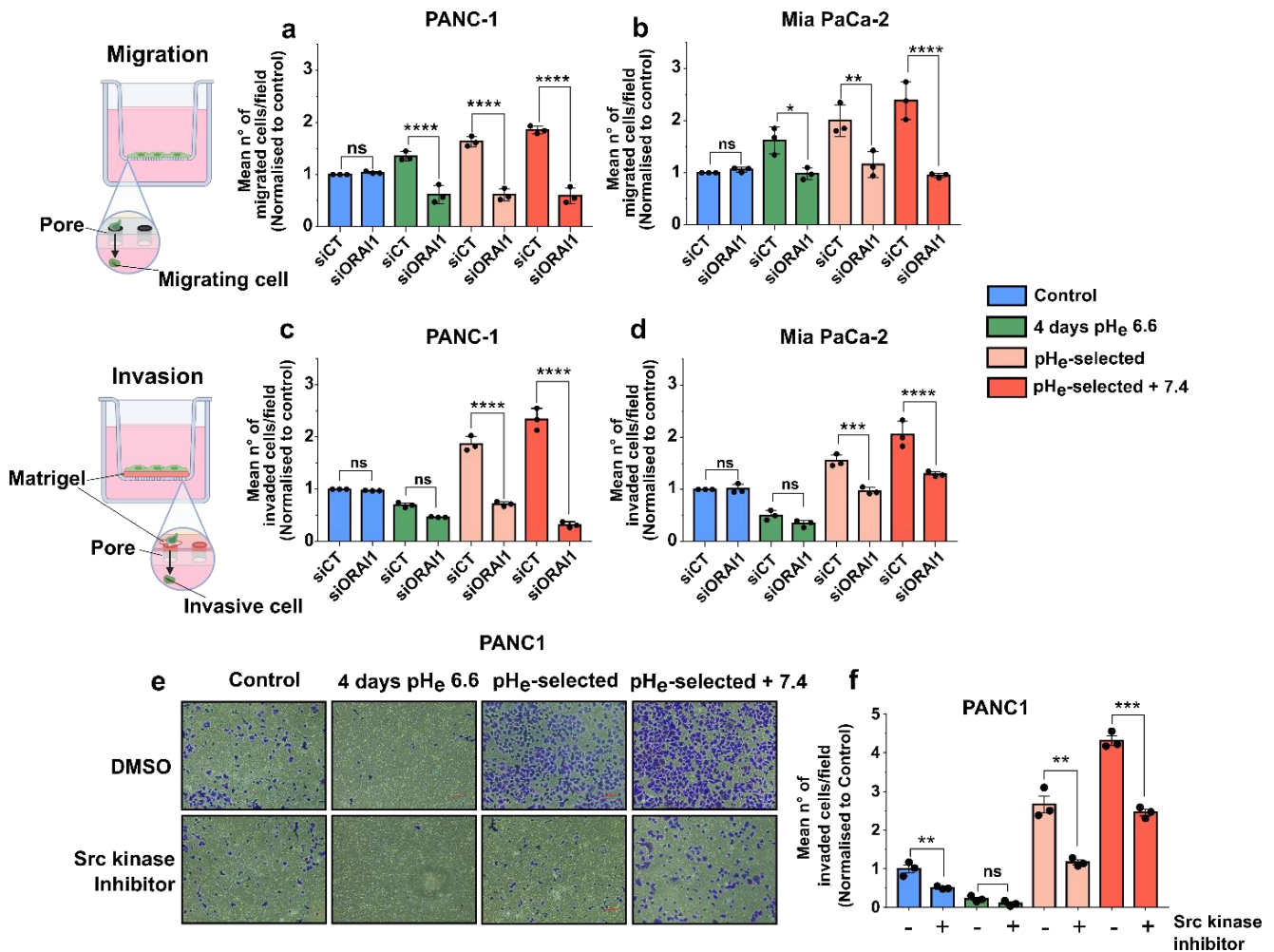


**Figure 7. Effect of ORAI1 silencing on cell migration and invasion in PANC-1 and Mia PaCa-2 cells and of Src kinase inhibition on cell adhesion and invasion in PANC-1 cells. a)** Quantification of the mean number of migrated cells of the transwell migration assay of cell models treated or not with siORAI1 in PANC-1 cells and **b)** Mia PaCa-2 cells. **c)** Quantification of the mean number of invasive cells of the transwell migration assay of cell models treated or not with siORAI1 in PANC-1 cells and **d)** Mia PaCa-2 cells. **e)** Representative microscopic images of transwell invasion

assay in the different PANC-1 cell models. **f)** Quantification of the mean number of invasive cells/field in the presence or absence (DMSO) of 5  $\mu$ M Src kinase inhibitor-1 in PANC-1 cell models. Data were reported as mean  $\pm$  SEM and are from 3 independent experiments. Data were analysed using Student *t*-test, \*  $p < 0.05$ , \*\*  $p < 0.01$ , \*\*\*  $p < 0.001$ , \*\*\*\*  $p < 0.0001$ .

Preliminary data allowed us to identify a potential downstream target involved in cancer cell invasion in PANC-1 cells, Src kinase, which role in cell invasion is well established, and that is  $\text{Ca}^{2+}$ -activated. The pharmacological inhibition of Src kinase using Src Inhibitor-1 inhibited cell invasion in all conditions tested, with the exception of short-term acid-treated PANC-1 cells, where Src kinase inhibition did not synergise with acidosis, as the inhibitory effect of  $\text{pH}_e$  was sufficient to almost completely abrogate cell invasion compared to control (Figure 7e, f).

## Discussion

The pro-tumour role of extracellular acidosis has been extensively demonstrated in the literature, as has the involvement of intracellular calcium signals in regulating various cellular processes that promote tumour progression. However, the hypothesis that tumour acidosis employs  $\text{Ca}^{2+}$  signalling as a preferential route for sustaining tumour progression has yet to be sufficiently explored. In this study, we employed previously characterised acidic PDAC cell models, which mimicked the different stages of acid selection and the successive step in metastasization by recovering  $\text{pH}_e$ -selected cells to  $\text{pH}_e$  7.4 (see Results I section of the manuscript) to unravel how tumour acidosis modulates cytosolic  $\text{Ca}^{2+}$  signals, with a particular focus on  $\text{Ca}^{2+}$  oscillations and Store-Operated  $\text{Ca}^{2+}$  entry (SOCE). We then explored the contribution of ORAI1, one of the major components of the SOCE, in PDAC cells' migratory and invasive abilities.

Our results showed a different  $\text{Ca}^{2+}$  response based on the acid exposure time and cell line. PANC-1 cells exposed to a short-term acidosis, mimicking the early stages of  $\text{pH}_e$  selection, showed enhanced basal  $\text{Ca}^{2+}$  levels, with the recovery of control-like cytosolic  $\text{Ca}^{2+}$  resting concentration with the long-term treatment and recovery to  $\text{pH}_e$  7.4 (Figure 4a, Supplementary Figure 1b). Previous studies showed that high basal  $\text{Ca}^{2+}$  levels are linked to mitochondrial  $\text{Ca}^{2+}$  overload and activation of the cytochrome c cascade, resulting in cell death in response to specific stimuli, in our case, low  $\text{pH}_e$ <sup>26</sup>. This might explain the decreased cell viability of PANC-1 4 days  $\text{pH}_e$  6.6 cells that we

previously observed (see Results I section of the manuscript). On the contrary, pH<sub>e</sub>-selected and those recovered to pH<sub>e</sub> 7.4 showed enhanced SOCE, which was supported by an increase in the ER Ca<sup>2+</sup> release (Figure 4c-f and Figure 4k and l). Several studies have reported that intra- and extracellular acidification negatively affects SOCE<sup>24,25,27-29</sup>. Most of these works were performed in non-cancer cells and with acute acidic exposition (range of minutes), assessing the effect of acidosis on SOC channels via electrophysiology experiments, supporting our results in the acute (200 seconds) and short-term (4 days) acidic treatment. However, the Ca<sup>2+</sup> response changed with the long-term acidosis (1 month), and the following recovery to pH<sub>e</sub> 7.4 suggests an adaptive response that may rely on the deregulation of SOCE components, such as ORAI proteins, to promote the increase of Ca<sup>2+</sup> influx. In accordance with this hypothesis, we found a tendency of upregulation of ORAI1 in PANC-1 pH<sub>e</sub>-selected cells that became significant following the recovery in pH<sub>e</sub> 7.4 (Figure 6a). In addition, these cells also downregulated ORAI2, a key component of SOCE in several cancer cell lines. Its overexpression was reported to reduce both ER Ca<sup>2+</sup> levels and SOCE in human glioblastoma cells, while its silencing enhanced SOCE amplitude<sup>30</sup>. This result was also reported in NCI-H23 lung cancer cells<sup>31</sup> and mouse T cells<sup>32</sup>, suggesting that PANC-1 pH<sub>e</sub>-selected + 7.4 cells might downregulate ORAI2 to support a major SOCE-mediated Ca<sup>2+</sup> influx. On the contrary, Ca<sup>2+</sup>-responses to low pH<sub>e</sub> differed in Mia PaCa-2 cells, in which basal Ca<sup>2+</sup> concentrations were not affected by acidic treatment (Figure 4b). We observed enhanced SOCE in all acidic models, despite the extent of Ca<sup>2+</sup> release from ER stores being strongly inhibited in the 4 days pH<sub>e</sub> 6.6 cell model (Figure 4m, n). Although no differences in ORAI1, ORAI2, and STIM1 mRNA expression were detected, all acidic models downregulated ORAI3, whose silencing was reported to increase SOCE in PDAC cell lines<sup>33</sup>. This might speculate that acidosis deregulates ORAI3 channel expression, leading to the increased SOCE observed in ORAI3-downregulated Mia PaCa-2 cells.

ORAI, STIM proteins, and, generally, SOCE are required to generate intracellular Ca<sup>2+</sup> oscillations in physiological and pathological contexts<sup>12,13,34,35</sup>. Several stimuli, including FBS, can trigger Ca<sup>2+</sup> oscillations. FBS contains several mitogens that activate IP3 synthesis via receptor-mediated PLC cleavage of PIP<sub>2</sub>, leading to IP3R-mediated ER Ca<sup>2+</sup> release, eliciting Ca<sup>2+</sup> waves in cooperation with CaMKII activity<sup>36</sup>. We report that PANC-1 cells generated SOCE-dependent Ca<sup>2+</sup>-oscillations following FBS treatment, while Mia PaCa-2 did not elicit any Ca<sup>2+</sup> waves (Figure 1a-c and Supplementary Figure 1a). The amplitude and frequency of these oscillations differed among the acidic models, showing the lowest frequency in the early stages of pH<sub>e</sub> selection (Figure 1a-c and

Figure 1f-i). They were also inhibited following acute acidic treatment (Figure 2). Kawanish and coworkers reported that  $\text{Na}^+$ -acetate-induced intracellular acidosis suppressed intracellular  $\text{Ca}^{2+}$  oscillations in rat hepatocytes<sup>37</sup>. Our previous work showed that PANC-1 cells slightly decreased their intracellular pH ( $\text{pH}_i$ ) following the 4 days-long acidic exposure (see Results I section of the manuscript). This suggests that acidic  $\text{pH}_e$ -induced internal acidification might affect  $\text{Ca}^{2+}$  waves. We also reported that PANC-1  $\text{Ca}^{2+}$  oscillations required SOCE for their initiation and maintenance (Figure 5). These results suggest that short-term acidosis might affect cytosolic  $\text{Ca}^{2+}$  oscillations by acidifying the intracellular milieu and affecting their initiation and maintenance by inhibiting ORAI1 and, thus, SOCE. Acid-selected PANC-1 cells showed an increase in ORAI1 mRNA levels, which  $\text{Ca}^{2+}$ -mediated entry might fuel the  $\text{Ca}^{2+}$ -oscillations compensating the inhibitory effect of acidic  $\text{pH}_e$ , restoring the fast frequencies observed in control cells.

At the molecular level, the frequency of the cytosolic  $\text{Ca}^{2+}$  oscillations must be decoded by specific  $\text{Ca}^{2+}$ -sensitive proteins to extrapolate the information carried and activate the specific cell response. Therefore, the frequency of these oscillations regulates the activity of the decoders.  $\text{Ca}^{2+}$  oscillations frequencies falling between 16 and 33 mHz, as observed for our control cells and assumed for  $\text{pH}_e$ -selected cells with and without recovery to  $\text{pH}_e$  7.4, can activate the translocation of NFAT transcription factor to the nucleus, where it regulates gene transcription<sup>38</sup>. NFAT is involved in the progression of several cancers, including PDAC<sup>39</sup>. We can then speculate a putative NFAT contribution in the enhanced aggressiveness of PANC-1 acid-selected cells (see Results I section of the manuscript), but that still needs to be verified. On the contrary, during the early stages of acid selection, PANC-1 cells showed slower  $\text{Ca}^{2+}$  waves characterised by a frequency lower than 3.5 mHz, a range decoded by other transcription factors, such as  $\text{NF-}\kappa\text{B}$ <sup>38</sup>.  $\text{NF-}\kappa\text{B}$  is  $\text{pH}$ -sensitive, and studies have demonstrated that it regulates the expression of ORAI1 and STIM1 in mast cells<sup>40</sup> and that its activation is regulated by SOCE-mediated  $\text{Ca}^{2+}$  entry in lymphocytes<sup>41</sup>. We hypothesise that the slow  $\text{Ca}^{2+}$  oscillations observed during the early stages of acid exposure might induce  $\text{NF-}\kappa\text{B}$  activation and promote ORAI1 upregulation as the acidic selection process continues.

Interestingly, ORAI1 seems to be a key transducer of TME acidosis signals to activate intracellular downstream pathways linked to PDAC progression, as its silencing only affected the migration and invasion of PDAC cells subjected to acid conditions, independently of the time of exposure (Figure 7a-d and Supplementary Figure 2). Preliminary data allowed us to identify Src kinase as a putative downstream target involved in cell-matrix adhesion and invasion in PANC-1

cells (Figure 7e,f). Sun et al. have reported that SOCE-mediated  $\text{Ca}^{2+}$  oscillations promote the invasion of melanoma cells by facilitating invadopodial precursor assembly via activating Src<sup>12</sup>. Moreover, pharmacological inhibition of Src decreases  $\text{Ca}^{2+}$  oscillations in HeLa cells, suggesting they are upstream of the MAP kinase cascade<sup>42</sup>. However, the dependency of Src activity on  $\text{Ca}^{2+}$  oscillations frequency remains to be elucidated.

## Conclusions

Tumour acidosis promotes the selection of PDAC cells characterised by an upregulation of SOCE, required for the generation of fast  $\text{Ca}^{2+}$  oscillations, which may trigger  $\text{Ca}^{2+}$ -dependent signalling pathways involved in PDAC progression (Figure 8).

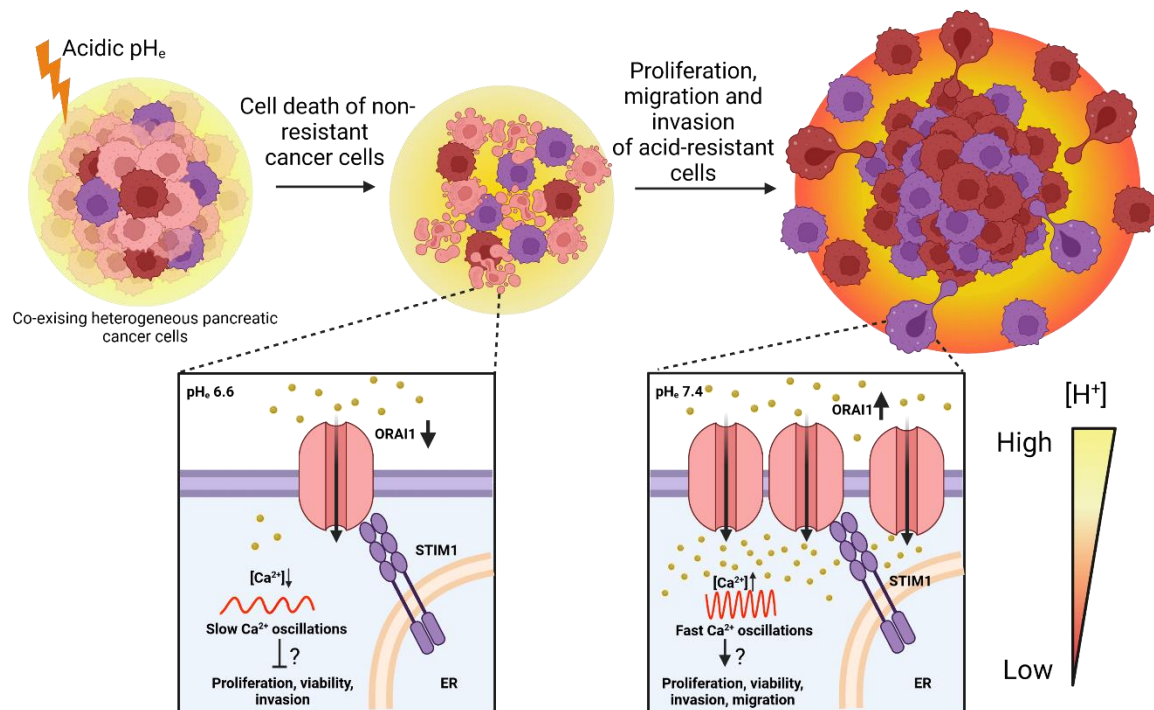


**Figure 8.** PDAC cells exposed to acidic extracellular conditions undergo a process of selection characterised by acid-induced genetic and phenotypic alterations, resulting in the selection of more aggressive PDAC cell phenotypes. The  $\text{Ca}^{2+}$  response to acidic  $\text{pH}_e$  are different along the acid-induced selection, as cells show enhanced basal calcium levels, decreased ORAI1 expression, SOCE and slower ORAI-1 mediated  $\text{Ca}^{2+}$  oscillations during the early stages of acidotic stress, which may contribute to the triggering of cell apoptosis and decreased growth and invasion. Acid selection and recovery to  $\text{pH}_e$  7.4 upregulates SOCE and recovers the fast  $\text{Ca}^{2+}$ -oscillations observed in control cells, which may enhance the malignancy features of acid-selected cells. The figure was created with [www.Biorender.com](http://www.Biorender.com).



## References

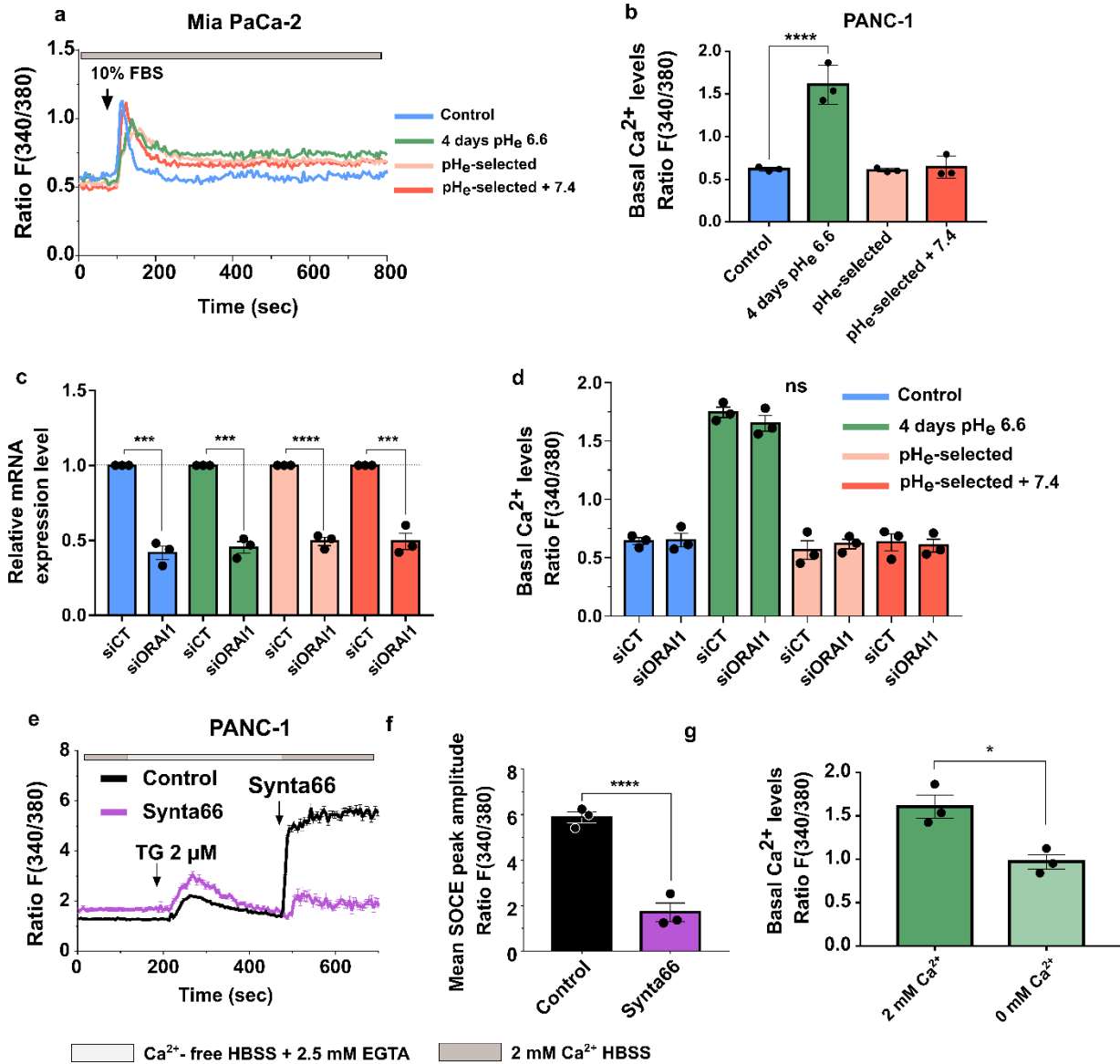
1. Sung, H. *et al.* Global Cancer Statistics 2020: GLOBOCAN Estimates of Incidence and Mortality Worldwide for 36 Cancers in 185 Countries. *CA A Cancer J Clin* **71**, 209–249 (2021).
2. Orth, M. *et al.* Pancreatic ductal adenocarcinoma: biological hallmarks, current status, and future perspectives of combined modality treatment approaches. *Radiat Oncol* **14**, 141 (2019).
3. Novak, I. & Praetorius, J. Fundamentals of Bicarbonate Secretion in Epithelia. in *Ion Channels and Transporters of Epithelia in Health and Disease* (eds. Hamilton, K. L. & Devor, D. C.) 187–263 (Springer New York, 2016). doi:10.1007/978-1-4939-3366-2\_5.
4. Pedersen, S. F., Novak, I., Alves, F., Schwab, A. & Pardo, L. A. Alternating pH landscapes shape epithelial cancer initiation and progression: Focus on pancreatic cancer. *BioEssays* **39**, 1600253 (2017).
5. Carvalho, T. M. A. *et al.* Tumor Microenvironment Features and Chemoresistance in Pancreatic Ductal Adenocarcinoma: Insights into Targeting Physicochemical Barriers and Metabolism as Therapeutic Approaches. *Cancers* **13**, 6135 (2021).
6. Boedtkjer, E. & Pedersen, S. F. The Acidic Tumor Microenvironment as a Driver of Cancer. *Annu. Rev. Physiol.* **82**, 103–126 (2020).
7. Pethő, Z., Najder, K., Bulk, E. & Schwab, A. Mechanosensitive ion channels push cancer progression. *Cell Calcium* **80**, 79–90 (2019).
8. Damaghi, M., Wojtkowiak, J. W. & Gillies, R. J. pH sensing and regulation in cancer. *Front. Physiol.* **4**, (2013).
9. Prevarskaya, N., Skryma, R. & Shuba, Y. Ion Channels in Cancer: Are Cancer Hallmarks Oncochannelopathies? *Physiological Reviews* **98**, 559–621 (2018).
10. Audero, M. M., Prevarskaya, N. & Fiorio Pla, A. Ca<sup>2+</sup> Signalling and Hypoxia/Acidic Tumour Microenvironment Interplay in Tumour Progression. *IJMS* **23**, 7377 (2022).
11. Rizaner, N. *et al.* Intracellular calcium oscillations in strongly metastatic human breast and prostate cancer cells: control by voltage-gated sodium channel activity. *Eur Biophys J* **45**, 735–748 (2016).

12. Sun, J. *et al.* STIM1- and Orai1-mediated Ca<sup>2+</sup> oscillation orchestrates invadopodium formation and melanoma invasion. *Journal of Cell Biology* **207**, 535–548 (2014).
13. Zhu, H. *et al.* Elevated Orai1 expression mediates tumor-promoting intracellular Ca<sup>2+</sup> oscillations in human esophageal squamous cell carcinoma. *Oncotarget* **5**, 3455–3471 (2014).
14. Sun, C. *et al.* Central role of IP3R2-mediated Ca<sup>2+</sup> oscillation in self-renewal of liver cancer stem cells elucidated by high-signal ER sensor. *Cell Death Dis* **10**, 396 (2019).
15. Dragoni, S. *et al.* Vascular Endothelial Growth Factor Stimulates Endothelial Colony Forming Cells Proliferation and Tubulogenesis by Inducing Oscillations in Intracellular Ca<sup>2+</sup> Concentration. *Stem Cells* **29**, 1898–1907 (2011).
16. Son, A. *et al.* Ca<sup>2+</sup> Influx Channel Inhibitor SARAF Protects Mice From Acute Pancreatitis. *Gastroenterology* **157**, 1660-1672.e2 (2019).
17. Hansen, M., Krabbe, S. & Novak, I. Purinergic Receptors and Calcium Signalling in Human Pancreatic Duct Cell Lines. *Cell Physiol Biochem* **22**, 157–168 (2008).
18. Young, S. H. & Rozengurt, E. Crosstalk between insulin receptor and G protein-coupled receptor signaling systems leads to Ca<sup>2+</sup> oscillations in pancreatic cancer PANC-1 cells. *Biochemical and Biophysical Research Communications* **401**, 154–158 (2010).
19. Chen, J. & Sanderson, M. J. Store-operated calcium entry is required for sustained contraction and Ca<sup>2+</sup> oscillations of airway smooth muscle: Store-operated Ca<sup>2+</sup> entry in airway smooth muscle Ca<sup>2+</sup> oscillations. *J Physiol* **595**, 3203–3218 (2017).
20. Kikuta, S. *et al.* Store-Operated Calcium Channels Are Involved in Spontaneous Slow Calcium Oscillations in Striatal Neurons. *Front. Cell. Neurosci.* **13**, 547 (2019).
21. Monteith, G. R., Prevarskaya, N. & Roberts-Thomson, S. J. The calcium–cancer signalling nexus. *Nat Rev Cancer* **17**, 373–380 (2017).
22. Ruffinatti, F. A. *et al.* Calcium signals: Analysis in time and frequency domains. *Journal of Neuroscience Methods* **199**, 310–320 (2011).
23. Ruffinatti, F. A., Gilardino, A., Lovisolo, D. & Ferraro, M. Spatial Wavelet Analysis of Calcium Oscillations in Developing Neurons. *PLoS ONE* **8**, e75986 (2013).

24. Malayev, A. & Nelson, D. J. Extracellular pH modulates the Ca<sup>2+</sup> current activated by depletion of intracellular Ca<sup>2+</sup> stores in human macrophages. *J. Membran Biol.* **146**, (1995).
25. Scrimgeour, N. R., Wilson, D. P. & Rychkov, G. Y. Glu106 in the Orai1 pore contributes to fast Ca<sup>2+</sup>-dependent inactivation and pH dependence of Ca<sup>2+</sup> release-activated Ca<sup>2+</sup> (CRAC) current. *Biochemical Journal* **441**, 743–753 (2012).
26. Pinton, P., Giorgi, C., Siviero, R., Zecchini, E. & Rizzuto, R. Calcium and apoptosis: ER-mitochondria Ca<sup>2+</sup> transfer in the control of apoptosis. *Oncogene* **27**, 6407–6418 (2008).
27. Beck, A., Fleig, A., Penner, R. & Peinelt, C. Regulation of endogenous and heterologous Ca<sup>2+</sup> release-activated Ca<sup>2+</sup> currents by pH. *Cell Calcium* **56**, 235–243 (2014).
28. Tsujikawa, H. *et al.* Identification of key amino acid residues responsible for internal and external pH sensitivity of Orai1/STIM1 channels. *Sci Rep* **5**, 16747 (2015).
29. Gavrieliouk, D. *et al.* Regulation of Orai1/STIM1 mediated ICRCAC by intracellular pH. *Sci Rep* **7**, 9829 (2017).
30. Scremin, E. *et al.* ORAI2 Down-Regulation Potentiates SOCE and Decreases A $\beta$ 2 Accumulation in Human Neuroglioma Cells. *IJMS* **21**, 5288 (2020).
31. Ay, A.-S., Benzerdjeb, N., Sevestre, H., Ahidouch, A. & Ouadid-Ahidouch, H. Orai3 Constitutes a Native Store-Operated Calcium Entry That Regulates Non Small Cell Lung Adenocarcinoma Cell Proliferation. *PLoS ONE* **8**, e72889 (2013).
32. Vaeth, M. *et al.* ORAI2 modulates store-operated calcium entry and T cell-mediated immunity. *Nat Commun* **8**, 14714 (2017).
33. Dubois, C. *et al.* Remodeling of Channel-Forming ORAI Proteins Determines an Oncogenic Switch in Prostate Cancer. *Cancer Cell* **26**, 19–32 (2014).
34. Yoast, R. E. *et al.* The native ORAI channel trio underlies the diversity of Ca<sup>2+</sup> signaling events. *Nat Commun* **11**, 2444 (2020).
35. Thiel, M., Lis, A. & Penner, R. STIM2 drives Ca<sup>2+</sup> oscillations through store-operated Ca<sup>2+</sup> entry caused by mild store depletion: STIM2 drives Ca<sup>2+</sup> oscillations through store-operated Ca<sup>2+</sup> entry. *The Journal of Physiology* **591**, 1433–1445 (2013).

36. Camors, E. & Valdivia, H. H. CaMKII regulation of cardiac ryanodine receptors and inositol triphosphate receptors. *Front. Pharmacol.* **5**, (2014).
37. Kawanishi, T., Nieminen, A. L., Herman, B. & Lemasters, J. J. Suppression of Ca<sup>2+</sup> oscillations in cultured rat hepatocytes by chemical hypoxia. *Journal of Biological Chemistry* **266**, 20062–20069 (1991).
38. Smedler, E. & Uhlén, P. Frequency decoding of calcium oscillations. *Biochimica et Biophysica Acta (BBA) - General Subjects* **1840**, 964–969 (2014).
39. Tong, Y. *et al.* Hypoxia-induced NFATc3 deSUMOylation enhances pancreatic carcinoma progression. *Cell Death Dis* **13**, 413 (2022).
40. Eylestein, A. *et al.* Transcription Factor NF- $\kappa$ B Regulates Expression of Pore-forming Ca<sup>2+</sup> Channel Unit, Orai1, and Its Activator, STIM1, to Control Ca<sup>2+</sup> Entry and Affect Cellular Functions. *Journal of Biological Chemistry* **287**, 2719–2730 (2012).
41. Berry, C. T., May, M. J. & Freedman, B. D. STIM- and Orai-mediated calcium entry controls NF- $\kappa$ B activity and function in lymphocytes. *Cell Calcium* **74**, 131–143 (2018).
42. Morita, M., Nakane, A., Fujii, Y., Maekawa, S. & Kudo, Y. High Cell Density Upregulates Calcium Oscillation by Increasing Calcium Store Content via Basal Mitogen-Activated Protein Kinase Activity. *PLoS ONE* **10**, e0137610 (2015).

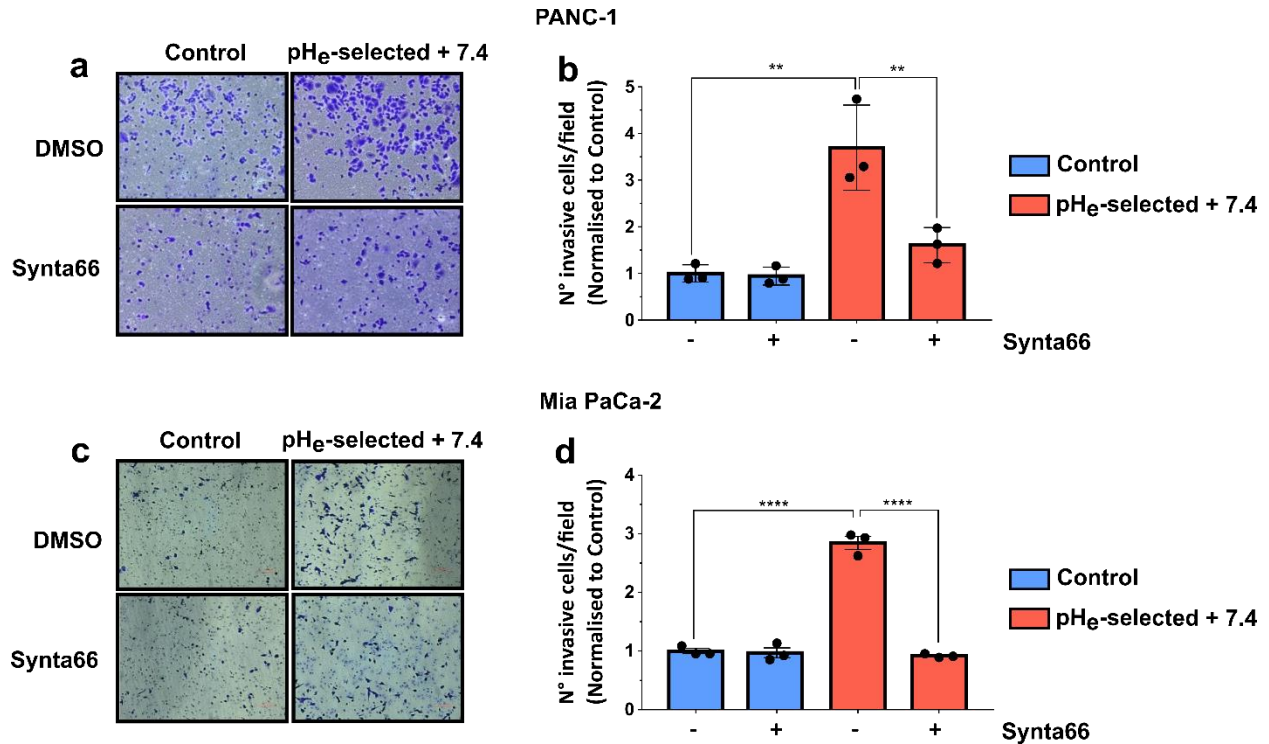
## Supplementary Figure 1



**a**) Representative traces of O/N starved Mia PaCa-2 cell models stimulated with 10% FBS to induce Ca<sup>2+</sup> oscillations. **b**) Quantification of the basal cytosolic Ca<sup>2+</sup> levels from starved-PANC-1 Ca<sup>2+</sup> oscillations traces. **c**) ORAI1 mRNA expression levels of PANC-1 cell models transfected with either siCT or siORAI1 with double-pulse technique and presented as fold change values obtained by RT-qPCR. ORAI1 gene levels were assessed 48h after the second pulse. The effects of siORAI1 in each cell model were compared to their respective control (siCT, dotted lines). Fold changes were quantified using the 2- $\Delta\Delta C_q$  method and normalised to HPRT reference gene. **d**) Quantification of the basal cytosolic Ca<sup>2+</sup> levels from Ca<sup>2+</sup> oscillations traces in PANC-1 cells transfected with siCT or siORAI1. **e**) Mean SOCE trace in PANC-1 cells treated or not with Synta66 (10 μM) to induce SOCE inhibition. **f**) Quantification of the mean SOCE peak

amplitude in PANC-1 vehicle cells (DMSO) and Synta66-treated cells. **g**) Quantification of the basal cytosolic  $\text{Ca}^{2+}$  levels from  $\text{Ca}^{2+}$  oscillations traces in PANC-1 cells exposed to short-term acidosis (4 days) in the presence of 2 mM  $\text{Ca}^{2+}$  or  $\text{Ca}^{2+}$ -free HBSS bathing solution. Data were reported as mean  $\pm$  SEM and are from 3 independent experiments. Data were analysed using Student t-test or One-way ANOVA with Dunnett's multiple comparison test, \*  $p < 0.05$ , \*\*\*  $p < 0.001$ , \*\*\*\*  $p < 0.0001$ .

## Supplementary Figure 2



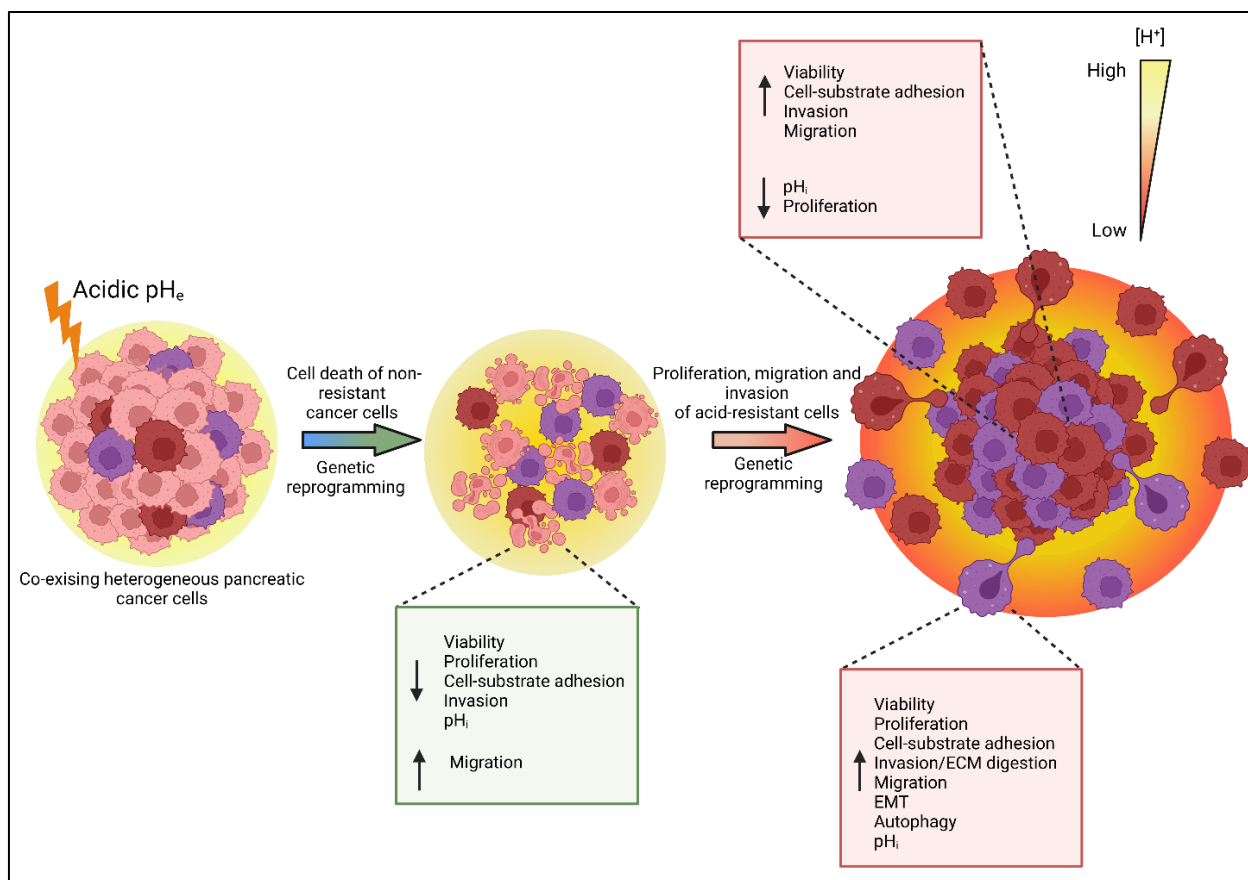
**a**) Representative microscopic images of PANC-1 control and pH<sub>e</sub>-selected + 7.4 invasive cells in the presence of 10  $\mu\text{M}$  Synta66 or control DMSO stained with crystal violet are shown. **b**) Quantification of PANC-1 control and pH<sub>e</sub>-selected + 7.4 cells that invaded through the matrigel-coated transwell in the presence of Synta66, indicating the number of cells of five representative areas per condition. **c**) Representative microscopic images of Mia PaCa-2 control and pH<sub>e</sub>-selected + 7.4 invasive cells in the presence of 10  $\mu\text{M}$  Synta66 or control DMSO, stained with crystal violet are shown. **d**) Quantification of Mia PaCa-2 control and pH<sub>e</sub>-selected + 7.4 cells that invaded through the matrigel-coated transwell in the presence of Synta66, indicating the number of cells of five representative areas per condition. Data were reported as mean  $\pm$  SEM and are from 3 independent experiments. Data were analysed using One-way ANOVA with Dunnett's multiple comparison tests, \*\*  $p < 0.01$ , \*\*\*\*  $p < 0.0001$ .

# Chapter IV

## Conclusion and perspectives

In this PhD thesis, different questions have been addressed for understanding the role of tumor acidosis in PDAC progression. In this chapter, the main results achieved will be presented, highlighting the challenges, and giving a global overview of the possible future work.

- I. *Acidic growth conditions promote epithelial-to-mesenchymal transition to select more aggressive PDAC cell phenotypes in vitro.*



**Graphical abstract:** PDAC cells exposed to acidic extracellular conditions undergo a process of selection, characterized by acid-induced genetic and phenotypic alterations. This results in increased cell death due to the cytotoxic effect of low  $pH_e$  and decrease of cell-substrate adhesion, proliferation and cell invasion. Along with the acid exposition, further genetic rewiring provides surviving cancer cells with more aggressive properties in terms of adhesion, migration, and invasion. Still limited proliferative capacities are overcome when cells are acclimated to  $pH_e$  7.4 following 1 month-long  $pH_e$  6.6 treatment. The figure was created with [www.Biorender.com](http://www.Biorender.com).

In our first work, we have explored the role of acidic pressure on genetic and phenotypic alterations of two PDAC cell lines, PANC-1 and Mia PaCa-2, by means of different in vitro techniques and RNA-sequencing. This work stemmed from the need of a comprehensive characterization of the effects of tumor acidosis on PDAC cells that would take into account the different stages of low  $pH_e$ -induced selection, from the early stages to the later ones. In fact, while the effects of acidic treatment have been previously described in different cancer cell types, only few recent studies have addressed this matter in pancreatic cancer<sup>259,315</sup>, therefore the evolution of PDAC to endure and adapt to prolonged acidotic microenvironmental stress is poorly understood. Moreover, the majority of the works have focused on the effects of acute extracellular acidification,



with expositions to low  $pH_e$  in the range of minutes to hours. This has only partially shed light on how tumor cells react to acid exposure, in particular because the TME is generally thought to become more acidic over time due to the extended latency of tumor formation. Despite several works have investigated the effects of acid adaptation in different cancer cell types, the cellular responses induced by acidosis are strictly cancer-type and cancer cell line- specific, due to the different tissue and cell expression/activity of the different  $pH_e$ -regulatory proteins.

Two other key aspects to take into consideration is the methodology for cell medium preparation with a specific target pH and the necessary distinction between acid adaptation and selection. Concerning the first aspect, when interpreting different results about the responses of cancer cells to acidosis, it is important to bear in mind the experimental procedures set up by each study to obtain the target pH in the cell culture medium and the closeness or otherwise to a physiological context. In fact, specific responses to acid exposure, as metabolic ones, can be different when they are induced by a reduction of the amount of bicarbonate or by an addition of lactate or HCl for acidification of the cell medium<sup>439</sup>, making difficult, if not impossible, the comparison among studies with different experimental procedures for reaching their target  $pH_e$ . For these reasons, we have decided to employ the  $CO_2/HCO_3^-$  buffer system, which is the most physiological relevant and stable<sup>440</sup>. This suggests that our results probably cannot be fully replicated in different experimental setting, such as by adopting lactate for acidifying the extracellular  $pH_e$ . However, this represents an interesting question that could be addressed in the future.

The second consideration regards the distinction between acid adaptation and acid selection and it is directly linked to the first consideration. A gradual change in  $pH_e$  over extended periods results in cell adaptation, as the slow pH modifications will allow cells to respond to these changes, while abrupt and large changes in  $pH_e$  will lead to cell selection, characterized by initial cell death and survival of a cancer subpopulation. Several studies have described the acid adaptation phenomenon, while fewer works have experimentally described the acid selection process, especially in PDAC. Therefore, we have decided to focus on acid selection, despite the difficulties faced in performing specific experiments with acid-selected cells that required a high number of cells, as the survival populations following the 1-month acid exposure are sparse.

The last reason that drove this work was the need of a comprehensive study underlying the effect of the TME acidification on PDAC cell invasion from the tumor acidic regions to areas with higher pHe, as those found at the boundaries of tumor-stroma. To this end, the PDAC cell model of acid selection and re-acclimation to physiological pHe was established, to evaluate the effect of this selection process on the promotion of the escape of cancer cells. This escape is driven by local invasion and represents a key step in tumor metastasis.

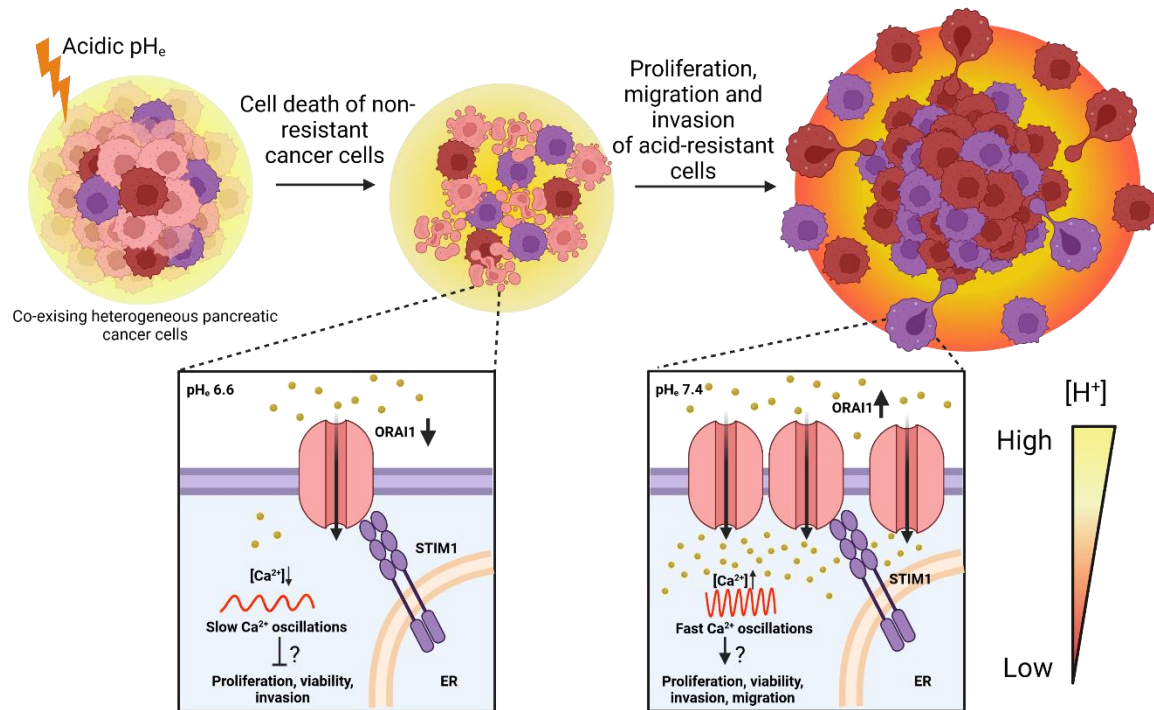
With these considerations in mind, we developed 3 different acidic models for each PDAC cell line for the study of the early stages of pHe-selection and the end stages of it, and the last model for mimicking the effect of acid selection on tumor cells escape from acidic regions. By performing different *in vitro* functional experiments and RNA-seq on PANC-1 cells, we demonstrated that low pH represents a stress factor during the early stages of selection, determining the cell death of “weaker” cancer cells with limited proliferative, adhesive and invasive capacities and selecting for cancer cells characterized by enhanced migratory and invasive abilities via EMT, although the proliferative capacity of 1 month-acid selected cells is still impaired. The recovery to pHe 7.4 for 2 weeks was sufficient to boost the proliferation of these cells, maintaining the increased migration and invasion and further promoting cancer cells escape by increased ECM degradation. Our work emphasized the key role of PDAC tumor acidosis in selecting aggressive cancer cell phenotypes with growth, migratory and invasive advantages, and promoting PDAC progression.

These results represent the first step upon which additional investigations can be conducted. The limitations of the *in vitro* could be overcome by employing scaffold-based three-dimensional (3D) multicellular pancreatic tumor models obtained with our different PDAC acidic models, which would better recapitulate *in vivo* the tumor cell environment. We are therefore aiming to assess the impact of acid selection on 3D spheroid invasion assays and go deeper in the more malignant phenotypes acquired by acid-selected cells by quantifying the chemoresistance of the different acidic models to therapeutic drugs, such as gemcitabine (GEM) and C18GEM, a lipophilic derivate of gemcitabine which represents a new potential therapeutic prodrug for PDAC. We are currently collaborating with the research group guided by Dr. Rosa Angela Cardone from Bari, Italy, to assess the effects of GEM and C18GEM on cell viability by using 3D organotypic cultures grown on an extracellular matrix composed of matrigel or collagen I. Moreover, experiments assessing the impact of these chemotherapy drugs on PDAC control and pHe-selected + 7.4 cells invasion are in progress. Finally, *in vivo* validation of the results is needed. This could be accomplished by using a

xenograft mouse model with PANC-1 control and  $pH_e$ -selected cells with or without recovery to  $pH_e$  7.4 cells. Another strategy could be to evaluate  $pH_e$ -selection induced aggressiveness in a syngeneic orthotopic murine model of PDAC using the Panc02 murine cancer cell lines, as Prof. Alves' group demonstrated that these murine cells share a similar aggressive phenotype as PANC-1  $pH_e$ -selected cells after acid-induced selection.

Another important aspect of being deepened is the correlation between the different cell phenotypes observed and the intracellular  $pH_i$  values of each cell model. It represents a key parameter for all types of cells, profoundly affecting several cell processes, including those promoting cancer progression<sup>441</sup>. It is also established that external acidosis affects the intracellular space, acidifying it in conditions of severe acidosis. In this context, the activity of proteins such as  $Na^+/HCO_3^-$ -cotransporter and  $Na^+/H^+$ -antiporter results essential to maintain the pH homeostasis of cancer cells and, therefore their expression and/or activity during the different stages of acid selection may give us important insights on  $pH_i$  regulation and the consequent cell phenotypic response to acidosis. For this purpose, we established a collaboration with the research group guided by Prof. Albrecht Schwab from Munster, Germany, for the performance of the  $NH_4^+$  prepulse technique to investigate  $Na^+$ -dependent  $H^+$  extrusion (e.g., mediated by the  $Na^+/HCO_3^-$ -cotransporter or  $Na^+/H^+$ -antiporter) and assess the activity of  $Na^+$ -dependent pH regulatory proteins in the different PDAC cell models.

***II.  $pH_e$ -sensitive Store-Operated  $Ca^{2+}$  channels signals contribute to tumor acidic microenvironment-induced PDAC cells' selection to more aggressive phenotypes.***



**Graphical abstract.** PDAC cells exposed to acidic extracellular conditions undergo a process of selection, characterized by acid-induced genetic and phenotypic alterations and which results in the selection of more aggressive PDAC cell phenotypes. The  $\text{Ca}^{2+}$  response to acidic  $\text{pH}_e$  are different along the acid-induce selection, as cells show enhanced basal calcium levels, decreased ORAI1 expression, SOCE and slower ORAI-1 mediated  $\text{Ca}^{2+}$  oscillations during the early stages of acidotic stress, which may contribute to the triggering of cell apoptosis and decreased growth and invasion. Acid selection and recovery to  $\text{pH}_e$  7.4 upregulates SOCE and recovers the fast  $\text{Ca}^{2+}$ -oscillations observed in control cells, which may enhance the malignancy features of acid-selected cells. The figure was created with [www.Biorender.com](http://www.Biorender.com).

In our second work, we explored the impact of tumor acidosis on intracellular  $\text{Ca}^{2+}$  signals in the previously established acidic models. Although the roles of tumor acidosis and  $\text{Ca}^{2+}$  signaling in cancer progression are well established, the hypothesis of acidic TME of pancreatic cancer employing  $\text{Ca}^{2+}$  signaling as preferential route for sustaining PDAC progression has not yet been sufficiently explored. Therefore, this study arose from the hypothesis of a synergic relationship between PDAC acidic microenvironment and  $\text{Ca}^{2+}$  signals. As for our previous work, there is a lack of studies focusing on the effect of the different stages of acid selection on the expression and activity of  $\text{Ca}^{2+}$ -permeable ion channels, in particular in PDAC. For our work, we have decided to focus on calcium oscillations as main players in different cancer-promoting processes<sup>289</sup>. A detailed

study revealed that  $\text{Ca}^{2+}$  oscillation in PANC-1 cells are dependent on Store-Operated  $\text{Ca}^{2+}$  Entry (SOCE). Starting from the acquired knowledge that SOCE, and therefore its components ORAI1 and STIM1, is  $\text{pH}_e$ -regulated, we employed  $\text{Ca}^{2+}$  imaging technique with Fura-2 for measuring of cytosolic  $\text{Ca}^{2+}$  levels, cell adhesion, migration and invasion assays, and siRNA and chemical inhibition of ORAI1 to demonstrated that PANC-1 cells generate slower FBS-induced and SOCE-dependent  $\text{Ca}^{2+}$  oscillations respect to control cells, correlated with the downregulation of SOCE and ORAI1 mRNA expression during the early stages of  $\text{pH}$ -selection. As the acidic exposure continues, we observed an increased in SOCE, which supported the generation of control-like and faster  $\text{Ca}^{2+}$  oscillations. Silencing of ORAI1 and its inhibition with Synta66 also showed that ORAI1-mediated  $\text{Ca}^{2+}$  influx might be involved in the enhanced migratory and invasive phenotypes of all the cell models exposed to acidic  $\text{pH}_e$ , as the different treatment for suppressing ORAI1 activity and function didn't affect control cells. Our work demonstrated that acid selection and recovery to physiological  $\text{pH}_e$  may employ ORAI1-mediated  $\text{Ca}^{2+}$  signals to promote cell migration and invasion in PDAC cells.

To validate the contribute of ORAI1 and other SOC channels in mediating the tumor acidosis responses in the context of PDAC progression, several additional questions must be addressed.

First, our main objective will be to work on both the upstream and downstream of ORAI1-mediated signaling, concentrating on the identification of the upstream molecular regulation behind ORAI1 deregulation in PANC-1 acidic models, and of a low  $\text{pH}_e$ - and  $\text{Ca}^{2+}$ -dependent signaling cascade implicated in the acquired malignancy of acid-selected cells. Concerning the upstream molecular mechanisms behind ORAI1 deregulation, our strategy involves the identification of  $\text{pH}_e$ -regulated transcription factors with  $\text{Ca}^{2+}$  signals-decoding properties which may regulate ORAI1 expression. Our putative candidate is NF- $\kappa$ B, which is known to be  $\text{pH}_e$ -sensitive, being activated by acidosis and playing and contributing to acidosis-induced invasion of MCF-7 and MDA-MB-231 breast cancer cells<sup>442</sup>. Moreover, NF- $\kappa$ B promotes the expression of ORAI1 and STIM1, in mast cells by binding to specific regions upstream of ORAI1 and STIM1 transcription start<sup>443</sup>. Calcium entry via  $\text{Ca}^{2+}$  release-activated ORAI1 channels also regulates NF- $\kappa$ B's activation and function in lymphocytes<sup>444</sup>. NF- $\kappa$ B is also a decoder of  $\text{Ca}^{2+}$  oscillations, being activated by a specific range of  $\text{Ca}^{2+}$  oscillations frequencies<sup>369</sup>. To study the potential feedback regulation between low  $\text{pH}$ , NF- $\kappa$ B and ORAI1-mediated  $\text{Ca}^{2+}$  oscillations, we will work at different levels. First, the acidic  $\text{pH}_e$ -mediated and  $\text{Ca}^{2+}$ -oscillations mediated NF- $\kappa$ B activity and cellular localization will be measured

in all PDAC control and acidic models via western blot, luciferase reporter assay and immunofluorescent staining, and by exploiting a fluorescence-tagged tracker of NF- $\kappa$ B translocation that it is being currently developed by the PHYCEL Laboratory, which will be transduced into cells and coupled to fluorescent Ca<sup>2+</sup> imaging, in order to allow the concomitance visualization of Ca<sup>2+</sup> oscillations and NF- $\kappa$ B translocation. Then, ORAI and STIM mRNA and protein levels will be also quantified in presence of NF- $\kappa$ B inhibitor, Wogonin, by means of qPCR and Western Blots. Vice versa, NF- $\kappa$ B activity and cellular localization will be measured using siORAI1 and siSTIM1. To verify if ORAI1-mediated Ca<sup>2+</sup> signals contribution in the enhanced aggressiveness in acidic selected models pass through NF- $\kappa$ B, the effects of NF- $\kappa$ B inhibition will be evaluated by means of transwell migration and invasion assays and 3D spheroids invasion assays.

On the other side, for the identification of the downstream signaling pathway triggered by ORAI1-mediated Ca<sup>2+</sup> signals in the PDAC acidic models, we will focus on NF- $\kappa$ B cascade-related proteins such as PI3K, ERK and Akt, and in other signaling molecules such as Src kinase, another decoder of Ca<sup>2+</sup> oscillations involved in the adhesion and invasion of all our PANC-1 models.

Another aspect to be deepen is the role of ORAI1, and potentially other ORAI and STIM channels, in the aggressive behaviors displayed by our acidic models, expanding the assessment of these Ca<sup>2+</sup>-channels/sensors in cell proliferation, chemosensitivity, invadopodia activity and viability, both in 2D and 3D cell cultures.

Beside SOC channels, we are currently started to develop a parallel project focusing on the role of other Ca<sup>2+</sup>-permeable channels in our characterized PANC-1 acidic models, which are TRPA1 and TRPM8. Our RNA-seq data have demonstrated that TRPA1 channels are downregulated in the PANC-1 “4 days pHe 6.6” (log<sub>2</sub> fold change TRPA1 = -1.546596874, *p*-value = 3.42E-05) and TRPA1 and TRP8 in “pHe-selected + 7.4” cells (log<sub>2</sub> fold change TRPA1 = -2.901223009, *p*-value = 8.49E-15; log<sub>2</sub> fold change TRPM8 = -1.385227926, *p*-value = 0.000233139), paving the way for further potential molecular targets that may be involved in the increased aggressiveness of PDAC cells following acidic selection. For this parallel work, we are collaborating with the research group of the Laboratory of Cellular and Molecular from Turin, Italy.

In conclusion, this project have highlighted the key role of PDAC tumor microenvironment and the acidosis-induced selection, which exacerbates the malignant phenotype and which is further increased after recovery to pHe 7.4, mimicking the stroma-tumor boundaries, where we can find higher pHe values and acid-adapted cells escape from tumor regions to metastasize. In this context,

Ca<sup>2+</sup>-signaling may act as important contributor in acid-selected enhanced migratory and invasive abilities acid-selection-induced upregulation of SOCE and probably with an involvement of Ca<sup>2+</sup> oscillations which have still to be clarified.

## **Annexe 1**



Review

# Ca<sup>2+</sup> Signalling and Hypoxia/Acidic Tumour Microenvironment Interplay in Tumour Progression

Madeline Magali Audero<sup>1,2</sup>, Natalia Prevarskaya<sup>1</sup> and Alessandra Fiorio Pla<sup>1,2,\*</sup> 

<sup>1</sup> U1003—PHYCEL—Laboratoire de Physiologie Cellulaire, Inserm, University of Lille, Villeneuve d'Ascq, 59000 Lille, France; madeline.audero@univ-lille.fr (M.M.A.); natacha.prevarskaya@univ-lille.fr (N.P.)

<sup>2</sup> Laboratory of Cellular and Molecular Angiogenesis, Department of Life Sciences and Systems Biology, University of Turin, 10123 Turin, Italy

\* Correspondence: alessandra.fiorio@unito.it; Tel.: +39-0116704660

**Abstract:** Solid tumours are characterised by an altered microenvironment (TME) from the physicochemical point of view, displaying a highly hypoxic and acidic interstitial fluid. Hypoxia results from uncontrolled proliferation, aberrant vascularization and altered cancer cell metabolism. Tumour cellular apparatus adapts to hypoxia by altering its metabolism and behaviour, increasing its migratory and metastatic abilities by the acquisition of a mesenchymal phenotype and selection of aggressive tumour cell clones. Extracellular acidosis is considered a cancer hallmark, acting as a driver of cancer aggressiveness by promoting tumour metastasis and chemoresistance via the selection of more aggressive cell phenotypes, although the underlying mechanism is still not clear. In this context, Ca<sup>2+</sup> channels represent good target candidates due to their ability to integrate signals from the TME. Ca<sup>2+</sup> channels are pH and hypoxia sensors and alterations in Ca<sup>2+</sup> homeostasis in cancer progression and vascularization have been extensively reported. In the present review, we present an up-to-date and critical view on Ca<sup>2+</sup> permeable ion channels, with a major focus on TRPs, SOC channels and PIEZO channels, which are modulated by tumour hypoxia and acidosis, as well as the consequent role of the altered Ca<sup>2+</sup> signals on cancer progression hallmarks. We believe that a deeper comprehension of the Ca<sup>2+</sup> signalling and acidic pH/hypoxia interplay will break new ground for the discovery of alternative and attractive therapeutic targets.

**Keywords:** Ca<sup>2+</sup> signalling; TRP channels; SOC channels; PIEZO channels; tumour acidic microenvironment; hypoxia; tumour progression



**Citation:** Audero, M.M.; Prevarskaya, N.; Fiorio Pla, A. Ca<sup>2+</sup> Signalling and Hypoxia/Acidic Tumour Microenvironment Interplay in Tumour Progression. *Int. J. Mol. Sci.* **2022**, *23*, 7377. <https://doi.org/10.3390/ijms23137377>

Academic Editors: Maria Beatrice Morelli and Amantini Consuelo

Received: 1 June 2022

Accepted: 27 June 2022

Published: 2 July 2022

**Publisher's Note:** MDPI stays neutral with regard to jurisdictional claims in published maps and institutional affiliations.



**Copyright:** © 2022 by the authors. Licensee MDPI, Basel, Switzerland. This article is an open access article distributed under the terms and conditions of the Creative Commons Attribution (CC BY) license (<https://creativecommons.org/licenses/by/4.0/>).

## 1. Introduction

### 1.1. Cancer Microenvironment: Focus on Tumour Acidic pH<sub>e</sub> and Hypoxia

Solid tumours are characterised by a dynamic microenvironment constituted by a variety of different non-cellular components, such as the extracellular matrix (ECM) components, circulating free DNA, and cell components, such as aberrant blood vessels, immune cells, tumour-associated fibroblasts (TAFs), endothelial cells, macrophages, pericytes, among others. In turn, the interaction with chemical and physical cues (hypoxia, tumour acidosis, high tumour interstitial stiffness), originates finally a peculiar chemical and physical environment that supports cancer progression [1].

A common feature of almost all advanced solid cancers is the presence of transient or permanent acidic and hypoxic tumour regions, which are a direct outcome of the cancer cells' metabolic pathways rearrangement, supporting their uncontrolled proliferation. This leads to a significant increase in cancer cells' anabolic activity and a reduction in the catabolic one, promoting the synthesis of amino acids, nucleotides, and lipids to back their growth. Indeed, according to Otto Warburg's work [2], cancer cells are characterised by an enhanced glycolytic breakdown of glucose to pyruvate and consequent NADPH and ATP production with respect to healthy cells, even in presence of oxygen and even considering the lower energy yield of pyruvate fermentation compared to oxidative respiration.



Nevertheless, it is important to underline that not all cancer cells are characterized by the Warburg effect, but it has been observed that cancer cells may have an opposite phenotype, with an increased mitochondrial oxidative activity [3]. The importance of mitochondrial activity in cancer cells is also explained by the oxidative phosphorylation increase observed when the Warburg effect is inhibited in cancer cells [3–5].

The metabolic rearrangement and fermentation of pyruvate resulting from glycolysis lead to high production of lactic acid, acidifying the intracellular environment. Hydrolysis of ATP also determines the release of protons ( $H^+$ ) in the intracellular space, contributing to its acidification [6–8]. Protonation has a severe negative impact on several enzymes and lipids, leading to a potential risk of impinging several cellular processes, including cell metabolism. It is therefore not surprising that cells use different systems to maintain the intracellular pH ( $pH_i$ ) within the physiological range of about 7.2. In cancer cells, a slightly more alkaline intracellular pH ( $pH$  7.4) has been observed, and evidence showed that this slight difference in  $pH_i$  between cancer cells and healthy cells promotes some of the hallmarks of cancer, such as cell death escape and proliferation [9–12]. To maintain this  $pH_i$  value, transformed cells have at their disposal an arsenal of overexpressed transporter proteins and pumps for protons and lactic acid extrusion to the extracellular milieu, resulting in its acidification. Examples of this transport system comprise monocarboxylate transporters (MCTs), major players in the transmembrane lactate trafficking,  $Na^+/H^+$  antiporters (NHE), vacuolar  $H^+$  ATPases, and carbonic anhydrases (CAs), mainly CAIX and CAXII, which role in cancer progression is well documented [13–17]. Acidic interstitial fluids are not only the result of the presence of lactic acid and protons but also of the  $CO_2$  derived from the cell respiration process in more oxygenated areas.  $CO_2$  can passively diffuse through the plasma membrane (PM), or it can be reversibly hydrated to  $HCO_3^-$  by the transmembrane Carbonic Anhydrase IX (CAIX) exofacial site and released in the tumour microenvironment with protons.  $Na^+/HCO_3^-$  cotransporters (NBCs) in the proximity of CAIX can mediate  $HCO_3^-$  influx for sustaining intracellular buffering, titrating cytosolic  $H^+$  [18,19]. It has to be noticed that the  $pH_i$  of cancer cells can drop significantly in presence of a strong acidic  $pH_e$ , giving rise to a heterogeneous  $pH_i$  landscape (due to the TME), where cancer cells resident in acidic regions will present quite a low  $pH_i$ , while cancer cells occupying moderate acidic  $pH_e$  areas will show a moderate alkaline  $pH_i$  [8]. It is therefore important to consider the tumour microenvironmental complexity to understand how cancer cells adapt to it, in order to possibly find new therapeutical targets. In addition to metabolic rearrangement, tumour acidosis can be further boosted by tumour-associated hypoxia, which leads to higher glycolytic cell metabolism rates. Hypoxia occurs in the context of tumours vascularized by insufficient vessels and/or vessels characterised by a poor capacity to diffuse oxygen and nutrients and to remove the metabolic waste products due to an altered process of angiogenesis, which leads to the formation of aberrant and dysfunctional vessels. Hypoxia is also the result of an increased oxygen demand from highly proliferating areas of the tumour, leading to intratumour hypoxia heterogeneity, with subregions of the tumour characterised by different oxygen concentrations and consumption. The irregular exposure to oxygen fluctuations is associated with adaptive mechanisms set in motion by cancer cells in order to promote their survival in that hostile environment. Indeed, hypoxia adaptation is linked to increased genomic instability and tumourigenesis [20] and to more aggressive cancer phenotypes in terms of tumour growth, drug and cell death resistance, angiogenesis and enhanced metastasis [21].

Hypoxia adaptation processes are initiated by a series of transcription factors belonging to the hypoxia-inducible factor family, in particular hypoxia-inducible factor 1 (HIF-1), which determines a gene expression reprogramming that affects cancer cell metabolism and processes which sustain its progression. HIF-1 is a heterodimer protein constituted by HIF-1 $\alpha$  and HIF-1 $\beta$  and this complex is not present in normoxic conditions. Although the  $\beta$  subunit is constitutively expressed in all cells, the HIF-1 $\alpha$  subunit is present only at low levels in all cells' cytoplasm due to the presence of two specific proline residues at positions 402 and 564 in the oxygen-dependent degradation (ODD) domain in the  $\alpha$

subunit. These residues are hydroxylated by prolyl hydroxylase protein (PHD) in presence of physiological oxygen levels, and this modification targets the subunit to degradation via the ubiquitin-proteasome pathway [22]. However, in hypoxic conditions, PHD is inhibited and therefore Pro402 and Pro564 are not hydroxylated, allowing HIF-1 $\alpha$  and HIF-1 $\beta$  to dimerize and translocate to the cell nucleus and the consequent activation of target genes transcription [22]. In addition to low O<sub>2</sub> concentrations, high intracellular lactate levels and specific growth factors or oncogenes can stabilise HIF-1 $\alpha$  as well, leading to the activation of HIF-1 $\alpha$ -target genes [23,24]. “Hypoxia-adaptive” responsive genes include glucose transporters, such as GLUT1/3, enzymes involved in anaerobic glycolysis, such as lactate dehydrogenase-A (LDHA), aldolase (ALDA), phosphoglycerate kinase-1 (PGK1), enolase (ENOL) and phosphofructokinase-1 (PFK-1), pyruvate dehydrogenase kinase 1 (PDK1), with consequent suppression of mitochondrial oxidative phosphorylation system (OXPHOS).

The hypoxia response is not limited to glycolytic flux, as it also enhances the expression of VEGF and other pro-angiogenic factors and promotes tumour progression by inducing epithelial–mesenchymal transition (EMT) [25], cell survival in moderate hypoxic conditions via autophagy, cell death via the same mechanism but in presence of severe hypoxic conditions [26], and by promoting cancer cells’ invasion and metastasis in acute hypoxic conditions (from minutes up to 72 h exposure *in vitro*). In particular hypoxia-mediated cell invasion is achieved by sustaining the mesenchymal phenotype, the expression of different metalloproteases (MMPs), lysyl oxidase (LOX), connective tissue growth factor (CTGF) and CAIX, NHE1 and MCTs [21], which contribute to pH regulation and enhance the acidification of the tumour microenvironment.

Hypoxia also plays a key role in chemoresistance, as reduced oxygen availability can affect not only drug delivery but also chemotherapeutics activity [27]. Moreover, the tumour hypoxic core is occupied by cancer cells with a hypoxia-induced stem cell-like phenotype, characterized by cell cycle arrest in the G1 phase and a quiescent state, representing a major problem for those chemotherapy agents which target rapidly proliferating cells [27–29]. Hypoxia also upregulates multidrug resistance genes [30–32].

Hypoxia sustains all these effects by activating different signalling pathways via HIF-1 $\alpha$ , such as the Wnt/ $\beta$ -catenin and TGF- $\beta$ /SMAD pathways, or in a HIF-1 $\alpha$ -independent manner, switching on MAPKs, AMPKs, PI3K/Akt/mTOR, NF- $\kappa$ B and Notch signalling transduction pathways [21,25], which are dependent also on intracellular Ca<sup>2+</sup> ions. All these mechanisms of cell adaptation to hypoxia determine the selection of highly aggressive clones, which pave the way for tumour expansion.

In addition to being affected by the hypoxic tumour microenvironment, acidic pH<sub>e</sub> has been observed to regulate HIF1 $\alpha$  and HIF2 $\alpha$  levels under normoxic conditions in glioma cells, promoting cancer stem cell maintenance [33], highlighting the feedback regulation and crosstalk between hypoxia and low pH<sub>e</sub>. Similarly to hypoxia, the acidic tumour microenvironment supports different hallmarks of cancer, such as drug resistance as previously described [34]. In addition, acidic TME plays an important role in immunoreactive processes and inflammation, by promoting the viability and fitness of pro-tumour M2 macrophages with respect to anti-tumour M1 macrophages [35], by inhibiting T and NK cells activation and inducing immune escape [36,37], by inducing a phenotypic shift in macrophages towards a tumour-promoting phenotype [38] and by increasing the tumour-promoting functions of tumour-associated neutrophils [39]. Moreover, acidic pH<sub>e</sub> fulfils its pro-tumour function through the enhancement of two other important hallmarks: cancer cell invasion and the ability to metastasise [40]. Studies in breast cancer and colon cancer have indeed demonstrated that invasive cell areas co-localise with acidic pH<sub>e</sub> regions [41], while studies in melanoma cells have shown that acidic pH<sub>e</sub> exposure increases their invasive abilities *in vitro* and the formation of pulmonary metastasis *in vivo* via a low pH<sub>e</sub>-promoted secretion of proteolytic enzymes and pro-angiogenic factors [42].

An explanatory example of the major role of acidosis in cancer progression is given by the unique pancreatic ductal adenocarcinoma (PDAC) microenvironment [43]. The

pancreatic duct is a net acid-base transporting epithelium, in which ductal cells secrete bicarbonate into the ductal lumen across the apical membrane. This transport is coupled to the extrusion of an equal amount of acid across the basolateral membrane, thereby physiological pancreatic interstitium is substantially acidic and epithelial cells are exposed to different extracellular pH ( $\text{pH}_e$ ) values. This process is intermittent in the healthy pancreas and associated with food intake. On the other hand, PDAC has been clearly associated with a hypoxic and acidic microenvironment with a dense desmoplastic stroma [43]. A challenging hypothesis is that, in combination with driver mutations, the alternating, but physiological,  $\text{pH}_e$  landscape in the pancreas and the intrinsic ability of pancreatic epithelial cells to adapt to different pH conditions, may act as a “preconditioning phenomenon” favouring the selection of specific cancer aggressive phenotypes which might promote PDAC arising and/or progression. In other words, once the specific mutations drive the ductal pancreatic cells’ transformation, cells would be already adapted and could even benefit from the adverse pH conditions and the combination of these factors may increase cell fitness to survive and become strongly aggressive in the hostile microenvironment [43].

In this context, it would be important to study the “transportome” alterations that are linked to hypoxia and to  $\text{pH}_e$  or  $\text{pH}_i$  alterations as possible targets for therapies. Indeed, many cancer hallmarks, such as cell proliferation, cell migration, invasion, and apoptosis resistance are driven by altered expression/regulation of ion transport proteins or ion channels, including acid–base transporters and  $\text{O}_2$ - and pH-sensitive channels, in particular,  $\text{Ca}^{2+}$ - and hypoxia- and pH-sensitive ion channels [43,44].

### 1.2. Calcium Signalling

Among different ions present in the intra- and extracellular environments,  $\text{Ca}^{2+}$  ions stand out for their functional importance as second messengers.  $\text{Ca}^{2+}$  ions have been observed to crosstalk with several cell signalling pathways by promoting different spatio-temporal  $\text{Ca}^{2+}$  patterns to selectively regulate innumerable physiological cell processes, ranging from cell differentiation, proliferation, migration, and programmed cell death to gene transcription, among others [45–47]. Its key role in signal transduction translates into the necessity of tight regulation of intracellular  $\text{Ca}^{2+}$  homeostasis, maintaining a low cytosolic free  $\text{Ca}^{2+}$  concentration (100 nM) with respect to the extracellular milieu (>1 mM) through the orchestrated work of several proteins that constitute the so-called  $\text{Ca}^{2+}$  signalling toolkit, including pumps ( $\text{Ca}^{2+}$  ATPases PMCA, SERCA) exchangers ( $\text{Na}^+/\text{Ca}^{2+}$  exchanger NCLX in mitochondria and NCX at the plasma membrane) or uniporters (MCU in mitochondria) and PM and ER  $\text{Ca}^{2+}$ -permeable channels. Calcium signals are modulated in time and space and differences in amplitude, frequency, duration, and location are transduced by cells to activate a specific response.

Thus, considering this multifaced role of  $\text{Ca}^{2+}$  ions, it is no surprise that alterations in  $\text{Ca}^{2+}$  homeostasis and  $\text{Ca}^{2+}$  channels expression and/or activity in cancer progression and vascularisation have been extensively reported by several works [44,48–57], making ion channels major players in cancer development (“Oncochannelopathies”) [58].

$\text{Ca}^{2+}$ -permeable channels represent pivotal molecular devices acting as microenvironmental sensors in the context of tumourigenesis and other diseases, being modulated by microenvironmental physicochemical cues, such as hypoxia and acidic  $\text{pH}_e$ . Thus, it is possible to speculate that acidic and hypoxic TME and  $\text{Ca}^{2+}$  signalling may work in synergy for the acquisition of aggressive cancer cell phenotypes. For this reason, a better understanding of the interplay between these players and the remodelling of  $\text{Ca}^{2+}$  signals induced by tumour acidic  $\text{pH}_e$  and hypoxia and translated to the cancer cells through the activity of  $\text{Ca}^{2+}$ -permeable ion channels and pumps may help to provide further comprehension of the mechanisms of cancer progression and novel putative therapeutic approaches. Indeed, hypoxia is often associated with a rise in intracellular  $\text{Ca}^{2+}$  levels in several types of cancer, via the upregulation of different  $\text{Ca}^{2+}$ -permeable channels and eventually potentiating cancer hallmarks [59,60] (see Section 2). In addition to hypoxia, acidic pH has been reported to regulate  $\text{Ca}^{2+}$ -permeable ion channels in a direct and indirect way, via specific  $\text{H}^+$  binding

sites or via competition with  $\text{Ca}^{2+}$  ions for binding sites as discussed below in Section 2. Data regarding the effects of  $\text{pH}_i$  on these channels is limited in the literature and refers principally to normal cells, whereas more data are available on the regulation of acidic  $\text{pH}_e$ , although different publications demonstrated the high variability of the effects of this microenvironmental parameter among different  $\text{Ca}^{2+}$  channels [44,57,61] (see also detailed discussion in Section 2).

In the next section, we will present an updated view of the recent literature on the role of Piezo channels, transient receptor potential  $\text{Ca}^{2+}$ -permeable ions channels (TRPs) and the so-called store-operated  $\text{Ca}^{2+}$  channels (SOCs) on normal and cancer cells, which activity and signalling transduction are directly affected by two features of the tumour microenvironment: hypoxia and acidosis. We will moreover illustrate the  $\text{Ca}^{2+}$  signalling pathways that may represent potential targets for cancer therapy.

## 2. Hypoxia and Acidic $\text{pH}_e$ -Dependent Regulation of $\text{Ca}^{2+}$ -Permeable Ion Channels in Normal and Cancer Cells

Hypoxia and acidic  $\text{pH}_e$  regulate the expression and/or activity of several  $\text{Ca}^{2+}$ -permeable channels, which are linked to tumour aggressiveness. Throughout the years, several publications have revealed the role of these two major players in the tumour microenvironment, proving a marked sensitivity to oxygen and  $\text{pH}_e$  of most TRPs, SOC and Piezo channels, which affects their functionality in different tissues. A detailed description of the updated literature on both normal and cancer cells will be presented in this section and Tables 1 and 2.

As summarized in Tables 1 and 2, the effects of tumour acidosis and tumour hypoxia vary significantly between the different calcium-permeable channels, and the information in the literature regarding certain channels is sometimes contradictory or limited to normal cells.

**Table 1.**  $\text{Ca}^{2+}$ -permeable ion channels regulation by acidic  $\text{pH}_e$ .

Ion Channel	Cell Type	Methodology	Acidic pH Value and Treatment Time	Effect of Low pH on Channel's Activity/Expression	Effect of Low pH on $\text{Ca}^{2+}$ Signals	Cellular Function	Ref.
Piezo1	Piezo1-transiently transfected HEK293 cells	Patch clamp $\text{Mn}^{2+}$ quenching assay	$\text{pH}_e$ 6.3–6.7, acute treatment	Stabilization of inactivated state, both acidic $\text{pH}_i$ and $\text{pH}_e$ inhibit channel's activity	Decreased $\text{Ca}^{2+}$ influx	Not assessed	[62]
	Murine pancreatic stellate cells (mPSCs)	$\text{Mn}^{2+}$ quenching assay mPSCs spheroids viability and apoptosis assay	$\text{pH}_e$ 6.6 and $\text{pH}_i$ 6.77 (obtained by 30 mM propionate) in acute treatment for $\text{Mn}^{2+}$ quenching assay, while 24 h long treatment for spheroid histology	Acidic $\text{pH}_e$ do not modify Piezo1 activity, while intracellular acidification inhibits channel's activity	Acidic $\text{pH}_e$ do not modify $\text{Ca}^{2+}$ influx, while intracellular acidification decreases $\text{Ca}^{2+}$ influx	Acidic $\text{pH}_e$ (6.6) impairs PSCs spheroid's integrity and viability, inducing cell apoptosis	[63]
TRPM2	Inducible TRPM2-overexpressing HEK293	Patch clamp	External solution with pH 5–8 superfused for 200 s. Internal solution with pH 6 superfused for 100 s; External solution with pH 3.5–6.5 in acute treatment or more prolonged periods ( $\geq 2$ min)	Extracellular acidification inactivates the channel in a voltage-dependent manner and $[\text{H}^+]$ -dependent manner. Intracellular acidification induces channel closure	Not assessed, but recovery from acidic pH-induced inactivation requires external $\text{Ca}^{2+}$ ions	Not assessed	[64]
	Human neutrophils	Patch clamp	External solution with pH 5 in acute treatment	External acidification negatively affects open probability and single-channel conductance, inducing channel closure	Not assessed	Not assessed	[64]
	TRPM2-overexpressing HEK293	Patch clamp	External solution with pH 3.5–6 in acute treatment	External acidification (up to pH 4.5) reversely decreases mean current amplitude in a $[\text{H}^+]$ -dependent manner, decreasing single-channel conductance	Not assessed	Not assessed	[65]
	TRPM2-overexpressing HEK293	Patch clamp	External solution with pH 4.0–6.5. Different time exposition based on protocol (from $<10$ s to $\geq 2$ min)	Acidic $\text{pH}_e$ inactivates open channels in an irreversible manner. Exposition to $\text{pH}_e$ 4–5 negatively affects channel activation.	Not assessed	Not assessed	[66]
	TRPM2-overexpressing HEK293	Patch clamp	External solution with pH 5.5, different exposition times (0, 30, 60, 90, and 120 s)	Irreversible inhibition after $\leq 60$ s exposure	Not assessed	Not assessed	[67]

Table 1. Cont.

Ion Channel	Cell Type	Methodology	Acidic pH Value and Treatment Time	Effect of Low pH on Channel's Activity/Expression	Effect of Low pH on Ca <sup>2+</sup> Signals	Cellular Function	Ref.
TRPM6	Pig isolated ventricular myocytes	Patch clamp	External solution with pH 5.5 and pH 6.5, ~5–10 min exposition	External acidification decreases channel's current amplitude in a pH <sub>e</sub> -dependent and voltage-independent manner. The inhibitory effect of acidic pH <sub>e</sub> is prevented by increasing intracellular pH buffering capacity	Not assessed	Not assessed	[68]
	TRPM6-overexpressing HEK293 cells	Patch clamp	External solution with pH 3–6, ~10 s-long exposition	External acidification increases channel's current amplitude in a pH <sub>e</sub> -dependent manner	Not assessed	Not assessed	[69]
	RBL-2H3 cells	Patch clamp	Acidification of intracellular side of membrane with ~200 s long 4–40 mM acetate treatment	Pre-incubation in 40 mM acetate solution inhibits TRPM7 current in a reversible manner	Not assessed	Not assessed	[70]
	TRPM7-overexpressing Chinese Hamster Ovary (CHO-K1) cells	Patch clamp	Internal and external solution with pH 5.6 and variable exposition (~200–500 s)	Internal and external acidification abolish channels' current	Not assessed	Not assessed	[70]
	TRPM7-overexpressing HEK293 cells	Patch clamp	Internal solution with pH 6.1 and ~10 min exposition	Internal acidification decreases TRPM7 currents' density	Not assessed	Not assessed	[71]
	Mouse hippocampal neurons	Patch clamp	External solution with pH 6.5, 2 min exposition	Extracellular acidification slows down channel's activation in a voltage-independent way	Not assessed	Not assessed	[72]
	TRPM7-overexpressing HEK293T cells	Patch clamp	External solution with pH 4 and pH 6, acute treatment	External acidification increases channel's current amplitude in a pH <sub>e</sub> -dependent manner	Not assessed	Not assessed	[69]
TRPM7	TRPM7-overexpressing HEK293T cells	Patch clamp	External solution with pH 3–7, ~50 s-long exposition	External acidification determines a significant increase in TRPM7 inward current in an [H <sup>+</sup> ] in a concentration-dependent manner	Not assessed	Not assessed	[73]
	Pig isolated ventricular myocytes	Patch clamp	External solution with pH 5.5 and pH 6.5, ~5–10 min exposition	External acidification decreases channel's current amplitude in a pH <sub>e</sub> -dependent and voltage-independent manner. The inhibitory effect of acidic pH <sub>e</sub> is prevented increasing intracellular pH buffering capacity	Not assessed	Not assessed	[68]
	Rat basophilic leukemia cells (RBL)	Patch clamp	External solution with pH 5.5, pH 6 and pH 6.5, ~1-min-long exposition	External acidification decreases channel's current amplitude in a pH <sub>e</sub> -dependent manner	Not assessed	Not assessed	[68]
	HeLa cells	Patch clamp Cell death assays (fluometric analysis of caspase 3/7 activation, electronic sizing of cell volume, and triple staining with Hoechst/acridine orange and propidium iodide assay.	External solution with pH 4 and pH 6, acute treatment for patch clamp experiments, and 1 h-long treatment with acidic pH <sub>e</sub> (4 and 6) for cell death assays	External acidification increases channel's current amplitude in a pH <sub>e</sub> -dependent manner	Not assessed	Acidosis promotes HeLa necrotic cell death	[74]
	Human atrial cardiomyocytes	Patch clamp	External solution with pH 4–6, acute treatment	External acidification increases channel's current amplitude in presence of divalent cations in the extracellular milieu	Not assessed	Not assessed	[75]
TRPV1	TRPV1-expressing HEK293 cells	Patch clamp	Acidic solution with pH 5.5 applied intracellularly for ~50 s	Acid treatment does not activate the channel in inside-out patches but potentiates 2-APB-evoked currents from the cytoplasmic side	Not assessed	Not assessed	[76]



Table 1. Cont.

Ion Channel	Cell Type	Methodology	Acidic pH Value and Treatment Time	Effect of Low pH on Channel's Activity/Expression	Effect of Low pH on Ca <sup>2+</sup> Signals	Cellular Function	Ref.
TRPV1	hTRPV1-transfected HEK293t cells	Calcium imaging	External solution with pH 4.3 and pH 6.1, ~4 min-long exposition	Acidic pH <sub>e</sub> activates TRPV1 channel	pH <sub>e</sub> 6.1 determines larger Ca <sup>2+</sup> transients with respect to pH <sub>e</sub> 4.3 in physiological extracellular Ca <sup>2+</sup> concentration, while, in presence of low extracellular Ca <sup>2+</sup> concentration, cells exposed to pH <sub>e</sub> 6.1 show reduced Ca <sup>2+</sup> entry respect to pH <sub>e</sub> 4.3 exposition	Not assessed	[77]
	Defolliculated <i>Xenopus laevis</i> oocytes, TRPV1-expressing HEK293 cells	Patch clamp	Extracellular solution with pH 6.4, cells pre-treated with acid bath solution for 2 min	Acidic pH <sub>e</sub> potentiates heat-evoked TRPV1 current in oocytes; potentiation of capsaicin and heat-evoked TRPV1 currents in HEK293 cells	Not assessed	Not assessed	[78]
	Primary human adult dermal lymphatic endothelial cell (HDLECs)	Cell viability assay Cell invasion assay in vitro tube formation assay Transwell cell migration assay	24 h long exposition to pH <sub>e</sub> 6.4, and 6 h long exposition for in vitro tube formation assay	Acidic pH <sub>e</sub> activates TRPV1 channel	Not assessed	Acidic pH <sub>e</sub> affects HDLECs morphology, increasing their migration and invasive abilities, proliferation and promoting lymphangiogenesis via acidosis-induced TRPV1 activation	[79]
TRPV2	TRPV2-expressing HEK293 cells	Patch clamp	Acute administration of extracellular solution with pH <sub>e</sub> 5.5 and 6	Extracellular acidosis potentiates the response of TRPV2 to 2-APB (and analogues) from the cytosolic side, while intracellular acidification and low pH <sub>e</sub> alone are not able to elicit any detectable current	Not assessed	Not assessed	[80]
TRPV3	TRPV3-expressing HEK293 cells	Patch clamp, calcium imaging	Acute administration of extracellular solution with pH <sub>e</sub> 5.5 and 6	Extracellular acidosis potentiates the response of TRPV3 to 2-APB (and analogues) from the cytosolic side. Intracellular acidification activates the channel, eliciting small but detectable currents	Extracellular acidosis increases Ca <sup>2+</sup> entry following 2-APB stimulation	Not assessed	[80]
	TRPV3-expressing HEK293 cells	Patch clamp Cell death assay (PI staining assay)	Intracellular administration of acidic solution with pH <sub>e</sub> 5.5 and glycolic acid. Extracellular solution with pH 5.5. Intracellular solution with pH 5.5–7.	Glycolic acid-induced intracellular proton release in presence of acidic solution activates the channel in a reversible way. Extracellular acidification does not activate TRPV3, while intracellular acidification alone activates the channel in a pH-dependent manner	Not assessed	Glycolic acid-induced acidification induces cell toxicity and cell death	[81]
	Human keratinocytes cells (HaCaT)	Patch clamp, cell death assay (PI staining assay)	Intracellular administration of acidic solution with pH <sub>e</sub> 5.5 and glycolic acid	Glycolic acid-induced intracellular proton release in presence of acidic solution potentiates the channel's response to 2-APB in a reversible manner	Not assessed	Glycolic acid-induced acidification induces cell toxicity and cell death	[81]
TRPV4	Chinese hamster ovary cells	Patch clamp	External solution with pH <sub>e</sub> 4, 5.5 and 6, acute treatment	Extracellular acidosis activates the channel in a pH <sub>e</sub> -dependent manner	Not assessed	Not assessed	[82]
	mTRPV4-overexpressing primary cultured mouse esophageal epithelial cells	Ca <sup>2+</sup> imaging	External solution with pH <sub>e</sub> 5, acute treatment	Not assessed	Extracellular acidic pH decreases Ca <sup>2+</sup> entry, lowering cytosolic Ca <sup>2+</sup> concentration	Not assessed	[83]
TRPV6	Jurkat cells	Patch clamp	External solution with pH 6, acute treatment	Extracellular acidosis suppresses TRPV6-mediated currents	Extracellular acidic pH reduces Ca <sup>2+</sup> entry, lowering cytosolic Ca <sup>2+</sup> concentration	Not assessed	[84]

Table 1. Cont.

Ion Channel	Cell Type	Methodology	Acidic pH Value and Treatment Time	Effect of Low pH on Channel's Activity/Expression	Effect of Low pH on Ca <sup>2+</sup> Signals	Cellular Function	Ref.
TRPA1	HEK-293t cells expressing hTRPA1, mTRPA1, or rTRPA1	Patch clamp Calcium imaging	Acidic solutions with pH 7.0, 6.4, 6.0, and 5.4, 30 s-long treatment in calcium imaging experiments	Extracellular acidosis activates inward currents via hTRPA1 and potentiates acrolein-evoked currents of hTRPA1 in a pH <sub>e</sub> -dependent and reversible manner, while failing to activate mouse and rodent TRPA1.	Extracellular acidosis increases Ca <sup>2+</sup> entry in hTRPA1, no effect on mTRPA1 and rTRPA1.	Not assessed	[85]
	DRG neurons derived from TRPV1/TRPA1-/- mice and overexpression hTRPA1	Calcium imaging	Acidic solutions with pH 5, 60 s-long treatment	Not assessed	Acidic pH <sub>e</sub> induces Ca <sup>2+</sup> entry	Not assessed	[85]
	Neuroblastoma ND7/23 cells expressing hTRPA1	Patch clamp	Acidic solution with pH 5, acute treatment	Acidic pH <sub>e</sub> activates hTRPA1	Not assessed	Not assessed	[85]
TRPC5	TRPC5-transiently transfected HEK293 cells	Patch Clamp	External acidic solution with pH 4.2, 5.5, 6.5, 7, ~100 s-long treatment	G protein-activated and spontaneous currents are potentiated by extracellular acidic pH by increasing the channel open probability, with a maximum effect at ~pH 6.5, while more acidic values inhibit the channel	Not assessed	Not assessed	[86]
TRPC4	TRPC4-transiently transfected HEK293 cells	Patch Clamp	External acidic solution with pH 4.2, 5.5, 6.5, 7, ~100 s-long treatment	G protein-activated currents are potentiated by extracellular acidic pH, with a maximum effect at ~pH 6.5 and complete inhibition at pH <sub>e</sub> 5.5	Not assessed	Not assessed	[86]
	mTRPC4-stably transfected HEK293 cells	Patch Clamp	External acidic solution with pH 6.8	Low pH <sub>i</sub> (6.75–6.25) accelerates G <sub>i/o</sub> -mediated TRPC4 activation, and this requires elevations in intracellular calcium concentration. Intracellular protons inhibit Englerin A-mediated TRPC4 activation	Not assessed	Not assessed	[87]
TRPC6	TRPC6-transiently transfected HEK293 cells	Patch Clamp	External acidic solution with pH 4.2, 5.5, 6.5, 7, ~100 s-long treatment	Acidic pH <sub>e</sub> inhibits channel's inward and outward currents starting from pH <sub>e</sub> 6.5 and the inhibition is potentiated by more acidic pH <sub>e</sub> values.	Not assessed	Not assessed	[86]
ORAI1/STIM1	Human macrophages	Patch clamp	External acidic solution with pH 6 and 8, ~200 s-long treatment	Extracellular acidosis inhibits ORAI1 channel in a pH <sub>e</sub> -dependent and reversible manner	Not assessed	Not assessed	[88]
	H4IIE rat liver cells overexpressing ORAI1 and STIM1	Patch clamp	External acidic solutions with pH 5.1 and 5.9	ORAI1 and STIM1-mediated I <sub>CRAC</sub> are inhibited by acidic pH <sub>e</sub> , with maximal effect at pH <sub>e</sub> 5.5	Not assessed	Not assessed	[89]
	RBL2H3 mast cell line, Jurkat T lymphocytes and heterologous ORAI1-2-3/STIM expressing HEK293 cells	Patch clamp	External and intracellular acidic solutions with pH 6 and 6.6	External and internal acidification inhibits IP3-induced I <sub>CRAC</sub> in RBL2H3 mast cell line, Jurkat T lymphocytes, and in heterologous ORAI/STIM-mediated I <sub>CRAC</sub> in HEK293 cells in a reversible manner	Not assessed	Not assessed	[90]
	ORAI1/STIM1-transiently transfected HEK293 cells	Patch Clamp	External acidic solution with pH 5.5	Acidic pH <sub>e</sub> inhibits ORAI1-2-3/STIM1 current amplitude in a reversible and pH-dependent manner, with a maximal effect at pH <sub>e</sub> 4.5	Not assessed	Not assessed	[91]
	ORAI1/STIM1-transiently transfected HEK293 cells	Patch Clamp	Intracellular acidic solution with pH 6.3	Intracellular acidosis inhibits ORAI1/STIM1 current, regulating the amplitude of the current and the Ca <sup>2+</sup> -dependent gating of the CRAC channels	Not assessed	Not assessed	[92]
	SH-SY5Y human neuroblastoma cells	Ca <sup>2+</sup> signals quantification by Mn <sup>2+</sup> quench technique	External acidic solution with pH 6.8 and 7 and 7.2. Different treatment time, ranging from ~3–4 min to ~8 min for carbachol-mediated Ca <sup>2+</sup> entry and ~7 min for thapsigargin-mediated Ca <sup>2+</sup> entry	Not assessed	Tumour acidic pH <sub>e</sub> inhibits carbachol- and thapsigargin-mediated Ca <sup>2+</sup> entry in a reversible manner, while intracellular acidification or alkalinization leads to no effects in carbachol-mediated Ca <sup>2+</sup> entry	Not assessed	[93]

Table 2. Ca<sup>2+</sup>-permeable ion channels regulation by hypoxia.

Ion Channel	Cell Type	Methodology	Hypoxia Technique and Treatment Time	Effect of Hypoxia on Channel's Activity/Expression	Effect of Hypoxia on Ca <sup>2+</sup> Signals	Cellular Function	Ref.
Piezo1	Mouse and human sickle red blood cells (RBCs)	Cell-attached and nystatin-permeabilized patch clamp Calcium imaging	Deoxygenation obtained by exposure with a superfusate gassed 30 min prior to the experiment with 100% N <sub>2</sub>	Deoxygenation activates a Ca <sup>2+</sup> - and cation-permeable conductance in a reversible manner, and this current is sensitive to inhibition by GsMTx-4; 1 mM	Increased Ca <sup>2+</sup> influx	Not assessed	[94]
	Pulmonary arterial endothelial cells (PASMCS) of patients with pulmonary arterial hypertension (PAH)	Calcium imaging EdU and cell counting proliferation assay Western Blot	/	Piezo1 expression and activity are increased in idiopathic pulmonary arterial hypertension and pulmonary arterial smooth muscle cells	Increased Ca <sup>2+</sup> influx and increased intracellular Ca <sup>2+</sup> release	Increased PAH-PASMCS' proliferation	[95]
	Pulmonary artery smooth muscle cells of mice and rats' models with experimental chronic hypoxia-induced pulmonary hypertension (PH) Human pulmonary artery endothelial cells (hPAECs)	Western Blot Calcium imaging	Hypoxia induced by incubation in 3% O <sub>2</sub> for 4 h–12 h or in 10% O <sub>2</sub> for a total of 6 weeks	Piezo1 is significantly upregulated in the lung tissue of PH rats and in chronic hypoxia-induced PH models. Piezo1 protein is transiently upregulated also in hPAECs after 6 h exposition to hypoxic conditions. Hypo-osmotic conditions upregulate Piezo1 protein levels in hPAECs	Hypo-osmotic upregulation of Piezo1 promotes Ca <sup>2+</sup> influx, promoting Akt and Erk signalling pathways activation, with downstream upregulation of Notch ligand	GsMTx4-mediated Piezo1 blockade partially reduces the chronic hypoxia-induced PH in mice with chronic hypoxia-induced pulmonary hypertension	[96]
TRPM2	TRPM2 WT and knockout (KO) neonatal hypoxic-ischemic (HI) brain injury mouse model	Western Blot	Hypoxia damage was induced in ischemic mice models by incubating the pups in a hypoxic chamber for 2 h	TRPM2 is acutely overexpressed 24 h after hypoxia-ischemic injury in brain tissue samples from mouse pups	Not assessed	Brain damage and inflammation are reduced in TRPM2 KO mice 7 days following hypoxic-ischemic brain injury. TRPM2 inhibits cell survival pathways after HI injury	[97]
	Primary cultures of rat cortical neurons subjected to oxidative stress	Calcium imaging Trypan Blue exclusion assay	Oxidative stress induced by 1 mM or 50 μM H <sub>2</sub> O <sub>2</sub> treatment	Not assessed	H <sub>2</sub> O <sub>2</sub> induces TRPM2-mediated intracellular calcium rise	SiTRPM2 prevents H <sub>2</sub> O <sub>2</sub> -mediated neuronal cell death	[98]
	TRPM2-overexpressing HEK293 cells	Whole-cell Patch Clamp	Hypoxia induced by cell incubation with gas mixture containing 5% O <sub>2</sub> for 30 and 60 min	TRPM2 activation is induced by 30- and 60-min exposure to hypoxic conditions	Not assessed	Hypoxia treatment enhances cell death, probably via TRPM2-mediated Ca <sup>2+</sup> influx	[99]
	ARPE-19 retinal pigment epithelial cells	Patch Clamp Calcium imaging Propidium iodide cell death assay	Hypoxia induced by CoCl <sub>2</sub> (200 μM) for 24 h	Hypoxia induces activation of TRPM2 currents and upregulates TRPM2 protein levels	Hypoxia induces TRPM2-mediated intracellular calcium rise	Hypoxia causes mitochondrial oxidative cell cytotoxicity and cell death via TRPM2-mediated Ca <sup>2+</sup> signals	[100]
	Primary IGR39 melanoma cells TRPM2-overexpressing HEK293 cells	Patch Clamp Calcium imaging	Treatment with chloramine-T (Chl-T) oxidant agent	Amount of 0.5 mM Chl-T activates TRPM2 in IGR39 and in TRPM2-expressing HEK293 cells	Chl-T treatments induce a significant increase in cytosolic Ca <sup>2+</sup> levels	Chl-T-induced TRPM2 activation and increased Ca <sup>2+</sup> influx activate BK and K <sub>Ca</sub> 3.1 potassium channels	[101]
	PC3 prostate cancer cells	Calcium imaging MTT and TUNEL assay	Treatment with 0.5 to 4 mM H <sub>2</sub> O <sub>2</sub> for 6 h	H <sub>2</sub> O <sub>2</sub> induces TRPM2 activation	H <sub>2</sub> O <sub>2</sub> treatment leads to TRPM2-mediated intracellular Ca <sup>2+</sup> increase in a concentration-dependent manner	H <sub>2</sub> O <sub>2</sub> induces TRPM2-Ca <sup>2+</sup> -CaMKII cascade that promotes ROS production, mitochondrial fragmentation, and inhibition of autophagy, inducing cell death	[102]



Table 2. Cont.

Ion Channel	Cell Type	Methodology	Hypoxia Technique and Treatment Time	Effect of Hypoxia on Channel's Activity/Expression	Effect of Hypoxia on Ca <sup>2+</sup> Signals	Cellular Function	Ref.
TRPM2	TRPM2-L and TRPM2-S-expressing SH-SY5Y neuroblastoma cells	Calcium imaging	Treatment with 250 $\mu$ M H <sub>2</sub> O <sub>2</sub> for 20 min	Not assessed	H <sub>2</sub> O <sub>2</sub> treatment leads to TRPM2-L-mediated intracellular Ca <sup>2+</sup> increase and a decrease in TRPM2-S	TRPM2-L-expressing cells show higher HIF-1/2 $\alpha$ levels with respect to TRPM2 short isoform and promote tumour growth in vivo	[103]
	Human breast cancer cells	Calcium imaging qPCR	Co-culture with neutrophils or H <sub>2</sub> O <sub>2</sub> treatment	Neutrophil-derived H <sub>2</sub> O <sub>2</sub> induces decrease in TRPM2 expression in H <sub>2</sub> O <sub>2</sub> -selected tumour cells	Not assessed	TRPM2 activation by neutrophil-derived H <sub>2</sub> O <sub>2</sub> and following Ca <sup>2+</sup> entry promotes cancer cells' death	[104]
TRPM6	Hepatic ischemia-reperfusion rat model	qPCR	Ischemia was obtained by 60 min clamping the left hepatic artery and the portal vein	TRPM6 expression is increased in liver tissue from ischemia-reperfusion rat model	Not assessed	Not assessed	[105]
TRPM7	TRPM7-overexpressing HEK293T cells Cortical neurons	Ca <sup>2+</sup> imaging Patch clamp PI cell death assay	Hypoxia induced by anaerobic chamber containing <0.2% O <sub>2</sub> atmosphere for 1, 1.5 and 2 h.	Hypoxia induces TRPM7 channel activation	Hypoxia increases Ca <sub>2+</sub> entry	Hypoxia-activated TRPM7 mediated-Ca <sup>2+</sup> entry determines cell death in cortical neurons	[106]
	Hepatic ischemia-reperfusion rat model	qPCR	Ischemia was obtained by 60 min clamping the left hepatic artery and the portal vein	TRPM7 expression is increased in liver tissue from ischemia-reperfusion rat model	Not assessed	Not assessed	[105]
TRPV1	HEK293T cells overexpressing rat TRPV1	Patch Clamp Calcium imaging	Hypoxic solution obtained by bubbling with 100% N <sub>2</sub> gas for at least 20 min before the perfusion (PO <sub>2</sub> , 3%)	Acute hypoxia weakly increases TRPV1 activity, but negatively affects capsaicin induced TRPV1 currents	Hypoxia leads to a slight increase in cytosolic Ca <sup>2+</sup> levels	Not assessed	[107]
	Rat DRG neurons hTRPV1/rTRPV1-expressing HEK293 cells	Whole-cell patch-clamp	Overnight (18–20 h) exposition to hypoxia (4% O <sub>2</sub> )	Overnight exposure to hypoxic/high glucose conditions increases TRPV1 mean peak current densities in both cell lines, without affecting its expression	Not assessed	Not assessed	[108]
	Rat pulmonary artery smooth muscle cells (PASMCs)	Calcium imaging qPCR Western Blot Wound Healing assay BrdU proliferation assay	24–48 h long exposition to hypoxia (1% and 10% O <sub>2</sub> )	Hypoxic conditions do not affect TRPV1 expression, but they increase TRPV1 activity	No assessed	Hypoxia-mediated TRPV1 activation enhances PASMCs migratory abilities and proliferation	[109]
	Human pulmonary artery smooth muscle cells (PASMCs)	Calcium imaging qPCR Western Blot Cell count proliferation assay	72 h long exposition to hypoxia (3% O <sub>2</sub> )	Chronic hypoxia upregulates both TRPV1 gene and protein levels	Chronic hypoxia increases cytosolic Ca <sup>2+</sup> levels	The proliferation of PASMCs is increased under hypoxia	[110]
	HepG2 and Huh-7 human hepatoma cell lines	RT-PCR Western Blot Flow cytometry	50, 100, 200, and 400 Mm H <sub>2</sub> O <sub>2</sub> treatment for 24 h	H <sub>2</sub> O <sub>2</sub> upregulates the expression of TRPV2 at mRNA and protein levels	Not assessed	Overexpression of TRPV2 promotes H <sub>2</sub> O <sub>2</sub> -induced cell death	[111]
TRPV3	Rat myocardial cells	MTT and Edu staining assay Western Blot Caspase-3 and LDH activity assay	12 h long exposition to hypoxia (1% O <sub>2</sub> )	TRPV3 is overexpressed in myocardial cells induced by ischemia/hypoxia	Not assessed	TRPV3 silencing protects cardiomyocytes from hypoxia-induced cell death and decreases the secretion of proinflammatory cytokines	[112]
	Primary rat pulmonary artery smooth muscle cells (PASMCs)	Western Blot Flow cytometry MTT assay	24 h long exposition to hypoxia (3% O <sub>2</sub> )	TRPV3 protein expression is enhanced in PASMCs from hypoxic rats	Not assessed	TRPV3 mediates hypoxia-induced PASMCs' proliferation via PI3K/AKT signalling	[113]

Table 2. Cont.

Ion Channel	Cell Type	Methodology	Hypoxia Technique and Treatment Time	Effect of Hypoxia on Channel's Activity/Expression	Effect of Hypoxia on Ca <sup>2+</sup> Signals	Cellular Function	Ref.
TRPV3	TRPV3-overexpressing HEK293	Patch Clamp	12 h long exposition to hypoxia (1% O <sub>2</sub> )	Pre-incubation in hypoxic conditions potentiates TRPV3 currents in response to 2-APB treatment	Not assessed	Not assessed	[114]
TRPV4	Rat cardiomyocytes	Western Blot qPCR Calcium imaging	6 h long exposition to hypoxia (95% N <sub>2</sub> ) in a controlled hypoxic chamber	TRPV4 gene and protein expression levels are increased after 6 h exposure to hypoxia	Hypoxia increases TRPV4-mediated Ca <sub>2+</sub> influx responses to 300 nM GSK	Hypoxia-mediated activation of TRPV <sub>4</sub> induces cytosolic Ca <sup>2+</sup> overload in cardiomyocytes, leading to ROS production and oxidative injury in vitro and in vivo	[115]
	Adult rat hippocampal astrocytes	Patch Clamp qPCR Western Blot Calcium imaging	Hypoxia/ischemia (H/I) is induced by occlusion of the common carotids in combination with hypoxic conditions (from 1 h up to 7 days, 6% O <sub>2</sub> )	TRPV4 mRNA and protein expression are significantly increased 1 h after H/I. H/I also activates TRPV4 channel	H/I enhances the response of 4aPDD, inducing TRPV4-mediated Ca <sup>2+</sup> oscillations	Not assessed	[116]
TRPA1	Several breast and lung cancer cell lines	Calcium imaging Cell viability and apoptosis assay via PI and Annexin IV staining	Treatment with 10 μM H <sub>2</sub> O <sub>2</sub> for 15 min for calcium measurements, 1, 20, and 100 μM for 72–96 h-long exposition for cell viability and cell death assays	H <sub>2</sub> O <sub>2</sub> treatment activates TRPA1 channel	H <sub>2</sub> O <sub>2</sub> treatment increases TRPA1-mediated calcium entry	TRPA1-mediated calcium entry promotes cell survival by upregulating anti-apoptotic pathways and promoting oxidative stress resistance	[117]
	Oligodendrocytes	Calcium imaging	Ischemia inducing solution	Not assessed	Ischemia-induced intracellular acidosis promotes Ca <sup>2+</sup> entry via TRPA1	Ischemia-induced intracellular acidosis and consequent Ca <sup>2+</sup> entry via TRPA1 mediate myelin damage	[118]
TRPC1	U-87 MG glioma cells	qPCR, western blot	Hypoxia induced by exposition to 1% O <sub>2</sub>	Not assessed	Not assessed	TRPC1 participates in hypoxia-induced VEGF gene and protein expression	[119]
	MDA-MB-468 breast cancer cells	qPCR, calcium imaging	Hypoxia induced by exposition to 1% O <sub>2</sub> for 24 h	Hypoxia upregulates TRPC1 via HIF1α	siTRPC1 reduces non-stimulated Ca <sup>2+</sup> entry and increases Store-Operated Ca <sup>2+</sup> entry in hypoxic conditions	TRPC1 overexpression promotes Snail EMT marker upregulation and decrease in claudin-4 epithelial marker in hypoxic conditions. TRPC1 regulates HIF-1α protein levels via Akt-dependent pathway and promotes hypoxia-induced STAT3 and EGFR phosphorylation. TRPC1 also regulates hypoxia-induced LC3BII levels via effects on EGFR.	[120]
TRPC5	MCF-7/WT and adriamycin-treated (MCF-7/ADM) human breast cancer cells	Western Blot, immunofluorescence,	Not assessed	Not assessed	Not assessed	TRPC5 promotes HIF-1α translocation to the nucleus and HIF-1α-mediated VEGF expression, boosting tumour angiogenesis	[121]

Table 2. Cont.

Ion Channel	Cell Type	Methodology	Hypoxia Technique and Treatment Time	Effect of Hypoxia on Channel's Activity/Expression	Effect of Hypoxia on Ca <sup>2+</sup> Signals	Cellular Function	Ref.
TRPC5	SW620 colon cancer cells	Western blot, transwell invasion, and migration assay, MTT proliferation assay	Not assessed	Not assessed	Not assessed	TRPC5 activates HIF-1alpha-Twist signalling to induce EMT, supporting colon cancer cells' migration, invasion, and proliferation	[122]
TRPC6	Murine pancreatic stellate cells (mPSCs)	Time-lapse single-cell random migration assay Bead-based cytokine assay qPCR Western Blot Ca <sup>2+</sup> signals quantification by Mn <sup>2+</sup> quench technique	24 h incubation in hypoxic conditions (1% O <sub>2</sub> , 5%CO <sub>2</sub> , and 94% N <sub>2</sub> ) or chemically induced hypoxia by pretreatment with 0.5 mmol/l DMOG	Hypoxic conditions enhance TRPC6 expression and activate the channel	Hypoxia stimulates Ca <sup>2+</sup> influx mediated by TRPC6 channels	Hypoxia-induced TRPC6 activation enhances mPSCs migration via secretion of pro-migratory factors	[123]
	Ix-2 human hepatic stellate cells (HSCs)	Calcium imaging qPCR Western Blot	Hypoxia induced by 100 µmol/L CoCl <sub>2</sub> treatment	Hypoxic conditions enhance TRPC6 expression and activate the channel	Hypoxia stimulates Ca <sup>2+</sup> influx mediated by TRPC6 channels	Hypoxia-induced TRPC6 activation and consequent calcium entry promote the synthesis of ECM proteins, which facilitate the fibrotic activation of HSCs	[124]
	Huh7 and HepG2 hepatocellular carcinoma cells (HCCs)	Confocal Calcium imaging Western Blot	Hypoxia induced by cell incubation in a low oxygen atmosphere with 1% O <sub>2</sub> , 5%CO <sub>2</sub> , and 94% N <sub>2</sub> for 6 h	Hypoxic conditions activate the channel	Hypoxia promotes calcium influx	Hypoxia-induced TRPC6-mediated calcium entry promotes HCCs drug resistance via STAT3 pathway	[125]
	U373MG and HMEC-1 glioblastoma cell lines	qPCR Western Blot Calcium imaging Proliferation assay Matrigel invasion assay Endothelial cell tube formation assay	Hypoxia induced by 100 µmol/L CoCl <sub>2</sub> treatment	Hypoxia enhances TRPC6 expression via Notch pathway	Hypoxia stimulates Ca <sup>2+</sup> influx mediated by TRPC6 channels	Hypoxia-induced TRPC6-mediated calcium entry promotes HCCs proliferation, colony formation, and invasion via NFAT pathway	[126]
ORAI1/STIM1	Primary Aortic Smooth Muscle Cells and HEK293 cells transfected with ORAI1 and STIM1	Patch Clamp Calcium imaging	Hypoxia was induced with 3 methods: (1) sodium dithionite (Na <sub>2</sub> S <sub>2</sub> O <sub>4</sub> ) treatment to 1 mM final concentration, pH adjustment to pH 7.4, and bubbling with 100% N <sub>2</sub> . (2) cell culture media with 30 min-long bubbling with 100% N <sub>2</sub> . (3) cell culture media with 30 min-long bubbling with 3% O <sub>2</sub>	Intracellular acidification induced by hypoxia in HEK293 cells leads to inhibition of SOCE by disrupting the electrostatic ORAI1/STIM1 binding and closing ORAI1 channel.	Hypoxia-induced intracellular acidification reduces SOCE in Primary Aortic Smooth Muscle Cells and HEK293 cells transfected with ORAI1 and STIM1	Not assessed	[92]
	A549 non-small cell lung cancer cells	Western Blot qPCR BrdU cell proliferation assay Calcium imaging Scrape-wound migration assay Matrigel transwell invasion assay	Hypoxia induced by Nicotine treatment for 48 h	Nicotine treatment-induced hypoxia determines ORAI1 overexpression at gene and protein levels	Nicotine treatment-induced hypoxia increases intracellular basal calcium levels and SOCE	Nicotine treatment-induced hypoxia increases A549 cells' proliferation and migration	[127]
	MDA-MB 231 and BT549 breast cancer cell lines and Human Microvascular Endothelial Cell line-1 (HMEC-1)	Western Blot qPCR Calcium imaging Migration assay (Wound healing and transwell migration assay) Matrigel transwell invasion assay Tube formation assay in vitro	Hypoxia induced by cell incubation in low oxygen atmosphere	Hypoxia promotes ORAI1 gene and protein upregulation via activation of Notch1 signalling	Hypoxia increases thapsigargin-induced SOCE, with consequent rise in cytosolic calcium entry	Hypoxia-induced ORAI1 overexpression and consequent increase in SOCE promote NFAT4 activation and enhance neuroblastoma cells' migration, invasion, and angiogenesis	[128]

Table 2. Cont.

Ion Channel	Cell Type	Methodology	Hypoxia Technique and Treatment Time	Effect of Hypoxia on Channel's Activity/Expression	Effect of Hypoxia on Ca <sup>2+</sup> Signals	Cellular Function	Ref.
ORAI1/STIM1	HCT-116 and SW480 human colon cancer cells and Human Microvascular Endothelial Cell line-1 (HMEC-1)	Western Blot qPCR Calcium imaging Transwell migration assay Matrigel transwell invasion assay Tube formation assay in vitro Cell attachment and detachment assays	Hypoxia induced by 100 µmol/L CoCl <sub>2</sub> treatment	Hypoxia promotes ORAI1 gene and protein upregulation via activation of Notch1 signalling	Hypoxia increases thapsigargin-induced SOCE	Hypoxia-induced ORAI1 overexpression and consequent increase in SOCE promote NFATc3 activation and enhance neuroblastoma cells' migration, invasion, and angiogenesis	[129]

### 2.1. Piezo Channels

Piezo proteins are mechanically activated non-selective cations channels identified over a decade ago by Patapoutian's group [130], a discovery that paved the way for various works that further clarified the role of these channels not only in the transduction of mechanical signals, but also in other physiological processes, and culminating in the 2021 Nobel Prize in Physiology or Medicine for David Julius and Ardem Patapoutian "for their discoveries of receptors for temperature and touch". Piezo channels play a key role in mechanotransduction, directly responding and integrating mechanical stimuli and forces from the cell environment into biological signals, leading to the activation of  $\text{Ca}^{2+}$ -dependent processes or cell depolarization in different organs [131]. Piezo channels are also involved in other physiological processes, exhaustively reviewed in [131].

The role of Piezo channels in cancer has been deepened in recent years, with several studies evidencing their importance in different types of cancer that originate from tissues subjected to mechanical stress [132]. Piezo1 and/or Piezo2 are overexpressed in several cancers of epithelial origin, where these channels act as oncogenes, enhancing carcinogenesis through different  $\text{Ca}^{2+}$ -dependent signalling pathways [133–137].

In addition to being sensitive to mechanical stimulation, Piezo1 is also regulated by protons. The work of Bae C. and colleagues in 2015 demonstrated that conditions of acidosis ( $\text{pH}_e$  6.3) inhibit Piezo1 by stabilizing its inactivated state [62]. A drop in extracellular pH and inactivation of Piezo1 might represent a protective mechanism in specific cell types, especially considering that low extracellular pH can promote intracellular acidification and, therefore, the activation of specific signalling pathways that result in cell death [138] (Table 1). This notion is supported by the study of Kuntze A. et al. of 2020, which demonstrated that extracellular acidosis-induced low intracellular pH ( $\text{pH}_i$  6.7) of pancreatic stellate cells (PSCs) inhibited the activity of Piezo1, reducing the  $\text{Ca}^{2+}$  influx in PSCs (Figure 1 and Table 1). In these conditions, Piezo1 activation with Yoda1 led to a loss of PSCs spheroid integrity and increased fragmentation, resulting virtually from  $\text{Ca}^{2+}$  overload and its induction of cell death. Therefore, extracellular acidosis-mediated intracellular pH drop and inactivation of Piezo1 might represent a protective mechanism for PSCs, in which  $\text{Ca}^{2+}$  fluxes are decreased and apoptosis is avoided [63].

Information about Piezo channels' regulation by low oxygen pressures is absent in cancer and the literature data are limited to a few works in red blood cells and pulmonary endothelial and smooth muscle cells, where the pathogenic role of Piezo1 was explored.

Stretch-activated cation channel expression, like Piezo1, has been reported in red blood cells (RBCs), where Piezo1 is expressed and localises at the cell membrane, where it regulates RBCs volume. This role assumes major relevance in pathological conditions, such as Sickle cell disease (SCD), where RBCs showed decreased deformability and higher intracellular  $\text{Ca}^{2+}$  levels with respect to normal red blood cells [139]. In sickle RBCs, low oxygen concentration led to the activation of transmembrane mechanosensitive ion channels. This activation originated a non-selective ion current named  $P_{\text{sickle}}$ , which activated the calcium-activated potassium channel  $\text{K}_{\text{Ca}3.1}$ , which initiates the dehydration cascade in sickle RBCs, responsible for potentiating haemoglobin aggregation [140]. Therefore,  $\text{Ca}^{2+}$  entry in sickle RBCs is necessary for their sickling, which is mediated by the opening of plasma membrane  $\text{Ca}^{2+}$ -permeable and mechanosensitive ion channels. In this context, Piezo1 can be suggested as a mediator of the non-selective ion current, as deoxygenation-induced  $P_{\text{sickle}}$  is abolished by GsMTx4, the tarantula spider toxin which is an inhibitor of mechanosensitive ion channels, including Piezo1 [94].

Recent works have shown that Piezo1 is upregulated in pulmonary arterial endothelial cells of patients with pulmonary arterial hypertension (PAH) and in pulmonary artery smooth muscle cells of mice and rats models with experimental chronic hypoxia-induced pulmonary hypertension (PH) [95,96]. Human pulmonary arterial endothelial cells showed maximal Piezo1 expression at 6 h hypoxic exposure, with a consequent increase in calpain-1 and calpain-2, both involved in PAH development [96]. Moreover, hypo-osmotic conditions upregulated Piezo1 protein levels in the same cells and promoted the activation of Akt

and Erk signalling pathways via Piezo1-induced  $\text{Ca}^{2+}$  entry, as demonstrated by siPiezo1 treatment, with downstream upregulation of Notch ligands [96]. The potential therapeutic effect of Piezo1 blockade in the mouse model with chronic hypoxia-induced PH was assessed by GsMTx4 treatment, which partially reduced the chronic hypoxia-induced PH [96]. These data support the role of Piezo1 in the remodelling of the pulmonary vasculature in PH.

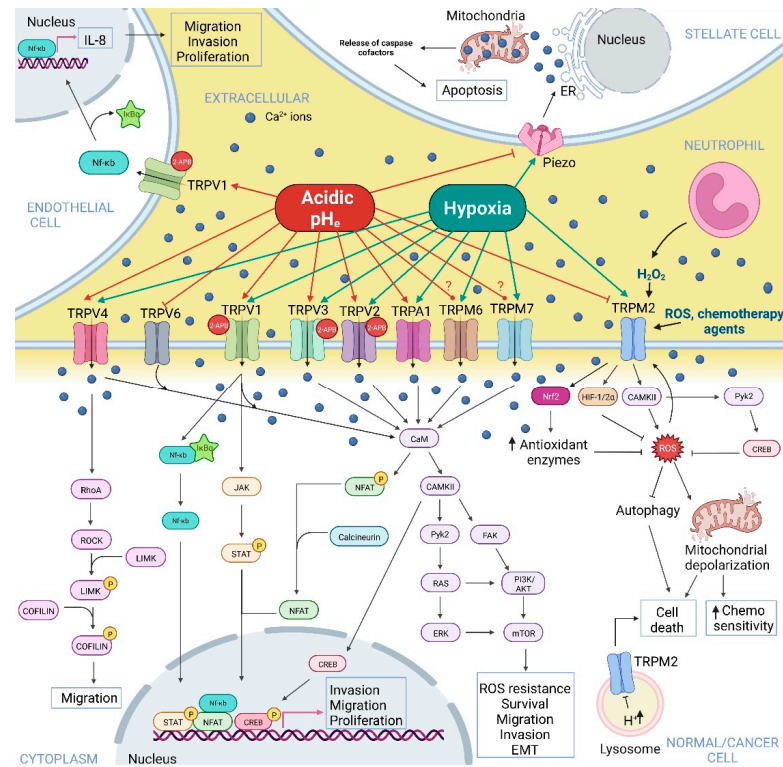


**Figure 1.** Overview of the effects of acidic  $\text{pH}_e$  and hypoxia on TRP and Piezo  $\text{Ca}^{2+}$ -permeable channels. The positive or negative effects of hypoxia and acidic  $\text{pH}_e$  on the  $\text{Ca}^{2+}$ -permeable channels were obtained from both normal and cancer cells-related studies, while the signalling pathways indicated were obtained uniquely from cancer cells-based investigations. The figure depicts Piezo-, TRPV-, TRPA1- and TRPM-mediated  $\text{Ca}^{2+}$ -dependent signalling pathways activated or inhibited by acidic  $\text{pH}_e$  and hypoxia and linked to tumour progression. TRPV (TRPV1–4, 6), TRPA1, and TRPM (TRPM6, 7) expressed in cell cancer’s plasma membrane are differentially regulated by acidic  $\text{pH}_e$ , being mostly activated by tumour acidosis, and transducing its signals to activate  $\text{Ca}^{2+}$ -dependent downstream effectors, such as NF- $\kappa$ B, JAK/STAT, PI3K/AKT, NFAT, ERK, and LIMK. TRPA1 is also activated by hypoxia. These effectors promote tumour cell migration, invasion, proliferation, survival, mesenchymal phenotype, and chemoresistance. TRPV6 channels’ activity is inhibited by tumour acidosis, as TRPM2, which inhibition avoids induction of cancer cell death and reduces chemosensitivity. Piezo channels embedded in stellate cells’ plasma membrane are inhibited by acidic  $\text{pH}_e$ , promoting stellate cells’ survival. TRPV1 activation in lymphatic endothelial cells promotes activation of NF- $\kappa$ B and upregulation of IL-8, a lymphangiogenic factor. CaM, calmodulin; CAMKII,  $\text{Ca}^{2+}$ /calmodulin-dependent protein kinase II; Pyk2, protein tyrosine kinase 2; RAS, Rat sarcoma virus; ERK, extracellular signal-regulated kinase; FAK, Focal Adhesion Kinase; PI3K, phosphoinositide 3-kinase; AKT, protein kinase B; mTOR, mammalian target of rapamycin; NF- $\kappa$ B, nuclear factor- $\kappa$ B; JAK, Janus kinases; STAT, signal transducer and activator of transcription; NFAT, nuclear factor of activated T-cells; RhoA, Ras homolog family member A; ROCK, Rho-associated protein kinase; LIMK, LIM domain kinase; CREB, C-AMP response element-binding protein. The question mark indicates contradictory results in the literature. Created with [BioRender.com](https://www.biorender.com), accessed on 20 June 2022.



## 2.2. Transient Receptor Potential Channels

Transient receptor potential (TRP) ion channels are a family of 28 different proteins in humans, mostly permeable to  $\text{Ca}^{2+}$  ions, characterized by a polymodal activation, and whose altered expression and/or functionality have been linked to several cancer types [54]. Several TRP channels are sensitive to changes in intra- and extracellular pH and to hypoxia (see Tables 1 and 2), altering  $\text{Ca}^{2+}$  downstream signalling pathways as described in the following paragraphs.

### 2.2.1. TRP Melastatin Subfamily

**TRPM2** is a non-selective cation channel localized at the plasma membrane and/or in lysosome compartments and permeable to  $\text{Ca}^{2+}$ ,  $\text{Mg}^{2+}$ , and monovalent cations. TRPM2 is activated by ADP-ribose (ADPR) and by intracellular  $\text{Ca}^{2+}$  increase associated with oxidative stress and reactive oxygen species (ROS) production [141–144].

TRPM2's activity is regulated by both intra- and extracellular pH. The work of Starkus and colleagues demonstrated that extracellular acidic pH ( $\text{IC}_{50}$  pH = 6.5) inhibited both inward and outward TRPM2 currents in TRPM2-overexpressing HEK293 cells in a voltage-dependent manner, by affecting the single-channel conductance, most probably due to the interaction of protons with outer pore and competing for binding sites with extracellular  $\text{Ca}^{2+}$  ions, as these ions attenuated the inhibitory effect of  $\text{pH}_e$  on TRPM2 [64]. These results were confirmed the same year by Du J. et al. and on the same cell line, although assuming a non-proton permeation through the channel [65], and by Yang W. et al. in 2010 [66], showing that low  $\text{pH}_e$ -mediated inhibition of TRPM2 might be induced by conformational changes following protons binding. Interestingly, extracellular acidic pH effects are species-dependent, with mTRPM2 channels showing less sensitivity to acidic  $\text{pH}_e$  compared to hTRPM2 [67] (see also Figure 1 and Table 1). Du J et al., as well as Starkus et al., also studied the intracellular acidic pH role showing a reversible inhibitory effect on the channel, inducing its closure without affecting single-channel conductance [64], probably by a mechanism of proton competition with the  $\text{Ca}^{2+}$  and ADPr binding site [65].

Several reports have highlighted the importance of the role of hypoxia in TRPM2's expression and activity, in particular in the context of hypoxia-induced brain damage, but with little evidence in tumour cells (Figure 1 and Table 2).

Concerning TRPM2's role in cerebral hypoxia, several comprehensive reviews have elucidated the current knowledge on this topic [145,146]. Huang and colleagues explored the TRPM2 pathological role in neonatal hypoxic-ischemic brain injury mouse model, demonstrating that genetic deletion of this channel had a long-term neuroprotective effect, reducing brain damage and inflammatory responses 7 days following the hypoxia-ischemic injury with respect to wild-type littermates. At the molecular level, TRPM2 was acutely overexpressed 24 h following hypoxia-ischemic injury in brain tissue samples from CD1 mouse pups and it inhibited pro-survival pathways in control mice by decreasing pAkt and pGSK-3 $\beta$  levels, exerting its protective role in TRPM2-null mice via Akt/Gsk-3 $\beta$  pathway [97]. In vitro TRPM2 silencing had a neuroprotective effect also in primary cultures of rat cortical neurons subjected to oxidative stress following brief  $\text{H}_2\text{O}_2$  exposure, reducing the intracellular calcium levels and preventing  $\text{H}_2\text{O}_2$ -mediated neuronal cell death [98]. In addition to neuronal cells, other works have explored hypoxia-induced activation of TRPM2 in other cell types, such as HEK-293 cells, where TRPM2 was activated after 30 and 60 min exposure to hypoxic conditions, leading potentially to an increased  $\text{Ca}^{2+}$  influx and oxidative stress, resulting in cell death [99], and retinal pigment epithelial cells, where 24 h-long exposure to hypoxia promoted ROS production and cell death via TRPM2-mediated  $\text{Ca}^{2+}$  influx [100].

In the context of tumourigenesis, TRPM2 is upregulated in several cancers where it mediates  $\text{Ca}^{2+}$ -dependent pathways promoting cell survival [147–152]. TRPM2 exerts this effect in particular by protecting cancer cells from oxidative stress by increasing their antioxidant defence. Indeed, although high levels of ROS are detected in almost all types of cancer, a precise balancing of their intracellular presence is required to avoid the toxic

effect of these reactive species, achieved through the expression of antioxidant proteins. TRPM2 channels act as ROS sensors, being activated by oxidative stress and switching on  $\text{Ca}^{2+}$ -dependent signalling pathways that lead to the enhanced activation of transcription factors involved in antioxidants' expression, (i.e., HIF-1/2 $\alpha$ ; CREB; Nrf2). These factors promote autophagy, DNA integrity, mitochondrial function, and ATP production [147] (Figure 1). Oxidative-stress-mediated TRPM2 activation and consequent rise in intracellular  $\text{Ca}^{2+}$  levels might promote cancer progression also by activating  $\text{Ca}^{2+}$ -dependent  $\text{K}^+$  channels, such as the large-conductance voltage-dependent BK channel and the medium-conductance voltage-independent  $\text{K}_{\text{Ca}3.1}$  channel, as reported in melanoma cells [101], which role in cancer hallmarks, such as cell viability and cell migration and invasion have been described [59]. However, other studies correlated TRPM2 expression with a higher sensitivity to chemotherapy. Indeed, an anti-survival role was highlighted in breast and colon cancer, where TRPM2 activation by chemotherapy agents resulted in  $\text{Ca}^{2+}$  entry, intracellular  $\text{Ca}^{2+}$  overload, and increased mitochondrial depolarisation, leading to cell death [153], and in prostate cancer, where  $\text{H}_2\text{O}_2$ -induced TRPM2 activation resulted in PC3 cells' death via  $\text{Ca}^{2+}$ -dependent inhibition of autophagy [102] (Figure 1). These results could be explained considering the differential role of full-length TRPM2 and its dominant-negative short isoform [103]. Chen and colleagues elucidated their role both in vitro and in vivo, demonstrating that full-length TRPM2 (TRPM2-L) had a protective role from oxidative stress by increasing antioxidant enzymes and pro-survival transcription factors, while the expression of the dominant-negative short isoform (TRPM2-S) reduced intracellular calcium influx in response to  $\text{H}_2\text{O}_2$  treatment and cell survival [103].

Another important consideration is the key role of TRPM2 in neutrophil-mediated cytotoxicity. Neutrophils secrete  $\text{H}_2\text{O}_2$ , which activates TRPM2 expressed on cancer cells' surfaces. This activation leads to  $\text{Ca}^{2+}$  influx in cancer cells, resulting in intracellular overload and induction of cell death, as was demonstrated in breast cancer cells [104] (Figure 1). Therefore, despite the pro-proliferative role of TRPM2 in several cancer cell lines, inhibition of its activity by tumour extracellular acidic pH might result in cancer cells' protection from neutrophil cytotoxicity, with overall major efficiency in dissemination. Finally, TRPM2 is also localised in lysosomal membranes, where the highly acidic pH inside the compartment might prevent TRPM2 activation and  $\text{Ca}^{2+}$  release from lysosomes to the cytosol, which may trigger apoptosis [154] (Figure 1). These works reinforce the concept that TRPM2 inhibition by acidic  $\text{pH}_e$  and activation by hypoxic conditions represent a protective mechanism for cancer cells.

**TRPM6** and **TRPM7** are both permeants mainly to  $\text{Mg}^{2+}$  ions and contribute to its homeostasis. These channels are also permeant to  $\text{Ca}^{2+}$  ions, increasing their intracellular concentration. TRPM7 has a unique structure as a "chanzyme" due to the presence of a kinase domain in its structure. TRPM6 has a tissue-specific expression and it is down-regulated in several cancer types, while TRPM7 is ubiquitously expressed and mostly upregulated in different malignancies, where it plays a key role in promoting different cancer hallmarks [155].

TRPM6 and TRPM7 channels' activity is modulated by both intra- and extracellular pH. For what concerns the effects of intracellular pH on TRPM7, the outward current density was decreased at low intracellular pH in HEK293 cells, with an  $\text{IC}_{50}$  of pH 6.32 and in the absence of  $\text{Mg}^{2+}$  [71]. This result was previously obtained also in RBL cells, where native TRPM7 currents were inhibited by intracellular acidification obtained by acetate treatment, and in TRPM7-overexpressing HEK293 cells in the same work [70]. Intracellular alkalinisation, induced by  $\text{NH}_4^+$  extracellular application, determined the induction of native TRPM7 current and the enhancement of its activity in RBL cells [70,71] (Table 1).

The effects of acidic  $\text{pH}_e$  (<6.0) on TRPM7 activity are quite controversial, with some evidence showing TRPM7 currents inhibition by low  $\text{pH}_e$  [68,70–72], others potentiation of TRPM7 inward current by strong acidic  $\text{pH}_e$  in HEK293 cells [69,73] and HeLa human cervical cells [74] (Table 1). The discrepancy of  $\text{pH}_e$  modulation on TRPM7 described by these works could be explained by taking into consideration the importance of  $\text{Ca}^{2+}$  and



Mg<sup>2+</sup> ions present in the extracellular milieu. According to the work of Mačianskienė R. et al., both TRPM7 outward and inward currents, expressed by cardiomyocytes, were potentiated in the acidic extracellular medium (pH < 6) containing divalent Ca<sup>2+</sup> and Mg<sup>2+</sup> ions, while the absence of these ions in the acidic extracellular medium resulted in the low p*H*<sub>e</sub>-mediated inhibition of TRPM7 currents in a voltage-independent manner [75]. It is hypothesized that protons and divalent cations compete for a binding site within the channel pore, and the absence of these cations might allow protons to permeate the channel and to bind to specific intracellular inhibitory sites, the same bound by intracellular protons, leading to channel inhibition [73,75].

Very few data are available for TRPM6, where contrasting data are reported, as for TRPM7. TRPM6 was indeed inhibited by extracellular acidity similarly to TRPM7 in isolated pig myocytes [68] but potentiated by extracellular acidic pH in HEK293 cells, even though the magnitude of increase in TRPM7 inward current was higher than that of TRPM6 [69] (Table 1).

Concerning TRPM6 and TRPM7 regulation by hypoxia, their expression is increased in a hepatic ischemia-reperfusion rat model [105], while hypoxia-induced TRPM7 overexpression and increased intracellular Mg<sup>2+</sup> concentrations were reported in rat hippocampal neurons in vitro [156]. TRPM7 sensitivity to hypoxia was also demonstrated by Tymianski and Mori group, showing that TRPM7 is activated by anoxic conditions or treatment with a hypoxic solution prepared by bubbling N<sub>2</sub> gas [106,157] (Table 2).

Although evidence of the effect of acidic pH and hypoxia on TRPM6/7 in cancer cells is still lacking, several works have demonstrated that TRPM7 is upregulated in various cancers and it is involved in the enhancement of a variety of cancer-related processes regulated by Ca<sup>2+</sup> signalling, such as proliferation, migration, invasion, cell death escape, and survival and epithelial–mesenchymal transition (EMT), via the activation of the Ras-ERK and the PI3K/AKT/mTOR signalling pathways [155] (Figure 1). Consequently, its activation by cancer-related extracellular acidic pH highlights its pivotal role in cancer progression.

## 2.2.2. TRP Vanilloid Subfamily

**TRPV1** is a non-selective cation channel with relatively high permeability to Ca<sup>2+</sup> ions, which is a major player in pain perception activated by different factors, including heat, inflammation, and acidic environment as revealed by David Julius, that shared the 2021 Nobel Prize for Physiology or Medicine [158–160]. Indeed, TRPV1 plays a key role in acidosis-induced pain, acting as a proton channel and being directly activated by protons [78,161].

Acidosis modulates TRPV1 activity, promoting its activation and potentiating its response to 2-APB, heat, and capsaicin (TRPV1 selective agonist) [76,78,80] (Table 1). hTRPV1 is indeed activated by mild acidosis (p*H*<sub>e</sub> 6.1) increasing intracellular Ca<sup>2+</sup> levels, while the channel is blocked in presence of strong acidic conditions [76]. T633 residue in the pore helix and V538 residue in the S3–S4 linker were identified as key residues involved in extracellular pH sensing [77]. Low p*H*<sub>e</sub> (<5.9) significantly potentiated heat and capsaicin-evoked response in HEK293 cells by increasing the channel's open probability at room temperature, therefore lowering the threshold for the channel activation, even in absence of chemical stimuli [78]. These data suggest that the potentiating effect of capsaicin and protons on TRPV1 are independent of each other and they are mediated by different TRPV1 residues (Table 1 and Figure 1). Concerning intracellular acidification, it enhanced TRPV1 currents evoked by 2-APB, without affecting the ones induced by capsaicin [80]. On the other hand, extracellular acidic pH activated TRPV1 and enhanced lymphatic endothelial cells' proliferative, migratory and invasive abilities via activation of NF-κB transcription factor and consequent upregulation of IL-8, a lymphangiogenic factor, contributing to lymphatic metastasis in tumour acidic microenvironment context [79] (Figure 1). The role of TRPV1 in cancer is dependent on the cancer type. TRPV1 is indeed upregulated in many cancers and it regulates different cancer cell processes, such as proliferation, cell

fate, migration, and invasion in a cancer type-specific manner, via the activation of different  $\text{Ca}^{2+}$ -dependent signalling pathways, such as PI3K/AKT, Ras-ERK and JAK/STAT signalling cascades and NF- $\kappa$ B activation [162], acting both as an anti-proliferative and pro-apoptotic factor in melanoma, colorectal, pancreatic and liver cancer, among others, and exerting a pro-tumour role in highly aggressive types of cancer [162] (Figure 1 and Figure 3). These pro- or anti-tumour effects of TRPV1 can be attributed to the different opening states available to the channel in response of different stimuli, exploiting each opening state's specific properties for the switching on of specific  $\text{Ca}^{2+}$ -dependent signalling pathways in different cancer cell types. Consequently, the  $\text{pH}_e$  regulation of TRPV1 might be considered as cell type, ligand, and context-specific, making it more difficult to identify its potential role as a pharmacological target.

Hypoxic TRPV1 modulation is reported in several publications, although cancer-related studies are lacking. Whole-cell patch clamp studies in HEK293T cells overexpressing rat TRPV1 showed that acute hypoxia weakly increased TRPV1 activity, but negatively affected capsaicin-induced TRPV1 currents. Hypoxia did not affect acidic  $\text{pH}_e$ -activated TRPV1 current. These results were confirmed by  $\text{Ca}^{2+}$  imaging experiments, where hypoxia induced a slight increase in cytosolic  $\text{Ca}^{2+}$  levels [107]. A stronger hypoxia-mediated TRPV1 activation was demonstrated in native rat sensory neurons and HEK293 cells expressing rat or human TRPV1, where chronic hypoxia (>24 h) did not affect the channel expression but potentiated TRPV1's activity via protein kinase C (PKC) $\epsilon$ - and HIF-1 $\alpha$ -dependent signalling pathways [108]. Parpaite and colleagues also showed on rat pulmonary artery smooth muscle cells (PASCs) that hypoxic conditions did not affect TRPV1 expression, but they increased TRPV1 activity probably via its translocation to the plasma membrane, enhancing PASCs' migratory abilities and proliferation [109]. Hypoxia-mediated changes in TRPV1 expression were instead reported in human PASCs, where chronic hypoxia upregulated both TRPV1 gene and protein levels, increasing intracellular  $\text{Ca}^{2+}$  levels and being involved in PASCs' proliferation [110] (Table 2).

In addition to TRPV1, also **TRPV2**, **TRPV3**, and **TRPV4** activity is modulated by acidic pH. **TRPV2** is an intracellular-resident non-selective cation channel that translocates to the cell membrane following PI3K activation. Once at the plasma membrane, TRPV2-mediated  $\text{Ca}^{2+}$  entry regulates different physiological cellular processes. TRPV2 deregulation has been linked to several types of cancer, where its activity supports its progression, in particular via the activation of the PI3K/AKT and the ERK signalling cascades, by escaping cell death and increasing proliferation, cell migration, and invasion [163]. TRPV2 is known to be insensitive to low  $\text{pH}_e$  alone [76,79], however, it has been demonstrated that acidic  $\text{pH}_e$  (6.0 and 5.5) potentiated TRPV2 currents in transiently transfected HEK293 cells that are evoked by 2-APB, increasing the channel's sensitivity to this ligand from the cytoplasmic side, as proved by inside-out patch configuration [80] (Table 1 and Figure 1).

Wang and colleagues did not report any change in TRPV2 expression following hypoxia exposure in human PASCs [110], but  $\text{H}_2\text{O}_2$ -mediated oxidative stress upregulated TRPV2 gene and protein expression in two different human hepatoma cell lines, with induction or cell death by activating pro-apoptotic proteins and by inhibiting pro-survival ones, and by enhancing the sensitivity of human hepatoma cells to oxidative stress-associated chemicals [111] (Table 2).

**TRPV3** is a non-selective calcium permeant cation channel mostly expressed in brain and skin, where it is involved in chemo-somatosensing. TRPV3 oncogenic activity was demonstrated in lung cancer, where TRPV3 expression was associated with short overall survival and  $\text{Ca}^{2+}$ -mediated increased proliferation via  $\text{Ca}^{2+}$ /calmodulin-dependent kinase II (CaMKII) [164]. As for TRPV2, acidic  $\text{pH}_e$  alone (pH 5.5) was not able to activate the channel in HEK293 cells, but only to potentiate the TRPV3 response to 2-APB and its analogues via acidification of the intracellular milieu, increasing cytosolic  $\text{Ca}^{2+}$  levels [80] (Table 1 and Figure 1). Moreover, cytosolic protons activated the channel, inducing small but detectable currents via different mechanisms with respect to 2-APB response potentiation, and indicating four residues in the S2–S3 linker to be implicated in the acid intracellular

activation of TRPV3 [80]. A more recent study from the same group has elucidated the mechanism of TRPV3 acid intracellular activation and extracellular inhibition. The authors identified Asp641 residue, localized in the selectivity filter, as a critical residue involved in TRPV3 extracellular acidic  $pH_e$  inhibition. Intracellular acidification protonated E682, E689, and D727 residues in the C-terminal, facilitating the channel's sensitization [165]. These data were also obtained by a previous work on TRPV3-transfected HEK293 and in HaCaT cells, where it was shown that TRPV3 is directly activated by glycolic acid-induced cytosolic acidification, inducing cell death, while extracellular acidification failed to activate the channel, resulting instead in decreased current amplitude [81] (Table 1 and Figures 1 and 3).

Concerning hypoxic regulation, no data on cancer cells is available. As for TRPV2, no differences in TRPV3 expression were reported in hypoxia exposed-PASMCs, but a recent work demonstrated TRPV3 upregulation in rat myocardial cells in response to ischemia/hypoxia treatment. To confirm the role of TRPV3 as a mediator of hypoxia-induced inflammation and apoptosis in rat myocardial cells, the authors reported that TRPV3 silencing protected cardiomyocytes from hypoxia-induced cell death and decreased the secretion of pro-inflammatory cytokines [112]. TRPV3 mediated hypoxia responses also in pulmonary artery smooth muscle cells, promoting their proliferation via PI3K/AKT signalling pathway [113], and hypoxia also robustly potentiated this channel current in TRPV3-overexpressing HEK293 cells in response to 2-APB treatment, without affecting the protein levels [114] (Table 2).

**TRPV4** is a heat-activated and mechanosensitive channel deregulated in different cancer cells, acting mostly as a pro-tumour factor, enhancing cancer cells' migration and metastasis through the activation of AKT and Rho/ROCK1/cofilin cascade, extracellular remodelling, proliferation and angiogenesis via activation of NFAT and PI3K signalling pathway [166–172], although a tumour-suppressive role has also been reported, especially in tumours expressing high TRPV4 levels [173,174] (Figures 1 and 3).

For what concerns TRPV4 regulation by pH, low extracellular pH ( $pH_e$  6) induced opening of transiently expressed TRPV4 in Chinese hamster ovary cells, with a maximal potentiation at  $pH_e$  4, as demonstrated by patch clamp current recording in absence of extracellular  $Ca^{2+}$  ions [82]. An opposite effect was observed in mouse oesophageal epithelial cells, where  $Ca^{2+}$  imaging experiments showed that the  $Ca^{2+}$  influx mediated by TRPV4 was abolished at  $pH_e$  5 [83] (Table 1). These opposite results might be explained considering the different techniques used by the two research groups and the experimental conditions in general. TRPV4 is a non-selective ion channel, permeable to protons when the extracellular solution is free from other divalent ions, such as  $Ca^{2+}$  ions. Since protons may compete with  $Ca^{2+}$  ions, a high extracellular proton concentration might lead to a decrease in  $Ca^{2+}$  influx but contributes to the gross TRPV4 current [83]. Collectively, considering the evidence outlined above, TRPV4's role in tumour biology is cancer type-specific and it might emerge as a potential drug target in the context of cancer treatment.

Regarding hypoxic TRPV4 regulation, no studies on cancer cells are present in the literature, but they are limited to other pathological states. In particular, its mRNA and protein expression levels were increased after 6 h long exposure to hypoxia in cardiomyocytes, inducing  $Ca^{2+}$  overload and enhancing oxidative injury [115]. TRPV4 plays also an important role in mediating hypoxia-induced pulmonary vasoconstriction (HPV) [175] and in the hypoxia/ischemia injury in the brain [116] (Table 2).

pH also regulates the activity of another component of the TRP vanilloid family, **TRPV6**, a highly  $Ca^{2+}$  selective channel (PCa/PNa~100) that is upregulated in different epithelial cancers, such as prostate, pancreatic, breast and ovarian cancer, in particular during early stages of tumour progression [176]. Several studies has revealed the positive effect of TRPV6 activity on tumour progression through the activation of  $Ca^{2+}$ -dependent signalling pathways [176], promoting cancer proliferation and cell survival in prostate cancer cells by activating the  $Ca^{2+}$ -dependent NFAT transcription factor [177,178], invasion of breast cancer cells through  $Ca^{2+}$ /Calmodulin (CaM)-dependent kinases, such as CaMKII [179,180],

cell survival, proliferation, and invasion in pancreatic cancer cells [181] and tumour growth in in vivo ovarian adenocarcinoma xenograft mouse model [182] (Figure 1 and Figure 3).

TRPV6 is a polymodal sensor that is regulated by different chemical and physical stimuli, including acidic  $\text{pH}_e$  and hypoxia. Alkaline  $\text{pH}_e$  positively modulated TRPV6's activity in Jurkat T-cells, where whole-cell patch-clamp experiments showed that solution at pH 8.2 determined the increase in TRPV6 activity and  $\text{Ca}^{2+}$  entry, while opposite effects were experienced for acidic  $\text{pH}_e$  (pH = 6), which reduced inward TRPV6 currents and  $\text{Ca}^{2+}$  influx in Jurkat T-cells [84] (Table 1).

Inhibition of TRPV6 by extracellular acidification might be explained considering TRPV6 expression in distinct stages of cancer progression. Tumours can be characterized by a more acidic extracellular microenvironment during late stages [183], phases in which TRPV6 expression is downregulated in some types of cancers, such as colon cancer [184]. However, the lack of further studies focusing on the effect of extracellular acid pH on TRPV6 activity makes a comprehensive understanding of the role of acid  $\text{pH}_e$  on TRPV6 in the context of tumour acidosis difficult.

As for many other TRPV channels, to date, there is extremely little information about TRPV6 modulation by hypoxia, especially in the tumorigenesis context, with a report of placental TRPV6 overexpression in hypoxic rats [185].

### 2.2.3. TRP Ankyrin Subfamily

**TRPA1** is a non-selective cation channel that functions as a polymodal sensor, and deregulation is observed in several malignancies in a tissue-specific manner [186]. TRPA1 has been described as highly sensitive to  $\text{O}_2$  and oxidants in vagal and sensory neurons. In particular, TRPA1 is activated in hypoxic conditions by the relief of the inhibition of prolyl hydroxylase (PDH) which is  $\text{O}_2$  sensitive [187].

The role of TRPA1 as a ROS sensor has been demonstrated also in cancer cells. The work of Takahashi et al. has demonstrated a key role of TRPA1 in promoting resistance to ROS-producing chemotherapies and oxidative stress tolerance in breast cancer cells via ROS-mediated TRPA1 activation and  $\text{Ca}^{2+}$ -CaM/PYK2 signalling pathway [117] (Table 2 and Figure 1). TRPA1 interaction with fibroblast growth factor receptor 2 (FGFR2) induces the activation of the receptor, promoting cancer cells' proliferation and invasion, prompting lung adenocarcinoma metastasis to the brain [188]. TRPA1 activation might also promote prostate cancer progression by triggering prostate cancer stromal cells' secretion of VEGF [189], a known mitogenic factor involved in the proliferation, migration and invasion of prostate cancer cells [190]. In line with those results, TRPA1 is indeed also an important player in promoting angiogenesis both in physiological retinal development as well as in prostate cancer-derived endothelial cells [191].

In addition to being activated by oxidants, TRPA1 is activated by several distinct exogenous and endogenous compounds [192] and by protons in the extracellular environment, on which regulation is specie dependent. HEK293 cells expressing human and rodent TRPA1 showed a specie-specific activation of the channel, where only hTRPA1 generated a membrane current when exposed to different extracellular acidic environments ( $\text{pH}_e$  6.4-5.4) reaching the maximal response at acidic  $\text{pH}_e$  5.4; this specific effect for hTRPA1 was confirmed by  $\text{Ca}^{2+}$  imaging experiments in HEK293 cells as well as in DRG neurons derived from TRPV1/TRPA1 $^{-/-}$  mice and in neuroblastoma ND7/23 cells expressing hTRPA1, where only hTRPA1 induced an increase in  $\text{Ca}^{2+}$  entry when exposed to acidic  $\text{pH}_e$ . This specie-specific activation of TRPA1 is due to valine and serine residues within transmembrane domains 5 and 6 [85] (Table 1).

TRPA1 can also be activated by intracellular acidification, as observed in the context of ischemia-induced acidification of the extracellular microenvironment in mice oligodendrocytes, with following acidification of the intracellular space and activation of TRPA1. This led to an increase in  $\text{Ca}^{2+}$  influx and damage to myelin [118] (Table 1). Altogether, these results and their role in cancer suggest that TRPA1 activation by acidic  $\text{pH}_e$  and hypoxia



may play a significant role in promoting cancer progression, highlighting its potential as a therapeutic target.

#### 2.2.4. TRP Canonical Subfamily

**TRPC1** is a non-selective cation channel, which assembles to form homo- and heteromeric channels with other members of the family, such as TRPC3, TRPC4 and TRPC5. TRPC1 upregulation has been reported in several cancers, such as pancreatic cancer, where it potentiates BxPc3 cells' migration via  $\text{Ca}^{2+}$ -dependent activation of PKC $\alpha$  [193], and breast cancer, where it exerts a pro-proliferative role in MCF-7 cells by mediating  $\text{Ca}^{2+}$  influx induced by  $\text{K}_{\text{Ca}3.1}$  activation [194] and via  $\text{Ca}^{2+}$ -dependent ERK1/2 activation [195]. TRPC1 also promotes human glioma cancer cells' proliferation via  $\text{Ca}^{2+}$  entry and supports tumour growth in vivo [196], and lung cancer differentiation, by promoting A549 cell proliferation [197]. TRPC1 also participates with ORAI1 channels in the induction of vimentin, a mesenchymal marker for epithelial–mesenchymal transition (EMT) [198] (Figures 2 and 3).

Although TRPC1 is not regulated by protons, several data demonstrated that TRPC1 expression is hypoxia-mediated. The study by Wang B. et al. in 2009 reported that TRPC1 is functionally expressed in U-87 malignant glioma cells under hypoxia, where it promoted the upregulation of VEGF expression, as VEGF mRNA levels were significantly decreased in presence of TRPC1 inhibitor or RNAi in hypoxic conditions [119] (Table 2 and Figure 2). VEGF has a central role in angiogenesis in both physiological and pathological conditions [199] and solid tumours are characterized by a hypoxic microenvironment, in which the lack of oxygen might promote VEGF expression, in order to induce angiogenesis and increase tumour oxygen supply. TRPC1 mediates hypoxia responses also in breast cancer cells, where HIF-1 $\alpha$  promoted its upregulation. In MDA-MB-468 breast cancer cells, TRPC1 is involved in the transactivation of the epidermal growth factor receptor (EGFR) during hypoxia, leading to the increase in LC3B autophagy marker [120]. Moreover, hypoxia-induced TRPC1 activation promoted epithelial–mesenchymal transition in the same cells, upregulating the mesenchymal marker snail and downregulating the epithelial marker claudin-4, promoting the hypoxia-induced EMT and, therefore, the aggressive and invasive phenotype of breast cancer cells [120] (Table 2 and Figure 2).

**TRPC5** is a  $\text{Ca}^{2+}$ -activated ion channel that is regulated by components of the tumour microenvironment, such as acidosis and supports hypoxia responses. In long-term adriamycin-treated breast cancer cells, TRPC5-mediated  $\text{Ca}^{2+}$  influx promoted HIF-1 $\alpha$  translocation in the nucleus and therefore the downstream transcription of HIF-1 $\alpha$ -regulated VEGF expression, highlighting its contribution to promoting breast cancer angiogenesis [121] (Table 2 and Figure 2). The same research group also validated TRPC5 role in mediating HIF-1 $\alpha$  response in tumour progression in colon cancer, where TRPC5 activated the HIF-1 $\alpha$ -Twist signalling pathway to promote EMT, migration and proliferation in SW620 colon cancer cells [122].

TRPC5 also acts as a  $\text{pH}_e$  sensor, as its spontaneous activity and G protein-activated currents are potentiated by extracellular acidic pH by increasing the channel open probability in presence of small changes of extracellular pH, with a maximum activity around  $\text{pH}_e$  6.5 and current inhibition starting from pH 5.5 [86] (Table 1).

Potentiation by acidic  $\text{pH}_e$  and involvement in HIF-1 $\alpha$  regulation demonstrates the interest of cancer cells in keeping TRPC5 channels active and over-expressed, in order to promote cancer-specific hallmarks, in particular chemoresistance. Indeed, the role of TRPC5 in promoting chemoresistance in different types of cancer is well known. In breast carcinoma cells, adriamycin-induced TRPC5 upregulation protects them from chemotherapy treatment, by inducing autophagy via an increase in cytosolic  $\text{Ca}^{2+}$  concentrations and activation of the  $\text{Ca}^{2+}$ -dependent CaMKK $\beta$ /AMPK $\alpha$ /mTOR pathway, promoting the cancer cell survival and tumour growth in vivo [200] (Figure 2). The work by Ma X. et al. in 2012 has also demonstrated in vitro and in vivo the critical role of this channel in promoting chemoresistance of adriamycin-resistant MCF-7 breast cancer cell line with the upregulation of another pump linked to drug resistance. TRPC5 overexpression resulted indeed in  $\text{Ca}^{2+}$

influx and activation of P-glycoprotein overproduction, a pump in charge of removing cytotoxic drugs from cells via  $\text{Ca}^{2+}$ /calmodulin/calcineurin-dependent NFATc3 signalling pathway [201]. The role of TRPC5 in therapy resistance is not confined to breast cancer, as its upregulation has been also identified in 5-fluorouracil resistant human colorectal cancer cells, where TRPC5 overexpression determines the overproduction of ATP-binding cassette subfamily B member 1 (ABCB1), a pump involved in drug resistance through the export of cytotoxic drugs, via  $\text{Ca}^{2+}$  entry and activation of  $\text{Ca}^{2+}$ -dependent Wnt/ $\beta$ -catenin signalling pathway and in a glycolysis-dependent manner [201–203] (Figure 2).

In addition to chemoresistance, TRPC5 expression was observed to be positively correlated with high proliferative, migratory, and invasive abilities of colon cancer cells, promoting the EMT through the HIF-1 $\alpha$ -Twist signalling pathway [122]. Therefore, these results demonstrate that the impact of the acid and hypoxic cancer microenvironment on the TRPC5 channel is aimed at its activation, thus promoting tumour progression (Figure 3).

Similar behaviour is shown by **TRPC4**, which shares high sequence similarity with TRPC5. TRPC4 is a  $\text{Ca}^{2+}$ - and G-coupled receptors-activated non-selective  $\text{Ca}^{2+}$  permeable cation channel [204]. TRPC4's role in cancer has been elucidated in the last years, being involved in promoting angiogenesis via cytosolic  $\text{Na}^+$  and  $\text{Ca}^{2+}$  rise [205,206] and proliferation [207], although a negative effect on A-498 renal cell carcinoma cells via Englerin A-mediated channel activation has been documented [208].

TRPC4-mediated currents are two-fold potentiated when exposed to  $\text{pH}_e$  6.5; however, lower pH leads to current inhibition starting from  $\text{pH}_e$  6, with complete current inhibition at  $\text{pH}_e$  5.5 [86].  $G_{i/o}$ -mediated TRPC4 activation is also accelerated by intracellular protons in an indirect way, regulating the kinetics of  $G_{i/o}$ -dependent TRPC4 activation, and it requires an increase in intracellular  $\text{Ca}^{2+}$  concentration. Intracellular protons do not act directly on the channel, as they inhibit TRPC4 activation by its direct agonist, Englerin A, but by acting on PLC $\delta$ 1 [87] (Table 1; Figures 2 and 3). No data are available to our knowledge about hypoxia regulation of TRPC4 expression and/or activity.

**TRPC6** is another TRPC member to be regulated by tumour microenvironmental clues, such as hypoxia. In fact, hypoxic conditions enhanced TRPC6 expression in murine pancreatic stellate cells, which constitute the major cellular components in pancreatic ductal adenocarcinoma's stroma, and which play a key role in generating PDAC's characteristic desmoplasia. TRPC6 promoted their activation and it was involved in the secretion of pro-migratory factors in presence of hypoxia [123]. Hypoxia upregulated TRPC6 mRNA expression in hepatocellular carcinoma cells, where TRPC6-mediated  $\text{Ca}^{2+}$  influx conferred drug resistance to these cells via the  $\text{Ca}^{2+}$ -dependent STAT3 signalling pathway in hypoxic conditions [125]. Hypoxia activated Notch1 and downstream TRPC6 expression also in glioma cells, with a consequent rise in cytosolic  $\text{Ca}^{2+}$  concentration and  $\text{Ca}^{2+}$ -dependent activation of the calcineurin-NFAT signalling pathway, promoting proliferation, cell invasion and angiogenesis under hypoxia [126] (Table 2, Figures 1 and 3). Hypoxia also upregulated TRPC6 in hepatic stellate cells via HIF-1 $\alpha$ /Notch1 pathway, leading to TRPC6-mediated  $\text{Ca}^{2+}$  influx and the downstream activation of  $\text{Ca}^{2+}$ -dependent nuclear factor of activated T-cells (NFAT) transcription factor and SMAD2/3-dependent TGF- $\beta$  signalling, which activation resulted in the expression of ECM proteins, such as collagen type I, that facilitate hepatic stellate cells' fibrotic activation and promotes hepatic fibrosis, strongly linked to arise of hepatocellular carcinoma [124] (Table 2; Figures 1 and 3).

Regarding the direct role of acidic extracellular pH (around pH 6.5), it is sufficient to inhibit TRPC6, and the inhibition increased in a pH-dependent manner, affecting both inward and outwards currents in HEK-transfected cells [86] (Table 1). This inhibitory effect of acidic  $\text{pH}_e$  might be explained considering the high TRPC6 levels expressed by pro-tumourigenic immune cells, such as neutrophils, where TRPC6-mediated calcium entry is required for CXCR2-mediated intermediary chemotaxis [209]. Consequently, inhibition of TRPC6 by acidic  $\text{pH}_e$  may impair neutrophils' migration and prevent them from leaving the acidic tumour microenvironment, thus contributing to its progression and metastasis by releasing ROS, secreting pro-tumour factors and inducing drug resistance [210]. Altogether,

these results suggest that the acidic  $pH_e$ -mediated potentiation of TRPC channels might be restricted to only some members, and it depends on the cell type expressing the channels.

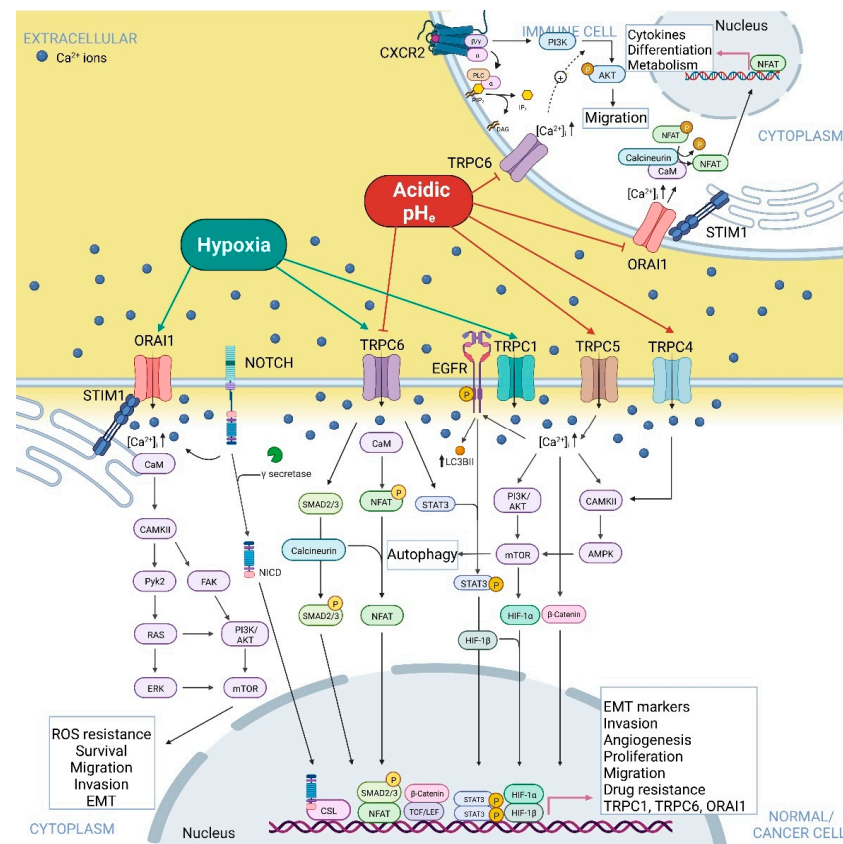


**Figure 2.** Overview of the effects of acidic  $pH_e$  and hypoxia on TRPC and Orai  $Ca^{2+}$ -permeable channels. The positive or negative effects of hypoxia and acidic  $pH_e$  on the  $Ca^{2+}$ -permeable channels were obtained from both normal and cancer cell-related studies, while the signalling pathways indicated were obtained uniquely from cancer cell-based investigations. The figure depicts TRPCs- and SOCs-mediated  $Ca^{2+}$ -dependent signalling pathways inhibited or activated by acidic  $pH_e$  or hypoxia and linked to tumour progression. TRPC (TRPC1, 4, 5) expressed in cancer cells' plasma membrane is all activated by acidic  $pH_e$  or hypoxia, transducing their signals to activate  $Ca^{2+}$ -dependent downstream effectors, such as SMAD2/3, NFAT, STAT3, HIF1, AMPK and  $\beta$ -catenin. These effectors promote tumour cell migration, angiogenesis, invasion, proliferation, mesenchymal phenotype and chemoresistance and the expression of TRPC1, via EGFR activation, and TRPC6 via Notch1 signalling pathway, in a mechanism of positive feedback regulation for both TRPC1 and TRPC6 channels. Immune cells expressing TRPC6 channels on plasma membrane show TRPC6's activity that is inhibited by acidic  $pH_e$ , reducing their migration. Orai1 channels function in immune cells is also negatively affected by acidic  $pH_e$ , impairing different processes needed for immune cells' anti-tumour activity. Hypoxia promotes both Orai1 expression, via Notch signalling pathway, and activation, leading to increased ROS resistance, migration, invasion, EMT and cell survival. CaM, calmodulin; CAMKII,  $Ca^{2+}$ /calmodulin-dependent protein kinase II; Pyk2, protein tyrosine kinase 2; RAS, rat sarcoma virus; ERK, extracellular signal-regulated kinase; FAK, focal adhesion kinase; PI3K, phosphoinositide 3-kinase; AKT, protein kinase B; mTOR, mammalian target of rapamycin; NICD, Notch intracellular domain; CSL, CBF1, suppressor of hairless, Lag-1; NFAT, nuclear factor of activated T-cells; STAT, signal transducers and activators of transcription; EGFR, epidermal growth factor receptor; HIF-1, hypoxia-inducible factor 1. Created with [BioRender.com](https://www.biorender.com), accessed on 20 June 2022.

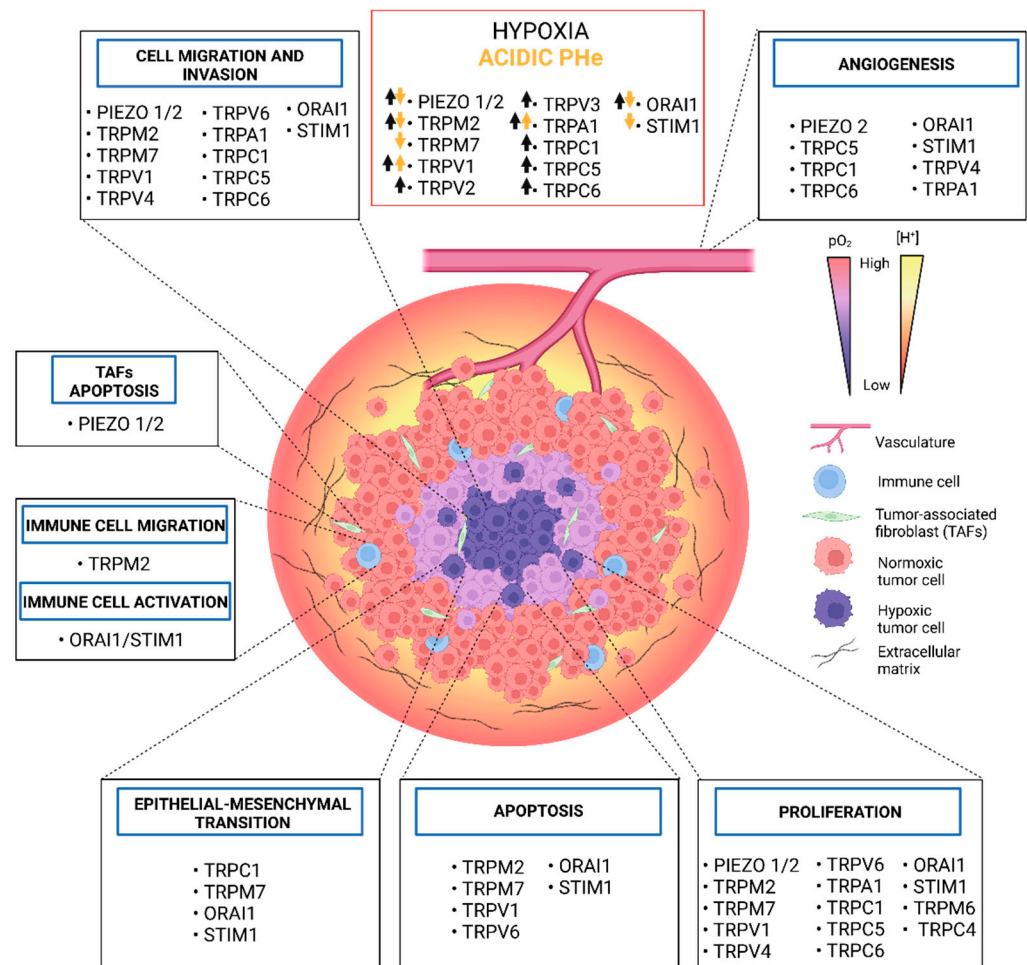


**Figure 3.** Schematic illustration of tumour microenvironment landscape. The increased tumour growth, the acidification of the extracellular space and aberrant vascularisation and limited O<sub>2</sub> supply origin a tumour core that is hypoxic and acidic, with limited supply of oxygen and nutrients from the blood vessels. Peripheral tumour cells are located in regions with a higher extracellular pH, a result of proximity to blood vessels and the possibility to wash out acidic waste products. TRP, Piezo and SOCs channels expressed in cancer, immune and stromal cells are presented in the corresponding black boxes with indication of their involvement in different cancer hallmarks, such as proliferation, migration, invasion, angiogenesis, and epithelial–mesenchymal transition. The red box contains the up-to-date information regarding the effect (up arrows = positive effect; down arrows = negative effect) of hypoxia and acid pHe on the activity and/or expression of calcium-permeable channels in cancer cells or tumour-associated cells.

### 2.3. Store-Operated Ca<sup>2+</sup> Channels

**ORAI**s are Ca<sup>2+</sup> release-activated Ca<sup>2+</sup> channels (CRAC) which are major players, with **STIM** proteins, in the mechanism known as store-operated Ca<sup>2+</sup> entry (SOCE), which mediates Ca<sup>2+</sup> entry into cells promoting the refilling of ER calcium stores as well as intracellular signalling, controlling both physiological and pathological processes such as inflammation, cell motility, cell proliferation, gene expression, apoptosis escape and cell invasion [211–213]. SOCE represents the main route of Ca<sup>2+</sup> entry in different types of cancer cells, contributing to several cancer hallmarks. Indeed, different works have highlighted the key role of SOCE in promoting the migration of different cancer cell lines, such as chemoresistant IGROV1 ovarian cancer cells by regulating focal adhesion turnover [214], SW480 colorectal carcinoma cells [215] and oral cancer cells through Akt/mTOR/NF-κB signalling [216]. Moreover, SOCE has been implicated in enhancing invasion of triple-negative breast cancer cells, as well as angiogenesis and migration, through NFAT4 signalling [128]



and through NFATc3 in colorectal cancer cells and tissues from patients [129], while in WM793 cells melanoma cells, SOCE-induced  $\text{Ca}^{2+}$  oscillations contribute to invadopodia formation via Src activation [217]. SOCE might promote invasion of cancer cells by inducing epithelial–mesenchymal transition, as observed in DU145 and PC3 prostate cancer cells [218] and BGC-803 and MKN-45 gastric cancer cells [219]. Store-operated channels (SOCs) in general play a key role also in the modulation of sensitivity to chemotherapy in a cancer type-specific manner, by promoting chemoresistance in breast cancer cells in the case of ORAI3 [220], ORAI1 and STIM1 in pancreatic ductal adenocarcinoma [212], ORAI1 in hepatocarcinoma [221], among others. SOCE also promotes extracellular vesicle formation, which is a signalling vector involved in the intercellular acquisition of multidrug resistance, in both malignant and non-malignant breast cancer cells via activation of calpain [222].

In addition to all these contributions to cancer progression, SOCE is regulated by hypoxia and pH. Several studies have demonstrated that intracellular and extracellular pH is able to modulate the activity of ORAI channels by affecting its coupling with STIM1 and/or by modifying its gating biophysical properties. The results obtained by numerous studies conducted on ORAI/STIM have clarified the concept that both intra- and extracellular acidic pH have an inhibitory effect on the activity of ORAIs, and on SOCE in general, while intra- and extracellular basic pH potentiate them. The notion that extracellular pH regulates native CRAC currents ( $I_{\text{CRAC}}$ ) was already known in 1995 when the work of Malayev A. and Nelson D.J. showed that acidic extracellular pH ( $\text{pH}_e = 6$ ) decreased the amplitude of inward  $\text{Ca}^{2+}$  currents while basic  $\text{pH}_e$  ( $\text{pH}_e = 8$ ) increased it in macrophages by using the patch clamp technique and that these changes were reversible and voltage-independent [88] (Table 1). More recently, inhibition by acidic  $\text{pH}_e$  was demonstrated in H4IIE rat liver cells overexpressing ORAI1 and STIM1 proteins, in which  $I_{\text{CRAC}}$  was inhibited completely at  $\text{pH}_e$  5.5 [89] (Table 1). In the same work, researchers identified E106, located in ORAI1's pore, as the residue responsible for pH dependence of CRAC currents, as E106D mutation in ORAI1 abolished the inhibition of  $I_{\text{CRAC}}$  by acidic  $\text{pH}_e$ . These results were also supported by the work of Beck A. and colleagues, which demonstrated that extracellular and intracellular acidification decreased the amplitude of IP3-induced endogenous  $I_{\text{CRAC}}$  in RBL2H3 mast cell line, in Jurkat T lymphocytes and in heterologous ORAI/STIM-mediated  $I_{\text{CRAC}}$  in HEK293 cells [90] (Table 1). In contrast to acidification, external alkalinisation increased both endogenous and overexpressed ORAI/STIM amplitude of  $I_{\text{CRAC}}$  ( $\text{pK}_a$  of 7.8 for RBL2H3 mast cells, 8.0 for Jurkat T lymphocytes and 7.9 for HEK293 cells). Other two key residues (D110 and D112) located in ORAI1's first extracellular loop have been proposed to contribute to some extent to  $\text{pH}_e$  sensitivity. Indeed, mutations of these residues to alanine prevented the alkalinisation-induced potentiation of  $I_{\text{CRAC}}$  and increased its amplitude in the presence of acidic  $\text{pH}_e$  [90]. Enhancement and the decrease in SOCs activity by external basic and acidic pH, respectively, were further confirmed in heterologous ORAI/STIM-mediated currents in HEK293 cells by Tsujikawa H. et al. in 2015, who have also demonstrated that E106 mediates  $\text{pH}_e$  sensitivity when  $\text{Ca}^{2+}$  is the permeant cation, while E190 when  $\text{Na}^+$  is the permeant cation [91] (Table 1). However, the effect of alkaline  $\text{pH}_i$  on  $I_{\text{CRAC}}$  is controversial. Indeed, alkaline  $\text{pH}_i$ -mediated potentiation of ORAI1/STIM1 activity was observed in other papers [91,223] (Table 1). These differences might be explained considering the type of intracellular  $\text{Ca}^{2+}$  buffer used [223]. Moreover, cytosolic alkalinisation led to SERCA inhibition, resulting in  $\text{Ca}^{2+}$  release from ER stores and activation of SOCs, with  $\text{Ca}^{2+}$  influx in NIH 3T3 cells [224]. Residual H155 located in the intracellular loop of ORAI1 is responsible for ORAI1/STIM1  $\text{pH}_i$  sensitivity, as mutation to phenylalanine decreased low  $\text{pH}_i$ -mediated  $I_{\text{CRAC}}$  inhibition and alkaline  $\text{pH}_i$ -mediated  $I_{\text{CRAC}}$  potentiation [91]. Since the effect of pH was the same in presence of all ORAI isoforms [90] and that both extracellular pH sensors (residues E106 and E190) and intracellular one (residue H155) are conserved in all three ORAI isoforms, it might suggest that the residues mentioned before act as common  $\text{pH}_i$  and  $\text{pH}_e$  sensors in ORAI1–2–3/STIM isoforms. In addition to H155, negatively charged amino acid residues in the STIM1 inactivation domain play an important role in  $\text{pH}_i$  sensitivity [223].

For what concerns hypoxia-mediated regulation of SOCs, intracellular acidification of primary aortic smooth muscle cells and HEK293 cells induced by hypoxia led to inhibition of SOCE by disrupting the electrostatic ORAI1/STIM1 binding and closing ORAI1 channel (Table 2 and Figure 2). Nonetheless, STIM1 remained associated with ORAI1 through the second binding site located between ORAI1's intracellular N-terminal tail and STIM1's STIM-ORAI activating region (SOAR), preventing the noxious hypoxia-mediated  $\text{Ca}^{2+}$  overload [92]. Therefore, intracellular hypoxia-mediated acidification might regulate SOCs activity by uncoupling ORAI1 and STIM1 and, consequently, reducing  $I_{\text{CRAC}}$  amplitude.

As ORAI/STIM mediate most of the  $\text{Ca}^{2+}$  signalling in cancer-induced acidosis, they play a key role in several pathological processes. In the cancer context, it was observed that SOCE is regulated by changes in extracellular pH, as acidification of tumour microenvironment suppressed both the carbachol-(CCH) and thapsigargin (TG)-mediated  $\text{Ca}^{2+}$  entry in neuroblastoma cells, while external alkalisation increased both the CCH- and the TG-induced  $\text{Ca}^{2+}$ -influx [93], therefore in accordance with the results obtained in non-cancer cells (Table 2 and Figure 2).

However, the work of Liu X. et al. of 2018 on triple-negative breast cancer cells (TNBCs) reported that hypoxia promoted the activation of Notch1 signalling, required for the upregulation of ORAI1 mRNA and protein levels in TNBCs (Table 2 and Figure 2). In addition, the upregulation of ORAI1 in hypoxia determined an increase in basal  $\text{Ca}^{2+}$  concentration and of thapsigargin-induced SOCE, which activated the downstream NFAT4 target, known to regulate the expression of cancer-related genes involved in its hallmarks [128]. The results of the same work showed that hypoxia enhanced invasion and TNBC migration via the Notch1/ORAI1/SOCE/NFAT4 pathway; therefore, ORAI1 and SOCE play a key role in promoting an aggressive phenotype. Same results were obtained in colon cancer cells by the same group of researchers, where potentiation of SOCE mediated by hypoxia-induced upregulation of ORAI1 determined the activation of NFATc3, enhancing hypoxia-induced invasion and angiogenesis in colon cancer cells [129]. The hypoxia-induced upregulation of SOCE components was also demonstrated in A549 and NCI-H292 non-small cell lung cancer cells, where nicotine treatment determined the upregulation of HIF-1 $\alpha$ , which increased the expression of the SOCE components TRPC1, TRPC6 and ORAI1. This translated into potentiation of SOCE and calcium entry, promoting lung cancer cells' proliferation [127].

Considering the acidosis and hypoxia-mediated effects presented, the inhibitory action of the tumour intra- and extracellular acidic pH on SOC channels seems to contradict the positive effect of SOCE on tumour progression. In particular, acidosis inhibition of SOCE does not correlate with the different studies demonstrating that ORAI/STIM and SOCE promote cancer development [225] and that also tumour acidosis and hypoxia support it by enhancing tumour cell migration, invasion and, therefore, its aggressive phenotype [40,226]. Possible explanations for the apparent counterproductive blockade of SOCE channels by the tumour's acidic pH lie in the fact that  $\text{Ca}^{2+}$  signalling not only promotes tumour progression and development by potentiation of its hallmarks but also contributes to its suppression by enhancing processes such as cell death, senescence and autophagy [49]. In addition, ORAI members assembly to form different combinations of heteromeric  $\text{Ca}^{2+}$  release-activated channels (CRACs) and the ratio of each ORAI member determines specific  $I_{\text{CRAC}}$  current properties and CRAC effects [227,228]. Therefore, the acidic pH of the tumour microenvironment may differently regulate heteromeric CRACs. Another point to consider is the key role of SOCE in immune cell activation [229]. The requirement of  $\text{Ca}^{2+}$  entry for antitumour immunity might explain the inhibitory effect of acidic tumour microenvironment on SOCE, in order to decrease immune cells' function and protect the tumour.

### 3. Concluding Remarks

The present review aimed to overview the crosstalk between major chemical components of the tumour microenvironment, hypoxia and acidic  $\text{pH}_e$ , and  $\text{Ca}^{2+}$ -permeable ion channels, summarizing the major  $\text{Ca}^{2+}$ -mediated signalling pathways that are involved

in hypoxia and acidic  $\text{pH}_e$  responses in cancer cells. We focused our attention mainly on not-voltage gated TRPs, SOCs as well as Piezo channels due to their role as polymodal sensors in the tumour microenvironment. In this perspective, the data presented showed that hypoxia has a positive effect on some TRP and ORAI1 channels (Figure 3), promoting their activation and their expression via different transcription factors. On the contrary, tumour acidosis modulation shows a higher variability, determining loss-of-function of specific  $\text{Ca}^{2+}$ -permeable ion channels expressed not only by cancer cells but also by immune cells, or potentiation or activation of others.

Although the separate roles of tumour acidosis, hypoxia and  $\text{Ca}^{2+}$  signalling in cancer progression are well established, less is known about their crosstalk in this context, with the majority of works cited in this review performed on normal cell lines and with a focus on acidic  $\text{pH}_e$  effect on  $\text{Ca}^{2+}$ -permeable ion channels' current via electrophysiology experiments. In addition, investigation of intracellular acidification-mediated regulation of  $\text{Ca}^{2+}$  signals and the  $\text{pH}_i$ -dependence of  $\text{Ca}^{2+}$ -permeable channels in cancer is rare, although it is well known that intracellular pH plays a more decisive role in regulating various biological processes and that this value is highly influenced by the extracellular pH. Based on the established knowledge about  $\text{Ca}^{2+}$ -dependent signalling pathways involved in tumour progression and on the information about the effects of hypoxia and acidosis on the activity and expression of different  $\text{Ca}^{2+}$ -permeable channels mostly available from normal or tumourigenic cells studies, the present review critically presented and discussed this crosstalk to elucidate and hypothesize which of TRPs, ORAIs and PIEZO channels  $\text{Ca}^{2+}$ -dependent signalling pathways could be activated or inhibited by hypoxia and tumour acidosis-mediated regulation of  $\text{Ca}^{2+}$ -permeable ion channels in cancer cells and involved in tumour progression, for the identification of potential molecular identities to target. In particular, the putative synergistic relationship between hypoxia, tumour acidosis and low  $\text{pH}_e$ -induced intracellular acidification and  $\text{Ca}^{2+}$  signals, the mechanisms of their interaction and their interdependence in tumours require further studies and clarifications, in order to fill the gap and promote a better understanding of the crosstalk between three major players in the cancer research field.

**Author Contributions:** Conceptualisation, M.M.A., A.F.P. and N.P.; methodology, M.M.A., A.F.P. and N.P.; investigation, M.M.A. and A.F.P.; writing—original draft preparation, M.M.A., A.F.P. and N.P.; writing—review and editing, M.M.A., A.F.P. and N.P.; visualisation, M.M.A., A.F.P. and N.P.; supervision, A.F.P. and N.P. All authors have read and agreed to the published version of the manuscript.

**Funding:** M.M.A. and N.P. are supported by the European Marie Skłodowska—Curie Innovative Training Network (ITN) pH and Ion Transport in Pancreatic Cancer—pHioniC (#GA 813834 pHioniC H 2020 MSCA ITN 2018). A.F.P. and M.M.A. are supported by PRIN 2017 “LIONESSE” project (#GA 754345) from the Italian Ministry for Education, University and Research. A.F.P., N.P. and M.M.A. are part of the Associated International Laboratory (CaPANCInv).

**Institutional Review Board Statement:** Not applicable.

**Informed Consent Statement:** Not applicable.

**Data Availability Statement:** Not applicable.

**Conflicts of Interest:** The authors declare no conflict of interest.

## References

1. Wei, R.; Liu, S.; Zhang, S.; Min, L.; Zhu, S. Cellular and Extracellular Components in Tumour Microenvironment and Their Application in Early Diagnosis of Cancers. *Anal. Cell. Pathol.* **2020**, *2020*, 6283796. [\[CrossRef\]](#)
2. Warburg, O. On the Origin of Cancer Cells. *Science* **1956**, *123*, 309–314. [\[CrossRef\]](#)
3. Cassim, S.; Vučetić, M.; Ždravević, M.; Pouyssegur, J. Warburg and Beyond: The Power of Mitochondrial Metabolism to Collaborate or Replace Fermentative Glycolysis in Cancer. *Cancers* **2020**, *12*, 1119. [\[CrossRef\]](#)
4. Marchiq, I.; Le Floch, R.; Roux, D.; Simon, M.-P.; Pouyssegur, J. Genetic Disruption of Lactate/H<sup>+</sup> Symporters (MCTs) and Their Subunit CD147/BASIGIN Sensitizes Glycolytic Tumour Cells to Phenformin. *Cancer Res.* **2015**, *75*, 171–180. [\[CrossRef\]](#)
5. Ždravević, M.; Brand, A.; Di Ianni, L.; Dettmer, K.; Reinders, J.; Singer, K.; Peter, K.; Schnell, A.; Bruss, C.; Decking, S.-M.; et al. Double Genetic Disruption of Lactate Dehydrogenases A and B Is Required to Ablate the “Warburg Effect” Restricting Tumour Growth to Oxidative Metabolism. *J. Biol. Chem.* **2018**, *293*, 15947–15961. [\[CrossRef\]](#)
6. Swietach, P.; Hulikova, A.; Vaughan-Jones, R.D.; Harris, A.L. New Insights into the Physiological Role of Carbonic Anhydrase IX in Tumour PH Regulation. *Oncogene* **2010**, *29*, 6509–6521. [\[CrossRef\]](#)
7. Petrova, V.; Annicchiarico-Petruzzelli, M.; Melino, G.; Amelio, I. The Hypoxic Tumour Microenvironment. *Oncogenesis* **2018**, *7*, 10. [\[CrossRef\]](#)
8. Boedtker, E.; Pedersen, S.F. The Acidic Tumour Microenvironment as a Driver of Cancer. *Annu. Rev. Physiol.* **2020**, *82*, 103–126. [\[CrossRef\]](#) [\[PubMed\]](#)
9. Webb, B.A.; Chimenti, M.; Jacobson, M.P.; Barber, D.L. Dysregulated PH: A Perfect Storm for Cancer Progression. *Nat. Rev. Cancer* **2011**, *11*, 671–677. [\[CrossRef\]](#)
10. Persi, E.; Duran-Frigola, M.; Damaghi, M.; Roush, W.R.; Aloy, P.; Cleveland, J.L.; Gillies, R.J.; Ruppin, E. Systems Analysis of Intracellular PH Vulnerabilities for Cancer Therapy. *Nat. Commun.* **2018**, *9*, 2997. [\[CrossRef\]](#) [\[PubMed\]](#)
11. Kazyken, D.; Lentz, S.I.; Fingar, D.C. Alkaline Intracellular PH (PHi) Activates AMPK–MTORC2 Signaling to Promote Cell Survival during Growth Factor Limitation. *J. Biol. Chem.* **2021**, *297*, 101100. [\[CrossRef\]](#) [\[PubMed\]](#)
12. Flinck, M.; Kramer, S.H.; Pedersen, S.F. Roles of PH in Control of Cell Proliferation. *Acta Physiol.* **2018**, *223*, e13068. [\[CrossRef\]](#) [\[PubMed\]](#)
13. Pérez-Tomás, R.; Pérez-Guillén, I. Lactate in the Tumour Microenvironment: An Essential Molecule in Cancer Progression and Treatment. *Cancers* **2020**, *12*, 3244. [\[CrossRef\]](#) [\[PubMed\]](#)
14. Flinck, M.; Kramer, S.H.; Schnipper, J.; Andersen, A.P.; Pedersen, S.F. The Acid-Base Transport Proteins NHE1 and NBCn1 Regulate Cell Cycle Progression in Human Breast Cancer Cells. *Cell Cycle* **2018**, *17*, 1056–1067. [\[CrossRef\]](#)
15. Rengifo Rodriguez, J.E.; Garcia-Perdomo, H.A. Role of Monocarboxylate Transporters in the Diagnosis, Progression, Prognosis, and Treatment of Prostate Cancer. *Turk. J. Urol.* **2020**, *46*, 413–418. [\[CrossRef\]](#)
16. Ward, C.; Meehan, J.; Gray, M.E.; Murray, A.F.; Argyle, D.J.; Kunkler, I.H.; Langdon, S.P. The Impact of Tumour PH on Cancer Progression: Strategies for Clinical Intervention. *Explor. Target. Anti-Tumour Ther.* **2020**, *1*, 71–100. [\[CrossRef\]](#)
17. Mboge, M.; Mahon, B.; McKenna, R.; Frost, S. Carbonic Anhydrases: Role in PH Control and Cancer. *Metabolites* **2018**, *8*, 19. [\[CrossRef\]](#)
18. Mookerjee, S.A.; Goncalves, R.L.S.; Gerencser, A.A.; Nicholls, D.G.; Brand, M.D. The Contributions of Respiration and Glycolysis to Extracellular Acid Production. *Biochim. Biophys. Acta BBA Bioenerg.* **2015**, *1847*, 171–181. [\[CrossRef\]](#)
19. Swietach, P. What Is PH Regulation, and Why Do Cancer Cells Need It? *Cancer Metastasis Rev.* **2019**, *38*, 5–15. [\[CrossRef\]](#)
20. Luoto, K.R.; Kumareswaran, R.; Bristow, R.G. Tumour Hypoxia as a Driving Force in Genetic Instability. *Genome Integr.* **2013**, *4*, 5. [\[CrossRef\]](#)
21. Muz, B.; de la Puente, P.; Azab, F.; Azab, A.K. The Role of Hypoxia in Cancer Progression, Angiogenesis, Metastasis, and Resistance to Therapy. *Hypoxia* **2015**, *3*, 83–92. [\[CrossRef\]](#) [\[PubMed\]](#)
22. Yang, C.; Zhong, Z.-F.; Wang, S.-P.; Vong, C.-T.; Yu, B.; Wang, Y.-T. HIF-1: Structure, Biology and Natural Modulators. *Chin. J. Nat. Med.* **2021**, *19*, 521–527. [\[CrossRef\]](#)
23. Doe, M.R.; Ascano, J.M.; Kaur, M.; Cole, M.D. Myc Posttranscriptionally Induces HIF1 Protein and Target Gene Expression in Normal and Cancer Cells. *Cancer Res.* **2012**, *72*, 949–957. [\[CrossRef\]](#) [\[PubMed\]](#)
24. Ippolito, L.; Morandi, A.; Giannoni, E.; Chiarugi, P. Lactate: A Metabolic Driver in the Tumour Landscape. *Trends Biochem. Sci.* **2019**, *44*, 153–166. [\[CrossRef\]](#)
25. Tam, S.Y.; Wu, V.W.C.; Law, H.K.W. Hypoxia-Induced Epithelial-Mesenchymal Transition in Cancers: HIF-1 $\alpha$  and beyond. *Front. Oncol.* **2020**, *10*, 486. [\[CrossRef\]](#)
26. Mazure, N.M.; Pouyssegur, J. Hypoxia-Induced Autophagy: Cell Death or Cell Survival? *Curr. Opin. Cell Biol.* **2010**, *22*, 177–180. [\[CrossRef\]](#)
27. Cosse, J.-P.; Michiels, C. Tumour Hypoxia Affects the Responsiveness of Cancer Cells to Chemotherapy and Promotes Cancer Progression. *Anti-Cancer Agents Med. Chem.* **2008**, *8*, 790–797. [\[CrossRef\]](#)
28. Muz, B.; de la Puente, P.; Azab, F.; Luderer, M.; Azab, A.K. Hypoxia Promotes Stem Cell-like Phenotype in Multiple Myeloma Cells. *Blood Cancer J.* **2014**, *4*, e262. [\[CrossRef\]](#)
29. Zhang, Q.; Han, Z.; Zhu, Y.; Chen, J.; Li, W. Role of Hypoxia Inducible Factor-1 in Cancer Stem Cells (Review). *Mol. Med. Rep.* **2020**, *23*, 17. [\[CrossRef\]](#)



30. Lv, Y.; Zhao, S.; Han, J.; Zheng, L.; Yang, Z.; Zhao, L. Hypoxia-Inducible Factor-1 $\alpha$  Induces Multidrug Resistance Protein in Colon Cancer. *Oncotargets Ther.* **2015**, *8*, 1941–1948. [[CrossRef](#)]
31. Li, D.-W.; Dong, P.; Wang, F.; Chen, X.-W.; Xu, C.-Z.; Zhou, L. Hypoxia Induced Multidrug Resistance of Laryngeal Cancer Cells via Hypoxia-Inducible Factor-1 $\alpha$ . *Asian Pac. J. Cancer Prev.* **2013**, *14*, 4853–4858. [[CrossRef](#)] [[PubMed](#)]
32. Li, J.; Wu, X.; Gan, L.; Yang, X.; Miao, Z. Hypoxia Induces Universal but Differential Drug Resistance and Impairs Anticancer Mechanisms of 5-Fluorouracil in Hepatoma Cells. *Acta Pharmacol. Sin.* **2017**, *38*, 1642–1654. [[CrossRef](#)] [[PubMed](#)]
33. Filatova, A.; Seidel, S.; Böğürçü, N.; Gräf, S.; Garvalov, B.K.; Acker, T. Acidosis Acts through HSP90 in a PHD/VHL-Independent Manner to Promote HIF Function and Stem Cell Maintenance in Glioma. *Cancer Res.* **2016**, *76*, 5845–5856. [[CrossRef](#)] [[PubMed](#)]
34. Wojtkowiak, J.W.; Verduzco, D.; Schramm, K.J.; Gillies, R.J. Drug Resistance and Cellular Adaptation to Tumour Acidic PH Microenvironment. *Mol. Pharm.* **2011**, *8*, 2032–2038. [[CrossRef](#)] [[PubMed](#)]
35. Lewis, C.E.; Pollard, J.W. Distinct Role of Macrophages in Different Tumour Microenvironments. *Cancer Res.* **2006**, *66*, 605–612. [[CrossRef](#)]
36. Pilon-Thomas, S.; Kodumudi, K.N.; El-Kenawi, A.E.; Russell, S.; Weber, A.M.; Luddy, K.; Damaghi, M.; Wojtkowiak, J.W.; Mulé, J.J.; Ibrahim-Hashim, A.; et al. Neutralization of Tumour Acidity Improves Antitumour Responses to Immunotherapy. *Cancer Res.* **2016**, *76*, 1381–1390. [[CrossRef](#)]
37. Brand, A.; Singer, K.; Koehl, G.E.; Kolitzus, M.; Schoenhammer, G.; Thiel, A.; Matos, C.; Bruss, C.; Klobuch, S.; Peter, K.; et al. LDHA-Associated Lactic Acid Production Blunts Tumour Immunosurveillance by T and NK Cells. *Cell Metab.* **2016**, *24*, 657–671. [[CrossRef](#)]
38. El-Kenawi, A.; Gatenbee, C.; Robertson-Tessi, M.; Bravo, R.; Dhillon, J.; Balagurunathan, Y.; Berglund, A.; Vishvakarma, N.; Ibrahim-Hashim, A.; Choi, J.; et al. Acidity Promotes Tumour Progression by Altering Macrophage Phenotype in Prostate Cancer. *Br. J. Cancer* **2019**, *121*, 556–566. [[CrossRef](#)]
39. Díaz, F.E.; Dantas, E.; Cabrera, M.; Benítez, C.A.; Delpino, M.V.; Duette, G.; Rubione, J.; Sanjuan, N.; Trevani, A.S.; Geffner, J. Fever-Range Hyperthermia Improves the Anti-Apoptotic Effect Induced by Low PH on Human Neutrophils Promoting a Proangiogenic Profile. *Cell Death Dis.* **2016**, *7*, e2437. [[CrossRef](#)]
40. Corbet, C.; Feron, O. Tumour Acidosis: From the Passenger to the Driver's Seat. *Nat. Rev. Cancer* **2017**, *17*, 577–593. [[CrossRef](#)]
41. Estrella, V.; Chen, T.; Lloyd, M.; Wojtkowiak, J.; Cornell, H.H.; Ibrahim-Hashim, A.; Bailey, K.; Balagurunathan, Y.; Rothberg, J.M.; Sloane, B.F.; et al. Acidity Generated by the Tumour Microenvironment Drives Local Invasion. *Cancer Res.* **2013**, *73*, 1524–1535. [[CrossRef](#)] [[PubMed](#)]
42. Rofstad, E.K.; Mathiesen, B.; Kindem, K.; Galappathi, K. Acidic Extracellular PH Promotes Experimental Metastasis of Human Melanoma Cells in Athymic Nude Mice. *Cancer Res.* **2006**, *66*, 6699–6707. [[CrossRef](#)] [[PubMed](#)]
43. Pedersen, S.F.; Novak, I.; Alves, F.; Schwab, A.; Pardo, L.A. Alternating PH Landscapes Shape Epithelial Cancer Initiation and Progression: Focus on Pancreatic Cancer. *BioEssays* **2017**, *39*, 1600253. [[CrossRef](#)] [[PubMed](#)]
44. Pethő, Z.; Najder, K.; Carvalho, T.; McMorro, R.; Todesca, L.M.; Rugi, M.; Bulk, E.; Chan, A.; Löwik, C.W.G.M.; Reshkin, S.J.; et al. PH-Channeling in Cancer: How PH-Dependence of Cation Channels Shapes Cancer Pathophysiology. *Cancers* **2020**, *12*, 2484. [[CrossRef](#)] [[PubMed](#)]
45. Islam, M.S. Calcium Signaling. In *Advances in Experimental Medicine and Biology*; Springer International Publishing: Cham, Switzerland, 2020; Volume 1131, ISBN 978-3-030-12456-4.
46. Berridge, M.J.; Bootman, M.D.; Roderick, H.L. Calcium Signalling: Dynamics, Homeostasis and Remodelling. *Nat. Rev. Mol. Cell Biol.* **2003**, *4*, 517–529. [[CrossRef](#)]
47. Clapham, D.E. Calcium Signaling. *Cell* **2007**, *131*, 1047–1058. [[CrossRef](#)]
48. Monteith, G.R.; Prevarskaya, N.; Roberts-Thomson, S.J. The Calcium–Cancer Signalling Nexus. *Nat. Rev. Cancer* **2017**, *17*, 373–380. [[CrossRef](#)]
49. Prevarskaya, N.; Ouadid-Ahidouch, H.; Skryma, R.; Shuba, Y. Remodelling of Ca<sup>2+</sup> Transport in Cancer: How It Contributes to Cancer Hallmarks? *Philos. Trans. R. Soc. B* **2014**, *369*, 20130097. [[CrossRef](#)]
50. Panda, S.; Chatterjee, O.; Roy, L.; Chatterjee, S. Targeting Ca<sup>2+</sup> Signaling: A New Arsenal against Cancer. *Drug Discov. Today* **2022**, *27*, 923–934. [[CrossRef](#)]
51. Negri, S.; Faris, P.; Berra-Romani, R.; Guerra, G.; Moccia, F. Endothelial Transient Receptor Potential Channels and Vascular Remodeling: Extracellular Ca<sup>2+</sup> Entry for Angiogenesis, Arteriogenesis and Vasculogenesis. *Front. Physiol.* **2020**, *10*, 1618. [[CrossRef](#)]
52. Scarpellino, G.; Munaron, L.; Cantelmo, A.R.; Fiorio Pla, A. Calcium-Permeable Channels in Tumour Vascularization: Peculiar Sensors of Microenvironmental Chemical and Physical Cues. In *From Malignant Transformation to Metastasis*; Stock, C., Pardo, L.A., Eds.; Reviews of Physiology, Biochemistry and Pharmacology; Springer International Publishing: Cham, Switzerland, 2020; Volume 182, pp. 111–137. ISBN 978-3-030-99799-1.
53. Catacuzzeno, L.; Sforza, L.; Esposito, V.; Limatola, C.; Franciolini, F. Ion Channels in Glioma Malignancy. In *Transportome Malfunction in the Cancer Spectrum*; Stock, C., Pardo, L.A., Eds.; Reviews of Physiology, Biochemistry and Pharmacology; Springer International Publishing: Cham, Switzerland, 2020; Volume 181, pp. 223–267. ISBN 978-3-030-90919-2.
54. Shapovalov, G.; Ritaine, A.; Skryma, R.; Prevarskaya, N. Role of TRP Ion Channels in Cancer and Tumourigenesis. *Semin. Immunopathol.* **2016**, *38*, 357–369. [[CrossRef](#)] [[PubMed](#)]

55. Seta, K.A.; Yuan, Y.; Spicer, Z.; Lu, G.; Bedard, J.; Ferguson, T.K.; Pathrose, P.; Cole-Strauss, A.; Kaufhold, A.; Millhorn, D.E. The Role of Calcium in Hypoxia-Induced Signal Transduction and Gene Expression. *Cell Calcium* **2004**, *36*, 331–340. [[CrossRef](#)] [[PubMed](#)]
56. Tajada, S. Calcium Permeable Channels in Cancer Hallmarks. *Front. Pharmacol.* **2020**, *11*, 19. [[CrossRef](#)] [[PubMed](#)]
57. Glitsch, M. Protons and  $\text{Ca}^{2+}$ : Ionic Allies in Tumour Progression? *Physiology* **2011**, *26*, 252–265. [[CrossRef](#)]
58. Prevarskaya, N.; Skryma, R.; Shuba, Y. Ion Channels in Cancer: Are Cancer Hallmarks Oncochannelopathies? *Physiol. Rev.* **2018**, *98*, 559–621. [[CrossRef](#)]
59. Girault, A.; Ahidouch, A.; Ouadid-Ahidouch, H. Roles for  $\text{Ca}^{2+}$  and  $\text{K}^{+}$  Channels in Cancer Cells Exposed to the Hypoxic Tumour Microenvironment. *Biochim. Biophys. Acta BBA Mol. Cell Res.* **2020**, *1867*, 118644. [[CrossRef](#)]
60. Shimoda, L.A.; Polak, J. Hypoxia. 4. Hypoxia and Ion Channel Function. *Am. J. Physiol. Cell Physiol.* **2011**, *300*, C951–C967. [[CrossRef](#)]
61. Glitsch, M. Mechano- and PH-Sensing Convergence on  $\text{Ca}^{2+}$ -Mobilising Proteins—A Recipe for Cancer? *Cell Calcium* **2019**, *80*, 38–45. [[CrossRef](#)]
62. Bae, C.; Sachs, F.; Gottlieb, P.A. Protonation of the Human PIEZO1 Ion Channel Stabilizes Inactivation. *J. Biol. Chem.* **2015**, *290*, 5167–5173. [[CrossRef](#)]
63. Kuntze, A.; Goetsch, O.; Fels, B.; Najder, K.; Unger, A.; Wilhelmi, M.; Sargin, S.; Schimmelpfennig, S.; Neumann, I.; Schwab, A.; et al. Protonation of Piezo1 Impairs Cell-Matrix Interactions of Pancreatic Stellate Cells. *Front. Physiol.* **2020**, *11*, 89. [[CrossRef](#)]
64. Starkus, J.G.; Fleig, A.; Penner, R. The Calcium-Permeable Non-Selective Cation Channel TRPM2 Is Modulated by Cellular Acidification: Proton-Induced Inhibition of TRPM2. *J. Physiol.* **2010**, *588*, 1227–1240. [[CrossRef](#)] [[PubMed](#)]
65. Du, J.; Xie, J.; Yue, L. Modulation of TRPM2 by Acidic PH and the Underlying Mechanisms for PH Sensitivity. *J. Gen. Physiol.* **2009**, *134*, 471–488. [[CrossRef](#)] [[PubMed](#)]
66. Yang, W.; Zou, J.; Xia, R.; Vaal, M.L.; Seymour, V.A.; Luo, J.; Beech, D.J.; Jiang, L.-H. State-Dependent Inhibition of TRPM2 Channel by Acidic PH. *J. Biol. Chem.* **2010**, *285*, 30411–30418. [[CrossRef](#)] [[PubMed](#)]
67. Zou, J.; Yang, W.; Beech, D.J.; Jiang, L.-H. A Residue in the TRPM2 Channel Outer Pore Is Crucial in Determining Species-Dependent Sensitivity to Extracellular Acidic PH. *Pflug. Arch. Eur. J. Physiol.* **2011**, *462*, 293–302. [[CrossRef](#)]
68. Gwanyanya, A.; Amuzescu, B.; Zakharov, S.I.; Macianskiene, R.; Sipido, K.R.; Bolotina, V.M.; Vereecke, J.; Mubagwa, K. Magnesium-Inhibited, TRPM6/7-like Channel in Cardiac Myocytes: Permeation of Divalent Cations and PH-Mediated Regulation: Cardiac TRPM6/7-like Channels. *J. Physiol.* **2004**, *559*, 761–776. [[CrossRef](#)] [[PubMed](#)]
69. Li, M.; Jiang, J.; Yue, L. Functional Characterization of Homo- and Heteromeric Channel Kinases TRPM6 and TRPM7. *J. Gen. Physiol.* **2006**, *127*, 525–537. [[CrossRef](#)]
70. Kozak, J.A.; Matsushita, M.; Nairn, A.C.; Cahalan, M.D. Charge Screening by Internal PH and Polyvalent Cations as a Mechanism for Activation, Inhibition, and Rundown of TRPM7/MIC Channels. *J. Gen. Physiol.* **2005**, *126*, 499–514. [[CrossRef](#)]
71. Chokshi, R.; Matsushita, M.; Kozak, J.A. Detailed Examination of  $\text{Mg}^{2+}$  and PH Sensitivity of Human TRPM7 Channels. *Am. J. Physiol. Cell Physiol.* **2012**, *302*, C1004–C1011. [[CrossRef](#)]
72. Chu, X.; Zhu, X.; Wei, W.; Li, G.; Simon, R.P.; MacDonald, J.F.; Xiong, Z. Acidosis Decreases Low  $\text{Ca}^{2+}$ -induced Neuronal Excitation by Inhibiting the Activity of Calcium-sensing Cation Channels in Cultured Mouse Hippocampal Neurons. *J. Physiol.* **2003**, *550*, 385–399. [[CrossRef](#)]
73. Jiang, J.; Li, M.; Yue, L. Potentiation of TRPM7 Inward Currents by Protons. *J. Gen. Physiol.* **2005**, *126*, 137–150. [[CrossRef](#)]
74. Numata, T.; Sato-Numata, K.; Okada, Y. TRPM7 Is Involved in Acid-Induced Necrotic Cell Death in a Manner Sensitive to Progesterone in Human Cervical Cancer Cells: Role of TRPM7 in Cervical Cancer Cell Death. *Physiol. Rep.* **2019**, *7*, e14157. [[CrossRef](#)] [[PubMed](#)]
75. Mačianskienė, R.; Almanaitytė, M.; Jekabsone, A.; Mubagwa, K. Modulation of Human Cardiac TRPM7 Current by Extracellular Acidic PH Depends upon Extracellular Concentrations of Divalent Cations. *PLoS ONE* **2017**, *12*, e0170923. [[CrossRef](#)] [[PubMed](#)]
76. Heber, S.; Ciotu, C.I.; Hartner, G.; Gold-Binder, M.; Ninidze, N.; Gleiss, A.; Kress, H.-G.; Fischer, M.J.M. TRPV1 Antagonist BCTC Inhibits PH 6.0-Induced Pain in Human Skin. *Pain* **2020**, *161*, 1532–1541. [[CrossRef](#)] [[PubMed](#)]
77. Ryu, S.; Liu, B.; Yao, J.; Fu, Q.; Qin, F. Uncoupling Proton Activation of Vanilloid Receptor TRPV1. *J. Neurosci.* **2007**, *27*, 12797–12807. [[CrossRef](#)]
78. Tominaga, M.; Caterina, M.J.; Malmberg, A.B.; Rosen, T.A.; Gilbert, H.; Skinner, K.; Raumann, B.E.; Basbaum, A.I.; Julius, D. The Cloned Capsaicin Receptor Integrates Multiple Pain-Producing Stimuli. *Neuron* **1998**, *21*, 531–543. [[CrossRef](#)]
79. Nakanishi, M.; Morita, Y.; Hata, K.; Muragaki, Y. Acidic Microenvironments Induce Lymphangiogenesis and IL-8 Production via TRPV1 Activation in Human Lymphatic Endothelial Cells. *Exp. Cell Res.* **2016**, *345*, 180–189. [[CrossRef](#)]
80. Gao, L.; Yang, P.; Qin, P.; Lu, Y.; Li, X.; Tian, Q.; Li, Y.; Xie, C.; Tian, J.; Zhang, C.; et al. Selective Potentiation of 2-APB-Induced Activation of TRPV1–3 Channels by Acid. *Sci. Rep.* **2016**, *6*, 20791. [[CrossRef](#)]
81. Cao, X.; Yang, F.; Zheng, J.; Wang, K. Intracellular Proton-Mediated Activation of TRPV3 Channels Accounts for the Exfoliation Effect of  $\alpha$ -Hydroxyl Acids on Keratinocytes. *J. Biol. Chem.* **2012**, *287*, 25905–25916. [[CrossRef](#)]
82. Suzuki, M.; Mizuno, A.; Kodaira, K.; Imai, M. Impaired Pressure Sensation in Mice Lacking TRPV4. *J. Biol. Chem.* **2003**, *278*, 22664–22668. [[CrossRef](#)] [[PubMed](#)]

83. Shikano, M.; Ueda, T.; Kamiya, T.; Ishida, Y.; Yamada, T.; Mizushima, T.; Shimura, T.; Mizoshita, T.; Tanida, S.; Kataoka, H.; et al. Acid Inhibits TRPV4-Mediated  $\text{Ca}^{2+}$  Influx in Mouse Esophageal Epithelial Cells: Acid-Sensitive TRPV4 in the Esophageal Epithelium. *Neurogastroenterol. Motil.* **2011**, *23*, 1020–e497. [[CrossRef](#)]
84. Cherezova, A.L.; Negulyaev, J.A.; Zenin, V.V.; Semenova, S.B. Extracellular PH Regulates the Entry of Calcium into Jurkat T-Cells. *Cell Tiss. Biol.* **2018**, *12*, 41–47. [[CrossRef](#)]
85. De la Roche, J.; Eberhardt, M.J.; Klinger, A.B.; Stanslowsky, N.; Wegner, F.; Koppert, W.; Reeh, P.W.; Lampert, A.; Fischer, M.J.M.; Leffler, A. The Molecular Basis for Species-Specific Activation of Human TRPA1 Protein by Protons Involves Poorly Conserved Residues within Transmembrane Domains 5 and 6. *J. Biol. Chem.* **2013**, *288*, 20280–20292. [[CrossRef](#)] [[PubMed](#)]
86. Semtner, M.; Schaefer, M.; Pinkenburg, O.; Plant, T.D. Potentiation of TRPC5 by Protons. *J. Biol. Chem.* **2007**, *282*, 33868–33878. [[CrossRef](#)] [[PubMed](#)]
87. Thakur, D.P.; Wang, Q.; Jeon, J.; Tian, J.; Zhu, M.X. Intracellular Acidification Facilitates Receptor-operated TRPC4 Activation through PLC $\delta$ 1 in a  $\text{Ca}^{2+}$ -dependent Manner. *J. Physiol.* **2020**, *598*, 2651–2667. [[CrossRef](#)]
88. Malayev, A.; Nelson, D.J. Extracellular PH Modulates the  $\text{Ca}^{2+}$  Current Activated by Depletion of Intracellular  $\text{Ca}^{2+}$  Stores in Human Macrophages. *J. Membr. Biol.* **1995**, *146*, 101–111. [[CrossRef](#)]
89. Scrimgeour, N.R.; Wilson, D.P.; Rychkov, G.Y. Glu106 in the Orai1 Pore Contributes to Fast  $\text{Ca}^{2+}$ -Dependent Inactivation and PH Dependence of  $\text{Ca}^{2+}$  Release-Activated  $\text{Ca}^{2+}$  (CRAC) Current. *Biochem. J.* **2012**, *441*, 743–753. [[CrossRef](#)]
90. Beck, A.; Fleig, A.; Penner, R.; Peinelt, C. Regulation of Endogenous and Heterologous  $\text{Ca}^{2+}$  Release-Activated  $\text{Ca}^{2+}$  Currents by PH. *Cell Calcium* **2014**, *56*, 235–243. [[CrossRef](#)]
91. Tsujikawa, H.; Yu, A.S.; Xie, J.; Yue, Z.; Yang, W.; He, Y.; Yue, L. Identification of Key Amino Acid Residues Responsible for Internal and External PH Sensitivity of Orai1/STIM1 Channels. *Sci. Rep.* **2015**, *5*, 16747. [[CrossRef](#)]
92. Mancarella, S.; Wang, Y.; Deng, X.; Landesberg, G.; Scalia, R.; Panettieri, R.A.; Mallilankaraman, K.; Tang, X.D.; Madesh, M.; Gill, D.L. Hypoxia-Induced Acidosis Uncouples the STIM-Orai Calcium Signaling Complex. *J. Biol. Chem.* **2011**, *286*, 44788–44798. [[CrossRef](#)]
93. Laskay, G.; Kálmán, K.; Van Kerkhove, E.; Steels, P.; Ameloot, M. Store-Operated  $\text{Ca}^{2+}$ -Channels Are Sensitive to Changes in Extracellular PH. *Biochem. Biophys. Res. Commun.* **2005**, *337*, 571–579. [[CrossRef](#)]
94. Vandorpe, D.H.; Xu, C.; Shmukler, B.E.; Otterbein, L.E.; Trudel, M.; Sachs, F.; Gottlieb, P.A.; Brugnara, C.; Alper, S.L. Hypoxia Activates a  $\text{Ca}^{2+}$ -Permeable Cation Conductance Sensitive to Carbon Monoxide and to GsMTx-4 in Human and Mouse Sickle Erythrocytes. *PLoS ONE* **2010**, *5*, e8732. [[CrossRef](#)] [[PubMed](#)]
95. Liao, J.; Lu, W.; Chen, Y.; Duan, X.; Zhang, C.; Luo, X.; Lin, Z.; Chen, J.; Liu, S.; Yan, H.; et al. Upregulation of Piezo1 (Piezo Type Mechanosensitive Ion Channel Component 1) Enhances the Intracellular Free Calcium in Pulmonary Arterial Smooth Muscle Cells from Idiopathic Pulmonary Arterial Hypertension Patients. *Hypertension* **2021**, *77*, 1974–1989. [[CrossRef](#)] [[PubMed](#)]
96. Wang, Z.; Chen, J.; Babicheva, A.; Jain, P.P.; Rodriguez, M.; Ayon, R.J.; Ravellette, K.S.; Wu, L.; Balistreri, F.; Tang, H.; et al. Endothelial Upregulation of Mechanosensitive Channel Piezo1 in Pulmonary Hypertension. *Am. J. Physiol. Cell Physiol.* **2021**, *321*, C1010–C1027. [[CrossRef](#)] [[PubMed](#)]
97. Huang, S.; Turlova, E.; Li, F.; Bao, M.; Szeto, V.; Wong, R.; Abussaud, A.; Wang, H.; Zhu, S.; Gao, X.; et al. Transient Receptor Potential Melastatin 2 Channels (TRPM2) Mediate Neonatal Hypoxic-Ischemic Brain Injury in Mice. *Exp. Neurol.* **2017**, *296*, 32–40. [[CrossRef](#)]
98. Kaneko, S.; Kawakami, S.; Hara, Y.; Wakamori, M.; Itoh, E.; Minami, T.; Takada, Y.; Kume, T.; Katsuki, H.; Mori, Y.; et al. A Critical Role of TRPM2 in Neuronal Cell Death by Hydrogen Peroxide. *J. Pharmacol. Sci.* **2006**, *101*, 66–76. [[CrossRef](#)]
99. Duzgun Ergun, D.; Dursun, S.; Pastaci Ozsobaci, N.; Hatirnaz Ng, O.; Naziroglu, M.; Ozelik, D. The Potential Protective Roles of Zinc, Selenium and Glutathione on Hypoxia-Induced TRPM2 Channel Activation in Transfected HEK293 Cells. *J. Recept. Signal Transduct.* **2020**, *40*, 521–530. [[CrossRef](#)]
100. Özkaya, D.; Naziroğlu, M.; Vanyorek, L.; Muhamad, S. Involvement of TRPM2 Channel on Hypoxia-Induced Oxidative Injury, Inflammation, and Cell Death in Retinal Pigment Epithelial Cells: Modulator Action of Selenium Nanoparticles. *Biol. Trace Elem. Res.* **2021**, *199*, 1356–1369. [[CrossRef](#)]
101. Ferrera, L.; Barbieri, R.; Picco, C.; Zuccolini, P.; Remigante, A.; Bertelli, S.; Fumagalli, M.R.; Zifarelli, G.; La Porta, C.A.M.; Gavazzo, P.; et al. TRPM2 Oxidation Activates Two Distinct Potassium Channels in Melanoma Cells through Intracellular Calcium Increase. *Int. J. Mol. Sci.* **2021**, *22*, 8359. [[CrossRef](#)]
102. Wang, Q.; Huang, L.; Yue, J. Oxidative Stress Activates the TRPM2- $\text{Ca}^{2+}$ -CaMKII-ROS Signaling Loop to Induce Cell Death in Cancer Cells. *Biochim. Biophys. Acta BBA Mol. Cell Res.* **2017**, *1864*, 957–967. [[CrossRef](#)]
103. Chen, S.; Hoffman, N.E.; Shanmughapriya, S.; Bao, L.; Keefer, K.; Conrad, K.; Merali, S.; Takahashi, Y.; Abraham, T.; Hirschler-Laszkiewicz, I.; et al. A Splice Variant of the Human Ion Channel TRPM2 Modulates Neuroblastoma Tumour Growth through Hypoxia-Inducible Factor (HIF)-1/2 $\alpha$ . *J. Biol. Chem.* **2014**, *289*, 36284–36302. [[CrossRef](#)]
104. Gershkovitz, M.; Caspi, Y.; Fainsod-Levi, T.; Katz, B.; Michaeli, J.; Khawaled, S.; Lev, S.; Polyansky, L.; Shaul, M.E.; Sionov, R.V.; et al. TRPM2 Mediates Neutrophil Killing of Disseminated Tumour Cells. *Cancer Res.* **2018**, *78*, 2680–2690. [[CrossRef](#)] [[PubMed](#)]
105. Bilecik, T.; Karateke, F.; Elkan, H.; Gokce, H. The Effects of TRPM2, TRPM6, TRPM7 and TRPM8 Gene Expression in Hepatic Ischemia Reperfusion Injury. *Eur. Rev. Med. Pharmacol. Sci.* **2019**, *23*, 3088–3095. [[PubMed](#)]



106. Aarts, M.; Iihara, K.; Wei, W.-L.; Xiong, Z.-G.; Arundine, M.; Cerwinski, W.; MacDonald, J.F.; Tymianski, M. A Key Role for TRPM7 Channels in Anoxic Neuronal Death. *Cell* **2003**, *115*, 863–877. [[CrossRef](#)]
107. Kim, K.S.; Yoo, H.Y.; Park, K.S.; Kim, J.K.; Zhang, Y.-H.; Kim, S.J. Differential Effects of Acute Hypoxia on the Activation of TRPV1 by Capsaicin and Acidic PH. *J. Physiol. Sci.* **2012**, *62*, 93–103. [[CrossRef](#)] [[PubMed](#)]
108. Ristoiu, V.; Shibasaki, K.; Uchida, K.; Zhou, Y.; Ton, B.-H.T.; Flonta, M.-L.; Tominaga, M. Hypoxia-Induced Sensitization of Transient Receptor Potential Vanilloid 1 Involves Activation of Hypoxia-Inducible Factor-1 Alpha and PKC. *Pain* **2011**, *152*, 936–945. [[CrossRef](#)] [[PubMed](#)]
109. Parpaite, T.; Cardouat, G.; Mauroux, M.; Gillibert-Duplantier, J.; Robillard, P.; Quignard, J.-F.; Marthan, R.; Savineau, J.-P.; Ducret, T. Effect of Hypoxia on TRPV1 and TRPV4 Channels in Rat Pulmonary Arterial Smooth Muscle Cells. *Pflug. Arch. Eur. J. Physiol.* **2016**, *468*, 111–130. [[CrossRef](#)]
110. Wang, Y.X.; Wang, J.; Wang, C.; Liu, J.; Shi, L.P.; Xu, M.; Wang, C. Functional Expression of Transient Receptor Potential Vanilloid-Related Channels in Chronically Hypoxic Human Pulmonary Arterial Smooth Muscle Cells. *J. Membr. Biol.* **2008**, *223*, 151–159. [[CrossRef](#)]
111. Ma, W.; Li, C.; Yin, S.; Liu, J.; Gao, C.; Lin, Z.; Huang, R.; Huang, J.; Li, Z. Novel Role of TRPV2 in Promoting the Cytotoxicity of H<sub>2</sub>O<sub>2</sub>-Mediated Oxidative Stress in Human Hepatoma Cells. *Free. Radic. Biol. Med.* **2015**, *89*, 1003–1013. [[CrossRef](#)]
112. Wang, J.; Chen, X.; Huang, W. MicroRNA-369 Attenuates Hypoxia-Induced Cardiomyocyte Apoptosis and Inflammation via Targeting TRPV3. *Braz. J. Med. Biol. Res.* **2021**, *54*, e10550. [[CrossRef](#)]
113. Zhang, Q.; Cao, Y.; Luo, Q.; Wang, P.; Shi, P.; Song, C.; Mingyao, E.; Ren, J.; Fu, B.; Sun, H. The Transient Receptor Potential Vanilloid-3 Regulates Hypoxia-Mediated Pulmonary Artery Smooth Muscle Cells Proliferation via PI3K/AKT Signaling Pathway. *Cell Prolif.* **2018**, *51*, e12436. [[CrossRef](#)]
114. Karttunen, S.; Duffield, M.; Scrimgeour, N.R.; Squires, L.; Lim, W.L.; Dallas, M.L.; Scragg, J.L.; Chicher, J.; Dave, K.A.; Whitelaw, M.L.; et al. Oxygen-Dependent Hydroxylation by Factor Inhibiting HIF (FIH) Regulates the TRPV3 Ion Channel. *J. Cell Sci.* **2015**, *128*, 225–231. [[CrossRef](#)] [[PubMed](#)]
115. Wu, Q.-F.; Qian, C.; Zhao, N.; Dong, Q.; Li, J.; Wang, B.-B.; Chen, L.; Yu, L.; Han, B.; Du, Y.-M.; et al. Activation of Transient Receptor Potential Vanilloid 4 Involves in Hypoxia/Reoxygenation Injury in Cardiomyocytes. *Cell Death Dis.* **2017**, *8*, e2828. [[CrossRef](#)] [[PubMed](#)]
116. Butenko, O.; Dzamba, D.; Benesova, J.; Honsa, P.; Benfenati, V.; Rusnakova, V.; Ferroni, S.; Anderova, M. The Increased Activity of TRPV4 Channel in the Astrocytes of the Adult Rat Hippocampus after Cerebral Hypoxia/Ischemia. *PLoS ONE* **2012**, *7*, e39959. [[CrossRef](#)]
117. Takahashi, N.; Chen, H.-Y.; Harris, I.S.; Stover, D.G.; Selfors, L.M.; Bronson, R.T.; Deraedt, T.; Cichowski, K.; Welm, A.L.; Mori, Y.; et al. Cancer Cells Co-Opt the Neuronal Redox-Sensing Channel TRPA1 to Promote Oxidative-Stress Tolerance. *Cancer Cell* **2018**, *33*, 985–1003.e7. [[CrossRef](#)]
118. Hamilton, N.B.; Kolodziejczyk, K.; Kougioumtzidou, E.; Attwell, D. Proton-Gated Ca<sup>2+</sup>-Permeable TRP Channels Damage Myelin in Conditions Mimicking Ischaemia. *Nature* **2016**, *529*, 523–527. [[CrossRef](#)]
119. Wang, B.; Li, W.; Meng, X.; Zou, F. Hypoxia Up-Regulates Vascular Endothelial Growth Factor in U-87 MG Cells: Involvement of TRPC1. *Neurosci. Lett.* **2009**, *459*, 132–136. [[CrossRef](#)] [[PubMed](#)]
120. Azimi, I.; Milevskiy, M.J.G.; Kaemmerer, E.; Turner, D.; Yapa, K.T.D.S.; Brown, M.A.; Thompson, E.W.; Roberts-Thomson, S.J.; Monteith, G.R. TRPC1 Is a Differential Regulator of Hypoxia-Mediated Events and Akt Signalling in PTEN-Deficient Breast Cancer Cells. *J. Cell Sci.* **2017**, *130*, 2292–2305. [[CrossRef](#)] [[PubMed](#)]
121. Zhu, Y.; Pan, Q.; Meng, H.; Jiang, Y.; Mao, A.; Wang, T.; Hua, D.; Yao, X.; Jin, J.; Ma, X. Enhancement of Vascular Endothelial Growth Factor Release in Long-Term Drug-Treated Breast Cancer via Transient Receptor Potential Channel 5-Ca<sup>2+</sup>-Hypoxia-Inducible Factor 1 $\alpha$  Pathway. *Pharmacol. Res.* **2015**, *93*, 36–42. [[CrossRef](#)] [[PubMed](#)]
122. Chen, Z.; Zhu, Y.; Dong, Y.; Zhang, P.; Han, X.; Jin, J.; Ma, X. Overexpression of TrpC5 Promotes Tumour Metastasis via the HIF-1 $\alpha$ -Twist Signaling Pathway in Colon Cancer. *Clin. Sci.* **2017**, *131*, 2439–2450. [[CrossRef](#)]
123. Nielsen, N.; Kondratska, K.; Ruck, T.; Hild, B.; Kovalenko, I.; Schimmelpfennig, S.; Welzig, J.; Sargin, S.; Lindemann, O.; Christian, S.; et al. TRPC6 Channels Modulate the Response of Pancreatic Stellate Cells to Hypoxia. *Pflug. Arch. Eur. J. Physiol.* **2017**, *469*, 1567–1577. [[CrossRef](#)]
124. Iyer, S.C.; Kannan, A.; Gopal, A.; Devaraj, N.; Halagowder, D. Receptor Channel TRPC6 Orchestrate the Activation of Human Hepatic Stellate Cell under Hypoxia Condition. *Exp. Cell Res.* **2015**, *336*, 66–75. [[CrossRef](#)] [[PubMed](#)]
125. Wen, L.; Liang, C.; Chen, E.; Chen, W.; Liang, F.; Zhi, X.; Wei, T.; Xue, F.; Li, G.; Yang, Q.; et al. Regulation of Multi-Drug Resistance in Hepatocellular Carcinoma Cells Is TRPC6/Calcium Dependent. *Sci. Rep.* **2016**, *6*, 23269. [[CrossRef](#)] [[PubMed](#)]
126. Chigurupati, S.; Venkataraman, R.; Barrera, D.; Naganathan, A.; Madan, M.; Paul, L.; Pattisapu, J.V.; Kyriazis, G.A.; Sugaya, K.; Bushnev, S.; et al. Receptor Channel TRPC6 Is a Key Mediator of Notch-Driven Glioblastoma Growth and Invasiveness. *Cancer Res.* **2010**, *70*, 418–427. [[CrossRef](#)] [[PubMed](#)]
127. Wang, Y.; He, J.; Jiang, H.; Zhang, Q.; Yang, H.; Xu, X.; Zhang, C.; Xu, C.; Wang, J.; Lu, W. Nicotine Enhances Store-operated Calcium Entry by Upregulating HIF-1 $\alpha$  and SOCC Components in Non-small Cell Lung Cancer Cells. *Oncol. Rep.* **2018**. [[CrossRef](#)]
128. Liu, X.; Wang, T.; Wang, Y.; Chen, Z.; Hua, D.; Yao, X.; Ma, X.; Zhang, P. Orai1 Is Critical for Notch-Driven Aggressiveness under Hypoxic Conditions in Triple-Negative Breast Cancers. *Biochim. Biophys. Acta BBA Mol. Basis Dis.* **2018**, *1864*, 975–986. [[CrossRef](#)]



129. Liu, X.; Wan, X.; Kan, H.; Wang, Y.; Yu, F.; Feng, L.; Jin, J.; Zhang, P.; Ma, X. Hypoxia-Induced Upregulation of Orai1 Drives Colon Cancer Invasiveness and Angiogenesis. *Eur. J. Pharmacol.* **2018**, *832*, 1–10. [[CrossRef](#)]
130. Coste, B.; Mathur, J.; Schmidt, M.; Earley, T.J.; Ranade, S.; Petrus, M.J.; Dubin, A.E.; Patapoutian, A. Piezo1 and Piezo2 Are Essential Components of Distinct Mechanically Activated Cation Channels. *Science* **2010**, *330*, 55–60. [[CrossRef](#)]
131. Parpaite, T.; Coste, B. Piezo Channels. *Curr. Biol.* **2017**, *27*, R250–R252. [[CrossRef](#)]
132. De Felice, D.; Alaimo, A. Mechanosensitive Piezo Channels in Cancer: Focus on Altered Calcium Signaling in Cancer Cells and in Tumour Progression. *Cancers* **2020**, *12*, 1780. [[CrossRef](#)]
133. Pardo-Pastor, C.; Rubio-Moscardo, F.; Vogel-González, M.; Serra, S.A.; Afthinos, A.; Mrkonjic, S.; Destaing, O.; Abenza, J.F.; Fernández-Fernández, J.M.; Trepát, X.; et al. Piezo2 Channel Regulates RhoA and Actin Cytoskeleton to Promote Cell Mechanobiological Responses. *Proc. Natl. Acad. Sci. USA* **2018**, *115*, 1925–1930. [[CrossRef](#)]
134. Chen, X.; Wanggou, S.; Bodalia, A.; Zhu, M.; Dong, W.; Fan, J.J.; Yin, W.C.; Min, H.-K.; Hu, M.; Draghici, D.; et al. A Feedforward Mechanism Mediated by Mechanosensitive Ion Channel PIEZO1 and Tissue Mechanics Promotes Glioma Aggression. *Neuron* **2018**, *100*, 799–815.e7. [[CrossRef](#)] [[PubMed](#)]
135. Yang, H.; Liu, C.; Zhou, R.-M.; Yao, J.; Li, X.-M.; Shen, Y.; Cheng, H.; Yuan, J.; Yan, B.; Jiang, Q. Piezo2 Protein: A Novel Regulator of Tumour Angiogenesis and Hyperpermeability. *Oncotarget* **2016**, *7*, 44630–44643. [[CrossRef](#)] [[PubMed](#)]
136. Zhang, J.; Zhou, Y.; Huang, T.; Wu, F.; Liu, L.; Kwan, J.S.H.; Cheng, A.S.L.; Yu, J.; To, K.F.; Kang, W. PIEZO1 Functions as a Potential Oncogene by Promoting Cell Proliferation and Migration in Gastric Carcinogenesis. *Mol. Carcinog.* **2018**, *57*, 1144–1155. [[CrossRef](#)] [[PubMed](#)]
137. Dombroski, J.A.; Hope, J.M.; Sarna, N.S.; King, M.R. Channeling the Force: Piezo1 Mechanotransduction in Cancer Metastasis. *Cells* **2021**, *10*, 2815. [[CrossRef](#)] [[PubMed](#)]
138. Martin, C.; Pedersen, S.F.; Schwab, A.; Stock, C. Intracellular PH Gradients in Migrating Cells. *Am. J. Physiol. Cell Physiol.* **2011**, *300*, C490–C495. [[CrossRef](#)]
139. Hertz, L.; Huisjes, R.; Llaudet-Planas, E.; Petkova-Kirova, P.; Makhro, A.; Danielczok, J.G.; Egee, S.; del Mar Mañú-Pereira, M.; van Wijk, R.; Vives Corrons, J.-L.; et al. Is Increased Intracellular Calcium in Red Blood Cells a Common Component in the Molecular Mechanism Causing Anemia? *Front. Physiol.* **2017**, *8*, 673. [[CrossRef](#)]
140. Wulff, H.; Castle, N.A. Therapeutic Potential of K<sub>Ca</sub>3.1 Blockers: Recent Advances and Promising Trends. *Expert Rev. Clin. Pharmacol.* **2010**, *3*, 385–396. [[CrossRef](#)]
141. Hara, Y.; Wakamori, M.; Ishii, M.; Maeno, E.; Nishida, M.; Yoshida, T.; Yamada, H.; Shimizu, S.; Mori, E.; Kudoh, J.; et al. LTRPC2 Ca<sup>2+</sup>-Permeable Channel Activated by Changes in Redox Status Confers Susceptibility to Cell Death. *Mol. Cell* **2002**, *9*, 163–173. [[CrossRef](#)]
142. Kolisek, M.; Beck, A.; Fleig, A.; Penner, R. Cyclic ADP-Ribose and Hydrogen Peroxide Synergize with ADP-Ribose in the Activation of TRPM2 Channels. *Mol. Cell* **2005**, *18*, 61–69. [[CrossRef](#)]
143. McHugh, D.; Flemming, R.; Xu, S.-Z.; Perraud, A.-L.; Beech, D.J. Critical Intracellular Ca<sup>2+</sup> Dependence of Transient Receptor Potential Melastatin 2 (TRPM2) Cation Channel Activation. *J. Biol. Chem.* **2003**, *278*, 11002–11006. [[CrossRef](#)]
144. Perraud, A.-L.; Takanishi, C.L.; Shen, B.; Kang, S.; Smith, M.K.; Schmitz, C.; Knowles, H.M.; Ferraris, D.; Li, W.; Zhang, J.; et al. Accumulation of Free ADP-Ribose from Mitochondria Mediates Oxidative Stress-Induced Gating of TRPM2 Cation Channels. *J. Biol. Chem.* **2005**, *280*, 6138–6148. [[CrossRef](#)] [[PubMed](#)]
145. Turlova, E.; Feng, Z.; Sun, H. The Role of TRPM2 Channels in Neurons, Glial Cells and the Blood-Brain Barrier in Cerebral Ischemia and Hypoxia. *Acta Pharmacol. Sin.* **2018**, *39*, 713–721. [[CrossRef](#)] [[PubMed](#)]
146. Mai, C.; Mankoo, H.; Wei, L.; An, X.; Li, C.; Li, D.; Jiang, L. TRPM2 Channel: A Novel Target for Alleviating Ischaemia-reperfusion, Chronic Cerebral Hypo-perfusion and Neonatal Hypoxic-ischaemic Brain Damage. *J. Cell. Mol. Med.* **2020**, *24*, 4–12. [[CrossRef](#)] [[PubMed](#)]
147. Miller, B.A. TRPM2 in Cancer. *Cell Calcium* **2019**, *80*, 8–17. [[CrossRef](#)]
148. Zhao, L.-Y.; Xu, W.-L.; Xu, Z.-Q.; Qi, C.; Li, Y.; Cheng, J.; Liu, L.-K.; Wu, Y.-N.; Gao, J.; Ye, J.-H. The Overexpressed Functional Transient Receptor Potential Channel TRPM2 in Oral Squamous Cell Carcinoma. *Sci. Rep.* **2016**, *6*, 38471. [[CrossRef](#)]
149. Zeng, X.; Sikka, S.C.; Huang, L.; Sun, C.; Xu, C.; Jia, D.; Abdel-Mageed, A.B.; Pottle, J.E.; Taylor, J.T.; Li, M. Novel Role for the Transient Receptor Potential Channel TRPM2 in Prostate Cancer Cell Proliferation. *Prostate Cancer Prostatic Dis.* **2010**, *13*, 195–201. [[CrossRef](#)]
150. Hopkins, M.M.; Feng, X.; Liu, M.; Parker, L.P.; Koh, D.W. Inhibition of the Transient Receptor Potential Melastatin-2 Channel Causes Increased DNA Damage and Decreased Proliferation in Breast Adenocarcinoma Cells. *Int. J. Oncol.* **2015**, *46*, 2267–2276. [[CrossRef](#)]
151. Almasi, S.; Sterea, A.M.; Fernando, W.; Clements, D.R.; Marcato, P.; Hoskin, D.W.; Gujar, S.; El Hiani, Y. TRPM2 Ion Channel Promotes Gastric Cancer Migration, Invasion and Tumour Growth through the AKT Signaling Pathway. *Sci. Rep.* **2019**, *9*, 4182. [[CrossRef](#)]
152. Almasi, S.; Kennedy, B.E.; El-Aghil, M.; Sterea, A.M.; Gujar, S.; Partida-Sánchez, S.; El Hiani, Y. TRPM2 Channel-Mediated Regulation of Autophagy Maintains Mitochondrial Function and Promotes Gastric Cancer Cell Survival via the JNK-Signaling Pathway. *J. Biol. Chem.* **2018**, *293*, 3637–3650. [[CrossRef](#)]
153. Guler, Y.; Ovey, I.S. Synergic and Comparative Effect of 5-Fluorouracil and Leucovorin on Breast and Colon Cancer Cells through TRPM2 Channels. *Bratisl. Lek. Listy* **2018**, *119*, 692–700. [[CrossRef](#)]

154. Lange, I.; Yamamoto, S.; Partida-Sanchez, S.; Mori, Y.; Fleig, A.; Penner, R. TRPM2 Functions as a Lysosomal  $\text{Ca}^{2+}$ -Release Channel in Cells. *Sci. Signal.* **2009**, *2*, ra23. [[CrossRef](#)] [[PubMed](#)]
155. Hantute-Ghesquier, A.; Haustrate, A.; Prevarskaya, N.; Lehen'kyi, V. TRPM Family Channels in Cancer. *Pharmaceuticals* **2018**, *11*, 58. [[CrossRef](#)] [[PubMed](#)]
156. Zhang, J.; Zhao, F.; Zhao, Y.; Wang, J.; Pei, L.; Sun, N.; Shi, J. Hypoxia Induces an Increase in Intracellular Magnesium via Transient Receptor Potential Melastatin 7 (TRPM7) Channels in Rat Hippocampal Neurons In Vitro. *J. Biol. Chem.* **2011**, *286*, 20194–20207. [[CrossRef](#)]
157. Mori, Y.; Takahashi, N.; Polat, O.K.; Kurokawa, T.; Takeda, N.; Inoue, M. Redox-Sensitive Transient Receptor Potential Channels in Oxygen Sensing and Adaptation. *Pflug. Arch. Eur. J. Physiol.* **2016**, *468*, 85–97. [[CrossRef](#)] [[PubMed](#)]
158. Caterina, M.J.; Leffler, A.; Malmberg, A.B.; Martin, W.J.; Trafton, J.; Petersen-Zeitz, K.R.; Koltzenburg, M.; Basbaum, A.I.; Julius, D. Impaired Nociception and Pain Sensation in Mice Lacking the Capsaicin Receptor. *Science* **2000**, *288*, 306–313. [[CrossRef](#)] [[PubMed](#)]
159. Reeh, P.W.; Fischer, M.J.M. Nobel Somatosensations and Pain. *Pflug. Arch. Eur. J. Physiol.* **2022**, *474*, 405–420. [[CrossRef](#)] [[PubMed](#)]
160. Storozhuk, M.V.; Moroz, O.F.; Zholos, A.V. Multifunctional TRPV1 Ion Channels in Physiology and Pathology with Focus on the Brain, Vasculature, and Some Visceral Systems. *BioMed Res. Int.* **2019**, *2019*, 5806321. [[CrossRef](#)]
161. Hellwig, N.; Plant, T.D.; Janson, W.; Schäfer, M.; Schultz, G.; Schaefer, M. TRPV1 Acts as Proton Channel to Induce Acidification in Nociceptive Neurons. *J. Biol. Chem.* **2004**, *279*, 34553–34561. [[CrossRef](#)]
162. Li, L.; Chen, C.; Chiang, C.; Xiao, T.; Chen, Y.; Zhao, Y.; Zheng, D. The Impact of TRPV1 on Cancer Pathogenesis and Therapy: A Systematic Review. *Int. J. Biol. Sci.* **2021**, *17*, 2034–2049. [[CrossRef](#)]
163. Siveen, K.S.; Nizamuddin, P.B.; Uddin, S.; Al-Thani, M.; Frenneaux, M.P.; Janahi, I.A.; Steinhoff, M.; Azizi, F. TRPV2: A Cancer Biomarker and Potential Therapeutic Target. *Dis. Markers* **2020**, *2020*, 8892312. [[CrossRef](#)]
164. Li, X.; Zhang, Q.; Fan, K.; Li, B.; Li, H.; Qi, H.; Guo, J.; Cao, Y.; Sun, H. Overexpression of TRPV3 Correlates with Tumour Progression in Non-Small Cell Lung Cancer. *Int. J. Mol. Sci.* **2016**, *17*, 437. [[CrossRef](#)] [[PubMed](#)]
165. Wang, H.; Yang, P.; Lu, Y.; Wang, J.; Jeon, J.; Wang, Q.; Tian, J.-B.; Zang, B.; Yu, Y.; Zhu, M.X. Mechanisms of Proton Inhibition and Sensitization of the Cation Channel TRPV3. *J. Gen. Physiol.* **2021**, *153*, e202012663. [[CrossRef](#)] [[PubMed](#)]
166. Lee, W.; Choong, L.; Jin, T.; Mon, N.; Chong, S.; Liew, C.; Putti, T.; Lu, S.; Harteneck, C.; Lim, Y. TRPV4 Plays a Role in Breast Cancer Cell Migration via  $\text{Ca}^{2+}$ -Dependent Activation of AKT and Downregulation of E-Cadherin Cell Cortex Protein. *Oncogenesis* **2017**, *6*, e338. [[CrossRef](#)] [[PubMed](#)]
167. Lee, W.H.; Choong, L.Y.; Mon, N.N.; Lu, S.; Lin, Q.; Pang, B.; Yan, B.; Krishna, V.S.R.; Singh, H.; Tan, T.Z.; et al. TRPV4 Regulates Breast Cancer Cell Extravasation, Stiffness and Actin Cortex. *Sci. Rep.* **2016**, *6*, 27903. [[CrossRef](#)]
168. Fiorio Pla, A.; Ong, H.L.; Cheng, K.T.; Brossa, A.; Bussolati, B.; Lockwich, T.; Paria, B.; Munaron, L.; Ambudkar, I.S. TRPV4 Mediates Tumour-Derived Endothelial Cell Migration via Arachidonic Acid-Activated Actin Remodeling. *Oncogene* **2012**, *31*, 200–212. [[CrossRef](#)]
169. Vellino, S.; Oddou, C.; Rivier, P.; Boyault, C.; Hiriart-Bryant, E.; Kraut, A.; Martin, R.; Coute, Y.; Knölker, H.-J.; Valverde, M.A.; et al. Crosstalk between the Calcium Channel TRPV4 and Reactive Oxygen Species Interlocks Adhesive and Degradative Functions of Invadosomes. *J. Cell Biol.* **2021**, *220*, e201910079. [[CrossRef](#)]
170. Wang, H.; Zhang, B.; Wang, X.; Mao, J.; Li, W.; Sun, Y.; Yuan, Y.; Ben, Q.; Hua, L.; Qian, A. TRPV4 Overexpression Promotes Metastasis through Epithelial–Mesenchymal Transition in Gastric Cancer and Correlates with Poor Prognosis. *Oncotargets Ther.* **2020**, *13*, 8383–8394. [[CrossRef](#)]
171. Li, X.; Cheng, Y.; Wang, Z.; Zhou, J.; Jia, Y.; He, X.; Zhao, L.; Dong, Y.; Fan, Y.; Yang, X.; et al. Calcium and TRPV4 Promote Metastasis by Regulating Cytoskeleton through the RhoA/ROCK1 Pathway in Endometrial Cancer. *Cell Death Dis.* **2020**, *11*, 1009. [[CrossRef](#)]
172. Thoppil, R.J.; Cappelli, H.C.; Adapala, R.K.; Kanugula, A.K.; Paruchuri, S.; Thodeti, C.K. TRPV4 Channels Regulate Tumour Angiogenesis via Modulation of Rho/Rho Kinase Pathway. *Oncotarget* **2016**, *7*, 25849–25861. [[CrossRef](#)]
173. Azimi, I.; Robitaille, M.; Armitage, K.; So, C.L.; Milevskiy, M.J.G.; Northwood, K.; Lim, H.F.; Thompson, E.W.; Roberts-Thomson, S.J.; Monteith, G.R. Activation of the Ion Channel TRPV4 Induces Epithelial to Mesenchymal Transition in Breast Cancer Cells. *Int. J. Mol. Sci.* **2020**, *21*, 9417. [[CrossRef](#)]
174. Peters, A.A.; Jamaludin, S.Y.N.; Yapa, K.T.D.S.; Chalmers, S.; Wiegman, A.P.; Lim, H.F.; Milevskiy, M.J.G.; Azimi, I.; Davis, F.M.; Northwood, K.S.; et al. Oncosis and Apoptosis Induction by Activation of an Overexpressed Ion Channel in Breast Cancer Cells. *Oncogene* **2017**, *36*, 6490–6500. [[CrossRef](#)] [[PubMed](#)]
175. Liu, L.; Guo, M.; Lv, X.; Wang, Z.; Yang, J.; Li, Y.; Yu, F.; Wen, X.; Feng, L.; Zhou, T. Role of Transient Receptor Potential Vanilloid 4 in Vascular Function. *Front. Mol. Biosci.* **2021**, *8*, 677661. [[CrossRef](#)] [[PubMed](#)]
176. Stewart, J.M. TRPV6 as A Target for Cancer Therapy. *J. Cancer* **2020**, *11*, 374–387. [[CrossRef](#)] [[PubMed](#)]
177. Lehen'kyi, V.; Flourakis, M.; Skryma, R.; Prevarskaya, N. TRPV6 Channel Controls Prostate Cancer Cell Proliferation via  $\text{Ca}^{2+}$ /NFAT-Dependent Pathways. *Oncogene* **2007**, *26*, 7380–7385. [[CrossRef](#)] [[PubMed](#)]
178. Raphaël, M.; Lehen'kyi, V.; Vandenberghe, M.; Beck, B.; Khalimonchik, S.; Vanden Abeele, F.; Farsetti, L.; Germain, E.; Bokhobza, A.; Mihalache, A.; et al. TRPV6 Calcium Channel Translocates to the Plasma Membrane via Orai1-Mediated Mechanism and Controls Cancer Cell Survival. *Proc. Natl. Acad. Sci. USA* **2014**, *111*, E3870–E3879. [[CrossRef](#)] [[PubMed](#)]

179. Kärki, T.; Rajakylä, E.K.; Acheva, A.; Tojkander, S. TRPV6 Calcium Channel Directs Homeostasis of the Mammary Epithelial Sheets and Controls Epithelial Mesenchymal Transition. *Sci. Rep.* **2020**, *10*, 14683. [[CrossRef](#)] [[PubMed](#)]
180. Dhennin-Duthille, I.; Gautier, M.; Faouzi, M.; Guilbert, A.; Brevet, M.; Vaudry, D.; Ahidouch, A.; Sevestre, H.; Ouadid-Ahidouch, H. High Expression of Transient Receptor Potential Channels in Human Breast Cancer Epithelial Cells and Tissues: Correlation with Pathological Parameters. *Cell. Physiol. Biochem.* **2011**, *28*, 813–822. [[CrossRef](#)]
181. Song, H.; Dong, M.; Zhou, J.; Sheng, W.; Li, X.; Gao, W. Expression and Prognostic Significance of TRPV6 in the Development and Progression of Pancreatic Cancer. *Oncol. Rep.* **2018**, *39*, 1432–1440. [[CrossRef](#)]
182. Xue, H.; Wang, Y.; MacCormack, T.J.; Lutes, T.; Rice, C.; Davey, M.; Dugourd, D.; Ilenchuk, T.T.; Stewart, J.M. Inhibition of Transient Receptor Potential Vanilloid 6 Channel, Elevated in Human Ovarian Cancers, Reduces Tumour Growth in a Xenograft Model. *J. Cancer* **2018**, *9*, 3196–3207. [[CrossRef](#)]
183. Sutoo, S.; Maeda, T.; Suzuki, A.; Kato, Y. Adaptation to Chronic Acidic Extracellular PH Elicits a Sustained Increase in Lung Cancer Cell Invasion and Metastasis. *Clin. Exp. Metastasis* **2020**, *37*, 133–144. [[CrossRef](#)]
184. Peleg, S.; Sellin, J.H.; Wang, Y.; Freeman, M.R.; Umar, S. Suppression of Aberrant Transient Receptor Potential Cation Channel, Subfamily V, Member 6 Expression in Hyperproliferative Colonic Crypts by Dietary Calcium. *Am. J. Physiol. Gastrointest. Liver Physiol.* **2010**, *299*, G593–G601. [[CrossRef](#)] [[PubMed](#)]
185. Yang, H.; An, B.-S.; Choi, K.-C.; Jeung, E.-B. Change of Genes in Calcium Transport Channels Caused by Hypoxic Stress in the Placenta, Duodenum, and Kidney of Pregnant Rats. *Biol. Reprod.* **2013**, *88*, 1–12. [[CrossRef](#)] [[PubMed](#)]
186. Park, Y.R.; Chun, J.N.; So, I.; Kim, H.J.; Baek, S.; Jeon, J.-H.; Shin, S.-Y. Data-Driven Analysis of TRP Channels in Cancer: Linking Variation in Gene Expression to Clinical Significance. *Cancer Genom. Proteom.* **2016**, *13*, 83–90.
187. Takahashi, N.; Kuwaki, T.; Kiyonaka, S.; Numata, T.; Kozai, D.; Mizuno, Y.; Yamamoto, S.; Naito, S.; Knevels, E.; Carmeliet, P.; et al. TRPA1 Underlies a Sensing Mechanism for O<sub>2</sub>. *Nat. Chem. Biol.* **2011**, *7*, 701–711. [[CrossRef](#)]
188. Berrout, J.; Kyriakopoulou, E.; Moparthi, L.; Hoge, A.S.; Berrout, L.; Ivan, C.; Lorger, M.; Boyle, J.; Peers, C.; Muench, S.; et al. TRPA1–FGFR2 Binding Event Is a Regulatory Oncogenic Driver Modulated by MiRNA-142-3p. *Nat. Commun.* **2017**, *8*, 947. [[CrossRef](#)]
189. Derouiche, S.; Mariot, P.; Warnier, M.; Vancauwenberghe, E.; Bidaux, G.; Gosset, P.; Mauroy, B.; Bonnal, J.-L.; Slomianny, C.; Delcourt, P.; et al. Activation of TRPA1 Channel by Antibacterial Agent Triclosan Induces VEGF Secretion in Human Prostate Cancer Stromal Cells. *Cancer Prev. Res.* **2017**, *10*, 177–187. [[CrossRef](#)]
190. Roberts, E.; Cossigny, D.A.F.; Quan, G.M.Y. The Role of Vascular Endothelial Growth Factor in Metastatic Prostate Cancer to the Skeleton. *Prostate Cancer* **2013**, *2013*, 418340. [[CrossRef](#)]
191. Bernardini, M.; Brossa, A.; Chinigo, G.; Grolez, G.P.; Trimaglio, G.; Allart, L.; Hulot, A.; Marot, G.; Genova, T.; Joshi, A.; et al. Transient Receptor Potential Channel Expression Signatures in Tumour-Derived Endothelial Cells: Functional Roles in Prostate Cancer Angiogenesis. *Cancers* **2019**, *11*, 956. [[CrossRef](#)]
192. Samanta, A.; Hughes, T.E.T.; Moiseenkova-Bell, V.Y. Transient Receptor Potential (TRP) Channels. In *Membrane Protein Complexes: Structure and Function*; Harris, J.R., Boekema, E.J., Eds.; Springer: Singapore, 2018; Volume 87, pp. 141–165, ISBN 978-981-10-7756-2.
193. Dong, H.; Shim, K.-N.; Li, J.M.J.; Estrema, C.; Ornelas, T.A.; Nguyen, F.; Liu, S.; Ramamoorthy, S.L.; Ho, S.; Carethers, J.M.; et al. Molecular Mechanisms Underlying Ca<sup>2+</sup>-Mediated Motility of Human Pancreatic Duct Cells. *Cell Physiol.* **2010**, *299*, 11. [[CrossRef](#)]
194. Faouzi, M.; Hague, F.; Geerts, D.; Ay, A.-S.; Potier-Cartreau, M.; Ahidouch, A.; Ouadid-Ahidouch, H. Functional Cooperation between KCa3.1 and TRPC1 Channels in Human Breast Cancer: Role in Cell Proliferation and Patient Prognosis. *Oncotarget* **2016**, *7*, 36419–36435. [[CrossRef](#)]
195. El Hiani, Y.; Ahidouch, A.; Lehen'kyi, V.; Hague, F.; Gouilleux, F.; Mentaverri, R.; Kamel, S.; Lassoued, K.; Brûlé, G.; Ouadid-Ahidouch, H. Extracellular Signal-Regulated Kinases 1 and 2 and TRPC1 Channels Are Required for Calcium-Sensing Receptor-Stimulated MCF-7 Breast Cancer Cell Proliferation. *Cell. Physiol. Biochem.* **2009**, *23*, 335–346. [[CrossRef](#)] [[PubMed](#)]
196. Bomben, V.C.; Sontheimer, H. Disruption of Transient Receptor Potential Canonical Channel 1 Causes Incomplete Cytokinesis and Slows the Growth of Human Malignant Gliomas: TRPC1 Channels Are Essential for Glioma Proliferation. *Glia* **2010**, *58*, 1145–1156. [[CrossRef](#)] [[PubMed](#)]
197. Jiang, H.-N.; Zeng, B.; Zhang, Y.; Daskoulidou, N.; Fan, H.; Qu, J.-M.; Xu, S.-Z. Involvement of TRPC Channels in Lung Cancer Cell Differentiation and the Correlation Analysis in Human Non-Small Cell Lung Cancer. *PLoS ONE* **2013**, *8*, e67637. [[CrossRef](#)] [[PubMed](#)]
198. Stewart, T.A.; Azimi, I.; Marcial, D.; Peters, A.A.; Chalmers, S.B.; Yapa, K.T.D.S.; Thompson, E.W.; Roberts-Thomson, S.J.; Monteith, G.R. Differential Engagement of ORAI1 and TRPC1 in the Induction of Vimentin Expression by Different Stimuli. *Lab. Invest.* **2020**, *100*, 224–233. [[CrossRef](#)] [[PubMed](#)]
199. Carmeliet, P. VEGF as a Key Mediator of Angiogenesis in Cancer. *Oncology* **2005**, *69*, 4–10. [[CrossRef](#)]
200. Zhang, P.; Liu, X.; Li, H.; Chen, Z.; Yao, X.; Jin, J.; Ma, X. TRPC5-Induced Autophagy Promotes Drug Resistance in Breast Carcinoma via CaMKK $\beta$ /AMPK $\alpha$ /MTOR Pathway. *Sci. Rep.* **2017**, *7*, 3158. [[CrossRef](#)]
201. Ma, X.; Cai, Y.; He, D.; Zou, C.; Zhang, P.; Lo, C.Y.; Xu, Z.; Chan, F.L.; Yu, S.; Chen, Y.; et al. Transient Receptor Potential Channel TRPC5 Is Essential for P-Glycoprotein Induction in Drug-Resistant Cancer Cells. *Proc. Natl. Acad. Sci. USA* **2012**, *109*, 16282–16287. [[CrossRef](#)]
202. Wang, T.; Chen, Z.; Zhu, Y.; Pan, Q.; Liu, Y.; Qi, X.; Jin, L.; Jin, J.; Ma, X.; Hua, D. Inhibition of Transient Receptor Potential Channel 5 Reverses 5-Fluorouracil Resistance in Human Colorectal Cancer Cells. *J. Biol. Chem.* **2015**, *290*, 448–456. [[CrossRef](#)]



203. Wang, T.; Ning, K.; Sun, X.; Zhang, C.; Jin, L.; Hua, D. Glycolysis Is Essential for Chemoresistance Induced by Transient Receptor Potential Channel C5 in Colorectal Cancer. *BMC Cancer* **2018**, *18*, 207. [[CrossRef](#)]
204. Plant, T.D.; Schaefer, M. TRPC4 and TRPC5: Receptor-Operated  $\text{Ca}^{2+}$ -Permeable Nonselective Cation Channels. *Cell Calcium* **2003**, *33*, 441–450. [[CrossRef](#)]
205. Veliceasa, D.; Ivanovic, M.; Hoepfner, F.T.-S.; Thumbikat, P.; Volpert, O.V.; Smith, N.D. Transient Potential Receptor Channel 4 Controls Thrombospondin-1 Secretion and Angiogenesis in Renal Cell Carcinoma: Thrombospondin-1 Loss in Renal Cancer. *FEBS J.* **2007**, *274*, 6365–6377. [[CrossRef](#)] [[PubMed](#)]
206. Song, H.B.; Jun, H.-O.; Kim, J.H.; Fruttiger, M.; Kim, J.H. Suppression of Transient Receptor Potential Canonical Channel 4 Inhibits Vascular Endothelial Growth Factor-Induced Retinal Neovascularization. *Cell Calcium* **2015**, *57*, 101–108. [[CrossRef](#)] [[PubMed](#)]
207. Zeng, B.; Yuan, C.; Yang, X.; Atkin, S.L.; Xu, S.-Z. TRPC Channels and Their Splice Variants Are Essential for Promoting Human Ovarian Cancer Cell Proliferation and Tumorigenesis. *Curr. Cancer Drug Targets* **2013**, *13*, 103–116. [[CrossRef](#)] [[PubMed](#)]
208. Carson, C.; Raman, P.; Tullai, J.; Xu, L.; Henault, M.; Thomas, E.; Yeola, S.; Lao, J.; McPate, M.; Verkuy, J.M.; et al. Englerin A Agonizes the TRPC4/C5 Cation Channels to Inhibit Tumour Cell Line Proliferation. *PLoS ONE* **2015**, *10*, e0127498. [[CrossRef](#)]
209. Lindemann, O.; Umlauf, D.; Frank, S.; Schimmelpfennig, S.; Bertrand, J.; Pap, T.; Hanley, P.J.; Fabian, A.; Dietrich, A.; Schwab, A. TRPC6 Regulates CXCR2-Mediated Chemotaxis of Murine Neutrophils. *J. Immunol.* **2013**, *190*, 5496–5505. [[CrossRef](#)]
210. Wu, L.; Saxena, S.; Awaji, M.; Singh, R.K. Tumour-Associated Neutrophils in Cancer: Going Pro. *Cancers* **2019**, *11*, 564. [[CrossRef](#)]
211. Prakriya, M. Store-Operated Orai Channels. In *Current Topics in Membranes*; Elsevier: Amsterdam, The Netherlands, 2013; Volume 71, pp. 1–32, ISBN 978-0-12-407870-3.
212. Kondratska, K.; Kondratskyi, A.; Yassine, M.; Lemonnier, L.; Lepage, G.; Morabito, A.; Skryma, R.; Prevarskaya, N. Orai1 and STIM1 Mediate SOCE and Contribute to Apoptotic Resistance of Pancreatic Adenocarcinoma. *Biochim. Biophys. Acta BBA Mol. Cell Res.* **2014**, *1843*, 2263–2269. [[CrossRef](#)]
213. Didiysova, M.; Zakrzewicz, D.; Magdolen, V.; Nagaraj, C.; Bálint, Z.; Rohde, M.; Preissner, K.T.; Wygrecka, M. STIM1/ORAI1-Mediated  $\text{Ca}^{2+}$  Influx Regulates Enolase-1 Exteriorization. *J. Biol. Chem.* **2015**, *290*, 11983–11999. [[CrossRef](#)]
214. Huang, H.-K.; Lin, Y.-H.; Chang, H.-A.; Lai, Y.-S.; Chen, Y.-C.; Huang, S.-C.; Chou, C.-Y.; Chiu, W.-T. Chemoresistant Ovarian Cancer Enhances Its Migration Abilities by Increasing Store-Operated  $\text{Ca}^{2+}$  Entry-Mediated Turnover of Focal Adhesions. *J. Biomed. Sci.* **2020**, *27*, 36. [[CrossRef](#)]
215. Zuccolo, E.; Laforenza, U.; Ferulli, F.; Pellavio, G.; Scarpellino, G.; Tanzi, M.; Turin, I.; Faris, P.; Lucariello, A.; Maestri, M.; et al. Stim and Orai Mediate Constitutive  $\text{Ca}^{2+}$  Entry and Control Endoplasmic Reticulum  $\text{Ca}^{2+}$  Refilling in Primary Cultures of Colorectal Carcinoma Cells. *Oncotarget* **2018**, *9*, 31098–31119. [[CrossRef](#)]
216. Singh, A.K. Orai-1 and Orai-2 Regulate Oral Cancer Cell Migration and Colonisation by Suppressing Akt/MTOR/NF- $\kappa$ B Signalling. *Life Sci.* **2020**, *261*, 118372. [[CrossRef](#)] [[PubMed](#)]
217. Sun, J.; Lu, F.; He, H.; Shen, J.; Messina, J.; Mathew, R.; Wang, D.; Sarnaik, A.A.; Chang, W.-C.; Kim, M.; et al. STIM1- and Orai1-Mediated  $\text{Ca}^{2+}$  Oscillation Orchestrates Invadopodium Formation and Melanoma Invasion. *J. Cell Biol.* **2014**, *207*, 535–548. [[CrossRef](#)] [[PubMed](#)]
218. Xu, Y.; Zhang, S.; Niu, H.; Ye, Y.; Hu, F.; Chen, S.; Li, X.; Luo, X.; Jiang, S.; Liu, Y.; et al. STIM1 Accelerates Cell Senescence in a Remodeled Microenvironment but Enhances the Epithelial-to-Mesenchymal Transition in Prostate Cancer. *Sci. Rep.* **2015**, *5*, 11754. [[CrossRef](#)] [[PubMed](#)]
219. Xia, J.; Wang, H.; Huang, H.; Sun, L.; Dong, S.; Huang, N.; Shi, M.; Bin, J.; Liao, Y.; Liao, W. Elevated Orai1 and STIM1 Expressions Upregulate MACC1 Expression to Promote Tumour Cell Proliferation, Metabolism, Migration, and Invasion in Human Gastric Cancer. *Cancer Lett.* **2016**, *381*, 31–40. [[CrossRef](#)]
220. Hasna, J.; Hague, F.; Rodat-Despoix, L.; Geerts, D.; Leroy, C.; Tulasne, D.; Ouadid-Ahidouch, H.; Kischel, P. Orai3 Calcium Channel and Resistance to Chemotherapy in Breast Cancer Cells: The P53 Connection. *Cell Death Differ.* **2018**, *25*, 693–707. [[CrossRef](#)]
221. Tang, B.-D.; Xia, X.; Lv, X.-F.; Yu, B.-X.; Yuan, J.-N.; Mai, X.-Y.; Shang, J.-Y.; Zhou, J.-G.; Liang, S.-J.; Pang, R.-P. Inhibition of Orai1-Mediated  $\text{Ca}^{2+}$  Entry Enhances Chemosensitivity of HepG2 Hepatocarcinoma Cells to 5-Fluorouracil. *J. Cell. Mol. Med.* **2017**, *21*, 904–915. [[CrossRef](#)]
222. Taylor, J.; Azimi, I.; Monteith, G.; Bebawy, M.  $\text{Ca}^{2+}$  Mediates Extracellular Vesicle Biogenesis through Alternate Pathways in Malignancy. *J. Extracell. Vesicles* **2020**, *9*, 1734326. [[CrossRef](#)]
223. Gavriliouk, D.; Scrimgeour, N.R.; Grigoryev, S.; Ma, L.; Zhou, F.H.; Barritt, G.J.; Rychkov, G.Y. Regulation of Orai1/STIM1 Mediated ICRC by Intracellular PH. *Sci. Rep.* **2017**, *7*, 9829. [[CrossRef](#)]
224. Li, S.; Hao, B.; Lu, Y.; Yu, P.; Lee, H.-C.; Yue, J. Intracellular Alkalinization Induces Cytosolic  $\text{Ca}^{2+}$  Increases by Inhibiting Sarco/Endoplasmic Reticulum  $\text{Ca}^{2+}$ -ATPase (SERCA). *PLoS ONE* **2012**, *7*, e31905. [[CrossRef](#)]
225. Prevarskaya, N.; Skryma, R.; Shuba, Y. Ion Channels and the Hallmarks of Cancer. *Trends Mol. Med.* **2010**, *16*, 107–121. [[CrossRef](#)]
226. Baghban, R.; Roshangar, L.; Jahanban-Esfahlan, R.; Seidi, K.; Ebrahimi-Kalan, A.; Jaymand, M.; Kolahian, S.; Javaheri, T.; Zare, P. Tumour Microenvironment Complexity and Therapeutic Implications at a Glance. *Cell Commun. Signal.* **2020**, *18*, 59. [[CrossRef](#)] [[PubMed](#)]
227. Bogeski, I.; Kummerow, C.; Al-Ansary, D.; Schwarz, E.C.; Koehler, R.; Kozai, D.; Takahashi, N.; Peinelt, C.; Griesemer, D.; Bozem, M.; et al. Differential Redox Regulation of Orai Ion Channels: A Mechanism to Tune Cellular Calcium Signaling. *Sci. Signal.* **2010**, *3*, ra24. [[CrossRef](#)] [[PubMed](#)]

228. Dubois, C.; Vanden Abeele, F.; Lehen'kyi, V.; Gkika, D.; Guarmit, B.; Lepage, G.; Slomianny, C.; Borowiec, A.S.; Bidaux, G.; Benahmed, M.; et al. Remodeling of Channel-Forming ORAI Proteins Determines an Oncogenic Switch in Prostate Cancer. *Cancer Cell* **2014**, *26*, 19–32. [[CrossRef](#)] [[PubMed](#)]
229. Xie, J.; Pan, H.; Yao, J.; Zhou, Y.; Han, W. SOCE and Cancer: Recent Progress and New Perspectives. *Int. J. Cancer* **2016**, *138*, 2067–2077. [[CrossRef](#)] [[PubMed](#)]

# Bibliography

1. Dolenšek, J., Pohorec, V., Rupnik, M. S. & Stožer, A. Pancreas Physiology. in *Challenges in Pancreatic Pathology* (ed. Seicean, A.) (InTech, 2017). doi:10.5772/65895.
2. Röder, P. V., Wu, B., Liu, Y. & Han, W. Pancreatic regulation of glucose homeostasis. *Exp Mol Med* **48**, e219–e219 (2016).
3. Pandiri, A. R. Overview of Exocrine Pancreatic Pathobiology. *Toxicol Pathol* **42**, 207–216 (2014).
4. Shi, C. & Liu, E. Anatomy, Histology, and Function of the Pancreas. in *Pathobiology of Human Disease* 2229–2242 (Elsevier, 2014). doi:10.1016/B978-0-12-386456-7.04902-9.
5. Overview of Exocrine Gland Physiology - Pancreatic and Salivary Glands - The Gastrointestinal System - Medical Physiology, 3rd Edition. <https://doctorlib.info/physiology/medical/227.html>.
6. Massey, M. K., Reiterman, M. J., Mourad, J. & Luckie, D. B. Is CFTR an exchanger?: Regulation of HCO<sub>3</sub>–Transport and extracellular pH by CFTR. *Biochemistry and Biophysics Reports* **25**, 100863 (2021).
7. Ishiguro, H. *et al.* physiology and Pathophysiology of bicarbonate secretion by pancreatic duct epithelium. **18** (2012).
8. Lee, M. G., Ohana, E., Park, H. W., Yang, D. & Muallem, S. Molecular Mechanism of Pancreatic and Salivary Gland Fluid and HCO<sub>3</sub><sup>-</sup> Secretion. *Physiological Reviews* **92**, 39–74 (2012).
9. Novak, I., Haanes, K. A. & Wang, J. Acid-base transport in pancreas—new challenges. *Front. Physiol.* **4**, (2013).
10. Kong, S. C., Gianuzzo, A., Novak, I. & Pedersen, S. F. Acid-base transport in pancreatic cancer: Molecular mechanisms and clinical potential. *Biochem. Cell Biol.* **92**, 449–459 (2014).
11. Novak, I. & Praetorius, J. Fundamentals of Bicarbonate Secretion in Epithelia. in *Ion Channels and Transporters of Epithelia in Health and Disease* (eds. Hamilton, K. L. & Devor, D. C.) 187–263 (Springer New York, 2016). doi:10.1007/978-1-4939-3366-2\_5.
12. Orth, M. *et al.* Pancreatic ductal adenocarcinoma: biological hallmarks, current status, and future perspectives of combined modality treatment approaches. *Radiat Oncol* **14**, 141 (2019).

13. Sung, H. *et al.* Global Cancer Statistics 2020: GLOBOCAN Estimates of Incidence and Mortality Worldwide for 36 Cancers in 185 Countries. *CA A Cancer J Clin* **71**, 209–249 (2021).
14. Kenner, B. J. *et al.* Early Detection of Pancreatic Cancer—a Defined Future Using Lessons From Other Cancers: A White Paper. *Pancreas* **45**, 1073–1079 (2016).
15. Siegel, R. L., Miller, K. D. & Jemal, A. Cancer statistics, 2020. *CA A Cancer J Clin* **70**, 7–30 (2020).
16. McGuigan, A. *et al.* Pancreatic cancer: A review of clinical diagnosis, epidemiology, treatment and outcomes. *WJG* **24**, 4846–4861 (2018).
17. Satoi, S., Yamamoto, T., Yamaki, S., Sakaguchi, T. & Sekimoto, M. Surgical indication for and desirable outcomes of conversion surgery in patients with initially unresectable pancreatic ductal adenocarcinoma. *Ann Gastroenterol Surg* **4**, 6–13 (2020).
18. Kruger, D., Lahoud, N., Yako, Y. Y., Devar, J. & Smith, M. Pancreatic ductal adenocarcinoma: Prognostic indicators of advanced disease. *PLoS ONE* **17**, e0262439 (2022).
19. Moshayedi, N., Escobedo, A. L., Thomassian, S., Osipov, A. & Hendifar, A. E. Race, sex, age, and geographic disparities in pancreatic cancer incidence. *JCO* **40**, 520–520 (2022).
20. Ayloo, S. & Molinari, M. Pancreatic manifestations in von Hippel–Lindau disease: A case report. *International Journal of Surgery Case Reports* **21**, 70–72 (2016).
21. H. Bekkali, N. & Oppong, K. Pancreatic ductal adenocarcinoma epidemiology and risk assessment: Could we prevent? Possibility for an early diagnosis. *Endosc Ultrasound* **6**, 58 (2017).
22. Zhou, B. *et al.* Early detection of pancreatic cancer: Where are we now and where are we going?: Early detection of pancreatic cancer. *Int. J. Cancer* **141**, 231–241 (2017).
23. Sun, H., Zhang, B. & Li, H. The Roles of Frequently Mutated Genes of Pancreatic Cancer in Regulation of Tumor Microenvironment. *Technol Cancer Res Treat* **19**, 153303382092096 (2020).
24. Esposito, I. Pathology of pancreatic ductal adenocarcinoma: Facts, challenges and future developments. *WJG* **20**, 13833 (2014).
25. Riva, G. *et al.* Histo-molecular oncogenesis of pancreatic cancer: From precancerous lesions to invasive ductal adenocarcinoma. *WJGO* **10**, 317–327 (2018).

26. Cortegoso Valdivia, P. *et al.* Diagnosis and management of intraductal papillary mucinous neoplasms of the pancreas. *Acta Bio Medica Atenei Parmensis* **89**, 147–152 (2018).
27. Tinder, T. L. *et al.* MUC1 Enhances Tumor Progression and Contributes Toward Immunosuppression in a Mouse Model of Spontaneous Pancreatic Adenocarcinoma. *The Journal of Immunology* **181**, 3116–3125 (2008).
28. Feldmann, G., Beaty, R., Hruban, R. H. & Maitra, A. Molecular genetics of pancreatic intraepithelial neoplasia. *J Hepatobiliary Pancreat Surg* **14**, 224–232 (2007).
29. Brosens, L. A. A., Hackeng, W. M., Offerhaus, G. J., Hruban, R. H. & Wood, L. D. Pancreatic adenocarcinoma pathology: changing “landscape”. **6**, 17 (2015).
30. Hackeng, W. M., Hruban, R. H., Offerhaus, G. J. A. & Brosens, L. A. A. Surgical and molecular pathology of pancreatic neoplasms. *Diagn Pathol* **11**, 47 (2016).
31. Murphy, S. J. *et al.* Genetic Alterations Associated With Progression From Pancreatic Intraepithelial Neoplasia to Invasive Pancreatic Tumor. *Gastroenterology* **145**, 1098-1109.e1 (2013).
32. Storz, P. Acinar cell plasticity and development of pancreatic ductal adenocarcinoma. *Nat Rev Gastroenterol Hepatol* **14**, 296–304 (2017).
33. Jones, S. *et al.* Core Signaling Pathways in Human Pancreatic Cancers Revealed by Global Genomic Analyses. *Science* **321**, 1801–1806 (2008).
34. Delpu, Y. *et al.* Genetic and Epigenetic Alterations in Pancreatic Carcinogenesis. *CG* **12**, 15–24 (2011).
35. Waters, A. M. & Der, C. J. KRAS: The Critical Driver and Therapeutic Target for Pancreatic Cancer. *Cold Spring Harb Perspect Med* **8**, a031435 (2018).
36. Huang, L., Guo, Z., Wang, F. & Fu, L. KRAS mutation: from undruggable to druggable in cancer. *Sig Transduct Target Ther* **6**, 386 (2021).
37. Hingorani, S. R. *et al.* Preinvasive and invasive ductal pancreatic cancer and its early detection in the mouse. *CANCER CELL* **16** (2003).
38. Collins, M. A. *et al.* Oncogenic Kras is required for both the initiation and maintenance of pancreatic cancer in mice. *J. Clin. Invest.* **122**, 639–653 (2012).



39. Guerra, C. *et al.* Chronic Pancreatitis Is Essential for Induction of Pancreatic Ductal Adenocarcinoma by K-Ras Oncogenes in Adult Mice. *Cancer Cell* **11**, 291–302 (2007).
40. van Heek, N. T. *et al.* Telomere Shortening Is Nearly Universal in Pancreatic Intraepithelial Neoplasia. *The American Journal of Pathology* **161**, 1541–1547 (2002).
41. Schutte, M. *et al.* Abrogation of the Rb/p16 Tumor-suppressive Pathway in Virtually All Pancreatic Carcinomas'. **5** (1997).
42. Wu, C., Yang, P., Liu, B. & Tang, Y. Is there a CDKN2A-centric network in pancreatic ductal adenocarcinoma? *OTT Volume* **13**, 2551–2562 (2020).
43. Aguirre, A. J. *et al.* Activated Kras and *Ink4a/Arf* deficiency cooperate to produce metastatic pancreatic ductal adenocarcinoma. *Genes Dev.* **17**, 3112–3126 (2003).
44. Redston, M. S., Caldas, C., Seymour, A. B., Hruban, R. H. & Kern, S. E. Homocopolymer Tracts in DNA Microdeletions. **9** (1994).
45. Maddalena, M. *et al.* TP53 missense mutations in PDAC are associated with enhanced fibrosis and an immunosuppressive microenvironment. *Proc. Natl. Acad. Sci. U.S.A.* **118**, e2025631118 (2021).
46. Weissmueller, S. *et al.* Mutant p53 Drives Pancreatic Cancer Metastasis through Cell-Autonomous PDGF Receptor  $\beta$  Signaling. *Cell* **157**, 382–394 (2014).
47. Klemke, L. *et al.* The Gain-of-Function p53 R248W Mutant Promotes Migration by STAT3 Deregulation in Human Pancreatic Cancer Cells. *Front. Oncol.* **11**, 642603 (2021).
48. Maitra, A. *et al.* Multicomponent Analysis of the Pancreatic Adenocarcinoma Progression Model Using a Pancreatic Intraepithelial Neoplasia Tissue Microarray. *Mod Pathol* **16**, 902–912 (2003).
49. Morton, J. P. *et al.* Mutant p53 drives metastasis and overcomes growth arrest/senescence in pancreatic cancer. *Proc. Natl. Acad. Sci. U.S.A.* **107**, 246–251 (2010).
50. Wilentz, R. E. *et al.* Loss of Expression of Dpc4 in Pancreatic Intraepithelial Neoplasia: Evidence That DPC4 Inactivation Occurs Late in Neoplastic Progression. **6** (2000).
51. Fullerton, P. T., Creighton, C. J. & Matzuk, M. M. Insights Into SMAD4 Loss in Pancreatic Cancer From Inducible Restoration of TGF- $\beta$  Signaling. *Molecular Endocrinology* **29**, 1440–1453 (2015).

52. Siegel, P. M. & Massagué, J. Cytostatic and apoptotic actions of TGF- $\beta$  in homeostasis and cancer. *Nat Rev Cancer* **3**, 807–820 (2003).
53. Kojima, K. *et al.* Inactivation of Smad4 Accelerates KrasG12D-Mediated Pancreatic Neoplasia. *Cancer Research* **67**, 8121–8130 (2007).
54. Bardeesy, N. *et al.* Smad4 is dispensable for normal pancreas development yet critical in progression and tumor biology of pancreas cancer. *Genes Dev.* **20**, 3130–3146 (2006).
55. Derynck, R. & Zhang, Y. E. Smad-dependent and Smad-independent pathways in TGF-b family signalling. **425**, 8 (2003).
56. Singh, G. *et al.* Sequential Activation of NFAT and c-Myc Transcription Factors Mediates the TGF- $\beta$  Switch from a Suppressor to a Promoter of Cancer Cell Proliferation. *Journal of Biological Chemistry* **285**, 27241–27250 (2010).
57. Apte, M. V. *et al.* Pancreatic stellate cells are activated by proinflammatory cytokines: implications for pancreatic fibrogenesis. *Gut* **44**, 534–541 (1999).
58. Wood, L. D., Yurgelun, M. B. & Goggins, M. G. Genetics of Familial and Sporadic Pancreatic Cancer. *Gastroenterology* **156**, 2041–2055 (2019).
59. Goggins, M., Hruban, R. H. & Kern, S. E. BRCA2 Is Inactivated Late in the Development of Pancreatic Intraepithelial Neoplasia. *The American Journal of Pathology* **156**, 1767–1771 (2000).
60. Andersen, D. K. *et al.* Diabetes, Pancreatogenic Diabetes, and Pancreatic Cancer. *Diabetes* **66**, 1103–1110 (2017).
61. Mier-Hicks, A. *et al.* Incidence, Management, and Implications of Visceral Thrombosis in Pancreatic Ductal Adenocarcinoma. *Clinical Colorectal Cancer* **17**, 121–128 (2018).
62. Wang, X. *et al.* Detection of KRAS Gene Mutations in Endoscopic Ultrasound-Guided Fine-Needle Aspiration Biopsy for Improving Pancreatic Cancer Diagnosis. *American Journal of Gastroenterology* **106**, 2104–2111 (2011).
63. Heger, U. *et al.* Induction chemotherapy in pancreatic cancer: CA 19-9 may predict resectability and survival. *HPB* **22**, 224–232 (2020).

64. Kapszewicz, M. & Małecka-Wojcieszko, E. Simple Serum Pancreatic Ductal Adenocarcinoma (PDAC) Protein Biomarkers—Is There Anything in Sight? *JCM* **10**, 5463 (2021).
65. Pu, N. *et al.* Alkaline Phosphatase-To-Albumin Ratio as a Prognostic Indicator in Pancreatic Ductal Adenocarcinoma after Curative Resection. *J. Cancer* **8**, 3362–3370 (2017).
66. Kanda, M. *et al.* Mutant TP53 in Duodenal Samples of Pancreatic Juice From Patients With Pancreatic Cancer or High-Grade Dysplasia. *Clinical Gastroenterology and Hepatology* **11**, 719-730.e5 (2013).
67. Mayerle, J. *et al.* Metabolic biomarker signature to differentiate pancreatic ductal adenocarcinoma from chronic pancreatitis. *Gut* **67**, 128–137 (2018).
68. Riva, F. *et al.* Clinical applications of circulating tumor DNA and circulating tumor cells in pancreatic cancer. *MOLECULAR ONCOLOGY* **13**.
69. Hidalgo, M. *et al.* Addressing the challenges of pancreatic cancer: Future directions for improving outcomes. *Pancreatology* **15**, 8–18 (2015).
70. Ducreux, M. *et al.* Cancer of the pancreas: ESMO Clinical Practice Guidelines for diagnosis, treatment and follow-up. *Annals of Oncology* **26**, v56–v68 (2015).
71. Michalski, C. W., Weitz, J. & Büchler, M. W. Surgery Insight: surgical management of pancreatic cancer. *Nat Rev Clin Oncol* **4**, 526–535 (2007).
72. Isaji, S. *et al.* International consensus on definition and criteria of borderline resectable pancreatic ductal adenocarcinoma 2017. *Pancreatology* **18**, 2–11 (2018).
73. van Veldhuisen, E. *et al.* Locally Advanced Pancreatic Cancer: Work-Up, Staging, and Local Intervention Strategies. *Cancers* **11**, 976 (2019).
74. Gillen, S., Schuster, T., Meyer zum Büschenfelde, C., Friess, H. & Kleeff, J. Preoperative/Neoadjuvant Therapy in Pancreatic Cancer: A Systematic Review and Meta-analysis of Response and Resection Percentages. *PLoS Med* **7**, e1000267 (2010).
75. Conroy, T. *et al.* FOLFIRINOX or Gemcitabine as Adjuvant Therapy for Pancreatic Cancer. *N Engl J Med* **379**, 2395–2406 (2018).
76. Von Hoff, D. D. *et al.* Increased Survival in Pancreatic Cancer with nab-Paclitaxel plus Gemcitabine. *N Engl J Med* **369**, 1691–1703 (2013).

77. Cloyd, J. M. *et al.* Neoadjuvant Therapy for Resectable and Borderline Resectable Pancreatic Cancer: A Meta-Analysis of Randomized Controlled Trials. *JCM* **9**, 1129 (2020).
78. Pappalardo, A. *et al.* Adjuvant Treatment in Pancreatic Cancer: Shaping the Future of the Curative Setting. *Front. Oncol.* **11**, 695627 (2021).
79. Akhtar, M., Haider, A., Rashid, S. & Al-Nabet, A. D. M. H. Paget's "Seed and Soil" Theory of Cancer Metastasis: An Idea Whose Time has Come. *Advances in Anatomic Pathology* **26**, 69–74 (2019).
80. Baghban, R. *et al.* Tumor microenvironment complexity and therapeutic implications at a glance. *Cell Commun Signal* **18**, 59 (2020).
81. Zhang, J. & Veeramachaneni, N. Targeting interleukin-1 $\beta$  and inflammation in lung cancer. *Biomark Res* **10**, 5 (2022).
82. Elyada, E. *et al.* Cross-Species Single-Cell Analysis of Pancreatic Ductal Adenocarcinoma Reveals Antigen-Presenting Cancer-Associated Fibroblasts. *Cancer Discovery* **9**, 1102–1123 (2019).
83. Dominguez, C. X. *et al.* Single-Cell RNA Sequencing Reveals Stromal Evolution into LRRC15+ Myofibroblasts as a Determinant of Patient Response to Cancer Immunotherapy. *Cancer Discovery* **10**, 232–253 (2020).
84. Peng, J. *et al.* Single-cell RNA-seq highlights intra-tumoral heterogeneity and malignant progression in pancreatic ductal adenocarcinoma. *Cell Res* **29**, 725–738 (2019).
85. Mizutani, Y. *et al.* Meflin-Positive Cancer-Associated Fibroblasts Inhibit Pancreatic Carcinogenesis. *Cancer Research* **79**, 5367–5381 (2019).
86. Wang, Y. *et al.* Single-cell analysis of pancreatic ductal adenocarcinoma identifies a novel fibroblast subtype associated with poor prognosis but better immunotherapy response. *Cell Discov* **7**, 36 (2021).
87. Bussard, K. M., Mutkus, L., Stumpf, K., Gomez-Manzano, C. & Marini, F. C. Tumor-associated stromal cells as key contributors to the tumor microenvironment. *Breast Cancer Res* **18**, 84 (2016).
88. Zhou, J. *et al.* Tumor-Associated Macrophages: Recent Insights and Therapies. *Front. Oncol.* **10**, 188 (2020).
89. Hanahan, D. & Weinberg, R. A. Hallmarks of Cancer: The Next Generation. *Cell* **144**, 646–674 (2011).

90. Carreau, A., Hafny-Rahbi, B. E., Matejuk, A., Grillon, C. & Kieda, C. Why is the partial oxygen pressure of human tissues a crucial parameter? Small molecules and hypoxia. *Journal of Cellular and Molecular Medicine* **15**, 1239–1253 (2011).
91. Böckelmann, L. C. & Schumacher, U. Targeting tumor interstitial fluid pressure: will it yield novel successful therapies for solid tumors? *Expert Opinion on Therapeutic Targets* **23**, 1005–1014 (2019).
92. Schaaf, M. B., Garg, A. D. & Agostinis, P. Defining the role of the tumor vasculature in antitumor immunity and immunotherapy. *Cell Death Dis* **9**, 115 (2018).
93. Hida, K., Maishi, N., Annan, D. & Hida, Y. Contribution of Tumor Endothelial Cells in Cancer Progression. *IJMS* **19**, 1272 (2018).
94. Erdreich-Epstein, A. *et al.* Integrins  $\alpha_v\beta_3$  and  $\alpha_v\beta_5$  Are Expressed by Endothelium of High-Risk Neuroblastoma and Their Inhibition Is Associated with Increased Endogenous Ceramide. **10** (2000).
95. Wikimedia Commons. [https://commons.wikimedia.org/wiki/Main\\_Page](https://commons.wikimedia.org/wiki/Main_Page).
96. Chen, Y. *et al.* Type I collagen deletion in  $\alpha$ SMA+ myofibroblasts augments immune suppression and accelerates progression of pancreatic cancer. *Cancer Cell* **39**, 548-565.e6 (2021).
97. Eble, J. A. & Niland, S. The extracellular matrix in tumor progression and metastasis. *Clin Exp Metastasis* **36**, 171–198 (2019).
98. Singh, P., Carraher, C. & Schwarzbauer, J. E. Assembly of Fibronectin Extracellular Matrix. *Annu. Rev. Cell Dev. Biol.* **26**, 397–419 (2010).
99. Efthymiou, G. *et al.* Shaping Up the Tumor Microenvironment With Cellular Fibronectin. *Front. Oncol.* **10**, 641 (2020).
100. *Tumor Microenvironment: Extracellular Matrix Components – Part B*. vol. 1272 (Springer International Publishing, 2020).
101. Lu, P., Takai, K., Weaver, V. M. & Werb, Z. Extracellular Matrix Degradation and Remodeling in Development and Disease. **24** (2011).
102. Freeman, C. & Hopwood, J. J. Catalytic properties and an integrated role in the lysosomal degradation of heparan sulphate. **282**, 10 (1992).

103. Kessenbrock, K., Plaks, V. & Werb, Z. Matrix Metalloproteinases: Regulators of the Tumor Microenvironment. *Cell* **141**, 52–67 (2010).
104. Klein, T. & Bischoff, R. Physiology and pathophysiology of matrix metalloproteases. *Amino Acids* **41**, 271–290 (2011).
105. Rangasamy, L., Geronimo, B. D., Ort, I., Ramos, A. & de Pascual-Teresa, B. Molecular Imaging Probes Based on Matrix Metalloproteinase Inhibitors (MMPi). 33 (2019).
106. Greco, M. R. *et al.* Protease activity at invadopodial focal digestive areas is dependent on NHE1-driven acidic pH. *Oncology Reports* **31**, 940–946 (2014).
107. Estrella, V. *et al.* Acidity Generated by the Tumor Microenvironment Drives Local Invasion. *Cancer Res* **73**, 1524–1535 (2013).
108. Tjomsland, V. *et al.* The Desmoplastic Stroma Plays an Essential Role in the Accumulation and Modulation of Infiltrated Immune Cells in Pancreatic Adenocarcinoma. *Clinical and Developmental Immunology* **2011**, 1–12 (2011).
109. Dougan, S. K. The Pancreatic Cancer Microenvironment. *Cancer J* **23**, 321–325 (2017).
110. Cannon, A. *et al.* Desmoplasia in pancreatic ductal adenocarcinoma: insight into pathological function and therapeutic potential. *Genes Cancer* **9**, 78–86 (2018).
111. Bachem, M. G. *et al.* Pancreatic carcinoma cells induce fibrosis by stimulating proliferation and matrix synthesis of stellate cells. *Gastroenterology* **128**, 907–921 (2005).
112. Bulle, A. & Lim, K.-H. Beyond just a tight fortress: contribution of stroma to epithelial-mesenchymal transition in pancreatic cancer. *Sig Transduct Target Ther* **5**, 249 (2020).
113. Hamada, S. *et al.* Pancreatic stellate cells enhance stem cell-like phenotypes in pancreatic cancer cells. *Biochemical and Biophysical Research Communications* **421**, 349–354 (2012).
114. Han, X. *et al.* Reversal of pancreatic desmoplasia by re-educating stellate cells with a tumour microenvironment-activated nanosystem. *Nat Commun* **9**, 3390 (2018).
115. Hartmann, N. *et al.* Prevailing Role of Contact Guidance in Intrastromal T-cell Trapping in Human Pancreatic Cancer. *Clinical Cancer Research* **20**, 3422–3433 (2014).

116. Begum, A. *et al.* The extracellular matrix and focal adhesion kinase signaling regulate cancer stem cell function in pancreatic ductal adenocarcinoma. *PLoS ONE* **12**, e0180181 (2017).
117. Carapuça, E. F. *et al.* Anti-stromal treatment together with chemotherapy targets multiple signalling pathways in pancreatic adenocarcinoma: Stroma and cancer co-targeting. *J. Pathol.* **239**, 286–296 (2016).
118. Ene-Obong, A. *et al.* Activated Pancreatic Stellate Cells Sequester CD8+ T Cells to Reduce Their Infiltration of the Juxtatumoral Compartment of Pancreatic Ductal Adenocarcinoma. *Gastroenterology* **145**, 1121–1132 (2013).
119. Muz, B., de la Puente, P., Azab, F. & Azab, A. K. The role of hypoxia in cancer progression, angiogenesis, metastasis, and resistance to therapy. *HP* **83** (2015) doi:10.2147/HP.S93413.
120. Yang, S.-L., Wu, C., Xiong, Z.-F. & Fang, X. Progress on hypoxia-inducible factor-3: Its structure, gene regulation and biological function (Review). *Molecular Medicine Reports* **12**, 2411–2416 (2015).
121. Holmquist-Mengelbier, L. *et al.* Recruitment of HIF-1 $\alpha$  and HIF-2 $\alpha$  to common target genes is differentially regulated in neuroblastoma: HIF-2 $\alpha$  promotes an aggressive phenotype. *Cancer Cell* **10**, 413–423 (2006).
122. Wang, G. L., Jiang, B. H., Rue, E. A. & Semenza, G. L. Hypoxia-inducible factor 1 is a basic-helix-loop-helix-PAS heterodimer regulated by cellular O<sub>2</sub> tension. *Proc. Natl. Acad. Sci. U.S.A.* **92**, 5510–5514 (1995).
123. Landázuri, M. O., Vara-Vega, A., Vitón, M., Cuevas, Y. & del Peso, L. Analysis of HIF-prolyl hydroxylases binding to substrates. *Biochemical and Biophysical Research Communications* **351**, 313–320 (2006).
124. Cockman, M. E. *et al.* Hypoxia Inducible Factor- $\alpha$  Binding and Ubiquitylation by the von Hippel-Lindau Tumor Suppressor Protein. *Journal of Biological Chemistry* **275**, 25733–25741 (2000).
125. Masson, N. *et al.* The FIH hydroxylase is a cellular peroxide sensor that modulates HIF transcriptional activity. *EMBO Rep* **13**, 251–257 (2012).
126. Wei, J. *et al.* Recent Advances in the Discovery of HIF-1 $\alpha$ -p300/CBP Inhibitors as Anti-Cancer Agents. *MRMC* **18**, (2018).
127. Geng, H. *et al.* HIF1 $\alpha$  Protein Stability Is Increased by Acetylation at Lysine 709. *Journal of Biological Chemistry* **287**, 35496–35505 (2012).

128. Hagen, T. Oxygen versus Reactive Oxygen in the Regulation of HIF-1  $\alpha$  : The Balance Tips. *Biochemistry Research International* **2012**, 1–5 (2012).
129. Premkumar, D. R. *et al.* Intracellular Pathways Linking Hypoxia to Activation of c-fos and AP-1. in *Oxygen Sensing* (eds. Lahiri, S., Prabhakar, N. R. & Forster, R. E.) vol. 475 101–109 (Springer US, 2002).
130. He, T.-L. *et al.* The c-Myc–LDHA axis positively regulates aerobic glycolysis and promotes tumor progression in pancreatic cancer. *Med Oncol* **32**, 187 (2015).
131. Karapetsas, A. *et al.* Biochemical and molecular analysis of the interaction between ERK2 MAP kinase and hypoxia inducible factor-1 $\alpha$ . *The International Journal of Biochemistry & Cell Biology* **43**, 1582–1590 (2011).
132. Khurana, A. *et al.* Regulation of the Ring Finger E3 Ligase Siah2 by p38 MAPK. *Journal of Biological Chemistry* **281**, 35316–35326 (2006).
133. Hou, P.-C. *et al.* Hypoxia-Induced Downregulation of DUSP-2 Phosphatase Drives Colon Cancer Stemness. *Cancer Research* **77**, 4305–4316 (2017).
134. Korbecki, J. *et al.* Chronic and Cycling Hypoxia: Drivers of Cancer Chronic Inflammation through HIF-1 and NF- $\kappa$ B Activation: A Review of the Molecular Mechanisms. *IJMS* **22**, 10701 (2021).
135. van Uden, P., Kenneth, N. S. & Rocha, S. Regulation of hypoxia-inducible factor-1 $\alpha$  by NF- $\kappa$ B. *Biochemical Journal* **412**, 477–484 (2008).
136. Hoesel, B. & Schmid, J. A. The complexity of NF- $\kappa$ B signaling in inflammation and cancer. *Mol Cancer* **12**, 86 (2013).
137. Culver, C. *et al.* Mechanism of Hypoxia-Induced NF- $\kappa$ B. *Mol Cell Biol* **30**, 4901–4921 (2010).
138. Scortegagna, M. *et al.* HIF-1 $\alpha$  regulates epithelial inflammation by cell autonomous NF $\kappa$ B activation and paracrine stromal remodeling. *Blood* **111**, 3343–3354 (2008).
139. Xu, L., Pathak, P. S. & Fukumura, D. Hypoxia-Induced Activation of p38 Mitogen-Activated Protein Kinase and Phosphatidylinositol 3'-Kinase Signaling Pathways Contributes to Expression of Interleukin 8 in Human Ovarian Carcinoma Cells. *Clinical Cancer Research* **10**, 701–707 (2004).



140. Sizemore, N., Leung, S. & Stark, G. R. Activation of Phosphatidylinositol 3-Kinase in Response to Interleukin-1 Leads to Phosphorylation and Activation of the NF- $\kappa$ B p65/RelA Subunit. *Mol Cell Biol* **19**, 4798–4805 (1999).
141. Nidai Ozes, O. *et al.* NF- $\kappa$ B activation by tumour necrosis factor requires the Akt serine–threonine kinase. *Nature* **401**, 82–85 (1999).
142. Tafani, M. *et al.* Up-regulation of pro-inflammatory genes as adaptation to hypoxia in MCF-7 cells and in human mammary invasive carcinoma microenvironment. *Cancer Science* **101**, 1014–1023 (2010).
143. Yasui, H. *et al.* Low-Field Magnetic Resonance Imaging to Visualize Chronic and Cycling Hypoxia in Tumor-Bearing Mice. *Cancer Research* **70**, 6427–6436 (2010).
144. Olbryt, M. *et al.* Global Gene Expression Profiling in Three Tumor Cell Lines Subjected to Experimental Cycling and Chronic Hypoxia. *PLoS ONE* **9**, e105104 (2014).
145. Gutsche, K. *et al.* Intermittent hypoxia confers pro-metastatic gene expression selectively through NF- $\kappa$ B in inflammatory breast cancer cells. *Free Radical Biology and Medicine* **101**, 129–142 (2016).
146. Chen, W.-L., Wang, C.-C., Lin, Y.-J., Wu, C.-P. & Hsieh, C.-H. Cycling hypoxia induces chemoresistance through the activation of reactive oxygen species-mediated B-cell lymphoma extra-long pathway in glioblastoma multiforme. *J Transl Med* **13**, 389 (2015).
147. Miao, Z.-F. *et al.* Influence of different hypoxia models on metastatic potential of SGC-7901 gastric cancer cells. *Tumor Biol.* **35**, 6801–6808 (2014).
148. Hsieh. Cycling hypoxia increases U87 glioma cell radioresistance via ROS induced higher and long-term HIF-1 signal transduction activity. *Oncol Rep* **24**, (2010).
149. Zhang, J., Zheng, L., Cao, J., Chen, B. & Jin, D. Inflammation induced by increased frequency of intermittent hypoxia is attenuated by tempol administration. *Braz J Med Biol Res* **48**, 1115–1121 (2015).
150. Nanduri, J. *et al.* HIF-1 $\alpha$  Activation by Intermittent Hypoxia Requires NADPH Oxidase Stimulation by Xanthine Oxidase. *PLoS ONE* **10**, e0119762 (2015).
151. Koong, A. C. *et al.* Pancreatic tumors show high levels of hypoxia. *International Journal of Radiation Oncology\*Biophysics* **48**, 919–922 (2000).

152. Koppenol, W. H., Bounds, P. L. & Dang, C. V. Otto Warburg's contributions to current concepts of cancer metabolism. *Nat Rev Cancer* **11**, 325–337 (2011).
153. Ying, H. *et al.* Oncogenic Kras Maintains Pancreatic Tumors through Regulation of Anabolic Glucose Metabolism. *Cell* **149**, 656–670 (2012).
154. Cao, L. *et al.* Glycometabolic rearrangements--aerobic glycolysis in pancreatic cancer: causes, characteristics and clinical applications. *J Exp Clin Cancer Res* **39**, 267 (2020).
155. Stern, R., Shuster, S., Neudecker, B. A. & Formby, B. Lactate Stimulates Fibroblast Expression of Hyaluronan and CD44: The Warburg Effect Revisited. *Experimental Cell Research* **276**, 24–31 (2002).
156. Husain, Z., Huang, Y., Seth, P. & Sukhatme, V. P. Tumor-Derived Lactate Modifies Antitumor Immune Response: Effect on Myeloid-Derived Suppressor Cells and NK Cells. *J.I.* **191**, 1486–1495 (2013).
157. Yalcin, A. *et al.* 6-phosphofructo-2-kinase/fructose 2,6-bisphosphatase-3 is required for transforming growth factor  $\beta$ 1-enhanced invasion of Panc1 cells in vitro. *Biochemical and Biophysical Research Communications* **484**, 687–693 (2017).
158. Hsu, M.-C. *et al.* Extracellular PKM2 induces cancer proliferation by activating the EGFR signaling pathway. *11* (2016).
159. Penny, H. L. *et al.* Warburg metabolism in tumor-conditioned macrophages promotes metastasis in human pancreatic ductal adenocarcinoma. *OncoImmunology* **5**, e1191731 (2016).
160. Zhao, H. *et al.* Up-regulation of glycolysis promotes the stemness and EMT phenotypes in gemcitabine-resistant pancreatic cancer cells. *J. Cell. Mol. Med.* **21**, 2055–2067 (2017).
161. Ji, S. *et al.* ALDOA functions as an oncogene in the highly metastatic pancreatic cancer. *Cancer Letters* **374**, 127–135 (2016).
162. Guillaumond, F. *et al.* Strengthened glycolysis under hypoxia supports tumor symbiosis and hexosamine biosynthesis in pancreatic adenocarcinoma. *Proc. Natl. Acad. Sci. U.S.A.* **110**, 3919–3924 (2013).
163. Sonveaux, P. *et al.* Targeting lactate-fueled respiration selectively kills hypoxic tumor cells in mice. *J. Clin. Invest.* JCI36843 (2008) doi:10.1172/JCI36843.

164. Shi, S. *et al.* VEGF Promotes Glycolysis in Pancreatic Cancer via HIF1? Up-Regulation. *CMM* **16**, 394–403 (2016).
165. Topalovski, M., Hagopian, M., Wang, M. & Brekken, R. A. Hypoxia and Transforming Growth Factor  $\beta$  Cooperate to Induce Fibulin-5 Expression in Pancreatic Cancer. *Journal of Biological Chemistry* **291**, 22244–22252 (2016).
166. Abdalla, M. Y. *et al.* Enhancing responsiveness of pancreatic cancer cells to gemcitabine treatment under hypoxia by heme oxygenase-1 inhibition. *Translational Research* **207**, 56–69 (2019).
167. Lang, M. *et al.* Arsenic trioxide plus PX-478 achieves effective treatment in pancreatic ductal adenocarcinoma. *Cancer Letters* **378**, 87–96 (2016).
168. Zhang, L. *et al.* Reactive Oxygen Species and Targeted Therapy for Pancreatic Cancer. *Oxidative Medicine and Cellular Longevity* **2016**, 1–9 (2016).
169. Yan, B. *et al.* Paracrine HGF/c-MET enhances the stem cell-like potential and glycolysis of pancreatic cancer cells via activation of YAP/HIF-1 $\alpha$ . *Experimental Cell Research* **371**, 63–71 (2018).
170. Zhu, H. *et al.* Upregulation of autophagy by hypoxia-inducible factor-1 $\alpha$  promotes EMT and metastatic ability of CD133+ pancreatic cancer stem-like cells during intermittent hypoxia. *Oncology Reports* **32**, 935–942 (2014).
171. Su, H.-T. *et al.* Stem Cell Marker Nestin Is Critical for TGF- $\beta$ 1-Mediated Tumor Progression in Pancreatic Cancer. *Molecular Cancer Research* **11**, 768–779 (2013).
172. Cao, J. *et al.* Hypoxia-driven paracrine osteopontin/integrin  $\alpha$ v $\beta$ 3 signaling promotes pancreatic cancer cell epithelial–mesenchymal transition and cancer stem cell-like properties by modulating forkhead box protein M1. *Mol Oncol* **13**, 228–245 (2019).
173. Shimojo, Y. *et al.* Attenuation of reactive oxygen species by antioxidants suppresses hypoxia-induced epithelial–mesenchymal transition and metastasis of pancreatic cancer cells. *Clin Exp Metastasis* **30**, 143–154 (2013).
174. Chen, S. *et al.* Hypoxia induces TWIST-activated epithelial–mesenchymal transition and proliferation of pancreatic cancer cells in vitro and in nude mice. *Cancer Letters* **383**, 73–84 (2016).

175. Yang, J. *et al.* HIF-2 $\alpha$  promotes epithelial-mesenchymal transition through regulating Twist2 binding to the promoter of E-cadherin in pancreatic cancer. *J Exp Clin Cancer Res* **35**, 26 (2016).
176. Miller, B. W. *et al.* Targeting the LOX / HYPOXIA axis reverses many of the features that make pancreatic cancer deadly: inhibition of LOX abrogates metastasis and enhances drug efficacy. *EMBO Mol Med* **7**, 1063–1076 (2015).
177. Audero, M. M., Prevarskaya, N. & Fiorio Pla, A. Ca<sup>2+</sup> Signalling and Hypoxia/Acidic Tumour Microenvironment Interplay in Tumour Progression. *IJMS* **23**, 7377 (2022).
178. Manoli, S. *et al.* The Activity of Kv 11.1 Potassium Channel Modulates F-Actin Organization During Cell Migration of Pancreatic Ductal Adenocarcinoma Cells. *Cancers* **11**, 135 (2019).
179. Ide, T. *et al.* Tumor–stromal cell interaction under hypoxia increases the invasiveness of pancreatic cancer cells through the hepatocyte growth factor/c-Met pathway. *Int. J. Cancer* **119**, 2750–2759 (2006).
180. Azoitei, N. *et al.* PKM2 promotes tumor angiogenesis by regulating HIF-1 $\alpha$  through NF- $\kappa$ B activation. *Mol Cancer* **15**, 3 (2016).
181. Niu, F. *et al.* LB-1 Exerts Antitumor Activity in Pancreatic Cancer by Inhibiting HIF-1 $\alpha$  and Stat3 Signaling: ROLE OF LB-1 IN PANCREATIC CANCER. *J. Cell. Physiol.* **230**, 2212–2223 (2015).
182. Kitamoto, S. *et al.* MUC1 enhances hypoxia-driven angiogenesis through the regulation of multiple proangiogenic factors. *Oncogene* **32**, 4614–4621 (2013).
183. Maruggi, M. *et al.* Absence of HIF1A Leads to Glycogen Accumulation and an Inflammatory Response That Enables Pancreatic Tumor Growth. *Cancer Research* **79**, 5839–5848 (2019).
184. Chang, L.-H., Pan, S.-L., Lai, C.-Y., Tsai, A.-C. & Teng, C.-M. Activated PAR-2 Regulates Pancreatic Cancer Progression through ILK/HIF- $\alpha$ -Induced TGF- $\alpha$  Expression and MEK/VEGF-A-Mediated Angiogenesis. *The American Journal of Pathology* **183**, 566–575 (2013).
185. Zhang, Z. *et al.* Hypoxia potentiates gemcitabine-induced stemness in pancreatic cancer cells through AKT/Notch1 signaling. *J Exp Clin Cancer Res* **37**, 291 (2018).
186. Yokoi, K. & Fidler, I. J. Hypoxia Increases Resistance of Human Pancreatic Cancer Cells to Apoptosis Induced by Gemcitabine. *Clinical Cancer Research* **10**, 2299–2306 (2004).

187. He, X. *et al.* Hypoxia regulates ABCG<sub>2</sub> activity through the activation of ERK1/2/HIF-1 $\alpha$  and contributes to chemoresistance in pancreatic cancer cells. *Cancer Biology & Therapy* **17**, 188–198 (2016).
188. Yoo, H. C. *et al.* A Variant of SLC1A5 Is a Mitochondrial Glutamine Transporter for Metabolic Reprogramming in Cancer Cells. *Cell Metabolism* **31**, 267-283.e12 (2020).
189. Persi, E. *et al.* Systems analysis of intracellular pH vulnerabilities for cancer therapy. *Nat Commun* **9**, 2997 (2018).
190. Hao, G., Xu, Z. P. & Li, L. Manipulating extracellular tumour pH: an effective target for cancer therapy. *RSC Adv.* **8**, 22182–22192 (2018).
191. Boedtker, E. & Pedersen, S. F. The Acidic Tumor Microenvironment as a Driver of Cancer. *Annu. Rev. Physiol.* **82**, 103–126 (2020).
192. Rohani, N. *et al.* Acidification of Tumor at Stromal Boundaries Drives Transcriptome Alterations Associated with Aggressive Phenotypes. *Cancer Res* **79**, 1952–1966 (2019).
193. Chiche, J. *et al.* Hypoxia-Inducible Carbonic Anhydrase IX and XII Promote Tumor Cell Growth by Counteracting Acidosis through the Regulation of the Intracellular pH. *Cancer Research* **69**, 358–368 (2009).
194. LaMonte, G. *et al.* Acidosis induces reprogramming of cellular metabolism to mitigate oxidative stress. *Cancer Metab* **1**, 23 (2013).
195. Filatova, A. *et al.* Acidosis Acts through HSP90 in a PHD/VHL-Independent Manner to Promote HIF Function and Stem Cell Maintenance in Glioma. *Cancer Res* **76**, 5845–5856 (2016).
196. Benej, M. *et al.* CA IX Stabilizes Intracellular pH to Maintain Metabolic Reprogramming and Proliferation in Hypoxia. *Front. Oncol.* **10**, 1462 (2020).
197. Swietach, P. What is pH regulation, and why do cancer cells need it? *Cancer Metastasis Rev* **38**, 5–15 (2019).
198. Damaghi, M., Wojtkowiak, J. W. & Gillies, R. J. pH sensing and regulation in cancer. *Front. Physiol.* **4**, (2013).
199. Malo, M. E. & Fliegel, L. Physiological role and regulation of the Na<sup>+</sup>/H<sup>+</sup> exchanger. *Can. J. Physiol. Pharmacol.* **84**, 1081–1095 (2006).

200. Denker, S. P., Huang, D. C., Orlowski, J., Furthmayr, H. & Barber, D. L. Direct Binding of the Na<sup>+</sup>-H<sup>+</sup> Exchanger NHE1 to ERM Proteins Regulates the Cortical Cytoskeleton and Cell Shape Independently of H<sup>+</sup> Translocation. *Molecular Cell* **6**, 1425–1436 (2000).
201. Lucien, F. *et al.* Hypoxia-induced mobilization of NHE6 to the plasma membrane triggers endosome hyperacidification and chemoresistance. *Nat Commun* **8**, 15884 (2017).
202. Kondapalli, K. C. *et al.* A leak pathway for luminal protons in endosomes drives oncogenic signalling in glioblastoma. *Nat Commun* **6**, 6289 (2015).
203. Busco, G. *et al.* NHE1 promotes invadopodial ECM proteolysis through acidification of the peri-invadopodial space. *FASEB j.* **24**, 3903–3915 (2010).
204. Cardone, R. A., Casavola, V. & Reshkin, S. J. The role of disturbed pH dynamics and the Na<sup>+</sup>/H<sup>+</sup> exchanger in metastasis. *Nat Rev Cancer* **5**, 786–795 (2005).
205. Greco, M. R. *et al.* Integrin-Linked Kinase Links Integrin Activation to Invadopodia Function and Invasion via the p(T567)-Ezrin/NHERF1/NHE1 Pathway. *IJMS* **22**, 2162 (2021).
206. Reshkin, S. J., A. Cardone, R. & Harguindey, S. Na<sup>+</sup>-H<sup>+</sup> Exchanger, pH Regulation and Cancer. *PRA* **8**, 85–99 (2012).
207. Brown, D. A., Melvin, J. E. & Yule, D. I. Critical role for NHE1 in intracellular pH regulation in pancreatic acinar cells. *American Journal of Physiology-Gastrointestinal and Liver Physiology* **285**, G804–G812 (2003).
208. Olszewski, U., Hlozek, M. & Hamilton, G. Activation of Na<sup>+</sup>/H<sup>+</sup> exchanger 1 by neurotensin signaling in pancreatic cancer cell lines. *Biochemical and Biophysical Research Communications* **393**, 414–419 (2010).
209. Wang, H., Cai, J., Du, S., Wei, W. & Shen, X. LAMC2 modulates the acidity of microenvironments to promote invasion and migration of pancreatic cancer cells via regulating AKT-dependent NHE1 activity. *Experimental Cell Research* **391**, 111984 (2020).
210. Cannone, S. *et al.* Cancer Associated Fibroblast (CAF) Regulation of PDAC Parenchymal (CPC) and CSC Phenotypes Is Modulated by ECM Composition. *Cancers* **14**, 3737 (2022).
211. Ouyang, H., Gore, J., Deitz, S. & Korc, M. microRNA-10b enhances pancreatic cancer cell invasion by suppressing TIP30 expression and promoting EGF and TGF- $\beta$  actions. *Oncogene* **33**, 4664–4674 (2014).

212. Cardone, R. A. *et al.* A Novel NHE1-Centered Signaling Cassette Drives Epidermal Growth Factor Receptor-Dependent Pancreatic Tumor Metastasis and Is a Target for Combination Therapy. *Neoplasia* **17**, 155–166 (2015).
213. Malinda, R. R. *et al.* TGF $\beta$  Signaling Increases Net Acid Extrusion, Proliferation and Invasion in Panc-1 Pancreatic Cancer Cells: SMAD4 Dependence and Link to Merlin/NF2 Signaling. *Frontiers in Oncology* **10**, 687 (2020).
214. Galenkamp, K. M. O. *et al.* Golgi Acidification by NHE7 Regulates Cytosolic pH Homeostasis in Pancreatic Cancer Cells. *Cancer Discov* **10**, 822–835 (2020).
215. Sandforth, L. *et al.* Impact of the Monocarboxylate Transporter-1 (MCT1)-Mediated Cellular Import of Lactate on Stemness Properties of Human Pancreatic Adenocarcinoma Cells. *Cancers* **12**, 581 (2020).
216. Baek, G. *et al.* MCT4 Defines a Glycolytic Subtype of Pancreatic Cancer with Poor Prognosis and Unique Metabolic Dependencies. *Cell Reports* **9**, 2233–2249 (2014).
217. Kong, S. C. *et al.* Monocarboxylate Transporters MCT1 and MCT4 Regulate Migration and Invasion of Pancreatic Ductal Adenocarcinoma Cells. *Pancreas* **45**, 1036–1047 (2016).
218. Wu, D.-H. *et al.* miR-124 Suppresses Pancreatic Ductal Adenocarcinoma Growth by Regulating Monocarboxylate Transporter 1-Mediated Cancer Lactate Metabolism. *Cell Physiol Biochem* **50**, 924–935 (2018).
219. Schneider, L. *et al.* The Na<sup>+</sup>/H<sup>+</sup> exchanger NHE1 is required for directional migration stimulated via PDGFR- $\alpha$  in the primary cilium. *The Journal of Cell Biology* **185**, 163–176 (2009).
220. Dovmark, T. H., Saccomano, M., Hulikova, A., Alves, F. & Swietach, P. Connexin-43 channels are a pathway for discharging lactate from glycolytic pancreatic ductal adenocarcinoma cells. *Oncogene* **36**, 4538–4550 (2017).
221. Wu, Z. *et al.* Emerging roles of the solute carrier family in pancreatic cancer. *Clinical and Translational Medicine* **11**, (2021).
222. Cappellesso, F. *et al.* Targeting the bicarbonate transporter SLC4A4 overcomes immunosuppression and immunotherapy resistance in pancreatic cancer. *Nat Cancer* **3**, 1464–1483 (2022).

223. Zhang, X., Tan, P., Zhuang, Y. & Du, L. hsa\_circRNA\_001587 upregulates SLC4A4 expression to inhibit migration, invasion, and angiogenesis of pancreatic cancer cells via binding to microRNA-223. *American Journal of Physiology-Gastrointestinal and Liver Physiology* **319**, G703–G717 (2020).
224. Ramirez, C., Hauser, A. D., Vucic, E. A. & Bar-Sagi, D. Plasma membrane V-ATPase controls oncogenic RAS-induced macropinocytosis. *Nature* **576**, 477–481 (2019).
225. Swietach, P., Hulikova, A., Vaughan-Jones, R. D. & Harris, A. L. New insights into the physiological role of carbonic anhydrase IX in tumour pH regulation. *Oncogene* **29**, 6509–6521 (2010).
226. Swietach, P., Patiar, S., Supuran, C. T., Harris, A. L. & Vaughan-Jones, R. D. The Role of Carbonic Anhydrase 9 in Regulating Extracellular and Intracellular pH in Three-dimensional Tumor Cell Growths. *Journal of Biological Chemistry* **284**, 20299–20310 (2009).
227. Becker, H. M. Carbonic anhydrase IX and acid transport in cancer. *Br J Cancer* **122**, 157–167 (2020).
228. Ong, C. H. C. *et al.* Hypoxia-regulated carbonic anhydrase IX (CAIX) protein is an independent prognostic indicator in triple negative breast cancer. *Breast Cancer Res* **24**, 38 (2022).
229. Li, Y., Dong, M., Sheng, W. & Huang, L. Roles of Carbonic Anhydrase IX in Development of Pancreatic Cancer. *Pathol. Oncol. Res.* **22**, 277–286 (2016).
230. McDonald, P. C. *et al.* Regulation of pH by Carbonic Anhydrase 9 Mediates Survival of Pancreatic Cancer Cells With Activated KRAS in Response to Hypoxia. *Gastroenterology* **157**, 823–837 (2019).
231. Futai, M., Sun-Wada, G.-H., Wada, Y., Matsumoto, N. & Nakanishi-Matsui, M. Vacuolar-type ATPase: A proton pump to lysosomal trafficking. *Proc. Jpn. Acad., Ser. B* **95**, 261–277 (2019).
232. Jefferies, K. C., Cipriano, D. J. & Forgac, M. Function, structure and regulation of the vacuolar (H<sup>+</sup>)-ATPases. *Archives of Biochemistry and Biophysics* **476**, 33–42 (2008).
233. Sun-Wada, G.-H. & Wada, Y. Role of vacuolar-type proton ATPase in signal transduction. *Biochimica et Biophysica Acta (BBA) - Bioenergetics* **1847**, 1166–1172 (2015).
234. O’Callaghan, K. M. *et al.* Heme-binding Protein HRG-1 Is Induced by Insulin-like Growth Factor I and Associates with the Vacuolar H<sup>+</sup>-ATPase to Control Endosomal pH and Receptor Trafficking. *Journal of Biological Chemistry* **285**, 381–391 (2010).



235. Sennoune, S. R. & Martinez-Zaguilan, R. Plasmalemmal vacuolar H<sup>+</sup>-ATPases in angiogenesis, diabetes and cancer. *J Bioenerg Biomembr* **39**, 427–433 (2007).
236. Elliott, I. A. *et al.* Lysosome inhibition sensitizes pancreatic cancer to replication stress by aspartate depletion. *Proc. Natl. Acad. Sci. U.S.A.* **116**, 6842–6847 (2019).
237. Chung, C. *et al.* The vacuolar-ATPase modulates matrix metalloproteinase isoforms in human pancreatic cancer. *Lab Invest* **91**, 732–743 (2011).
238. Hayashi, Y., Katayama, K., Togawa, T., Kimura, T. & Yamaguchi, A. Effects of bafilomycin A1, a vacuolar type H<sup>+</sup> ATPase inhibitor, on the thermosensitivity of a human pancreatic cancer cell line. *International Journal of Hyperthermia* **22**, 275–285 (2006).
239. Gatenby, R. A. & Brown, J. Mutations, evolution and the central role of a self-defined fitness function in the initiation and progression of cancer. *Biochimica et Biophysica Acta (BBA) - Reviews on Cancer* **1867**, 162–166 (2017).
240. Massonneau, J. *et al.* Suboptimal extracellular pH values alter DNA damage response to induced double-strand breaks. *FEBS Open Bio* **8**, 416–425 (2018).
241. Jayanth, V. R., Bayne, M. T. & Varnes, M. E. Effects of Extracellular and Intracellular pH on Repair of Potentially Lethal Damage, Chromosome Aberrations and DNA Double-Strand Breaks in Irradiated Plateau-Phase A549 Cells. *Radiation Research* **139**, 152 (1994).
242. Xiao, H., Li, T.-K., Yang, J.-M. & Liu, L. F. Acidic pH induces topoisomerase II-mediated DNA damage. *Proc. Natl. Acad. Sci. U.S.A.* **100**, 5205–5210 (2003).
243. Zhang, H. Y., Hormi-Carver, K., Zhang, X., Spechler, S. J. & Souza, R. F. In Benign Barrett's Epithelial Cells, Acid Exposure Generates Reactive Oxygen Species That Cause DNA Double-Strand Breaks. *Cancer Research* **69**, 9083–9089 (2009).
244. McBrian, M. A. *et al.* Histone Acetylation Regulates Intracellular pH. *Molecular Cell* **49**, 310–321 (2013).
245. Flinck, M., Kramer, S. H. & Pedersen, S. F. Roles of pH in control of cell proliferation. *Acta Physiol* **223**, e13068 (2018).
246. Lagadic-Gossmann, D., Huc, L. & Lecreur, V. Alterations of intracellular pH homeostasis in apoptosis: origins and roles. *Cell Death Differ* **11**, 953–961 (2004).

247. Zhu, L. *et al.* ASIC1 inhibition impairs the proliferation and migration of pancreatic stellate cells induced by pancreatic cancer cells. *neo* **68**, 174–179 (2021).
248. Jin, C. *et al.* Over-expression of ASIC1a promotes proliferation via activation of the  $\beta$ -catenin/LEF-TCF axis and is associated with disease outcome in liver cancer. *Oncotarget* **8**, 25977–25988 (2016).
249. Glitsch, M. Protons and  $\text{Ca}^{2+}$ : Ionic Allies in Tumor Progression? *Physiology* **26**, 252–265 (2011).
250. Hjelmeland, A. B. *et al.* Acidic stress promotes a glioma stem cell phenotype. *Cell Death Differ* **18**, 829–840 (2011).
251. Hu, P. *et al.* Acidosis enhances the self-renewal and mitochondrial respiration of stem cell-like glioma cells through CYP24A1-mediated reduction of vitamin D. *Cell Death Dis* **10**, 25 (2019).
252. Végran, F., Boidot, R., Michiels, C., Sonveaux, P. & Feron, O. Lactate Influx through the Endothelial Cell Monocarboxylate Transporter MCT1 Supports an NF- $\kappa$ B/IL-8 Pathway that Drives Tumor Angiogenesis. *Cancer Research* **71**, 2550–2560 (2011).
253. De Saedeleer, C. J. *et al.* Lactate Activates HIF-1 in Oxidative but Not in Warburg-Phenotype Human Tumor Cells. *PLoS ONE* **7**, e46571 (2012).
254. Huang, S. *et al.* Acidic stress induces apoptosis and inhibits angiogenesis in human bone marrow-derived endothelial progenitor cells. *Oncol Lett* (2017) doi:10.3892/ol.2017.6947.
255. Faes, S. *et al.* Acidic pH reduces VEGF-mediated endothelial cell responses by downregulation of VEGFR-2; relevance for anti-angiogenic therapies. *Oncotarget* **7**, 86026–86038 (2016).
256. Peppicelli, S., Bianchini, F., Torre, E. & Calorini, L. Contribution of acidic melanoma cells undergoing epithelial-to-mesenchymal transition to aggressiveness of non-acidic melanoma cells. *Clin Exp Metastasis* **31**, 423–433 (2014).
257. Riemann, A. *et al.* Extracellular Acidosis Modulates the Expression of Epithelial-Mesenchymal Transition (EMT) Markers and Adhesion of Epithelial and Tumor Cells. *Neoplasia* **21**, 450–458 (2019).
258. Suzuki, A., Maeda, T., Baba, Y., Shimamura, K. & Kato, Y. Acidic extracellular pH promotes epithelial mesenchymal transition in Lewis lung carcinoma model. *Cancer Cell Int* **14**, 129 (2014).
259. Wu, T.-C. *et al.* Identification of distinct slow mode of reversible adaptation of pancreatic ductal adenocarcinoma to the prolonged acidic pH microenvironment. *J Exp Clin Cancer Res* **41**, 137 (2022).

260. Corbet, C. & Feron, O. Tumour acidosis: from the passenger to the driver's seat. *Nat Rev Cancer* **17**, 577–593 (2017).
261. Hofschröder, V. *et al.* Extracellular protonation modulates cell-cell interaction mechanics and tissue invasion in human melanoma cells. *Sci Rep* **7**, 42369 (2017).
262. Stock, C. & Pedersen, S. F. Roles of pH and the Na<sup>+</sup>/H<sup>+</sup> exchanger NHE1 in cancer: From cell biology and animal models to an emerging translational perspective? *Seminars in Cancer Biology* **43**, 5–16 (2017).
263. Chen, Y., Chen, C.-H., Tung, P.-Y., Huang, S.-H. & Wang, S.-M. An acidic extracellular pH disrupts adherens junctions in HepG2 cells by Src kinases-dependent modification of E-cadherin. *J. Cell. Biochem.* **108**, 851–859 (2009).
264. Li, S. *et al.* Acidic pH regulates cytoskeletal dynamics through conformational integrin  $\beta$ 1 activation and promotes membrane protrusion. *Biochimica et Biophysica Acta (BBA) - Molecular Basis of Disease* **1864**, 2395–2408 (2018).
265. Stock, C. & Schwab, A. Protons make tumor cells move like clockwork. *Pflügers Arch - Eur J Physiol* **458**, 981–992 (2009).
266. Moellering, R. E. *et al.* Acid treatment of melanoma cells selects for invasive phenotypes. *Clin Exp Metastasis* **25**, 411–425 (2008).
267. Debreova, M. *et al.* CAIX Regulates Invadopodia Formation through Both a pH-Dependent Mechanism and Interplay with Actin Regulatory Proteins. *IJMS* **20**, 2745 (2019).
268. Lee, S.-H. *et al.* Carbonic anhydrase IX is a pH-stat that sets an acidic tumour extracellular pH in vivo. *Br J Cancer* **119**, 622–630 (2018).
269. Wojtkowiak, J. W., Verduzco, D., Schramm, K. J. & Gillies, R. J. Drug Resistance and Cellular Adaptation to Tumor Acidic pH Microenvironment. *Mol. Pharmaceutics* **8**, 2032–2038 (2011).
270. Brand, A. *et al.* LDHA-Associated Lactic Acid Production Blunts Tumor Immunosurveillance by T and NK Cells. *Cell Metabolism* **24**, 657–671 (2016).
271. Colegio, O. R. *et al.* Functional polarization of tumour-associated macrophages by tumour-derived lactic acid. *Nature* **513**, 559–563 (2014).

272. Ishikawa, T. *et al.* Influence of pH on Heat-Induced Aggregation and Degradation of Therapeutic Monoclonal Antibodies. *Biological & Pharmaceutical Bulletin* **33**, 1413–1417 (2010).
273. Gerweck, L. E., Vijayappa, S. & Kozin, S. Tumor pH controls the *in vivo* efficacy of weak acid and base chemotherapeutics. *Mol Cancer Ther* **5**, 1275–1279 (2006).
274. Blaszczyk, W. & Swietach, P. What do cellular responses to acidity tell us about cancer? *Cancer Metastasis Rev* **40**, 1159–1176 (2021).
275. Wojtkowiak, J. W. *et al.* Chronic Autophagy Is a Cellular Adaptation to Tumor Acidic pH Microenvironments. *Cancer Res* **72**, 3938–3947 (2012).
276. Marino, M. L. *et al.* Autophagy Is a Protective Mechanism for Human Melanoma Cells under Acidic Stress. *J. Biol. Chem.* **287**, 30664–30676 (2012).
277. Andreucci, E. *et al.* The acidic tumor microenvironment drives a stem-like phenotype in melanoma cells. *J Mol Med* **98**, 1431–1446 (2020).
278. Peppicelli, S. *et al.* Anoikis Resistance as a Further Trait of Acidic-Adapted Melanoma Cells. *Journal of Oncology* **2019**, 1–13 (2019).
279. Damaghi, M. & Gillies, R. Phenotypic changes of acid-adapted cancer cells push them toward aggressiveness in their evolution in the tumor microenvironment. *Cell Cycle* **16**, 1739–1743 (2017).
280. Yao, J. *et al.* Cancer Cell Acid Adaptation Gene Expression Response Is Correlated to Tumor-Specific Tissue Expression Profiles and Patient Survival. *Cancers* **12**, 2183 (2020).
281. Klein, C. A. Selection and adaptation during metastatic cancer progression. *Nature* **501**, 365–372 (2013).
282. Fortunato, A. *et al.* Natural Selection in Cancer Biology: From Molecular Snowflakes to Trait Hallmarks. *Cold Spring Harb Perspect Med* **7**, a029652 (2017).
283. Leroi, A. M., Koufopanou, V. & Burt, A. Cancer selection. *Nat Rev Cancer* **3**, 226–231 (2003).
284. Hwang, I. K. *et al.* Presence of pancreatic intraepithelial neoplasia-3 in a background of chronic pancreatitis in pancreatic cancer patients. *Cancer Sci* **106**, 1408–1413 (2015).
285. P. U. Reber, A. G. Patel, M. T. Toy. Feline Model of Chronic Obstructive Pancreatitis: Effects of Acute Pancreatic Duct Decompression on Blood Flow and Interstitial pH. *Scandinavian Journal of Gastroenterology* **34**, 439–444 (1999).

286. Pedersen, S. F., Novak, I., Alves, F., Schwab, A. & Pardo, L. A. Alternating pH landscapes shape epithelial cancer initiation and progression: Focus on pancreatic cancer. *BioEssays* **39**, 1600253 (2017).
287. Berridge, M. J., Lipp, P. & Bootman, M. D. The versatility and universality of calcium signalling. *Nat Rev Mol Cell Biol* **1**, 11–21 (2000).
288. Pratt, S. J., Hernández-Ochoa, E. & Martin, S. S. Calcium signaling: breast cancer's approach to manipulation of cellular circuitry. *Biophys Rev* **12**, 1343–1359 (2020).
289. Monteith, G. R., Prevarskaya, N. & Roberts-Thomson, S. J. The calcium–cancer signalling nexus. *Nat Rev Cancer* **17**, 373–380 (2017).
290. Cahalan, M. D. STIMulating store-operated Ca<sup>2+</sup> entry. *Nat Cell Biol* **11**, 669–677 (2009).
291. Wuytack, F., Raeymaekers, L. & Missiaen, L. PMR1/SPCA Ca<sup>2+</sup> pumps and the role of the Golgi apparatus as a Ca<sup>2+</sup> store. *Pflugers Arch - Eur J Physiol* **446**, 148–153 (2003).
292. Noble, D. & Herchuelz, A. Role of Na/Ca exchange and the plasma membrane Ca<sup>2+</sup>-ATPase in cell function: Conference on Na/Ca Exchange. *EMBO Rep* **8**, 228–232 (2007).
293. Panda, S., Chatterjee, O., Roy, L. & Chatterjee, S. Targeting Ca<sup>2+</sup> signaling: A new arsenal against cancer. *Drug Discovery Today* **27**, 923–934 (2022).
294. Pethő, Z., Najder, K., Bulk, E. & Schwab, A. Mechanosensitive ion channels push cancer progression. *Cell Calcium* **80**, 79–90 (2019).
295. Prevarskaya, N., Skryma, R. & Shuba, Y. Ion Channels in Cancer: Are Cancer Hallmarks Oncochannelopathies? *Physiological Reviews* **98**, 559–621 (2018).
296. Lin, R. *et al.* TRPM2 promotes the proliferation and invasion of pancreatic ductal adenocarcinoma. *Mol Med Report* (2018) doi:10.3892/mmr.2018.8816.
297. Bauer, I. *et al.* The NAD<sup>+</sup>-dependent Histone Deacetylase SIRT6 Promotes Cytokine Production and Migration in Pancreatic Cancer Cells by Regulating Ca<sup>2+</sup> Responses. *Journal of Biological Chemistry* **287**, 40924–40937 (2012).
298. Yee, N. S., Zhou, W. & Liang, I.-C. Transient receptor potential ion channel Trpm7 regulates exocrine pancreatic epithelial proliferation by Mg<sup>2+</sup>-sensitive Socs3a signaling in development and cancer. *Disease Models & Mechanisms* **4**, 240–254 (2011).

299. Yee, N. S., Chan, A. S., Yee, J. D. & Yee, R. K. TRPM7 and TRPM8 Ion Channels in Pancreatic Adenocarcinoma: Potential Roles as Cancer Biomarkers and Targets. *Scientifica* **2012**, 1–8 (2012).
300. Yee, N. S. *et al.* Aberrant over-expression of TRPM7 ion channels in pancreatic cancer: required for cancer cell invasion and implicated in tumor growth and metastasis. *Biology Open* **4**, 507–514 (2015).
301. Rybarczyk, P. *et al.* Transient receptor potential melastatin-related 7 channel is overexpressed in human pancreatic ductal adenocarcinomas and regulates human pancreatic cancer cell migration. *Int. J. Cancer* **131**, E851–E861 (2012).
302. Yee, N. S., Zhou, W. & Lee, M. Transient receptor potential channel TRPM8 is over-expressed and required for cellular proliferation in pancreatic adenocarcinoma. *Cancer Letters* **297**, 49–55 (2010).
303. Cucu, D. *et al.* Characterization of Functional Transient Receptor Potential Melastatin 8 Channels in Human Pancreatic Ductal Adenocarcinoma Cells. *Pancreas* **43**, 795–800 (2014).
304. Liu, J. *et al.* Silencing of TRPM8 inhibits aggressive tumor phenotypes and enhances gemcitabine sensitivity in pancreatic cancer. *Pancreatology* **18**, 935–944 (2018).
305. Du, J. *et al.* Elevated Transient Receptor Potential Melastatin 8 (TRPM8) Expression Is Correlated with Poor Prognosis in Pancreatic Cancer. *Med Sci Monit* **24**, 3720–3725 (2018).
306. Ulăreanu, R. *et al.* N-glycosylation of the transient receptor potential melastatin 8 channel is altered in pancreatic cancer cells. *Tumour Biol.* **39**, 101042831772094 (2017).
307. Kim, M.-H., Seo, J. B., Burnett, L. A., Hille, B. & Koh, D.-S. Characterization of store-operated Ca<sup>2+</sup> channels in pancreatic duct epithelia. *Cell Calcium* **54**, 266–275 (2013).
308. Dong, H. *et al.* Molecular mechanisms underlying Ca<sup>2+</sup>-mediated motility of human pancreatic duct cells. **299**, 11 (2010).
309. Hartel, M. Vanilloids in pancreatic cancer: potential for chemotherapy and pain management. *Gut* **55**, 519–528 (2006).
310. Huang, J., Liu, J. & Qiu, L. Transient receptor potential vanilloid 1 promotes EGFR ubiquitination and modulates EGFR/MAPK signalling in pancreatic cancer cells. *Cell Biochem Funct* **38**, 401–408 (2020).

311. Zhang, L. P., Ma, F., Abshire, S. M. & Westlund, K. N. Prolonged high fat/alcohol exposure increases TRPV4 and its functional responses in pancreatic stellate cells. *American Journal of Physiology-Regulatory, Integrative and Comparative Physiology* **304**, R702–R711 (2013).
312. Zaccagnino, A. *et al.* In silico analysis of the transportome in human pancreatic ductal adenocarcinoma. *Eur Biophys J* **45**, 749–763 (2016).
313. Song, H. *et al.* Expression and prognostic significance of TRPV6 in the development and progression of pancreatic cancer. *Oncol Rep* (2018) doi:10.3892/or.2018.6216.
314. Tawfik, D. *et al.* The A818–6 system as an in-vitro model for studying the role of the transportome in pancreatic cancer. *BMC Cancer* **20**, 264 (2020).
315. Schnipper, J. *et al.* Acid Adaptation Promotes TRPC1 Plasma Membrane Localization Leading to Pancreatic Ductal Adenocarcinoma Cell Proliferation and Migration through Ca<sup>2+</sup> Entry and Interaction with PI3K/CaM. *Cancers* **14**, 4946 (2022).
316. Storck, H. *et al.* Ion channels in control of pancreatic stellate cell migration. *Oncotarget* **8**, (2017).
317. Nielsen, N. *et al.* TRPC6 channels modulate the response of pancreatic stellate cells to hypoxia. *Pflugers Arch - Eur J Physiol* **469**, 1567–1577 (2017).
318. Kondratska, K. *et al.* Orai1 and STIM1 mediate SOCE and contribute to apoptotic resistance of pancreatic adenocarcinoma. *Biochimica et Biophysica Acta (BBA) - Molecular Cell Research* **1843**, 2263–2269 (2014).
319. Khan, H. Y. *et al.* Calcium Release-Activated Calcium (CRAC) Channel Inhibition Suppresses Pancreatic Ductal Adenocarcinoma Cell Proliferation and Patient-Derived Tumor Growth. *Cancers* **12**, 750 (2020).
320. Zhou, J. *et al.* Identification of chemoresistance-related mRNAs based on gemcitabine-resistant pancreatic cancer cell lines. *Cancer Medicine* **9**, 1115–1130 (2020).
321. Wang, J. *et al.* STIM1 overexpression in hypoxia microenvironment contributes to pancreatic carcinoma progression. *Cancer Biology & Medicine* **16**, 100 (2019).
322. Dubois, C. *et al.* ORAI3 silencing alters cell proliferation and promotes mitotic catastrophe and apoptosis in pancreatic adenocarcinoma. *Biochimica et Biophysica Acta (BBA) - Molecular Cell Research* **1868**, 119023 (2021).

323. Kuntze, A. *et al.* Protonation of Piezo1 Impairs Cell-Matrix Interactions of Pancreatic Stellate Cells. *Front. Physiol.* **11**, 89 (2020).
324. Fels, B., Nielsen, N. & Schwab, A. Role of TRPC1 channels in pressure-mediated activation of murine pancreatic stellate cells. *Eur Biophys J* **45**, 657–670 (2016).
325. Sauter, D. R. P., Novak, I., Pedersen, S. F., Larsen, E. H. & Hoffmann, E. K. ANO1 (TMEM16A) in pancreatic ductal adenocarcinoma (PDAC). *Pflugers Arch - Eur J Physiol* **467**, 1495–1508 (2015).
326. Crottès, D. *et al.* TMEM16A controls EGF-induced calcium signaling implicated in pancreatic cancer prognosis. *Proc. Natl. Acad. Sci. U.S.A.* **116**, 13026–13035 (2019).
327. Wang, Q. *et al.* TMEM16A Ca<sup>2+</sup>-activated Cl<sup>-</sup> channel inhibition ameliorates acute pancreatitis via the IP3R/Ca<sup>2+</sup>/NFκB/IL-6 signaling pathway. *Journal of Advanced Research* **23**, 25–35 (2020).
328. Zhu, S. *et al.* ASIC1 and ASIC3 contribute to acidity-induced EMT of pancreatic cancer through activating Ca<sup>2+</sup>/RhoA pathway. *Cell Death Dis* **8**, e2806–e2806 (2017).
329. Feske, S. *et al.* A mutation in Orai1 causes immune deficiency by abrogating CRAC channel function. *Nature* **441**, 179–185 (2006).
330. Vig, M. *et al.* CRACM1 Is a Plasma Membrane Protein Essential for Store-Operated Ca<sup>2+</sup> Entry. *Science* **312**, 1220–1223 (2006).
331. Zhang, S. L. *et al.* Genome-wide RNAi screen of Ca<sup>2+</sup> influx identifies genes that regulate Ca<sup>2+</sup> release-activated Ca<sup>2+</sup> channel activity. *Proc. Natl. Acad. Sci. U.S.A.* **103**, 9357–9362 (2006).
332. Yeromin, A. V. *et al.* Molecular identification of the CRAC channel by altered ion selectivity in a mutant of Orai. *Nature* **443**, 226–229 (2006).
333. Mercer, J. C. *et al.* Large Store-operated Calcium Selective Currents Due to Co-expression of Orai1 or Orai2 with the Intracellular Calcium Sensor, Stim1. *Journal of Biological Chemistry* **281**, 24979–24990 (2006).
334. Chalmers, S. B. & Monteith, G. R. ORAI channels and cancer. *Cell Calcium* **74**, 160–167 (2018).
335. Frischauf, I. *et al.* Cooperativeness of Orai Cytosolic Domains Tunes Subtype-specific Gating. *Journal of Biological Chemistry* **286**, 8577–8584 (2011).
336. Rothberg, B. S., Wang, Y. & Gill, D. L. Orai Channel Pore Properties and Gating by STIM: Implications from the Orai Crystal Structure. *Sci. Signal.* **6**, (2013).



337. Derler, I. *et al.* The Extended Transmembrane Orai1 N-terminal (ETON) Region Combines Binding Interface and Gate for Orai1 Activation by STIM1. *Journal of Biological Chemistry* **288**, 29025–29034 (2013).
338. Hou, X., Burstein, S. R. & Long, S. B. Structures reveal opening of the store-operated calcium channel Orai. *eLife* **7**, e36758 (2018).
339. Hogan, P. G. & Rao, A. Store-operated calcium entry: Mechanisms and modulation. *Biochemical and Biophysical Research Communications* **460**, 40–49 (2015).
340. Zhou, Y., Ramachandran, S., Oh-hora, M., Rao, A. & Hogan, P. G. Pore architecture of the ORAI1 store-operated calcium channel. *Proc. Natl. Acad. Sci. U.S.A.* **107**, 4896–4901 (2010).
341. Bokhobza, A. Study of ORAI protein remodeling with CRISPR and quantitative microscopy. (Université de Lille, 2022).
342. Takahashi, Y. *et al.* Essential role of the N-terminus of murine Orai1 in store-operated Ca<sup>2+</sup> entry. *Biochemical and Biophysical Research Communications* **356**, 45–52 (2007).
343. Desai, P. N. *et al.* Multiple types of calcium channels arising from alternative translation initiation of the *Orai1* message. *Sci. Signal.* **8**, (2015).
344. Fukushima, M., Tomita, T., Janoshazi, A. & Putney, J. W. Alternative translation initiation gives rise to two isoforms of *orai1* with distinct plasma membrane mobilities. *Journal of Cell Science* jcs.104919 (2012) doi:10.1242/jcs.104919.
345. Dörr, K. *et al.* Cell type-specific glycosylation of Orai1 modulates store-operated Ca<sup>2+</sup> entry. *Sci. Signal.* **9**, (2016).
346. Roos, J. *et al.* STIM1, an essential and conserved component of store-operated Ca<sup>2+</sup> channel function. *Journal of Cell Biology* **169**, 435–445 (2005).
347. Liou, J. *et al.* STIM Is a Ca<sup>2+</sup> Sensor Essential for Ca<sup>2+</sup>-Store-Depletion-Triggered Ca<sup>2+</sup> Influx. *Current Biology* **15**, 1235–1241 (2005).
348. Spassova, M. A. *et al.* STIM1 has a plasma membrane role in the activation of store-operated Ca<sup>2+</sup> channels. *Proc. Natl. Acad. Sci. U.S.A.* **103**, 4040–4045 (2006).
349. Zbidi, H. *et al.* STIM1 and STIM2 Are Located in the Acidic Ca<sup>2+</sup> Stores and Associates with Orai1 upon Depletion of the Acidic Stores in Human Platelets. *Journal of Biological Chemistry* **286**, 12257–12270 (2011).

350. Collins, H. E., Zhang, D. & Chatham, J. C. STIM and Orai Mediated Regulation of Calcium Signaling in Age-Related Diseases. *Front. Aging* **3**, 876785 (2022).
351. Putney, J., W. Origins of the concept of store-operated calcium entry. *Front Biosci* **S3**, 980 (2011).
352. Noble, M. *et al.* Structural Mechanisms of Store-Operated and Mitochondrial Calcium Regulation: Initiation Points for Drug Discovery. *IJMS* **21**, 3642 (2020).
353. Casteels, R. & Droogmans, G. Exchange characteristics of the noradrenaline-sensitive calcium store in vascular smooth muscle cells or rabbit ear artery. *The Journal of Physiology* **317**, 263–279 (1981).
354. Putney, J. W. *et al.* The functions of store-operated calcium channels. *Biochimica et Biophysica Acta (BBA) - Molecular Cell Research* **1864**, 900–906 (2017).
355. Hoth, M. & Penner, R. Depletion of intracellular calcium stores activates a calcium current in mast cells. *Nature* **355**, 353–356 (1992).
356. Hoth, M. Calcium and barium permeation through calcium release-activated calcium (CRAC) channels. *Pflügers Arch* **430**, 315–322 (1995).
357. Zweifach, A. & Lewis, R. S. Rapid inactivation of depletion-activated calcium current (ICRAC) due to local calcium feedback. *Journal of General Physiology* **105**, 209–226 (1995).
358. Brough, G. H. *et al.* Contribution of endogenously expressed Trp1 to a Ca<sup>2+</sup>-selective, store-operated Ca<sup>2+</sup> entry pathway. *FASEB j.* **15**, 1704–1710 (2001).
359. Rosado, J. A. Discovering the mechanism of capacitative calcium entry. *American Journal of Physiology-Cell Physiology* **291**, C1104–C1106 (2006).
360. Sun, Y., Birnbaumer, L. & Singh, B. B. TRPC1 regulates calcium-activated chloride channels in salivary gland cells. *J. Cell. Physiol.* **230**, 2848–2856 (2015).
361. Liao, Y. *et al.* Functional interactions among Orai1, TRPCs, and STIM1 suggest a STIM-regulated heteromeric Orai/TRPC model for SOCE/Icrac channels. *Proc. Natl. Acad. Sci. U.S.A.* **105**, 2895–2900 (2008).
362. Cheng, K. T., Liu, X., Ong, H. L., Swaim, W. & Ambudkar, I. S. Local Ca<sup>2+</sup> Entry Via Orai1 Regulates Plasma Membrane Recruitment of TRPC1 and Controls Cytosolic Ca<sup>2+</sup> Signals Required for Specific Cell Functions. *PLoS Biol* **9**, e1001025 (2011).

363. Lis, A. *et al.* CRACM1, CRACM2, and CRACM3 Are Store-Operated Ca<sup>2+</sup> Channels with Distinct Functional Properties. *Current Biology* **17**, 794–800 (2007).
364. Bandara, S., Malmersjö, S. & Meyer, T. Regulators of Calcium Homeostasis Identified by Inference of Kinetic Model Parameters from Live Single Cells Perturbed by siRNA. *Sci. Signal.* **6**, (2013).
365. Leon-Aparicio, D. *et al.* Orai3 channel is the 2-APB-induced endoplasmic reticulum calcium leak. *Cell Calcium* **65**, 91–101 (2017).
366. Inayama, M. *et al.* Orai1–Orai2 complex is involved in store-operated calcium entry in chondrocyte cell lines. *Cell Calcium* **57**, 337–347 (2015).
367. Vaeth, M. *et al.* ORAI2 modulates store-operated calcium entry and T cell-mediated immunity. *Nat Commun* **8**, 14714 (2017).
368. Yoast, R. E. *et al.* The native ORAI channel trio underlies the diversity of Ca<sup>2+</sup> signaling events. *Nat Commun* **11**, 2444 (2020).
369. Smedler, E. & Uhlén, P. Frequency decoding of calcium oscillations. *Biochimica et Biophysica Acta (BBA) - General Subjects* **1840**, 964–969 (2014).
370. Dolmetsch, R. E., Xu, K. & Lewis, R. S. Calcium oscillations increase the efficiency and specificity of gene expression. *Nature* **392**, 933–936 (1998).
371. Perez, J. F. & Sanderson, M. J. The Frequency of Calcium Oscillations Induced by 5-HT, ACH, and KCl Determine the Contraction of Smooth Muscle Cells of Intrapulmonary Bronchioles. *Journal of General Physiology* **125**, 535–553 (2005).
372. Gu, X. & Spitzer, N. C. Distinct aspects of neuronal differentiation encoded by frequency of spontaneous Ca<sup>2+</sup> transients. *Nature* **375**, 784–787 (1995).
373. Debir, B., Meaney, C., Kohandel, M. & Unlu, M. B. The role of calcium oscillations in the phenotype selection in endothelial cells. *Sci Rep* **11**, 23781 (2021).
374. De Young, G. W. & Keizer, J. A single-pool inositol 1,4,5-trisphosphate-receptor-based model for agonist-stimulated oscillations in Ca<sup>2+</sup> concentration. *Proc. Natl. Acad. Sci. U.S.A.* **89**, 9895–9899 (1992).
375. Sneyd, J. *et al.* On the dynamical structure of calcium oscillations. *Proc Natl Acad Sci USA* **114**, 1456–1461 (2017).

376. Dolmetsch, R. E. & Lewis, R. S. Signaling between intracellular Ca<sup>2+</sup> stores and depletion-activated Ca<sup>2+</sup> channels generates [Ca<sup>2+</sup>]<sub>i</sub> oscillations in T lymphocytes. *Journal of General Physiology* **103**, 365–388 (1994).
377. Liu, X., Liao, D. & Ambudkar, I. S. Distinct Mechanisms of [Ca<sup>2+</sup>]<sub>i</sub> Oscillations in HSY and HSG Cells: Role of Ca<sup>2+</sup> Influx and Internal Ca<sup>2+</sup> Store Recycling. *J. Membrane Biol.* **181**, 185–193 (2001).
378. Bird, G. St. J. & Putney, J. W. Capacitative calcium entry supports calcium oscillations in human embryonic kidney cells: Calcium entry and oscillations. *The Journal of Physiology* **562**, 697–706 (2005).
379. Wedel, B., Boyles, R. R., Putney, J. W. & Bird, G. S. Role of the store-operated calcium entry proteins Stim1 and Orai1 in muscarinic cholinergic receptor-stimulated calcium oscillations in human embryonic kidney cells: Stim1, Orai1 and calcium oscillations. *The Journal of Physiology* **579**, 679–689 (2007).
380. Zhang, X. *et al.* A calcium/cAMP signaling loop at the ORAI1 mouth drives channel inactivation to shape NFAT induction. *Nat Commun* **10**, 1971 (2019).
381. Boie, S., Chen, J., Sanderson, M. J. & Sneyd, J. The relative contributions of store-operated and voltage-gated Ca<sup>2+</sup> channels to the control of Ca<sup>2+</sup> oscillations in airway smooth muscle: Store-operated and voltage-gated Ca<sup>2+</sup> channels in airway smooth muscle. *J Physiol* **595**, 3129–3141 (2017).
382. Ong, H. L. *et al.* STIM2 enhances receptor-stimulated Ca<sup>2+</sup> signaling by promoting recruitment of STIM1 to the endoplasmic reticulum–plasma membrane junctions. *Sci. Signal.* **8**, (2015).
383. Thiel, M., Lis, A. & Penner, R. STIM2 drives Ca<sup>2+</sup> oscillations through store-operated Ca<sup>2+</sup> entry caused by mild store depletion: STIM2 drives Ca<sup>2+</sup> oscillations through store-operated Ca<sup>2+</sup> entry. *The Journal of Physiology* **591**, 1433–1445 (2013).
384. Emrich, S. M. *et al.* Omnitemporal choreographies of all five STIM/Orai and IP3Rs underlie the complexity of mammalian Ca<sup>2+</sup> signaling. *Cell Reports* **34**, 108760 (2021).
385. Sun, J. *et al.* STIM1- and Orai1-mediated Ca<sup>2+</sup> oscillation orchestrates invadopodium formation and melanoma invasion. *Journal of Cell Biology* **207**, 535–548 (2014).
386. Zhu, H. *et al.* Elevated Orai1 expression mediates tumor-promoting intracellular Ca<sup>2+</sup> oscillations in human esophageal squamous cell carcinoma. *Oncotarget* **5**, 3455–3471 (2014).

387. Sun, C. *et al.* Central role of IP3R2-mediated Ca<sup>2+</sup> oscillation in self-renewal of liver cancer stem cells elucidated by high-signal ER sensor. *Cell Death Dis* **10**, 396 (2019).
388. Dragoni, S. *et al.* Vascular Endothelial Growth Factor Stimulates Endothelial Colony Forming Cells Proliferation and Tubulogenesis by Inducing Oscillations in Intracellular Ca<sup>2+</sup> Concentration. *Stem Cells* **29**, 1898–1907 (2011).
389. Kume, K., Chen, L., Lee, J. & Müschen, M. Autonomous Ca<sup>2+</sup> Oscillations Reflect Oncogenic Signaling in B-ALL Cells. *Blood* **134**, 1253–1253 (2019).
390. Wang, L. *et al.* Prostate Cancer Incidence and Mortality: Global Status and Temporal Trends in 89 Countries From 2000 to 2019. *Front. Public Health* **10**, 811044 (2022).
391. Chen, R. *et al.* Cav1.3 channel  $\alpha 1D$  protein is overexpressed and modulates androgen receptor transactivation in prostate cancers. *Urologic Oncology: Seminars and Original Investigations* **32**, 524–536 (2014).
392. Perrouin Verbe, M.-A., Bruyere, F., Rozet, F., Vandier, C. & Fromont, G. Expression of store-operated channel components in prostate cancer: the prognostic paradox. *Human Pathology* **49**, 77–82 (2016).
393. Derouiche, S. *et al.* Bisphenol A stimulates human prostate cancer cell migration via remodelling of calcium signalling. *SpringerPlus* **2**, 54 (2013).
394. Zhou, Y. *et al.* Suppression of STIM1 inhibits the migration and invasion of human prostate cancer cells and is associated with PI3K/Akt signaling inactivation. *Oncology Reports* **38**, 2629–2636 (2017).
395. Crumbaker, M., Khoja, L. & Joshua, A. AR Signaling and the PI3K Pathway in Prostate Cancer. *Cancers* **9**, 34 (2017).
396. Xu, Y. *et al.* STIM1 accelerates cell senescence in a remodeled microenvironment but enhances the epithelial-to-mesenchymal transition in prostate cancer. *Sci Rep* **5**, 11754 (2015).
397. Flourakis, M. *et al.* Orai1 contributes to the establishment of an apoptosis-resistant phenotype in prostate cancer cells. *Cell Death Dis* **1**, e75–e75 (2010).
398. Berry, P. A., Birnie, R., Droop, A. P., Maitland, N. J. & Collins, A. T. The calcium sensor STIM1 is regulated by androgens in prostate stromal cells. *Prostate* **71**, 1646–1655 (2011).

399. Liu, G. *et al.* Up-regulation of Orai1 expression and store operated Ca<sup>2+</sup> entry following activation of membrane androgen receptors in MCF-7 breast tumor cells. *BMC Cancer* **15**, 995 (2015).
400. Kashyap, D. *et al.* Global Increase in Breast Cancer Incidence: Risk Factors and Preventive Measures. *BioMed Research International* **2022**, 1–16 (2022).
401. Gueder, N. *et al.* sp<sup>2</sup>-Iminosugar  $\alpha$ -glucosidase inhibitor 1- C -octyl-2-oxa-3-oxocastanospermine specifically affected breast cancer cell migration through Stim1,  $\beta$ 1-integrin, and FAK signaling pathways. *J Cell Physiol* **232**, 3631–3640 (2017).
402. Yang, S., Zhang, J. J. & Huang, X.-Y. Orai1 and STIM1 Are Critical for Breast Tumor Cell Migration and Metastasis. *Cancer Cell* **15**, 124–134 (2009).
403. Motiani, R. K. *et al.* Orai3 is an estrogen receptor  $\alpha$ -regulated Ca<sup>2+</sup> channel that promotes tumorigenesis. *FASEB j.* **27**, 63–75 (2013).
404. Hu, J. *et al.* Downregulation of transcription factor Oct4 induces an epithelial-to-mesenchymal transition via enhancement of Ca<sup>2+</sup> influx in breast cancer cells. *Biochemical and Biophysical Research Communications* **411**, 786–791 (2011).
405. Davis, F. M. *et al.* Non-Stimulated, Agonist-Stimulated and Store-Operated Ca<sup>2+</sup> Influx in MDA-MB-468 Breast Cancer Cells and the Effect of EGF-Induced EMT on Calcium Entry. *PLoS ONE* **7**, e36923 (2012).
406. Azimi, I. *et al.* Pharmacological inhibition of store-operated calcium entry in MDA-MB-468 basal A breast cancer cells: consequences on calcium signalling, cell migration and proliferation. *Cell. Mol. Life Sci.* **75**, 4525–4537 (2018).
407. Liu, X. *et al.* Orai1 is critical for Notch-driven aggressiveness under hypoxic conditions in triple-negative breast cancers. *Biochimica et Biophysica Acta (BBA) - Molecular Basis of Disease* **1864**, 975–986 (2018).
408. Hasna, J. *et al.* Orai3 calcium channel and resistance to chemotherapy in breast cancer cells: the p53 connection. *Cell Death Differ* **25**, 693–707 (2018).
409. Babaer, D. *et al.* High salt induces P-glycoprotein mediated treatment resistance in breast cancer cells through store operated calcium influx. *Oncotarget* **9**, 25193–25205 (2018).
410. Schmidt, S. *et al.* Enhanced Orai1 and STIM1 expression as well as store operated Ca<sup>2+</sup> entry in therapy resistant ovary carcinoma cells. *Oncotarget* **5**, 4799–4810 (2014).

411. Abdelazeem, K. N. M. *et al.* Upregulation of Orai1 and STIM1 expression as well as store-operated Ca<sup>2+</sup> entry in ovary carcinoma cells by placental growth factor. *Biochemical and Biophysical Research Communications* **512**, 467–472 (2019).
412. Huang, H.-K. *et al.* Chemoresistant ovarian cancer enhances its migration abilities by increasing store-operated Ca<sup>2+</sup> entry-mediated turnover of focal adhesions. *J Biomed Sci* **27**, 36 (2020).
413. Soboloff, J., Zhang, Y., Minden, M. & Berger, S. A. Sensitivity of myeloid leukemia cells to calcium influx blockade. *Experimental Hematology* **30**, 1219–1226 (2002).
414. Cabanas, H. *et al.* Deregulation of calcium homeostasis in Bcr-Abl-dependent chronic myeloid leukemia. *Oncotarget* **9**, 26309–26327 (2018).
415. Piwocka, K., Vejda, S., Cotter, T. G., O’Sullivan, G. C. & McKenna, S. L. Bcr-Abl reduces endoplasmic reticulum releasable calcium levels by a Bcl-2-independent mechanism and inhibits calcium-dependent apoptotic signaling. *Blood* **107**, 4003–4010 (2006).
416. Ritchie, M. F., Yue, C., Zhou, Y., Houghton, P. J. & Soboloff, J. Wilms Tumor Suppressor 1 (WT1) and Early Growth Response 1 (EGR1) Are Regulators of STIM1 Expression. *Journal of Biological Chemistry* **285**, 10591–10596 (2010).
417. Owen, C., Fitzgibbon, J. & Paschka, P. The clinical relevance of Wilms Tumour 1 (WT1) gene mutations in acute leukaemia. *Hematol. Oncol.* n/a-n/a (2009) doi:10.1002/hon.931.
418. Inoue, K. *et al.* Wilms’ Tumor Gene (WT1) Competes With Differentiation-Inducing Signal in Hematopoietic Progenitor Cells. *Blood* **91**, 2969–2976 (1998).
419. Hoover, P. J. & Lewis, R. S. Stoichiometric requirements for trapping and gating of Ca<sup>2+</sup> release-activated Ca<sup>2+</sup> (CRAC) channels by stromal interaction molecule 1 (STIM1). *Proc. Natl. Acad. Sci. U.S.A.* **108**, 13299–13304 (2011).
420. Diez-Bello, R., Jardin, I., Salido, G. M. & Rosado, J. A. Orai1 and Orai2 mediate store-operated calcium entry that regulates HL60 cell migration and FAK phosphorylation. *Biochimica et Biophysica Acta (BBA) - Molecular Cell Research* **1864**, 1064–1070 (2017).
421. Zhu, M. *et al.* Store-operated Ca<sup>2+</sup> entry regulates glioma cell migration and invasion via modulation of Pyk2 phosphorylation. *J Exp Clin Cancer Res* **33**, 98 (2014).

422. Hernando-Pérez, E. *et al.* Differential Ca<sup>2+</sup> responses and store operated Ca<sup>2+</sup> entry in primary cells from human brain tumors. *Biochimica et Biophysica Acta (BBA) - Molecular Cell Research* **1868**, 119060 (2021).
423. Aulestia, F. J. *et al.* Quiescence status of glioblastoma stem-like cells involves remodelling of Ca<sup>2+</sup> signalling and mitochondrial shape. *Sci Rep* **8**, 9731 (2018).
424. Terrié, E. *et al.* Store-Operated Calcium Channels Control Proliferation and Self-Renewal of Cancer Stem Cells from Glioblastoma. *Cancers* **13**, 3428 (2021).
425. Motiani, R. K. *et al.* STIM1 and Orai1 mediate CRAC channel activity and are essential for human glioblastoma invasion. *Pflugers Arch - Eur J Physiol* **465**, 1249–1260 (2013).
426. Feldman, B., Fedida-Metula, S., Nita, J., Sekler, I. & Fishman, D. Coupling of mitochondria to store-operated Ca<sup>2+</sup>-signaling sustains constitutive activation of protein kinase B/Akt and augments survival of malignant melanoma cells. *Cell Calcium* **47**, 525–537 (2010).
427. Fedida-Metula, S. *et al.* Lipid rafts couple store-operated Ca<sup>2+</sup> entry to constitutive activation of PKB/Akt in a Ca<sup>2+</sup>/calmodulin-, Src- and PP2A-mediated pathway and promote melanoma tumor growth. *Carcinogenesis* **33**, 740–750 (2012).
428. Stanisz, H. *et al.* Inverse regulation of melanoma growth and migration by Orai1/STIM2-dependent calcium entry. *Pigment Cell Melanoma Res.* **27**, 442–453 (2014).
429. Umemura, M. *et al.* Store-Operated Ca<sup>2+</sup> Entry (SOCE) Regulates Melanoma Proliferation and Cell Migration. *PLoS ONE* **9**, e89292 (2014).
430. Hooper, R. *et al.* Novel Protein Kinase C-Mediated Control of Orai1 Function in Invasive Melanoma. *Mol Cell Biol* **35**, 2790–2798 (2015).
431. Gross, S. *et al.* Suppression of Ca<sup>2+</sup> signaling enhances melanoma progression. *The EMBO Journal* **41**, (2022).
432. Akella, N. M., Ciraku, L. & Reginato, M. J. Fueling the fire: emerging role of the hexosamine biosynthetic pathway in cancer. *BMC Biol* **17**, 52 (2019).
433. Derler, I. *et al.* Cholesterol modulates Orai1 channel function. *Sci. Signal.* **9**, (2016).



434. Woods, N. *et al.* Fendiline inhibits proliferation and invasion of pancreatic cancer cells by interfering with ADAM10 activation and  $\beta$ -catenin signaling. *Oncotarget* **6**, 35931–35948 (2015).
435. Kutschat, A. P., Johnsen, S. A. & Hamdan, F. H. Store-Operated Calcium Entry: Shaping the Transcriptional and Epigenetic Landscape in Pancreatic Cancer. *Cells* **10**, 966 (2021).
436. Strobel, O., Neoptolemos, J., Jäger, D. & Büchler, M. W. Optimizing the outcomes of pancreatic cancer surgery. *Nat Rev Clin Oncol* **16**, 11–26 (2019).
437. Carvalho, T. M. A. *et al.* Tumor Microenvironment Features and Chemoresistance in Pancreatic Ductal Adenocarcinoma: Insights into Targeting Physicochemical Barriers and Metabolism as Therapeutic Approaches. *Cancers* **13**, 6135 (2021).
438. Zheng, T., Jäättelä, M. & Liu, B. pH gradient reversal fuels cancer progression. *The International Journal of Biochemistry & Cell Biology* **125**, 105796 (2020).
439. Gao, J. *et al.* Differential metabolic responses in breast cancer cell lines to acidosis and lactic acidosis revealed by stable isotope assisted metabolomics. *Sci Rep* **10**, 21967 (2020).
440. Michl, J., Park, K. C. & Swietach, P. Evidence-based guidelines for controlling pH in mammalian live-cell culture systems. *Commun Biol* **2**, 144 (2019).
441. Webb, B. A., Chimenti, M., Jacobson, M. P. & Barber, D. L. Dysregulated pH: a perfect storm for cancer progression. *Nat Rev Cancer* **11**, 671–677 (2011).
442. Gupta, S. C., Singh, R., Pochampally, R., Watabe, K. & Mo, Y.-Y. Acidosis promotes invasiveness of breast cancer cells through ROS-AKT-NF- $\kappa$ B pathway. *Oncotarget* **5**, 12070–12082 (2014).
443. Eylestein, A. *et al.* Transcription Factor NF- $\kappa$ B Regulates Expression of Pore-forming Ca<sup>2+</sup> Channel Unit, Orai1, and Its Activator, STIM1, to Control Ca<sup>2+</sup> Entry and Affect Cellular Functions. *Journal of Biological Chemistry* **287**, 2719–2730 (2012).
444. Berry, C. T., May, M. J. & Freedman, B. D. STIM- and Orai-mediated calcium entry controls NF- $\kappa$ B activity and function in lymphocytes. *Cell Calcium* **74**, 131–143 (2018).